Characterising the genetic architecture of common elastic tissue disorders using UK Biobank

A thesis submitted to the University of Oxford in partial fulfilment of the requirements for the degree of

Doctor of Philosophy

Molecular and Cellular Medicine

Dr Waheed-Ul-Rahman Ahmed

Green Templeton College

NDORMS

Trinity Term 2024

Abstract

Background

Elastic fibres are key extracellular matrix (ECM) components that provide elasticity to tissues throughout the body, allowing them to recover after deformation. Derangement of elastic fibres lead to cutaneous and systemic disorders that show elastic tissue pathology. To distinguish between rarer disorders of elastic tissue, and common disease, I have coined the term '*elastopathies*.' Common elastopathies such as hiatus hernia, diverticular disease, haemorrhoids, inguinal hernia, varicose veins, female genital prolapse, umbilical hernia, aneurysmal disease, emphysema, pneumothorax, rectal prolapse, and femoral hernia, have a complex aetiology where genetic predisposition and environmental factors interplay to influence overall phenotypic expression. These elastopathies are highly prevalent and exert a significant healthcare and socioeconomic burden. However, their genetic basis remains poorly defined, with limited putative genes identified.

Method

To unravel the genetic architecture of the 12 elastopathies identified in the UK Biobank resource (hiatus hernia, diverticular disease, haemorrhoids, inguinal hernia, varicose veins, female genital prolapse, umbilical hernia, aneurysmal disease, emphysema, pneumothorax, rectal prolapse, and femoral hernia), genome-wide association study (GWAS) testing was performed across ~400,000 genotyped participants from the UK Biobank resource, with replication from ~410,000 participants from 23andMe, Inc. (California) for the varicose veins analysis. All 12 elastopathies were studied

independently, and then combined in a final pan-elastopathy GWA study to identify the shared genetic architecture of common elastopathies in UK Biobank. A disparate analysis was performed combining all four types of hernia in a pan-hernia analysis to identify shared genetics. Genes and pathways were prioritised using a suite of bioinformatic approaches, and pharmacological targets identified using the Open Targets Platform. A genetic risk score was constructed to examine the genetic burden among participants with severe disease. For the pan-hernia analysis, multi-trait and multivariate meta-analysis approaches were deployed to uncover the shared genetic susceptibility to multiple hernia phenotypes. For the pan-elastopathy analysis, an individual patient data (IPD) meta-analysis was performed and the latent elastopathy phenotype was analysed using genomic structural equation modelling (SEM) to uncover shared genetic biology.

Results

Performing the largest two-stage GWAS of varicose veins in 810,625 participants, forty-nine signals at 46 susceptibility loci were discovered, including 29 previously unreported associations. Next, through (at the time) the first-ever GWA study of haemorrhoids in over 400,000 participants, 13 signals at 12 novel loci were discovered to associate with haemorrhoids. Association analysis of inguinal, femoral, umbilical, and hiatus hernia individually yielded 58 signals at 38 loci (34 new) associated with the four hernia phenotypes. When combined in a multi-trait meta-analysis, 12 biologically relevant putative loci were discovered to associate with multiple hernia phenotypes, demonstrating novel and robust evidence of shared susceptibility to hernia. Of significance, the genetic risk scoring correlated with disease severity across the varicose veins, haemorrhoids, and pan-hernia analyses, with patients undergoing

surgery having a higher genetic burden than those managed non-surgically. Lastly, studying the 12 elastopathies in a pan-elastopathy IPD meta-analysis, 18 susceptibility loci were discovered to associate with the pan-elastopathy phenotype which were not discovered when the 12 elastopathies were studied individually. Moreover, employing common factor analysis to unveil the latent elastopathy phenotype, a further four loci were discovered to be integral to a shared genetic risk towards elastopathies. Collectively, over 250 independent susceptibility loci were discovered to associate with the 12 elastopathies, which were mapped to over 500 putative genes, many of which demonstrated profound evidence of a shared genetic biology, therapeutic tractability and clustered in pathways pertaining to core matrisomal components and ECM homeostasis.

Conclusion

Prioritised genes and pathways demonstrate significant biological plausibility, and represent promising candidates for further investigation of elastic tissue biology and potential pharmacological targeting. The genetic risk score correlated with disease across varicose veins, haemorrhoids and hernia disorders, representing an important proof-of-principle for the future use of genetic risk scoring in personalised medicine approaches to surgical disorders. Lastly, studying the 12 elastic tissue disorders together, a novel category of pathologically linked disorders defined by elastic tissue dysfunction were discovered— the elastopathies. To this end, this thesis advances the field of study around elastopathies and complex trait genetics.

Dedicated to the memory of my late grandfather,

Master Muhammad Yunus Bhatti

(1924 - 1990)

إِنَّا لِلّٰهِ وَإِنَّـا إِلَيْهِ رَاجِعُونَ

Though we never met, your remarkable focus on the importance of education as a teacher in my ancestral village of Hill Kalan, Kotli, Azad Jammu and Kashmir, shaped my family and my journey. Your legacy guided me to Oxford.

Acknowledgements

الْحَمْدُ لِلَّهِ الَّذِي بِنِعْمَتِهِ تَتِمُّ الصَّالِحَاتُ

All praise is due to Allah (God), by whose honour and majesty, deeds of virtue are accomplished.

I am deeply grateful to Allah (the most glorified) for granting me the opportunity to study at the University of Oxford, where I have been able to learn without bounds and deepen my understanding of medicine. As an NHS doctor, I have witnessed first-hand the impact of health inequalities. It is my hope that my research on elastopathies will contribute to closing these gaps, ensuring better care for the millions in the UK afflicted by these devastating diseases and for those most in need.

I owe my sincerest and deepest gratitude to my supervisors, Professor Dominic Furniss, Mr Akira Wiberg, and Professor Krina Zondervan, for their invaluable mentorship, patience, and unwavering belief in me over the past five years. I have learned more under your guidance than I could have known possible, and you gave me far more time and support than two DPhil students would ever warrant. Your expertise, generosity, and encouragement have shaped me into a better doctor, scientist, and person, and I will carry the lessons you taught me throughout my career and life.

It is easy to follow the path well-trodden, and hence I consider myself deeply fortunate to have been within a minute's walk from Dr Michael Ng and Mr Akira Wiberg. Your expertise in GWAS proved invaluable at many critical junctures throughout my DPhil journey. Thank you for your patience with my questions, for bouncing ideas, and for enduring my late-night emails with such grace.

A heartfelt thank you to my Director of Graduate Studies at NDORMS, Professor Afsie Sabokbar, whose kindness and support have meant a lot to me. You have been a second mother to me at the Botnar, always looking out for my wellbeing and facilitating my return to Oxford after my Master's. Your pastoral care for myself and other students has been invaluable and cannot be overstated.

I owe my deepest gratitude to my wife, Saira Noor Hassan, and my 17-month-old son, Muhammad Yunus Waheed. Saira, you have been my unwavering pillar of support through the toughest years of my life. We got married during the early stages of my DPhil, and throughout these years, despite all the challenges—moving homes, balancing life with a new child, and my work as a doctor—you never asked for much, even when you deserved so much more. Your endless patience, love, and encouragement kept me going, especially when I felt like giving up. You made it possible for me to persevere, even when you were pregnant and caring for our child. This DPhil journey has been as much yours as it has been mine.

My son Yunus, your presence filled even the hardest days with joy and purpose. Your laughter and lightness inspired me to keep pushing forward, and I will make you as proud of me as I am of you.

At the heart of it all, I owe an immeasurable debt to my parents, Manzoor Ahmad Bhatti and Robina Kausar Bhatti, for their endless sacrifices and unwavering support. Your courage to leave your home and family in Kashmir to build a better life in England, and the countless struggles you faced, have defined who I am today. Your perseverance, and the values of hard work, humility, prayer and being in the service of those in need, have profoundly influenced my worldview. Coming to Oxford is the realisation of a dream that you made possible, and I will never forget the sacrifices you endured to get me here.

Lastly, to my best friend, Akmal Ali, and all the friends I've made at Oxford—thank you for your support and camaraderie throughout this journey. I have enjoyed every minute of my time in Oxford and learned more than I knew possible and made memories that I will cherish for the rest of my life.

Preface

This thesis is a collection of the research work carried out by myself in the Botnar Research Centre, Nuffield Department of Orthopaedics, Rheumatology and Musculoskeletal Sciences (NDORMS), University of Oxford, between October 2019 and October 2024, under the supervision of Professor Dominic Furniss, Mr Akira Wiberg, and Professor Krina Zondervan.

Every piece of work that is described in this thesis was conducted solely by me, with the exception of the following:

- Mr Akira Wiberg performed the quality control (QC) of the UK Biobank resource that was used in all chapters, and ran the initial association analysis for varicose veins (**Chapter 2**).
- Dr Michael Ng performed the case-control matching and developed the codes to run the metaUSAT analysis for the pan-hernia study (**Chapter 4**).
- Dr Sam Kleeman performed the common factor analysis using summary data I generated for the pan-elastopathy study (**Chapter 5).**

- **Chapter 2** is part of a manuscript titled *'Genome-wide association analysis and replication in 810,625 individuals with varicose veins'* (Nat Commun **13**, 3065 (2022)).
- **Chapter 3** has been presented at the European Society of Coloproctology (ESCP) 2020 International Conference and the Association of Surgeons In Training (ASiT) 2021 Conference: *"Genome-Wide Association Analysis In 401,583 Individuals Identifies Novel Therapeutic Targets for Haemorrhoids"* (Br J Surg, **108**, s6 (2021)).
- **Chapter 4** is part of a manuscript titled *"Shared genetic architecture of hernias: A genome-wide association study with multivariable meta-analysis of multiple hernia phenotypes"* (PLoS ONE 17(12): e0272261 (2022)).
- **Chapter 5** is being prepared in manuscript form for submission to a peer-reviewed journal.

I state the research described herein is original, though the work of others is cited with appropriate references in-text. No part of this research has previously been submitted for the conferral of a degree outside of the University of Oxford. However, **Chapter 2**, **Chapter 3**, and **Chapter 4** are presented *as is* from the prior MSc viva on 9th October 2020 based on the dispensation outcome from the MSD Education Committee on the 19th January 2021.

Dr Waheed-Ul-Rahman Ahmed

Oct 2024

Abbreviations

AAA: Abdominal Aortic Aneurysm

α-SMA: Alpha-Smooth Muscle Actin

ANNOVAR: Annotate Variation

ANOVA: Analysis of Variance

BOLT-LMM: Bayesian Optimized Likelihood Tree with a Linear Mixed Model

BMP: Bone Morphogenetic Protein

CAD: Coronary Artery Disease

CADD: Combined Annotation Dependent Depletion

CCN: Cellular Communication Network

cDNA: Complimentary DNA

COPD: Chronic Obstructive Pulmonary Disease

DD: Diverticular Disease

DNA: Deoxyribonucleic Acid

EAF: Effect Allele Frequency

ECM: Extracellular Matrix

EDS: Ehlers-Danlos syndrome

eQTL: Expression Quantitative Trait Locus

FDR: False Discovery Rate

FUMA: Functional Mapping and Annotation of GWAS

GDF: Growth Differentiation Factor

GERA: Genetic Epidemiology Research on Adult Health and Aging

GERP: Genomic Evolutionary Rate Profiling

GO: Gene Ontology

GORD: Gastro-Oesophageal Reflux Disease

GRM: Genetic Relationship Matrix

GWA: Genome-Wide Association

GWAMA: Genome-Wide Association Meta-Analysis

GWAS: Genome-Wide Association Study

HEIDI: Heterogeneity In Dependent Instrument

HyPrColoc: Hypothesis Prioritisation in Multi-Trait Colocalisation

IBD: Identity-by-descent

IndSigSNPs: Independent significant SNPs

IPD: Individual Patient Data

LD: Linkage Disequilibrium

LDS: Loeys-Dietz Syndrome

LDHub: Linkage Disequilibrium Hub

LDSC: Linkage Disequilibrium Score Regression

MAGMA: Multi-Marker Analysis of Genomic Annotation

MAF: Minor Allele Frequency

MFS: Marfan Syndrome

MHC: Major Histocompatibility Complex

MiRNA: Micro RNA

MMP: Matrix Metalloproteinase

MSigDB: Molecular Signatures Database

MTAG: Multi-Trait Analysis of GWAS

OPCS: Office of Population Censuses and Surveys Classification of Interventions and Procedures

OR: Odds Ratio

Pan-UKBB: Pan-UK Biobank

PHF2: Plant Homeodomain Finger Protein 2

PSP: Primary Spontaneous Pneumothorax

PXE: Pseudoxanthoma Elasticum

QC: Quality Control

RDB: RegulomeDB

SAIGE: Scalable and Accurate Implementation of Generalized Mixed Model

SIFT: Sorting Intolerant From Tolerant

SMR: Summary-Based Mendelian Randomisation

SNP: Single Nucleotide Polymorphism

SVAS: Supravalvular Aortic Stenosis

TAA: Thoracic Aortic Aneurysm

TGF: Transforming Growth Factor

TIMPs: Tissue Inhibitors of Metalloproteinases

VEGF: Vascular Endothelial Growth Factor

VA-MVP: Veterans Affairs Million Veteran Programme

vSMC: Vascular Smooth Muscle Cell

VVs: Varicose Veins

WBS: Williams-Beuren Syndrome

WMS: Weill-Marchesani Syndrome

WT1: Wilms Tumour 1

Table of Contents

Chapter 1: Introduction

1.1. Introduction

1.1.1. The extracellular matrix

The extracellular matrix (ECM) is a complex three-dimensional network comprising ~1 - 1.5% of the mammalian proteome.[1] The ECM is a highly complex and dynamic organ central to all tissues; it is continuously remodelled to regulate tissue homeostasis.[2] Aside from its mechanical and architectural properties, via cell-ECM and ECM-cell interactions the ECM receives and transmits signals between cells, meaning it plays an important role in vital cellular processes such as adhesion, proliferation, migration, differentiation and apoptosis.[3] The ECM can be sub-divided into two fundamental constituents: i) the interstitial connective tissue matrix (encapsulates cells), ii) the basement membrane (separates epithelium from stroma) (**Figure 1.1**).[4] The core matrisome* comprises ~300 proteins, including 43 collagen subunits, ~200 glycoproteins and ~36 proteoglycans.[1] Collagens are the most abundant ECM protein, able to fold into different sized trimeric, coiled coil rods that impart structural integrity to the ECM of several tissues, including tendon (fibres), bone and cartilage (organic matrices), basement membrane (laminar sheets), vitreous humour (viscous matrix), and the dermis and capsules of organs (interstitial matrices).[5]

Another central structural component of the ECM is elastin, a glycoprotein constituent that confers elasticity to tissues and complements the function of collagens. Other extensively studied glycoproteins include fibronectins, laminins, thrombospondins, fibulins and tenascins.[6] Glycoproteins have a myriad of functions including ECM

* A complete 'parts list' of all the proteins that make up the extracellular matrix (ECM) and proteins that have the ability to contribute to the ECM in different scenarios.

assembly, and importantly can act as integral membrane proteins (such as the integrins) where they are central to ECM-cell interactions and regulate fundamental cellular processes, often via growth factor signalling.[3] The glycoprotein family of ECM proteins comprise a characteristic repeating oligosaccharide chain attached covalently to amino acid side-chains. Another constituent of the core matrisome is the proteoglycan family which, among other attributes, have important space-filling and lubrication properties due to their constituent glycosaminoglycan (GAG) chains which are strongly negatively charged.[7] Well-known proteoglycans include versican (anti-adhesion molecule in blood vessels and other tissues), perlecan (endothelial barrier function), aggrecan (major proteoglycan in cartilage), and fibromodulin (epidermis).[1]

Figure 1.1. The extracellular matrix (ECM). The ECM consists of two components: an interstitial matrix and a basement membrane. The mammalian matrisome is the complete 'parts list' of ECM proteins that comprise the ECM. Adapted from Bonnans (2014).[4]

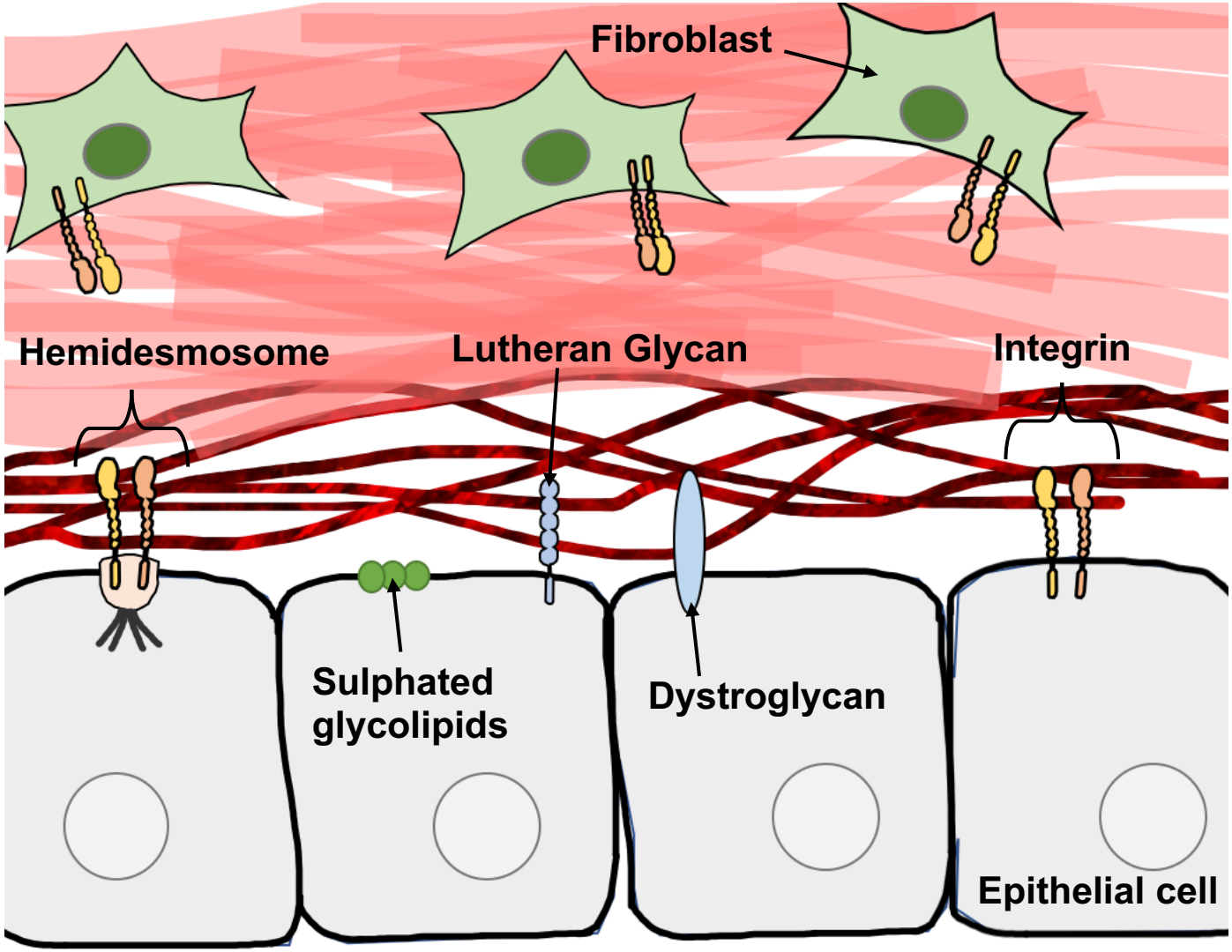

Interstitial matrix

- Collagens (Collagen I)
- Elastin
- GAGs
- Fibronectin
- PGs
- Tenascin C

Basement Membrane

- Laminins
- Collagen IV
- Heparan sulphate PGs (Perlecan, aggrecan)
- Nidogen
- Entactin

1.1.2. Maintenance of the extracellular matrix

The ECM represents a dynamic network with high turnover; it is continuously synthesised, modified, re-assembled and degraded.[8] This turnover is kept under tight control to maintain normal connective tissue function and homeostasis, particularly during injury. Perturbed ECM remodelling can precipitate morphological changes which can lead to pathology.[4] Disruptions in coordinated ECM synthesis or degradation can result in disorders of ECM accumulation (such as fibrotic disorders or malignancy[9]) or breakdown (such as herniae, diverticular disease, haemorrhoids, varicose veins, aneurysms, and pelvic organ prolapse[10]). Remodelling of the structure, composition, and distribution of the ECM involves chemical and enzymatic cross-linking, and cleavage by proteolytic enzymes that are intimately involved in this process.[4] This includes the complex interactions of four groups of proteases:

i) Matrix metalloproteinases

The Matrix metalloproteinases (MMPs) are the main enzyme in matrix degradation, they are synergistically able to digest all ECM macromolecules.[4] MMPs are metal-binding proteases that are secreted as latent precursors (*zymogens*) and activated by extracellular activation (most commonly cleavage). The MMP family comprises 23 members, with the majority being secreted and a small proportion being membranous. MMPs consist of three major groups: collagenases, gelatinases, and stromelysins (reviewed in Reynolds (2014)[11]). Their coordinated activity is necessary for tissue homeostasis; during injury, disease, or inflammation, secretion and activation of MMPs is heightened. Aside from ECM remodelling, MMPs are involved in the cleavage

and activation of ECM-bound or intrinsic growth factors, and therefore have wide-ranging activities.[12]

ii) Adamalysins

The adamalysin family comprise ADAMs (a disintegrin and metalloproteinases), ADAMTS (ADAMs with a thrombospondin motif), and ADAMTSL (ADAMTS-like) proteins.[4] They are membranous or secreted enzymes that function in shedding ECM proteins adjacent to cell membranes, and partake in cell–cell fusion, adhesion and intracellular signalling.[13] A unique feature of adamalysins are their potential adhesion and protease domains, enabling them to partake in a plethora of biological functions, including the formation, remodelling, and degradation of components of the ECM.[14]

iii) Meprins

Meprins are part of the astacin family of membrane-bound and secreted zinc metalloproteinases. They are multi-domain and comprise two subunits - meprin-α and meprin-β.[4] Meprins are key shedding proteins that work at the cell membrane (predominantly meprin-β) or are secreted into peri-cellular space (meprin-α) and work to hydrolyse cell surface and ECM proteins, biologically active peptides, and cytokines.[4] Indeed, meprin synthesis is necessary for the activation of interleukins IL1β and IL18 [15,16] and for the dissemination of leucocytes through the ECM, and therefore has important roles in inflammation.[17,18] Meprins have further roles in the cleavage and maturation of a diverse range of ECM substrates, including collagen IV[4], pro-collagens I[19] and III[20], pro-ADAM-10[21], fibronectin[4], kallikrein[22], nidogen[4]; as well as the maturation of several growth factors (namely EGF and VEGFA) and proteases, including MMPs -3 and -9.[23]

iv) Metalloproteinase inhibitors

Dynamic remodelling and repair of the ECM necessitates careful control of the activity of ECM-degrading metalloproteinases to ensure that excessive and pathological breakdown of the tissue matrix and cell surface molecules is avoided.[3,4] Metalloproteinase inhibitors therefore play a fundamental role in ECM composition and homeostasis. Four members of the tissue inhibitor of metalloproteinase (TIMP) family have been cloned (TIMPs 1 to 4), which counteract the function of both the matrix- (MMPs) and disintegrin- metalloproteinases (ADAMs and ADAMTSs).[24] TIMPs have a number of sites at which they can form complexes with metalloproteinases, enabling them to selectively and preferentially bind and inhibit specific metalloproteinases. The metalloproteinase:TIMP ratio of tissues therefore governs the overall composition of ECM, and is tightly regulated by cytokines, growth factors, and hormones, many of which are cell-specific and others which are ubiquitous (e.g. Transforming Growth Factor β (TGF-β)).[25] Furthermore, enzymes such a LOX, LOXL1 and transglutaminases are involved in the cross-linking of ECM components and support the role of TIMPs in stiffening the ECM.[26]

1.1.3. The elastic tissue

The tissues of several organs need to be robust and extensible to perform their normal physiological roles, such as large arterial vessels during systole, the respiratory tree during inspiration, and the bowel during peristalsis.[27] The elastic properties of tissues are provided by the distribution of elastic fibres throughout their ECM. The vast majority of the mature elastic fibre (~90%) is represented by a central amorphous, insoluble component (elastin), attached to (and interspersed by) a longitudinally aligned 10-15nm thick micro-fibrillar sheet.[28] The tubular microfibril structure consists of several glycoproteins, importantly fibrillin and micro-fibril-associated glycoprotein, which function as an organising scaffold to buttress the homogenous elastin.[27] The elastin precursor, tropoelastin, is secreted into the pericellular space where it is assembled into loose chains by being placed onto the fibrillar scaffold and cross-linked into elastin fibres.[29] On account of this cross-linking, elastin is the *sole* protein in the human matrisome which imparts elastic recoil to tissues and organs.[30] As well as being stabilised by cross-linking, elastic fibres are promoted and stabilised by proteins such as the fibulins which link elastic fibres to cells.[31]

Alongside elastic properties which enable elastic tissues to recover after deformation, these tissues require tensile reinforcement to resist applied loads and to prevent overstretch.[29] The ECM of different tissues therefore comprises a varying proportion of amorphous elastin and proteoglycans, which impart matrix resilience, and collagens, which provide tensile strength as determined by the mechanical needs of the tissue.[32] Elastic fibres may represent a small component of some tissues (~2-4%

of the dry weight of skin), or they can play a more significant role in others, such as in larger arteries, where elastic fibres constitute over 50% of the ECM architecture.[29]

The most abundant collagen, Type I collagen, exists in most mammalian tissues as closely-packed thick fibrils arranged in a superhelix.[12] Reticular collagen fibres are represented by Type III collagens; these fibres are coarse, branched, and segmented. They cross-link into a fine meshwork (reticulin), and support soft tissues such as the liver, bone marrow, and lymphatic vessels.[33] Collagen can also exist in non-fibrous forms in ground substance[12], such as in the amorphous ground substance of hyalin and articular cartilage (Type II collagen) and the basal laminae (Type IV collagen).[33] The ECM fibres of different tissues can therefore be divided into an elastin system and a collagenous system[34], each working in sync to endow overall physiological functionality and character to different tissues.

1.1.4. Disorders of the elastic tissue

Disruption in the tightly controlled balance between elastic and collagen fibre composition and other matrix components can impact tissue homeostasis, and therefore the intrinsic molecular and physiological properties of tissues.[35] Indeed, elastic and collagen fibres represent a great challenge to tissue repair due to their molecular complexity and requirement of chaperone proteins for synthesis.[36] Disorders of elastic tissue are therefore common, and encompass a phenotypic spectrum of disease. Detailed study of genetic disorders that disrupt ECM assembly or homeostasis has enabled a greater understanding of the extensive molecular network that underpins normal tissue matrix biology.[30]

Genetic disorders of connective tissue broadly pertain to the assembly of elastin or collagen fibres. The prototypic disorders of elastin assembly are the cutis laxa (CL) syndromes, Marfan Syndrome (MFS) and MFS-like syndromes, and pseudoxanthoma elasticum (PXE).[33] CL syndromes are characterised by abnormal elastic fibres causing loose, redundant hypoelastic skin with poor elastic recoil. Several subtypes of inherited CL exist, each with variable severity and clinical features, including skin laxity, herniae, aortic aneurysms, and bladder diverticula, among others (**Table 1.1**).[37] Autosomal dominant forms of MFS result from a mutation in the fibrillin-1 gene (FBN1), which is the core component of the microfibril layer of elastic fibres that is heavily involved in the sequestration and bioavailability of Transforming Growth Factor Beta (TGF-β) peptides.[38] MFS is typified by cardiovascular, musculoskeletal, and ocular manifestations, with aortic aneurysms and dissection being a prominent cause of mortality in these patients.[39] PXE is an autosomal recessive disease caused by loss-

of-function mutations of ABCC6 (ATP Binding Cassette Subfamily C Member 6), a putative transmembrane receptor.[33] PXE affects tissues rich in elastic fibres, causing fragmentation and ectopic mineralisation of elastic fibres.[40] The cardinal features of PXE are skin elasticity, ocular neovascularisation, and cardiovascular manifestations, such as early arteriosclerosis and cardiac failure. Other disorders of elastin assembly include supravalvular aortic stenosis (SVAS), Williams-Beuren Syndrome (WBS), Weil-Marchesani Syndrome (WMS), congenital contractural arachnodactyly (Beals Syndrome), and geleophysic dysplasia.[41]

Disorders of collagen assembly, which alter collagen formation, impact almost all tissues and organ systems of the body and present with a range of phenotypes depending on the disruption of different collagen subtypes.[30,42] The most well-known disorders of collagen assembly are Ehlers-Danlos Syndromes (EDS), which are a group of collagen and collagen-related disorders showing clinical and genetic heterogeneity.[30] Patients with EDS broadly demonstrate cutaneous, ligamentous and articular abnormalities, as well as abnormalities of the vasculature and internal organs.[30] More specifically, the commonest features of EDS are of skin hyper-extensibility, fragility of tissues, and joint hypermobility (the 13 most common EDS subtypes are listed in **Table 1.2**).[42] Twenty-nine collagen types have been described, with several collagen types known to be associated with disease (**Table 1.3**).[42]

The elastic and connective tissue disorders mentioned thus far are heritable, and are caused largely by the disruption of a single gene (monogenic). Monogenic disorders are often rare, highly-penetrant, syndromic forms of disease; for example, MFS has a prevalence of ~1.5 - 17.2 per 100,000[43] and EDS has a prevalence of ~4 to 20 per

100,000.[44] Complex disorders, on the other hand, represent the vast majority of human disease, and consist of both genetic (multiple alleles at distinct loci each with a small effect on phenotype[45]) and non-genetic contributors which together impart overall disease susceptibility. Complex disorders can have a prevalence of *at least* 1 in 3, meaning their disease burden is far greater on a population level and they have a higher societal cost.

Complex disorders of the elastic tissue, like monogenic disease, can impact every organ of the body. These conditions typically manifest as a group of common diseases characterised by impaired elastic recoil of tissues. To distinguish these prevalent disorders from rare syndromic forms of elastic tissue disease, I have coined the term '*elastopathies'*, and from hereinafter will refer to them collectively under this grouping.

In the UK Biobank, I have identified 12 such elastopathies originating from a primary elastic tissue pathology origin (See **Figure 1.2**).[46] The study of the genetic contributions to elastopathies is limited, this includes hiatus hernia, diverticular disease, haemorrhoids, inguinal hernia, varicose veins, female genital prolapse, umbilical hernia, aneurysms, emphysema, pneumothorax, rectal prolapse, and femoral hernia, which are the focus of this thesis. Candidate gene studies have largely failed to identify extensive genetic culprits[47,48], and research efforts and funding devoted to understanding the pathobiology behind these disorders, in particular the genetic basis, has been limited.[49] **Sections 1.1.5** through **1.1.7** will cover in further detail the background behind varicose veins, haemorrhoids, and herniae; with **Section 1.1.8** discussing the remaining six elastopathies: diverticular disease, female

genital prolapse, aneurysmal disease, emphysema, pneumothorax, and rectal prolapse.

Table 1.1. Cutis laxa sub-types and clinical manifestations. Clinical manifestations are ordered according to how typical they are across all ten cutis laxa sub-types. Table adapted from Berk (2011).[37]

	ADCL	ARCL-IA	ARCL-IB	ARCL-IIA	ARCL-IIB	ARCL-III	XLCL	MACS	URDS	ATS
Genetic defect	***ELN***	***FBLN4***	***FBLN5***	***ATP6V0A2***	***PYCR1***	**-**	***ATP7A***	***RIN2***	***LTBP4***	***SLC2A10***
Skin laxity	+++	++	+++	+++	+++	+++	+++	+++	+++	+++
Hernia	++	+++	+++	+++	++	++	+++	+	+++	++
Joint laxity		+		+++	+++	++	++	+++	++	+++
Postnatal growth delay		++	+	+++	+++	+++	+		+++	
Prominent ears	+++	+	+++				++		+	+
Scoliosis				++	+	++	++	+++		++
Hypotonia		+		+++		++	++		+++	
Delayed motor development		+	+	+++		+++	+++			
Retrognathia		+++		+++	+++				+++	+++
Emphysema	++	++	+++						+++	
Aortic aneurysm	++	+++		+						++
Arterial tortuosity		+++	+				++			+++
Mental retardation				+++	+++	+++	+++			
Bladder diverticula			+	+			+++		+++	
Patent anterior fontanelle				+++		++	++		++	
IUGR				+++	+++	+++			+	
Congenital hip dislocation		+		+	+++	++				
Hypertelorism		+++							+++	++
Osteoporosis					++		++	+		
Athetoid movements					+	+++				
Corneal opacification					+	+++				
SVAS			+++							
Glycosylation defects				++						
Occipital horns							+++			
Short and broad clavicles							+++			
Macrocephaly								+++		
Alopecia								+++		
Gingival hyperplasia								+++		

ADCL, Autosomal dominant cutis laxa; ARCL, autosomal recessive cutis laxa; ATS, arterial tortuosity syndrome; DBS, De Barsy syndrome; IUGR, intrauterine growth retardation; MACS, macrocephaly-alopecia-cutis laxa-scoliosis syndrome; SVAS, supravalvular aortic stenosis; URDS, Urban-Rifkin-Davis syndrome; XLCL, X-linked cutis laxa; +, rare; ++, not uncommon; +++, Common; blank, not present.

Table 1.2. The different subtypes of Ehlers-Danlos Syndrome (EDS). The 13 EDS subtypes categorised according to the latest latest 2017 international classification of EDS.[50] Table adapted from Meester (2017).[51]

EDS subtype	Gene	Key clinical features
EDS disorders of collagen structure and processing		
Classical	*COL5A/COL5A2*	Skin hyper-elasticity and hypermobile joints
Vascular	*COL3A1*	Skin and vascular fragility, characteristic facies
Athrochalasia	*COL1A/COL1A2*	Severe hypermobile joints, congenital hip dislocation, skin hyper-elasticity
Dermatosparaxis	*ADAMTS2*	Extreme skin fragility, mild hypermobile joints, characteristic facies
Cardiac-valvular	*COL1A2*	Severe cardiac valve abnormalities defects, hypermobile joints, skin hyper-elasticity
EDS disorders of collagen folding and cross-linking		
Kypho-scoliotic	*PLOD1/FKBP14*	Kyphoscoliosis, hypermobile joints, muscular atrophy
EDS disorders of myomatrix structure and function		
Classical-like	*TNXB*	Skin hyper-elasticity, hypermobile joints, skin fragility
Myopathic	*COL12A1*	Muscular atrophy, proximal joint contractures, distal joint hypermobility
EDS disorders of GAG synthesis		
Spondylo-dysplastic	*B4GALT7/B3GALT6*	Short stature, muscle atrophy, bowing of limbs
Musculo-contractural	*CHST14/DSE*	Congenital contractures, characteristic facies, skin fragility.
EDS disorders of the complement pathway		
Periodontal	*C1R/C1S*	Severe periodontitis, lack of attached gingiva, pretibial plaques
EDS disorders of intracellular processes		
Spondylo-dysplastic	*SLC39A13*	Short stature, muscular atrophy, bowing of limbs
Brittle Cornea syndrome	*ZNF469/PRDM5*	Thin cornea, keratoconus, keratoglobus, blue sclerae
EDS disorders that remain unresolved		
Hypermobile	?	Hypermobile joints, skin hyper-elasticity, smooth velvety skin

Table 1.3. The collagen genes associated with disease. Collagen genes are arranged according to type. Table adapted from Jobling (2014).[42]

Collagen gene	Collagen type	Anatomic areas of expression	Associated Disorders
COL1A1	**Type I**	Most connective tissue, skin, tendon, ligament, bone	Caffey disease EDS classical and athrochalasia types OI types I, II, III, IV
COL1A2			EDS athrochalasia and cardiac-valvular types OI Types II, III, IV
COL2A1	**Type II** **Type XI**	Cartilage, nucleus pulposus, vitreous, cornea, inner ear	Achondrogenesis II/hypochondrogenesis Kneist dysplasia Osteoarthritis with mild chondrodysplasia Platyspondylic lethal skeletal dysplasia, Torrence type Sponyloepiphyseal dysplasia congenita Spondyloepimetaphyseal dysplasia, Strudwick type Stickler syndrome type 1, non-syndromic ocular type
COL3A1	**Type III**	Most connective tissue, especially vessels, skin and tendons	EDS vascular type EDS hypermobile type
COL4A1	**Type IV**	Basement membranes	Brain small vessel disease with Axenfeld–Reiger anomaly and haemorrhage Hereditary angiopathy with nephropathy, aneurysm and muscle cramps Porencephaly I
COL4A2			Porencephaly 2
COL4A3			Alport syndrome, AD and AR types
COL4A4			Benign familial haematuria
COL4A5			Alport syndrome, X-linked
COL4A6			Diffuse leiomyomatosis with Alport syndrome
COL5A1	**Type V**	Most connective tissue, especially skin, bone, tendon, cornea, placenta and foetal membranes	EDS classical type EDS brittle cornea syndrome
COL6A1	**Type VI**	Most connective tissue, tendons, contributes to cell matrix adhesion in skeletal muscle	Bethlem myopathy Ullrich congenital muscular dystrophy
COL7A1	**Type VII**	Anchoring fibrils in dermo-epidermal junctions	Epidermolysis bullosa dystrophica, autosomal recessive and dominant types, bart type, inversa type, pruriginosa type, pretibial type
COL9A1	**Type IX**	Cartilage, vitreous, retina, inner ear	MED Type VI Stickler syndrome Type IV, autosomal recessive
COL9A2			MED Type II Stickler syndrome Type V, autosomal recessive
COL9A3			MED Type III Multiple epiphyseal dysplasia with myopathy

COL10A1	**Type X**	Hypertrophic chondrocytes in calcifying cartilage	Metaphyseal chondrodysplasia, Schmid type
COL11A1	**Type XI**	Cartilage, nucleus pulposus, vitreous, cornea, inner ear	Stickler syndrome, Type II, AD Fibrochondrogenesis Marshal syndrome
COL11A2		Cartilage, nucleus pulposus, inner ear	Stickler syndrome, Type III, AD Fibrochondrogenesis Deafness, AD and AR Weissenbacker–Zweymuller syndrome
COL17A1	**Type XVII**	Component of hemidesmosomes	Junctional epidermolysis bullosa, non-Herlitz type
COL18A1	**Type XVIII**	Basement membranes	Knobloch syndrome

AD, autosomal dominant; AR, autosomal recessive EDS, Ehlers-Danlos Syndrome; MED, Multiple epiphyseal dysplasia; OI, Osteogenesis imperfecta;

Figure 1.2. Complex disorders with a primary elastic tissue pathology (the elastopathies). A diagram depicting 12 elastopathies in which elastin dysfunction leads to pathology as identified in UK Biobank. Other disorders with secondary elastic tissue involvement have not been included. Vector image from Pixabay – no attribution license.

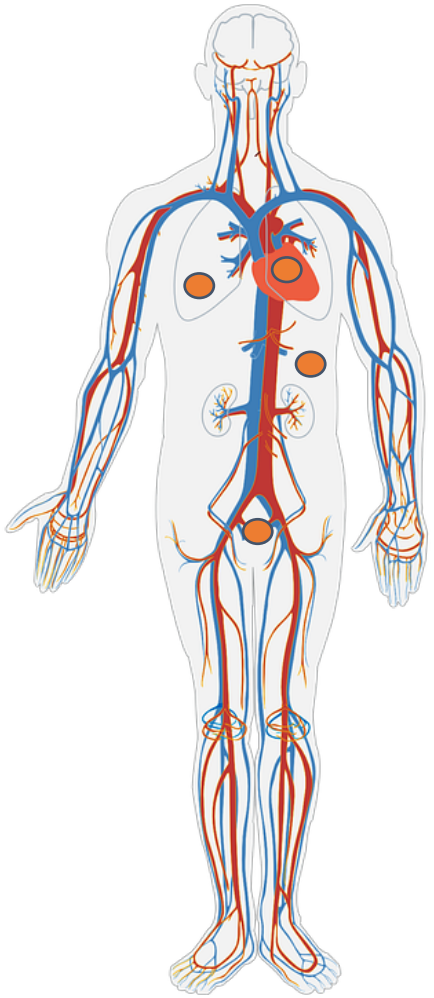

The cardiovascular system
- Varicose veins
- Aneurysm

The respiratory system
- Emphysema
- Pneumothorax

The gastrointestinal system
- Hiatus hernia
- Diverticular disease
- Haemorrhoidal disease
- Inguinal hernia
- Umbilical hernia
- Femoral hernia

The reproductive system
- Female genital prolapse
- Rectal prolapse

1.1.5. Varicose veins as a complex disease model

Varicose veins are tortuous, dilated (> 3mm diameter), and palpable veins that are a highly prevalent clinical presentation of chronic venous disease (CVD) (**Figure 1.3**). CVD is classified clinically according to the universal Clinical Etiological Anatomical Pathophysiological (CEAP) classification system which aids research and reporting around CVD (**Table 1.4**).[52]

Figure 1.3. Extensive varicose veins affecting the leg. Image from the Wellcome Collection Gallery. St Bartholomew's Hospital Archives & Museum SBHB MU/14/51/4. Photo number: L0061468. Licensed under CC-BY-4.0.

Varicose veins are estimated to affect 25 - 33% of females and 10 - 20% of males[53,54], and temporal trend data demonstrate a growing disease prevalence.[55] The Bonn Vein

Study demonstrated that chronic venous insufficiency leads to significant skin changes in around 3 - 14% of cases[56], including oedema, lipodermatosclerosis, skin ulcers, and infrequently amputation.[57] Each year in the US, at least 20,556 patients receive a new diagnosis of venous ulceration[58], with chronic venous insufficiency responsible for ~72% of these.[59] Despite established treatment protocols, 25-50% of venous ulcers of the leg continue unhealed after six months of therapy[60], and the annual cost of managing venous leg ulcers in the USA is ~$14.9 billion.[61] Each year around 2% of healthcare expenditure in the UK is directly attributable to the management of varicose veins and its complications, which represents ~10-30% of the workload of district nurses.[62] The cost of venous-related illness on society at large is extensive: each year 4.5 million work days in the US *alone* are lost to venous-related illness.[63] Varicose veins therefore lead to significant economic and societal health costs.

Presently there are no medical treatments for varicose veins, with management restricted to surgical intervention (Marsden *et al*.[64] summarise NICE Guidance around the diagnosis and management of varicose veins). Endovenous ablative techniques are the first-line treatment for symptomatic varicose veins[64]; however, recurrence of varicosities following surgery is as high as 20%, meaning it is no better than open truncal stripping surgery.[65] Thus, for a significant subset of patients, varicose veins are complicated by ongoing sequelae and significantly impact patient-reported quality of life[58], requiring repeat intervention.

The aetiopathology of varicose veins is multifactorial (**Figure 1.4**).[66] A widely recognised theory is that varicose veins develop from valvular insufficiency which causes haemodynamic backflow and stasis, resulting in venous hypertension; this

precipitates vessel wall alterations as well as inflammation and activation of the venous wall.[67,68] However, the exact sequence of pathological events is not well understood and shows significant heterogeneity between patients[67,68], suggesting varicose veins are a complex disorder with several concomitant susceptibilities which lead to overall pathology. Risk factors for varicose veins established from large epidemiological studies include older age, female sex, obesity, height, orthostatic professions, a history of deep vein thrombosis, and a positive family history.[69,70]

Up to 85% of varicose veins patients report a positive family history[71], and among offspring with one affected parent the familial standardised incidence ratio is 2.39[72], with a narrow-sense heritability of ~17%.[73] Moreover, genetic factors contribute to 30-40% of femoral vein capacity and elasticity (a predisposing phenotypic contributor to varicose veins).[74] This suggests that inherent venous characteristics, and thus varicose vein pathology, are at least *in part* under genetic control.[75] Moreover, several candidate gene and linkage studies have identified putative genes implicated in varicose veins biology, including *FOXC2* (Forkhead Box C2), *THBD* (Thrombomodulin), *DMN* (Desmulin), and *MTHFR* (methylenetetrahydrofolate reductase) genes. Through an analysis of cDNA (complementary DNA) libraries comparing varicose veins with normal veins, Lee *et al.*[76] identified differential expression in several ECM proteins, including tubulin, lumican, and versican.

Three previous genome-wide association studies (GWAS) of varicose veins have been described in the literature (as of September 2020 (Completion of **Chapter 2**). Ellinghaus *et al.*[77] identified two genome-wide significant susceptibility loci at *EFEMP1* and *KCNH8,* in their discovery cohort of 323 cases and 4,619 controls and

independent replication in 1,946 cases and 3,146 control participants. Fukaya *et al*.[78] performed a GWAS in 9,577 cases and 327,959 control participants from the UK Biobank, identifying 30 additional signals (27 loci) associated with varicose veins. This study, however, has two main limitations. Firstly, cases were defined only by the International Classification of Diseases (ICD) 9th or 10th edition codes, meaning that thousands of cases defined by operative intervention codes were misclassified as controls. Secondly, the genetic associations discovered were not tested in an independent replication cohort.[78] Shadrina *et al*.(2019)[79] subsequently performed a summary level GWAS using publicly-available online UK Biobank summary data from the Neale Lab (http://www.nealelab.is/) and Gene ATLAS[80] (http://geneatlas.roslin.ed.ac.uk/) (no access to patient level data), identifying 12 loci, all of which had been identified in the previous analysis by Fukaya and colleagues[78] and lacked replication. Following completion of our varicose veins study described in **Chapter 2** (September 2020 (published online June 2022[81])), a further three GWAS studies were performed for varicose veins. Lee *et al.*[82] (May 2022), performed a single-stage association analysis in 96 cases and 1000 controls from Taiwan, however due to low power and mismatched controls, only 6 suggestive variants were identified, none of which reached the genome-wide significance threshold ($P < 5\times10^{-8}$). Moreover, 'healthy' controls were identified through a self-report questionnaire which asked only whether controls had cardiovascular disease and not specifically questions pertaining to varicose veins or venous ulcerations, a nuance the lay public is likely to miss, and likely increased type II error among controls. Levin *et al*.[83] (09 Jan 2023) subsequently performed a GWAS of varicose veins in a total of 49,765 cases and 1,334,301 controls using the Veterans Affairs Million Veteran Programme (VA-MVP) and summary data from eMERGE, UK Biobank, FinnGen and BioBank Japan.; they

identified 139 loci to reach genome-wide significance. However, despite using around 1.4 million participants in the meta-analysis, the team were only able to identify 49,765 cases (3.6% case prevalence), suggesting a significant proportion of cases remain unidentified. This is likely contributed by two factors: i. the sole reliance on diagnostic medical codes and not surgical codes to identify patients, ii. the VA-MVP being a predominantly male cohort (>90%), whilst varicose veins have a female predominance worldwide. Subsequently, Helkkula *et al.*[84] (18 Jan 2023) published a GWAS of 17,027 cases and 190,028 controls in FinnGen, identifying 50 loci ($P < 5\times10^{-8}$), including a low-frequency missense variant (rs201955556-T) in *GJD3* which is protective in the Finnish population. However, this key finding was not replicated in summary data available from other European or Asian biobanks, and the authors concluded it was a Finnish-specific variant, though this is a noteworthy assumption.

Table 1.4. Updated 2020 CEAP classification system and reporting standard for chronic venous disease. The CEAP (Clinical-Etiological-Anatomic-Pathophysiologic) classification standard to describe patients with chronic venous disorders (CVD). The system is based on the clinical manifestations of CVD and a current understanding of its aetiology, pathophysiology, and anatomical involvement. This table is based on the latest revised 2020 CEAP classification published by the American Venous Forum.[52]

CEAP Classification 2020

Clinical classification	
C_0	No visible or palpable signs of venous disease
C_1	Telangiectasias or reticular veins
C_2	Varicose veins
C_{2r}	Recurrent varicose veins
C_3	Oedema
C_4	Changes in skin and subcutaneous tissue secondary to CVD
C_{4a}	Pigmentation or eczema
C_{4b}	Lipodermatosclerosis or atrophie blanche
C_{4c}	Corona phlebectatica
C_5	Healed
C_6	Active venous ulcer
C_{6r}	Recurrent active venous ulcer
(A)etiologic classification	
E_p	Primary
E_s	Secondary
E_{si}	Secondary – intravenous
E_{se}	Secondary – extravenous
E_c	Congenital
E_n	No cause identified
Anatomic classification	
A_s	**Superficial** Tel Telangiectasia Ret Reticular veins GSVa Great saphenous vein above knee GSVb Great saphenous vein below knee SSV Small saphenous vein AASV Anterior accessory saphenous vein NSV Nonsaphenous vein

A_d	**Deep**
	IVC Inferior vena cava CIV Common iliac vein IIV Internal iliac vein EIV External iliac vein PELV Pelvic veins CFV Common femoral vein DFV Deep femoral vein FV Femoral vein POPV Popliteal vein TIBV Crural (tibial) vein PRV Peroneal vein ATV Anterior tibial vein PTV Posterior tibial vein MUSV Muscular veins GAV Gastrocnemius vein SOV Soleal vein
A_p	**Perforator**
	TPV Thigh perforator vein CPV Calf perforator vein
A_n	**No venous anatomic location identified**
Patho-physiologic classification	
P_r	Reflux
P_o	Obstruction
$P_{r,o}$	Reflux and obstruction
P_n	No pathophysiology identified

Figure 1.4. Pathophysiology of varicose veins. The pathophysiology of varicose veins is highly complex, and the order of pathological events is a topic of debate. Outlined below are the most well-defined contributors to varicose veins pathobiology, alongside predisposing factors such as age, sex, weight, height, and genetics.[68] Image courtesy of the National Health Lung and Blood Institute (NIH)®, Sep 2017. Image modified by *Jmarchn*, made available by Wikimedia commons, under a CC-BY-SA-3.0 license.

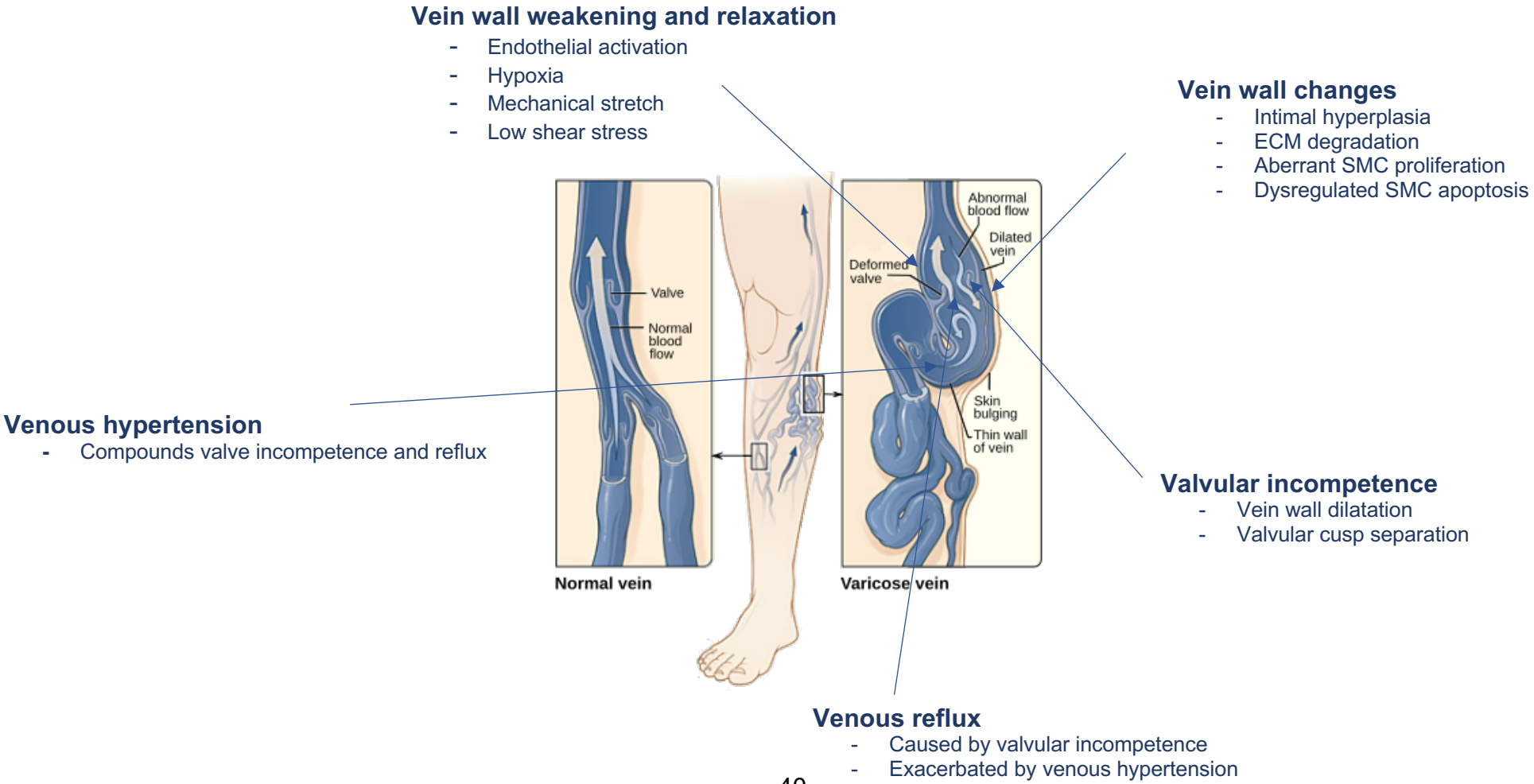

1.1.6. Haemorrhoids as a complex disease model

Haemorrhoids (*piles*) results from the enlargement of the haemorrhoidal veins and distal displacement of the anal cushions (**Figure 1.5**).[85] Haemorrhoidal veins are normal structures that play an important role in faecal continence[86]; at rest they are full of blood, acting as a plug and contribute 15-20% of resting anal pressure.[87]

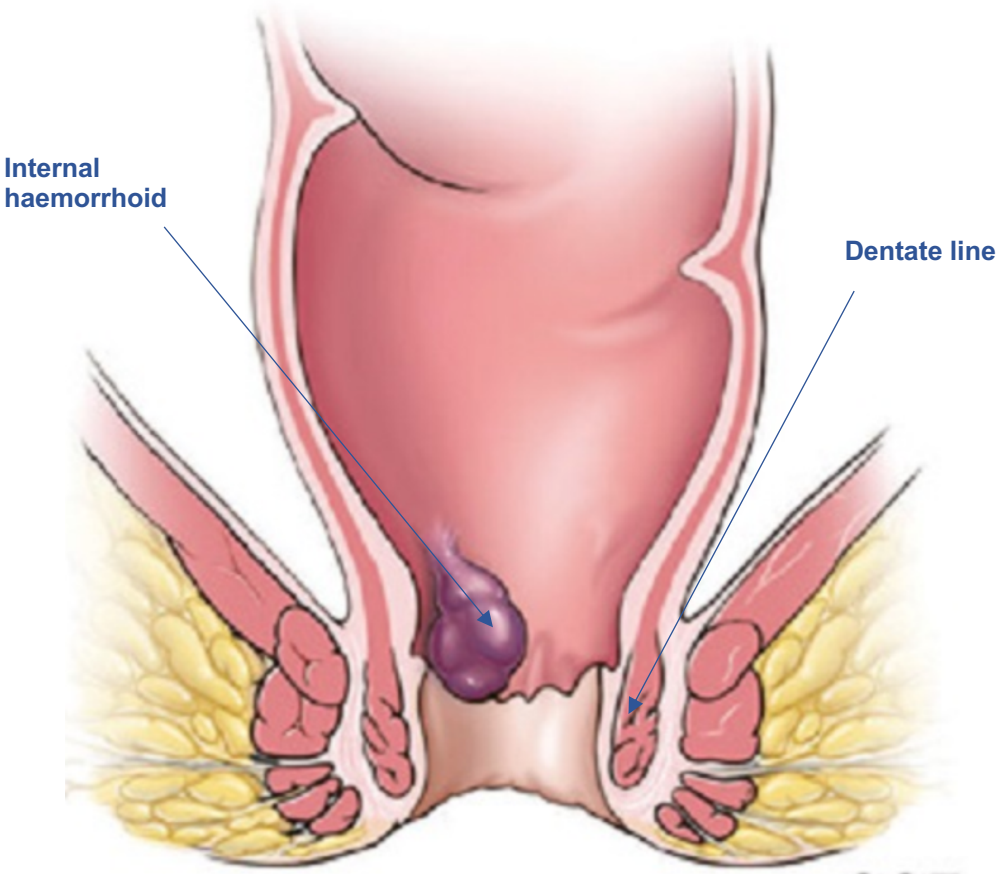

Figure 1.5. An internal haemorrhoid. The schematic depicts a Grade I internal haemorrhoid. Internal haemorrhoids are those originating above the dentate line and external haemorrhoids are those originating below. Image adapted from ConsultQD (Cleveland Clinic). Image made available by Wikimedia Commons, Under a CC-0-1.0 License.

Haemorrhoids are the third most common outpatient gastrointestinal diagnosis[88], reported incidentally in 40%[89] of Americans after screening colonoscopies and 86% of proctoscopies in rectal surgery clinics[90], with an estimated worldwide prevalence ranging from 4.4% to 36.4%.[91–93] Symptomatic haemorrhoidal disease* occurs in ~10-30% of patients with enlarged haemorrhoids[94], representing 3.3 million ambulatory care visits annually in the USA.[89] Crosland and Jones found only 41% of patients in general practice reporting rectal bleeding had sought medical advice for it[95], suggesting the actual incidence of haemorrhoidal disease is likely much higher due to the associated anxiety, as well as personal and cultural stigma.[96] Haemorrhoidal disease can also co-exist with serious pathology, or can often be misdiagnosed in its place.[97] General practice prescriptions for topical treatments for haemorrhoidal disease have been found to increase in the year prior to a rectal cancer diagnosis.[98] It is therefore important that correct diagnoses for haemorrhoids are made and that risk of more serious proximal pathology is ruled out.[99]

Internal haemorrhoid severity is commonly graded according to the Goligher Classification System **(Table 1.5)**.[100] Management of haemorrhoidal disease is directed by the severity of symptoms and degree of prolapse (**Figure 1.6**)[99], and is predicted to increase 23% over the next 20 years.[101] Conservative approaches for early stage haemorrhoidal disease can include fibre supplementation[102], lifestyle modification and topical preparations, with only limited data existing for their long-term benefit. Surgical intervention is the mainstay of treatment for haemorrhoidal disease,

* Haemorrhoidal disease is the symptomatic presentation of pathologically enlarged haemorrhoids (i.e. dilated haemorrhoidal veins). Most patients with enlarged haemorrhoids report no symptoms and therefore do not have haemorrhoidal disease.

with over 35,000 surgical interventions performed for haemorrhoidal disease in England in 2018-19.[103] Surgical interventions include outpatient procedures, principally rubber band ligation (RBL) which is associated with bleeding[104], pain, and high-recurrence rates (particularly in haemorrhoids with significant prolapse) which can be as high as 49%.[105] Radical surgery requiring general anaesthesia is the definitive treatment for high-grade haemorrhoidal disease that does not respond to outpatient treatment, and is particularly effective in larger prolapsed haemorrhoids[106]; however it is associated with short and long-term complications.[107,108] Thus, for a significant proportion of patients, haemorrhoidal disease significantly impacts their quality of life.

The aetiology of haemorrhoids has been a source of debate and discussion over the centuries.[102] Haemorrhoids are thought to have a complex multi-factorial aetiology, with four theories proposed (**Figure 1.7)**: the varicose vein theory* (which is the least accepted of all four[109]), the internal anal sphincter (IAS) hypertonicity theory†, the (anal cushion) vascular hyperplasia theory‡ (both of which have been postulated to increase resting pressure in the anal canal), the vascular theory§, and the more widely accepted sliding anal lining theory** (thought to be caused by disruption of the stromal component of the anal canal and rectal redundancy).[109,110] It is likely that several of these factors are at play in a complex manner, each imparting a heightened risk of haemorrhoids. Risk factors for haemorrhoids[86] include middle-age (peak prevalence

* Varicose vein theory – that haemorrhoids are varicosities, however this is now obsolete as haemorrhoids and anorectal varices are not the same.
† IAS hypertonicity theory – that haemorrhoids are caused by an increased resting anal pressure due to IAS hypertonicity.
‡ Vascular hyperplasia theory – that haemorrhoidal cushions are corpus cavernosum recti and maintain anal continence.
§ Vascular theory – that haemorrhoids occur due to hypertension in the portal venous system.
** Sliding anal-lining theory – that haemorrhoids are caused by a displacement of the anal lining mucosa of the anal cushions due to ECM fragmentation

of 45-65, following a Gaussian distribution[91]), male sex, prolonged straining (due to constipation), hard stool, a low-fibre diet, pregnancy, obesity, high socioeconomic status and associated conditions[86] such as irritable bowel syndrome[111], herniae[112,113], varicose veins[114,115], genitourinary prolapse[116,117], diverticular disease.[118,119], and other elastopathies[112,120] Several studies have pointed towards a positive family history as a contributor to haemorrhoids aetiopathology; however, at the time of completing the study described in **Chapter 3** (September 2020), no studies had performed heritability estimates for haemorrhoids.[86,121–123] The existing literature has largely overlooked the role of genetic susceptibility in haemorrhoids development[124], whilst the genetic contributions of other anorectal and associated disorders have been studied in detail.[125,126] Since completion of **Chapter 3**, Zheng *et al.*[127] (April 2021) have performed a large GWAS meta-analysis of haemorrhoids in 944,133 participants (218,920 cases and 725,213 matched controls) from 23andMe, UK Estonian Genome Centre, Michigan Genomics Initiative, and Genetic Epidemiology Research on Aging (GERA). The meta-analysis identified a compelling hereditary component to haemorrhoids, estimating the SNP-based heritability at ~5% and uncovering 5,480 genome-wide significant variants at 102 independent susceptibility loci. The study implicated the ECM, elasticity of the connective tissue, smooth muscle function, gut motility, as well as the circulatory system to be intimately involved in the pathogenesis of haemorrhoids.

Table 1.5. **Goligher classification for internal haemorrhoids**. Internal haemorrhoids severity is commonly classified according to a four-grade system which describes the prominence of the haemorrhoidal veins and the degree of prolapse. Adapted from Cataldo (2005).[128]

Grade	Physical findings
I	Engorged and hyperaemic haemorrhoidal veins – no prolapse
II	Haemorrhoidal cushions prolapse into anal canal during defecation – spontaneous reduction
III	Haemorrhoidal cushion prolapse into anal during defecation, but remain prolapsed – manual reduction
IV	Entirely exteriorised haemorrhoids, permanently prolapsed – manual reduction not effective

Figure 1.6. **Evidence-based treatment algorithm for Grade I-IV haemorrhoidal disease**. Adapted from the recent European Society of Coloproctology guideline for haemorrhoidal disease.[99] RBL, Rubber Band Ligation; DG-HAL, Doppler-Guided Haemorrhoidal Artery Ligation.

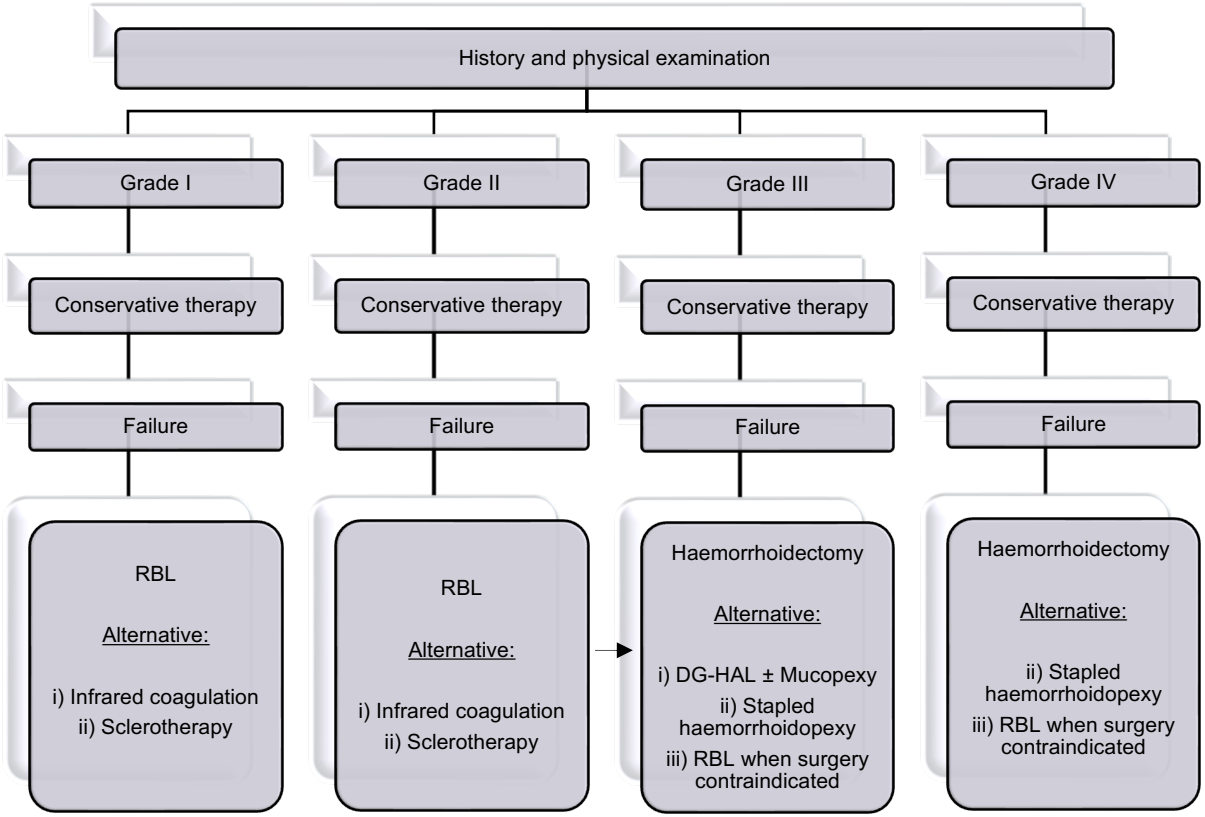

Figure 1.7. The pathogenesis of haemorrhoids. The five commonly held theories around the pathogenesis of haemorrhoids are provided below, alongside an explanation contextualising each theory.

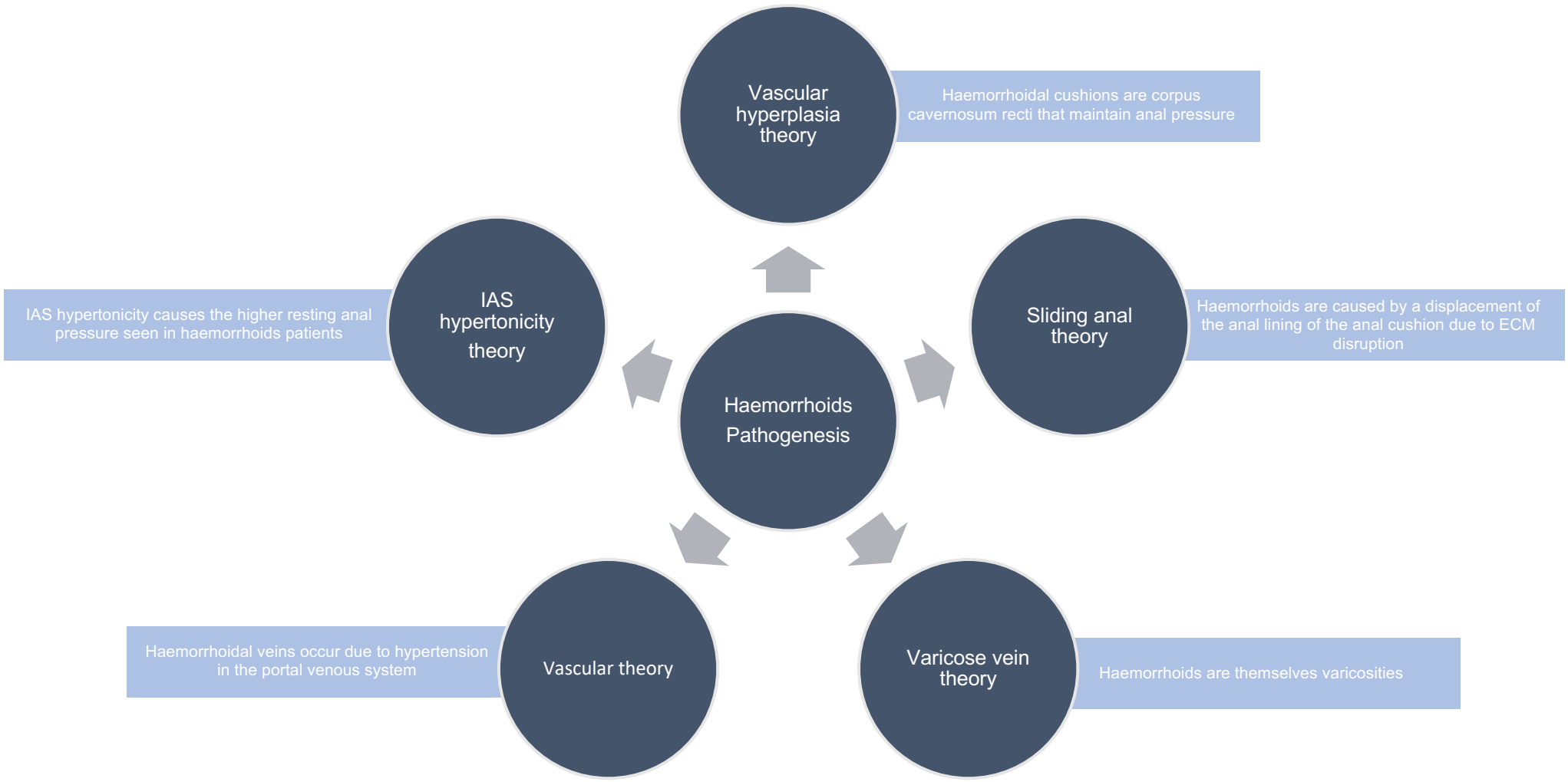

1.1.7. Herniae as a complex disease model

Herniae are a group of conditions characterised by the abnormal protrusion of an organ from the native anatomic cavity in which it resides. Abdominal wall hernia (AWH) represent the majority of hernia types (**Figure 1.8**), though herniae can occur outside the abdominal wall: principally hiatus hernia, which involves protrusion of the abdominal contents through the diaphragm into the mediastinum. The prevalence of AWHs are ~100 to 300 per 100,000 of the population, and each year, at least 20 million AWHs are repaired worldwide[129,130]. Inguinal hernia represents around three-quarters of all herniae[130], with a lifetime risk of 27% in males and 3% in females.[131] In England, over 135,000 surgical procedures were performed in 2019 for AWHs[132], making it one of the most commonly performed elective operations.[133]

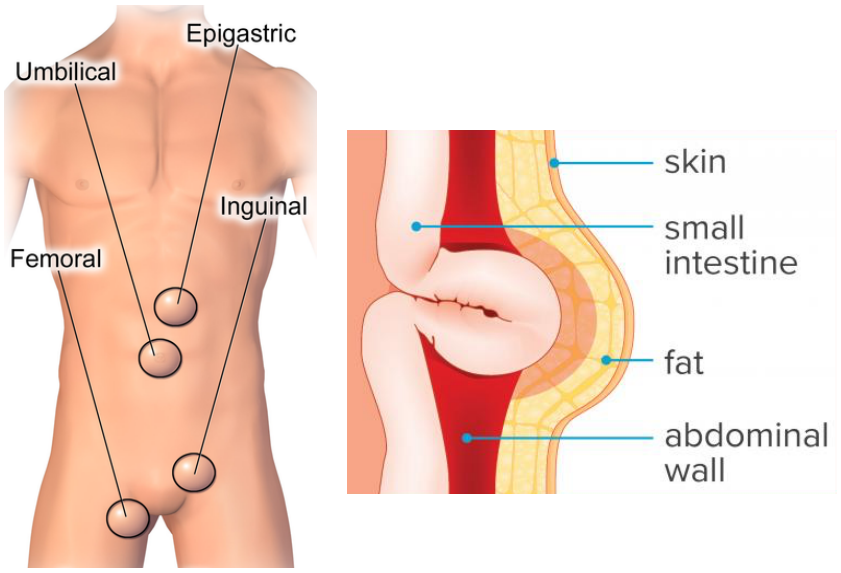

Figure 1.8. Common abdominal wall herniae. A schematic depicting common sites of hernia. *Image on the left made available by Wikimedia Commons under a CC-BY-SA-4.0 license. OTRS ticket #2019081910003902. Image on the right adapted from Medial News Today.* Image made available by Wikimedia Commons, Under a CC-0-1.0 License.

Up to a third of abdominal wall and hiatus hernia patients are symptomatic.[134] The main clinical manifestation of hiatus hernia is gastro-oesophageal reflux disease (GORD), and the cornerstone of medical therapy is to alleviate symptoms by inhibiting gastric secretions.[135] Symptomatic AWH can present with swelling, a feeling of heaviness in the abdomen, burning sensations, sharp pain, and discomfort on coughing, activity and defaecation, with sudden onset severe pain and an irreducible lump suggestive of strangulation (a surgical emergency).[136] Surgery is the definitive treatment for symptomatic AWH; however, it is associated with complications including chronic postoperative pain, seroma or haematoma, infection, and failure of surgical repair.[137,138] Reoperation rate for inguinal hernia recurrence is non-negligible at 12.3% at five years and 23.1% at 13 years.[139] Recurrence is lower and return to work is faster among prosthetic mesh repairs compared to sutured repairs[140,141], however mesh-related complications are common– including contraction, erosion and infection.[141,142] In the case of femoral hernia, diagnostic difficulties result in these herniae often being misdiagnosed. Up to 35-40% of these patients are not diagnosed until there is strangulation or bowel obstruction requiring emergency hernia repair (associated with high mortality rates).[143–145] Surgical management of AWHs can therefore be challenging, with high recurrence rates and risks of complication that can significantly reduce patients' quality of life. This emphasises a growing need to improve our understanding of hernia aetiopathology (**Figure 1.9**), which may guide new therapeutic avenues to improve patient outcomes.

Alongside the shared risk factors of age, sex, and body mass index, family history is a major contributor to hernia pathology. A positive family history is associated with an

eight-fold increased risk of groin hernia[146,147], and is implicated in an increased susceptibility to contralateral and recurrent inguinal hernia.[148–150] Among patients with a sibling with a surgically treated AWH, Zöller *et al.*[151], demonstrated the concordant standardised incidence ratio of inguinal hernia (1.97), femoral hernia (3.40), umbilical hernia (3.61), incisional hernia (2.24) and epigastric hernia (5.57). The characteristic presence of hernia in several genetic syndromes, including MFS[48], EDS[48] and CL syndromes (**Table 1.1**)[32], provide further evidence for an underlying genetic cause. Zöller *et al.*[151] also found several discordant risks to be over 2, suggesting a strong shared familial susceptibility among all five AWHs, with the greatest familial susceptibility shared between femoral and inguinal hernia. These results are supported by several clinical studies which identify a common co-occurrence of multiple hernia subtypes.[152,153] Indeed, patients with a first-degree relative with inguinal hernia are at more risk of femoral, umbilical, incisional and epigastric herniae.[154]

It is therefore likely that identifiable genetic risk factors may selectively predispose to distinct hernia pathology and even multiple hernia risk. However, at the time of completing **Chapter 4** (Sep 2020; subsequently published Dec 2022[155]) no studies had characterised the genetic basis of non-congenital hernia and only a handful of gene studies had identified molecular candidates.[156–162] At the time of completion of the analysis described in **Chapter 4**, only one GWAS of inguinal hernia (identifying four loci) had been performed[163], and a GWAS of GORD in 6,750 participants did not identify any genome-wide significant loci.[164]

Since this time, five additional GWA studies have been performed for hernia phenotypes of varying approaches:

i. Wei *et al.*[165] *(11 Aug 2021)* performed a discrete GWAS of four abdominal wall herniae (inguinal hernia, femoral hernia, umbilical hernia, and incisional hernia) in a total of 367,394 participants in UK Biobank. They demonstrated a notable genetic component to these complex disorders and found the estimated heritability for inguinal hernia to be 12%, femoral hernia to be 6%, umbilical hernia to be 16%, and incisional hernia to be 7%. The study confirmed four previously identified loci associated with inguinal hernia and identified 57 additional genome-wide-significant loci, including 55 loci for inguinal hernia, three for femoral hernia, five for umbilical hernia, and three for incisional hernia. Three of these loci were associated with multiple hernia phenotypes, including 1q41, and two loci at 2p16. Importantly, this study did not conduct a formal multivariable multi-trait GWAS meta-analysis of the four hernia phenotypes to uncover the shared genetic architecture to hernia formation, and did not include hiatus hernia, focussing instead on abdominal wall hernia. The inclusion of incisional hernia as a disease phenotype confounds the results significantly as this cohort are enriched for those patients having had surgery, and the team did not include surgery as a covariate in the analysis.

ii. Hikino *et al*.[166] *(12 Aug 2021)* subsequently performed a trans-ethnic GWAS meta-analysis of inguinal hernia in 1,983 cases and 12,507 controls from BioBank Japan and 15,995 cases and 361,617 White European controls from the UK Biobank (total 17,978 cases and 374124 controls). They identified 23 genome-wide significant loci, including five newly loci following meta-analysis—most importantly, they identified a compelling shared genetic architecture

across both populations (trans-ethnic genetic correlation 0.77 (SE = 0.26)) and identified genes over-represented in ECM pathways, including two transethnic variants near the elastin gene significantly associated with inguinal hernia in both populations.

iii. Choquet *et al.*[167] *(Jan 2022)* performed a large-scale ancestry-stratified and sex-stratified GWAS meta-analysis of inguinal hernia in 513,120 participants (35,774 cases and 477,346 controls) from the UK Biobank and GERA of Hispanic and Latino, African, East Asian and European descent. Independent replication of top-associated variants was performed in 728,418 participants from 23andMe (33,491 cases and 694,927 controls). This study identified 41 new replicated loci associated with inguinal hernia, including two loci associated with African ancestry, and eight loci demonstrating sex-specific effects, with *MYO1D* and *ZBTB7C* associated with inguinal hernia in females but not males.

iv. Fadista *et al.*[168] *(Jun 2022)* performed a GWAS in a total of 65,492 cases from the UK Biobank with documented ICD9/10 codes, surgical codes, or interview self-report codes for at least one of five hernia phenotypes (inguinal, femoral, umbilical, hiatus, and incisional hernia) and 343,101 controls without medical codes for hernia pathology. Follow-up replication studies were performed for inguinal hernia in 23,803 cases from four datasets: FinnGen, Estonian Biobank, iPSYCH, and the diverticular study. In total, 81 independent genome-wide significant loci were identified to associate with one of the five hernia types, including 26 loci which associated with multiple hernia phenotypes.

v. Campbell *et al.*[169] *(Oct 2022)* performed a two-stage GWAS in UK Biobank for hiatus hernia in a total of 367,399 participants (36,351 cases, 331,048 controls),

identifying 245 variants at 14 independent susceptibility loci to associate with hiatus hernia. However, an important limitation in this study was that the replication was not performed in a geographically distinct cohort, but in a random sub-section of the UK Biobank participants (20%), meaning this was not a true replication study.

Figure 1.9. Pathophysiology of abdominal wall hernia. Summarised below are contributors of abdominal wall hernia pathology as highlighted by Abrahamson.[170] Image made available by Wikimedia Commons, under a CC-0-1.0 license.

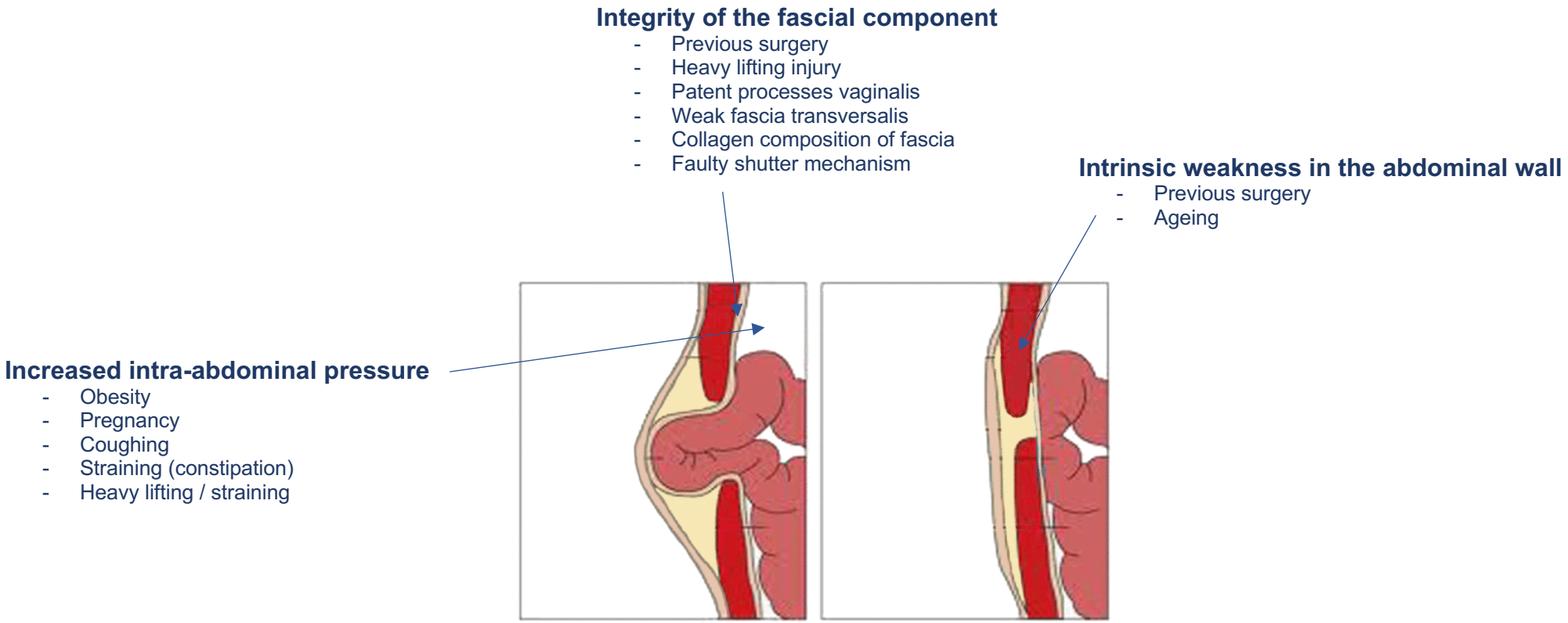

1.1.8. Other disorders as elastopathies

Elastic tissues within large bowel, the pelvic cavity, arteries, and lung parenchyma are necessary to provide elasticity and resilience to allow these structures to handle mechanical stress, the lack of which leads to pathology. Other elastopathies include diverticular disease, female genital prolapse, aneurysmal disease, emphysema, pneumothorax, and rectal prolapse. Whilst these disorders are not typically grouped together in clinical practice, I hypothesise that they may share a common pathophysiological mechanism alongside the disorders previously mentioned. Below, I outline briefly the role of genetic and environmental contributions to these six elastopathies.

Diverticular disease

Colonic diverticulosis is a condition affecting around 1/3rd of the Western world with an increasing global prevalence.[171] Diverticulosis is characterised by small pouches, or diverticula, forming in the walls of the large intestine, most commonly the descending and sigmoid colon among Westerners.[172] The majority of patients with colonic diverticuloses remain asymptomatic throughout their lives, with a quarter of patients developing symptomatic diverticulosis (diverticular disease)[172], and the most common complication in ~4% of patients being acute diverticulitis.[173,174]

Diverticular disease is an age-related condition affecting over 65% of patients by age 85[175], with females presenting later than males[176], but having higher rates of diverticulitis and worse mortality outcomes.[177] Existing treatment options for diverticular disease include fibre supplementation and lifestyle changes, as well as

antibiotics, and inevitably surgery and lengthy hospital stay in complicated disease. In Europe alone over 800,000 patients annually are admitted to hospital with diverticular disease, with an associated inpatient mortality rate of 1.5 - 3%[178], representing a significant societal burden.[179] The pathophysiology of diverticular disease is complex, the most substantial factors include colonic wall abnormalities (elastic and muscular tissue disruption and ageing leading to structural weakness), disordered colonic motility, poor diet and lifestyle, as well as genetics which is thought to be the most significant driver, with a heritability ~40% based on full-sibling risk.[180] Whilst four genome-wide association studies (GWAS) to date have identified in excess of 150 independent loci, the vast majority of heritability risk for diverticular disease remains unaccounted for.[180–183]

Female genital prolapse

Female pelvic organ prolapse (POP) is characterised by the caudal descent of one or more pelvic organs, causing protrusion into the vagina or past the introitus.[184] Under normal physiology, a myriad of scaffolding mechanisms exist to prevent prolapse, including bony structures, pelvic floor muscles, endopelvic fascia and connective and elastic tissue, the disruption of which can lead to POP.[185] The spectrum of prolapse demonstrated in POP ranges from no prolapse (Stage 0) to maximal descent and complete vaginal eversion (Stage IV).[186] Female genital prolapse is associated with a substantial symptom burden, particularly when prolapsing extends beyond the hymenal plane (stages II - IV), resulting in morbidity and a high symptom burden, including vaginal heaviness, pain, urinary storage and voiding dysfunction, incontinence, constipation, and sexual impairment.[187] POP is a prevalent condition diagnosed in ~40% of postmenopausal women[188], and 7 - 26% of women when

restricted to diagnoses where prolapsing is overt (stages II-IV).[189,190] Around 12 - 19% of women with POP require surgical intervention by age 80[191], however there is a high recurrence following surgery in around 10-30% of women.[192] POP is the primary indication for a fifth of all hysterectomies (the commonest indication in postmenopausal women)[193]; in the USA alone, over 300,000 surgeries are performed each year for POP.[194] Established environmental factors for POP include old age, obesity, vaginal childbirth, parity, and previous hysterectomy. Increasingly, genetic factors are understood to contribute to disease risk with a greater risk of POP among first-degree relatives[195], and a greater twin similarity among monozygotic twins than dizygotic twins and a corresponding heritability of ~40% for POP.[196] To date, three genome-wide association studies have identified a combined 26 loci for female genital prolapse, however a large proportion of the genetic contribution for female POP remains to be understood.[197–199]

Aneurysmal disease

Arterial aneurysmal disease is the localised pathological dilatation of arterial vessels to greater than 150% of their original segment diameter.[200] Aneurysmal disease can occur throughout the arterial network. Most commonly, aneurysms arise in the abdominal aorta (AAA), with a prevalence of 8% of men aged over 65[201], as well as intracranial aneurysms, with an unruptured prevalence of 3.2% of the global population.[202] Less frequently, aneurysms can occur in the thoracic aorta (TAA) (prevalence of 5.3 per 100,000[203]), in the peripheral arteries (including popliteal and femoral aneurysms, and rarely in visceral arteries (prevalence unknown). Diffuse aneurysmal disease is an established phenomena in literature[204], with around a sixth of patients with a primary aneurysm having concomitant disease.[204] Whilst localised

factors can initiate pathological dilatation across individual arterial network segments, a systemic propensity driven by genetic and environmental contributions is likely the main driver behind aneurysm formation.[205] Indeed, emerging evidence suggests a generalised arteriomegaly and disruption of the entire vascular tree in aneurysmal disease patients.[206]

Due to the burden of AAAs on the population, clinical screening programmes exist for men over the age of 65 in the UK. Screening has been highly successful, leading to a halving of in-hospital mortality.[207] At present however, no national screening programmes exist for cerebral, thoracic, peripheral or visceral aneurysmal disease and as a result these are identified incidentally or following spontaneous rupture.[208,209] Around 95% of patients with thoracic aneurysms are asymptomatic before an acute rupture event, with a mortality of over 90%, and therefore their exact epidemiology is challenging to establish.[210] Risk factors for aneurysm vary across the arterial network, with atherosclerosis being the most significant risk factor for AAA and descending TAAs, however systemic connective tissue dysfunction is associated most strongly with ascending TAA. Tobacco smoking and hypertension are a driver of cerebral and femoral aneurysms, and advancing age is a prominent cause of popliteal aneurysms.[211,212]

An important non-modifiable risk is the role of molecular genetics in aneurysm formation. Indeed, multiple genetic syndromes are associated with aneurysmal disease, including Ehlers-Danlos Syndrome, Marfan's syndrome, Loeys-Dietz syndrome, polycystic kidney disease, neurofibromatosis type 1, Turner syndrome, and alpha-1 anti-trypsin deficiency. Aside from causal gene mutations, a plethora of

susceptibility genes have been identified through GWAS which predispose to aneurysmal disease across the vascular tree[213–216], though a significant proportion of the genetic contribution to aneurysmal disease remains undiscovered.

Emphysema

Pulmonary emphysema is a form of chronic obstructive pulmonary disease (COPD), causing progressive airflow limitation. Emphysema results from irreversible destruction of lung parenchyma distal to the terminal bronchioles leading to loss of elasticity of alveoli causing air trapping, dilatation of air spaces and impaired gas exchange. COPD is the third most common cause of mortality in the world with over 212 million reported cases[217,218], representing a significant strain on global health systems.[219] Emphysema patients typically present with chronic, progressively-worsening exertional dyspnoea, cough, and excessive sputum production. Emphysema often goes undiagnosed, or it is diagnosed late in the course of the disease (with a peak prevalence at age 65[220]) due to frequent requirement of spirometry evidence to confirm diagnosis. At present, no disease-modifying treatments exist for emphysema with smoking cessation, lifestyle modification, and symptom control being the focus of clinical strategies to slow disease progression.[221,222] The most prominent risk factor for emphysema is tobacco smoking, however inhalation of smoke from biomass fuel, as well as accelerated ageing, social deprivation, tuberculosis, and family history are important drivers of disease.[219] COPD clusters in families with an estimated heritability of ~30%[223,224], and a multitude of Mendelian conditions presenting with emphysema, such as alpha-1 antitrypsin deficiency, cutis laxa, and cerebral aneurysm-cirrhosis syndrome. Several GWAS studies for emphysema, and measures of COPD, such as FEV1/FEVC ratio,

quantification of CT imaging findings have identified susceptibility loci for emphysema. However, to date, no studies have studied emphysema alongside other elastic tissue disorders using GWAS to find cross-trait susceptibility loci.

Pneumothorax

Pneumothorax results from air leaking into the pleural cavity, usually due to communication between the alveoli and the pleura, the atmosphere and the pleura, or gas-forming bacterium within the pleura. Clinically, pneumothorax can be defined as occurring spontaneously or non-spontaneously.[225] Primary spontaneous pneumothorax (PSP) has traditionally been defined as the presence of air in the pleural cavity in the absence of precipitating lung pathology, trauma, or an iatrogenic cause.[226] However, increasingly, data suggests the presence of an underlying pleuro-pulmonary pathology in all spontaneous pneumothoraces.[227] Others risk factors for PSP include being of a tall stature, low BMI, tobacco and cannabis smoking, living at high altitude, family history, and connective tissue dysfunction.[228] Disruption of connective tissue leads to defects in the formation of the visceral pleura making it more prone to changes in intrapleural pressures, as well as predisposing to pulmonary blebs, bullae and cysts.[229] PSP has an incidence of ~12.5 per 100,000 people annually[230], with a peak incidence at 35 years of age.[231] Whilst the majority of spontaneous pneumothoraces can be managed without chest drain insertion, global research collaboration to stratify low-risk patients at first presentation has failed to provide consensus.[232] For around 30 - 50% of PSP patients, there is recurrence of pneumothorax[233,234], with the greatest risk within the first year.[235] More robust biomarkers for risk stratification at first presentation are therefore required to identify those patients at greater risk.[236] Intriguingly, ~10 - 12% of spontaneous pneumothorax

patients have a first degree relative with pneumothorax, with these patients invariably having a higher rate of recurrence at first presentation.[237–239] Indeed, several syndromic presentations typified by connective tissue dysfunction include pneumothorax as part of their cluster of symptoms, including Birt-Hogg-Dubé syndrome, Loeys-Dietz Syndrome, cutis laxa, Ehlers-Danlos syndrome (vascular-type), Marfan syndrome, alpha-1 anti-trypsin deficiency, among others. Genetic contributions may therefore represent an important aspect of risk prognostication in identifying pneumothorax patients, and particularly those at a higher risk of phenotypically severe disease associated with recurrence and surgical intervention. Monogenic variants responsible for pneumothorax are only present in ~10% of PSP cases, contributing only minimally to the heritability of pneumothorax.[236] This suggests that common risk genes may play a more pronounced role in disease susceptibility. Only a single GWAS in 92 cases and 129 controls has been performed for PSP; however this study failed to identify any genome-wide significant susceptibility loci.[240] To date, no study has employed the use of biobank-scale datasets to uncover the genetic basis of pneumothorax, providing an important opportunity to uncover the genetic basis of pneumothorax and other elastopathies.

Rectal prolapse

Rectal prolapse involves the funnel-shaped infolding of the rectal wall after defecation which follows a disease spectrum: from a high rectal prolapse, descending into the anal canal (low anal), or in its most severe form, protruding externally from the anal canal.[241] Rectal prolapse has a prevalence of ~0.5% of the general population[242], being more common amongst women than men, with a peak age of incidence in women at age 70, and under 40 in men.[242,243] The natural history of rectal prolapse

has been described[244], with high grade internal rectal prolapse tending to progress on to full-thickness external rectal prolapse across a period of ~10 years. In its least severe form, low grade internal rectal prolapse tends to be largely asymptomatic, however as it progresses to external rectal prolapse, patients frequently experience symptoms of obstructed defecation, faecal incontinence, and bleeding.[241,245,246] For early stage asymptomatic rectal prolapse (Grade I - II), rectal prolapse requires only conservative management such as fibre supplementation and laxative therapy. For more advanced rectal prolapse (Grades III (High Anal) - V (External)), surgery remains the only viable strategy for symptomatic disease as these patients will invariably develop irreversible faecal incontinence.[247] However, despite over a hundred individual operations to manage rectal prolapse, no consensus exists around approach (abdominal versus perineal) or the use of mesh[248], sutures, or with or without resection.[249] Moreover, recurrence rates are very high at around 10%[249], with no difference between approaches. Risk factors for rectal prolapse include advancing age, female sex, a history of vaginal delivery, and chronic constipation. Though, over a quarter of patients with rectal prolapse are nulliparous or males, suggesting additional factors, namely connective tissue dysfunction are at play in the pathobiology of rectal prolapse.[250] Indeed, Keane and colleagues found a perturbed Type I : III collagen ratio in nulliparous women compared to parous women with stress urinary incontinence.[251] Whilst the genetics of pelvic organ prolapse has been studied extensively[195], to date no data has determined the contribution of genetic risk in the pathobiology of rectal prolapse.

1.1.9. Genome-wide association study

The study of the influence of genetics in complex disorders relies on approaches beyond familial linkage studies. Genome-wide association studies (GWAS) are the current best way to study the polygenic architecture of these disorders (a field known as complex trait genetics). GWAS seeks to identify the correlation between genetic variation in regions of the genome (in particular common single-nucleotide polymorphisms (SNPs)*) and disease status. The first landmark GWA study, performed by Klein *et al*.[252] in 2005, investigated associations for age-related macular degeneration in a total cohort of 96 cases and 60 controls of white origin, identifying two significant SNP variants in a region of *CFH*, a regulator of innate immunity.[253] Twenty years on, considerable strides in rapid, low-budget SNP array and high throughput sequencing technology have been made.[254] This, alongside sizable advances in data storage capacities have enabled association analysis across a much larger number of genetic variants, and across increasingly larger population sizes — facilitating the largest association analysis to date in 2,370,390 participants.[255] As of 26th August 2020, a total of 4,681 association studies for 5,506 unique diseases and traits have been catalogued by the National Human Genome Research Institute–European Bioinformatics Institute (NHGRI-EBI) GWAS Catalog.[256] GWAS is central to this thesis, hence a brief overview of its principles is warranted.

Modern SNP arrays genotype around ~0.5 to 1 million variants, capturing ~1% of variation in the human genome. GWAS leverages the principle of linkage

* The most common form of genetic variation resulting from a change (polymorphism) of a single nucleotide. The term SNPs, variants, and markers are used synonymously in the context of GWAS.

disequilibrium (LD) at the population level – the non-random association between genetic markers at different loci – meaning SNPs that are adjacent to each other are generally inherited together during recombination events.[257] Coordinated international research consortiums such as the 1000 Genomes Project[258] and the HapMap Project[259] have been successful in cataloguing SNPs that capture common genomic variation across different populations and their structural relation to one another. This development has been pivotal in facilitating imputation of ungenotyped SNPs from those that have been typed, meaning common variants in an individual can be predicted from lower-coverage SNP arrays.

The full-breadth of steps involved in a GWAS study are detailed by Hardy and Singleton[260]. Briefly, a GWA study comprises a case-control comparison for each typed or imputed variant between a population of cases* and a population of controls†. Statistical analysis is performed to examine the frequency of each allele in the two populations to look for significant association (See **Figure 1.10**). To account for multiple-testing and to control false positive rate, a genome-wide statistical significance threshold is set a $P < 5\times10^{-8}$ (0.05/ 1,000,000). GWAS is therefore rooted in an experimental, hypothesis-free and gene-agnostic methodology, identifying common variants that confer modest, incremental risk towards a disease phenotype at multiple loci (median odds ratio (OR) ~1.33 per SNP) (**Figure 1.11**).

Significant GWAS-associated variants, in themselves, are a location marker for disease, and are not indicative of a particular gene candidate. Indeed, for two-thirds

* participants that have the trait or disease in question
† participants that do not have a particular trait or disease

of associated loci, the prioritised gene is not the nearest gene to the most associated SNP at a locus.[261] Therefore functional annotation and mapping of loci is an important step to unravelling the genetic architecture of a disease and to prioritise actionable variants that can support functional validation experiments and therapeutic targeting.[262]

Several limitations are inherent to GWAS methodology: the most striking is that the vast majority of associated variants reside in non-coding or intergenic regions[263], and therefore for a significant proportion of GWAS hits, it is unclear how these loci play a role in disease biology. Another important limitation is that for complex disorders, a significant proportion of heritability are ascribed to rare genetic variation which are not captured within GWAS analyses, meaning there is significant missing heritability for complex traits that is difficult to attribute.[264] Moreover, to date, 88.9% of GWAS participants across all studies have been from European ancestry[265], meaning the transferability of GWAS results to non-European populations is restricted.[266] This is highlighted by the significantly lower predictive capabilities of polygenic risk scores (derived from European populations) when examined in non-Europeans.[267] Moreover, significantly more genetic variation is present in non-European populations, which are unfortunately under-studied, meaning that current efforts are deprived of variants that are common in non-Europeans. Clearly there is much progress to be made in this regard, with efforts such as the GWAS Diversity Monitor[265] (gwasdiversitymonitor.com) and programmes such as the African Genome Variation Project, GemomeAsia 100K and H3Africa, representing important steps towards greater diversity in GWAS studies.

Despite its many limitations, the access to large summary statistics datasets and international collaborations has grown exponentially in the last few years which has enabled the genetic community to make great strides in understanding complex disease genetics through GWAS. Perhaps the most striking GWAS successes have been for auto-immune, metabolic and psychiatric disease.[261] Type II Diabetes Mellitus (T2DM) for instance is the most studied trait of all GWA studies (147 studies, 3% of all GWA studies)[256], leading to the identification of 2486 individual SNP associations.[256] This includes the identification of a loss-of-function mutation in *SLC30A8* (encodes a zinc transport ion channel expressed in beta cells) which is protective for TD2M, and has driven pharmaceutical efforts to develop ZnT-8 antagonists which are currently being investigated.[268] Other benefits of GWAS, include the utility of GWAS-derived variants as genetic predictors (polygenic risk scoring)[269], which have enabled the development of promising risk scoring tools for diseases such as glaucoma[270], and which may foreseeably be implemented on a population scale as more participants are genotyped (for example, by direct-to-consumer companies such as 23andMe) and as genetic databases acquire greater population sizes to improve their predictive capabilities.

The very first GWA studies in small cohorts of < 1000 participants often failed to capture the full extent of heritability of complex disorders, however we are now in an era of powerful association studies of over 1 million participants. The development of large population-based initiatives over the past five years, have been necessary to advance GWAS research efforts. The UK Biobank is a prospective cohort study of ~500,000 participants of white British ancestry that have had whole genome genotyping and linkage to their electronic medical records and represents the principal

data source used in this thesis to uncover the genetic architecture of common elastopathies[46]

Figure 1.10. Method for GWA Study designs. Calculation example illustrating the methodology behind GWA studies. The genotype counts for SNP 1 are taken from the 9p21 SNP as identified in the Wellcome Trust Case Control Consortium Study (2007) of seven common diseases.[271] The figure shows the G allele of SNP1 is significantly (P <5e-8) over-represented among cases compared to controls and may be a marker for disease. Adapted and made available by Wikimedia Commons under a CC-BY-3.0 license.

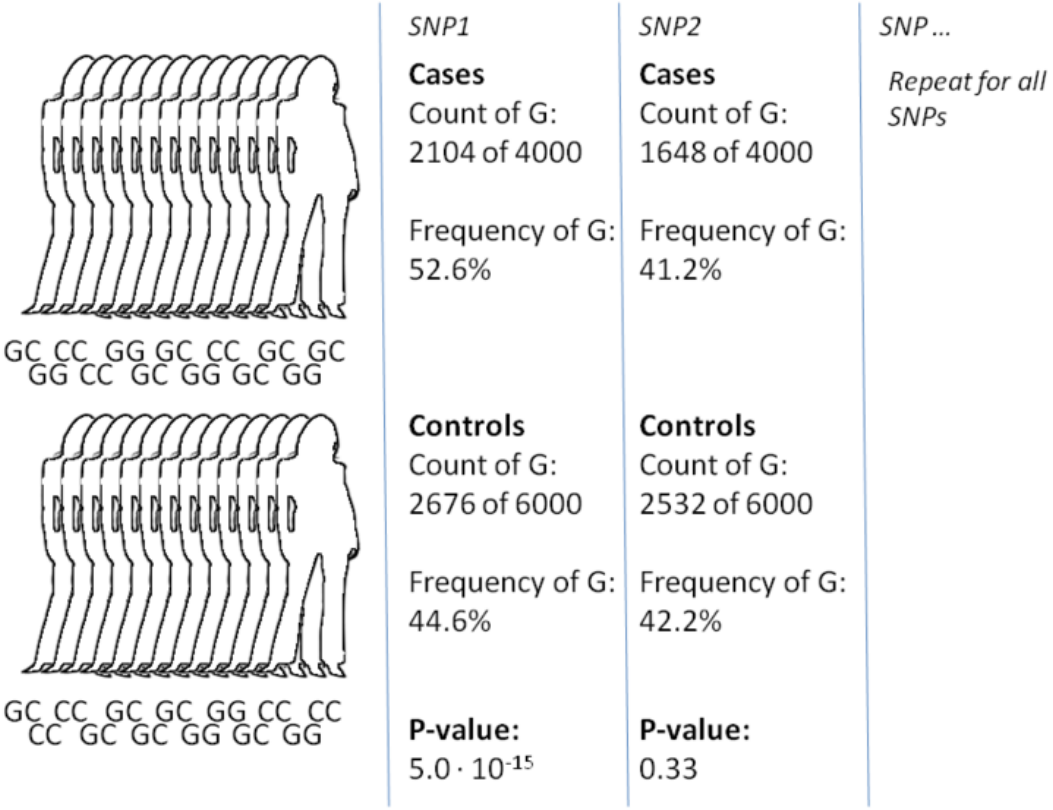

Figure 1.11. Spectrum of disease allelic effects identified by GWAS. A GWAS is positioned to identify common variants each with small effect sizes (OR < 1.5), each contributing to overall disease risk. Adapted from Bush (2012)[272] and made available by Wikimedia Commons under a CC-BY-2.5 license.

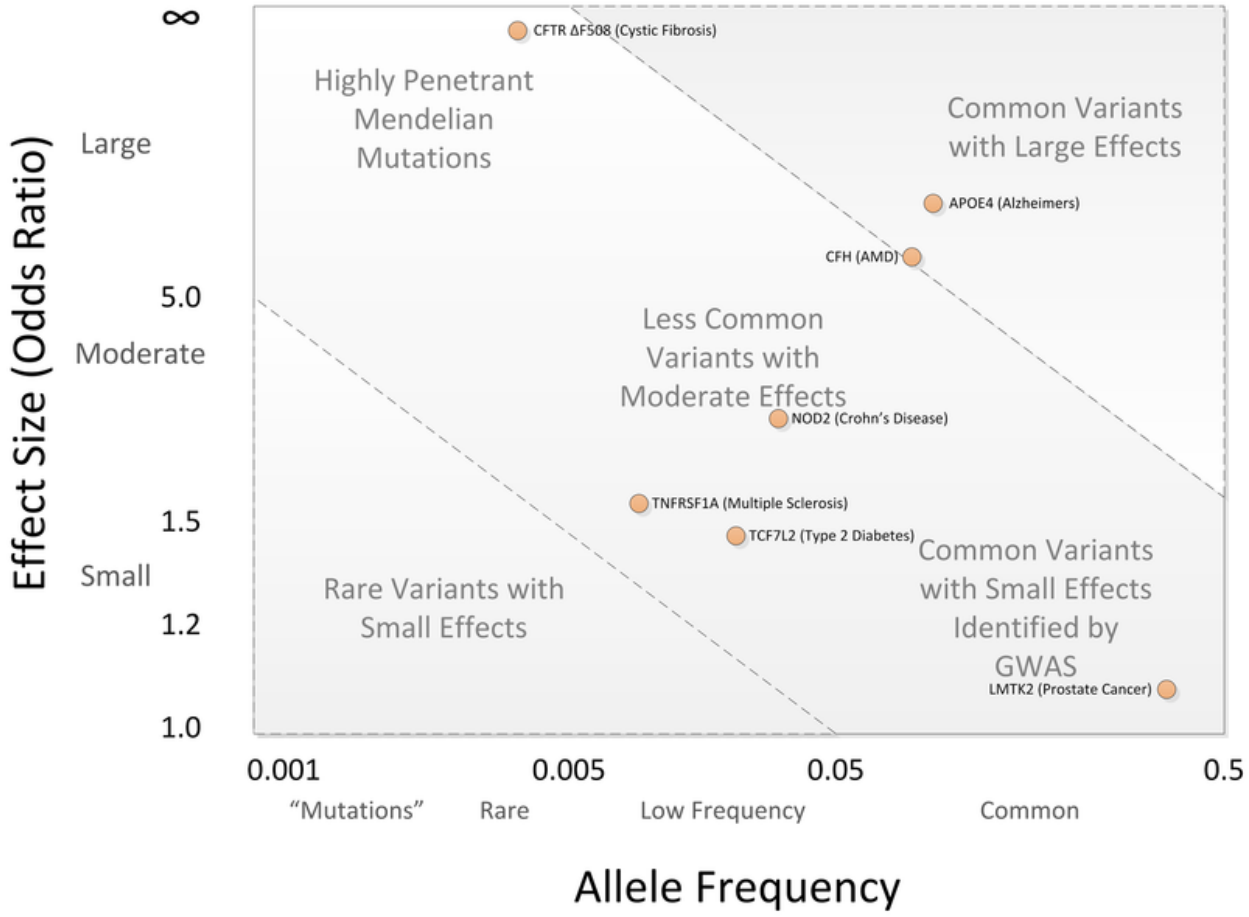

1.1.10. Scope of thesis

My thesis is titled ‘Characterising the genetic architecture of complex elastic tissue disorders in UK Biobank’. It is important to define ‘genetic architecture’ and ‘complex elastic tissue disorders’:

i) *Genetic architecture* – pertains to the “characteristics of genetic variation that are responsible for heritable phenotypic variability[273].” It comprises the full extent of genetic variants that affect a trait, the frequency of these variants in the population, the effect size of each variant, and the variants’ interaction with each other and the environment.[273]

ii) *Complex elastic tissue disorders* – it is important to note that there is no recognised classification of ‘elastic tissue disorders’, and the term is often used synonymously with connective tissue disorders. However, to distinguish the two, elastic tissue disorders herein refers to acquired diseases pertaining to significant involvement of elastic fibre dysfunction in their pathobiology and the resultant loss of resilience and elasticity of tissues.[32] To hone in on this detail further, I will hereinafter refer to complex elastic tissue disorders as ‘elastopathies’ in order to distinguish common disease from rarer syndromic forms of disease that are typically associated with the former terminology. The elastopathies being investigated in this thesis are 12: hiatus hernia, diverticular disease, haemorrhoids, inguinal hernia, varicose veins, female genital prolapse, umbilical hernia, aneurysmal disease, emphysema, pneumothorax, rectal prolapse, and femoral hernia

To this end, the chapters that follow have these broad aims:

i) **Chapter 2** – map the genetic architecture of varicose veins through a two-stage GWAS and prioritise candidate genes that are important in its pathobiology. Additionally, to perform bioinformatic functional analyses and construct a genetic risk score for the prognostication of varicose veins.

ii) **Chapter 3** – map the genetic architecture of haemorrhoidal disease through (at the time) the first-ever GWAS, and prioritise candidate genes that are important in its pathobiology. Additionally, to perform bioinformatic functional analyses and construct a genetic risk score for the prognostication of haemorrhoidal disease.

iii) **Chapter 4** – map the genetic architecture of four hernia sub-types individually (inguinal, femoral, umbilical and hiatus hernia) and through multi-trait meta-analysis approaches, elucidate the shared genetic biology between multiple hernia subtypes. To construct a genetic risk score for the prognostication of hernia individually and for multiple hernia risk.

iv) **Chapter 5** – outline the genetic architecture of the 12 elastopathies from the UK Biobank (hiatus hernia, diverticular disease, haemorrhoids, inguinal hernia, varicose veins, female genital prolapse, umbilical hernia, aneurysmal disease, emphysema, pneumothorax, rectal prolapse, and femoral hernia) and look for evidence of shared genetics between the disorders. To perform an individual patient data meta-analysis and structural equation modelling of the elastopathy phenotype to uncover shared risk.

1.1.11. Funding

The author is recipient to scholarships from the Aziz Foundation, Wolfson Foundation and Royal College Surgeons of England for the work described in this thesis. The author also receives stipendiary support from the National Institute of Health Research (NIHR) Oxford Biomedical Research Centre (Musculoskeletal theme). Previously, the author was funded by summer vacation studentships from the British Association of Plastic, Reconstructive and Aesthetic Surgeons (BAPRAS) and the Royal College of Surgeons of Edinburgh (RCSEd) for work pertaining to **Chapter 2** of this thesis. The mentioned funding bodies have at no stage had any influence on the study and results reported herein.

1.2. Chapter references

1. Hynes, R. O. & Naba, A. Overview of the matrisome-An inventory of extracellular matrix constituents and functions. *Cold Spring Harb. Perspect. Biol.* **4**, (2012).
2. Hynes, R. O. The extracellular matrix: Not just pretty fibrils. *Science* **326**, 1216–1219 (2009).
3. Frantz, C., Stewart, K. M. & Weaver, V. M. The extracellular matrix at a glance. *J. Cell Sci.* **123**, 4195–4200 (2010).
4. Bonnans, C., Chou, J. & Werb, Z. Remodelling the extracellular matrix in development and disease. *Nature Reviews Molecular Cell Biology* **15**, 786–801 (2014).
5. Miller, R. T. Mechanical properties of basement membrane in health and disease. *Matrix Biology* **57**–**58**, 366–373 (2017).
6. Naba, A. *et al.* The matrisome: In silico definition and in vivo characterization by proteomics of normal and tumor extracellular matrices. *Mol. Cell. Proteomics* **11**, (2012).
7. Yue, B. Biology of the extracellular matrix: An overview. *Journal of Glaucoma* **23**, S20–S23 (2014).
8. Lu, P., Takai, K., Weaver, V. M. & Werb, Z. Extracellular Matrix degradation and remodeling in development and disease. *Cold Spring Harb. Perspect. Biol.* **3**, (2011).
9. Cox, T. R. & Erler, J. T. Remodeling and homeostasis of the extracellular matrix: Implications for fibrotic diseases and cancer. *DMM Disease Models and Mechanisms* **4**, 165–178 (2011).
10. Raffetto, J. D. Pathophysiology of Chronic Venous Disease and Venous Ulcers.

Surgical Clinics of North America **98**, 337–347 (2018).

11. Reynolds, J. J., Hembry, R. M. & Meikle, M. C. Connective tissue degradation in health and periodontal disease and the roles of matrix metalloproteinases and their natural inhibitors. *Advances in dental research* **8**, 312–319 (1994).
12. Ricard-Blum, S. The Collagen Family. *Cold Spring Harb. Perspect. Biol.* **3**, 1–19 (2011).
13. Mead, T. J. & Apte, S. S. ADAMTS proteins in human disorders. *Matrix Biology* **71**–**72**, 225–239 (2018).
14. Kelwick, R., Desanlis, I., Wheeler, G. N. & Edwards, D. R. The ADAMTS (A Disintegrin and Metalloproteinase with Thrombospondin motifs) family. *Genome Biol.* **16**, 113 (2015).
15. Herzog, C. *et al.* Meprin A and meprin α generate biologically functional IL-1β from pro-IL-1β. *Biochem. Biophys. Res. Commun.* **379**, 904–908 (2009).
16. Banerjee, S. & Bond, J. S. Prointerleukin-18 is activated by meprin β in vitro and in vivo in intestinal inflammation. *J. Biol. Chem.* **283**, 31371–31377 (2008).
17. Sun, Q., Jin, H. J. & Bond, J. S. Disruption of the meprin α and β genes in mice alters homeostasis of monocytes and natural killer cells. *Exp. Hematol.* **37**, 346–356 (2009).
18. Crisman, J. M., Zhang, B., Norman, L. P. & Bond, J. S. Deletion of the Mouse Meprin β Metalloprotease Gene Diminishes the Ability of Leukocytes to Disseminate through Extracellular Matrix. *J. Immunol.* **172**, 4510–4519 (2004).
19. Broder, C. *et al.* Metalloproteases meprin α and meprin β are C- and N-procollagen proteinases important for collagen assembly and tensile strength. *Proc. Natl. Acad. Sci. U. S. A.* **110**, 14219–14224 (2013).
20. Kronenberg, D. *et al.* Processing of procollagen III by meprins: New players in

extracellular matrix assembly. *J. Invest. Dermatol.* **130**, 2727–2735 (2010).

21. Jefferson, T. *et al.* The substrate degradome of meprin metalloproteases reveals an unexpected proteolytic link between meprin β and ADAM10. *Cell. Mol. Life Sci.* **70**, 309–333 (2013).
22. Ohler, A., Debela, M., Wagner, S., Magdolen, V. & Becker-Pauly, C. Analyzing the protease web in skin: Meprin metalloproteases are activated specifically by KLK4, 5 and 8 vice versa leading to processing of proKLK7 thereby triggering its activation. in *Biological Chemistry* **391**, 455–460 (Biol Chem, 2010).
23. Geurts, N. *et al.* Meprins process matrix metalloproteinase-9 (MMP-9)/gelatinase B and enhance the activation kinetics by MMP-3. *FEBS Lett.* **586**, 4264–4269 (2012).
24. Nagase, H., Visse, R. & Murphy, G. Structure and function of matrix metalloproteinases and TIMPs. *Cardiovascular Research* **69**, 562–573 (2006).
25. Arpino, V., Brock, M. & Gill, S. E. The role of TIMPs in regulation of extracellular matrix proteolysis. *Matrix Biology* **44**–**46**, 247–254 (2015).
26. Lucero, H. A. & Kagan, H. M. Lysyl oxidase: An oxidative enzyme and effector of cell function. *Cellular and Molecular Life Sciences* **63**, 2304–2316 (2006).
27. Midwood, K. S. & Schwarzbauer, J. E. Elastic Fibers : Building Bridges Between Cells and Their Matrix. *Curr. Biol.* **12**, 279–281 (2002).
28. Mecham, R. P. Elastin in lung development and disease pathogenesis. *Matrix Biol.* **73**, 6–20 (2018).
29. Rosenbloom, J., Abrams, W. R. & Mecham, R. Extracellular matrix 4: The elastic fiber. *FASEB J.* **7**, 1208–1218 (1993).
30. Harrison, P. & Wordsworth, P. Metabolic bone disease and inherited disorders of bone and connective tissue. in *The Rheumatology Handbook* 247–298

(Imperial College Press, 2011). doi:10.1142/9781848163218_0005

31. Yanagisawa, H. *et al.* Fibulin-5 is an elastin-binding protein essential for elastic fibre development in vivo. *Nature* **415**, 168–171 (2002).

32. Kielty, C. M. Elastic fibres in health and disease. *Expert Rev. Mol. Med.* **8**, 1–23 (2006).

33. Vanakker, O., Callewaert, B., Malfait, F. & Coucke, P. The Genetics of Soft Connective Tissue Disorders. *Annu. Rev. Genomics Hum. Genet.* **16**, 229–255 (2015).

34. Montes, G. S. Structural biology of the fibres of the collagenous and elastic systems. *Cell Biol. Int.* **20**, 15–27 (1996).

35. Milewicz, D. M., Urban, Z. & Boyd, C. *Genetic disorders of the elastic fiber system*. *Matrix Biology* **19**, (2000).

36. Shifren, A. & Mecham, R. P. The stumbling block in lung repair of emphysema: Elastic fiber assembly. in *Proceedings of the American Thoracic Society* **3**, 428–433 (2006).

37. Berk, D. R., Bentley, D. D., Bayliss, S. J., Lind, A. & Urban, Z. Cutis laxa: A review. *J. Am. Acad. Dermatol.* **66**, 842.e1-842.e17 (2012).

38. Benke, K. *et al.* The role of transforming growth factor-beta in Marfan syndrome. *Cardiol. J.* **20**, 227–234 (2013).

39. Landis, B. J., Veldtman, G. R. & Ware, S. M. Genotype-phenotype correlations in Marfan syndrome. **103**, (2017).

40. Christiano, A. M. & Uitto, J. Molecular pathology of the elastic fibers. in *Journal of Investigative Dermatology* **103**, S53–S57 (1994).

41. Baldwin, A. K., Simpson, A., Steer, R., Cain, S. A. & Kielty, C. M. Elastic fibres in health and disease. *Expert Rev. Mol. Med.* **15**, (2013).

42. Jobling, R. *et al.* The collagenopathies: Review of clinical phenotypes and molecular correlations. *Curr. Rheumatol. Rep.* **16**, (2014).

43. Kodolitsch, Y. Von *et al.* Perspectives on the revised ghent criteria for the diagnosis of marfan syndrome. *Appl. Clin. Genet.* **8**, 137–155 (2015).

44. Germain, D. P. Ehlers-Danlos syndrome type IV. *Orphanet Journal of Rare Diseases* **2**, 32 (2007).

45. Mitteroecker, P., Cheverud, J. M. & Pavlicev, M. Multivariate analysis of genotype–phenotype association. *Genetics* **202**, 1345–1363 (2016).

46. Bycroft, C. *et al.* The UK Biobank resource with deep phenotyping and genomic data. *Nature* **562**, 203–209 (2018).

47. Grant, Y., Onida, S. & Davies, A. Genetics in chronic venous disease. *Phlebol. J. Venous Dis.* **32**, 3–5 (2017).

48. Barnett, C., Langer, J. C., Hinek, A., Bradley, T. J. & Chitayat, D. Looking past the lump: genetic aspects of inguinal hernia in children. *Journal of Pediatric Surgery* **44**, 1423–1431 (2009).

49. Mann, M., Tendulkar, A., Birger, N., Howard, C. & Ratcliffe, M. B. National Institutes of Health Funding for Surgical Research. *Ann. Surg.* **247**, 217–221 (2008).

50. Malfait, F. *et al.* The 2017 international classification of the Ehlers–Danlos syndromes. *Am. J. Med. Genet. Part C Semin. Med. Genet.* **175**, 8–26 (2017).

51. Meester, J. A. N. *et al.* Differences in manifestations of Marfan syndrome, Ehlers-Danlos syndrome, and Loeys-Dietz syndrome. *Ann. Cardiothorac. Surg.* **6**, 582–594 (2017).

52. Lurie, F. *et al.* The 2020 update of the CEAP classification system and reporting standards. *J. Vasc. Surg. Venous Lymphat. Disord.* **8**, 342–352 (2020).

53. Beebe-Dimmer, J. L., Pfeifer, J. R., Engle, J. S. & Schottenfeld, D. The epidemiology of chronic venous insufficiency and varicose veins. *Ann. Epidemiol.* **15**, 175–184 (2005).

54. Evans, C. J., Fowkes, F. G. R., Ruckley, C. V. & Lee, A. J. Prevalence of varicose veins and chronic venous insufficiency in men and women in the general population: Edinburgh Vein Study. *J. Epidemiol. Community Health* **53**, 149–153 (1999).

55. Heit, J. A. *et al.* Trends in the incidence of venous stasis syndrome and venous ulcer: A 25-year population-based study. *J. Vasc. Surg.* **33**, 1022–1027 (2001).

56. Rabe, E. *et al.* Bonn Vein Study by the German Society of Phlebology: Epidemiological study to investigate the prevalence and severity of chronic venous disorders in the urban and rural residential populations. *Phlebologie* **32**, 1–14 (2003).

57. Anwar, M. A. *et al.* A review of familial, genetic, and congenital aspects of primary varicose vein disease. *Circ. Cardiovasc. Genet.* **5**, 460–466 (2012).

58. Smith, J. J., Garratt, A. M., Guest, M., Greenhalgh, R. M. & Davies, A. H. Evaluating and improving health-related quality of life in patients with varicose veins. *J. Vasc. Surg.* **30**, 710–719 (1999).

59. Bergqvist, D., Lindholm, C. & Nelzen, O. Chronic leg ulcers: The impact of venous disease. *J. Vasc. Surg.* **29**, 752–755 (1999).

60. Singer, A. J., Tassiopoulos, A. & Kirsner, R. S. Evaluation and Management of Lower-Extremity Ulcers. *N. Engl. J. Med.* **377**, 1559–1567 (2017).

61. Rice, J. B. *et al.* Burden of venous leg ulcers in the United States. *J. Med. Econ.* **17**, 347–356 (2014).

62. Laing, W. Chronic Venous Diseases of the Leg. *Office of Health Economics:*

London (1992). Available at: https://www.ohe.org/publications/chronic-venous-diseases-leg. (Accessed: 1st January 2020)

63. Stanley, J. C. *et al.* Vascular surgery in the United States: Workforce issues: Report of the Society for Vascular Surgery and the International Society for Cardiovascular Surgery, North American Chapter, Committee on Workforce Issues. *J. Vasc. Surg.* **23**, 172–181 (1996).

64. Marsden, G., Perry, M., Kelley, K. & Davies, A. H. Diagnosis and management of varicose veins in the legs: Summary of NICE guidance. *BMJ (Online)* **347**, (2013).

65. O'Donnell, T. F., Balk, E. M., Dermody, M., Tangney, E. & Iafrati, M. D. Recurrence of varicose veins after endovenous ablation of the great saphenous vein in randomized trials. *Journal of Vascular Surgery: Venous and Lymphatic Disorders* **4**, 97–105 (2016).

66. Segiet, O. A. *et al.* Biomolecular mechanisms in varicose veins development. *Annals of Vascular Surgery* **29**, 377–384 (2015).

67. Raffetto, J. D. & Khalil, R. A. Mechanisms of varicose vein formation: Valve dysfunction and wall dilation. *Phlebology* **23**, 85–89 (2008).

68. Lim, C. S. & Davies, A. H. Pathogenesis of primary varicose veins. *Br. J. Surg.* **96**, 1231–1242 (2009).

69. Lee, A. J., Evans, C. J., Allan, P. L., Ruckley, C. V & Fowkes, F. G. R. Lifestyle factors and the risk of varicose veins: Edinburg Vein Study. *J. Clin. Epidemiol.* **56**, 171–179 (2003).

70. Sisto, T. *et al.* Prevalence and risk factors of varicose veins in lower extremities: Mini-Finland health survey. *Eur. J. Surgery, Acta Chir.* **161**, 405–414 (1995).

71. Scott TE, LaMorte WW, Gorin DR, M. J. Risk factors for chronic venous

insufficiency: a dual case-control study. *J. Vasc. Surg.* **22**, 622–8 (1995).

72. Zöller, B., Ji, J., Sundquist, J. & Sundquist, K. Family history and risk of hospital treatment for varicose veins in Sweden. *Br. J. Surg.* **99**, 948–953 (2012).

73. Fiebig, A. *et al.* Heritability of chronic venous disease. *Hum. Genet.* **127**, 669–674 (2010).

74. Molnár, A. Á. *et al.* Heritability of venous biomechanics. *Arterioscler. Thromb. Vasc. Biol.* **33**, 152–157 (2013).

75. Brinsuk, M., Tank, J., Luft, F. C., Busjahn, A. & Jordan, J. Heritability of Venous Function in Humans. *Arterioscler. Thromb. Vasc. Biol.* **24**, 207–211 (2004).

76. Lee, S. *et al.* Gene Expression Profiles in Varicose Veins Using Complementary DNA Microarray. *Dermatologic Surg.* **31**, 391–395 (2006).

77. Ellinghaus, E. *et al.* Genome-wide association analysis for chronic venous disease identifies EFEMP1 and KCNH8 as susceptibility loci. *Sci. Rep.* **7**, 1–9 (2017).

78. Fukaya, E. et al. Clinical and Genetic Determinants of Varicose Veins. *Circulation* 1–12 (2018). doi:10.1161/CIRCULATIONAHA.118.035584

79. Shadrina, A. *et al.* Polymorphisms of genes involved in inflammation and blood vessel development influence the risk of varicose veins. *Clin. Genet.* 1–23 (2018). doi:10.1111/cge.13362

80. Canela-Xandri, O., Rawlik, K. & Tenesa, A. An atlas of genetic associations in UK Biobank. *Nat. Genet. 2018 5011* **50**, 1593–1599 (2018).

81. Ahmed, W. U. R. *et al.* Genome-wide association analysis and replication in 810,625 individuals with varicose veins. *Nat. Commun. 2022 131* **13**, 1–11 (2022).

82. Lee, M. L. *et al.* A genome-wide association study for varicose veins. *Phlebology*

37, 267–278 (2022).

83. Levin, M. G. *et al.* Genetics of varicose veins reveals polygenic architecture and genetic overlap with arterial and venous disease. *Nat. Cardiovasc. Res. 2023 21* **2**, 44–57 (2023).

84. Helkkula, P. *et al.* Genome-wide association study of varicose veins identifies a protective missense variant in GJD3 enriched in the Finnish population. *Commun. Biol. 2023 61* **6**, 1–12 (2023).

85. Henry, MM; Swash, M. *Coloproctology and the pelvic floor: Pathophysiology and management*. *Butterworths* (Butterworths, 1985).

86. Loder, P. B., Nicholls, R. J. & Phillips, A. K. S. *Haemorrhoids: pathology, pathophysiology and aetiology*. *British Journal of Surgery* **81**, (1994).

87. Banov, L., Knoepp, L. F., Erdman, L. H. & Alia, R. T. Management of hemorrhoidal disease. *J. S. C. Med. Assoc.* **81**, 398–401 (1985).

88. Sandler, R. S. & Peery, A. F. Rethinking What We Know About Hemorrhoids. *Clinical Gastroenterology and Hepatology* **17**, 8–15 (2019).

89. Everhart, J. E. & Ruhl, C. E. Burden of Digestive Diseases in the United States Part II: Lower Gastrointestinal Diseases. *Gastroenterology* **136**, 741–754 (2009).

90. Haas, P. A., Haas, G. P., Schmaltz, S. & Fox, T. A. The prevalence of hemorrhoids. *Dis. Colon Rectum* **26**, 435–439 (1983).

91. Johanson, J. F. & Sonnenberg, A. The prevalence of hemorrhoids and chronic constipation. An epidemiologic study. *Gastroenterology* **98**, 380–386 (1990).

92. ACHESON, R. M. Haemorrhoids in the adult male; a small epidemiological study. *Guys. Hosp. Rep.* **109**, 184–195 (1960).

93. Gazet, J. C., Redding, W. & Rickett, J. W. The prevalence of haemorrhoids. A

preliminary survey. *Proc. R. Soc. Med.* **63 Suppl**, 78–80 (1970).

94. Abramowitz, L. *et al.* The European Journal of General Practice The prevalence of proctological symptoms amongst patients who see general practitioners in France The prevalence of proctological symptoms amongst patients who see general practitioners in France. (2014). doi:10.3109/13814788.2014.899578
95. Crosland, A. & Jones, R. Rectal bleeding: Prevalence and consultation behaviour. *BMJ* **311**, 486 (1995).
96. Shi, Y. *et al.* Factors influencing patient delay in individuals with haemorrhoids: A study based on theory of planned behavior and common sense model. *J. Adv. Nurs.* **75**, 1018–1028 (2019).
97. Ristvedt, S. L. *et al.* Delayed treatment for rectal cancer. *Dis. Colon Rectum* **48**, 1736–1741 (2005).
98. Hansen, P. L., Hjertholm, P. & Vedsted, P. Increased diagnostic activity in general practice during the year preceding colorectal cancer diagnosis. *Int. J. Cancer* **137**, 615–624 (2015).
99. Tol, R. R. *et al.* European Society of ColoProctology: guideline for haemorrhoidal disease. *Color. Dis.* **22**, 650–662 (2020).
100. Lohsiriwat, V. Approach to Hemorrhoids. doi:10.1007/s11894-013-0332-6
101. Etzioni, D. A., Beart, R. W., Madoff, R. D. & Ault, G. T. Impact of the Aging Population on the Demand for Colorectal Procedures. *Dis. Colon Rectum* **52**, 583–590 (2009).
102. Altomare, D. F. & Giuratrabocchetta, S. Conservative and surgical treatment of haemorrhoids. *Nature Reviews Gastroenterology and Hepatology* **10**, 513–521 (2013).
103. Hospital Admitted Patient Care Activity 2018-19 - NHS Digital. Available at:

https://digital.nhs.uk/data-and-information/publications/statistical/hospital-admitted-patient-care-activity/2018-19. (Accessed: 4th August 2020)

104. Iyer, V. S., Shrier, I. & Gordon, P. H. Long-term outcome of rubber band ligation for symptomatic primary and recurrent internal hemorrhoids. *Dis. Colon Rectum* **47**, 1364–1370 (2004).

105. Brown, S. R. *et al.* Haemorrhoidal artery ligation versus rubber band ligation for the management of symptomatic second-degree and third-degree haemorrhoids (HubBLe): a multicentre, open-label, randomised controlled trial. *Lancet* **388**, 356–364 (2016).

106. Shanmugam V, Thaha MA, Rabindranath KS, Campbell KL, Steele RJ, L. M. Rubber band ligation versus excisional haemorrhoidectomy for haemorrhoids. *Cochrane Database Syst Rev* **3**, (2005).

107. Bleday R, Pena JP, Rothenberger DA, Goldberg SM, B. J. Symptomatic hemorrhoids: Current incidence and complications. *Dis. Colon Rectum* **35**, 477–481 (1992).

108. Sardinha, T. C. & Corman, M. L. Hemorrhoids. *Surgical Clinics of North America* **82**, 1153–1167 (2002).

109. Margetis, N. Pathophysiology of internal hemorrhoids. *Ann. Gastroenterol.* **32**, 264–272 (2019).

110. Pata, F. *et al.* Anatomy, Physiology and Pathophysiology of Haemorrhoids. *Rev. Recent Clin. Trials* **15**, (2020).

111. Favreau, C., Siproudhis, L., Eleouet, M., Bouguen, G. & Bretagne, J. F. Underlying functional bowel disorder may explain patient dissatisfaction after haemorrhoidal surgery. *Color. Dis.* **14**, 356–361 (2012).

112. Salnikova, L. E., Khadzhieva, M. B. & Kolobkov, D. S. Biological findings from

the PheWAS catalog: focus on connective tissue-related disorders (pelvic floor dysfunction, abdominal hernia, varicose veins and hemorrhoids). *Hum. Genet.* **135**, 779–795 (2016).

113. Abramson, J. H., Gofin, J., Hopp, C., Makler, A. & Epstein, L. M. The epidemiology of inguinal hernia. A survey in western Jerusalem. *J. Epidemiol. Community Health* **32**, 59–67 (1978).
114. Ekici, U., Kartal, A. & Ferhatoglu, M. F. Association Between Hemorrhoids and Lower Extremity Chronic Venous Insufficiency. *Cureus* **11**, (2019).
115. Burkitt, D. P. Varicose Veins Deep Vein Thrombosis, and Haemorrhoids: Epidemiology and Suggested Aetiology. *Br. Med. J.* **2**, 556 (1972).
116. Heslop, J. PILES AND RECTOCELES. *ANZ J. Surg.* **57**, 935–938 (1987).
117. Miedel, A., Tegerstedt, G., Mæhle-Schmidt, M., Nyrén, O. & Hammarström, M. Nonobstetric Risk Factors for Symptomatic Pelvic Organ Prolapse. *Obstet. Gynecol.* **113**, 1089–1097 (2009).
118. Humphreys, D. M. Diverticular disease: Three studies: Part I—Relation to other disorders and fibre intake. *Br. Med. J.* **1**, 424–425 (1976).
119. S, R. J. vd L. G. D. Diverticular disease. Pathology and clinical aspects based on 368 autopsy cases. *Zentralbl Chir* **116**, 991–8 (1991).
120. Willis, S., Junge, K., Ebrahimi, R., Prescher, A. & Schumpelick, V. Haemorrhoids - a collagen disease? *Color. Dis.* **12**, 1249–1253 (2010).
121. Bruch, H. P. & Roblick, U. J. Pathophysiologie des Hämorrhoidalleidens. *Chirurg* **72**, 656–659 (2001).
122. Khan, N. M. M. Injection sclerotherapy versus electrocoagulation in the management outcome of early haemorrhoids - PubMed. *J Pak Med Assoc* **56**, 579–582 (2006).

123. Yildiz, T., Aydin, D. B., Ilce, Z., Yucak, A. & Karaaslan, E. External hemorrhoidal disease in child and teenage: Clinical presentations and risk factors. *Pakistan J. Med. Sci.* **35**, 696–700 (2019).

124. Kaidar-Person, O., Person, B. & Wexner, S. D. Hemorrhoidal Disease: A Comprehensive Review. *Journal of the American College of Surgeons* **204**, 102–117 (2007).

125. Bogaert, J. & Prenen, H. Molecular genetics of colorectal cancer. *Annals of Gastroenterology* **27**, 9–14 (2014).

126. Cleynen, I. *et al.* Inherited determinants of Crohn's disease and ulcerative colitis phenotypes: A genetic association study. *Lancet* **387**, 156–167 (2016).

127. Zheng, T. *et al.* Genome-wide analysis of 944 133 individuals provides insights into the etiology of haemorrhoidal disease. *Gut* **70**, 1538–1549 (2021).

128. Cataldo, P. *et al.* Practice Parameters for the Management of Hemorrhoids (Revised). *Dis. Colon Rectum* **48**, 189–194 (2005).

129. Bay-Nielsen, M. *et al.* Quality assessment of 26 304 herniorrhaphies in Denmark: A prospective nationwide study. *Lancet* **358**, 1124–1128 (2001).

130. Kingsnorth, A. N. & LeBlanc, K. A. *Management of Abdominal Hernias*. (Springer London, 2013). doi:10.1007/978-1-84882-877-3

131. Primatesta, P. & Goldacre, M. J. Inguinal hernia repair: Incidence of elective and emergency surgery, readmission and mortality. *Int. J. Epidemiol.* **25**, 835–839 (1996).

132. NHS Digital. NHS Hospital Admitted Patient Care Activity, 2018-19: Procedures and Interventions. Available at: https://digital.nhs.uk/data-and-information/publications/statistical/hospital-admitted-patient-care-activity/2018-19. (Accessed: 10th September 2020)

133. Abbott, T. E. F. *et al.* Frequency of surgical treatment and related hospital procedures in the UK: A national ecological study using hospital episode statistics. *Br. J. Anaesth.* **119**, 249–257 (2017).

134. Hair, A., Paterson, C., Wright, D., Baxter, J. N. & O'Dwyer, P. J. What effect does the duration of an inguinal hernia have on patient symptoms? *J. Am. Coll. Surg.* **193**, 125–129 (2001).

135. Roman, S. & Kahrilas, P. J. The diagnosis and management of hiatus hernia. *BMJ (Online)* **349**, (2014).

136. Jenkins, J. T. & O'Dwyer, P. J. Inguinal hernias. *BMJ* **336**, 269–272 (2008).

137. Simons, M. P. *et al.* European Hernia Society guidelines on the treatment of inguinal hernia in adult patients. *Hernia* **13**, 343–403 (2009).

138. Poelman, M. M. *et al.* EAES Consensus Development Conference on endoscopic repair of groin hernias. *Surgical Endoscopy* **27**, 3505–3519 (2013).

139. Flum, D. R., Horvath, K. & Koepsell, T. Have outcomes of incisional hernia repair improved with time? A population-based analysis. *Ann. Surg.* **237**, 129–135 (2003).

140. Scott, N. *et al.* Open Mesh versus non-Mesh for groin hernia repair. *Cochrane Database Syst. Rev.* (2001). doi:10.1002/14651858.cd002197

141. Smart, N. J., Marshall, M. & Daniels, I. R. Biological meshes: A review of their use in abdominal wall hernia repairs. *Surgeon* **10**, 159–171 (2012).

142. Köckerling, F. *et al.* What is the evidence for the use of biologic or biosynthetic meshes in abdominal wall reconstruction? *Hernia* **22**, 249–269 (2018).

143. Dahlstrand, U., Wollert, S., Nordin, P., Sandblom, G. & Gunnarsson, U. Emergency femoral hernia repair: A study based on a national register. *Ann. Surg.* **249**, 672–676 (2009).

144. Koch, A., Edwards, A., Haapaniemi, S., Nordin, P. & Kald, A. Prospective evaluation of 6895 groin hernia repairs in women. *Br. J. Surg.* **92**, 1553–1558 (2005).

145. Nilsson, H., Stylianidis, G., Haapamäki, M., Nilsson, E. & Nordin, P. Mortality after groin hernia surgery. *Ann. Surg.* **245**, 656–660 (2007).

146. Lau, H., Fang, C., Yuen, W. K. & Patil, N. G. Risk factors for inguinal hernia in adult males: A case-control study. *Surgery* **141**, 262–266 (2007).

147. Burcharth, J., Pommergaard, H. C. & Rosenberg, J. The inheritance of groin hernia: A systematic review. *Hernia* **17**, 183–189 (2013).

148. Ikeda, H. *et al.* Risk of contralateral manifestation in children with unilateral inguinal hernia: Should hernia in children be treated contralaterally? *J. Pediatr. Surg.* **35**, 1746–1748 (2000).

149. Jansen, P. L., Klinge, U., Jansen, M. & Junge, K. Risk factors for early recurrence after inguinal hernia repair. *BMC Surg.* **9**, 18 (2009).

150. Maddox, M. M. & Smith, D. P. A long-term prospective analysis of pediatric unilateral inguinal hernias: Should laparoscopy or anything else influence the management of the contralateral side? *J. Pediatr. Urol.* **4**, 141–145 (2008).

151. Zöller, B., Ji, J., Sundquist, J. & Sundquist, K. Shared and nonshared familial susceptibility to surgically treated inguinal hernia, femoral hernia, incisional hernia, epigastric hernia, and umbilical hernia. *J. Am. Coll. Surg.* **217**, (2013).

152. Glassow, F. Femoral hernia. Review of 2,105 repairs in a 17 year period. *Am. J. Surg.* **150**, 353–356 (1985).

153. De Luca, L. *et al. Relationship Between Hiatal Hernia and Inguinal Hernia*. *Digestive Diseases and Sciences* **49**, (2004).

154. Liem, M. S. L., Van Der Graaf, Y., Beemer, F. A. & Van Vroonhoven, T. J. M. V.

Increased risk for inguinal hernia in patients with Ehlers-Danlos syndrome. *Surgery* **122**, 114–115 (1997).

155. Ahmed, W. U. R. *et al.* Shared genetic architecture of hernias: A genome-wide association study with multivariable meta-analysis of multiple hernia phenotypes. *PLoS One* **17**, e0272261 (2022).
156. Sezer, S. *et al.* Association of collagen type I alpha 1 gene polymorphism with inguinal hernia. *Hernia* **18**, 507–512 (2014).
157. Han, Q. *et al.* Functional sequence variants within the SIRT1 gene promoter in indirect inguinal hernia. *Gene* **546**, 1–5 (2014).
158. Zhang, Y. *et al.* Genetic analysis of the TBX2 gene promoter in indirect inguinal hernia. *Hernia* **18**, 513–517 (2014).
159. Zhang, Y. *et al.* Genetic analysis of the TBX1 gene promoter in indirect inguinal hernia. *Gene* **535**, 290–293 (2014).
160. Antoniou, G. A. *et al.* Assessment of insertion/deletion polymorphism of the angiotensin-converting enzyme gene in abdominal aortic aneurysm and inguinal hernia. *Vascular* **21**, 1–5 (2013).
161. Wang, D., Han, Y., Xu, X., Chen, J. & Chen, Y. Matrix Metalloproteinases (MMP-2) and Tissue Inhibitors of Metalloproteinases (TIMP-2) in Patients with Inguinal Hernias. *World J. Surg.* 1–8 (2020). doi:10.1007/s00268-020-05674-0
162. Mao, Y. *et al.* A network analysis revealed the essential and common downstream proteins related to inguinal hernia. *PLoS One* **15**, e0226885 (2020).
163. Jorgenson, E. *et al.* A genome-wide association study identifies four novel susceptibility loci underlying inguinal hernia. *Nat. Commun.* **6**, (2015).
164. Bonfiglio, F. *et al.* A meta-analysis of reflux genome-wide association studies in 6750 Northern Europeans from the general population. *Neurogastroenterol.*

Motil. **29**, (2017).

165. Wei, J. *et al.* Identification of fifty-seven novel loci for abdominal wall hernia development and their biological and clinical implications: results from the UK Biobank. *Hernia* **26**, 335–348 (2022).
166. Hikino, K. *et al.* Susceptibility loci and polygenic architecture highlight population specific and common genetic features in inguinal hernias: genetics in inguinal hernias. *EBioMedicine* **70**, (2021).
167. Choquet, H. *et al.* Ancestry- and sex-specific effects underlying inguinal hernia susceptibility identified in a multiethnic genome-wide association study meta-analysis. *Hum. Mol. Genet.* **31**, 2279–2293 (2022).
168. Fadista, J. *et al.* Comprehensive genome-wide association study of different forms of hernia identifies more than 80 associated loci. *Nat. Commun. 2022 131* **13**, 1–11 (2022).
169. Campbell, M. *et al.* Identification of 14 novel susceptibility loci for diaphragmatic hernia development and their biological and clinical implications: results from the UK Biobank. *Surg. Endosc.* **36**, 7647–7651 (2022).
170. Abrahamson, J. *GROIN HERNIA SURGERY ETIOLOGY AND PATHOPHYSIOLOGY OF PRIMARY AND RECURRENT GROIN HERNIA FORMATION*.
171. Bugiantella, W. *et al.* Left colon acute diverticulitis: an update on diagnosis, treatment and prevention. *Int. J. Surg.* **13**, 157–164 (2015).
172. Tursi, A. *et al.* Colonic diverticular disease. *Nat. Rev. Dis. Prim. 2020 61* **6**, 1–23 (2020).
173. Miller, A. S. *et al.* The Association of Coloproctology of Great Britain and Ireland consensus guidelines in emergency colorectal surgery. *Colorectal Dis.* **23**, 476–

547 (2021).

174. Sartelli, M. *et al.* 2020 update of the WSES guidelines for the management of acute colonic diverticulitis in the emergency setting. *World J. Emerg. Surg.* **15**, (2020).

175. Painter, N. S. & Burkitt, D. P. Diverticular Disease of the Colon, a 20th Century Problem. *Clin. Gastroenterol.* **4**, 3–21 (1975).

176. McConnell, E. J., Tessier, D. J. & Wolff, B. G. Population-based incidence of complicated diverticular disease of the sigmoid colon based on gender and age. *Dis. Colon Rectum* **46**, 1110–1114 (2003).

177. Sell, N. M. *et al.* Are There Variations in Mortality From Diverticular Disease By Sex? *Dis. Colon Rectum* **63**, 1285–1292 (2020).

178. Delvaux, M. Diverticular disease of the colon in Europe: epidemiology, impact on citizen health and prevention. *Aliment. Pharmacol. Ther.* **18 Suppl 3**, 71–74 (2003).

179. Peery, A. F. *et al.* Burden and Cost of Gastrointestinal, Liver, and Pancreatic Diseases in the United States: Update 2021. *Gastroenterology* **162**, 621–644 (2022).

180. Wu, Y. *et al.* 150 risk variants for diverticular disease of intestine prioritize cell types and enable polygenic prediction of disease susceptibility. *Cell genomics* **3**, (2023).

181. Maguire, L. H. *et al.* Genome-wide association analyses identify 39 new susceptibility loci for diverticular disease. *Nat. Genet.* **50**, 1359–1365 (2018).

182. Zheng, T. *et al.* Genome-wide analysis of 944 133 individuals provides insights into the etiology of haemorrhoidal disease. *Gut* **70**, 1538–1549 (2021).

183. Joo, Y. Y. *et al.* Multi-ancestry genome- and phenome-wide association studies

of diverticular disease in electronic health records with natural language processing enriched phenotyping algorithm. *PLoS One* **18**, (2023).

184. Barber, M. D. Pelvic organ prolapse. *BMJ* **354**, (2016).
185. Moalli, P. A., Debes, K. M., Meyn, L. A., Howden, N. S. & Abramowitch, S. D. Hormones Restore Biomechanical Properties of the Vagina and Supportive Tissues After Surgical Menopause in Young Rats. *Am. J. Obstet. Gynecol.* **199**, 161.e1 (2008).
186. Persu, C., Chapple, C. R., Cauni, V., Gutue, S. & Geavlete, P. Pelvic Organ Prolapse Quantification System (POP–Q) – a new era in pelvic prolapse staging. *J. Med. Life* **4**, 75 (2011).
187. Barber, M. D. Pelvic organ prolapse. *BMJ* **354**, (2016).
188. Hendrix, S. L. *et al.* Pelvic organ prolapse in the Women's Health Initiative: Gravity and gravidity. *Am. J. Obstet. Gynecol.* **186**, 1160–1166 (2002).
189. Swift, S. *et al.* Pelvic Organ Support Study (POSST): The distribution, clinical definition, and epidemiologic condition of pelvic organ support defects. *Am. J. Obstet. Gynecol.* **192**, 795–806 (2005).
190. Gutman, R. E., Ford, D. E., Quiroz, L. H., Shippey, S. H. & Handa, V. L. Is there a pelvic organ prolapse threshold that predicts pelvic floor symptoms? *Am. J. Obstet. Gynecol.* **199**, 683.e1-683.e7 (2008).
191. Wu, J. M., Matthews, C. A., Conover, M. M., Pate, V. & Jonsson Funk, M. Lifetime risk of stress urinary incontinence or pelvic organ prolapse surgery. *Obstet. Gynecol.* **123**, 1201–1206 (2014).
192. Nygaard, I. *et al.* Long-term Outcomes Following Abdominal Sacrocolpopexy for Pelvic Organ Prolapse. *JAMA* **309**, 2016–2024 (2013).
193. Whiteman, M. K. *et al.* Inpatient hysterectomy surveillance in the United States,

2000-2004. *Am. J. Obstet. Gynecol.* **198**, 34.e1-34.e7 (2008).

194. Smith, F. J., Holman, C. D. A. J., Moorin, R. E. & Tsokos, N. Lifetime risk of undergoing surgery for pelvic organ prolapse. *Obstet. Gynecol.* **116**, 1096–1100 (2010).

195. Chiaffarino, F. *et al.* Reproductive factors, family history, occupation and risk of urogenital prolapse. *Eur. J. Obstet. Gynecol. Reprod. Biol.* **82**, 63–67 (1999).

196. Altman, D., Forsman, M., Falconer, C. & Lichtenstein, P. Genetic Influence on Stress Urinary Incontinence and Pelvic Organ Prolapse. *Eur. Urol.* **54**, 918–923 (2008).

197. Allen-Brady, K. *et al.* Identification of six loci associated with pelvic organ prolapse using genome-wide association analysis. *Obstet. Gynecol.* **118**, 1345–1353 (2011).

198. Olafsdottir, T. *et al.* Genome-wide association identifies seven loci for pelvic organ prolapse in Iceland and the UK Biobank. *Commun. Biol.* **3**, (2020).

199. Pujol-Gualdo, N. *et al.* Advancing our understanding of genetic risk factors and potential personalized strategies for pelvic organ prolapse. *Nat. Commun.* **13**, (2022).

200. Shaw, P. M., Loree, J. & Gibbons, R. C. Abdominal Aortic Aneurysm. *StatPearls* (2024).

201. Nordon, I. M., Hinchliffe, R. J., Loftus, I. M. & Thompson, M. M. Pathophysiology and epidemiology of abdominal aortic aneurysms. *Nat. Rev. Cardiol. 2010 82* **8**, 92–102 (2010).

202. Jersey, A. M. & Foster, D. M. Cerebral Aneurysm. *Man. Neuroanesthesia Essentials* 281–282 (2023). doi:10.1201/9781315154367-35

203. Gouveia e Melo, R. *et al.* Incidence and Prevalence of Thoracic Aortic

Aneurysms: A Systematic Review and Meta-analysis of Population-Based Studies. *Semin. Thorac. Cardiovasc. Surg.* **34**, 1–16 (2022).

204. van Laarhoven, C. J. H. C. M. *et al.* Systematic Review of the Co-Prevalence of Arterial Aneurysms Within the Vasculature. *Eur. J. Vasc. Endovasc. Surg.* **61**, 473–483 (2021).
205. van't Hof, F. N. G. *et al.* Shared genetic risk factors of intracranial, abdominal, and thoracic aneurysms. *J. Am. Heart Assoc.* **5**, (2016).
206. Johnsen, S. H. *et al.* Relation of common carotid artery lumen diameter to general arterial dilating diathesis and abdominal aortic aneurysms: the Tromsø Study. *Am. J. Epidemiol.* **169**, 330–338 (2009).
207. Mani, K. *et al.* Treatment of abdominal aortic aneurysm in nine countries 2005-2009: a vascunet report. *Eur. J. Vasc. Endovasc. Surg.* **42**, 598–607 (2011).
208. Erbel, R. *et al.* 2014 ESC guidelines on the diagnosis and treatment of aortic diseases. *Eur. Heart J.* **35**, 2873–2926 (2014).
209. Hiratzka, L. F. *et al.* 2010 ACCF/AHA/AATS/ACR/ASA/SCA/SCAI/SIR/STS/SVM guidelines for the diagnosis and management of patients with Thoracic Aortic Disease: a report of the American College of Cardiology Foundation/American Heart Association Task Force on Practice Guidelines, American Association for Thoracic Surgery, American College of Radiology, American Stroke Association, Society of Cardiovascular Anesthesiologists, Society for Cardiovascular Angiography and Interventions, Society of Interventional Radiology, Soc. *Circulation* **121**, (2010).
210. Bossone, E. & Eagle, K. A. Epidemiology and management of aortic disease: aortic aneurysms and acute aortic syndromes. *Nat. Rev. Cardiol. 2020 185* **18**, 331–348 (2020).

211. Kuzmik, G. A., Sang, A. X. & Elefteriades, J. A. Natural history of thoracic aortic aneurysms. *J. Vasc. Surg.* **56**, 565–571 (2012).

212. Isselbacher, E. M. Thoracic and abdominal aortic aneurysms. *Circulation* **111**, 816–828 (2005).

213. Bakker, M. K. *et al.* Genome-wide association study of intracranial aneurysms identifies 17 risk loci and genetic overlap with clinical risk factors. *Nat. Genet. 2020 5212* **52**, 1303–1313 (2020).

214. Wu, C. *et al.* Identifying novel risk genes in intracranial aneurysm by integrating human proteomes and genetics. *Brain* **147**, 2817–2825 (2024).

215. Roychowdhury, T. *et al.* Genome-wide association meta-analysis identifies risk loci for abdominal aortic aneurysm and highlights PCSK9 as a therapeutic target. *Nat. Genet. 2023 5511* **55**, 1831–1842 (2023).

216. Klarin, D. *et al.* Genome-wide association study of thoracic aortic aneurysm and dissection in the Million Veteran Program. *Nat. Genet. 2023 557* **55**, 1106–1115 (2023).

217. Gershon, A. S., Warner, L., Cascagnette, P., Victor, J. C. & To, T. Lifetime risk of developing chronic obstructive pulmonary disease: A longitudinal population study. *Lancet* **378**, 991–996 (2011).

218. Safiri, S. *et al.* Burden of chronic obstructive pulmonary disease and its attributable risk factors in 204 countries and territories, 1990-2019: results from the Global Burden of Disease Study 2019. *BMJ* **378**, (2022).

219. Barnes, P. J. *et al.* Chronic obstructive pulmonary disease. *Nat. Rev. Dis. Prim. 2015 11* **1**, 1–21 (2015).

220. Lozano, R. *et al.* Global and regional mortality from 235 causes of death for 20 age groups in 1990 and 2010: A systematic analysis for the Global Burden of

Disease Study 2010. *Lancet* **380**, 2095–2128 (2012).

221. Salvi, S. S. & Barnes, P. J. Chronic obstructive pulmonary disease in non-smokers. *Lancet* **374**, 733–743 (2009).

222. Romieu, I. *et al.* Improved Biomass Stove Intervention in Rural Mexico. *https://doi.org/10.1164/rccm.200810-1556OC* **180**, 649–656 (2012).

223. Ingebrigtsen, T. *et al.* Genetic influences on chronic obstructive pulmonary disease - A twin study. *Respir. Med.* **104**, 1890–1895 (2010).

224. McCloskey, S. C. *et al.* Siblings of Patients With Severe Chronic Obstructive Pulmonary Disease Have a Significant Risk of Airflow Obstruction. *https://doi.org/10.1164/ajrccm.164.8.2105002* **164**, 1419–1424 (2012).

225. Zarogoulidis, P. *et al.* Pneumothorax: from definition to diagnosis and treatment. *J. Thorac. Dis.* **6**, S372 (2014).

226. Sahn, S. A. & Heffner, J. E. Spontaneous Pneumothorax. *N. Engl. J. Med.* **342**, 868–874 (2000).

227. Louw, E. H., Shaw, J. A. & Koegelenberg, C. F. N. New insights into spontaneous pneumothorax: A review. *African J. Thorac. Crit. care Med.* **27**, 18–22 (2021).

228. Haynes, D. & Baumann, M. H. Pleural controversy: aetiology of pneumothorax. *Respirology* **16**, 604–610 (2011).

229. Neptune, E. R. *et al.* Dysregulation of TGF-beta activation contributes to pathogenesis in Marfan syndrome. *Nat. Genet.* **33**, 407–411 (2003).

230. Gupta, D. *et al.* Epidemiology of pneumothorax in England. *Thorax* **55**, 666–671 (2000).

231. Bobbio, A. *et al.* Epidemiology of spontaneous pneumothorax: gender-related differences. *Thorax* **70**, 653–658 (2015).

232. Kelly, A. M. & Druda, D. Comparison of size classification of primary spontaneous pneumothorax by three international guidelines: a case for international consensus? *Respir. Med.* **102**, 1830–1832 (2008).

233. Brims, F. J. H. & Maskell, N. A. Ambulatory treatment in the management of pneumothorax: a systematic review of the literature. *Thorax* **68**, 664–669 (2013).

234. Walker, S. P. *et al.* Recurrence rates in primary spontaneous pneumothorax: a systematic review and meta-analysis. *Eur. Respir. J.* **52**, (2018).

235. Sadikot, R. T., Greene, T., Meadows, K. & Arnold, A. G. Recurrence of primary spontaneous pneumothorax. *Thorax* **52**, 805–809 (1997).

236. Nikolić, M. Z. & Marciniak, S. J. Familial pneumothorax. *Univ. Coll. London* doi:10.1186/ISRCTN79151659

237. Liu, Y., Xing, H., Huang, Y., Meng, S. & Wang, J. Familial spontaneous pneumothorax: importance of screening for Birt-Hogg-Dubé syndrome. *Eur. J. Cardiothorac. Surg.* **57**, 39–45 (2020).

238. Graham, R. B., Nolasco, M., Peterlin, B. & Garcia, C. K. Nonsense mutations in folliculin presenting as isolated familial spontaneous pneumothorax in adults. *Am. J. Respir. Crit. Care Med.* **172**, 39–44 (2005).

239. Baumann, M. H. & Noppen, M. Pneumothorax. *Respirology* **9**, 157–164 (2004).

240. Sousa, I. *et al.* Multicentric Genome-Wide Association Study for Primary Spontaneous Pneumothorax. *PLoS One* **11**, e0156103 (2016).

241. Collinson, R., Cunningham, C., D'Costa, H. & Lindsey, I. Rectal intussusception and unexplained faecal incontinence: findings of a proctographic study. *Colorectal Dis.* **11**, 77–83 (2009).

242. Bordeianou, L. *et al.* Clinical Practice Guidelines for the Treatment of Rectal Prolapse. *Dis. Colon Rectum* **60**, 1121–1131 (2017).

243. Madiba, T. E., Baig, M. K. & Wexner, S. D. Surgical Management of Rectal Prolapse. *Arch. Surg.* **140**, 63–73 (2005).

244. Wijffels, N. A., Collinson, R., Cunningham, C. & Lindsey, I. What is the natural history of internal rectal prolapse? *Color. Dis.* **12**, 822–830 (2010).

245. Farouk, R. & Duthie, G. S. Rectal prolapse and rectal invagination. *Eur. J. Surg.* **164**, 323–332 (1998).

246. Dvorkin, L. S. *et al.* Rectal intussusception in symptomatic patients is different from that in asymptomatic volunteers. *Br. J. Surg.* **92**, 866–872 (2005).

247. Cunin, D. *et al.* No surgery for full-thickness rectal prolapse: what happens with continence? *World J. Surg.* **37**, 1297–1302 (2013).

248. Alam, N. N., Narang, S. K., Köckerling, F., Daniels, I. R. & Smart, N. J. Rectopexy for Rectal Prolapse. *Front. Surg.* **2**, 163153 (2015).

249. Senapati, A. *et al.* PROSPER: a randomised comparison of surgical treatments for rectal prolapse. *Color. Dis.* **15**, 858–868 (2013).

250. Marshman, D., Percy, J., Fielding, I. & Delbridge, L. RECTAL PROLAPSE: RELATIONSHIP WITH JOINT MOBILITY. *Aust. N. Z. J. Surg.* **57**, 827–829 (1987).

251. Keane, D. P., Sims, T. J., Abrams, P. & Bailey, A. J. Analysis of collagen status in premenopausal nulliparous women with genuine stress incontinence. *BJOG An Int. J. Obstet. Gynaecol.* **104**, 994–998 (1997).

252. Klein, R. J. *et al.* Complement factor H polymorphism in age-related macular degeneration. *Science (80-.).* **308**, 385–389 (2005).

253. Rodríguez De Córdoba, S., Esparza-Gordillo, J., Goicoechea De Jorge, E., Lopez-Trascasa, M. & Sánchez-Corral, P. The human complement factor H: Functional roles, genetic variations and disease associations. *Molecular*

Immunology **41**, 355–367 (2004).

254. Margulies, M. *et al.* Genome sequencing in microfabricated high-density picolitre reactors. *Nature* **437**, 376–380 (2005).

255. Baselmans, B. M. L. *et al.* Multivariate genome-wide analyses of the well-being spectrum. *Nat. Genet.* **51**, 445–451 (2019).

256. D., W. *et al.* The NHGRI GWAS Catalog, a curated resource of SNP-trait associations. *Nucleic Acids Res.* **42**, D1001–D1006

257. Slatkin, M. Linkage disequilibrium - Understanding the evolutionary past and mapping the medical future. *Nature Reviews Genetics* **9**, 477–485 (2008).

258. Auton, A. *et al.* A global reference for human genetic variation. *Nature* **526**, 68–74 (2015).

259. Frazer, K. A. *et al.* A second generation human haplotype map of over 3.1 million SNPs. *Nature* **449**, 851–861 (2007).

260. Hardy, J. & Singleton, A. Genomewide association studies and human disease. *N. Engl. J. Med.* **360**, 1759–1768 (2009).

261. Visscher, P. M. *et al.* 10 Years of GWAS Discovery: Biology, Function, and Translation. *Am. J. Hum. Genet.* **101**, 5–22 (2017).

262. Breen, G. *et al.* Translating genome-wide association findings into new therapeutics for psychiatry. *Nature Neuroscience* **19**, 1392–1396 (2016).

263. Maurano, M. T. *et al.* Systematic localization of common disease-associated variation in regulatory DNA. *Science (80-.).* **337**, 1190–1195 (2012).

264. Mayhew, A. J. & Meyre, D. Assessing the Heritability of Complex Traits in Humans: Methodological Challenges and Opportunities. *Curr. Genomics* **18**, (2017).

265. Mills, M. C. & Rahal, C. The GWAS Diversity Monitor tracks diversity by disease

in real time. *Nature Genetics* **52**, 242–243 (2020).

266. Martin, A. R. *et al.* Human Demographic History Impacts Genetic Risk Prediction across Diverse Populations. *Am. J. Hum. Genet.* **100**, 635–649 (2017).
267. Duncan, L. *et al.* Analysis of polygenic risk score usage and performance in diverse human populations. *Nat. Commun.* **10**, 1–9 (2019).
268. Flannick, J. *et al.* Loss-of-function mutations in SLC30A8 protect against type 2 diabetes. *Nat. Genet.* **46**, 357–363 (2014).
269. Evans, D. M., Visscher, P. M. & Wray, N. R. Harnessing the information contained within genome-wide association studies to improve individual prediction of complex disease risk. *Hum. Mol. Genet.* **18**, 3525–3531 (2009).
270. Craig, J. E. *et al.* Multitrait analysis of glaucoma identifies new risk loci and enables polygenic prediction of disease susceptibility and progression. *Nat. Genet.* **52**, 160–166 (2020).
271. Burton, P. R. *et al.* Genome-wide association study of 14,000 cases of seven common diseases and 3,000 shared controls. *Nature* **447**, 661–678 (2007).
272. Bush, W. S. & Moore, J. H. Chapter 11: Genome-Wide Association Studies. *PLoS Comput. Biol.* **8**, e1002822 (2012).
273. Timpson, N. J., Greenwood, C. M. T., Soranzo, N., Lawson, D. J. & Richards, J. B. Genetic architecture: The shape of the genetic contribution to human traits and disease. *Nature Reviews Genetics* **19**, 110–124 (2018).

Chapter 2: Genome-wide association analysis of varicose veins

2.1. Introduction

2.1.1. Rationale and aims

As discussed in **Chapter 1**, varicose veins represent a common disorder with a high socioeconomic burden and associated patient morbidity.[1] There are currently no medical treatments for varicose veins, and endovenous surgical approaches to manage symptomatic varicose veins are associated with high recurrence.[2] The majority of varicose veins patients report a positive family history[3], thus demonstrating the importance of genetic susceptibility to varicose veins. However to date, relatively few genes have been implicated through candidate gene studies and GWAS approaches.[4–7] The aim of this chapter is to advance our understanding of the genetic architecture of varicose veins and discover clinically relevant biological pathways and potential molecular targets associated with varicose veins. This will be achieved by undertaking the largest two-stage GWAS of varicose veins using the UK Biobank cohort, with independent replication in a cohort from 23andMe, Inc.

2.2. Methods

2.2.1. Ethics and consent

UK Biobank received research ethics approval from the North West Research Ethics Committee (MREC) (11/NW/0382), in accordance with the Declaration of Helsinki. Informed consent was obtained to collate and disseminate genotype data for all study participants for the purposes of medical research. The work presented in this thesis was performed under UK Biobank study ID 10948. All 23andMe participants were from the userbase of 23andMe, Inc. (Sunnyvale, California) — a direct-to-consumer personal genomics company. Genotyping of participants was performed by the 23andMe Personal Genome Service. All 23andMe research participants included in this chapter completed an online questionnaire and provided informed consent for their genotype data to be used for research purposes, under a protocol approved by the external AAHRPP-accredited IRB, Ethical and Independent Review Services (E&I Review).

2.2.2. Study population and phenotype definition

UK Biobank is a population-level resource: a multicentre prospective cohort study of 488,377 UK participants aged 40-69 years recruited from 2006 to 2010.[8] Participants were invited to the study centre to provide written consent, complete a touch-screen questionnaire, and take part in a computer-based interview; physical and functional measures were also obtained, alongside genetic samples for whole genome genotyping.[9] Participants' genotype data was linked with their electronic medical

records to permit deep phenotyping.[9] The characteristics of the full UK Biobank cohort are described in detail elsewhere.[10]

In the discovery analysis, varicose vein cases were identified from the UK Biobank data showcase (ukbiobank.ac.uk) using diagnostic, operative and self-report codes. Cases for varicose veins were defined if participants had at least one of the following four codes (specific codes are in parentheses and **Table 2.1**)

1. Primary and/or secondary ICD-10 codes for varicose veins (I83)
2. Primary and/or secondary OPCS code for varicose vein surgery: (L84-L88)
3. Self-reported operation code for varicose vein surgery (1479)
4. Self-reported non-cancer illness code for varicose veins (1494)

In summary, 27,165 participants from the UK Biobank cohort had at least one of the above codes and were classified as varicose vein cases. Participants without any of these codes were designated as controls.

Table 2.1. Codes used for varicose veins case definition in UK Biobank. The total number of participants with each of the diagnostic codes is shown below. A total of 27,165 participants possessed at least one of the diagnostic codes for varicose veins.

Source of Data	UK Biobank Data Field	Code	Description	N
Primary ICD-10	41202	I83.0	Varicose veins of lower extremities with ulcer	12195
		I83.1	Varicose veins of lower extremities with inflammation	
		I83.2	Varicose veins of lower extremities with both ulcer and inflammation	
		I83.9	Varicose veins of lower extremities without ulcer or inflammation	
Secondary ICD-10	41204	As above	As above	1168
Primary OPCS	41200	L84	Combined operations on varicose vein of leg	12528
		L85	Ligation of varicose vein of leg	
		L86	Injection into varicose vein of leg	
		L87	Other operations on varicose vein of leg	
		L88	Transluminal operations on varicose vein of leg	
Secondary OPCS	41210	As above	As above	8116
Non-cancer illness (self-report)	20002	1494	Varicose veins	2266
Operation (self-report)	20004	1479	Varicose vein surgery	20115
Total (excluding overlaps)				**27165**

Following quality control (outlined in **Section 2.2.4. Quality control**), the final discovery analysis consisted of 22,473 cases and 379,183 controls.

In the 23andMe replication cohort, participants provided answers to the varicose veins-related question, *'Do you have varicose veins on your legs?' (Yes/Not Sure/No)*. Self-reported varicose veins cases were defined if they answered, *'yes'* to the above question, while controls were identified as those that answered *'No'.* Using this approach, in the final replication analysis, a total of 113,041 self-reported varicose veins cases and 295,928 control participants were included.

2.2.3. Genotyping

Genome-wide genotyping data was made available for 488,377 participants in the UK Biobank cohort.[9] The initial 49,950 participants were genotyped on the Affymetrix UK BiLEVE Axiom array (807,411 genotyped variants), with the second batch of 438,427 participants from the cohort genotyped on the Affymetrix UK Biobank Axiom array (825,927 genotyped variants). The two arrays were almost identical, sharing over 95% marker content. The present study is based on the third release of the UK Biobank cohort (July 2017), which contained the complete set of genotypes for the 488,377 participants (805,426 directly genotyped variants).

The 23andMe independent replication cohort was genotyped using one of four custom arrays (v1/v2, v3, v4, v5). Illumina HumanHap550+ BeadChip was used for v1/v2 (1,680 cases, 4,882 controls) and the Illumina OmniExpress+ BeadChip was used for v3 (21,342 cases, 56,448 controls). For v4 a fully customised array (58,883 cases,

148,637 controls) was used, and for v5, the Illumina Infinium Global Screening Array was implemented (31,136 cases, 85,961 controls). Successive arrays contained significant overlap between all previous array chips.

2.2.4. Quality control

Quality control (QC) for the UK Biobank discovery cohort used a combination of UK Biobank's own QC and additional layers of more stringent QC performed locally by the Furniss Group. The full protocol has been described in detail elsewhere (**Figure 2.1**).[11] Briefly, all SNPs with a call rate < 90% were removed. This was followed by sample-level QC — participants were excluded if: (i) they demonstrated heterozygosity > 3 S.D. from the mean (calculated using UK Biobank's PCA-adjusted heterozygosity values, Data Field 22004); (ii) there was disparity between genetically inferred sex (Data Field 22001) and self-reported sex (Data Field 31) or participants with aneuploidy of sex chromosomes (Data Field 22019); and (iii) had a call rate < 98%. Further, all participants who were not white British in ancestry (based on principal component analysis (PCA) and self-reported ethnicity (Data Field 22006)) were excluded.

Following PCA, 86,693 participants were excluded from the discovery GWAS analysis. Using a linear mixed model implemented in BOLT-LMM[12] enabled the inclusion of related participants.

Next, SNP-level QC was performed, following which 230,562 SNPs were excluded based on: (i) a call rate < 98%, (ii) Hardy-Weinberg Equilibrium (HWE) $P < 1\times10^{-4}$, (iii)

minor allele frequency (MAF) < 0.01. Six participants were further excluded because they were visual outliers when autosomal heterozygosity was plotted against call rate. The post-QC discovery GWAS therefore consisted of 401,667 participants and 547,011 directly genotyped variants (**Figure 2.1**).

In the 23andMe replication analysis, samples were restricted to participants from European ancestry determined through an analysis of local ancestry.[13] A maximal set of unrelated participants was chosen for each analysis using a segmental identity-by-descent (IBD) estimation algorithm. Participants were defined as related if they shared more than 700 cM IBD, including regions where the two participants share either one or both genomic segments IBD. When selecting participants for case/ control phenotype analyses, the selection process was designed to always maximise case sample size by preferentially retaining cases over controls. Specifically, if both an individual case and an individual control were found to be related, then the case was retained in the analysis. Variant QC was implemented independently to genotyped and imputed GWAS results. The SNPs failing QC were flagged based on multiple criteria, namely HWE P-value, call rate, imputation R-square and test statistics of batch effects.

Figure 2.1. Overview of Quality Control. **A**) Flowchart summarising the quality control (QC) protocol. Excluded SNPs are in blue panels on the left and excluded participants are in green panels on the right. [1]Pre-QC exclusions: 3 participants with invalid IDs and sex, and 8 participants who have withdrawn from UK Biobank were excluded prior to QC. [2]Pre-association exclusions: 11 participants who were not present in UK Biobank's sample file accompanying the BGEN files were excluded prior to association. **B)** Principal Component Analysis (PCA) for demonstration of ethnicity of UK Biobank participants. The UK Biobank cohort was merged with publicly available data from the 1000 Genomes Project and PCA was performed using flashpca. Participants identified by UK Biobank as having white British ancestry are coloured in lime green, and the remaining UK Biobank participants are in grey. In this graph of principal component 1 vs principal component 2, a near-perfect overlap can be seen between the UK Biobank "white British" participants and both GBR (British in England and Scotland - light brown) and CEU (Utah residents with Northern and Western European ancestry - magenta) participants from the 1000 Genomes Project. Figure modified from Wiberg, *et al*.[11]

a

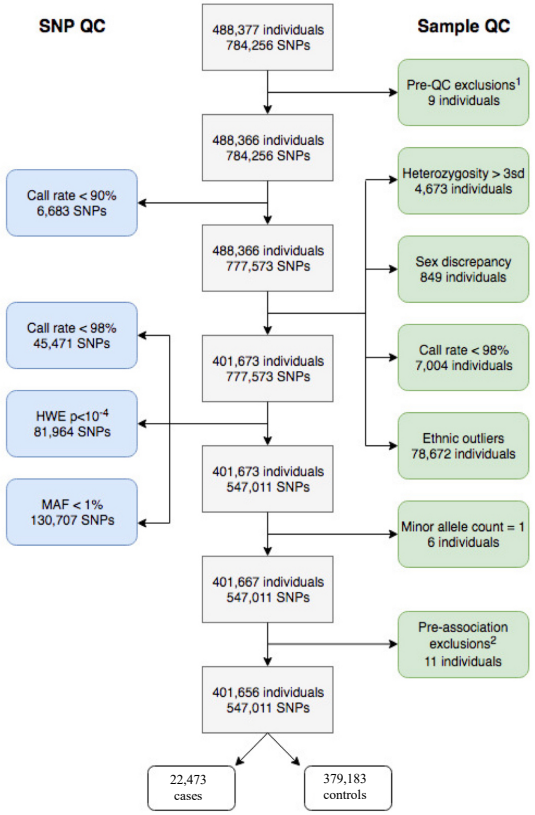

b

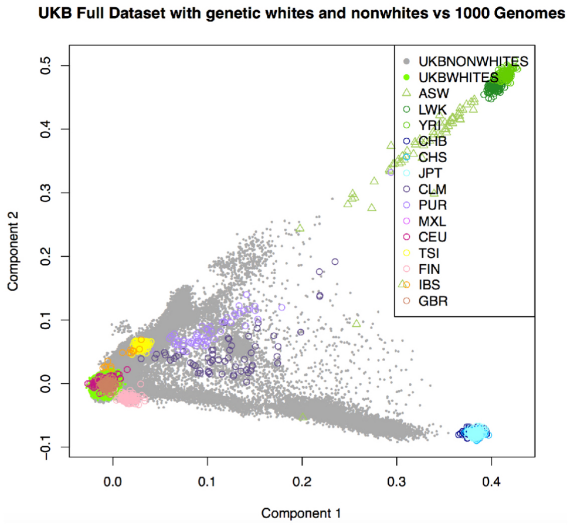

2.2.5. Imputation

UK Biobank autosome phasing was performed centrally using a 1000 Genomes Consortium[14] Phase 3 reference panel in SHAPEIT3[15], and is described in detail elsewhere.[9] The ~800,000 directly genotyped variants in the full UK Biobank cohort were imputed to 92,693,895 autosomal markers using a combination reference panel from the Haplotype Reference Consortium[9], the 1000 Genomes Project and the UK10K Project.[14,16] After the quality control checks (detailed in **2.2.4. Quality control**), low-quality (imputation INFO Score < 0.9) and rare (MAF < 0.01) variants from the imputation dataset were excluded, leaving ~9 million variants for the final discovery association analysis (discussed further in **2.2.6. Association analysis**).

In the 23andMe replication analysis, out-of-sample modified versions of the Beagle graph-based haplotype phasing algorithm[17] and Eagle2[18] algorithm were implemented to phase samples. The samples were imputed against a single unified imputation reference panel combining the 1000 Genomes Phase 3 haplotypes[14] with the UK10K project imputation reference panel[16] using Minimac3.[19]

2.2.6. Association analysis

In the UK Biobank discovery analysis, genome-wide association testing was performed across a total of 8,944,547 SNPs (547,011 directly genotyped (MAF ≥ 0 .01) and 8,397,536 imputed SNPs using a linear mixed non-infinitesimal model implemented in BOLT-LMM v2.323.[12] The reference human genome assembly used was GRCh37 (hg19) and linkage disequilibrium scores were obtained from

participants of European-ancestry extracted from the BOLT-LMM package.[12] To account for residual population structure, adjustments were included in the model for the covariates: genetic sex and genotyping platform. Association testing was implemented by linear regression assuming an additive allelic effect using imputed allelic dosages. BOLT-LMM[12] implements a linear regression and hence outputs a beta regression coefficient (with an associated standard error) for case-control outcomes - odds ratios for each variant were computed using the following equation:

$$\ln(OR) = \frac{\beta}{\mu(1-\mu)}$$

Where β is the beta regression coefficient calculated by BOLT LMM[12], and μ is the fraction of the cases in the sample (μ = 0.0593).

Conditional regression analysis was performed in BOLT-LMM for the top signal at each of the genome-wide significant loci from the association analysis (except the MHC region due to the high density of genes and high linkage of variants).[12] The conditional regression model regressed on genetic sex and genotyping platform, with the genotypic dosage of the top signal as calculated by QCTOOL 2.0 as a third covariate (see **2.2.15. URLs**). If any genome-wide significant signals remained at that locus, this process was repeated iteratively (by adding the genotypic dosage of the top residual signal as a further covariate), until no genome-wide significant signal remained.

In the 23andMe replication analysis, summary statistics were generated though logistic regression assuming an additive model for allelic effects. Association analysis

was performed by regressing on age, sex, the first five principal components, and the genotyping platform.

The lead 118 independent variants from the discovery analysis were tested for association with varicose veins in 23andMe. A Bonferroni-corrected $P < 4.24\times10^{-4}$ (0.05/118) was defined as the significant threshold for replication. Replication data for 108 of 118 variants were available in the 23andMe summary statistics: nine variants did not meet the SNP quality control within 23andMe, and one variant (10:79677281_CA_C) was not identified. A fixed-effects meta-analysis of each of the top independent variants was performed in Genome-Wide Association Meta-Analysis (GWAMA) software.[20]

2.2.7. Genomic risk loci definition

Risk loci interpretation of the genetic associations was performed within the platform FUMA GWAS v1.3.3 (*Functional Mapping and Annotation of Genome-Wide Association Studies,* see **2.1.15 URLs**).[21] Independent significant SNPs (IndSigSNPs) were first established by identifying all genome-wide significant SNPs ($P < 5\times10^{-8}$) and those that were independent from each other at $r^2 < 0.6$. These IndSigSNPs were then represented by lead SNPs, a proportion of IndSigSNPs that were in linkage equilibrium with each other at $r^2 < 0.1$. Lead SNPs were manually selected in FUMA as those independent signals emerging from the conditional regression analysis (Refer to **2.2.6. Association analysis**), and subsequent positional and eQTL gene mapping was based on these variants (see **2.2.9. Candidate gene mapping**). Independent genomic risk loci were identified as physical genomic regions around lead SNPs (Lead

SNPs that were < 250kb apart were merged), with genome risk loci borders established by identifying variants in linkage disequilibrium ($r^2 \geq 0.6$) of one of the IndSigSNPs. A single independent genomic risk locus was defined as the genomic region housing all variants (defined as candidate variants) in linkage with each IndSigSNP. Novel risk loci were those risk loci that had not been previously related to varicose veins in the NHGRI-EBI catalogue of published genome-wide association studies.[22]

2.2.8. Functional annotation of SNPs

Functional mapping and annotation of the associated SNPs was performed in FUMA *SNP2GENE* v1.3.6[21], an online platform that collates external databases to provide comprehensive annotation information for functional interpretation (**2.1.15 URLs**). For all analyses, the summary statistics from the UK Biobank discovery cohort were used with default settings. All candidate genes in each defined genomic risk locus in linkage disequilibrium with an IndSigSNP ($r^2 \geq 0.6$), a $P < 5\times10^{-2}$, and MAF > 0.01 were included in the FUMA *SNP2GENE* annotation. FUMA *SNP2GENE* uses each candidate variant's genomic location and effect/non-effect allele to collate functional annotation data from established genetic annotation databases[21], including ANNOVAR[23], RegulomeDB[24], CADD[25], and 15-core chromatin state categories.[26] ANNOVAR was queried to identify the gene location and function of candidate variants.[23] Combined Annotation Dependent Depletion (CADD) is a tool for scoring the deleteriousness of candidate variants and their likelihood to affect protein structure or function.[25] A CADD score ≥ 12.37 is the suggested threshold for a predicted pathogenic variant[27], with a scaled CADD score > 20 indicative of a variant in the top

1% of deleterious variants in the human genome, and a score > 30 indicating a variant in the top 0.1% of deleterious variants.[25] RegulomeDB is a resource that uses eQTL data and chromatin marks to highlight DNA features and regulatory elements in non-coding genomic regions.[24] RegulomeDB scores are categorical and range from 1a to 7, with a score of 1a indicative of a variant with the highest possibility of affecting transcription factor binding and linked to expression of a gene target (i.e. EQTL + TF Binding + matched TF motif + matched DNase Footprint + DNase peak).[24] Chromatin state annotations refer to the accessibility of genomic regions to transcriptional effects. The 15-core chromatin state model (NIH Roadmap Epigenomes Consortium[26]), provides a reference epigenomic landscape of the human genome based on a core-set of 5 chromatin marks assayed across 127 epigenomes (H3K4me3, H3K4me1, H3K36me3, H3K27me3 and H3K9me3).[26] The 15-states capture key interactions between chromatin marks, with a score of 1 to 7 indicative of a region of open chromatin, and a score of 1 denoting a region with the highest accessibility (i.e. an active transcription start site).[26] Exonic SNPs were investigated further using gnomAD and Ensembl genome browsers to uncover non-synonymous functionality (Refer to **2.2.15. URLs**).[28]

2.2.9. Candidate gene mapping

To map candidate variants identified in the GWAS to genes, four gene mapping approaches were implemented - positional mapping[21], eQTL mapping[21], MAGMA genome-wide, gene association analysis (GWGAS)[29], and summary-based mendelian randomisation (SMR)[30]:

i) Positional mapping - the candidate variants at each locus were mapped to protein-coding genes that lay within a genomic window of 10kb on either side of the variant.

ii) eQTL mapping was used to map candidate variants within each locus to a gene if it had a genome-wide significant eQTL association ($P < 5\times10^{-8}$, FDR < 0.05) for that gene* in tibial artery tissue from the GTEx repository[21], based on having a cis-eQTL within 1MB of the gene. (Tibial artery tissue was chosen for this analysis as it was thought to be the closest surrogate for lower limb venous tissue out of all 53 tissue types present in GTEx).

iii) A MAGMA v1.07[29] genome-wide gene association test was implemented in FUMA *SNP2GENE*.[21] This mapped at least one SNP from the GWAS individually to 18,733 protein-coding genes obtained from Ensembl build 85.[28] To map variants to these genes across the genome, a strict Bonferroni correction was implemented to account for multiple-testing ($P < 2.67\times10^{-6}$ (i.e. 0.05/18733)). A Quantile-Quantile plot for the GWGAS was generated and genes whose P-values reached genome-wide significance were additionally labelled in a Manhattan plot.

iv) SMR was used to identify genes with expression levels associated with varicose veins due to pleiotropy.[30] The association between a gene's expression in tibial artery tissue (eQTL data taken from GTEx V7 tibial artery[21]) and varicose veins was analysed using the top-associated eQTL for each gene as a genetic instrument. SMR significant genes (P_{SMR} < 0.05/ number of probes) are those providing evidence of pleiotropy†,

*in other words, allelic variation at the SNP is associated with altered gene expression levels
†i.e. the expression of a gene and that of a trait are influenced by the same causal variant at the gene locus

but also of co-localisation*.[30] To examine for heterogeneity in SMR estimates and to untangle pleiotropy from co-localisation, a HEterogeneity In Dependent Instrument (HEIDI) test was implemented[30], with SNPs passing the HEIDI test (a $P_{HEIDI} < 0.05$/ number of P_{SMR}-significant Probes) associated with varicose veins through pleiotropy (rather than co-localisation); and therefore identifying genes whose expression levels mediate the association between SNPs and varicose veins.

2.2.10. Gene set, tissue and pathway analyses

Gene-set analysis was performed in MAGMA v1.07[29] (implemented in FUMA *SNP2GENE*[21]), with the full distribution of SNP P-values from the GWGAS analysis (described in **Section 2.2.9**) that lay positionally within the start and end points of a protein-coding gene (predefined distances were set to 0kb on both sides). Using competitive testing for gene set enrichment, 15,496 gene sets obtained from MSigDB v8.0[31] were tested (5500 curated gene sets and 9996 GO terms). Curated gene sets were derived from nine data sources[31], including KEGG, REACTOME and BioCarta and GO terms made up of three categories: biological processes, cellular components and molecular function. To account for multiple testing, enrichment across the gene sets was corrected to account for the number of gene sets tested ($P < 3.23 \times 10^{-6}$ (0.05/ 15496)). Enrichment of the overlap between GWAS variants and those reported in previous GWAS within the NIH GWAS Catalog were also examined[22], with enrichment P-values for the proportion of overlap in the genes determined.

*possibility that SNPs controlling gene expression are in LD with those associated with the traits

MAGMA tissue expression analysis[29] was performed to test the relationship between GWAS associations (the full distribution of SNP p-values were used in the gene-property analysis) and highly expressed genes from individual tissues in the GTEx v8 30 general tissue types collection and 54 specific tissue types collection separately.[21] Gene property analysis was implemented using the averaged expression of genes in each tissue type as a covariate[29], and gene expression values depicted as log2-transformed average RPKM per tissue type after winsorized at 50 based on the GTEx RNA-seq data.[21]

The above described gene set and tissue expression analyses were then repeated within FUMA *GENE2FUNC* v1.3.5d[21], to specifically hone in on the functionality of *only* the genes prioritised directly from the four candidate gene mapping approaches (i.e. a credible set of genes)* (described in **Section 2.2.9.**). Gene set enrichment analyses of the gene sets within MSigDB v8.0[31] were tested, and gene property and tissue enrichment analyses within GTEx consortium tissue was also performed distinctly for the prioritised varicose veins associated genes.[21]

Using eXploring Genomic Relations (XGR) software[32], pathway enrichment analysis of the prioritised genes was performed to highlight canonical pathways that were enriched. A hypergeometric distribution test was performed and adjusted FDR < 0.05 used to highlight prioritised gene sets. No restriction on overlap between the input genes was in place.

* i.e. genes *specifically* prioritised through one of the four described gene mapping approaches and *not* only from the GWGAS test performed in MAGMA (which is what FUMA *SNP2GENE* does) using the full distribution of P-values of variants throughout the genome to identify enriched candidate genes.

2.2.11. SNP-based heritability analysis

Using Linkage Disequilibrium Score (LDSC) regression[33], the LD intercept and mean chi-squared test score for the varicose veins GWAS was calculated, with the attenuation score calculated using the equation: (LDSC intercept - 1)/ (mean χ^2 - 1). LDSC was used to produce a SNP-based heritability estimate for varicose veins in UK Biobank and 23andMe (h^2_g).[34] This approach derived the heritability for varicose veins by regressing each variants association statistic onto its LD Score*. h^2_g is a measure of genetic variance defined as the proportion of phenotypic variance explained by all or selected SNPs on a genotyping array. For the LDSC calculations[33], we harmonised the varicose veins GWAS summary statistics to include 1,170,823 variants that were well-imputed in the HapMap 3 panel and LD pruned ($r^2 < 0.1$) with long range LD regions removed to avoid capturing excess variance of LD regions. A two-step estimator cut-off of 30 was set to remove SNPs with large effect sizes.[33]

2.2.12. Genetic correlation analysis

Using the varicose veins summary statistics, we performed a genetic correlation analysis in the LD Hub database v1.9.3.[34] LD Hub is a centralised database of summary-level GWAS results for 832 diseases/traits from several publicly-available consortia.[34] 176 preselected traits across nine trait categories from the LDHub database were tested for correlation with varicose veins: metabolites, glycaemic traits, autoimmune diseases, anthropometric traits, smoking behaviour, lipids, cardiometabolic traits, reproductive traits and haematological traits. Trait categories

* i.e. 'The sum of LD r^2 measured with all other SNPs'.

were pre-defined based on associations in the literature. Genetic correlations (r_g) between the traits were defined by regression on each variant's Z-score product from the two phenotypes, against its LDSC.[33] To account for multiple testing, a Bonferroni correction of $P < 5.56\times10^{-3}$ (0.05/9) was applied.

2.2.13. Drug-target enrichment analysis

Genes prioritised through the gene-mapping approaches were queried in the Open Targets Platform.[35] The Open Targets Platform is a comprehensive data integration resource for access to and visualisation of potential therapeutics targets with associated disorders.[35] Drug targets may be proteins, protein complexes or RNA molecules as identified by the Human Gene Nomenclature Committee (HGNC), with integration from Ensembl (protein-coding genes)[28]. Relationships between gene targets and diseases are collated by mapping to Experiment Factor Ontology (EFO) terms. [35] Open Targets Platform determines the tractability of proteins encoded by the prioritised genes to therapeutic targeting, or whether they are under investigation in clinical trials (data extracted from clinicaltrials.gov). The Platform summarises the available evidence for target-disease associations using a plethora of information for target and disease. Fisher's exact test was used to determine the overlap of varicose veins prioritised genes with pharmacologically active drug targets in several diseases, with a nominal $P < 5\times10^{-2}$ indicative of significance.[35]

2.2.14. Genetic risk score

Genetic risk score profiles for the UK Biobank cohort were calculate via a weighted genetic risk score (wGRS), based on the top independent variants at each replicated risk locus. The wGRS was compared between between six groups of participants from the GWAS: i) all cases vs all controls; ii) surgical cases vs non-surgical cases; iii) cases with ulceration vs cases with no ulceration. Surgical cases were defined as those with OPCS (*Office of Population Censuses and Surveys Classification of Interventions and Procedures*) or self-reported operative codes. Ulceration cases were those that had a primary and/or secondary ICD-10 codes for varicose veins with ulceration (I83.0 and I83.2) (detailed in **2.2.4. Quality control**). The following formula was implemented[36]:

$$wGRS = \sum_{i=1}^{n} W_i X_i$$

where i is the lead SNP at each genomic risk locus, n is the total number of lead SNPs in the GWAS (n = 49), W_i is the weighting for each of the SNPs (the natural logarithm of the odds ratio for each effect allele), and X_i is the number of effect alleles each individual possesses for each SNP. Each subject's risk allele was used to compute a SNP dosage (QCTOOL v2). wGRS calculations and unpaired t-testing between the different subgroups was performed in R v3.3.1 (see URLs).

2.2.15. URLs

ANNOVAR, www.annovar.openbioinformatics.org/en/latest/; BOLT-LMM, www.data.broadinstitute.org/alkesgroup/BOLT-LMM/; CADD, cadd.gs.washington.edu/; Ensembl, www.ensembl.org/index.html; flashpca,

github.com/gabraham/flashpca/; FUMA, www.fuma.ctglab.nl/; GERP, www.mendel.stanford.edu/SidowLab/downloads/gerp/; GnomAD, www.gnomad.broadinstitute.org/; GTEx Portal, www.gtexportal.org/home/; GWAMA, www.genomics.ut.ee/en/tools/gwama; Human Genome Variation Society (HGVS), www.varnomen.hgvs.org/; HRC, www.haplotype-reference-consortium.org/ ; LD Hub, www.ldsc.broadinstitute.org/ldhub/; LD Link, www.ldlink.nci.nih.gov/; MAGMA, www.ctg.cncr.nl/software/magma; Open Targets Platform, www.targetvalidation.org/; PLINK, www.pngu.mgh.harvard.edu/~purcell/plink/; Polyphen-2, www.genetics.bwh.harvard.edu/pph2;

QCTOOL,www.well.ox.ac.uk/~gav/qctool_v2/#overview; R, www.r-project.org; RegulomeDB, www.regulomedb.org/; SHAPEIT3, jmarchini.org/shapeit3/; SIFT, www.sift.bii.a-star.edu.sg/; UK Biobank, www.ukbiobank.ac.uk/; XGR, www.galahad.well.ox.ac.uk:3040; 1000 Genomes Project, www.1000genomes.org; 23andMe, https://research.23andme.com/

2.3. Results

2.3.1. Forty-six replicated varicose veins susceptibility loci

The overall two-stage association analysis workflow is provided in **Figure 2.2**. The discovery cohort consisted of 22,473 cases and 379,183 controls of white British ancestry from the UK Biobank dataset. Association testing yielded genome-wide significant associations at 109 risk loci (12,391 variants). A further nine independent signals at eight loci were identified through conditional regression analysis. The λ_{GC} demonstrated inflation (1.25), with the LDSC regression intercept (1.06) and attenuation ratio (0.13) in keeping with the expectations of polygenicity and large sample size (**Figure 2.3-A**).[33]

The 118 lead independent signals at the 109 risk loci were tested in the 23andMe association analysis consisting of 113,041 self-reported varicose vein cases and 295,928 controls. Here again, the LDSC intercept demonstrated moderate inflation (λ = 1.13, S.E. = 0.01). Forty-nine of 118 variants demonstrated significant association with varicose veins at a Bonferroni-corrected threshold of $P < 4.24\times10^{-4}$ (**Table 2.2**). Thus, in total 49 independent significant associations at 46 risk loci were identified (**Figure 2.3-B**; regional Locus Zoom plots for all 49 signals are presented in **Figure 2.4).** Across both cohorts, allelic effects were concordant at all 49 replicated variants, with minimal evidence of heterogeneity between the two association studies at all loci (Q-statistic > 0.05). Eighteen of the 45 risk loci were previously reported, and 28 are novel (Table 1). Sixty-nine variants (at 63 risk loci) did not replicate, and are therefore

not included in subsequent post-association analyses. These can be found in **Appendix Table 2.1**.

Figure 2.2. Varicose veins GWA study design and analysis workflow. A two-stage GWAS conducted in UK Biobank, with replication of the lead independent variants variants within the 23andMe replication cohort. Of the 118 tested variants, data on 117 variants were available for replication in the 23andMe Cohort, of which 108 passed QC within the replication cohort (see **2.2.6. Association Analysis**). Forty-nine independent variants at 46 loci met the Bonferroni-corrected threshold in the replication cohort, and subsequently were interrogated further in multiple analyses.

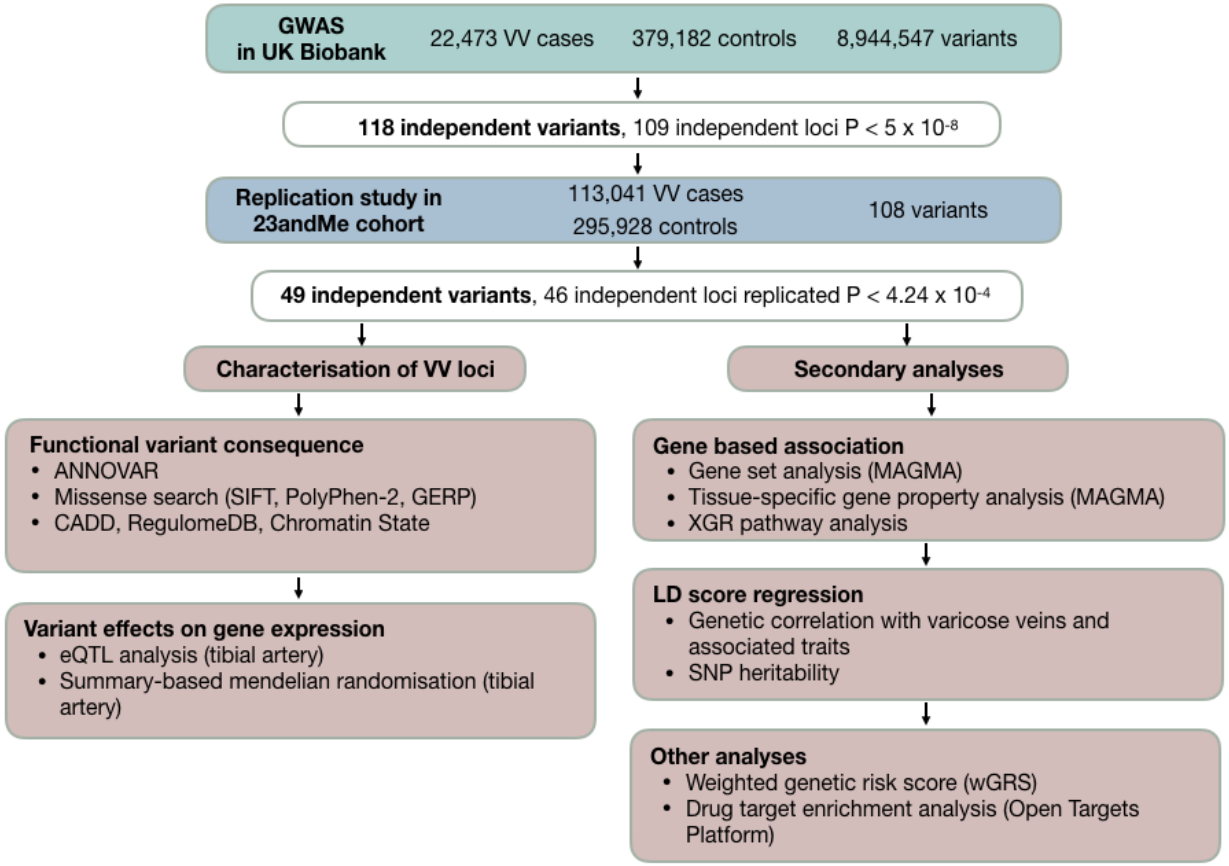

Table 2.2. Forty-nine significant variants at 46 susceptibility loci associated with varicose veins in a two-stage GWAS of 135,514 cases and 675,111 controls from the UK Biobank and 23andMe, Inc.

SNP					Discovery GWAS in UK Biobank				Replication GWAS in 23andMe				Meta-Analysis		
Chr	SNP	Position*	EA†	NEA‡	EAF§	INFO‖	OR#	P-Value	EAF§	INFO‖	OR#	P-Value	OR#	P-Value	Candidate genes
1	rs11121615	10825577	C	T	0.31	0.984	1.32 (1.30-1.35)	1.40×10^{-158}	0.32	0.944	1.57 (1.48-1.67)	2.72×10^{-50}	1.35 (1.32-1.38)	6.95×10^{-201}	*CASZ1*
1	**rs7518191**	**115603413**	**T**	**C**	**0.30**	**0.986**	**1.07 (1.05-1.09)**	**2.30×10^{-10}**	**0.31**	**0.998**	**1.14 (1.08-1.21)**	**5.72×10^{-6}**	**1.08 (1.06-1.10)**	**6.90×10^{-14}**	***TSPAN2***
1	**rs17712208****	**214150445**	**A**	**T**	**0.04**	**G**	**1.13 (1.07-1.19)**	**3.00×10^{-6}**	**0.03**	**0.687**	**1.50 (1.25-1.81)**	**1.71×10^{-5}**	**1.15 (1.10-1.21)**	**1.68×10^{-8}**	***PROX1***
1	**rs340875**	**214158986**	**G**	**C**	**0.48**	**0.993**	**1.07 (1.05-1.09)**	**2.30×10^{-11}**	**0.50**	**0.993**	**1.27 (1.20-1.34)**	**3.22×10^{-18}**	**1.09 (1.07-1.11)**	**4.22×10^{-20}**	***PROX1***
1	**rs2820464**	**219693220**	**A**	**G**	**0.34**	**0.997**	**1.07 (1.04-1.09)**	**3.60×10^{-10}**	**0.32**	**0.997**	**1.16 (1.09-1.22)**	**6.91×10^{-7}**	**1.07 (1.05-1.10)**	**4.48×10^{-14}**	**-**
2	rs9967884	30488183	A	G	0.77	0.995	1.10 (1.07-1.12)	1.60×10^{-15}	0.78	0.986	1.20 (1.12-1.28)	4.99×10^{-8}	1.11 (1.08-1.13)	1.40×10^{-20}	*LBH*
2	rs3791679	56096892	A	G	0.77	G	1.07 (1.04-1.09)	1.90×10^{-8}	0.76	G	1.22 (1.15-1.30)	4.42×10^{-10}	1.08 (1.06-1.11)	1.59×10^{-13}	*EFEMP1*
2	rs2861819	68489221	C	G	0.66	0.996	1.17 (1.15-1.20)	2.10×10^{-56}	0.65	0.925	1.40 (1.32-1.49)	1.04×10^{-29}	1.20 (1.17-1.22)	2.65×10^{-77}	*PPP3R1*
2	**rs4849044**	**112898933**	**C**	**T**	**0.51**	**0.991**	**1.07 (1.05-1.09)**	**2.00×10^{-11}**	**0.50**	**0.990**	**1.12 (1.06-1.18)**	**5.78×10^{-5}**	**1.07 (1.05-1.09)**	**1.98×10^{-14}**	***FBLN7***
2	**rs17819430**	**118886398**	**C**	**A**	**0.96**	**0.991**	**1.15 (1.10-1.21)**	**5.00×10^{-9}**	**0.96**	**0.979**	**1.40 (1.22-1.61)**	**1.63×10^{-6}**	**1.18 (1.13-1.23)**	**1.51×10^{-12}**	***INSIG2***
2	**rs55889669**	**173194747**	**A**	**G**	**0.19**	**0.994**	**1.08 (1.05-1.11)**	**3.60×10^{-10}**	**0.19**	**0.977**	**1.20 (1.12-1.29)**	**2.62×10^{-7}**	**1.09 (1.07-1.12)**	**2.89×10^{-14}**	**-**
3	**rs844176**	**14827080**	**G**	**A**	**0.89**	**0.974**	**1.11 (1.07-1.14)**	**1.60×10^{-10}**	**0.89**	**0.966**	**1.18 (1.08-1.29)**	**1.81×10^{-4}**	**1.11 (1.08-1.15)**	**3.39×10^{-13}**	***FGD5***
3	rs2713575	128294355	G	A	0.50	0.980	1.11 (1.09-1.13)	7.30×10^{-28}	0.50	0.999	1.21 (1.15-1.28)	5.02×10^{-12}	1.12 (1.10-1.14)	1.82×10^{-36}	*GATA2*
3	**rs9877579**	**188058716**	**C**	**T**	**0.26**	**0.986**	**1.07 (1.05-1.10)**	**7.90×10^{-11}**	**0.26**	**0.983**	**1.14 (1.07-1.21)**	**3.21×10^{-5}**	**1.08 (1.06-1.10)**	**5.84×10^{-14}**	***LPP***
4	rs28558138	26818080	G	C	0.58	0.979	1.14 (1.12-1.16)	2.00×10^{-40}	0.58	0.890	1.21 (1.14-1.28)	8.71×10^{-11}	1.15 (1.13-1.17)	9.35×10^{-49}	*TBC1D19*
4	**rs56155140**	**57824451**	**A**	**G**	**0.19**	**G**	**1.09 (1.07-1.12)**	**6.50×10^{-13}**	**0.19**	**0.996**	**1.21 (1.13-1.29)**	**5.17×10^{-8}**	**1.11 (1.08-1.13)**	**8.30×10^{-18}**	***IGFBP7***
4	**rs1471251**	**87976359**	**A**	**T**	**0.60**	**0.993**	**1.06 (1.04-1.08)**	**4.50×10^{-8}**	**0.61**	**0.987**	**1.12 (1.06-1.18)**	**5.31×10^{-5}**	**1.06 (1.04-1.08)**	**8.33×10^{-11}**	***AFF1***

4	**rs34154818**	**89726823**	**A**	**AT**	**0.55**	**0.980**	**1.05 (1.03-1.08)**	**4.90×10^{-8}**	**0.53**	**0.951**	**1.14 (1.08-1.21)**	**2.25×10^{-6}**	**1.06 (1.04-1.08)**	**2.13×10^{-11}**	***FAM13A***
4	**rs10007409**	**120142306**	**C**	**T**	**0.69**	**0.999**	**1.06 (1.04-1.08)**	**3.20×10^{-8}**	**0.68**	**0.990**	**1.21(1.14-1.28)**	**1.12×10^{-10}**	**1.07 (1.05-1.10)**	**2.09×10^{-13}**	***USP53***
4	**rs11728719**	**186696172**	**A**	**C**	**0.76**	**0.978**	**1.08 (1.05-1.10)**	**3.00×10^{-11}**	**0.77**	**0.958**	**1.15 (1.08-1.23)**	**1.63×10^{-5}**	**1.09 (1.06-1.11)**	**1.65×10^{-14}**	***SORBS2***
5	**rs57253948**	**38754162**	**G**	**A**	**0.06**	**G**	**1.12 (1.07-1.16)**	**3.70×10^{-8}**	**0.06**	**0.989**	**1.32 (1.18-1.47)**	**1.15×10^{-6}**	**1.14 (1.09-1.18)**	**1.05×10^{-11}**	**-**
5	rs3749748	127350549	T	C	0.25	0.992	1.16 (1.13-1.18)	5.60×10^{-39}	0.24	0.964	1.42 (1.33-1.51)	3.69×10^{-27}	1.18 (1.16-1.21)	1.06×10^{-56}	*FBN2, SLC12A2*
5	rs11135046	158230013	G	T	0.46	0.995	1.12 (1.10-1.14)	1.60×10^{-32}	0.45	0.992	1.16 (1.10-1.23)	5.81×10^{-8}	1.13 (1.11-1.15)	1.33×10^{-38}	*EBF1*
6	rs7773004	26267755	A	G	0.51	0.998	1.09 (1.07-1.11)	6.00×10^{-20}	0.50	0.984	1.18 (1.12-1.25)	1.38×10^{-9}	1.10 (1.08-1.12)	2.33×10^{-26}	*HFE*
6	**rs11967262**	**43760327**	**C**	**G**	**0.51**	**0.996**	**1.06 (1.04-1.08)**	**5.20×10^{-9}**	**0.51**	**0.990**	**1.34 (1.27-1.42)**	**8.13×10^{-27}**	**1.09 (1.07-1.11)**	**1.45×10^{-19}**	***VEGFA***
6	rs1936800	127436064	C	T	0.47	G	1.06 (1.04-1.08)	2.60×10^{-9}	0.49	0.986	1.20 (1.13-1.26)	7.26×10^{-11}	1.07 (1.05-1.09)	8.29×10^{-15}	*RSPO3*
8	**rs34022079**	**6648676**	**C**	**T**	**0.64**	**0.975**	**1.07 (1.05-1.09)**	**8.20×10^{-11}**	**0.63**	**0.888**	**1.62 (1.52-1.71)**	**4.59×10^{-58}**	**1.11 (1.09-1.14)**	**1.61×10^{-29}**	**-**
8	rs10504825	87567848	C	A	0.41	G	1.07 (1.05-1.09)	7.20×10^{-13}	0.41	0.997	1.14 (1.08-1.21)	1.55×10^{-6}	1.08 (1.06-1.10)	6.51×10^{-17}	*CPNE3*
9	**rs78216177**	**232148**	**C**	**G**	**0.14**	**0.992**	**1.10 (1.07-1.13)**	**3.70×10^{-11}**	**0.14**	**0.988**	**1.16 (1.08-1.25)**	**1.28×10^{-4}**	**1.10 (1.08-1.13)**	**5.80×10^{-14}**	***DOCK8***
9	**rs753085**	**117045447**	**G**	**A**	**0.73**	**0.994**	**1.06 (1.04-1.09)**	**1.50×10^{-8}**	**0.73**	**0.995**	**1.14 (1.07-1.21)**	**4.11×10^{-5}**	**1.07 (1.05-1.09)**	**2.17×10^{-11}**	***COL27A1***
9	rs10817762	118161597	A	C	0.52	0.994	1.08 (1.06-1.10)	1.80×10^{-16}	0.52	0.994	1.14 (1.08-1.20)	2.05×10^{-6}	1.09 (1.07-1.11)	1.02×10^{-20}	*TNC*
10	**rs61863928**	**64449549**	**G**	**T**	**0.62**	**0.955**	**1.06 (1.04-1.08)**	**3.00×10^{-8}**	**0.64**	**0.887**	**1.37 (1.29-1.45)**	**4.22×10^{-25}**	**1.09 (1.07-1.11)**	**1.51×10^{-17}**	**-**
11	**rs79465012**	**128258136**	**C**	**T**	**0.93**	**G**	**1.13 (1.09-1.17)**	**9.70×10^{-11}**	**0.93**	**0.842**	**1.28 (1.14-1.44)**	**2.46×10^{-5}**	**1.14 (1.10-1.18)**	**1.08×10^{-13}**	**-**
12	**rs7308356**	**50539611**	**G**	**A**	**0.63**	**0.997**	**1.08 (1.06-1.11)**	**4.10×10^{-16}**	**0.62**	**0.997**	**1.14 (1.08-1.21)**	**2.93×10^{-6}**	**1.09 (1.07-1.11)**	**3.02×10^{-20}**	***CERS5***
12	**rs1054852**	**124496316**	**G**	**A**	**0.38**	**0.904**	**1.06 (1.04-1.08)**	**1.60×10^{-8}**	**0.37**	**0.927**	**1.29 (1.21-1.36)**	**1.44×10^{-17}**	**1.08 (1.06-1.11)**	**2.87×10^{-16}**	***DNAH10OS***
13	**rs41286076**	**73634859**	**T**	**C**	**0.26**	**0.998**	**1.08 (1.05-1.10)**	**1.10×10^{-11}**	**0.25**	**0.977**	**1.14 (1.07-1.21)**	**5.64×10^{-5}**	**1.08 (1.06-1.11)**	**1.06×10^{-14}**	***KLF5***
14	**rs72683923**	**50735947**	**C**	**T**	**0.02**	**G**	**1.22 (1.14-1.30)**	**1.40×10^{-8}**	**0.02**	**0.721**	**2.38 (1.90-2.99)**	**1.06×10^{-13}**	**1.28 (1.20-1.37)**	**3.62×10^{-14}**	***CDKL1***
15	rs11852492	96167544	T	C	0.84	0.999	1.12 (1.09-1.15)	8.90×10^{-18}	0.83	0.994	1.20 (1.11-1.29)	1.49×10^{-6}	1.13 (1.10-1.15)	3.30×10^{-22}	-
16	**rs11076178**	**57146402**	**T**	**C**	**0.11**	**0.986**	**1.09 (1.06-1.12)**	**2.10×10^{-8}**	**0.11**	**0.905**	**1.18 (1.08-1.28)**	**3.16×10^{-4}**	**1.10 (1.07-1.13)**	**1.05×10^{-10}**	***CPNE2***

16	rs111350029**	88796770	G	GGGA GGC	0.14	0.910	1.24 (1.20-1.27)	1.90×10^{-48}	0.14	0.810	1.57 (1.44-1.71)	7.82×10^{-25}	1.27 (1.23-1.30)	7.39×10^{-66}	*PIEZO1, GALNS*
16	rs11646394**	88812279	C	A	0.87	0.995	1.19 (1.16-1.23)	2.30×10^{-34}	0.88	0.924	1.47 (1.35-1.61)	5.00×10^{-18}	1.22 (1.18-1.25)	3.62×10^{-46}	*PIEZO1, GALNS*
16	rs2002833	88842117	G	A	0.33	0.988	1.19 (1.17-1.22)	1.10×10^{-65}	0.31	0.988	1.43 (1.35-1.52)	8.55×10^{-34}	1.22 (1.19-1.24)	2.47×10^{-90}	*PIEZO1, GALNS*
17	**rs6503321**	**2096580**	**A**	**G**	**0.38**	**0.999**	**1.06 (1.04-1.08)**	**3.80×10^{-8}**	**0.37**	**0.990**	**1.14 (1.08-1.21)**	**3.28×10^{-6}**	**1.07 (1.05-1.08)**	**1.77×10^{-11}**	***SMG6***
17	rs638538	68216128	A	C	0.27	0.979	1.11 (1.09-1.14)	6.90×10^{-23}	0.28	0.994	1.19 (1.12-1.26)	1.79×10^{-8}	1.12 (1.10-1.14)	5.85×10^{-29}	*KCNJ2*
17	rs9895127	70029808	T	C	0.43	0.987	1.10 (1.08-1.12)	6.40×10^{-22}	0.44	0.989	1.16 (1.10-1.22)	1.48×10^{-7}	1.11 (1.09-1.13)	2.88×10^{-27}	*AC007461.1*
19	**rs12609241**†**	**16360926**	**G**	**A**	**0.75**	**0.990**	**1.07 (1.05-1.10)**	**3.00×10^{-10}**	**0.75**	**0.950**	**1.33 (1.25-1.42)**	**1.84×10^{-18}**	**1.10 (1.08-1.12)**	**1.32×10^{-18}**	***KLF2***
20	rs3787184	50157837	A	G	0.83	0.978	1.16 (1.13-1.19)	3.10×10^{-32}	0.82	0.949	1.17 (1.09-1.26)	1.32×10^{-5}	1.16 (1.14-1.19)	2.51×10^{-36}	*NFATC2*
20	**rs76602912**	**57459868**	**T**	**C**	**0.98**	**G**	**1.25 (1.18-1.33)**	**7.50×10^{-13}**	**0.97**	**0.857**	**1.52 (1.26-1.83)**	**1.41×10^{-5}**	**1.28 (1.20-1.36)**	**3.56×10^{-16}**	***GNAS***
20	rs6062619	62683002	A	G	0.73	0.952	1.10 (1.08-1.12)	1.90×10^{-17}	0.73	0.824	1.27 (1.19-1.36)	4.97×10^{-13}	1.11 (1.09-1.14)	5.48×10^{-25}	*SOX18*

*Based on NCBI Genome Build 37 (hg19). †The effect allele. ‡The alternate (non-effect) allele. §The effect allele frequency in the study population. ||The imputation quality score; G= genotyped SNP. #Odds ratio (95% confidence intervals). OR > 1 indicative of increased risk with effect allele. **denotes four residual significant signals following conditional regression analysis at the lead SNP. **†At this locus, 19p13.11, the lead SNP in the UK Biobank cohort was rs451367 ($P_{discovery} = 2.10\times10^{-10}$), however, this did not replicate in 23andMe ($P_{replication} = 0.47$; Appendix Table 2.1) - the independent residual signal, rs12609241 shown here, did however replicate. Bold variants represent loci not previously reported.

Figure 2.3. Results of genome-wide association study in varicose veins. A) Quantile-Quantile plot of observed vs. expected P-values for the association analysis for varicose veins. B) Manhattan plot showing genome-wide P-values plotted against position on each of the autosomes. The dark blue, light blue, and green dots refer to the discovery cohort in UK Biobank, with the red dots corresponding to the forty-nine variants from the 23andMe cohort at each replicated locus. The dark blue peaks correspond to the 46 loci that replicated in the 23andMe cohort at a Bonferroni-corrected threshold of $P < 4.24 \times 10^{-4}$. Candidate genes at each locus are named above each signal, with newly discovered genetic loci in blue, and previously described loci in black.

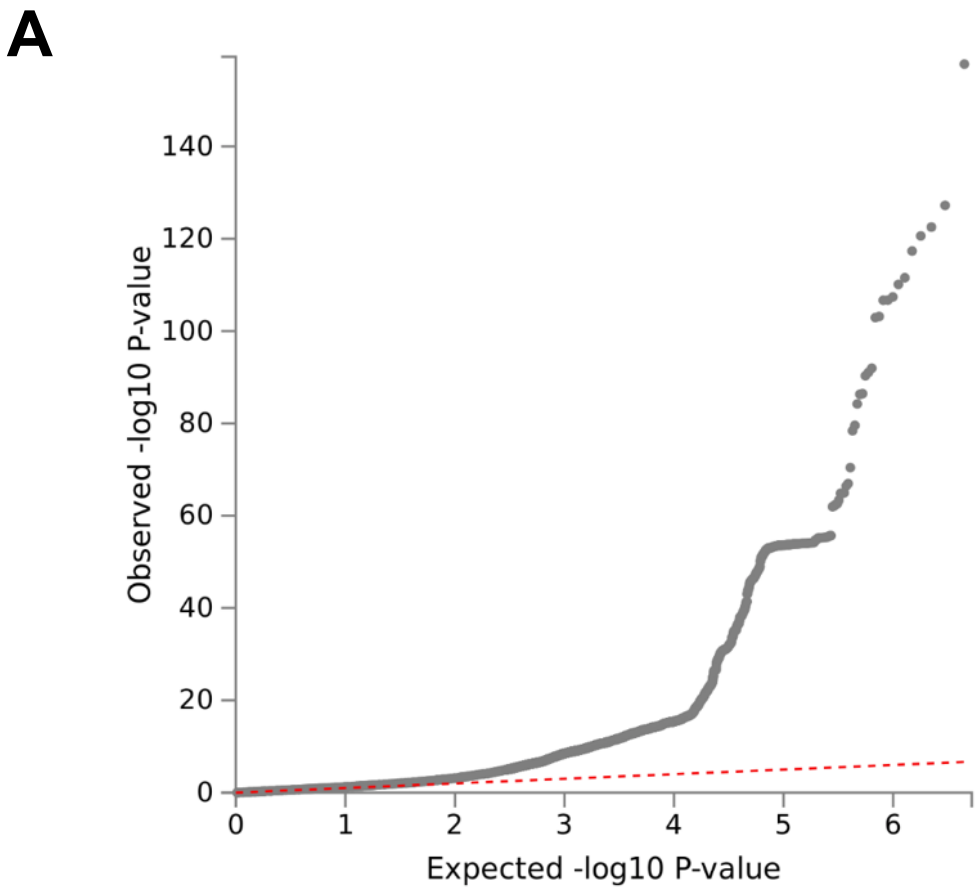

B

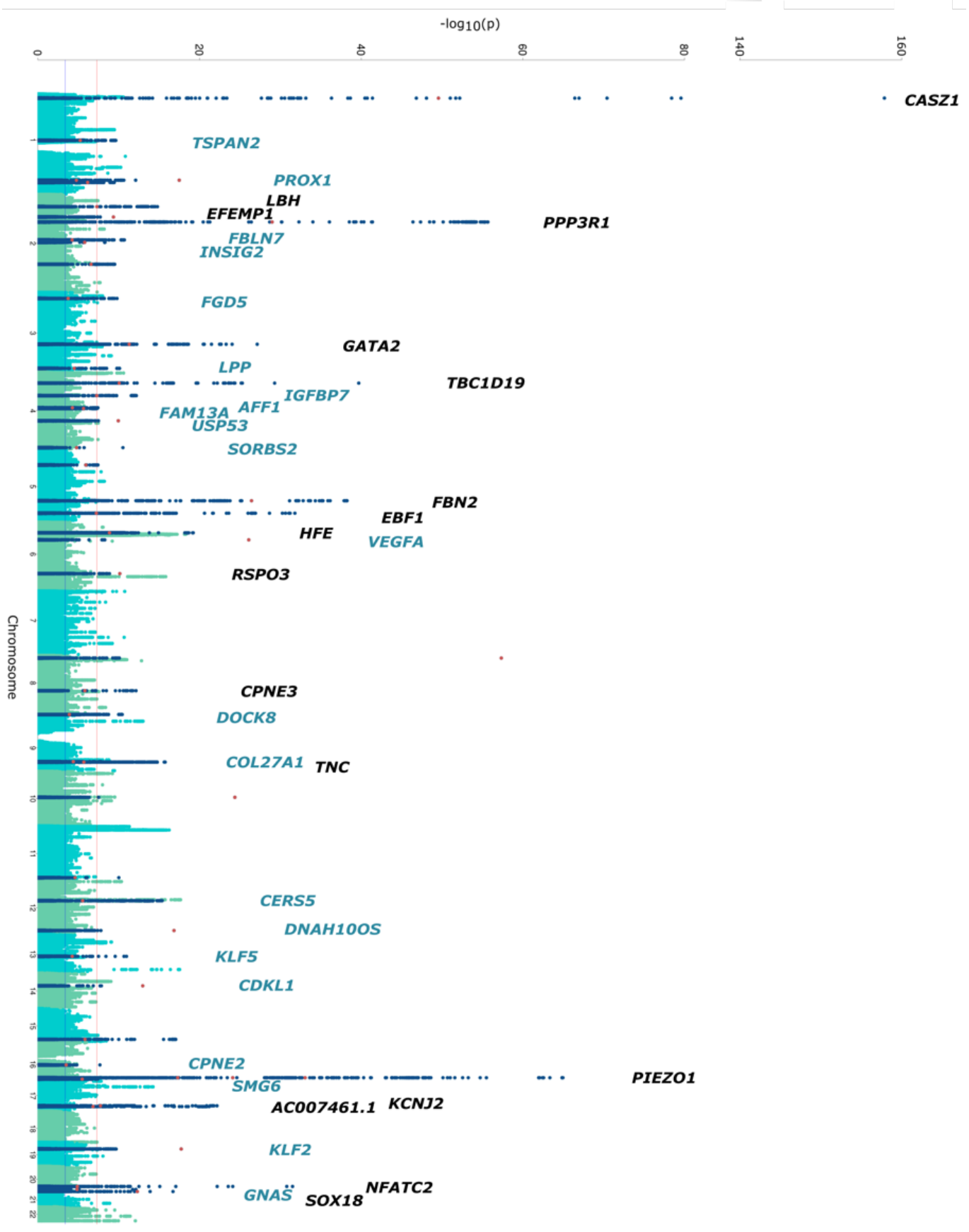
-log10(p)
0
20
40
60
80
140
160
Chromosome
1
2
3
4
5
6
7
8
9
10
11
12
13
14
15
16
17
18
19
20
21
22
CASZ1
TSPAN2
PROX1
LBH
EFEMP1
PPP3R1
FBLN7
INSIG2
FGD5
GATA2
LPP
TBC1D19
IGFBP7
FAM13A
AFF1
USP53
SORBS2
FBN2
EBF1
HFE
VEGFA
RSPO3
CPNE3
DOCK8
COL27A1
TNC
CERS5
DNAH10OS
KLF5
CDKL1
CPNE2
PIEZO1
SMG6
AC007461.1
KCNJ2
KLF2
GNAS
SOX18
NFATC2

Figure 2.4. Regional Locus Zoom plots of all varicose veins associated signals. LocusZoom plots of the 49 independent genome-wide significant variants at the 46 replicated varicose veins associated susceptibility loci. Plots are ordered by chromosome number and genomic position. SNP position is shown on the x-axis, and strength of association on the y-axis (-$\log_{10}$ P-value). The linkage disequilibrium (LD) relationship between the lead SNP and the surrounding SNPs is indicated by the r^2 legend. In the lower panel of each sub-figure, genes within 500kb on either side of the index SNP are shown. The position on each chromosome is depicted in relation to Human Genome build hg19 (GRCh37). Note: variants rs34154818 and rs111350029 did not exist in the 1000 genomes reference panel and therefore r^2 values could not be generated

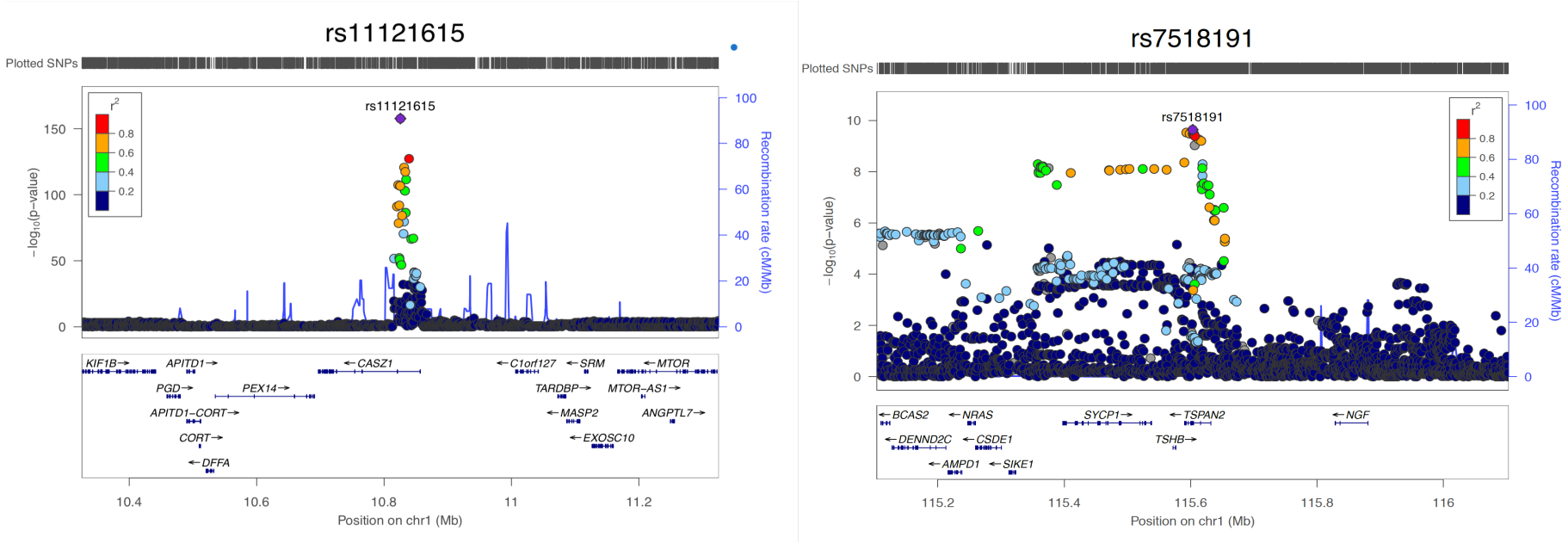

rs17712208

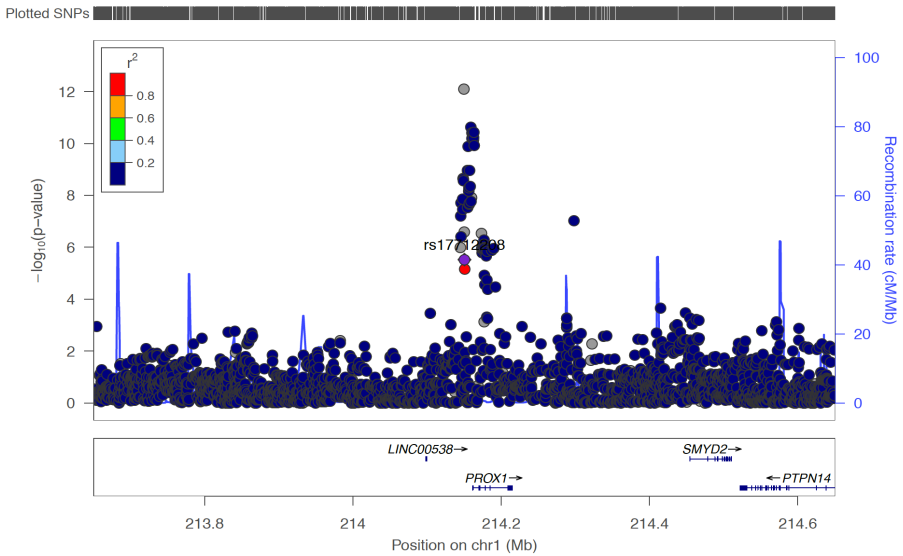

rs340875

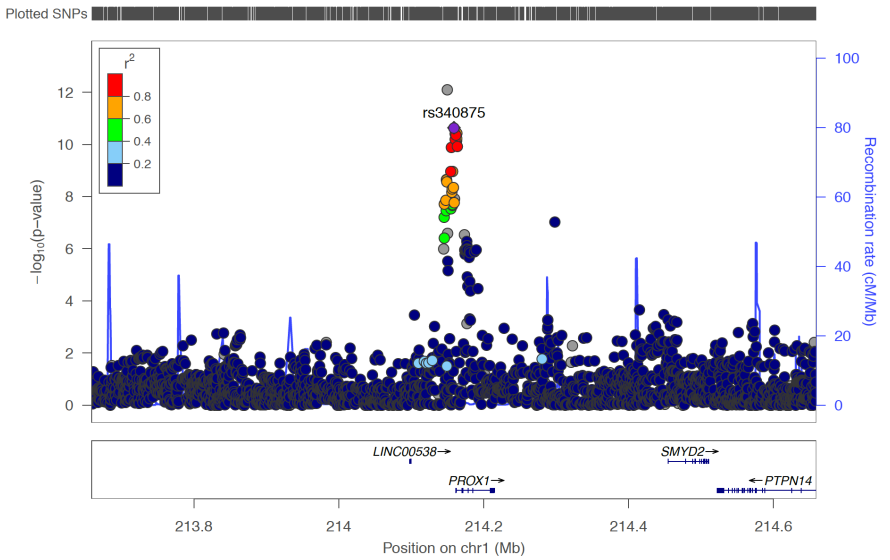

rs2820464

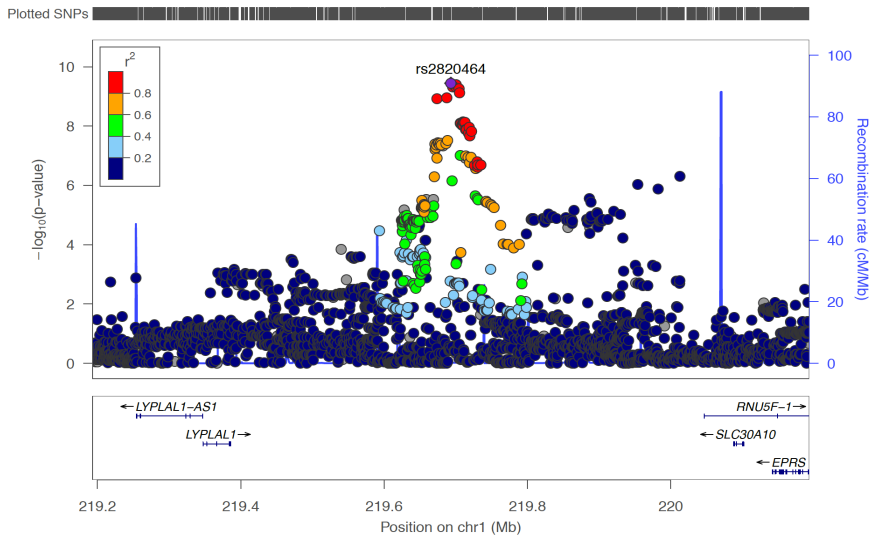

rs9967884

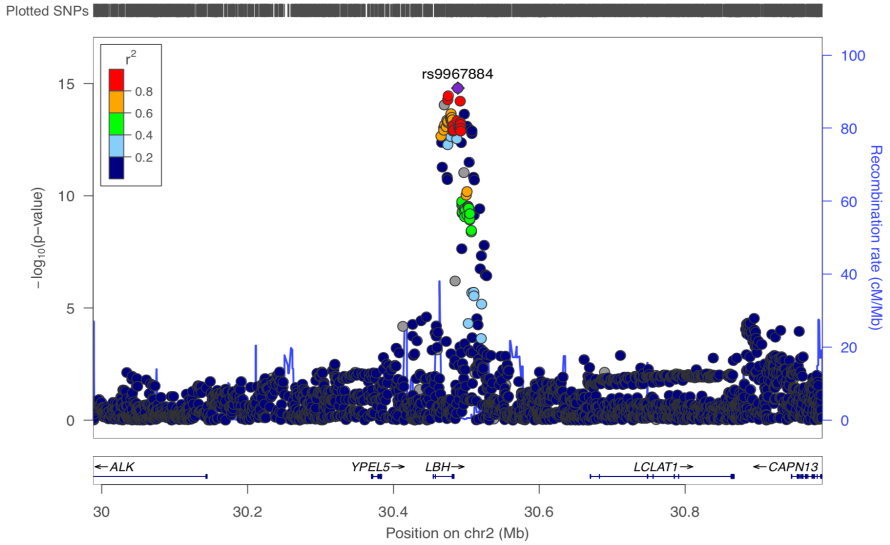

rs3791679

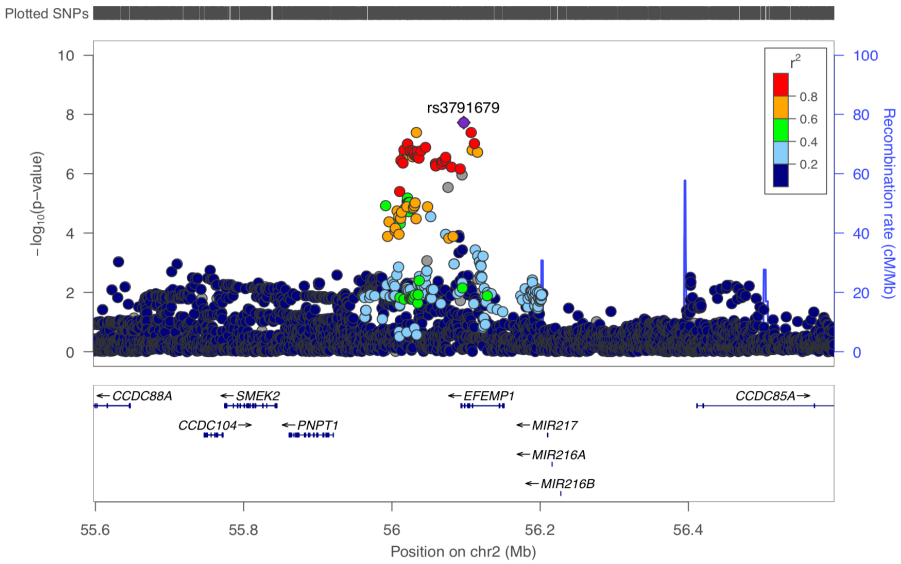

rs2861819

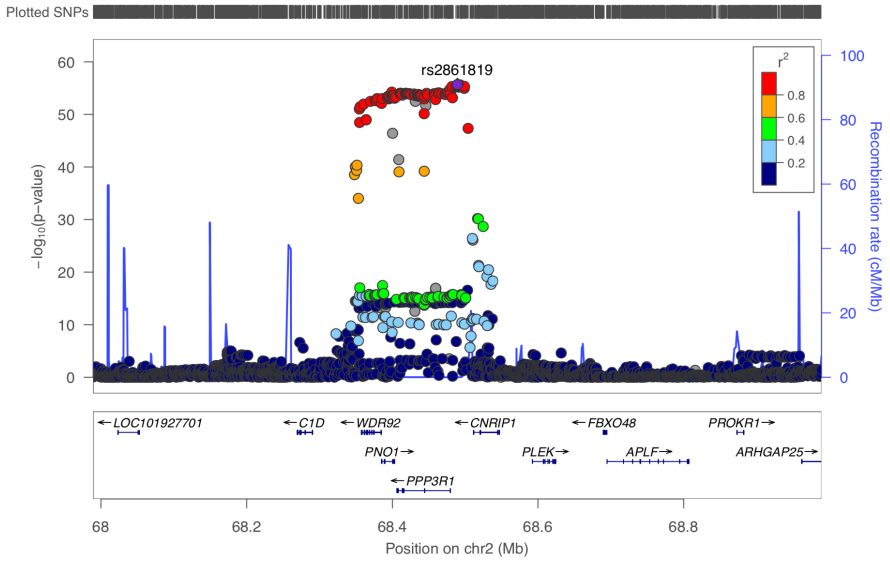

rs4849044

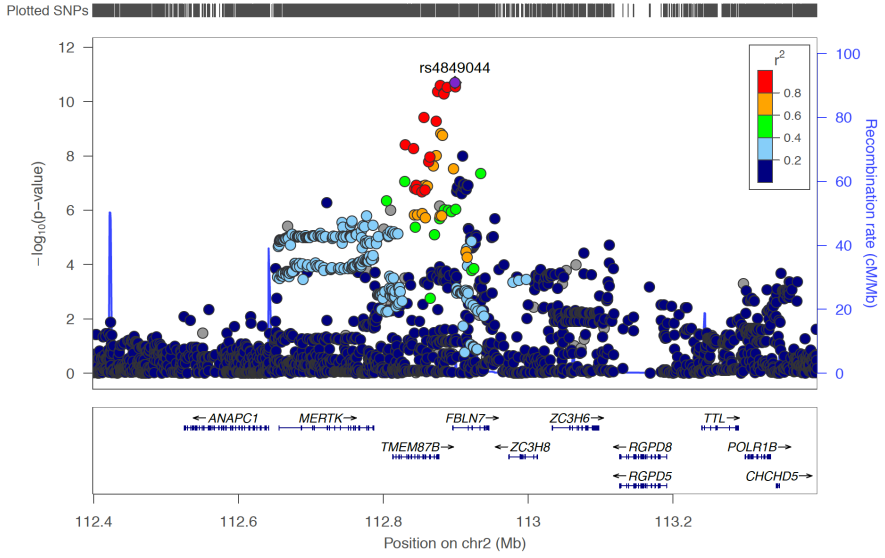

rs17819430

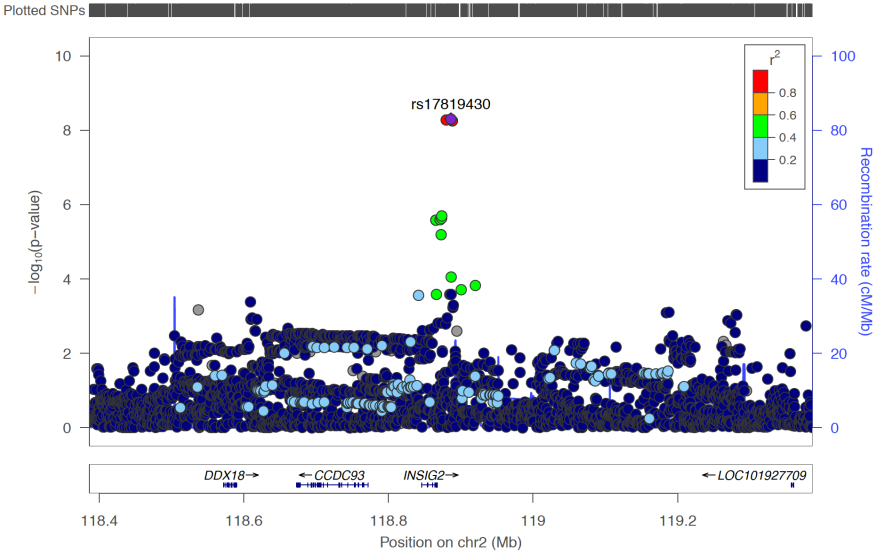

rs55889669

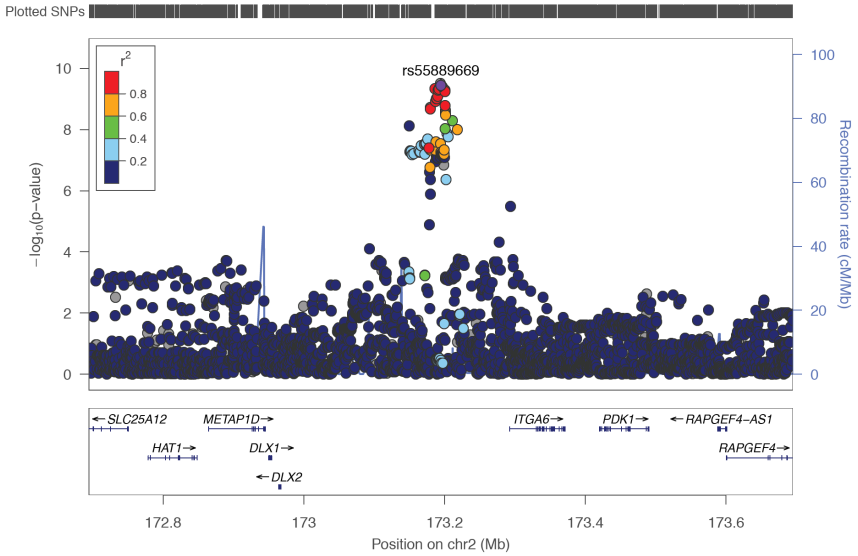

rs844176

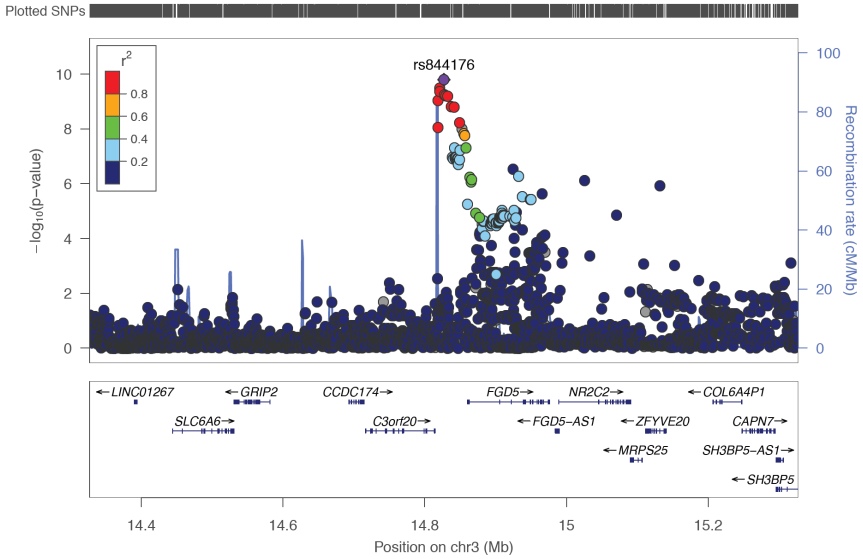

rs2713575

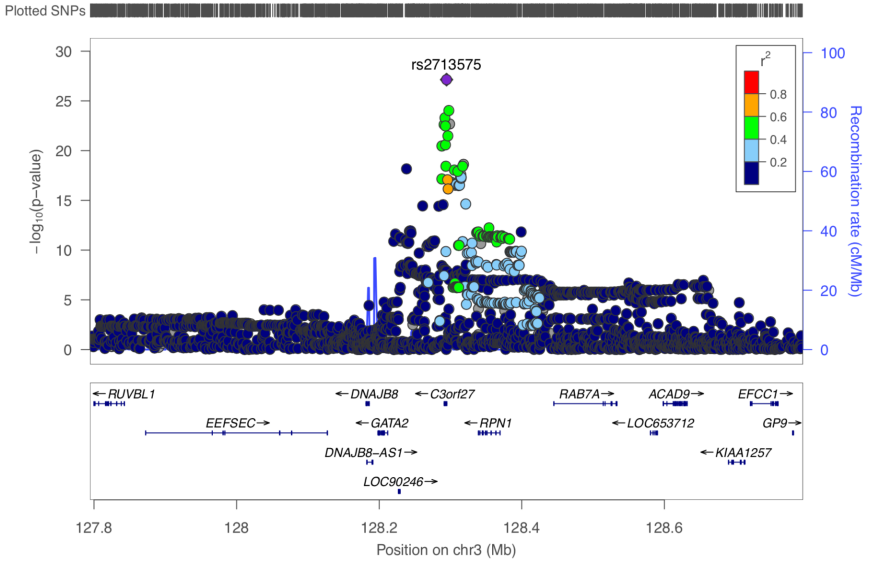

rs9877579

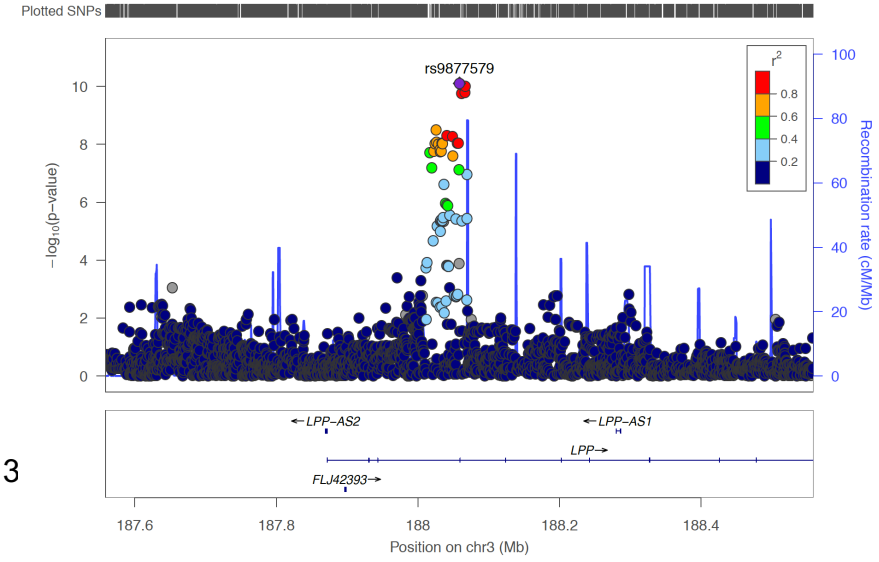

rs28558138

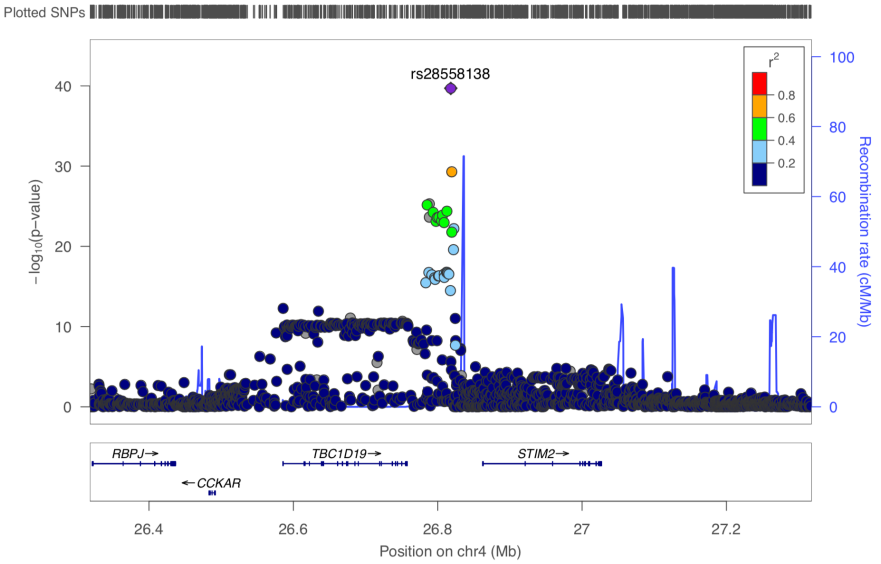

rs56155140

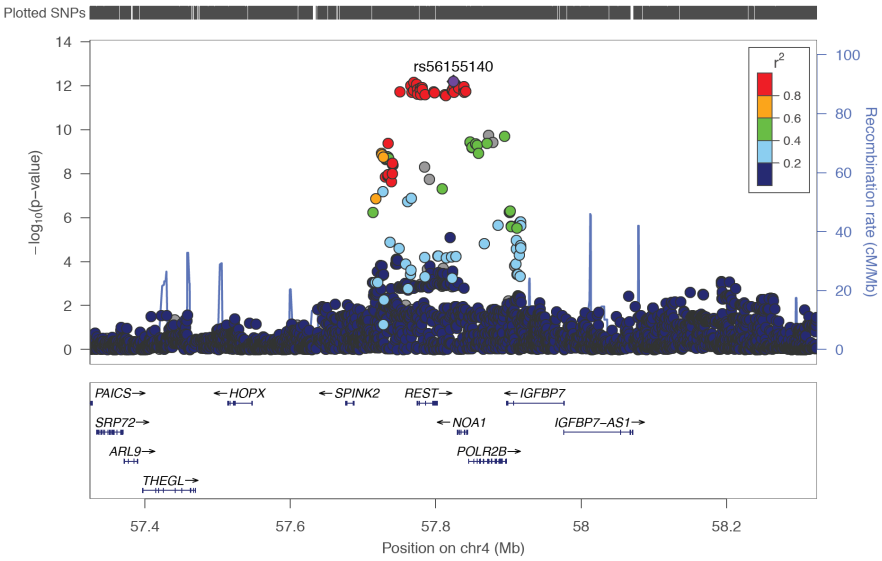

rs1471251

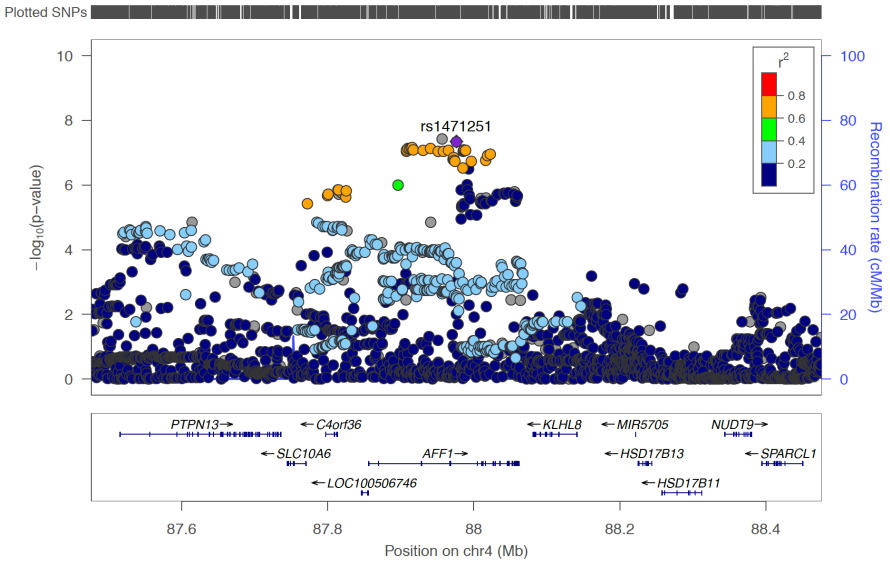

rs34154818

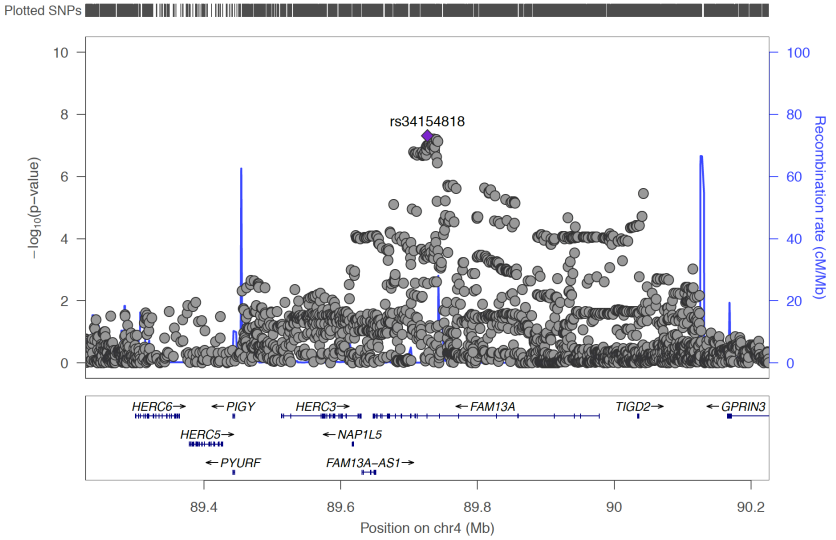

rs10007409

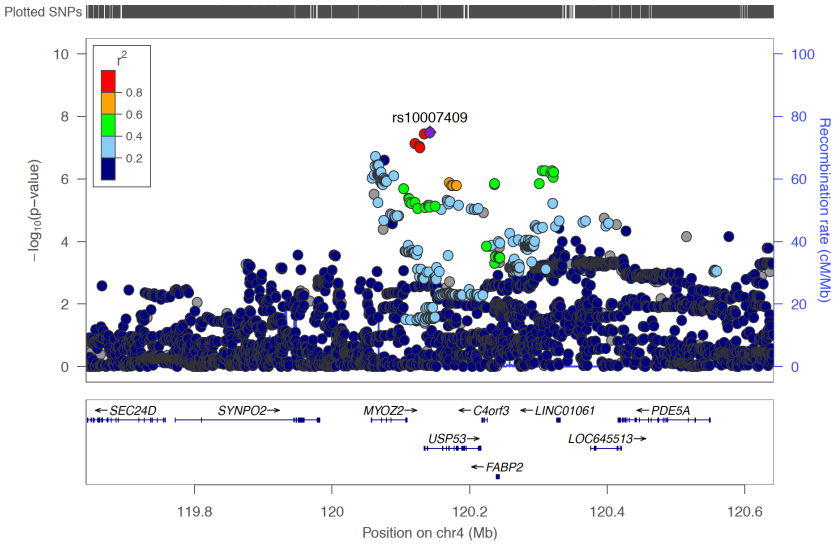

rs11728719

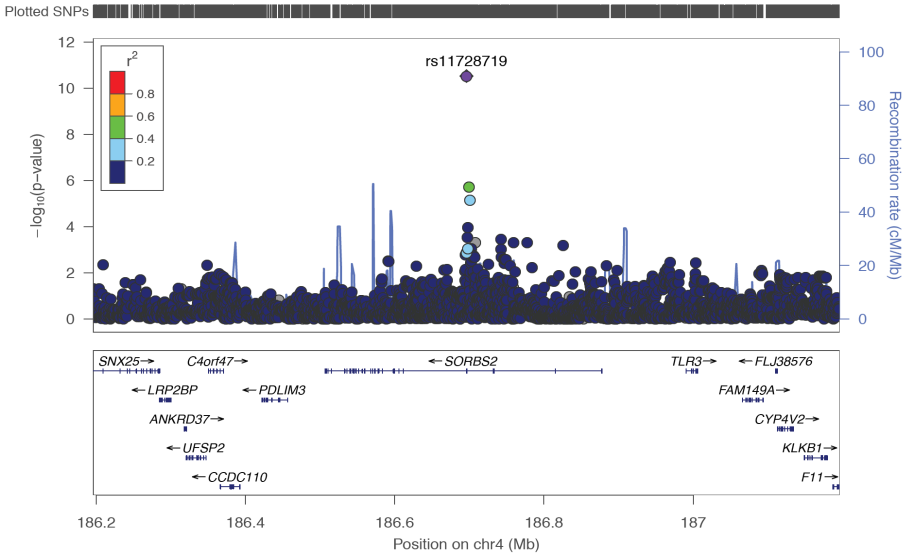

rs57253948

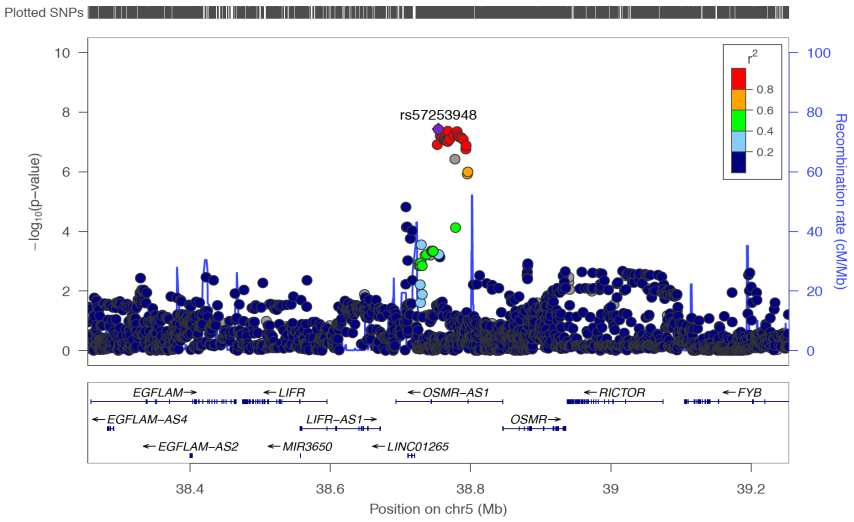

rs3749748

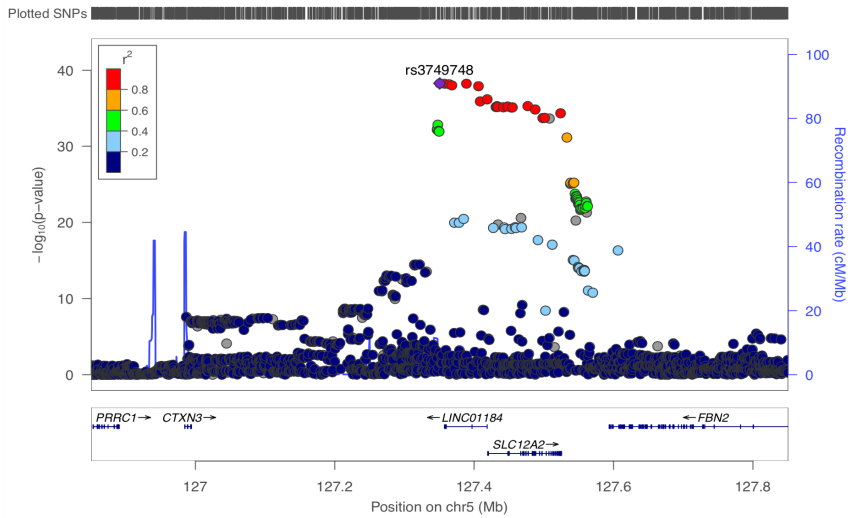

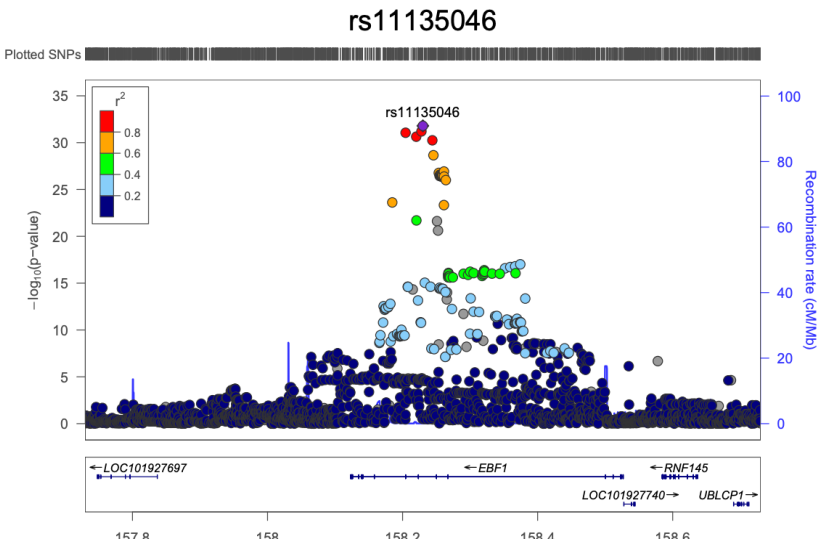
rs11135046
Plotted SNPs
rs11135046
r²
0.8
0.6
0.4
0.2
−log10(p−value)
Recombination rate (cM/Mb)
LOC101927697
EBF1
RNF145
LOC101927740
UBLCP1

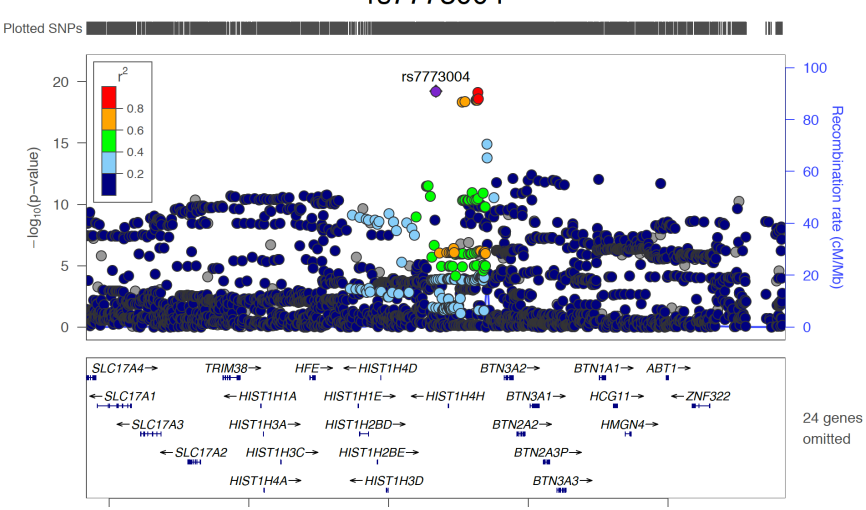
rs7773004
Plotted SNPs
rs7773004
r²
0.8
0.6
0.4
0.2
−log10(p−value)
Recombination rate (cM/Mb)
SLC17A4
TRIM38
HFE
HIST1H4D
BTN3A2
BTN1A1
ABT1
SLC17A1
HIST1H1A
HIST1H1E
HIST1H4H
BTN3A1
HCG11
ZNF322
SLC17A3
HIST1H3A
HIST1H2BD
BTN2A2
HMGN4
SLC17A2
HIST1H3C
HIST1H2BE
BTN2A3P
HIST1H4A
HIST1H3D
BTN3A3
24 genes
omitted

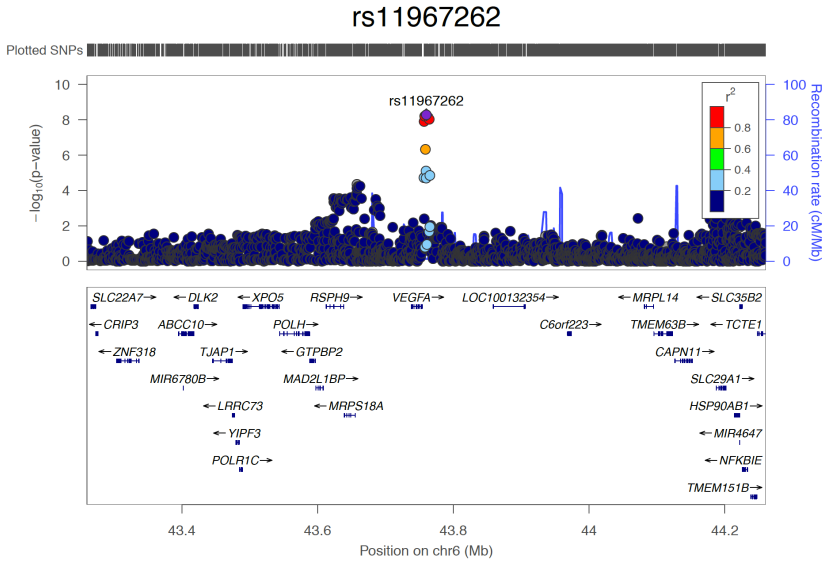
rs11967262
Plotted SNPs
rs11967262
r²
0.8
0.6
0.4
0.2
−log10(p−value)
Recombination rate (cM/Mb)
SLC22A7
DLK2
XPO5
RSPH9
VEGFA
LOC100132354
MRPL14
SLC35B2
CRIP3
ABCC10
POLH
C6orf223
TMEM63B
TCTE1
ZNF318
TJAP1
GTPBP2
CAPN11
MIR6780B
MAD2L1BP
SLC29A1
LRRC73
MRPS18A
HSP90AB1
YIPF3
MIR4647
POLR1C
NFKBIE
TMEM151B
43.4
43.6
43.8
44
44.2
Position on chr6 (Mb)

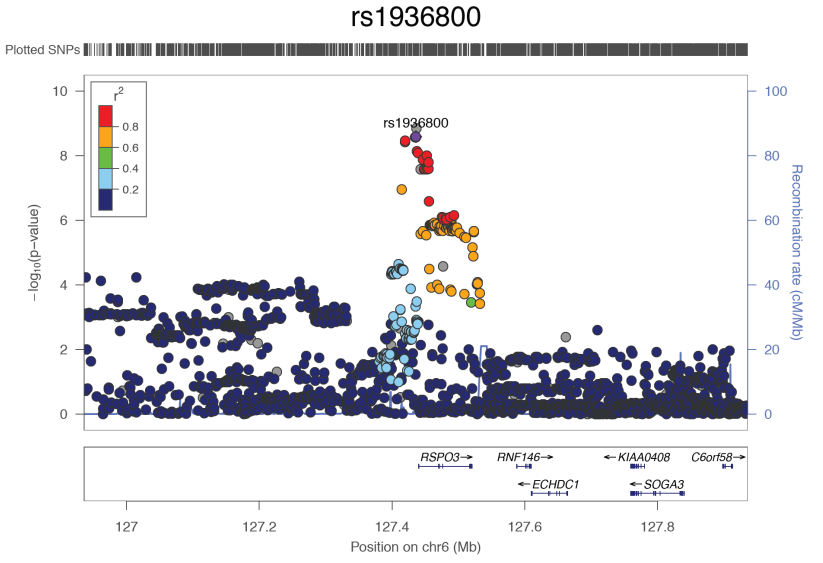
rs1936800
Plotted SNPs
rs1936800
r²
0.8
0.6
0.4
0.2
−log10(p−value)
Recombination rate (cM/Mb)
RSPO3
RNF146
KIAA0408
C6orf58
ECHDC1
SOGA3
127
127.2
127.4
127.6
127.8
Position on chr6 (Mb)

rs34022079

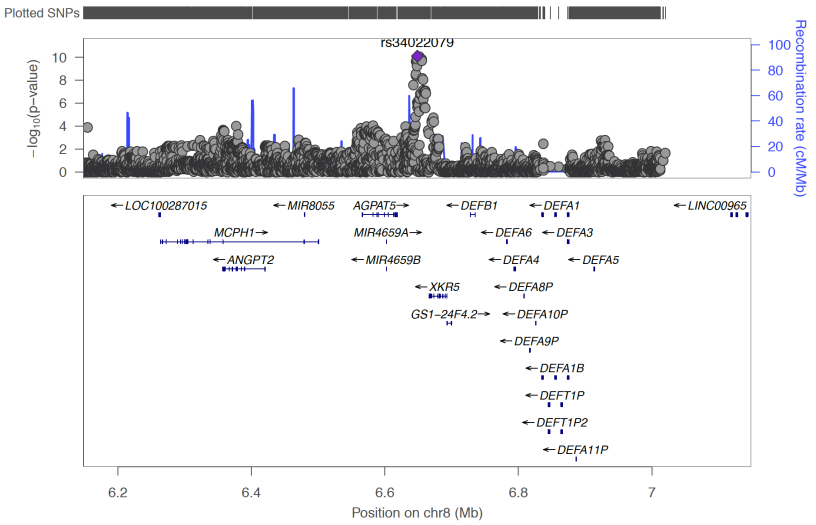

rs10504825

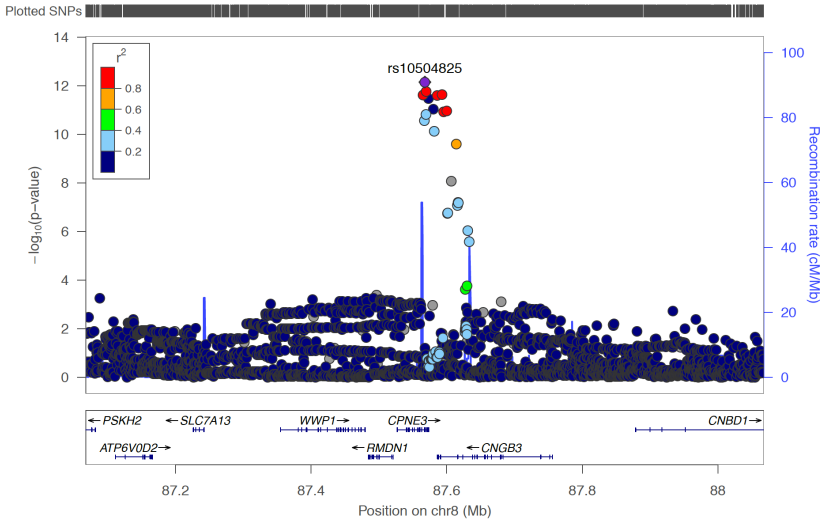

rs78216177

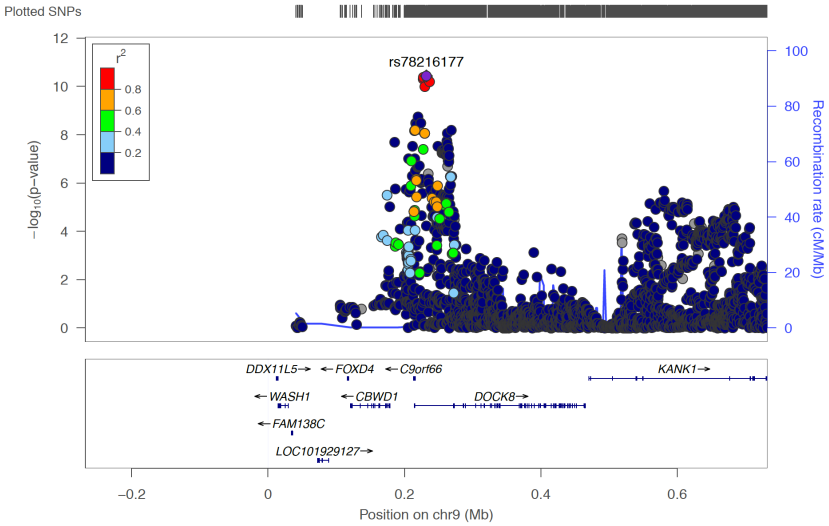

rs753085

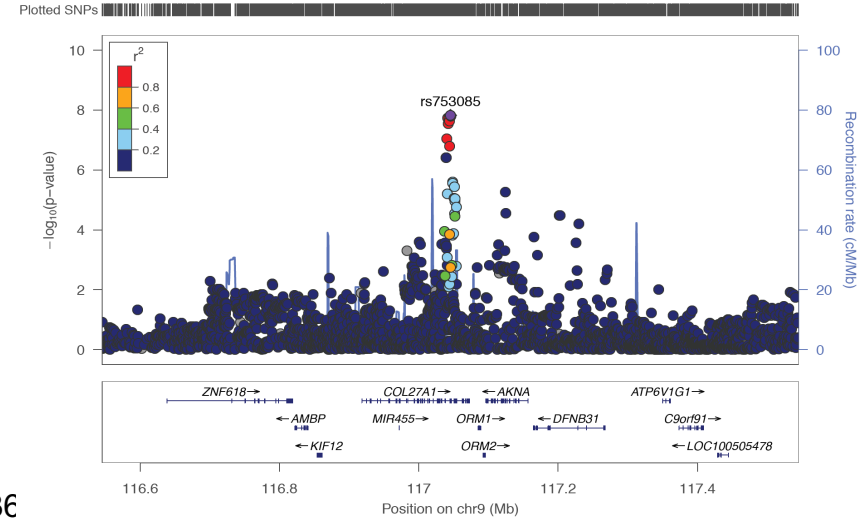

rs10817762

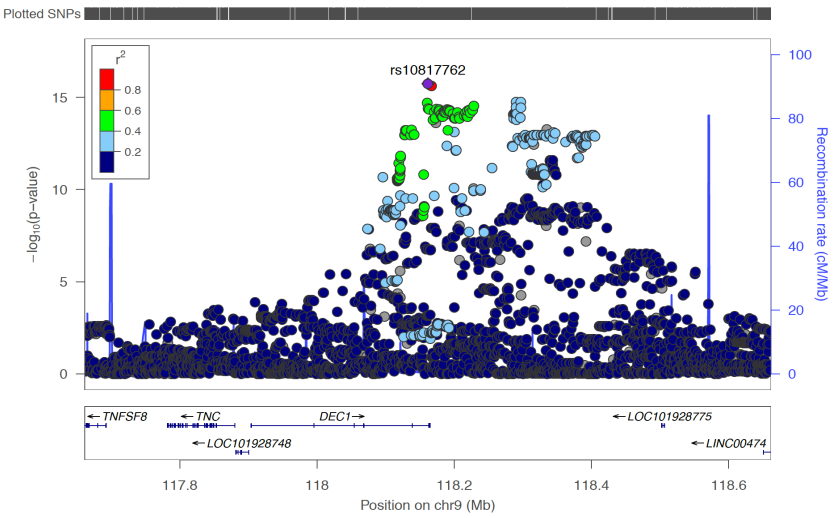

rs61863928

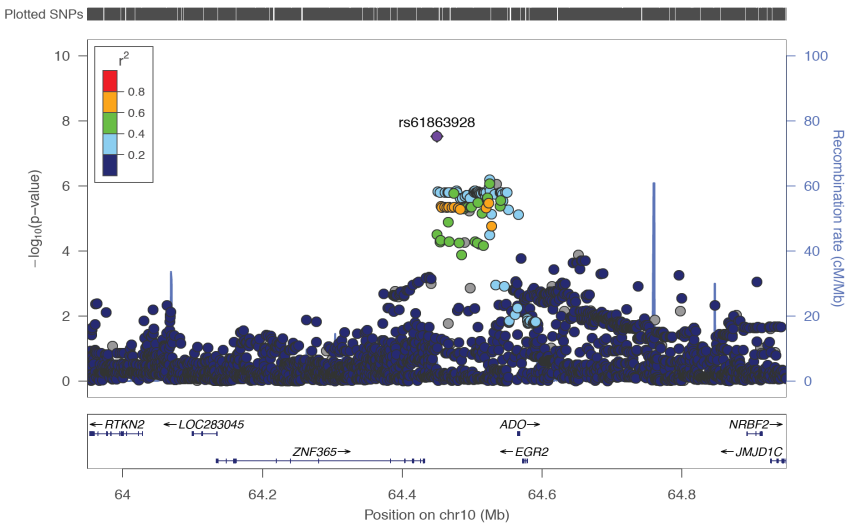

rs79465012

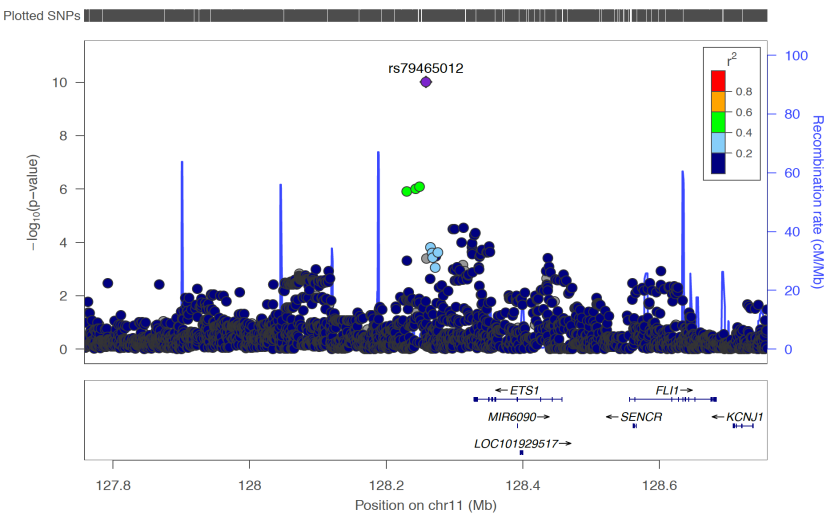

rs7308356

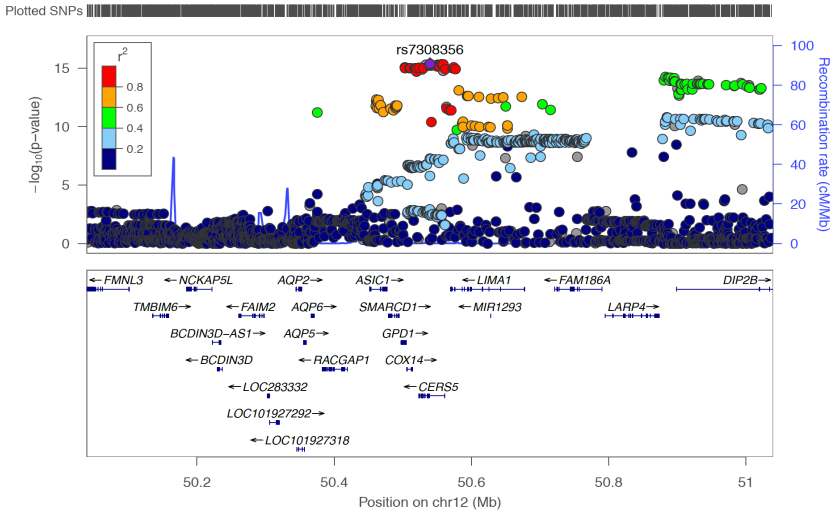

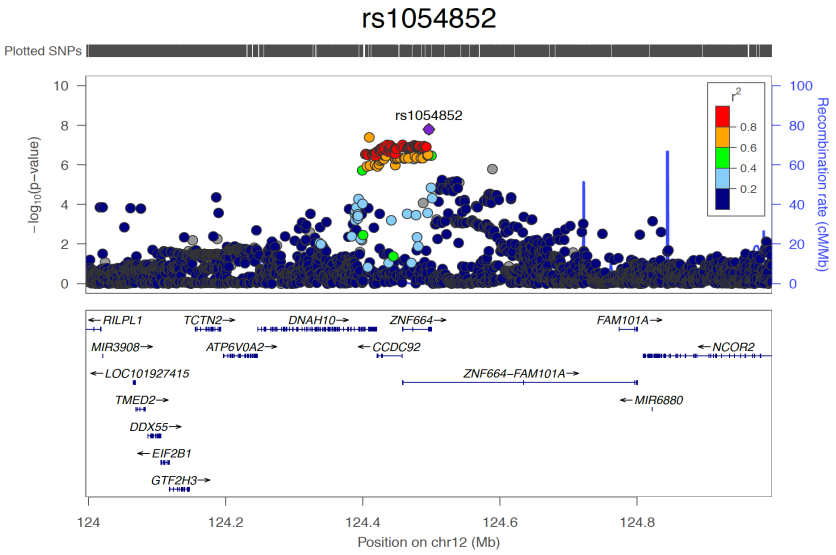
rs1054852
Plotted SNPs
rs1054852
r^2
0.8
0.6
0.4
0.2
$-\log_{10}$(p-value)
Recombination rate (cM/Mb)
RILPL1
TCTN2
DNAH10
ZNF664
FAM101A
MIR3908
ATP6V0A2
CCDC92
NCOR2
LOC101927415
ZNF664–FAM101A
TMED2
MIR6880
DDX55
EIF2B1
GTF2H3
Position on chr12 (Mb)

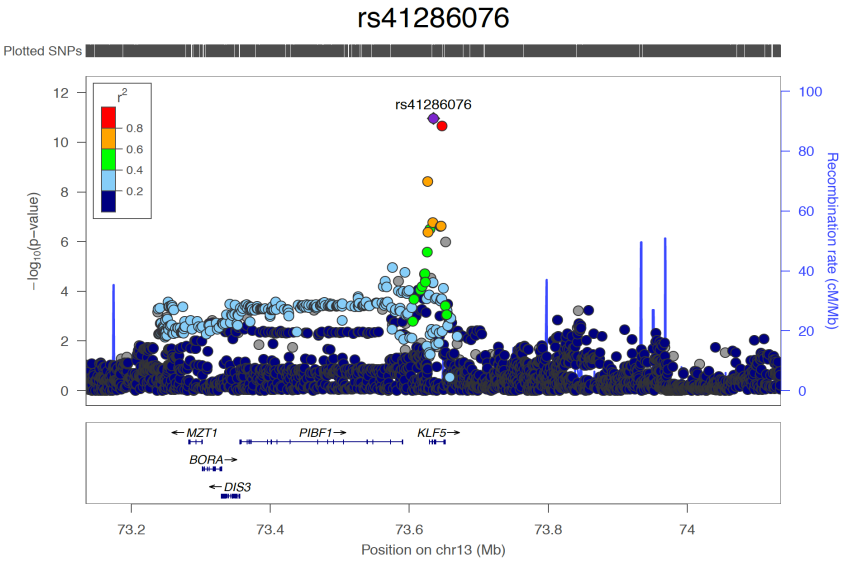
rs41286076
Plotted SNPs
rs41286076
r^2
0.8
0.6
0.4
0.2
$-\log_{10}$(p-value)
Recombination rate (cM/Mb)
MZT1
PIBF1
KLF5
BORA
DIS3
Position on chr13 (Mb)

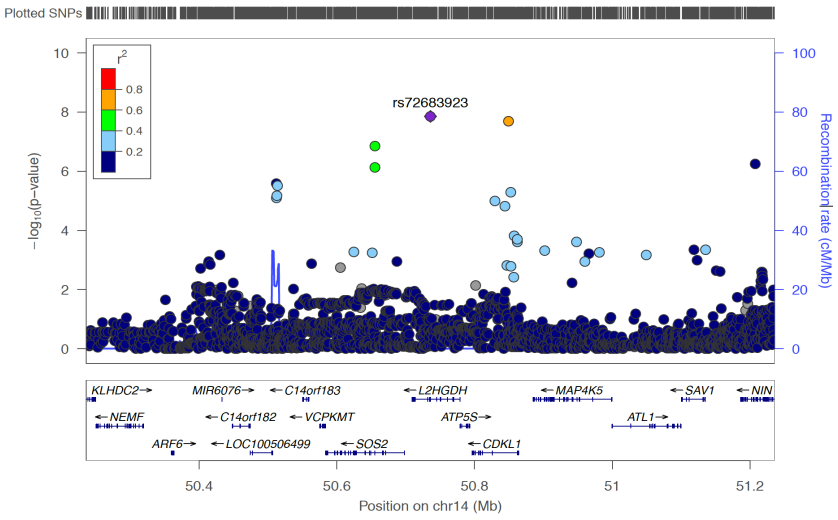
rs72683923
Plotted SNPs
rs72683923
r^2
0.8
0.6
0.4
0.2
$-\log_{10}$(p-value)
Recombination rate (cM/Mb)
KLHDC2
MIR6076
C14orf183
L2HGDH
MAP4K5
SAV1
NIN
NEMF
C14orf182
VCPKMT
ATP5S
ATL1
ARF6
LOC100506499
SOS2
CDKL1
Position on chr14 (Mb)

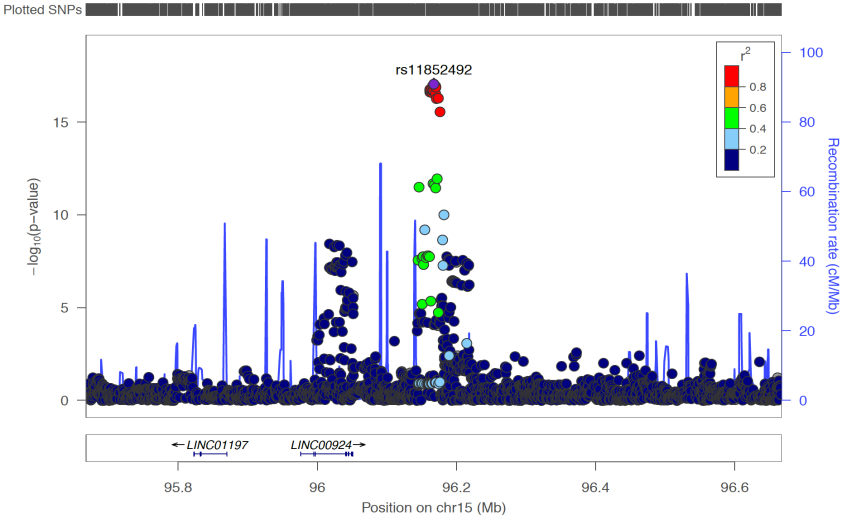
rs11852492
Plotted SNPs
rs11852492
r^2
0.8
0.6
0.4
0.2
$-\log_{10}$(p-value)
Recombination rate (cM/Mb)
LINC01197
LINC00924
Position on chr15 (Mb)

rs11076178

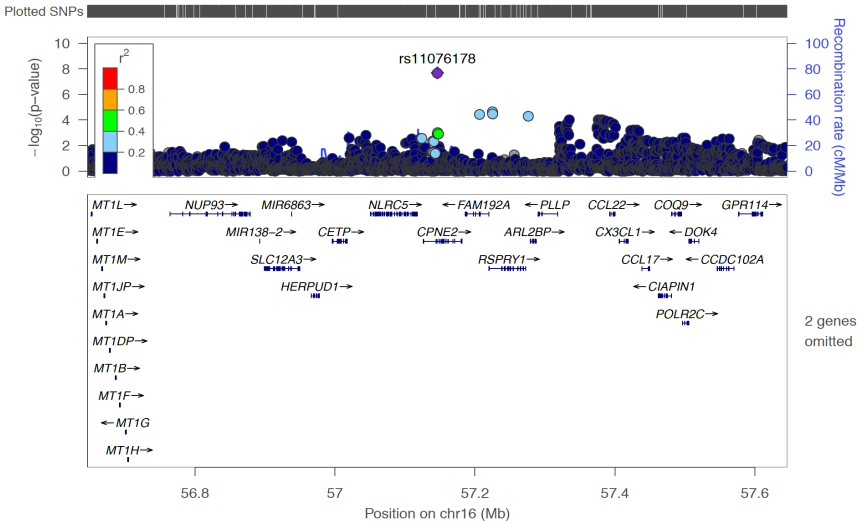

rs111350029

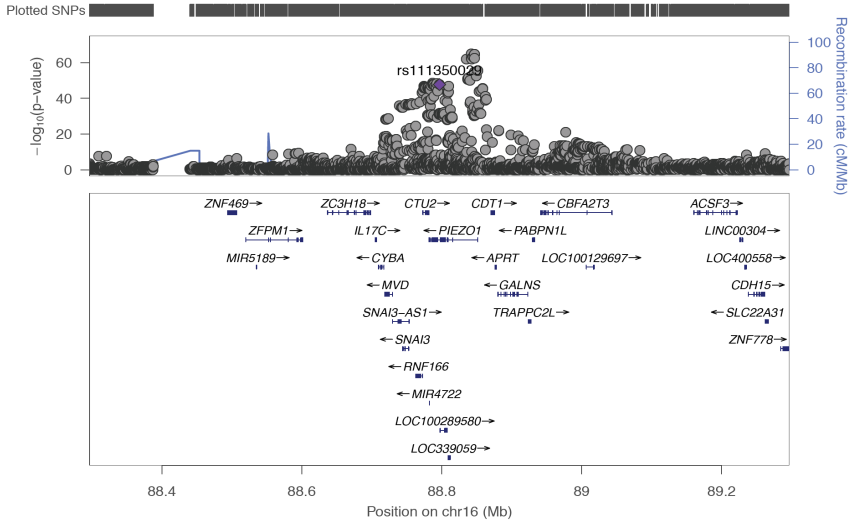

rs11646394

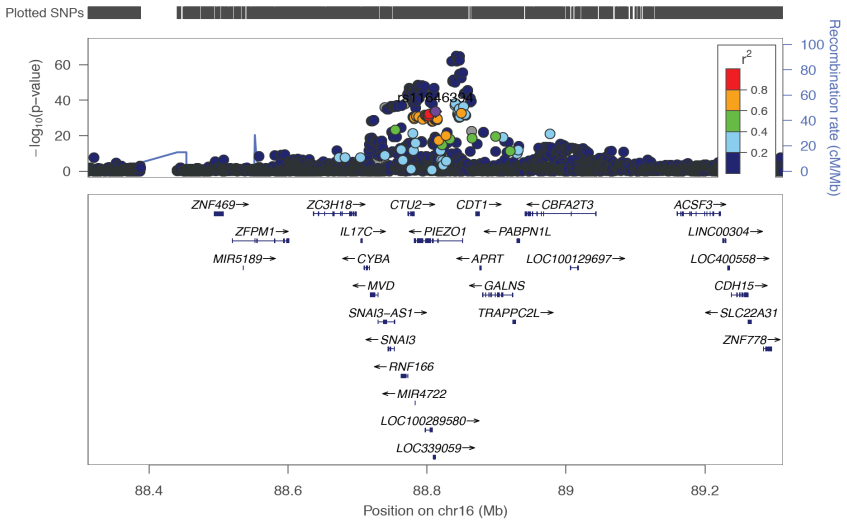

rs2002833

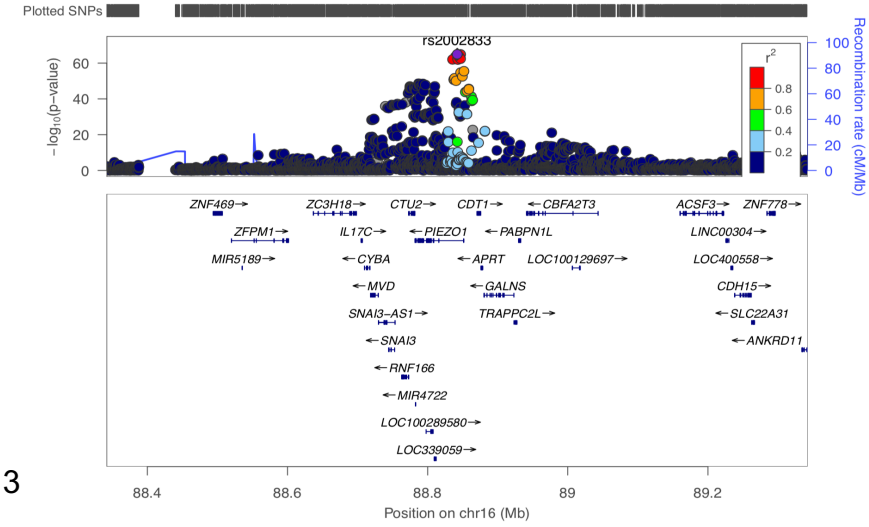

rs6503321

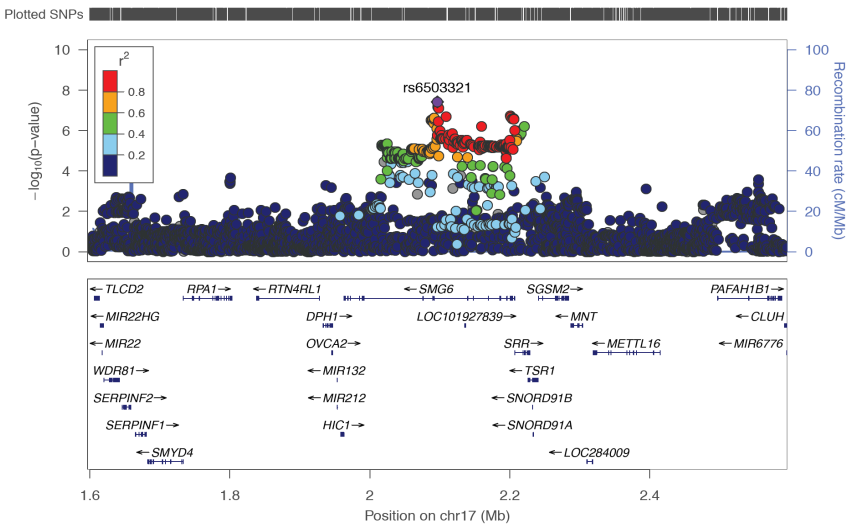

rs638538

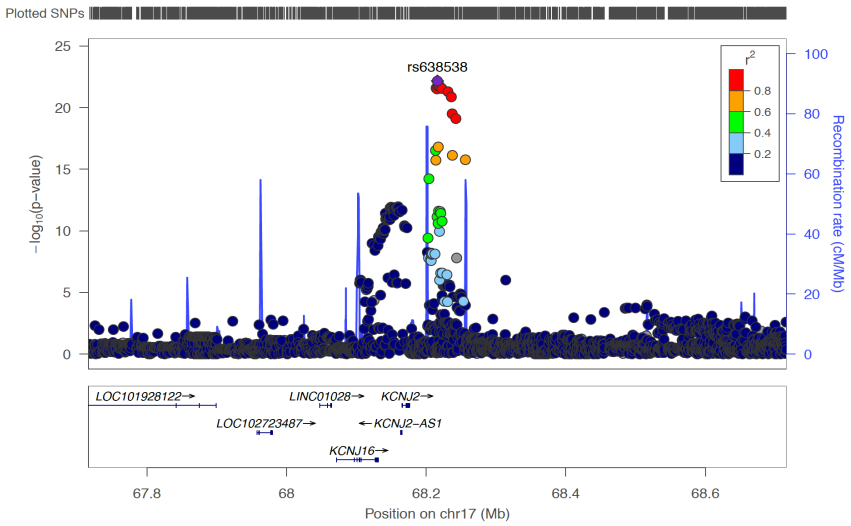

rs9895127

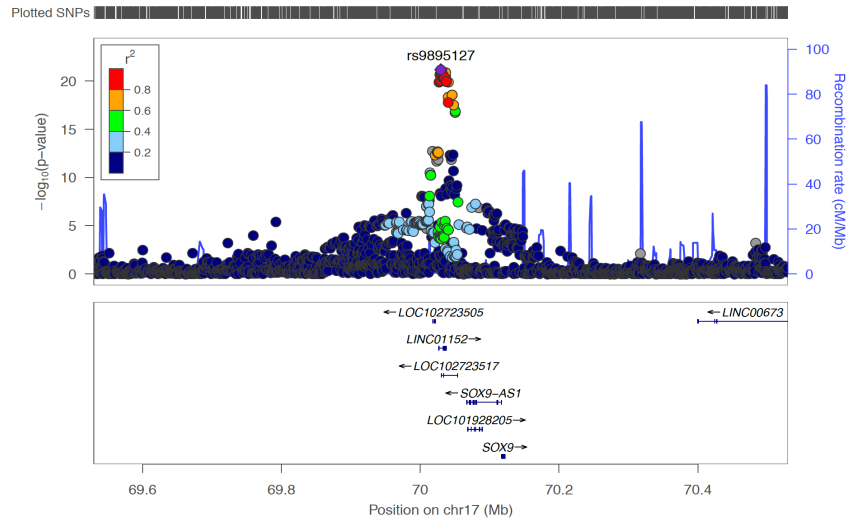

rs12609241

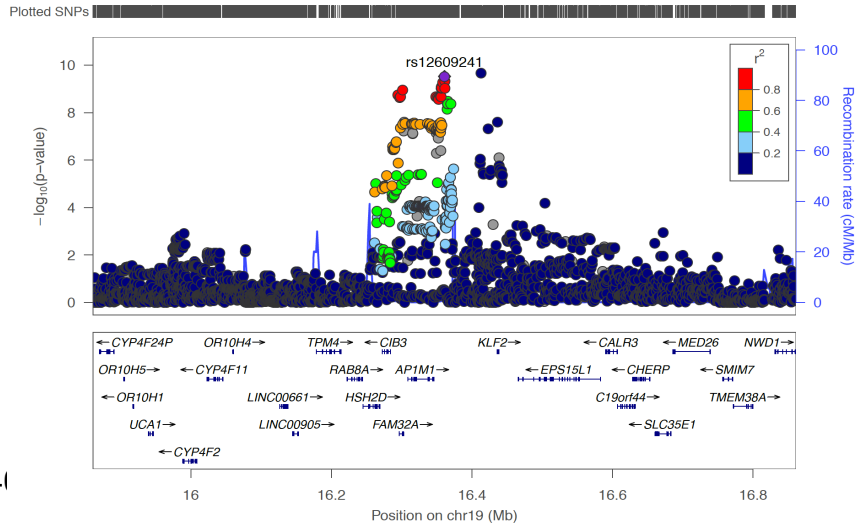

rs3787184

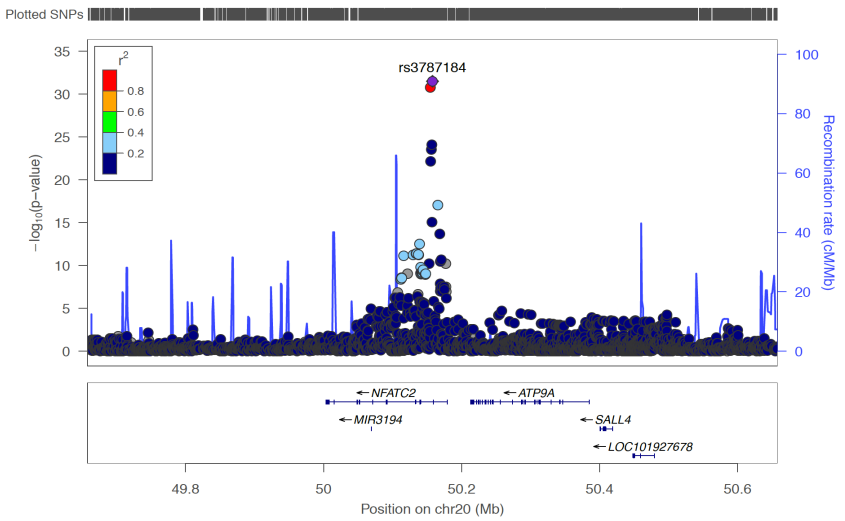

rs76602912

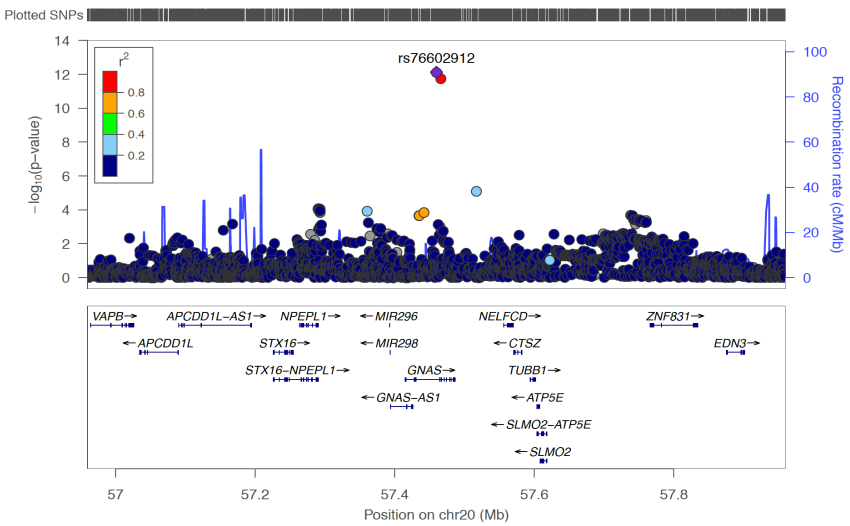

rs6062619

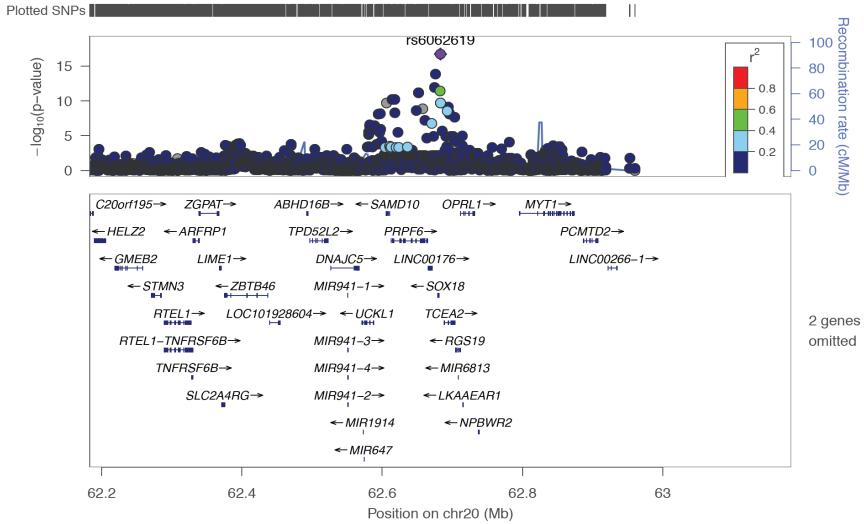

2.3.2. *In silico* annotation

FUMA[21] was used to interrogate and annotate SNPs at the susceptibility loci, identifying 5,315 genome-wide significant candidate SNPs from the discovery cohort associated with varicose veins at 45 of the 46 replicated loci (**Figure 2.5**). ~2% of candidate variants (n = 103) were exonic, of which 47 were synonymous and 56 were non-synonymous (52 missenses, two stop gains, one splice site variant, and one frameshift variant). Four missense variants were non-synonymous and predicted to alter protein structure and/or function and demonstrated modest linkage with the index replicated variant at three loci ($r^2 \geq 0.22$ and $D' \geq 0.75$) – 12q13.12 (rs7308356), 16q24.3 (rs2002833) and 17q24.3 (rs9895127) (**Appendix Table 2.2**). This includes rs12303082-T/G ($P = 2.0\times10^{-9}$, OR = 1.06, $r^2_{index} = 0.27$, $D'_{index} = 0.92$) which resides within a highly conserved region (Genomic evolutionary rate profiling (GERP) score: 0.83) of *FAM186A*, causing a p.Lys187Gln amino acid substitution which is predicted to be deleterious and alter protein function (SIFT[37]: 0.01, PolyPhen-2[38]: 0.91). Another missense variant, rs7184427-A/G ($P = 9.1\times10^{-40}$, OR = 1.19, $r^2_{index} = 0.22$, $D'_{index} = 0.75$), results in a predicted deleterious p.Val250Ala substitution within *PIEZO1* (SIFT[37]: 0.00). *PIEZO1* encodes a mechanosensitive cation channel involved in the detection of vascular shear stress, and was previously associated with varicose veins and lymphoedema.[5,39]

Of the intronic and intergenic variants (n = 4294, 80.8%) highlighted by ANNOVAR[23] (**Figure 2.5**), 3,735 (87.0%) lie in open chromatin regions. 163 of the intronic and intergenic variants show evidence of functionality with a CADD Score[25] ≥ 12.37 (**Appendix Table 2.3**), of which 17 also demonstrate regulatory potential with an

RDB[24] score of 2b or less (*likely to affect binding*) and eight with an RDB score of 1f or less (*likely to affect binding and linked to expression of a gene target* (i.e. an eQTL)) (**Appendix Table 2.3**).

Figure 2.5. Functional annotation of the genome-wide significant variants at the forty-six varicose veins-associated loci. Functional consequences of the SNPs on genes were obtained by performing ANNOVAR gene-based annotation using Ensembl genes (build 85) in FUMA. A) CADD scores, B) RegulomeDB scores and C) 15-core chromatin state were annotated to all 5,315 SNPs in 1000G phase 3 by FUMA through matching chromosome, position, reference, and alternative alleles. D) Positional classification of the 5,315 SNPs.

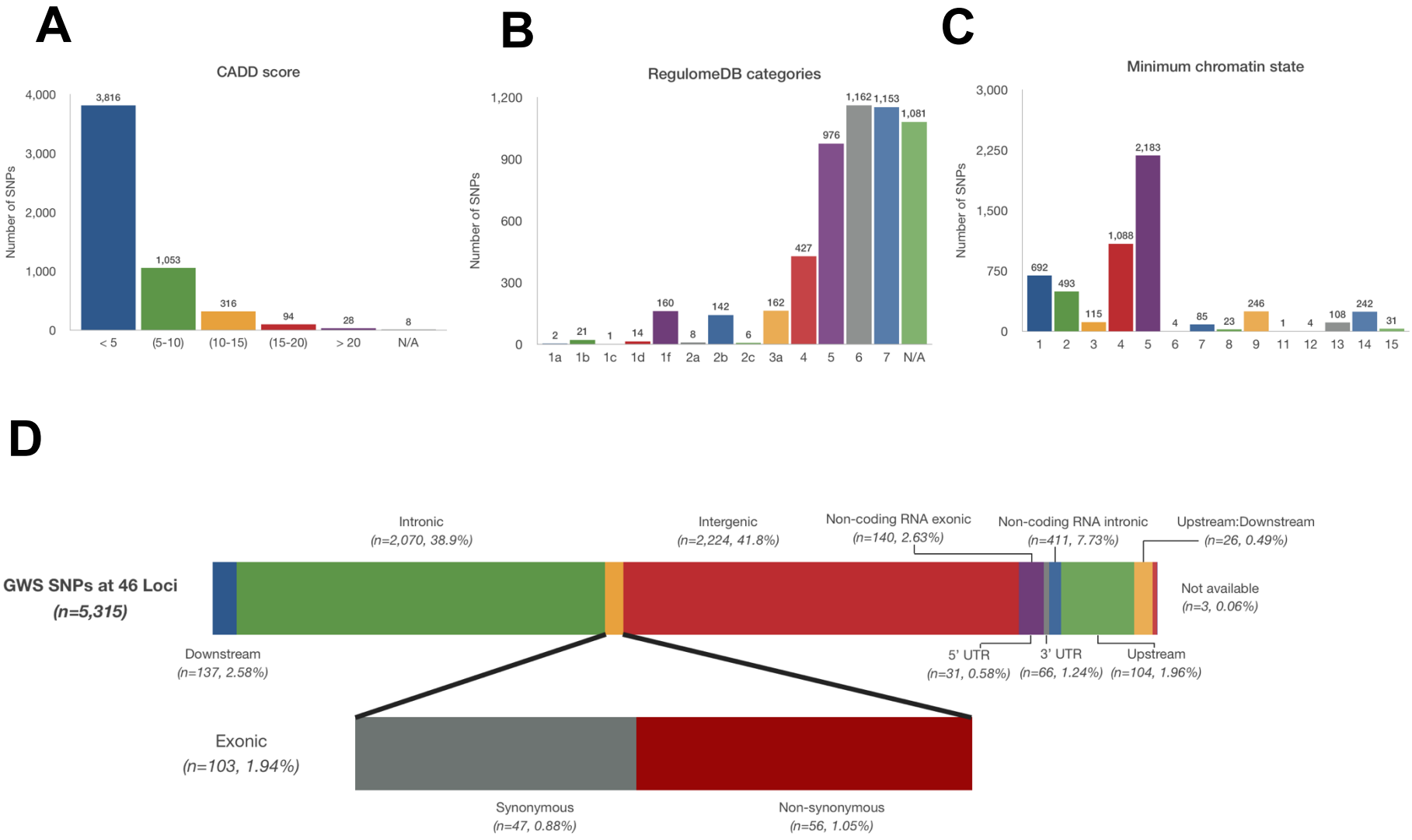

2.3.3. Gene mapping

204 putative genes were mapped to 38 replicated loci based on genomic proximity at these loci.[21] Eighty genes were prioritised based on their association with variants that are known to alter expression of these genes (eQTLs) within tibial artery tissue from the GTEx consortium v8.0[40] ($P_{eqtl} < 5\times10^{-8}$). Of these, 30 were *not* positionally mapped (i.e. they reside outside the 10kb positional proximity window). A genome-wide, gene-based association study (GWGAS) implemented in MAGMA v1.07[29] prioritised 248 protein-coding genes significantly associated with varicose veins at a Bonferroni-corrected P-value < 2.67×10^{-6}; of which, 117 lay within the confines of the replicated loci (**Figure 2.6**; **Figure 2.7**; **Appendix Table 2.4**).

Summary-based mendelian randomisation (SMR) analysis[30] was performed using eQTL data from GTEx v8[40] tibial artery tissue as an instrumental variable to test association between gene expression levels and varicose veins. SMR testing was performed across 4,946 probes with a cis-eQTL P < 5×10^{-8}; with the threshold for significance set at $P_{SMR} < 1.01\times10^{-5}$. Forty-four putative genes passed this stringent correction and were subsequently tested via a HEIDI analysis to exclude associations with varicose veins through linkage disequilibrium or co-localisation. Twenty-seven SMR-significant genes passed the HEIDI test ($P_{HEIDI} \geq 1.12\times10^{-3}$ (0.05/44)) (**Appendix Table 2.5**), 14 of which lay within the varicose veins susceptibility loci and therefore associated with varicose veins through pleiotropy.

In summary, 237 unique genes were mapped to 39 of 46 varicose vein susceptibility loci by at least one of the four mapping strategies, 61 of which were novel putative

genes (**Table 2.3**). Substantial overlap was found across the mapping strategies, with the majority of genes (54.9%, n = 130) being mapped by two or more approaches. Thirty-six genes were prioritised by three mapping approaches, and six genes (*ATF1, AP1M1, DNAH10OS, FBLN7, LBH, WDR92*) were mapped to the varicose veins susceptibility loci by all four mapping approaches (**Figure 2.8**).

Figure 2.6. MAGMA gene-based association study quantile-quantile plot. Quantile-Quantile (Q-Q) plot for the genome-wide, gene-based association test computed by MAGMA v1.07.[29]

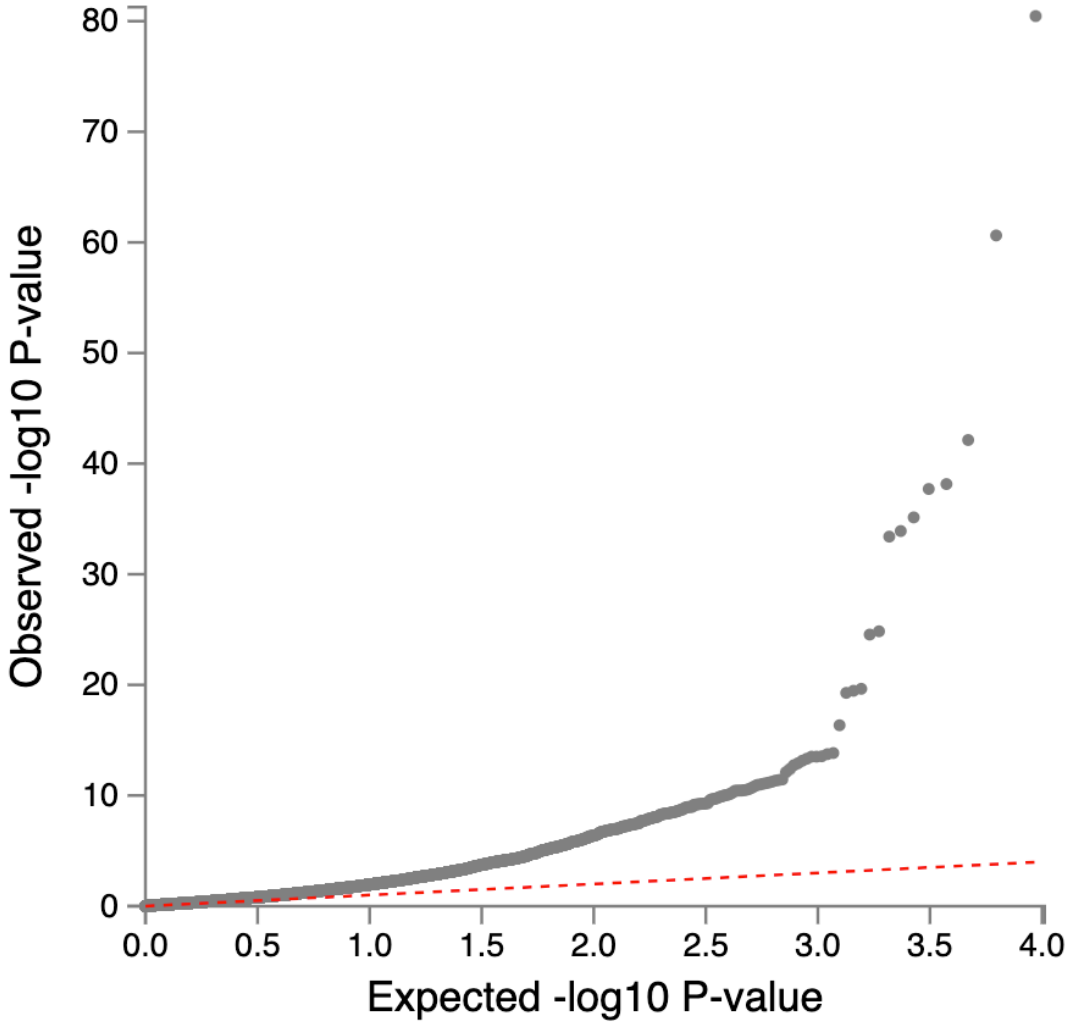

Figure 2.7. MAGMA genome-wide, gene-based association study Manhattan plot. Manhattan plot for the MAGMA GWGAS for varicose veins. The dotted red line indicates the threshold for genome-wide significance ($P < 2.68 \times 10^{-6}$). 248 genes reached genome-wide significance in this analysis, with the top-ten enriched MAGMA genes are annotated in the Manhattan plot.

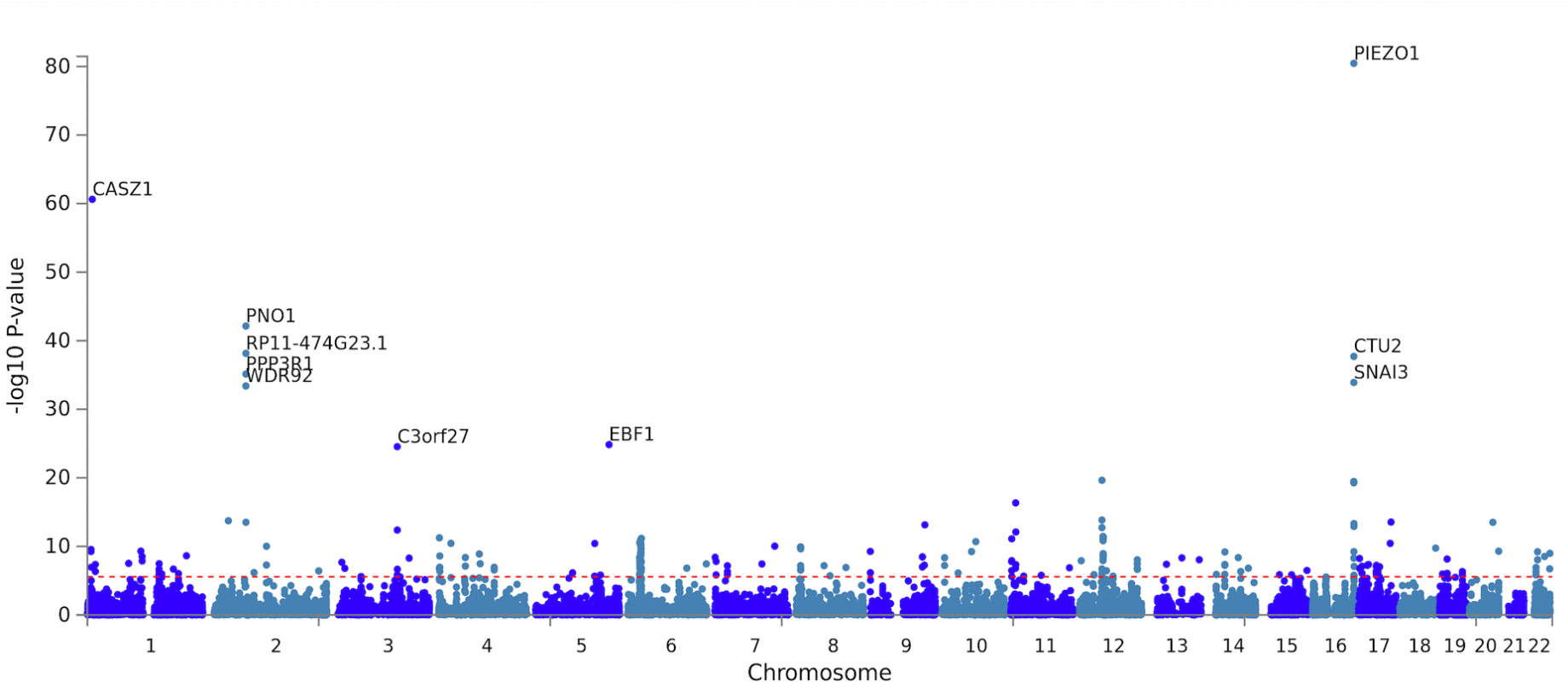

Figure 2.8. Venn diagram for the 237 genes prioritised at the varicose veins associated loci. 237 unique genes were mapped to thirty-nine of the 46 associated loci by one or more gene mapping strategies. 204 genes were mapped via positional mapping, 80 genes were mapped via eQTL mapping, 14 genes were mapped by SMR, and 117 genes were mapped by MAGMA. Overlap between the four different mapping strategies is shown in the Venn diagram. See **Appendix Table 2.6** for a complete list of all prioritised genes.

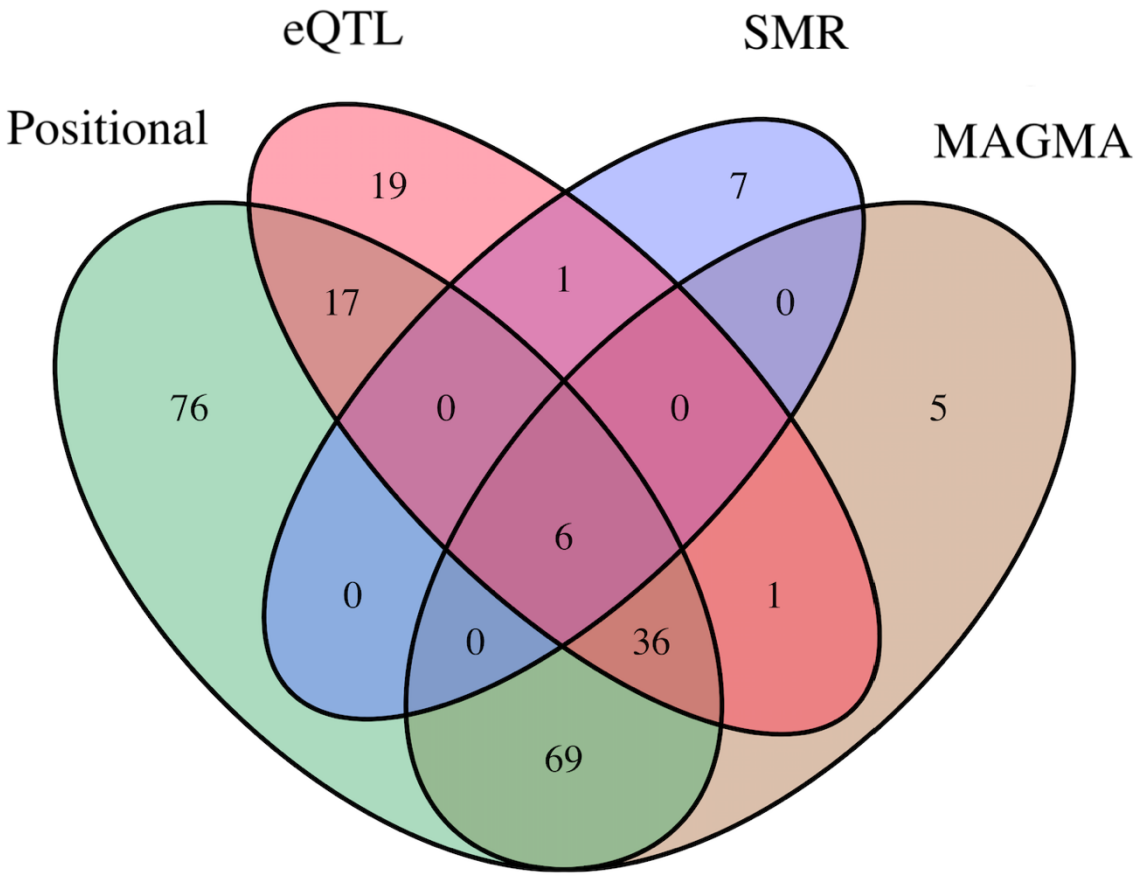

2.3.4. Gene set, pathway and tissue-specific enrichment

To delineate gene sets and enriched pathways at which the 237 prioritised genes converged, gene-set analysis was conducted in MAGMA v1.07.[29] Four Gene Ontology (GO) gene sets were significantly over-represented in the summary statistics: Cardiovascular Development ($P = 1.56\times10^{-8}$, n = 666); Tube Morphogenesis ($P = 9.35\times10^{-8}$, n =778); Blood Vessel Morphogenesis ($P = 9.39\times10^{-7}$, n = 555); and Tube Development ($P = 1.68\times10^{-6}$, n = 956) (**Appendix Table 2.7**). MAGMA[29] tissue-specific gene property analysis of 54 specific tissue types from the GTEx v8.0 consortium[40] demonstrated significant gene expression in all three vascular tissue types present in GTEx — Coronary Artery ($P = 6.23\times10^{-7}$, 2nd most enriched), Tibial Artery ($P = 1.05\times10^{-6}$, 3rd most enriched) and Aorta ($P = 3.92\times10^{-5}$, 8th most enriched) (**Figure 2.9-A**). MAGMA tissue enrichment within GTEx 30 general tissue types[40] also demonstrated blood vessel tissue to be highly enriched ($P = 3.8\times10^{-4}$, 3rd most enriched) (**Figure 2.9-B**). Next, performing enrichment analysis of the 237 prioritised genes within eXploring Genomic Relations (XGR),[32] six canonical pathways were significantly over-represented. This included genes in pathways pertaining to extracellular matrix biology, the VEGF and VEGFR signalling network, and intracellular Ca^{2+} signalling in the T-Cell Receptor (TCR) Pathway (**Table 2.4**).

Figure 2.9. MAGMA tissue expression analysis. MAGMA Tissue Expression Analysis of varicose veins GWAS-summary data, implemented in FUMA in A) 54 specific and B) 30 general tissue types. This analysis tests the relationship between highly expressed genes in a specific tissue and the genetic associations from the GWAS. Gene-property analysis is performed using average expression of genes per tissue type as a gene covariate. Gene expression values are log2 transformed average RPKM (Read Per Kilobase Per Million) per tissue type after winsorization at 50, and are based on GTEx v8 RNA-Seq data across 54 specific tissue types and 30 general tissue types. The dotted line indicates the Bonferroni-corrected α level, and the tissues that meet this significance threshold are highlighted in red.

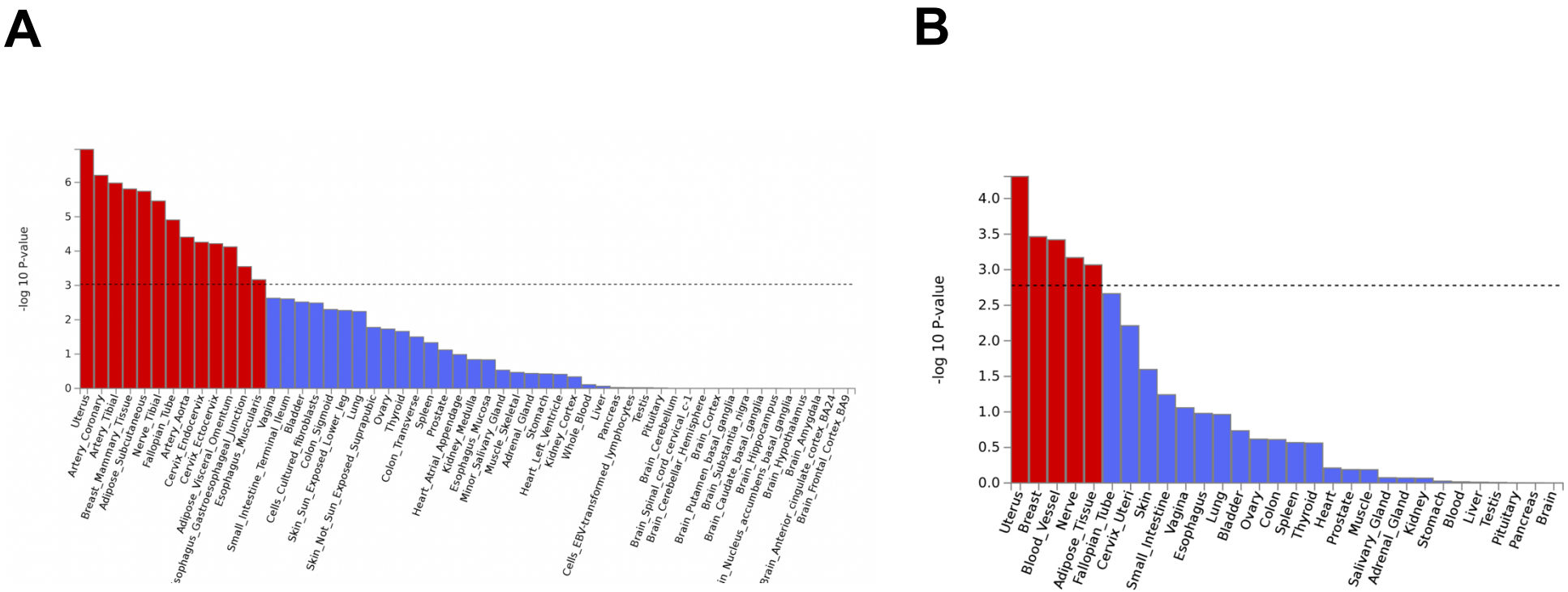

Table 2.4. Gene-based enrichment analysis for varicose veins associated genes in eXploring Genomic Relations (XGR).

Biological Process	Z-Score	P-Value	FDR	Number of overlapped genes	Genes
Alpha9 beta1 integrin signalling events	3.85	0.0012	0.032	*2*	*TNC, VEGFA*
Genes encoding structural ECM glycoproteins	3.39	0.0012	0.032	*6*	*EFEMP1, FBLN7, FBN2, IGFBP7, RSPO3, TNC*
Calcium signalling in the CD4+ TCR pathway	3.5	0.0019	0.032	*2*	*NFATC2, PPP3R1*
Ensemble of genes encoding core extracellular matrix including ECM glycoproteins, collagens and proteoglycans	3.11	0.0019	0.032	*7*	*COL27A1, EFEMP1, FBLN7, FBN2, IGFBP7, RSPO3, TNC*
Non-canonical WNT signalling pathway	3.29	0.0025	0.035	*2*	*MAPK10, NFATC2*
VEGF and VEGFR signalling network	3.11	0.0032	0.036	*1*	*VEGFA*

2.3.5 Genetic correlations with varicose veins associated phenotypes

The total contribution of common SNP variants to the varicose veins phenotype was calculated using LDSC Regression.[33] Using LD Scores from ~1.2 million variants found in European populations, the SNP-based heritability* (h^2g) for varicose veins in the discovery population was estimated to be 5.03% (S.E. = 0.30%). The h^2_g was found to be near-identical in the independent 23andMe cohort (h^2_g = 5.40%, S.E. = 0.30%).

Correlation testing between the polygenic architecture of varicose veins and 171 publicly available traits (nine trait categories) from the LDHub database[34] were calculated using LDSC regression.[33] Of the nine trait categories tested, two categories (anthropometric and autoimmune) contained traits that met the Bonferroni-corrected significance threshold (**Appendix Table 2.8**). All twelve significant traits positively correlated with varicose veins (**Figure 2.10**), eleven of which belonged to the anthropometric category (pertaining to height and weight phenotypes). In the autoimmune trait category, systemic lupus erythematosus was discovered to be correlated with varicose veins, demonstrating ~19% genetic overlap ($P = 4.2\times10^{-3}$, r_g = 0.195). Of note, Morris *et al.* previously found variant rs17321999-C at 2p23.1 to be associated with systemic lupus erythematosus ($P = 2.22\times10^{-16}$, OR = 0.83)[41], which is also significantly associated with varicose veins in the discovery analysis ($P = 3.20\times10^{-14}$, OR = 1.09), and is in high linkage with the lead SNP at locus 2p23.1, rs9967884 (r^2 = 0.87).

* i.e. the total phenotypic variance between the population attributable to the SNPs identified in this GWAS

Figure 2.10. Genetic correlation between varicose veins and other phenotypes from the LDHub Database. All twelve significant traits ($P < 5.56\times10^{-3}$) are positively correlated with varicose veins. The consortium and ethnicity for each study is provided in parentheses. *EGG, Early Growth Genetics Consortium; GIANT, Genetic Investigation of ANthropometric Traits Consortium ; Alkes, Alkes Group (Harvard T.H Chan School of Public Health); NA, Not Applicable. Eur, European ethnicity; Mi, Mixed ethnicity.*

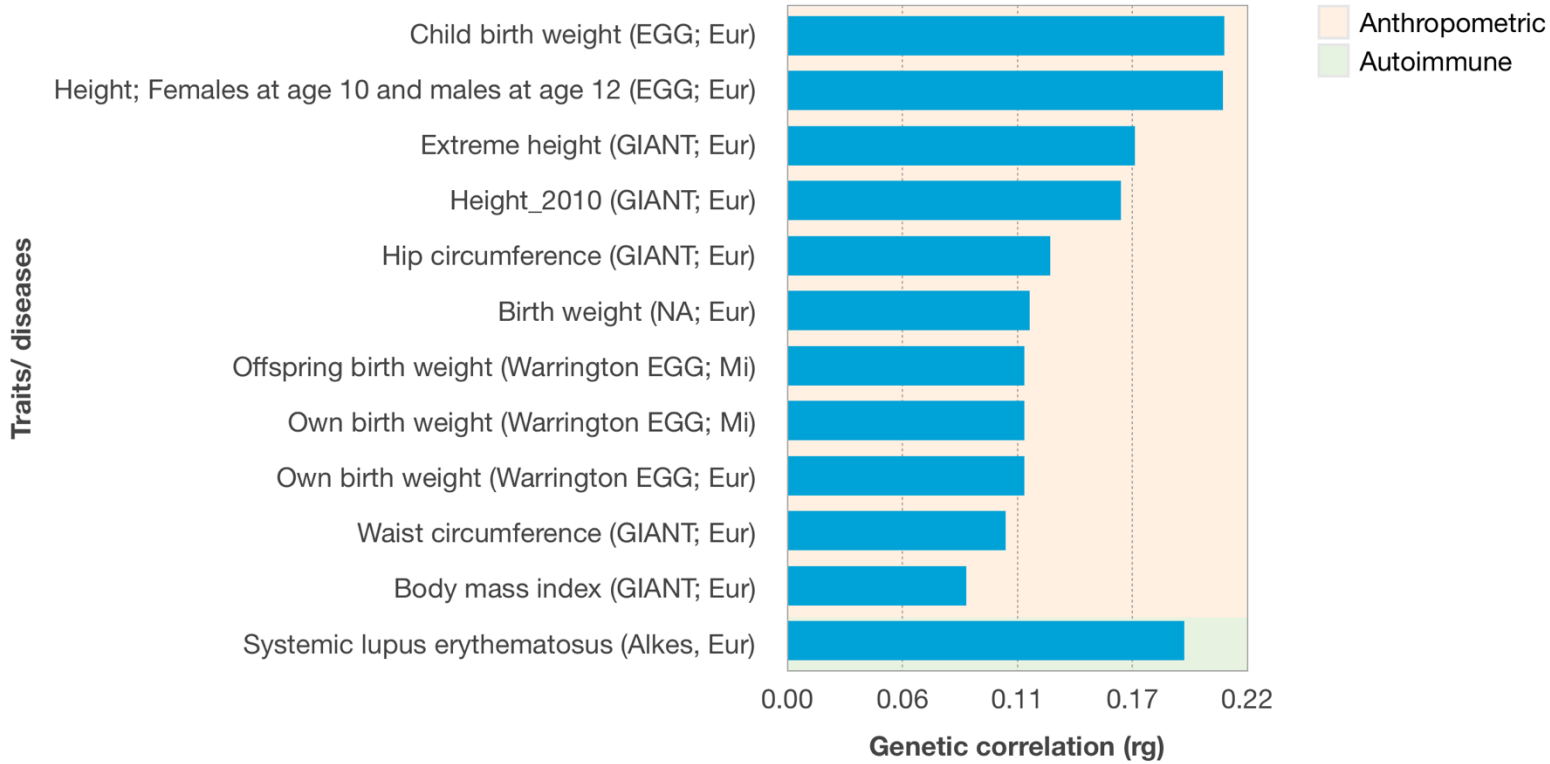

2.3.6. Drug target enrichment analysis

The Open Targets Platform investigated the potential for therapeutic targeting of the protein products of 200 of the 237 prioritised genes.[35] Forty-two therapeutic pathways reached nominal significance ($P < 5\times10^{-2}$), with the Butyrophillin family interactions pathway demonstrating top enrichment ($P = 2.6\times10^{-7}$, six drug targets), followed by the Calcineurin-NFAT pathway ($P= 9.4\times10^{-4}$, two targets), and the Transcriptional regulation by RUNX1 pathway (highest number of enriched targets (n = 14), $P = 1.6\times10^{-3}$) (**Appendix Table 2.9**). Pharmacological tractability data for 105 gene targets were available, with 65 predicted to be tractable to antibody targeting to a high confidence, and 26 genes predicted to be tractable to small molecule targeting (**Appendix Table 2.10**). Eight genes had the highest level of evidence as pharmacologically active targets, with known pharmaceutical interactions (*CDK10, COL27A1, GABBR1, KCNJ2, MAPK10, OPRL1, TNC and VEGFA*) (**Appendix Table 2.11**). This includes *VEGFA*, which is a target for several antibody, protein and oligosaccharide agents which are currently under phase two, three and four clinical trials (clinicaltrials.gov) for several ocular vascular disorders.

2.3.7. Genetic risk score for varicose veins

The 49 independent significant signals associated with varicose veins were used to calculate a weighted genetic risk score (wGRS) for all 401,667 participants in UK Biobank. As expected, the wGRS for varicose veins cases (5.179) was higher than in controls (4.986; $P = 9.90 \times 10^{-324}$). Moreover, varicose veins cases that had undergone surgery had a higher wGRS (5.185) compared to varicose veins cases that had not undergone a surgical procedure to manage their disease (5.076; $P = 2.46 \times 10^{-13}$). Varicose veins cases without ulceration (5.184) were found to have a higher wGRS than cases with ulceration (5.092; $P = 3.65 \times 10^{-5}$) (**Table 2.5**).

Table 2.5. Weighted genetic risk score for varicose veins in the UK Biobank cohort

Group	VVs cases	Controls	P-value†	VVs cases with operation code	VVs cases without operation code	P-value§	VVs cases with ulceration code	VVs cases without ulceration code	P-value±
N	22,473	379,183		21,407	1,066		596	21877	
Mean wGRS* (standard deviation)	5.179 (0.454)	4.986 (0.451)	9.90×10^{-324}	5.185 (0.453)	5.076 (0.468)	2.46×10^{-13}	5.092 (0.543)	5.184 (0.543)	3.65×10^{-5}

*VVs, Varicose veins. *wGRS: weighted genetic risk score. †Unpaired two-tailed t-test between VVs cases and controls. §Unpaired two-tailed t-test between VVs cases with an operation code and VVs cases without an operation code. ±Unpaired two-tailed t-test between VVs cases with an ulceration code and VVs cases without an ulceration code.*

2.4. Discussion

2.4.1. Summary

Varicose veins are a major national health burden, resulting in significant patient morbidity and large healthcare costs, with treatment restricted to surgical intervention and compounded by high recurrence. There is a growing need to understand the biology of varicose veins in order to guide new therapeutic approaches. The present study represents hitherto the largest and most comprehensive association analysis of varicose veins, involving 135,514 cases and 675,111 controls. The association study identified twenty-eight novel risk loci (29 novel signals), and independently replicated 18 of 29 previously reported (but non-replicated) loci (20 of 32 known signals). The suite of *in silico* analyses used provide robust evidence of functional variants in varicose veins-associated genomic regions. Moreover, strong enrichment for genes expressed in the extracellular matrix, immune cell signalling and circulatory system development was demonstrated in the pathway analyses. Of note, a new genetic correlation between the polygenic architecture of varicose veins and systemic lupus erythematosus was discovered. Several prioritised genes show potential for pharmacological targeting, and are currently under active study in other disease models. Finally, the weighted genetic risk score correlated with a more severe prognosis – a fundamental step in facilitating personalised medicine approaches to varicose veins.

The 46 risk loci contain genes that cluster into five functional categories: angiogenesis and lymphangiogenesis, smooth muscle cell biology, extracellular matrix regulation, the immune response, and apoptosis (**Appendix Table 2.12**).

2.4.2. Angiogenesis

Angiogenesis plays a central role in the development and maintenance of healthy veins. Disruption in normal angiogenic processes can lead to varicose veins[42], potentially because of a failure to develop properly-formed venous walls and valves, or to repair defects following vascular stress injury.

The analysis yielded a total of nine presumed angiogenesis-related varicose veins susceptibility loci, most interestingly rs11967262 at 6p21.1 ($P_{meta} = 1.45\times10^{-19}$, OR = 1.09), which resides in an intergenic region ~7kb upstream of vascular endothelial growth factor A (*VEGFA*). VEGFA is a critical regulator of angiogenesis, and is fundamental to conserving the integrity and functionality of the vessel wall.[43] Binding to its receptor VEGR2, VEGFA functions as a selective endothelial mitogen, inducing endothelial cell proliferation, migration and differentiation. Hypoxia and mechanical stretch are key inducers of VEGFR2 expression via activation of the HIF pathway, which itself has been implicated in varicose veins.[44] VEGFA and VEGFR2 expression are considerably heightened in varicose vein walls compared to normal vein, especially in varicose veins complicated by thrombophlebitis.[45] VEGFA also functions as a potent vascular permeability factor[46], which is posited to lead to varicose vein progression and complications via fenestration of the endothelium.[47] The increased microvascular permeability may therefore be an important feature in the progression of varicose veins to chronic venous insufficiency (oedema and venous ulceration).[47] Plasma levels of VEGFA have also been shown to be significantly amplified in varicose veins patients.[48] VEGFA may therefore be implicated in the pathogenesis of varicose veins via its vasodilatory effects, which are thought to decrease vessel tone and lead

to stasis, as well as oxygen free radical release, causing weakness of the vessel wall.[47] VEGFA intriguingly also promotes inflammation via expression of vascular and intracellular adhesion molecules on endothelial cells, connecting angiogenesis to immune dysfunction.[49]

Furthermore, rs2713575 ($P_{meta} = 1.82\times10^{-36}$, OR = 1.12) at 3q21.3 lies in an intronic region near *GATA2*. *GATA2* is a haematopoietic transcription factor necessary for vascular integrity that acts downstream of VEGF, and has been demonstrated to regulate VEGF-induced angiogenesis and lymphangiogenesis.[50] The VEGF axis may therefore be a promising candidate for therapeutic targeting in the treatment of varicose veins. To this end, several anti-VEGFA agents were enriched in our drug-target enrichment analysis, and are currently being investigated in randomised trials for the treatment of several proliferative retinopathies and retinal vein occlusion.

2.4.3. Lymphangiogenesis

Positional and MAGMA mapping highlighted genes at four loci relating to lymphangiogenesis. Indeed, the lymphatic system develops from veins, and its function is intimately linked to the venous circulation, draining extracellular fluid back into circulation. It is therefore feasible that similar genetic defects may result in either lymphoedema, varicose veins, or a combination of the two conditions. rs340875, (P_{meta} = 4.22×10^{-20}, OR = 1.09) is ~2kb upstream of *PROX1*, a master inducer gene necessary for the development of lymphatic vasculature.[51] PROX1 knock-out mice are deficient of lymphatic vasculature.[52] Of significance, during developmental lymphangiogenesis, *PROX1* has been shown to be necessary for the formation of lymphovenous valves.[53,54] This suggests that PROX1 dysfunction may predispose to varicose vein development by causing defects in venous valves. Furthermore, PROX1 is co-expressed and functions alongside the transcription factor FOXC2 in lymphatic valve forming cells at the earliest stage of lymphatic development.[55] Mutations in *FOXC2* cause hereditary lymphoedema-distichiasis, a disease which is characterised by varicose veins and peripheral lymphoedema – highlighting genetic overlap between the two disorders.[56] Previous twin studies have demonstrated linkage of the FOXC2 region with varicose veins[57,58], however the present study did not yield evidence of association between varicose veins and *FOXC2*.

2.4.4. Extracellular matrix regulation

Varicose veins show deposition of extracellular matrix (ECM) in the perivascular space – possibly a compensatory mechanism to buttress an already weakened wall.[59] Moreover, intimal hypertrophy and an increased vessel diameter (characteristic features of ECM disruption) are also seen in varicose veins.[60] This luminal dilatation in varicose veins, alongside valve ring enlargement, is thought to compromise the ability of venous valves to co-apt, compounding venous reflux and leading to stasis and venous hypertension.[4] Of note, a marked imbalance of the structural ECM proteins, collagen and elastin is seen in varicose veins, with a preponderance of collagen compared to normal veins.[61] Redundancy in the connective tissue components of the valves or venous wall may therefore predispose to varicose veins pathology.

The prioritised genes significantly overlapped with canonical pathways relating to ECM components, including Collagen Type XXVII Alpha 1 Chain (*COL27A1*), EGF-containing Fibulin-like Extracellular Matrix Protein 1 (*EFEMP1)* and Fibulin-7 (*FBLN7*).

rs753085 ($P = 2.17\times10^{-11}$, OR = 1.07) resides within an intronic region of Collagen Type XXVII Alpha 1 Chain (*COL27A1*). COL27A1 is a fibrillar collagen in the extracellular matrices of several tissues, including blood vessels.[62] Diminished expression of *COL27A1* has been demonstrated in varicose vein samples.[63] The drug enrichment analysis demonstrated the potential candidacy of COL27A1 as a therapeutic target for varicose vein prevention or treatment, with multiple pharmaceutical agents currently being investigated in several clinical trials.

Another lead signal, rs4849044, lies in an intronic region of *FBLN7* at 2q13 (P_{meta} = 1.98×10^{-14}, OR = 1.07). Fibulins are secreted glycoproteins that stabilise the ECM and are expressed in matrices, elastic fibres and basement membranes.[64] FBLN7 is a cell adhesion molecule that interacts with extracellular matrix proteins, and is highly expressed in blood vessels. The C-terminal fragment of FBLN7 (FBLN7-C) demonstrates anti-angiogenic activity, binding to venous endothelium and disrupting tube formation and vessel sprouting.[65] Of note, *FBLN7* was mapped to the 2q13 locus by all four mapping strategies, and contains eQTL variants which associate *FBLN7* to varicose veins through pleiotropy in the SMR analysis, demonstrating its candidacy as a potential functional player in varicose veins biology.

My study replicated the previously reported association between rs3791679 and varicose veins ($P = 1.59\times10^{-13}$, OR = 1.08), mapped to *EFEMP1*.[66] *EFEMP1* encodes another member of the fibulin family, fibulin-3[67], which is highly expressed in venous endothelia. Fibulin-3 antagonises vascular development through its effect on decreasing expression of the matrix metalloproteinases, MMP2 and MMP3, and increasing expression of MMP inhibitors (TIMPs) in endothelial tissue.[68] To this end, varicose veins have been found to demonstrate a characteristic reduction in expression of MMP2, and heightened expression of TIMP1 and MMP1 protein levels within the saphenofemoral junction.[69] Altered expression of these enzymes may therefore precipitate inherent weakness in the vein wall, predisposing patients to varicose veins. rs3791679 is a notable polymorphism at this locus, with 45 associations across 12 traits, including carpal tunnel syndrome, joint hypermobility, and several anthropometric measures of BMI and height (which have been previously

associated with varicose veins in epidemiological studies).[11,70,71] Consistently, the LDSC genetic correlation analysis demonstrated striking genetic overlap between varicose veins and height and weight phenotypes. Moreover, the drug enrichment analysis identified fibulin-3 to be tractable to antibody targeting with high confidence, and metformin has been previously demonstrated to perturb fibulin-3 levels through inhibition at the transcriptional level.[72] Fibulin-3 therefore necessitates further study as a potential therapeutic target for varicose veins.

2.4.5. Immune response

Heightened expression of inflammatory mediators has been observed in varicose veins compared to normal veins.[4] Specifically, varicose vein walls show increased mast cells, monocytes and macrophages compared to normal veins.[4] Chronic inflammation in the vein wall has therefore been postulated to be a key feature of varicose vein biology.[60]

The association analysis defined five inflammation-associated risk loci, in particular rs78216177 ($P_{meta} = 5.80\times10^{-14}$, OR = 1.10), which lies in an intron of *DOCK8*. *DOCK8* plays a significant role in the innate and adaptive immune systems, with *DOCK8* deletion strongly associated with Hyper-IgE syndrome, a type of primary immunodeficiency that affects multiple systems including the vasculature.[73] Indeed, vascular abnormalities in hyper-IgE syndrome include arterial dilating pathology, aneurysmal changes, and abnormalities in great vessels. These occur in a different vascular territory to varicose veins, and are thought to have overlapping pathological features.

Using publicly available GWAS data, a substantial genetic overlap between varicose veins and systemic lupus erythematosus was discovered. Lead variant rs1471251 ($P = 8.33\times10^{-11}$, OR = 1.06) is an eQTL of *AFF1,* and has been associated with systemic lupus erythematosus.[74] Supporting this shared polygenic architecture, the C allele of SNP variant rs17321999, which associates significantly with varicose veins, also increases the risk of systemic lupus.[41]

Canonical pathway analysis within XGR demonstrated enrichment for *Intracellular calcium signalling in the CD4+ T-Cell Receptor (TCR) pathway* ($P = 1.9\times10^{-3}$, $Z = 3.5$), specifically highlighting Nuclear Factor of Activated T-Cells, Cytoplasmic, Calcineurin-Dependent 2 (*NFATC2*) and Protein Phosphatase 3 Regulatory Subunit B, Alpha (*PPP3R1*) which are closely involved in this pathway. Two significant signals were discovered at: i) 20q13.2 – an intronic region of *NFATC2* (rs3787184 ($P_{meta} = 2.51\times10^{-36}$, OR = 1.16)) and ii) 2p14 – an intergenic region ~19kb upstream of *PPP3R1* (rs2861819 ($P_{meta} = 2.65\times10^{-77}$, OR = 1.20)). *PPP3R1* encodes Calcineurin subunit B type 1, a Ca^{2+} influx-induced serine/threonine-specific phosphatase, which, alongside NFAT transcription factors, regulates the activation of native T-Cells.[75] Varicose veins are characterised by clustering and infiltration of T lymphocytes[59], which are distributed proximate to the venous valve agger*.[76] Therefore, altered calcium signalling in T-Cells through aberrant *PPP3R1* and *NFATC2* signalling may be involved in the valvular pathology depicted in varicose veins.

* a fibroelastic structure located at the base of venous valves where media meets adventitia

2.4.6. Vascular smooth muscle cell proliferation and migration

Varicose vein walls demonstrate a pathologically altered phenotype defined by vein wall remodelling, consisting of vascular smooth muscle cell (vSMC) hypertrophy, proliferation and migration into intima.[77–79] VSMCs in varicose veins are disarranged and undergo de-differentiation from a contractile to a synthetic phenotype. These changes impair the normal contractile function of SMCs in varicose vein tissue.[78,79] My study implicates for the first time in GWAS, genes that might be intimately involved in this process.

Six loci related to vSMC proliferation and migration were identified, most notably rs7518191 at 1p13.2 (P_{meta} = 6.90×10^{-14}, OR = 1.07) which lies in an intron of Tetraspanin 2 (*TSPAN2*), and is an eQTL for *TSPAN2* in several tissues, including tibial artery (P_{eQTL} = 1.3×10^{-6}). Tetraspanins are expressed at cell surfaces where they function in cell adhesion, cell migration, proliferation and differentiation.[80] *TSPAN2* is selectively enriched in vSMCs within blood vessels; its expression is closely associated with vSMC differentiation.[80] However, *TSPAN2* expression is inhibited when the vSMC undergoes phenotypic modulation in diseased human vessel, which could perhaps lead to the vSMC de-differentiation and migration observed in varicose veins.[81,82]

2.4.7. Apoptosis

Varicose veins demonstrate a significantly reduced expression of components in the intrinsic apoptotic pathway, specifically of bax and Caspase 9.[59] Furthermore, reduction in *Cyclin-D1* and over-expression of *BCL2* has also been demonstrated in the media and intima of varicose veins compared to normal tissue.[83] De-differentiation of vSMC away from a contractile phenotype in varicose veins is thought to be caused by, or at least exacerbated by, disruption in apoptosis.[83,84] Apoptosis may therefore be a contributory factor in the pathogenesis of varicose veins.

The GWAS identified two novel apoptosis-related loci. rs7308356 ($P_{meta} = 3.02\times10^{-20}$, OR = 1.09) is in a highly conserved intronic region within Ceramide Synthase 5 (*CERS5*), where it is a known eQTL for CERS5.[85] Ceramides are a key group of enzymes which are involved in cell death, differentiation and senescence.[86,87] *CERS5* overexpression facilitates apoptosis and autophagy, and it is overexpressed in several tumours, including colorectal and colon cancers.[88] Inhibition of CERS5 could prevent the normal apoptotic response of damaged endothelium following vascular injury.

rs72683923 ($P = 3.62\times10^{-14}$, OR = 1.28), is an exonic synonymous SNP in cyclin-dependent kinase-like 1 (CDKL1), which interacts with cyclin to regulate cell cycle, differentiation and apoptosis[89]. CDKL1 disruption inhibits cell proliferation, promoting apoptosis in breast cancer and melanoma. Further, *in vitro* knockout of CDKL1 suppresses cell proliferation and promotes apoptosis.[90] Therefore, one can postulate that decreased CDKL1 activity in endothelial cells may lead to increased apoptosis and predispose to varicose veins development.

2.4.8. Genetic risk score

In the USA, over two million participants have advanced chronic venous disease[91], and around half a million require invasive surgical procedures annually. The weighted genetic risk score derived from the replicated signals was found to correlate with disease severity, with varicose veins cases managed surgically possessing a higher genetic burden than those managed non-surgically. This finding suggests that those who were *phenotypically* severe were also *genotypically* more susceptible. This represents a proof-of-principle, demonstrating the feasibility for data-driven prognostication in enabling the identification of varicose veins cases that are more likely to require surgical intervention. This could foreseeably guide medical and surgical management, such as the use of early preventive approaches in high risk participants; these might include prophylactic compression stockings or early ablation procedures to mitigate risk of venous ulceration. Indeed, the efficacy of early endovenous ablation in improving outcomes of venous leg ulcers has been shown.[92] However, among cases with ulceration, the wGRS did not correlate with severity, suggesting i) other variants not identified in this study may be involved in ulceration risk, ii) ulceration may be less sensitive to genetic contributions and more a product of non-genetic risk factors (such as orthostatic professions), or iii) this part of the study was underpowered to detect ulceration-specific loci, given there were only 596 cases with ulceration (2.65% of overall cases).

2.4.9 Strengths and limitations

Several limitations of the present study must be recognised. Firstly, while the discovery cohort in UK Biobank used a combination of hospital diagnostic, operative and self-report codes, varicose veins cases in the 23andMe cohort were defined *solely* by self-report codes, meaning that the phenotyping for the replication study was necessarily less stringent. Moreover, instead of performing a formal meta-analysis between the discovery and replication GWAS, the association of only the 118 independent lead GWS SNPs from the UK Biobank cohort were independently tested. Thus, sub-threshold signals in the discovery analysis that may have reached significance in the replication GWAS, or under meta-analysis, were not identified. Finally, the unavailability of the full summary statistics for the replication GWAS restricted our *in silico* analyses to the summary statistics from the discovery GWAS alone.

However, several strengths go in some way to lend credence to the study findings. The present study was performed in a total of 135,514 cases and 675,111 controls, representing the largest association study of varicose veins by a substantial margin. Moreover, the false positive rate was rigidly controlled by reporting only the loci that were associated in the discovery cohort at genome-wide levels of significance *and* that subsequently replicated in 23andMe, hence the 49 variants reported here are likely to represent true signals. This notion is substantiated by the fact that the associated loci mapped to a plethora of biologically plausible genes, which show clustering across several connected pathways. This study represents a fundamental step in the use of genetic risk scoring in enabling better prognostication and decision-making in the management of varicose veins.

In this study, the inclusion of operative codes for phenotyping in the UK Biobank discovery cohort enabled a considerably larger number of cases to be identified than a previous GWAS that also used the UK Biobank resource but relied solely on ICD diagnostic codes (22,473 cases vs 9,577 cases).[5] As a fundamental principle of case ascertainment in surgical diseases, it is necessary to identify participants that have undergone surgery for a disease: given the inevitable risk of complications, surgery is generally reserved for participants at the phenotypically severe end of the disease that may have failed non-surgical treatment. The weighted genetic risk score demonstrates that varicose veins cases that had undergone surgery were also, on the whole, genotypically more severe. This finding lends further validity to the forty-nine identified signals.

2.5. Conclusion

This chapter presents the largest association study of varicose veins, a common disease associated with significant patient morbidity, reduced quality-of-life, and high socioeconomic burden. Forty-nine variants at 46 susceptibility loci were discovered to associate with varicose veins, with associated genomic regions mapped to new genes and pathways that are involved in angiogenesis, lymphangiogenesis, extracellular matrix regulation, inflammation, vascular smooth muscle cell activity, and apoptosis. Identified genes and pathways demonstrate striking representation along biologically viable pathways, suggesting they are eminently plausible contributors to the pathogenesis of varicose veins. A number of genes represent promising candidates for further investigation of venous biology. Notably, *VEGFA*, *COL27A1*, *EFEMP1*, *PPP3R1* and *NFATC2* represent probable 'key players' as potential therapeutic targets in the treatment of varicose veins. Lastly, the demonstration that genetic risk score correlates with disease severity represents a fundamental step towards improved prognostication of varicose veins patients.

2.6. Chapter References

1 Laing W. Chronic Venous Diseases of the Leg. Off. Heal. Econ. London. 1992. https://www.ohe.org/publications/chronic-venous-diseases-leg (accessed Jan 1, 2020).

2 O'Donnell TF, Balk EM, Dermody M, Tangney E, Iafrati MD. Recurrence of varicose veins after endovenous ablation of the great saphenous vein in randomized trials. J. Vasc. Surg. Venous Lymphat. Disord. 2016; **4**: 97–105.

3 Scott TE, LaMorte WW, Gorin DR MJ. Risk factors for chronic venous insufficiency: a dual case-control study. *J Vasc Surg* 1995; **22**: 622–8.

4 Lim CS, Davies AH. Pathogenesis of primary varicose veins. *Br J Surg* 2009; **96**: 1231–42.

5 Fukaya E et al. Clinical and Genetic Determinants of Varicose Veins. *Circulation* 2018; : 1–12.

6 Shadrina AS, Sharapov SZ, Shashkova TI, Tsepilov YA. Varicose veins of lower extremities: Insights from the first large-scale genetic study. *PLoS Genet* 2019; **15**: e1008110.

7 Ellinghaus E, Ellinghaus D, Krusche P, *et al.* Genome-wide association analysis for chronic venous disease identifies EFEMP1 and KCNH8 as susceptibility loci. *Sci Rep* 2017; **7**. DOI:10.1038/srep45652.

8 Allen NE, Sudlow C, Peakman T, Collins R. UK biobank data: Come and get it. Sci. Transl. Med. 2014; **6**. DOI:10.1126/scitranslmed.3008601.

9 Bycroft C, Freeman C, Petkova D, *et al.* The UK Biobank resource with deep phenotyping and genomic data. *Nature* 2018; **562**: 203–9.

10 Sudlow C, Gallacher J, Allen N, *et al.* UK Biobank: An Open Access Resource

for Identifying the Causes of a Wide Range of Complex Diseases of Middle and Old Age. *PLoS Med* 2015; **12**. DOI:10.1371/journal.pmed.1001779.

11 Wiberg A, Ng M, Schmid AB, *et al.* A genome-wide association analysis identifies 16 novel susceptibility loci for carpal tunnel syndrome. *Nat Commun* 2019; **10**: 1–12.

12 Loh PR, Tucker G, Bulik-Sullivan BK, *et al.* Efficient Bayesian mixed-model analysis increases association power in large cohorts. *Nat Genet* 2015; **47**: 284–90.

13 Durand EY, Do CB, Mountain JL, Macpherson JM. Ancestry Composition: A Novel, Efficient Pipeline for Ancestry Deconvolution. *bioRxiv* 2014; : 010512.

14 Auton A, Abecasis GR, Altshuler DM, *et al.* A global reference for human genetic variation. Nature. 2015; **526**: 68–74.

15 O'Connell J, Sharp K, Shrine N, *et al.* Haplotype estimation for biobank-scale data sets. *Nat Genet* 2016; **48**: 817–20.

16 Walter K, Min JL, Huang J, *et al.* The UK10K project identifies rare variants in health and disease. *Nature* 2015; **526**: 82–9.

17 Browning SR, Browning BL. Rapid and accurate haplotype phasing and missing-data inference for whole-genome association studies by use of localized haplotype clustering. *Am J Hum Genet* 2007; **81**: 1084–97.

18 Loh PR, Palamara PF, Price AL. Fast and accurate long-range phasing in a UK Biobank cohort. *Nat Genet* 2016; **48**: 811–6.

19 Das S, Forer L, Schönherr S, *et al.* Next-generation genotype imputation service and methods. *Nat Genet* 2016; **48**: 1284–7.

20 Mägi R, Morris AP. GWAMA: Software for genome-wide association meta-analysis. *BMC Bioinformatics* 2010; **11**. DOI:10.1186/1471-2105-11-288.

21 Watanabe K, Taskesen E, Van Bochoven A, Posthuma D. Functional mapping and annotation of genetic associations with FUMA. *Nat Commun* 2017; **8**: 1–10.

22 D. W, J. M, J. M, *et al.* The NHGRI GWAS Catalog, a curated resource of SNP-trait associations. *Nucleic Acids Res*; **42**: D1001–6.

23 Wang KLMHH. ANNOVAR: functional annotation of genetic variants from high-throughput sequencing data. *Nucleic Acids Res* 2010; **38**: e164.

24 Boyle AP, Hong EL, Hariharan M, *et al.* Annotation of functional variation in personal genomes using RegulomeDB. *Genome Res* 2012; **22**: 1790–7.

25 Rentzsch P, Witten D, Cooper GM, Shendure J, Kircher M. CADD: predicting the deleteriousness of variants throughout the human genome. *Nucleic Acids Res* 2018; **47**: D886–94.

26 Ernst J, Kellis M. Chromatin-state discovery and genome annotation with ChromHMM. *Nat Protoc* 2017; **12**: 2478–92.

27 Kircher M, Witten DM, Jain P, O'roak BJ, Cooper GM, Shendure J. A general framework for estimating the relative pathogenicity of human genetic variants. *Nat Genet* 2014; **46**: 310–5.

28 Cunningham F, Achuthan P, Akanni W, *et al.* Ensembl 2019. *Nucleic Acids Res* 2019; **47**: D745–51.

29 de Leeuw CA, Mooij JM, Heskes T, Posthuma D. MAGMA: Generalized Gene-Set Analysis of GWAS Data. *PLoS Comput Biol* 2015; **11**: 1–20.

30 Zhu Z, Zhang F, Hu H, *et al.* Integration of summary data from GWAS and eQTL studies predicts complex trait gene targets. *Nat Genet* 2016; **48**: 481–7.

31 Liberzon A, Birger C, Thorvaldsdóttir H, Ghandi M, Mesirov JP, Tamayo P. The Molecular Signatures Database Hallmark Gene Set Collection. *Cell Syst* 2015; **1**: 417–25.

32 Fang H, Knezevic B, Burnham KL, Knight JC. XGR software for enhanced interpretation of genomic summary data, illustrated by application to immunological traits. *Genome Med* 2016; **8**: 1–20.

33 Bulik-Sullivan B, Loh PR, Finucane HK, *et al.* LD score regression distinguishes confounding from polygenicity in genome-wide association studies. *Nat Genet* 2015; **47**: 291–5.

34 Zheng J, Erzurumluoglu AM, Elsworth BL, *et al.* LD Hub: A centralized database and web interface to perform LD score regression that maximizes the potential of summary level GWAS data for SNP heritability and genetic correlation analysis. *Bioinformatics* 2017; **33**: 272–9.

35 Carvalho-Silva D, Pierleoni A, Pignatelli M, *et al.* Open Targets Platform: new developments and updates two years on. *Nucleic Acids Res* 2019; **47**: D1056–65.

36 De Jager PL, Chibnik LB, Cui J, *et al.* Integration of genetic risk factors into a clinical algorithm for multiple sclerosis susceptibility: a weighted genetic risk score. *Lancet Neurol* 2009; **8**: 1111–9.

37 Ng PC, Henikoff S. SIFT: predicting amino acid changes that affect protein function. *Nucleic Acids Res* 2003; **31**: 3812–4.

38 Adzhubei IA, Schmidt S, Peshkin L, *et al.* A method and server for predicting damaging missense mutations. Nat. Methods. 2010; **7**: 248–9.

39 Lukacs V, Mathur J, Mao R, *et al.* Impaired PIEZO1 function in patients with a novel autosomal recessive congenital lymphatic dysplasia. *Nat Commun* 2015; **6**: 1–7.

40 Aguet F, Brown AA, Castel SE, *et al.* Genetic effects on gene expression across human tissues. *Nature* 2017; **550**: 204–13.

41 Morris DL, Sheng Y, Zhang Y, *et al.* Genome-wide association meta-analysis in Chinese and European individuals identifies ten new loci associated with systemic lupus erythematosus. *Nat Genet* 2016; **48**: 940–6.

42 Chang MY, Chiang PT, Chung YC, *et al.* Apoptosis and Angiogenesis in Varicose Veins Using Gene Expression Profiling. *Fooyin J Heal Sci* 2009; **1**: 85–91.

43 Ferrara N. Molecular and biological properties of vascular endothelial growth factor. J. Mol. Med. 1999; **77**: 527–43.

44 Lim CS, Kiriakidis S, Sandison A, Paleolog EM, Davies AH. Hypoxia-inducible factor pathway and diseases of the vascular wall. J. Vasc. Surg. 2013; **58**: 219–30.

45 Kowalewski R, Małkowski A, Sobolewski K, Gacko M. Vascular endothelial growth factor and its receptors in the varicose vein wall Czynnik wzrostu śródbłonka naczyniowego i jego receptory w ścianie żylaków kończyn. 2011.

46 Esser S, Wolburg K, Wolburg H, Breier G, Kurzchalia T, Risau W. Vascular endothelial growth factor induces endothelial fenestrations in vitro. *J Cell Biol* 1998; **140**: 947–59.

47 Hollingsworth SJ, Powell GL, Barker SGE, Cooper DG. Primary varicose veins: Altered transcription of VEGF and its receptors (KDR, flt-1, soluble flt-1) with sapheno-femoral junction incompetence. *Eur J Vasc Endovasc Surg* 2004; **27**: 259–68.

48 Howlader MH, Coleridge Smith PD. Relationship of plasma vascular endothelial growth factor to CEAP clinical stage and symptoms in patients with chronic venous disease. *Eur J Vasc Endovasc Surg* 2004; **27**: 89–93.

49 Kim I, Moon SO, Kim SH, Kim HJ, Koh YS, Koh GY. Vascular Endothelial

Growth Factor Expression of Intercellular Adhesion Molecule 1 (ICAM-1), Vascular Cell Adhesion Molecule 1 (VCAM-1), and E-selectin through Nuclear Factor-κB Activation in Endothelial Cells. *J Biol Chem* 2001; **276**: 7614–20.

50 Spinner MA, Sanchez LA, Hsu AP, *et al.* GATA2 deficiency: A protean disorder of hematopoiesis, lymphatics, and immunity. *Blood* 2014; **123**: 809–21.

51 Harvey NL, Srinivasan RS, Dillard ME, *et al.* Lymphatic vascular defects promoted by Prox1 haploinsufficiency cause adult-onset obesity. *Nat Genet* 2005; **37**: 1072–81.

52 Wigle JT, Oliver G. Prox1 function is required for the development of the murine lymphatic system. *Cell* 1999; **98**: 769–78.

53 Bazigou E, Lyons OTA, Smith A, *et al.* Genes regulating lymphangiogenesis control venous valve formation and maintenance in mice. *J Clin Invest* 2011; **121**: 2984–92.

54 Sathish Srinivasan R, Oliver G. Prox1 dosage controls the number of lymphatic endothelial cell progenitors and the formation of the lymphovenous valves. *Genes Dev* 2011; **25**: 2187–97.

55 Sabine A, Agalarov Y, Maby-ElHajjami H, *et al.* Mechanotransduction, PROX1, and FOXC2 Cooperate to Control Connexin37 and Calcineurin during Lymphatic-Valve Formation. *Dev Cell* 2012; **22**: 430–45.

56 Fang J, Dagenais SL, Erickson RP, *et al.* Mutations in FOXC2 (MFH-1), a forkhead family transcription factor, are responsible for the hereditary lymphedema-distichiasis syndrome. *Am J Hum Genet* 2000; **67**: 1382–8.

57 Serra R, Buffone G, De Franciscis A, *et al.* A genetic study of chronic venous insufficiency. *Ann Vasc Surg* 2012; **26**: 636–42.

58 Mellor RH, Brice G, Stanton AWB, *et al.* Mutations in FOXC2 Are Strongly

Associated With Primary Valve Failure in Veins of the Lower Limb. 2007; : 1912–21.

59 Segiet OA, Brzozowa-Zasada M, Piecuch A, Dudek D, Reichman-Warmusz E, Wojnicz R. Biomolecular mechanisms in varicose veins development. *Ann Vasc Surg* 2015; **29**: 377–84.

60 Oklu R, Habito R, Mayr M, *et al.* Pathogenesis of varicose veins. *J Vasc Interv Radiol* 2012; **23**: 33–9.

61 Gandhi RH, Irizarry E, Nackman GB, Halpern VJ, Mulcare RJ, Tilson MD. Analysis of the connective tissue matrix and proteolytic activity of primary varicose veins. *J Vasc Surg* 1993; **18**: 814–20.

62 Pace JM, Corrado M, Missero C, Byers PH. Identification, characterization and expression analysis of a new fibrillar collagen gene, COL27A1. *Matrix Biol* 2003; **22**: 3–14.

63 Markovic JN, Shortell CK. Genomics of varicose veins and chronic venous insufficiency. Semin. Vasc. Surg. 2013; **26**: 2–13.

64 De Vega S, Iwamoto T, Yamada Y. Fibulins: Multiple roles in matrix structures and tissue functions. Cell. Mol. Life Sci. 2009; **66**: 1890–902.

65 De Vega S, Suzuki N, Nonaka R, *et al.* A C-terminal fragment of fibulin-7 interacts with endothelial cells and inhibits their tube formation in culture. *Arch Biochem Biophys* 2014; **545**: 148–53.

66 Ellinghaus E, Ellinghaus D, Krusche P, *et al.* Genome-wide association analysis for chronic venous disease identifies EFEMP1 and KCNH8 as susceptibility loci. *Sci Rep* 2017; **7**: 1–9.

67 Zhang Y, Marmorstein LY. Focus on molecules: Fibulin-3 (EFEMP1). Exp. Eye Res. 2010; **90**: 374–5.

68 Albig AR, Neil JR, Schiemann WP. Fibulins 3 and 5 antagonize tumor angiogenesis in vivo. *Cancer Res* 2006; **66**: 2621–9.

69 Parra JR, Cambria RA, Hower CD, *et al.* Tissue inhibitor of metalloproteinase-1 is increased in the saphenofemoral junction of patients with varices in the leg. *J Vasc Surg* 1998; **28**: 669–75.

70 Lee AJ, Evans CJ, Allan PL, Ruckley C V, Fowkes FGR. Lifestyle factors and the risk of varicose veins: Edinburg Vein Study. *J Clin Epidemiol* 2003; **56**: 171–9.

71 Sisto T, Reunanen A, Laurikka J, *et al.* Prevalence and risk factors of varicose veins in lower extremities: Mini-Finland health survey. *Eur J Surgery, Acta Chir* 1995; **161**: 405–14.

72 Gao L-B, Tian S, Gao H-H, Xu Y-Y. Metformin inhibits glioma cell U251 invasion by downregulation of fibulin-3. *Neuroreport* 2013; **24**: 504–8.

73 Engelhardt KR, McGhee S, Winkler S, *et al.* Large deletions and point mutations involving the dedicator of cytokinesis 8 (DOCK8) in the autosomal-recessive form of hyper-IgE syndrome. *J Allergy Clin Immunol* 2009; **124**. DOI:10.1016/j.jaci.2009.10.038.

74 Okada Y, Shimane K, Kochi Y, *et al.* A Genome-Wide Association Study Identified AFF1 as a Susceptibility Locus for Systemic Lupus Eyrthematosus in Japanese. *PLoS Genet* 2012; **8**: e1002455.

75 Lewis RS. Calcium Signaling Mechanisms in T Lymphocytes. *Annu Rev Immunol* 2001; **19**: 497–521.

76 Sayer GL, Smith PDC. Immunocytochemical Characterisation of the Inflammatory Cell Infiltrate of Varicose Veins. *Eur J Vasc Endovasc Surg* 2004; **28**: 479–83.

77 Jacobs BN, Andraska EA, Obi AT, Wakefield TW. Pathophysiology of varicose veins. *J Vasc Surg Venous Lymphat Disord* 2017; **5**: 460–7.

78 Wali MA, Eid RA. Smooth muscle changes in varicose veins: An ultrastructural study. *J Smooth Muscle Res* 2001; **37**: 123–35.

79 Wali MA, Eid RA. Intimal changes in varicose veins: An ultrastructural study. *J Smooth Muscle Res* 2002; **38**: 63–74.

80 Todd SC, Doctor VS, Levy S. Sequences and expression of six new members of the tetraspanin/TM4SF family. *Biochim Biophys Acta - Gene Struct Expr* 1998; **1399**: 101–4.

81 Zhao J, Wu W, Zhang W, *et al.* Selective expression of TSPAN2 in vascular smooth muscle is independently regulated by TGF-b1/smad and myocardin/serum response factor. *FASEB J* 2017; **31**: 2576–91.

82 Halayko AJ, Solway J. Invited review: Molecular mechanisms of phenotypic plasticity in smooth muscle cells. J. Appl. Physiol. 2001; **90**: 358–68.

83 Ascher E, Jacob T, Hingorani A, Gunduz Y, Mazzariol F, Kallakuri S. Programmed cell death (apoptosis) and its role in the pathogenesis of lower extremity varicose veins. In: Annals of Vascular Surgery. Springer New York, 2000: 24–30.

84 Ascher E, Jacob T, Hingorani A, Tsemekhin B, Gunduz Y. Expression of molecular mediators of apoptosis and their role in the pathogenesis of lower-extremity varicose veins. *J Vasc Surg* 2001; **33**: 1080–6.

85 Brachtendorf S, Wanger RA, Birod K, *et al.* Chemosensitivity of human colon cancer cells is influenced by a p53-dependent enhancement of ceramide synthase 5 and induction of autophagy. *Biochim Biophys Acta - Mol Cell Biol Lipids* 2018; **1863**: 1214–27.

86 Hannun YA. Functions of ceramide in coordinating cellular responses to stress. *Science (80-)* 1996; **274**: 1855–9.

87 Hannun YA, Obeid LM. Sphingolipids and their metabolism in physiology and disease. Nat. Rev. Mol. Cell Biol. 2018; **19**: 175–91.

88 Chen L, Chen H, Li Y, Li L, Qiu Y, Ren J. Endocannabinoid and ceramide levels are altered in patients with colorectal cancer. *Oncol Rep* 2015; **34**: 447–54.

89 Montini E, Andolfi G, Caruso A, *et al.* Identification and characterization of a novel serine-threonine kinase gene from the Xp22 region. *Genomics* 1998; **51**: 427–33.

90 Wang Y, Huang Q. Downregulation of CDKL1 promotes gastric cell apoptosis through inhibiting cell growth and colony formation. 2017.

91 Gloviczki P, Comerota AJ, Dalsing MC, *et al.* The care of patients with varicose veins and associated chronic venous diseases: Clinical practice guidelines of the Society for Vascular Surgery and the American Venous Forum. *J Vasc Surg* 2011; **53**: 2S-48S.

92 Gohel MS, Heatley F, Liu X, *et al.* A randomized trial of early endovenous ablation in venous ulceration. *N Engl J Med* 2018; **378**: 2105–14.

.

2.7. Chapter Appendix

The appendix for this chapter is provided as an online supplement at the following URL: **bit.ly/WAhmed_C2Appendix**

Table of Contents

Chapter 3: Genome-wide association analysis of haemorrhoids

3.1. Introduction

3.1.1. Rationale and aims

In **Chapter 1**, I substantiate haemorrhoids disease as a complex disorder with a multi-factorial aetiology, including elastic tissue dysfunction (the sliding anal lining theory).[1,2] Several studies report a positive family history among patients with haemorrhoids[3–6], however heritability estimates are lacking for haemorrhoids, as are, candidate genes involved in its pathobiology. The aim of this chapter is to undertake the first ever genome-wide association study (GWAS) of haemorrhoids to advance our understanding of the genetic architecture of haemorrhoids and to discover clinically-relevant biologic pathways, prioritise targets for therapeutic development, and to enhance personalised medicine approaches to haemorrhoids through genetic risk scoring.

3.2. Methods

3.2.1. Ethics and consent

The research and consent procedures of the UK Biobank are provided in **Chapter 2 (Section 2.2.1.)**.[7]

3.2.2. Study participants

A complete description of the study participants of the UK Biobank cohort are provided in **Chapter 2 (Section 2.2.2.)**.[8]

Haemorrhoids cases were defined as such if they had at least one of the following diagnostic or operative codes consistent with haemorrhoids (**Table 3.1)**:

1. Primary and/or secondary ICD-10 codes for haemorrhoids *(I84.0, I84.1, I84.2, I84.3, I84.4, I84.5, I84.7, I84.8, I84.9, K64.0, K64.1, K64.2, K64.3, K64.8 and K64.9)*
2. Primary and/or secondary OPCS code for haemorrhoids surgery *(H51.1, H51.3, H51.8, H51.9, H52, H53.2, H53.3, H53.8, H53.9, L70.3)*
3. Self-reported operation code for haemorrhoids surgery *(1483)*
4. Self-reported non-cancer illness code for haemorrhoids *(1505)*

In total, 39,950 UK Biobank participants had at least one diagnostic or operative code indicative of haemorrhoids and were therefore defined as cases.

Table 3.1. Diagnostic codes used for haemorrhoids case definition. The total number of participants with each of the diagnostic codes are described below. A total of 39,950 participants possessed at least one of the diagnostic codes for haemorrhoids.

Source of Data	UK Biobank Data Field	Code	Description	N
Primary ICD-10	41202	I84.0	Internal thrombosed haemorrhoids	19019
		I84.1	Internal haemorrhoids with other complications	
		I84.2	Internal haemorrhoids without complication	
		I84.3	External thrombosed haemorrhoids	
		I84.4	External haemorrhoids with other complications	
		I84.5	External haemorrhoids without complication	
		I84.7	Unspecified thrombosed haemorrhoids	
		I84.8	Unspecified haemorrhoids with other complications	
		I84.9	Unspecified haemorrhoids without complication	
		K64.0	First degree haemorrhoids	
		K64.1	Second degree haemorrhoids	
		K64.2	Third degree haemorrhoids	
		K64.3	Fourth degree haemorrhoids	
		K64.8	Other specified haemorrhoids	
		K64.9	Haemorrhoids, unspecified	
Secondary ICD-10	41204	As above	As above	16425
Primary OPCS	41200	H51.1	Haemorrhoidectomy	10198
		H51.3	Stapled haemorrhoidectomy	
		H51.8	Other specified excision of haemorrhoid	
		H51.9	Unspecified excision of haemorrhoid	
		H52	Destruction of haemorrhoid	
		H53.2	Forced manual dilation of anus for haemorrhoid	
		H53.3	Manual reduction of prolapsed haemorrhoid	
		H53.8	Other specified other operations on haemorrhoid	
		H53.9	Unspecified other operations on haemorrhoid	
		L70.3	Ligation of artery NEC	
Secondary OPCS	41210	As above	As above	2491

Non-cancer illness (self-report)	20002	1505	Haemorrhoids / piles	2283
Operation (self-report)	20004	1483	Haemorrhoidectomy / piles surgery/ banding of piles	9662
Total unique cases (excluding overlap)				**39950**

Of the 39,950 haemorrhoids cases identified in UK Biobank, 31,652 cases passed quality control (outlined in **3.2.4 Quality Control**), with the remaining 369,931 post-QC participants that did not possess a diagnostic or operative code indicative of haemorrhoids being defined as controls.

3.2.3. Genotyping

A complete description of the genotyping procedure for the UK Biobank cohort is provided in **Chapter 2 (Section 2.2.3.)**. [8]

3.2.4 Quality control

A complete description of the quality control (QC) procedure implemented centrally by UK Biobank and locally by our group is provided in **Chapter 2 (Section 2.2.4.).**

After central (UK Biobank)[8], and local QC implementation, 86,794 participants from the GWAS analysis and 230,562 genotyped SNPs were excluded (**Figure 3.1**). In

summary, 547,011 genotyped variants and 401,583 participants of white British ancestry passed the QC and were included in the subsequent association analysis (See **3.2.6 Association Analysis**).

Figure 3.1. Overview of quality control pipeline. Excluded SNPs are presented in the blue panels and excluded samples are in the green panels. [1]Pre-QC exclusions: 3 participants with invalid IDs and sex, and 8 participants who had withdrawn from the study were excluded prior to QC. [2]Pre-association exclusions: 11 participants who were not present in UK Biobank's sample file accompanying the imputed genotype data were excluded prior to association, alongside 73 participants who subsequently withdrew consent for participation in UK Biobank.

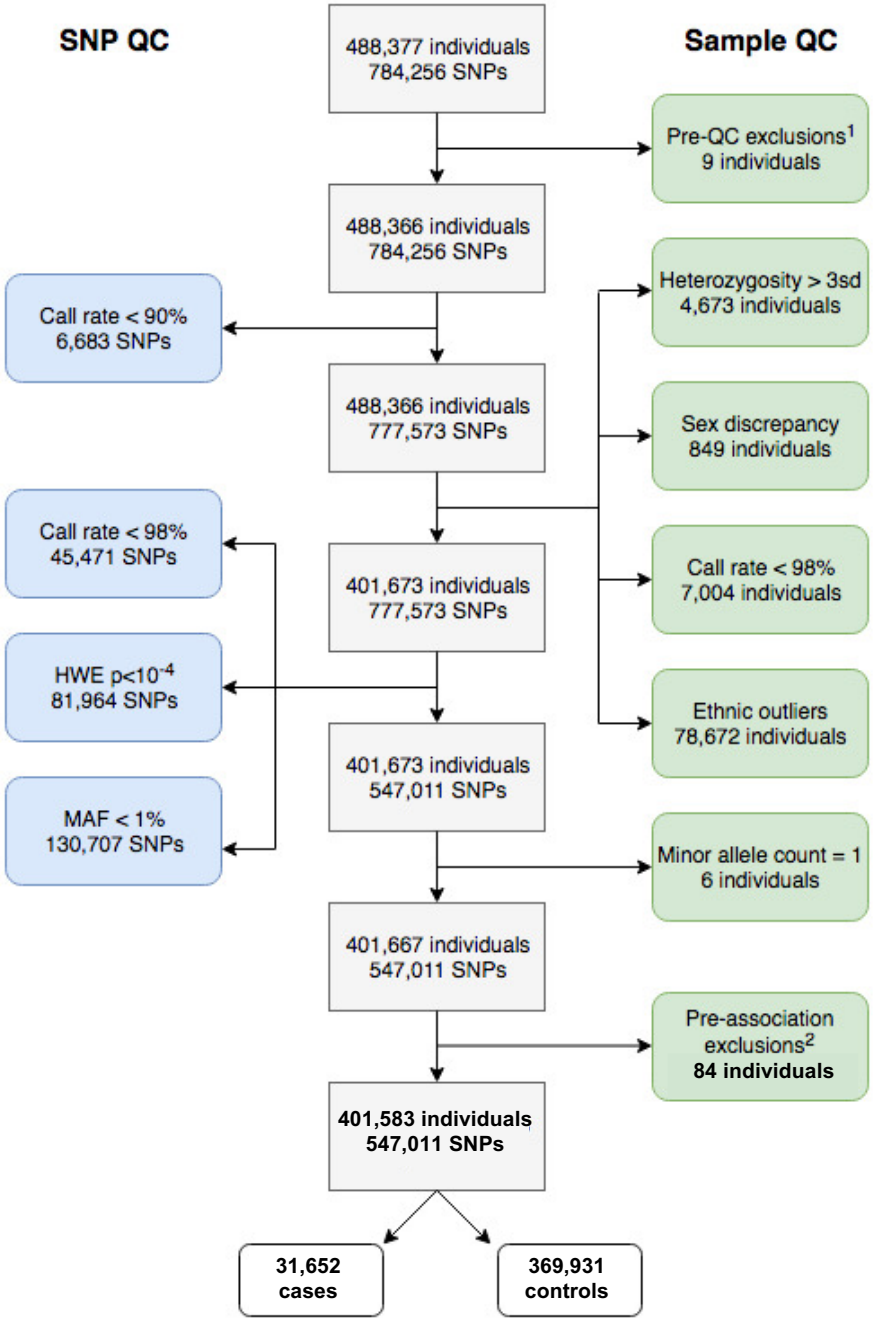

3.2.5. Imputation

A complete description of the imputation methodology is provided in **Chapter 2 (Section 2.2.5)**.[8]

3.2.6. Association analysis

Genome-wide association testing was performed across a total of 8,944,561 SNPs (547,011 directly genotyped (MAF ≥ 0 .01) and 8,397,550 imputed SNPs (MAF ≥ 0.01, INFO Imputation score ≥ 0.90)) using a linear mixed non-infinitesimal model implemented in BOLT-LMM v2.323.[9,10]

Further methodological details pertaining to the association analysis performed for haemorrhoids in this chapter are provided in **Chapter 2 (Section 2.2.13)**.

3.2.7. Genomic risk loci definition

A complete description of the methods used for genomic risk loci definition is provided in **Chapter 2 (Section 2.2.7)**.

3.2.8. Functional annotation of SNPs

A complete description of the methods used for the functional annotation of variants is provided in **Chapter 2 (Section 2.2.8)**.

3.2.9. Candidate gene mapping

A complete description of the methods used for candidate gene mapping approach is provided in **Chapter 2 (Section 2.2.9)**.

3.2.10. Gene set, tissue and pathway analyses

This section follows the methodology described in **Chapter 2 (Section 2.2.10)**.

3.2.11. SNP-based heritability analysis

Methodological details on the SNP heritability analysis is described in **Chapter 2 (Section 2.2.11.)**.

3.2.12. Genetic correlation analysis

Full methodological details regarding the genetic correlation analysis are consistent with, and provided in, **Chapter 2 (Section 2.2.12.)**.

89 traits across thirteen trait categories from the LDHub[11] database were tested for correlation with haemorrhoids: anthropometric, autoimmune, cancer, education, haematological, hormone, lipids, personality, psychiatric, reproductive, sleeping, smoking behaviour. Traits categories were pre-defined based on associations in the literature. To account for multiple testing, a Bonferroni correction of $P < 3.8\times10^{-3}$ (0.05/13) was applied.

3.2.13. Drug-target enrichment analysis

The drug-target enrichment analysis performed for haemorrhoids in this chapter followed the methods described in **Chapter 2 (Section 2.2.13.).**[12]

3.2.14. Genetic risk score

The weighted genetic risk score (wGRS) methodology implemented in this chapter mirrors those described in **Chapter 2** (**Section 2.2.14.)**. The wGRS was compared between four groups of participants from the GWAS: i) all cases vs all controls; ii) surgical cases vs non-surgical cases.

3.2.15. URLs

ANNOVAR, www.annovar.openbioinformatics.org/en/latest/; BOLT-LMM, www.data.broadinstitute.org/alkesgroup/BOLT-LMM/; CADD, cadd.gs.washington.edu/; ENSEMBL, www.ensembl.org/index.html; flashpca, github.com/gabraham/flashpca/; FUMA, www.fuma.ctglab.nl/; GERP, http://mendel.stanford.edu/SidowLab/downloads/gerp/; GTEx Portal, www.gtexportal.org/home/; GWAMA, www.genomics.ut.ee/en/tools/gwama; Human Genome Variation Society (HGVS), www.varnomen.hgvs.org/; HRC, www.haplotype-reference-consortium.org/ ; LD Hub, www.ldsc.broadinstitute.org/ldhub/; LD Link, www.ldlink.nci.nih.gov/; MAGMA, www.ctg.cncr.nl/software/magma; Open Targets Platform, www.targetvalidation.org/; PLINK,

www.pngu.mgh.harvard.edu/~purcell/plink/; Polyphen-2, www.genetics.bwh.harvard.edu/pph2; QCTOOL,www.well.ox.ac.uk/~gav/qctool_v2/#overview; R, www.r-project.org; RegulomeDB, www.regulomedb.org/; SHAPEIT3, jmarchini.org/shapeit3/; SIFT, www.sift.bii.a-star.edu.sg/; UK Biobank, www.ukbiobank.ac.uk/; XGR, www.galahad.well.ox.ac.uk:3040; 1000 Genomes Project, www.1000genomes.org;

3.3. Results

3.3.1. Twelve novel haemorrhoids associated loci

A single-stage genome-wide association analysis was performed in UK Biobank consisting of 31,652 cases and 369,931 controls of white British ancestry. The analytic workflow for the GWAS is provided in **Figure 3.2**. Association testing for haemorrhoids was conducted across 547,011 directly genotyped SNPs (MAF ≥ 0 .01) and 8,397,550 imputed SNPs (MAF ≥ 0.01, INFO Imputation score ≥ 0.90).[10] The analysis yielded genome-wide level associations ($P < 5\times10^{-8}$) at 12 risk loci (882 variants). Conditional regression analysis demonstrated an additional independent residual signal at locus 7q11.23 (rs77689666, $P_{Cond} = 2.90\times10^{-9}$, OR = 1.10). Thus, in summary, 13 independent signals at 12 novel risk loci associated with haemorrhoids (**Table 3.2**). The λ_{GC} demonstrated moderate inflation (1.15), however the LDSC intercept of 1.01 and an attenuation ratio of 0.07 suggests that this is due to the large sample size of the cohort and polygenicity, rather than population stratification (**Figure 3.3**).[13]

The most significant association signal from the GWAS came from locus 9q34.2 (index SNP rs687621, $P = 3.3\times10^{-26}$, OR = 1.10) which was mapped in the genome-wide, gene-based MAGMA test to *CACFD1*. *CACFD1* encodes the flower membrane protein, human flower (hFWE), the negative expression of which has been found to reduce tumour growth and metastasis, and impart sensitisation to chemotherapy.[14] Of the 13 index variants, the variant described above, rs687621, was genotyped with the remaining twelve imputed variants having robust imputation scores of between 0.913 and 0.998. All index variants were common, with minor allele frequencies in Europeans ranging from 6% to 49%. Odds ratios for the effect alleles range from 1.05

to 1.13 which is in keeping with the effect sizes typically seen in other GWAS (median OR ~1.33) (A Manhattan plot is provided in **Figure 3. 4**). Regional plots for all 13 associated loci are provided in **Figure 3.5**.

Figure 3.2. Haemorrhoids GWA study design and analysis workflow. A single-stage GWAS of haemorrhoids was conducted in UK Biobank, identifying 13 independent variants, which were interrogated further in subsequent analyses.

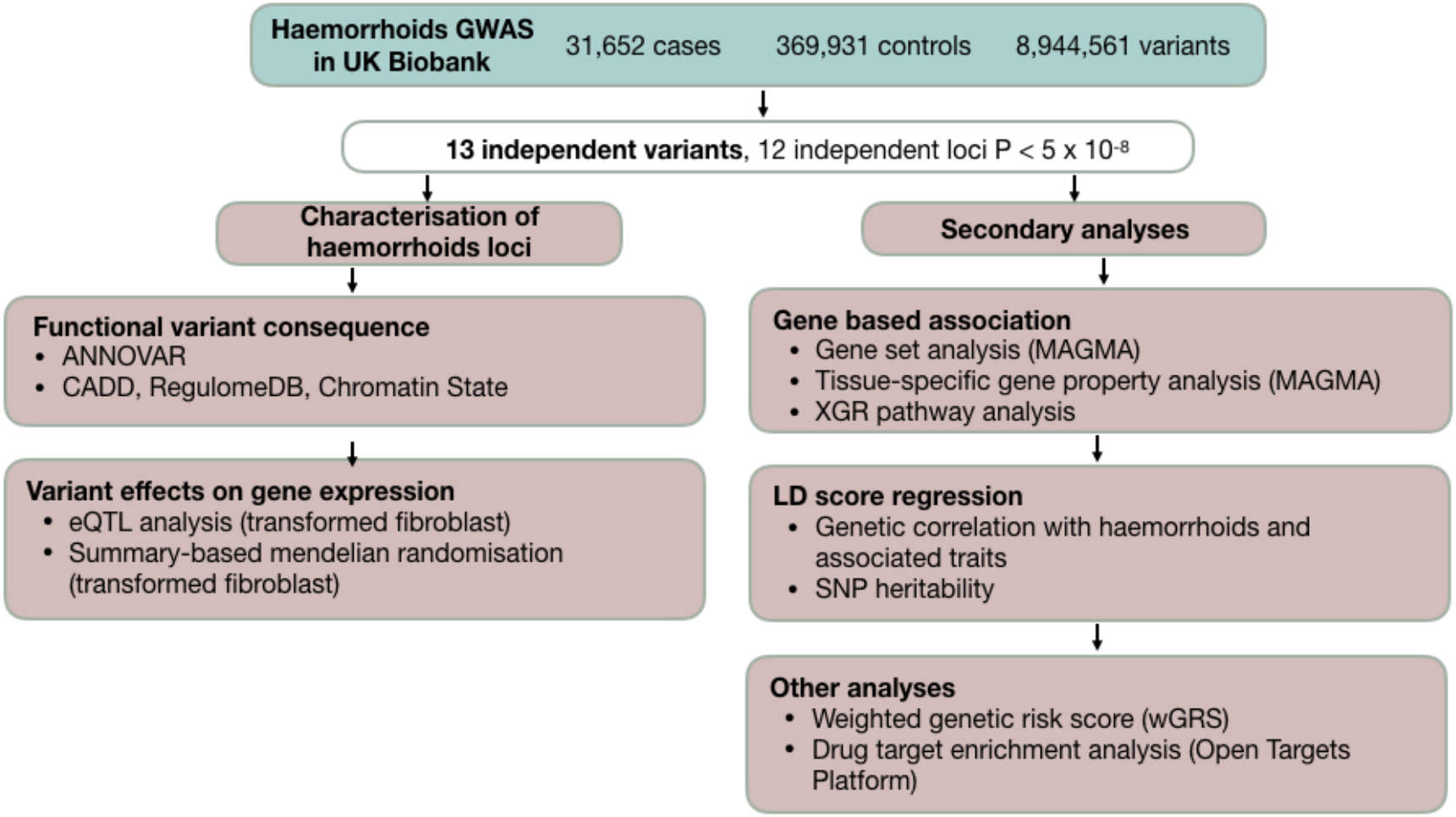

Table 3.2. Thirteen novel signals at 12 loci significantly associated with haemorrhoids in 31,652 cases and 369,931 controls in UK Biobank

Chromosome	Position[a]	rsID	EA[b]	NEA[c]	EAF[d]	Info[e]	OR (95% CI)	P-value	Mapped genes[f]
1	204559707	rs10900600	T	G	0.69	0.995	1.06 (1.04-1.07)	1.50×10^{-9}	*LRRN2, MDM4±, PIK3C2B*
2	67881931	rs114233333	C	G	0.06	0.995	1.11 (1.07-1.14)	7.90×10^{-9}	-
5	37422640	rs112047495	T	C	0.64	0.997	1.06 (1.04-1.08)	6.10×10^{-11}	*C5orf42±, NIPBL±, NUP155±, WDR70±*
5	50759375	rs17824230	G	C	0.87	0.989	1.07 (1.05-1.10)	2.10×10^{-8}	-
7	73306093	rs75606842	A	G	0.22	0.977	1.07 (1.05-1.09)	1.00×10^{-10}	-
7#	73434287	rs77689666	G	A	0.06	0.990	1.10 (1.07-1.14)	2.90×10^{-9}	*ELN±*
7	100632790	rs4556017	C	T	0.15	0.984	1.08 (1.06-1.11)	9.10×10^{-12}	*ACHE, MUC3A, MUC12*
8	71651344	rs4612371	G	C	0.46	0.913	1.05 (1.03-1.07)	4.00×10^{-8}	*LACTB2, XKR9±*
8	105879946	rs12375337	T	A	0.31	0.996	1.05 (1.04-1.07)	4.20×10^{-9}	*RP11-127H5.1±*
9	22124504	rs1333047	A	T	0.51	0.998	1.06 (1.04-1.08)	4.60×10^{-12}	-
9	136137065	rs687621	A	G	0.68	G	1.10 (1.08-1.12)	3.30×10^{-26}	*CACFD1*
12	66409367	rs11176001	C	A	0.87	0.990	1.13 (1.10-1.15)	4.70×10^{-22}	-
15	67441750	rs72743461	A	C	0.24	0.998	1.06 (1.04-1.08)	1.60×10^{-8}	*RP11-342M21.2, SMAD3±*

[a]Based on NCBI Genome Build 37 (hg19).
[b]The effect allele.
[c]The non-effect allele.
[d]The effect allele frequency.
[e]The SNP INFO score for imputed SNPs; G = genotyped SNP.
[f]The 17 genes (in alphabetical order) prioritised at these loci based on positional mapping, eQTL mapping and MAGMA gene mapping (see Methods).
[±]Where overlap in gene mapping strategies occurred, the gene(s) with the highest level of overlap are depicted.
[#]Denotes a residual significant signal following conditional regression analysis at the lead SNP at the locus.

Figure 3.3. Quantile-quantile (Q-Q) plot of associated variants.

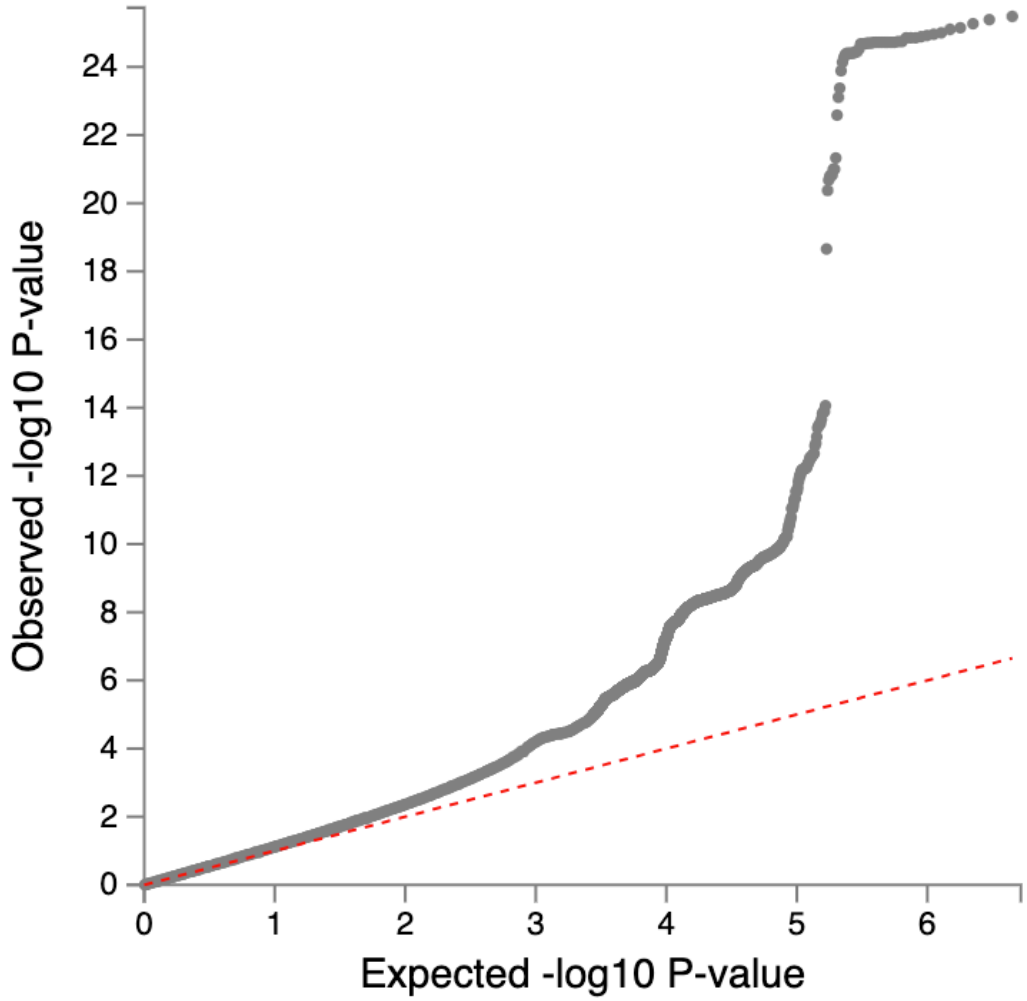

Figure 3.4. Results of the genome-wide association study in haemorrhoids. A Manhattan plot showing genomic position on each of the autosomes plotted against association signal strength (-$\log_{10}$ P-value). The red line refers to the genome-wide significance threshold of $P < 5\times10^{-8}$. Of the prioritised genes (described elsewhere in this chapter), the most promising gene candidate is highlighted in the Manhattan plot based on literature. Bold genes are those that were prioritised using the four mapping strategies; *CDKN2B-AS1* was prioritised based on a detailed literature search of proximal genes at this locus.

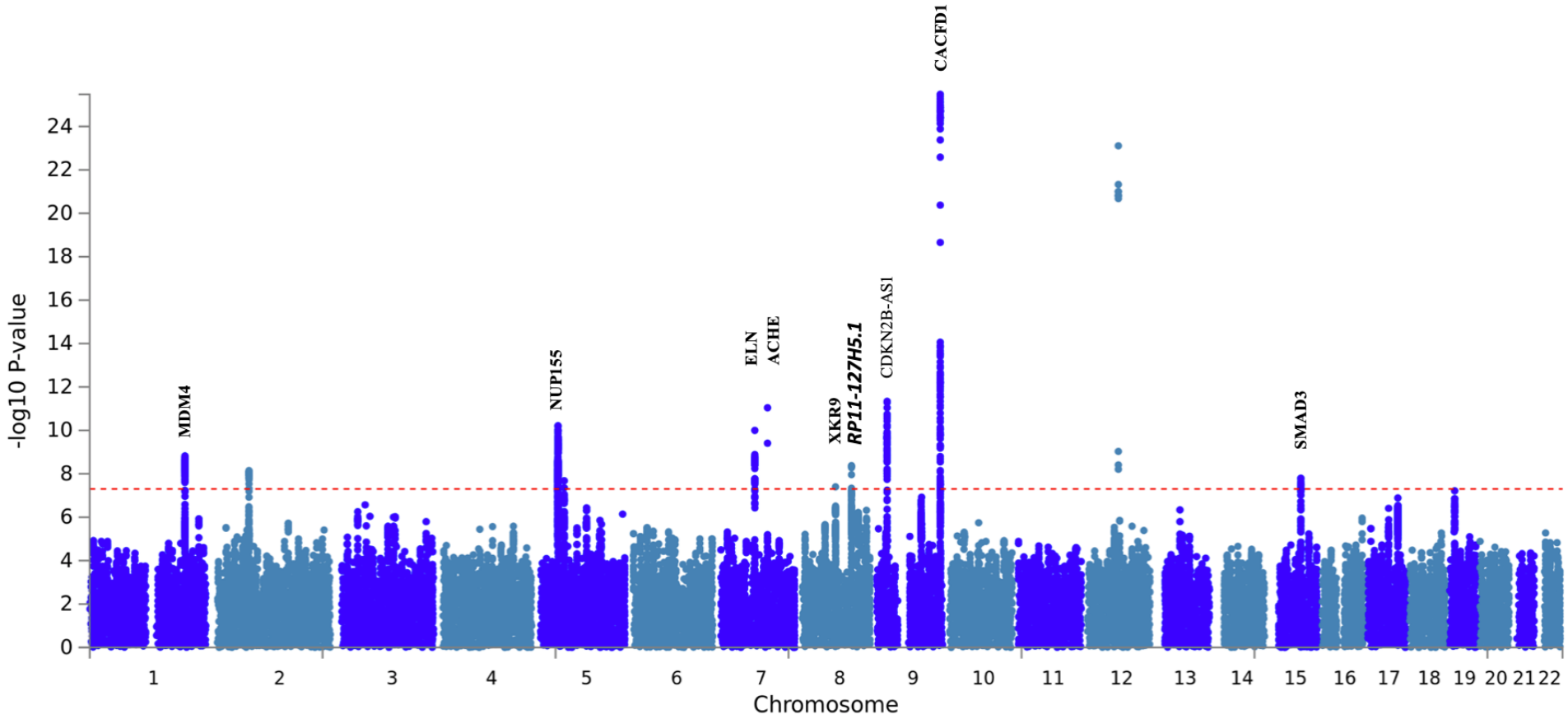

Figure 3.5. Regional Locus Zoom plots of all haemorrhoids associated signals. LocusZoom plots of the 13 independent genome-wide significant variants at the 12 haemorrhoids associated susceptibility loci. Plots are ordered by chromosome number and genomic position. SNP position is shown on the x-axis, and strength of association on the y-axis (-$\log_{10}$ P-value). The linkage disequilibrium (LD) relationship between the lead SNP and the surrounding SNPs is indicated by the r^2 legend. In the lower panel of each sub-figure, genes within 500kb on either side of the index SNP are shown. The position on each chromosome is depicted in relation to Human Genome build hg19 (GRCh37).

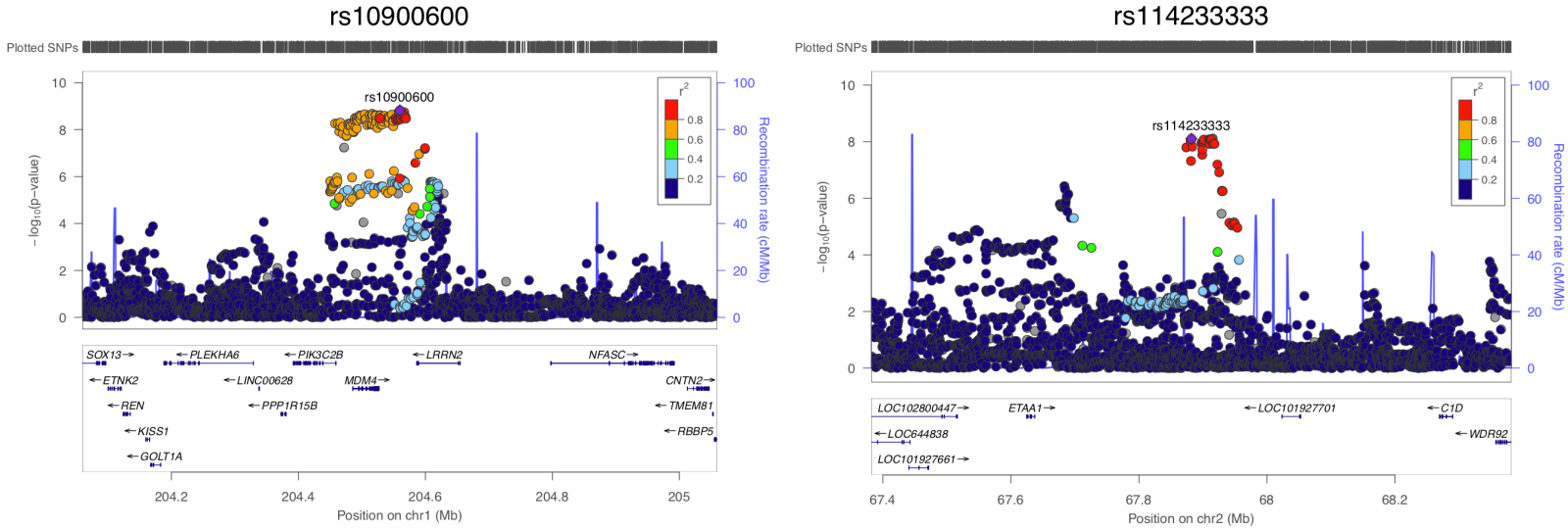

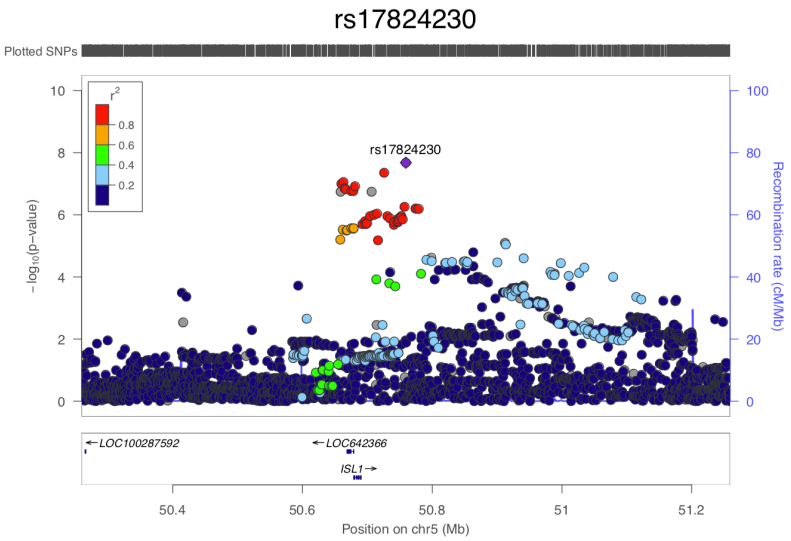
rs17824230
Plotted SNPs
rs17824230
$-\log_{10}$(p-value)
Recombination rate (cM/Mb)
LOC100287592
LOC642366
ISL1
Position on chr5 (Mb)

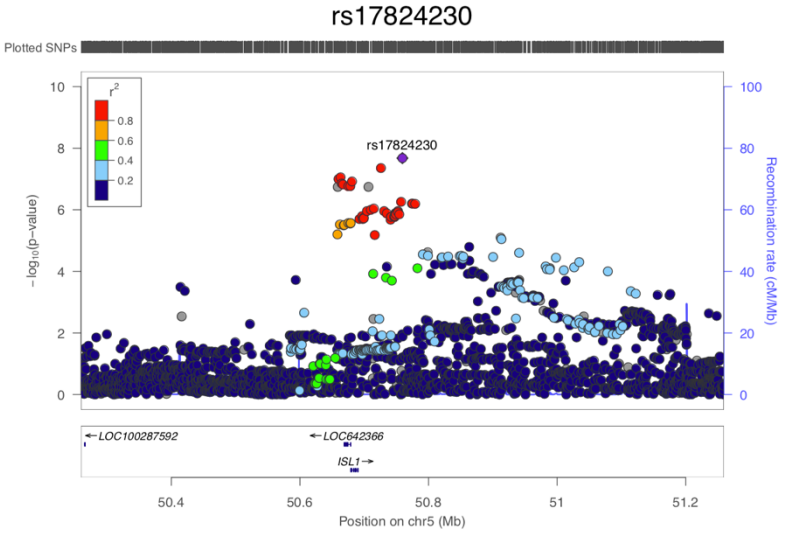
rs17824230
Plotted SNPs
rs17824230
$-\log_{10}$(p-value)
Recombination rate (cM/Mb)
LOC100287592
LOC642366
ISL1
Position on chr5 (Mb)

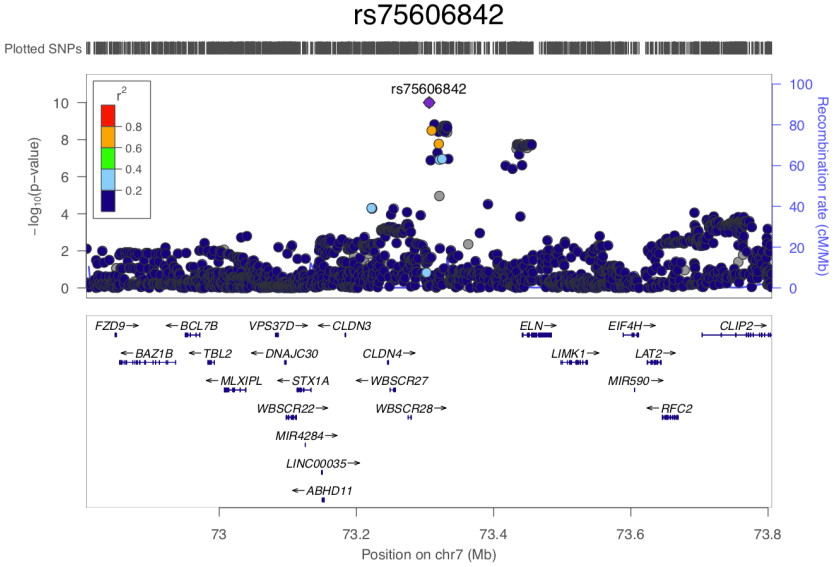
rs75606842
Plotted SNPs
rs75606842
$-\log_{10}$(p-value)
Recombination rate (cM/Mb)
FZD9
BCL7B
VPS37D
CLDN3
ELN
EIF4H
CLIP2
BAZ1B
TBL2
DNAJC30
CLDN4
LIMK1
LAT2
MLXIPL
STX1A
WBSCR27
MIR590
WBSCR22
WBSCR28
RFC2
MIR4284
LINC00035
ABHD11
Position on chr7 (Mb)

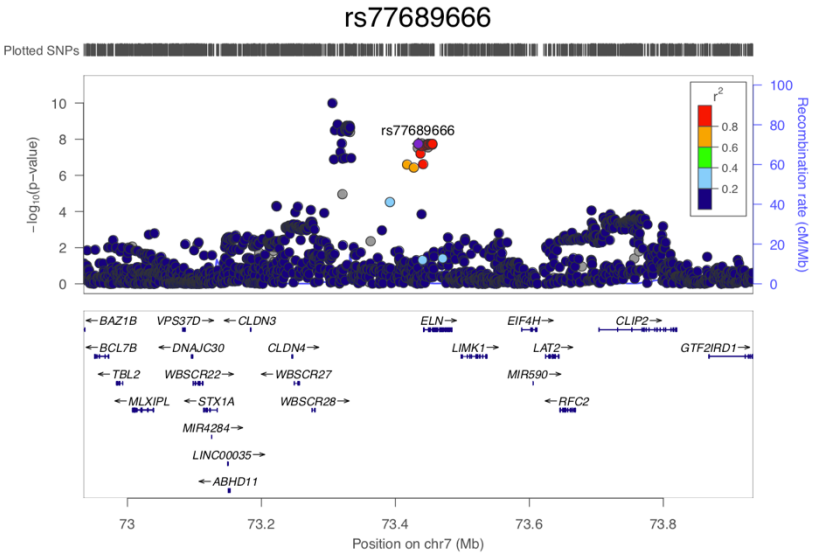
rs77689666
Plotted SNPs
rs77689666
$-\log_{10}$(p-value)
Recombination rate (cM/Mb)
BAZ1B
VPS37D
CLDN3
ELN
EIF4H
CLIP2
BCL7B
DNAJC30
CLDN4
LIMK1
LAT2
GTF2IRD1
TBL2
WBSCR22
WBSCR27
MIR590
MLXIPL
STX1A
WBSCR28
RFC2
MIR4284
LINC00035
ABHD11
Position on chr7 (Mb)

rs4556017

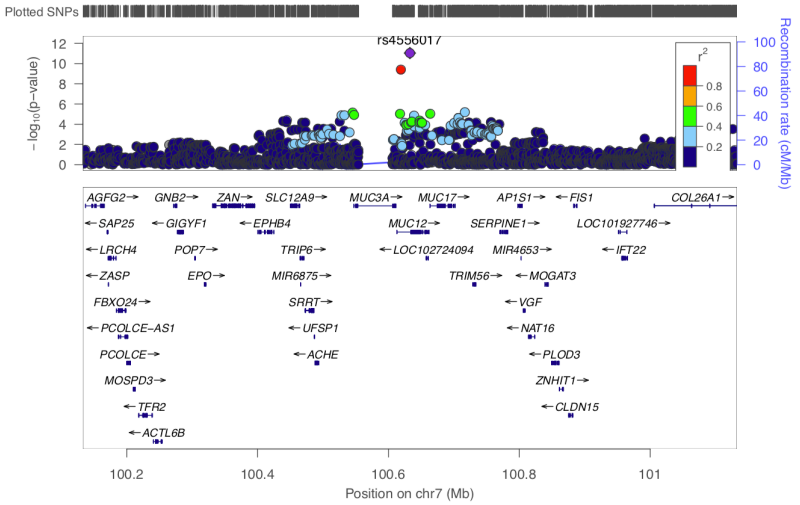

rs4612371

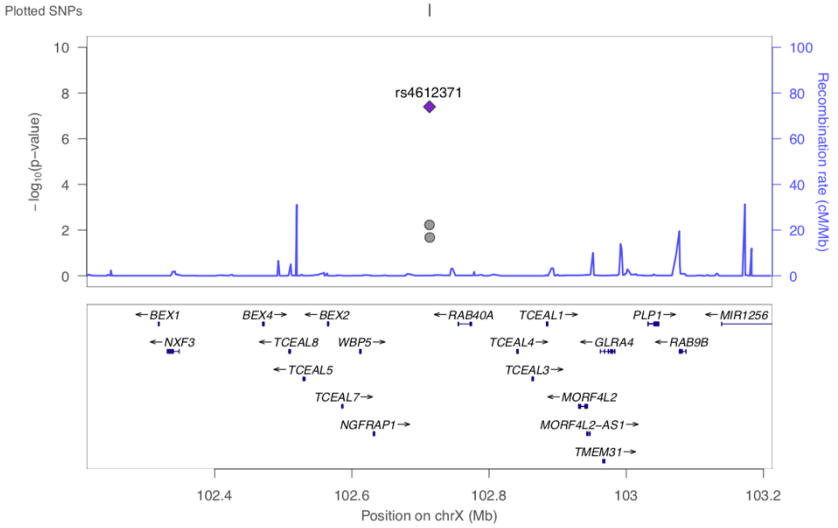

rs12375337

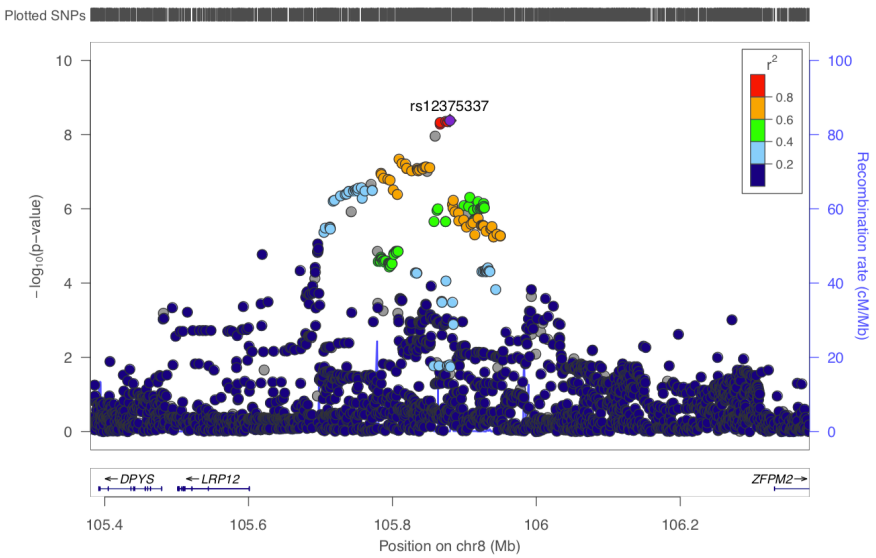

rs1333047

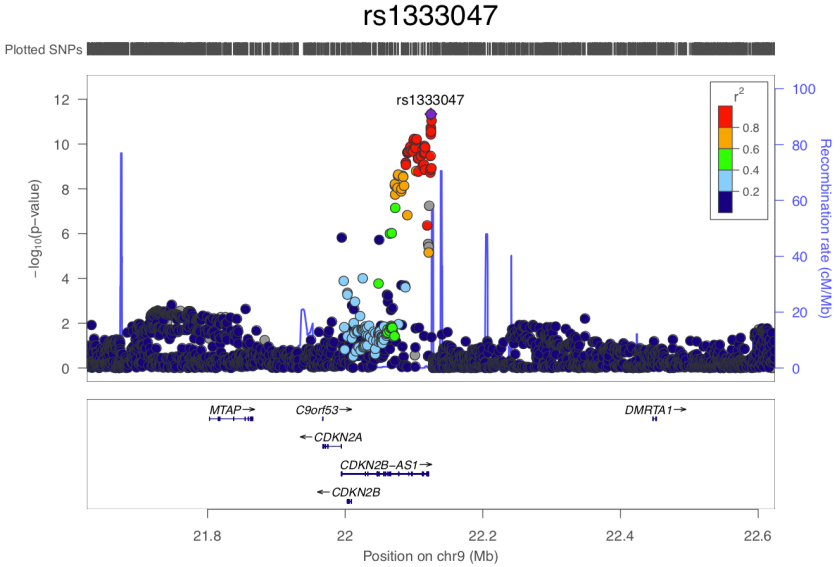

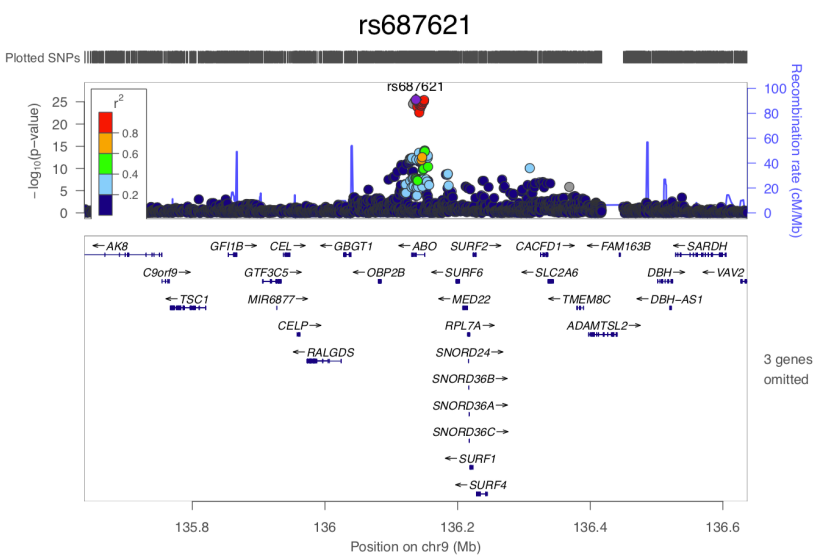
rs687621
Plotted SNPs
rs687621
$-\log_{10}$(p-value)
Recombination rate (cM/Mb)
r^2
0.8
0.6
0.4
0.2
AK8
GFI1B
CEL
GBGT1
ABO
SURF2
CACFD1
FAM163B
SARDH
C9orf9
GTF3C5
OBP2B
SURF6
SLC2A6
DBH
VAV2
TSC1
MIR6877
MED22
TMEM8C
DBH-AS1
CELP
RPL7A
ADAMTSL2
RALGDS
SNORD24
SNORD36B
SNORD36A
SNORD36C
SURF1
SURF4
3 genes omitted
135.8
136
136.2
136.4
136.6
Position on chr9 (Mb)

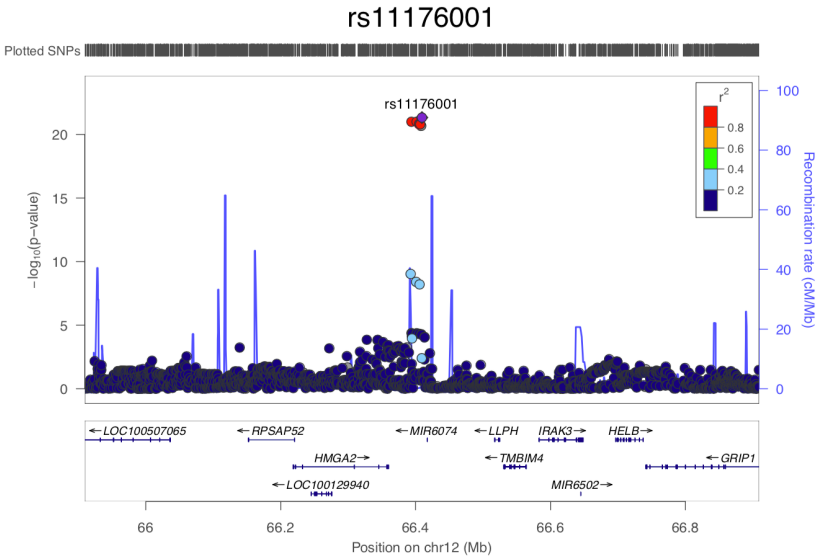
rs11176001
Plotted SNPs
rs11176001
$-\log_{10}$(p-value)
Recombination rate (cM/Mb)
r^2
0.8
0.6
0.4
0.2
LOC100507065
RPSAP52
MIR6074
LLPH
IRAK3
HELB
HMGA2
TMBIM4
GRIP1
LOC100129940
MIR6502
66
66.2
66.4
66.6
66.8
Position on chr12 (Mb)

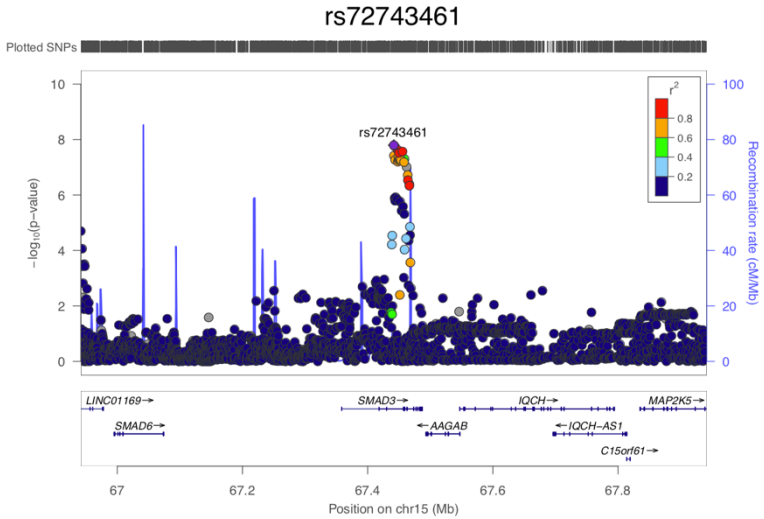
rs72743461
Plotted SNPs
rs72743461
$-\log_{10}$(p-value)
Recombination rate (cM/Mb)
r^2
0.8
0.6
0.4
0.2
LINC01169
SMAD3
IQCH
MAP2K5
SMAD6
AAGAB
IQCH-AS1
C15orf61
67
67.2
67.4
67.6
67.8
Position on chr15 (Mb)

3.3.2. *In silico* annotation

Localising associated SNPs using ANNOVAR[15] implemented in FUMA GWAS (Functional Mapping and Annotation of GWAS) v1.3.3[16] yielded 609 genome-wide significant ($P < 5\times10^{-8}$) candidate SNPs (956 in total) across the 12 risk loci (**Figure 3.6**).[15,16] All variants were non-coding, with the majority lying in intronic and intergenic regions (76.5%, n = 466), and a proportion annotated as intronic or exonic non-coding RNAs (20.9%, n = 127) (**Figure 3.6**). Of the 466 intronic-intergenic variants, 98.9% (n = 461) resided in open chromatin regions depicted by a minimum 15-core chromatin state of 1 to 7 in 127 tissue/cell types from the Roadmap Epigenomics Consortium ChroHMM model.[17] 33 intronic-intergenic candidate variants had a CADD score[18] ≥ 12.37 suggesting they may be deleterious (**Appendix Table 3.1.**), of which 16 were genome-wide significant – four of these demonstrated potential regulatory activity depicted by a RegulomeDB[19] score of 2b or less (*likely to affect binding):* rs7532236 (*RP11-430C7.4*), rs11750212 (*WDR70*), rs1866316 (*SMAD3*), rs17293632 (*SMAD3*).

Figure 3.6. Functional annotation of the 956 candidate SNPs at the 12 haemorrhoids associated risk loci. Functional consequences of the SNPs on genes were obtained by performing ANNOVAR gene-based annotation using Ensembl genes (build 85) in FUMA. A) CADD scores, B) RegulomeDB scores and C) 15-core chromatin state were annotated to all 956 SNPs in 1000G phase 3 by FUMA through matching chromosome, position, reference, and alternative alleles. D) Positional classification of the 956 SNPs.

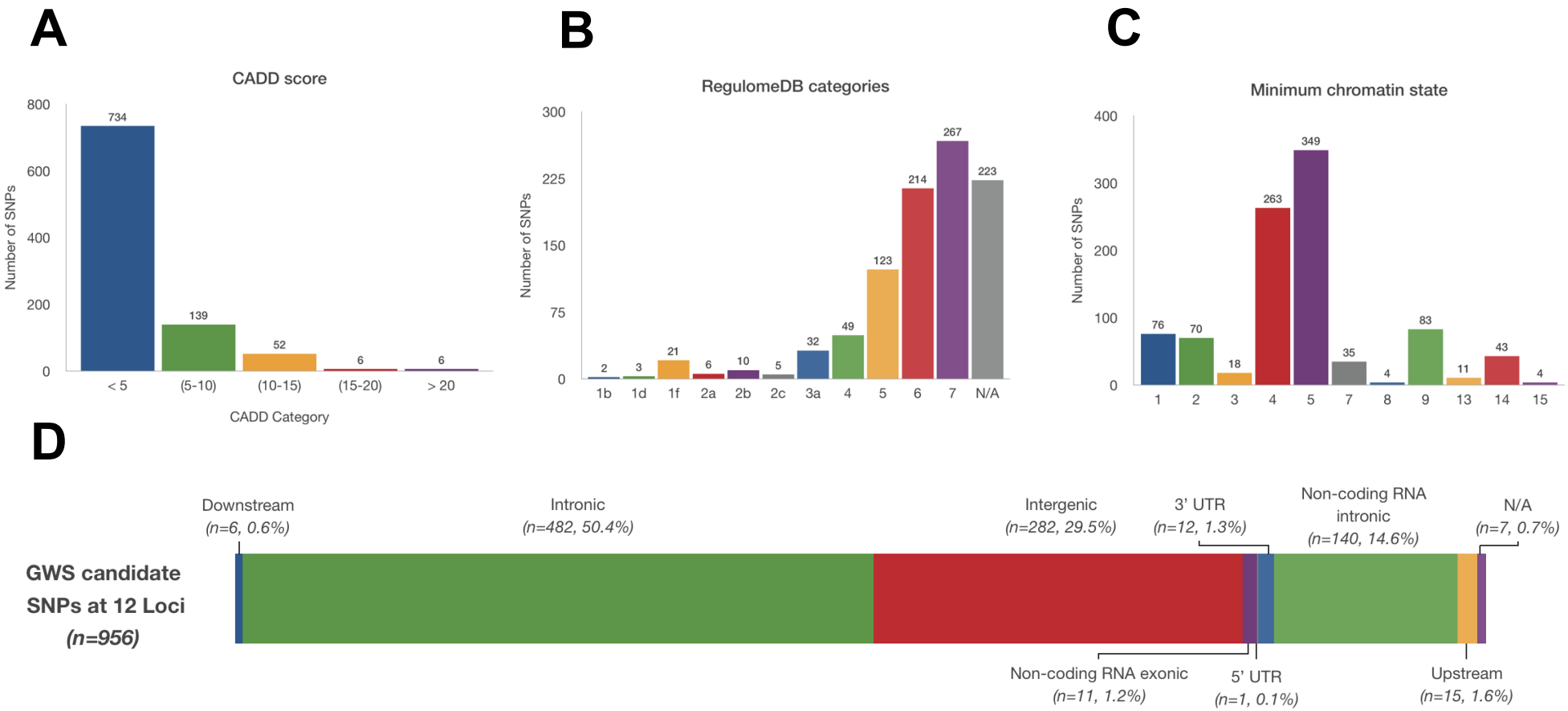

3.3.3. Gene mapping

Candidate SNPs in FUMA v1.3.3[16] were mapped positionally to 13 protein-coding genes based on genomic proximity. Three genes were prioritised based on containing variants that are known to affect expression of these genes (eQTLs) within fibroblast tissue from the GTEx consortium[20] and GENCORD collection[21] or skeletal muscle tissues from the GTEx consortium[20] ($P_{eqtl} < 5\times10^{-8}$) — two of these genes (*ACHE*, *LACTB2*) were *not* prioritised in the positional or subsequent MAGMA mapping approaches (i.e. lay outside the confines of the 10kb positional window from the lead SNP and were not picked up in the genome-wide gene association test). Performing a genome-wide, gene-based association test in MAGMA v1.07[22], 18 genes reached the genome-wide significance threshold in MAGMA ($P < 2.64\times10^{-6}$), 11 of which resided within the realms of our susceptibility loci (**Appendix Table 3.2.**), with two genes (*LRRN2* and *CACFD1*) being prioritised only at this genome-wide gene mapping level (**Figures 3.7 and 3.8**). The fourth strategy, summary-based mendelian randomisation (SMR)[23] identified no genes that met the SMR-significance threshold ($P < 0.05/4323 = 2.68\times10^{-6}$) and associated with haemorrhoids through pleiotropy.

In summary, 17 unique genes were mapped to eight of the 12 haemorrhoids susceptibility loci by at least one mapping approach. Nine genes were mapped by two or more gene-mapping strategies, with one gene (*XKR9*), being mapped by three gene-mapping approaches (**Table 3.3 and Figure 3.9**).

Figure 3.7. MAGMA gene-based association analysis Quantile-Quantile plot. Quantile-Quantile (Q-Q) plot for the genome-wide, gene-based association test computed by MAGMA v1.07.[22]

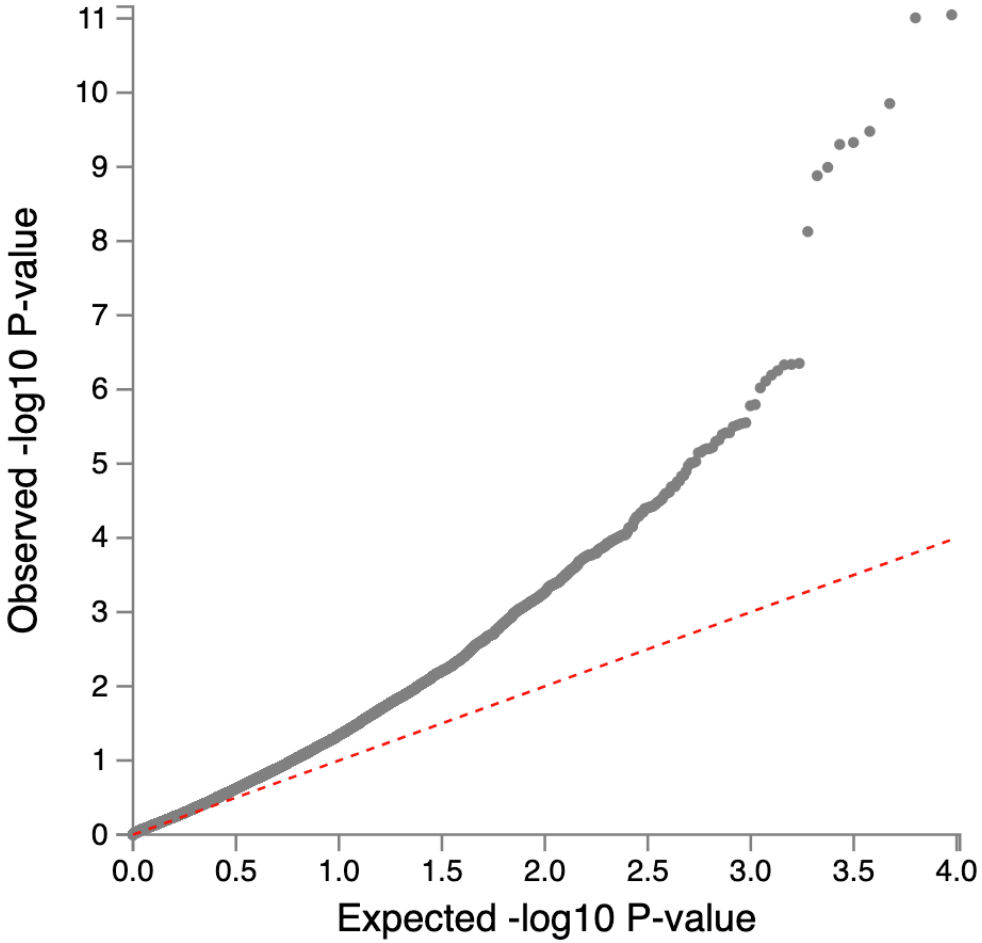

Figure 3.8. MAGMA gene-based association analysis Manhattan plot. Manhattan plot for the genome-wide, gene-based association test computed by MAGMA v1.07.[22] Input SNPs were mapped to 18918 protein coding genes. Genome wide significance (red dashed line in the plot) was defined at $P = 2.64 \times 10^{-6}$ (0.05/18918). The 18 significant MAGMA genome-wide associated genes are depicted above the red line; 11 of the 18 MAGMA mapped genes resided within the realms of the 12 genomic risk loci.

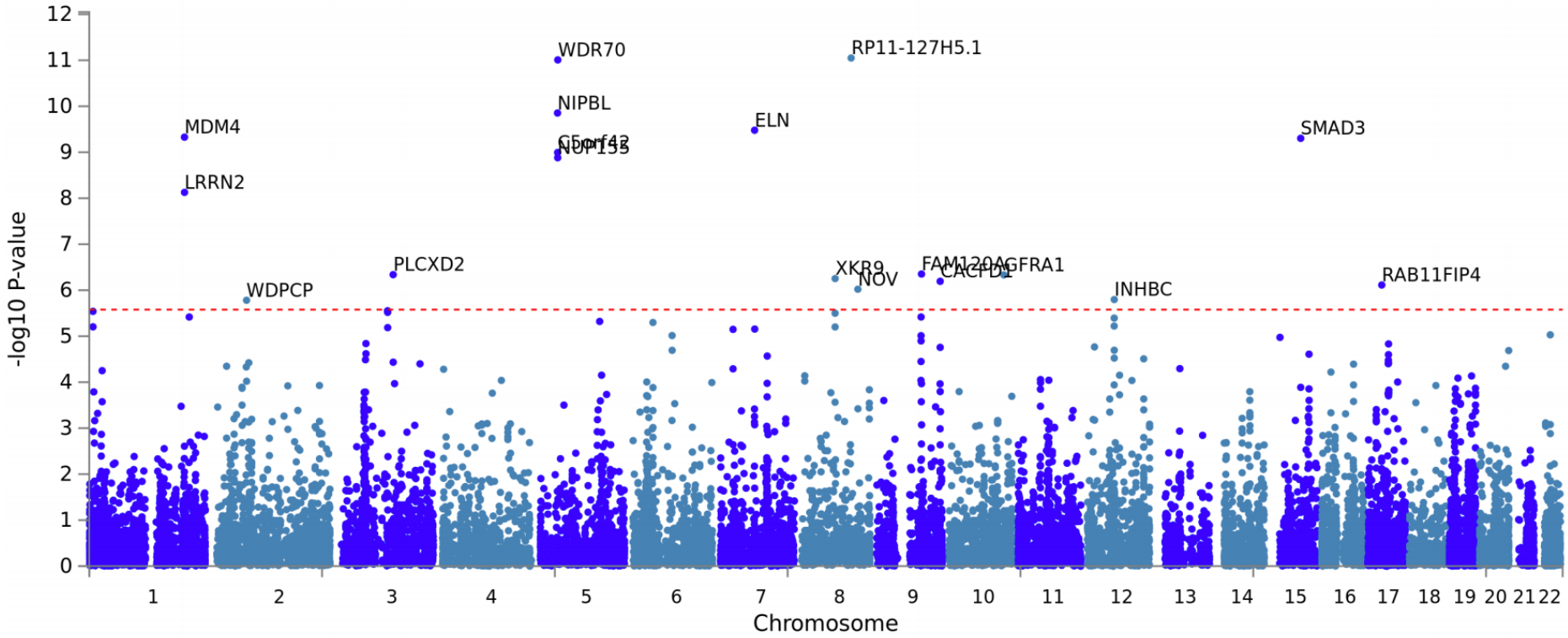

Table 3.3. Genes mapped to the haemorrhoids associated loci using the four mapping strategies. 17 unique genes were mapped to eight of the 12 associated loci by one or more gene mapping strategies (see Methods). 13 genes were mapped via positional mapping in FUMA, 3 genes were mapped via eQTL mapping in FUMA, 11 genes were mapped using MAGMA. No genes were mapped using SMR. Overlap between the four different mapping strategies is shown.

Chromosome	Lead SNP	Position	13 FUMA Positionally Mapped Genes	3 FUMA eQTL Mapped Genes	11 MAGMA Mapped Genes	Number of Gene Mapping Approaches
1	rs10900600	204559707			LRRN2	1
1	rs10900600	204559707	*MDM4*		*MDM4*	2
1	rs10900600	204559707	*PIK3C2B*			1
5	rs112047495	37422640	*C5ORF42*		*C5ORF42*	2
5	rs112047495	37422640	*NIPBL*		*NIPBL*	2
5	rs112047495	37422640	*NUP155*		*NUP155*	2
5	rs112047495	37422640	*WDR70*		*WDR70*	2
7	rs77689666	73434287	*ELN*		*ELN*	2
7	rs4556017	100632790		*ACHE*		1
7	rs4556017	100632790	*MUC3A*			1
7	rs4556017	100632790	*MUC12*			1
8	rs4612371	71651344		*LACTB2*		1
8	rs4612371	71651344	*XKR9*	*XKR9*	*XKR9*	3
8	rs12375337	105879946	*RP11-127H5.1*		*RP11-127H5.1*	2
9	rs687621	136137065			*CACFD1*	1
15	rs72743461	67441750	*RP11-342M21.2*			1
15	rs72743461	67441750	*SMAD3*		*SMAD3*	2

Figure 3.9. Venn diagram for the 17 mapped genes prioritised at the haemorrhoids associated loci. 17 unique genes were mapped to eight of the 12 associated loci by one or more gene mapping strategies (see Methods). 13 genes were mapped via positional mapping in FUMA, 3 genes were mapped via eQTL mapping in FUMA, 11 genes were mapped using MAGMA. No genes were mapped using SMR. Overlap between the three different mapping strategies is shown in the Venn diagram.

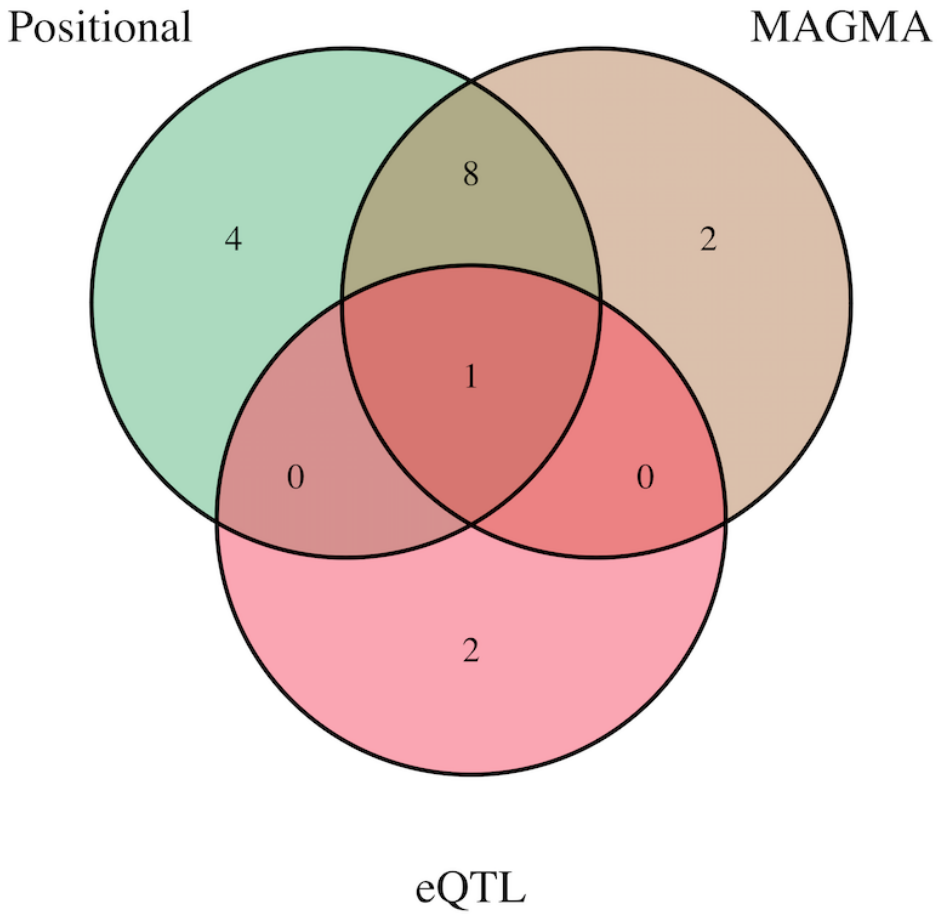

3.3.4. Gene set, pathway and tissue-specific enrichment

Gene-set analysis in MAGMA v1.07[22] determined the convergence of MAGMA prioritised genes within 15,496 gene sets (5500 curated gene sets and 9995 GO terms) from MSigDB v8.0. [24] One curated gene set was significantly enriched: '*Genes up-regulated and displaying increased copy number in glioblastoma samples (TCGA_Glioblastoma_Copy_Number_Up (M5536))'* ($P = 7.15\times10^{-8}$, n = 72 genes) (**Appendix Table 3.3.**). Moreover, tissue expression analysis in MAGMA[22] using GTEx v8.0 30 general tissue types[20] demonstrated blood vessel to be the most enriched tissue ($P = 3.07\times10^{-6}$), with all three vascular tissue types being significantly enriched in the separate GTEx v8.0 54 tissue types expression analysis[20]: Tibial Artery ($P = 5.20\times10^{-6}$, most enriched tissue), Aorta ($P = 7.83\times10^{-5}$, 3rd most enriched tissue), Coronary Artery ($P = 2.64\times10^{-4}$, 6th most enriched tissue) (**Figure 3.10**). Moreover, of all remaining significantly enriched non-vascular tissues across both general and specific GTEx tissues; all tissues reside in hollow organs where smooth muscle plays an important role in function (namely uterus, oesophagus, oesophago-gastric junction, and cervix).

Performing gene set enrichment analysis in FUMA *GENE2FUNC*[16] demonstrated the 17 prioritised genes to cluster in several GWAS Catalog reported genes. Striking enrichment was noted of 11 of 18 prioritised genes in gene sets for six phenotypes reported in the GWAS Catalog[25], most significantly diverticular disease ($P = 3.20\times10^{-4}$, 2nd most significant, *SMAD3*, *WDR70*, *ELN*, *LACTB2*) and fracture non-union ($P = 3.20\times10^{-4}$; *ACHE*, *MUC3A*, *MUC12*). Pathway analysis in eXploring Genomic Relations (XGR)[26] furthermore yielded five enriched canonical pathways including

those related to regulation of cytoplasmic and nuclear SMAD2/3 signalling ($P = 4.8\times10^{-4}$, $Z = 5.21$, $FDR = 7.1\times10^{-3}$) extracellular matrix biology. ($P = 3.6\times10^{-3}$, $Z = 2.88$, $FDR = 1.3\times10^{-2}$) (**Table 3.4)**. Moreover, gene expression heatmap of the 17 prioritised genes in both GTEx v8.0[20] 30 general tissue types and 54 specific tissue types demonstrated *ELN* and *SMAD3* genes to have the highest expression in blood vessel tissue (**Figure 3.11**).

Figure 3.10. MAGMA tissue expression analysis. Tissue Expression Analysis of haemorrhoids GWAS data computed by MAGMA v1.07. A) 54 specific and B) 30 general tissue types. This analysis examines the relationship between genes containing significant genetic associations from the MAGMA association test and their expression levels across various tissues from the GTEx consortium. Gene-property analysis is performed using average expression of genes per tissue type as a gene covariate. Gene expression values are log2 transformed average RPKM (Read Per Kilobase Per Million) per tissue type after winsorization at 50, and are based on GTEx v8 RNA-Seq data across 54 specific tissue types and 30 general tissue types. The dotted line indicates the Bonferroni-corrected α level, and the tissues that meet this significance threshold are highlighted in red.

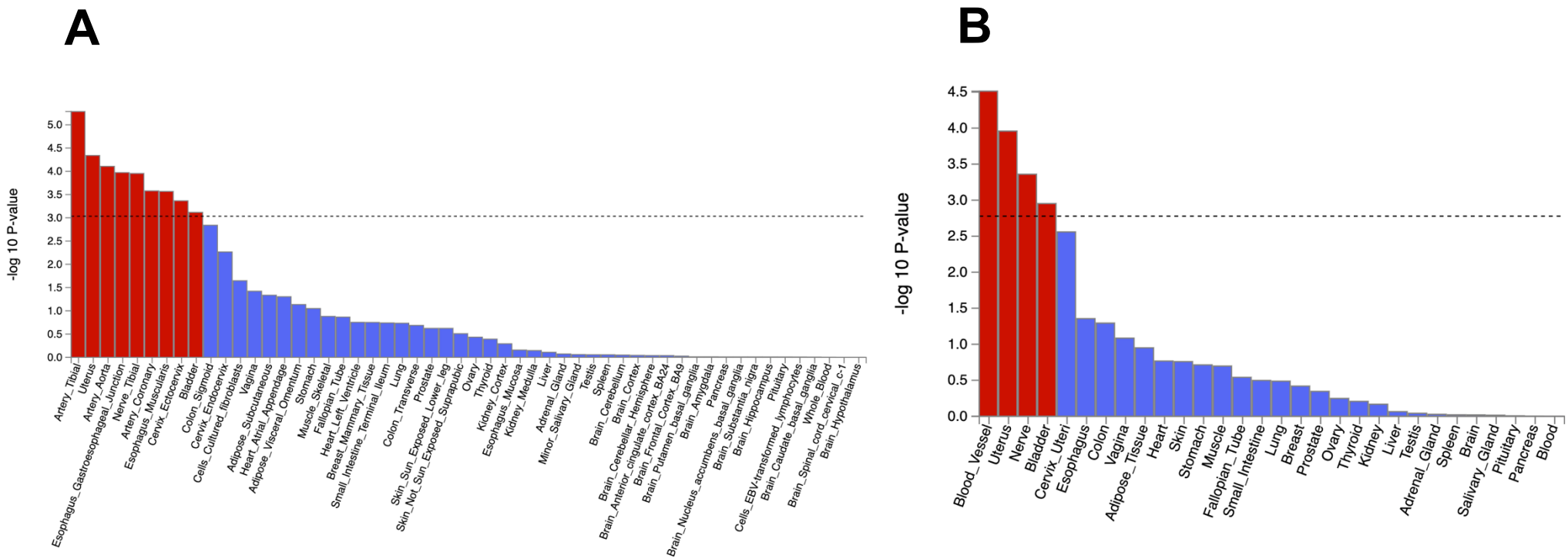

Table 3.4. Gene-based enrichment analysis in XGR. Pathway analysis of the 17 prioritised haemorrhoids associated genes was performed in eXploring Genomic Relations (XGR) for canonical pathways using a hypergeometric distribution test.

Biological Process	Z-Score	P-Value	FDR	Number of overlapped genes	Genes
Regulation of cytoplasmic and nuclear SMAD2/3 signalling	5.21	4.8×10^{-4}	7.1×10^{-2}	1	*SMAD3*
Genes encoding proteins affiliated structurally or functionally to extracellular matrix proteins	2.88	3.6×10^{-3}	1.3×10^{-2}	2	*MUC12, MUC3A*
Signalling events mediated by Stem cell factor receptor (c-Kit)	2.77	4.5×10^{-3}	1.3×10^{-2}	1	*PIK3C2B*
p53 pathway	2.56	5.7×10^{-3}	1.3×10^{-2}	1	*MDM4*
ATF-2 transcription factor network	2.56	5.7×10^{-3}	1.3×10^{-2}	1	*ACHE*

Figure 3.11. Heatmap of gene expression of the 17 prioritised genes across GTEx tissues. The average expression of the 17 prioritised genes at the haemorrhoids associated loci across A) 54 specific and B) 30 general GTEx v8.0 tissue types are shown. Average expression value per tissue type per gene are shown following winsorization at 50 and log 2 transformation with pseudocount 1. Expression value is depicted in Transcripts per Million, and both genes and tissues have been ordered by hierarchical clustering.

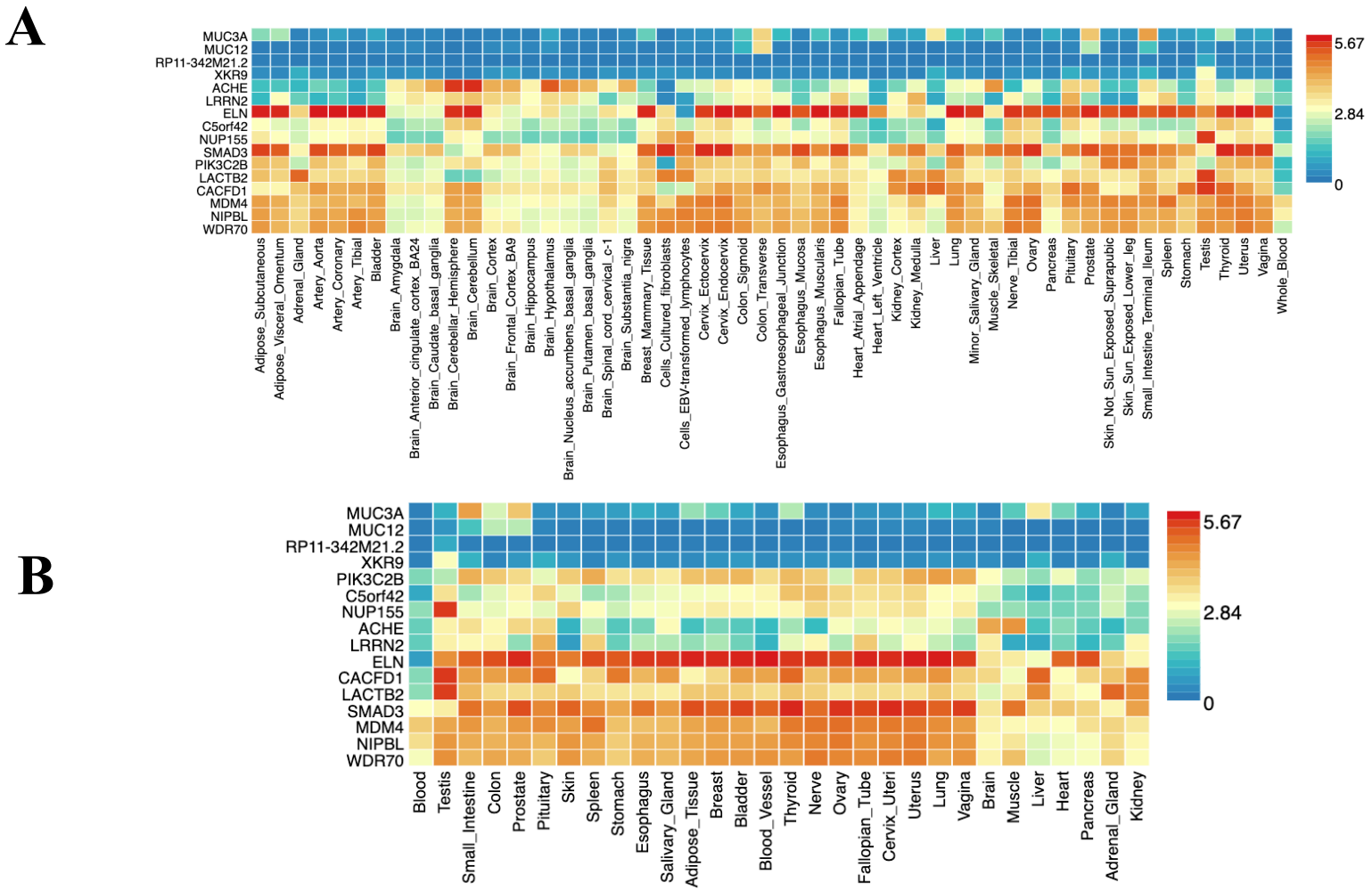

3.3.5 Genetic correlations with haemorrhoids associated phenotypes

The contribution of common variants to haemorrhoids risk were examined using LD Score regression[27]. Using LD scores from ~1.2 million variants found in European populations, the SNP-based heritability (h^2_{SNP}) for haemorrhoids was estimated in the UK Biobank population to be 2.37% (S.E. = 0.18%). Correlation testing between haemorrhoids and other traits using GWAS summary statistics from LD Hub highlighted fifteen traits/diseases across seven trait categories significantly associated with haemorrhoids ($P_{bon} < 3.85\times10^{-3}$).[11]

Of the 89 traits tested across seven trait categories (**Appendix Table 3.4.**), 15 traits across seven trait categories were significantly correlated ($P_{bon} < 3.85\times10^{-3}$). Four categories (personality, psychiatric, sleeping, anthropometric) contained traits that were positively correlated with haemorrhoids (**Figure 3.12**). Traits closely related to mental health were amongst those positively correlated with haemorrhoids; with neuroticism sharing a genetic overlap of ~20 - 26%, depressive symptoms ~19%, and insomnia ~15%. The largest quantity of positively-associated traits was in the anthropometric category, with several measures relating to bodyweight sharing a genetic overlap of between 11 and 17%.

Of note, the reproductive category contained traits that were both positively and negatively correlated with haemorrhoids, with number of children ever born (parity status) having a positive correlation (~20% genetic overlap) and age at first birth having a negative genetic correlation (-20%). In the cognitive and education trait categories, several measures of literacy and cognitive performance negatively

correlated with haemorrhoids (years of schooling -12-17% and intelligence -14% genetic overlap).

Figure 3.12. Genetic correlation between haemorrhoids and other traits and diseases. Genetic correlation (r_g) between haemorrhoids and publicly available phenotypes in LD Hub, using LDSC regression. Fifteen traits met a Bonferroni-corrected significance $P_{bon} < 3.85 \times 10^{-3}$ and are depicted. GPC, Genetics of Personality Consortium; SSGAC, Social Science Genetics Association Consortium.

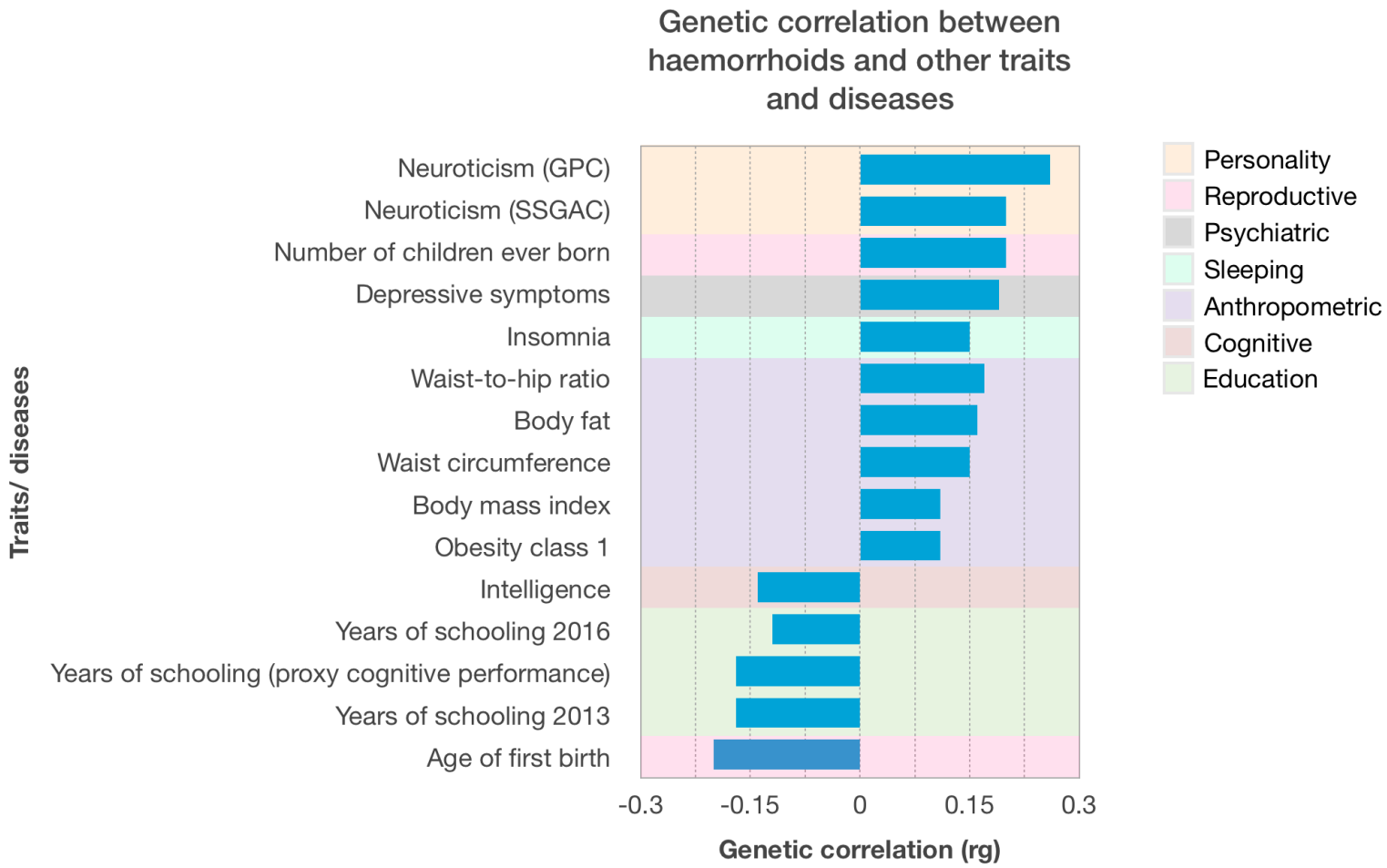

3.3.6. Drug target enrichment analysis

Interrogation within the Open Targets Platform underlined the potential for therapeutic targeting of the protein products of 16 of the 17 prioritised genes. Forty-eight drug pathways reached a nominal significance threshold (**Appendix Table 3.5.**), with the mucin drug targets MUC12 and MUC3A in the '*Defective GALNT3 causes familial hyperphosphataemic tumoral calcinosis (HFTC)*' pathway being most enriched ($P = 3.3\times10^{-4}$). Pharmacological tractability data for 13 gene targets were available, with three (*ACHE*, *PIK3C2B* and *SMAD3*) predicted tractable to small molecule targeting and six predicted tractable by antibody targeting to a high confidence (*ACHE*, *ADRA2B*, *ELN*, *MUC12*, *MUC3A*, *PIK3C2B*) (**Figure 3.13**). Three gene targets were pharmacologically active with 43 known pharmaceutical interactions (*ACHE*, *ADRA2B*, *ELN*), with ADRA2B (encoded by *RP11-127H5.1*) having the most drug interactions (n= 30), followed by ACHE (n= 12) and ELN (n= 1) (**Appendix Table 3.6.**). Of note, the structural protein ELN is an established target by the elastin proteolytic enzyme, vonapanitase, which has been independently investigated in five completed, stage 1-3 clinical trials (clinicaltrials.gov) for the management of chronic kidney disease.

Figure 3.13. Tractability information for gene targets in the drug-target enrichment analysis. Of the 17 prioritised genes interrogated in the Open Targets Platform, tractability information on 13 genes was available; the tractability of each of these genes to small molecule and/or antibody targeting is shown in the below figure.

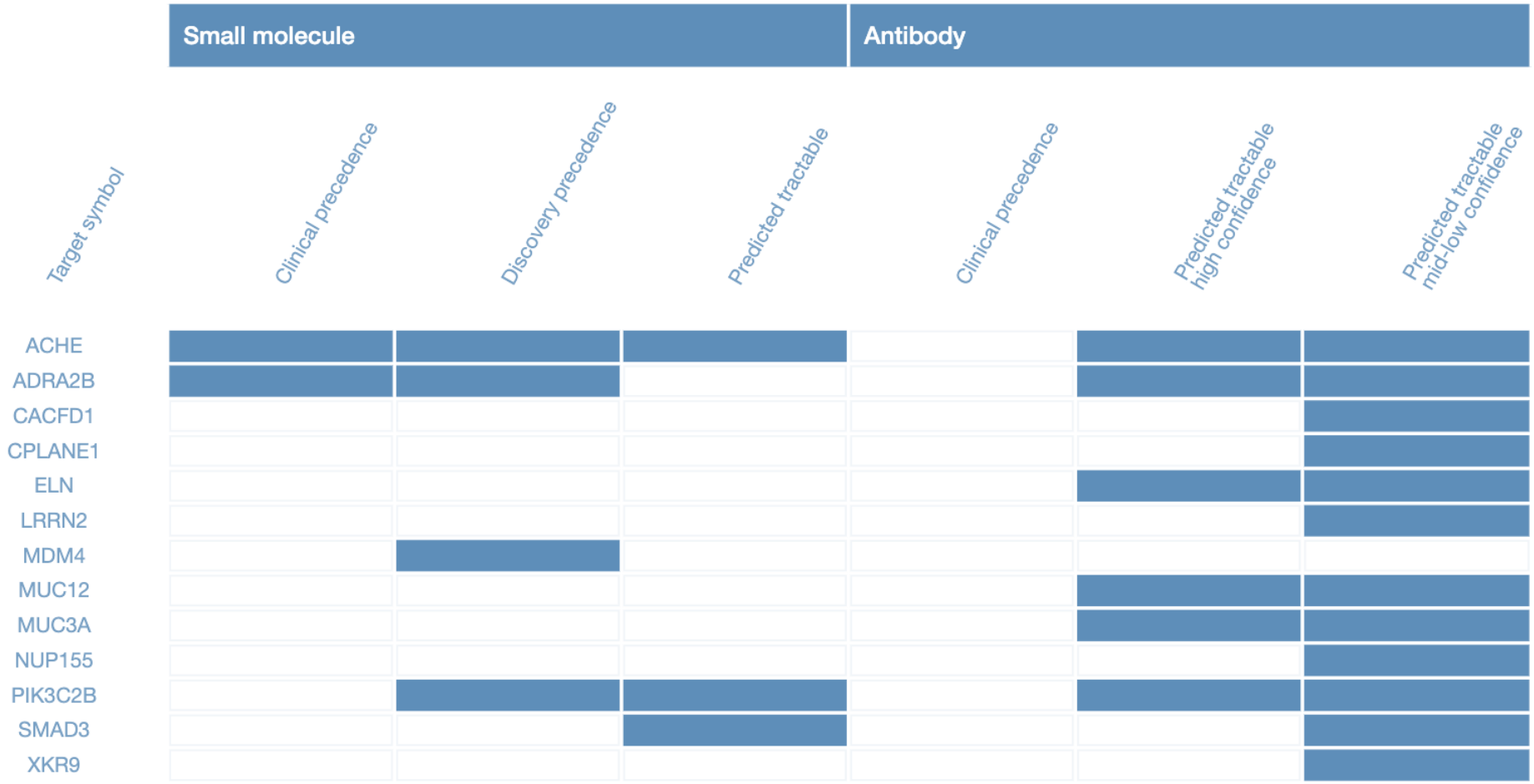

3.3.7. Genetic risk score for haemorrhoids

The 13 independent significant signals associated with haemorrhoids were used to calculate a weighted genetic risk score (wGRS) for all 401,658 participants in UK Biobank. As expected, the wGRS for haemorrhoids cases (0.856) was higher than in controls (0.835; $P = 7.63\times10^{-135}$). Moreover, the haemorrhoids cases that had undergone surgery had a higher wGRS (0.865) compared to haemorrhoids cases that had not undergone a surgical procedure to manage their disease (0.848; $P = 4.58\times10^{-27}$) (**Table 3.5**).

Table 3.5. Weighted genetic risk score for haemorrhoids in the UK Biobank cohort

Group	Haemorrhoids cases	Controls	P-Value†	Haemorrhoids cases with operation code	Haemorrhoids cases without operation code	P-Value§
N	31,652	369,931		14,735	16,917	
Mean wGRS* (standard deviation)	0.835 (0.144)	0.856 (0.145)	7.63×10^{-135}	0.865 (0.145)	0.848 (0.145)	4.58×10^{-27}

*wGRS: weighted genetic risk score. †Unpaired two-tailed t-test between haemorrhoids cases and controls. §Unpaired two-tailed t-test between haemorrhoids cases with an operation code and haemorrhoids cases without an operation code.

3.4. Discussion

3.4.1. Summary

Haemorrhoids are a major health burden associated with high morbidity, reduced quality-of-life, and high healthcare costs.[28] Effective medical therapies are lacking in the armamentarium of the colorectal surgeon and are increasingly required. Performing the first genome-wide association analysis of haemorrhoids to date, in 31,652 cases and 369,931 control, 13 independent susceptibility signals reaching genome-wide significance at 12 risk loci were identified. Further, using *in silico* analyses, strong evidence of functionality in the haemorrhoids-associated regions was demonstrated; showing that genes in these associated regions are significantly enriched for expression in vascular tissue, tissues associated with hollow organs with a high preponderance of smooth muscle, and extracellular matrix regulation pathways. Genetic correlation analyses demonstrated a strong and positive genetic correlation between haemorrhoids and several mental-health related phenotypes, parity status, and weight. Genetic risk scoring of patients with haemorrhoids undergoing surgery correlated with a more severe phenotype - representing a first step in personalised medicine approaches to managing haemorrhoids. The majority of prioritised genes demonstrate pharmaceutical potential, with three genes (*ACHE*, *ADRA2B*, *ELN*) under investigation in active pharmaceutical research efforts.

3.4.2. Extracellular Matrix Remodelling

Haemorrhoids are fibrovascular cushions in the rectal mucosa which constitute a complex arrangement of smooth muscle, connective tissue and elastic fibres with arteriovenous communications.[29] Anatomical studies demonstrate haemorrhoidal veins and the surrounding musculature to be supported by an extracellular lattice of longitudinally organised collagen and elastic fibres.[30] Diseased haemorrhoid tissue has been shown to have an abnormal ratio of type I to III collagen[31], suggesting a role for collagen metabolism and resulting mechanical instability and loss of tensile strength as contributors to haemorrhoid disease pathobiology.[31,32] Indeed, haemorrhoid disease has also been reported in patients with Ehlers-Danlos Syndrome (which is characterised by mutations in collagen genes).[33] The ECM of the anal submucosa degrades with age, with adult anal specimens found to have a less structured appearance of collagen fibres[34] — this also aligns with the peak incidence of haemorrhoids in middle to old age.[35]

In the ECM of connective tissues, collagen (tensile strength) works in concert with elastin (elastic recoil) to determine the geometric arrangement and mechanical properties of tissues. Indeed matrix metalloproteinases (MMPs) negatively regulate ECM composition, and gene expression of MMPs -1, -2 and -3 have been shown to be increased in grade I and II haemorrhoids disease with MMPs -2, -8, -9 and NGAL levels shown to be elevated in grade 3 haemorrhoids.[32] Studied to a lesser degree in the biology of haemorrhoids is the contribution of elastin. The association analysis identified rs77689666-G ($P = 2.90\times10^{-9}$, OR = 1.10, EAF = 0.06), a variant residing in an intergenic region at 7q11.23, ~8kb upstream of *ELN*. *ELN* encodes elastin, which

is the core component of elastic fibres and provides elastic recoil to tissues such as haemorrhoidal veins. This is supported by the fact *ELN* was the most differentially-expressed gene in blood vessel tissue of all 17 prioritised genes, highlighting its roles in the elasticity of vascular tissues. Moreover, the drug-target enrichment analyses revealed elastin to be among the three prioritised genes targets with confirmed pharmaceutical interactions. XGR pathway analysis enriched canonical gene sets involved in structural components of the ECM. Disruption of the muscular and elastic constituents of haemorrhoids is thought to lead to distal shifting of the vascular padding (sliding anal lining theory[2]), a common feature of haemorrhoid disease.[36] Loss of integrity of the ECM, and in particular of elastin during ageing has been posited as an important pathway in the pathobiology of haemorrhoids.[30] Elastin may therefore represent an important player in the biology of haemorrhoids. Moreover, collagen and elastin expression in rectal submucosa has also been shown to be significantly reduced in obstructive defecation syndrome[37], another disorder of rectum.

Epidemiological observations have highlighted haemorrhoids to be associated with other disorders of connective tissue, namely: hernia[38], varicose veins[39,40], , genitourinary prolapse[41,42], and diverticular disease.[43,44] The G minor allele of SNP rs77689666 also significantly associates with and confers risk in Europeans for diverticular disease in a previous GWAS by Maguire[45] ($P = 1.65\times10^{-9}$, OR = 1.11) and in the hernia GWAS ($P = 3.2\times10^{-10}$, OR = 1.08) (*Please refer to* ***Chapter 4***). These results are consistent with the hypothesis of a degree of shared pathophysiology between haemorrhoids and other associated elastic tissue disorders.

3.4.3. TGFβ-Signalling Pathway

The transforming growth factor-β (TGF-β) signalling pathway plays a central role in normal physiological and disease processes via regulation of core cellular processes such as growth, differentiation, migration, apoptosis, and ECM remodelling.[46,47] The TGF-β signalling pathway constitutes a complex family of 33 polypeptide growth factors, including Smads which are key intracellular mediators of the response to TGF-β in ECM-producing mesenchymal cells (myofibroblasts and fibroblasts).[48,49] Target genes known to be Smad-responsive include key fibrillar ECM glycoproteins such as collagen and fibronectin, MMPs, and tissue inhibitors of MMPs (TIMP-1). [50–53] Indeed, TGF-β signalling, has been shown to play a central pathogenic role in the development of aortic aneurysm in Marfan syndrome.[54]

SNP rs72743461-A is significantly associated with haemorrhoids, a variant residing within intron 1 of *SMAD3* at 15q22.33 ($P = 1.6\times10^{-8}$, OR = 1.06, EAF = 0.24). The TGF-β/Smad3 signalling pathway is a key component of tissue fibrogenesis[52], acting as a potent stimulator of ECM protein accumulation.[55–58] Of note, two intronic variants were identified residing < 1kb from - and in high linkage with - the lead SNP at this locus: rs17293632 ($P = 1.7\times10^{-8}$, OR = 1.06, EAF = 0.24, $r^2 = 1.00$) and rs1866316 ($P = 3.8\times10^{-8}$, OR = 1.05, EAF = 0.30, $r^2 = 0.71$) which are among the top four variants from the GWAS predicted *both* deleterious (CADD score[18] = 22.6 and 14.4, respectively) and demonstrating strong regulatory potential (RegulomeDB[19] score = 2A and 2B, respectively). Disruption of TGF-β/Smad3 signalling pathway through loss of Smad3 is thought to reduce fibrogenic mesenchymal cell activation and confer resistance to the development of colorectal fibrosis[59], and induce resistance to tissue

fibrosis in other organs[52] (such as skin[60], kidney[61], lung[62], and liver[63]). One can therefore hypothesise that overexpression of *SMAD3,* and activation of the TGF-β/Smad3 signalling pathway disrupts the ECM architecture of haemorrhoidal veins and may therefore predispose to risk of haemorrhoids development. Aside from its role in ECM regulation, the TGF-β-signalling pathway is a fundamental pathway involved in colorectal cancer risk[64], with SMAD3 in particular having been demonstrated to associate with survival in colorectal cancer.[65] Several variants in *SMAD3* have been shown to be associated with differential miRNA expression levels in both normal colorectal mucosa as well as tumour tissue.[66]

Endoglin (CD105) is a membrane glycoprotein expressed in vascular endothelial cells where it forms a core component of the receptor that binds TGF-β1 and TGF-β3. Endoglin is a proliferation-associated antigen on vascular endothelium and is a specific marker for neovascularisation.[67,68] Haemorrhoids samples have been found to have overexpression of endoglin[69]; supporting the involvement of the TGF-β signalling pathway in haemorrhoids and also suggesting a role for neovascularisation as well as extracellular matrix disruption in haemorrhoids biology.

3.4.4. Internal anal sphincter tonicity

Freckner and Euler[70] suggest the internal anal sphincter (IAS) to contribute as much as 85% of resting anal pressure in normal individuals. Prevailing manometric studies have demonstrated the presence of ultra-slow waves and high resting pressures in the anal canal of patients with haemorrhoids; which has been suggested to be due to IAS hypertonicity[71–73] (with one study by Teramoto also describing external AS hypertrophy[74]). High resting anal pressure in the anal canal are thought to impair venous return from haemorrhoidal veins during defecation.[1] Hancock demonstrated resting anal pressures to decline after manual anal dilation, further supporting the role of IAS hypertonicity in haemorrhoids pathobiology.[75]

The association analysis discovered rs4556017-T ($P = 9.10\times10^{-12}$, OR = 1.08, EAF = 0.15), which resides in intron 1 of *MUC12* at 7q22.1. Via eQTL mapping, rs4556017 was identified to be a robust eQTL for *ACHE* (~140kb upstream from *MUC12*) in GTEx v8 aorta tissue ($P_{eQTL}= 1.8\times10^{-15}$, FDR = 5.55×10^{-39}). *ACHE* encodes acetylcholinesterase which catalyses the degradation of acetylcholine in the neuromuscular junction leading to termination of synaptic transmission. Acetylcholine is thought to relax smooth muscle in the IAS by stimulating NO synthesis.[76] Detailed 3D reconstruction of the human autonomic innervation of the IAS has been previously performed.[77] NO is the predominant inhibitory neurotransmitter of non-adrenergic non-cholinergic enteric neurones that mediate relaxation of the IAS during defecation.[78] Over-expression of the *ACHE* gene in patients with haemorrhoids may therefore have some role to play in the pathobiology of haemorrhoids by imparting a higher resting anal pressure via reduced inhibitory signalling of the IAS tone. The ACHE gene

product was found to have confirmed pharmaceutical interactions in the drug-target enrichment analysis. Indeed, injection of botulinum toxin into the anal sphincter — which prevents release of acetylcholine from presynaptic nerve endings and noradrenaline from sympathetic nerve endings[79]—has been shown to be highly effective in rapid relief of pain from thrombosed external haemorrhoids (thought to be due to a reduction in anal resting pressure).[80] ACHE may therefore represent an early target and warrant further research as a potential therapeutic avenue for haemorrhoids disease.

It is encouraging that through eQTL mapping, this study has implicated for the first time, a biological candidate in support of the IAS hypertonicity theory. However, an important caveat is that several studies have failed to identify differences in IAS thickness in patients with haemorrhoids compared to healthy controls.[81,82] This suggests alternative factors may be contributing to the high anal pressure in patients with haemorrhoids. The vascular hyperplasia theory proposed by Stelzner[29], represents an alternative view implicating a role for vascular distension and increased pressure of the anal cushions themselves in the increased anal pressure seen in patients with haemorrhoids. Sun et al[100], demonstrated in their study that the high anal pressure in patients with haemorrhoids were indeed due to higher pressure in the *vascular cushions*, rather than the IAS. However, it is very likely that *both* these factors hold part of the truth and contribute to overall increased anal pressures seen in haemorrhoids.

3.4.5. Haemorrhoids and arterial dilating diseases

rs1333047 is an intergenic variant that resides ~4kb upstream of *CDKN2B-AS1* (CDKN2B Antisense RNA 1), located near the *CDKN2B-CDKN2A* gene cluster. This region at 9p21.3 is known to be heavily associated with cardiovascular disease, endometriosis, periodontitis, glaucoma, colorectal cancer, and several aneurysm phenotypes. Striking overlap between the lead SNP at this *CDKN2B-AS1* region and variants previously known to be associated with several aneurysm phenotypes is noted (all variants significantly associated with haemorrhoids and in high LD (r^2 > ~0.8) with rs1333047). All associated variants reside in an ~4.2kb window adjacent to rs1333047: Abdominal aortic aneurysm: rs10757278[83] (P = 2.2×10^{-11}, r^2 = 0.97), rs10757274[84] (P = 1.9×10^{-10}, r^2 = 0.84) ; intracranial aneurysm: rs10733376[85] (P = 2.6 $\times10^{-10}$, r^2 = 0.87), rs10757272[86] (P = 8.5 $\times10^{-10}$, r^2 = 0.85) & rs6475606 (P = 1×10^{-8}, r^2 = 0.79); and combined intracranial, abdominal and thoracic aneurysms (pleiotropy): rs7866503[87] (P = 2.1×10^{-10}, r^2 = 0.86). The dilating venous disorders (namely haemorrhoids, varicose veins, varicoceles) are a phenomenon which occur in a different vascular territory - and with differing clinical manifestations - to the dilating arterial disorders, namely arterial aneurysms and coronary artery ectasia. However, it is understood that they share an overlapping pathobiology, with pathological weakness in vascular wall conferring disease risk.[88] Implicated and shared pathological processes underpinning both arterial and venous dilating disease include ECM remodelling[2,89], oxidative stress[90], increased inflammatory processes[91,92], and increased NO stimulation[93,94] in the vessel wall.

This finding lends support and brings together the previous associations implicated in ECM remodelling, TGF-β signalling and IAS tonicity. Lastly, in an analysis of the pheWAS catalogue, Salnikova, *et al*.[95] identified a pronounced signal (rs4977574, P = 7.0×10^{-4}) at *CDKN2B-AS1*, associated with 2796 haemorrhoids cases and 642 female stress urinary incontinence patients. It is encouraging that in this GWA study, variant rs4977574 at *CDKN2B-AS1* was significantly associated with haemorrhoids and in high LD with the lead SNP at this locus (P = 1.9×10^{-10}, r^2 = 0.84).

3.4.6. Haemorrhoids and colorectal cancer

Cancer of the haemorrhoidal veins is rare[96], however haemorrhoids can often occur alongside colorectal cancer. Rectal bleeding is a common symptom in haemorrhoids; it can be indicative of benign pathology but also of proximal pathology.[97] Discriminating haemorrhoids from anorectal malignancy can be difficult, with coincidental pathology occurring in a large proportion of patients, especially in the elderly.[98] These results support the need for great care in investigating these patients to ensure malignancy (or inflammatory bowel disease) is ruled out.[99] Several studies have previously demonstrated the preponderance of haemorrhoids in colorectal cancer patients[100], and while this may have an associated risk of confounding (due to similar symptomatology), it is an important observation nonetheless.

Of the 12 risk loci associated with haemorrhoids in this study, eight loci are mapped to genes which are associated with malignancy, of which six loci are associated with colorectal malignancy. Mucins are epithelial glycoproteins that are highly-expressed in colorectal cancer.[101] The mucins MUC3A (transmembrane mucin) and MUC12 (membrane-bound mucin) - to which rs4556017 is mapped - are evolutionarily related to each other and thought to be down-regulated in colorectal cancers.[102] ELN (lead SNP: rs77689666) is a component of ECM glycoproteins and is implicated in the tumour microenvironment. ELN gene expression is increased in colorectal tumours, with MMP9 gene expression found to be elevated and MMP12 gene expression down-regulated.[103] Slattery *et al.*[104] found variants in *SMAD3* to confer colon cancer-specific survival. Locus 8q13.3 (lead SNP rs4612371) was eQTL mapped to *LACTB2* via associated SNP rs6999140 in several vascular and cultured fibroblast tissues (GTEx

v8.0 Tibial Artery, P_{eQTL} = 7.34×10^{-17}, FDR = 2.16×10^{-15}; GTEx v8.0 Cells Cultured Fibroblasts, P_{eQTL} = 1.11×10^{-8}, FDR = 2.03×10^{-9}; GTEX v8.0 Aorta Artery, P_{eQTL} = 2.22×10^{-8}, FDR = 1.34×10^{-5})). A recurrent in-frame gene fusion of *LACTB2-NCOA2* has been found to promote colorectal carcinogenesis via inactivation of the negative growth regulatory gene *NCOA2* in colorectal cancer.[105] MDM4 and the nucleoporin Nup155 are intimately involved in in the p53 pathway — with MDM4 regulating p53 activity and Nup155 acting as a p53 repression target.[106] Finally, *CACFD1* mapped by rs687621 (P=3.3×10^{-26}, OR=1.10), encodes human flower (hFWE) - inhibition of flower protein expression has been found to reduce tumour growth and metastasis, including imparting sensitivity to chemotherapy.[14]

3.4.7. Heritability and genetic correlations of haemorrhoids disease

Despite being a highly common condition with a significant global health burden[99], to date, no family or twin studies have attempted to demonstrate the population variance for haemorrhoids disease attributable to genetic differences. Indeed several studies have suggested haemorrhoids has *no* familial component[2,107], or that any familial component is confounded by common lifestyle habits[108] or sufferers increased awareness of their parents' anal health.[3] Through LDSC regression[27], the SNP-based heritability (h^2_g) for haemorrhoids - based on ~10% of the common frequency variants in the GWAS - was found to be 2.37% (0.18%). Since common variation accounts for a small proportion of the overall narrow-sense heritability of complex diseases[109], it is likely that this analysis does not capture the *full* extent of the heritability for haemorrhoids. In this large cohort, haemorrhoids has been found to have a notable genetic architecture, with several significantly associated putative and biologically-plausible risk loci.

Genetic correlation analyses identified several traits which significantly correlated with haemorrhoids. A striking positive correlation was seen between haemorrhoids and weight-related phenotypes (Genetic overlap 11 - 17%). This is supported by the fact that obesity is an independent risk factor for haemorrhoids[110,111]; postulated to impede venous return through increased intraabdominal pressure, and imparting increased stress on rectal musculature.[111] To this end, pregnancy is also a risk factor for haemorrhoids for these reasons[3], and thought to also be compounded by hormonal changes.[3] The correlation analysis highlighted parity status (*number of children ever born*) to be positively correlated (~20% genetic overlap) with haemorrhoids and age

of first birth to be negatively correlated (-20%) with haemorrhoids. These findings are likely due to the fact that a younger age of birth relates to a higher parity status, increasing risk of haemorrhoids.

Several mental-health related phenotypes (neuroticism, depression, and insomnia) were among the most significant and positively correlated (~15 - 26% genetic overlap) with haemorrhoids. Recurrent haemorrhoid symptoms such as anal bleeding, itchiness and pain - made worse by high recurrence following surgery - may impact quality-of-life in patients with haemorrhoids. Lee *et al*. demonstrate in a national cross-sectional study (n = 17,228 (2480 haemorrhoids cases)), that both self-reported depression and physician diagnosed depression significantly correlate with haemorrhoids.[111] A genetic susceptibility to haemorrhoids may therefore include a heightened risk of mental health sequelae in these patients.

3.4.8. Genetic risk score for haemorrhoids correlates with disease severity

In the USA (1999), ~23 million adults (~13% of the USA population) were projected to have haemorrhoids[112], of which 21% (7.7 million) were estimated to have had surgical intervention for haemorrhoids.[113] The genetic risk score derived from the association signals was higher among patients with haemorrhoids requiring surgery (therefore likely to represent the phenotypically more severe end of the disease spectrum), than those managed outwith surgery. This provides the proof-of-concept that the use of genetic risk scoring may enable pinpointing of patients that have a genetic susceptibility towards more severe haemorrhoidal disease that is likely to require surgical intervention. This could foreseeably enable early lifestyle modification, such as weight loss and increased fibre intake, which may show greater impact early in the disease course[32], and moreover enable early intervention when symptoms appear and guide surgical plans.

3.4.9. Strengths and limitations

There are several limitations that warrant further discussion. In the GWAS of varicose veins (**Chapter 2**), ~1/3 of all discovery loci from UK Biobank replicated in an independent cohort. Independent replication of this haemorrhoids GWAS is therefore necessary to control the false positive rate. Further, an independent cohort would enable the genetic risk score to be validated externally, limiting bias. Another weakness is that the genetic factors may be a small contributor to overall disease risk – this suggests that environmental factors, in concert with genetic factors, contribute to overall haemorrhoids disease risk. In the absence of current family or twin studies, and the use of common variation in this study, it is likely that this analysis has underestimated the full extent of the heritability of haemorrhoids.

Several strengths go in some way to lend credence to the study findings. Firstly, the use of the UK Biobank has enabled among the largest study to date of this disease model in the literature, allowing the identification of several robust signals. The rigorous bioinformatic analyses employed has enabled characterisation of biologically viable candidates which demonstrate natural clustering and are supported by previous studies. Lastly, the genetic risk score provides a partial validation of the association, paving the way for genetic risk stratification in personalised medicine approaches to haemorrhoids.

3.5. Conclusion

This study represents the first association analysis of haemorrhoids, a disease with a substantial global prevalence, patient morbidity, and high attributed healthcare costs. Moreover, several of the loci appear to cluster in shared pathways which demonstrate biological plausibility, including extracellular matrix remodelling, TGF-β signalling, and internal anal sphincter hypertonicity. These results lend credence to the study findings and are an important step in highlighting core players in haemorrhoids pathobiology. The weighted genetic risk score correlated with disease severity, indicating that individuals with a higher genetic burden were more likely to be on the phenotypic extreme of haemorrhoids – an important step in personalised medicine approaches to haemorrhoids. Further independent replication analyses and characterisation of loci through functional work are required to characterise these pathways further.

3.6. Chapter References

1. Margetis, N. Pathophysiology of internal hemorrhoids. *Ann. Gastroenterol.* **32**, 264–272 (2019).
2. Pata, F. *et al.* Anatomy, Physiology and Pathophysiology of Haemorrhoids. *Rev. Recent Clin. Trials* **15**, (2020).
3. Loder, P. B., Nicholls, R. J. & Phillips, A. K. S. *Haemorrhoids: pathology, pathophysiology and aetiology*. *British Journal of Surgery* **81**, (1994).
4. Bruch, H. P. & Roblick, U. J. Pathophysiologie des Hämorrhoidalleidens. *Chirurg* **72**, 656–659 (2001).
5. Khan, N. M. M. Injection sclerotherapy versus electrocoagulation in the management outcome of early haemorrhoids - PubMed. *J Pak Med Assoc* **56**, 579–582 (2006).
6. Yildiz, T., Aydin, D. B., Ilce, Z., Yucak, A. & Karaaslan, E. External hemorrhoidal disease in child and teenage: Clinical presentations and risk factors. *Pakistan J. Med. Sci.* **35**, 696–700 (2019).
7. Sudlow, C. *et al.* UK Biobank: An Open Access Resource for Identifying the Causes of a Wide Range of Complex Diseases of Middle and Old Age. *PLoS Med.* **12**, (2015).
8. Bycroft, C. *et al.* The UK Biobank resource with deep phenotyping and genomic data. *Nature* **562**, 203–209 (2018).
9. Loh, P. Mixed-model association for biobank-scale datasets. **50**, 906–908 (2018).
10. Loh, P. R. *et al.* Efficient Bayesian mixed-model analysis increases association power in large cohorts. *Nat. Genet.* **47**, 284–290 (2015).
11. Zheng, J. *et al.* LD Hub: A centralized database and web interface to perform

LD score regression that maximizes the potential of summary level GWAS data for SNP heritability and genetic correlation analysis. *Bioinformatics* **33**, 272–279 (2017).

12. Carvalho-Silva, D. *et al.* Open Targets Platform: new developments and updates two years on. *Nucleic Acids Res.* **47**, D1056–D1065 (2019).
13. Bulik-Sullivan, B. *et al.* LD score regression distinguishes confounding from polygenicity in genome-wide association studies. *Nat. Genet.* **47**, 291–295 (2015).
14. Madan, E. *et al.* Flower isoforms promote competitive growth in cancer. *Nature* **572**, 260–264 (2019).
15. Wang, K. L. M. H. H. ANNOVAR: functional annotation of genetic variants from high-throughput sequencing data. *Nucleic Acids Res.* **38**, e164 (2010).
16. Watanabe, K., Taskesen, E., Van Bochoven, A. & Posthuma, D. Functional mapping and annotation of genetic associations with FUMA. *Nat. Commun.* **8**, 1–10 (2017).
17. Ernst, J. & Kellis, M. Chromatin-state discovery and genome annotation with ChromHMM. *Nat. Protoc.* **12**, 2478–2492 (2017).
18. Rentzsch, P., Witten, D., Cooper, G. M., Shendure, J. & Kircher, M. CADD: predicting the deleteriousness of variants throughout the human genome. *Nucleic Acids Res.* **47**, D886–D894 (2018).
19. Boyle, A. P. *et al.* Annotation of functional variation in personal genomes using RegulomeDB. *Genome Res.* **22**, 1790–1797 (2012).
20. Aguet, F. *et al.* Genetic effects on gene expression across human tissues. *Nature* **550**, 204–213 (2017).
21. Popadin, K. Y. *et al.* Gene Age Predicts the Strength of Purifying Selection

Acting on Gene Expression Variation in Humans. *AJHG* **95**, 660–674 (2014).

22. de Leeuw, C. A., Mooij, J. M., Heskes, T. & Posthuma, D. MAGMA: Generalized Gene-Set Analysis of GWAS Data. *PLoS Comput. Biol.* **11**, 1–20 (2015).
23. Zhu, Z. *et al.* Integration of summary data from GWAS and eQTL studies predicts complex trait gene targets. *Nat. Genet.* **48**, 481–487 (2016).
24. Liberzon, A. *et al.* The Molecular Signatures Database Hallmark Gene Set Collection. *Cell Syst.* **1**, 417–425 (2015).
25. D., W. *et al.* The NHGRI GWAS Catalog, a curated resource of SNP-trait associations. *Nucleic Acids Res.* **42**, D1001–D1006
26. Fang, H., Knezevic, B., Burnham, K. L. & Knight, J. C. XGR software for enhanced interpretation of genomic summary data, illustrated by application to immunological traits. *Genome Med.* **8**, 1–20 (2016).
27. Bulik-Sullivan, B. *et al.* An atlas of genetic correlations across human diseases and traits. *Nat. Genet.* **47**, 1236–1241 (2015).
28. Burkitt, D. P. & Graham-Stewart, C. W. Haemorrhoids-postulated pathogenesis and proposed prevention. *Postgrad. Med. J.* **51**, 631–636 (1975).
29. STELZNER, F. THE CORPUS CAVERNOSUM RECTI. *Dis. Colon Rectum* **7**, 398–9 (1964).
30. Lierse, W. Anatomie und Pathophysiologie des Haemorrhoidalleidens. *Langenbecks Arch Chir 1989;* **1989**, 769–72 (1989).
31. Willis, S., Junge, K., Ebrahimi, R., Prescher, A. & Schumpelick, V. Haemorrhoids - a collagen disease? *Color. Dis.* **12**, 1249–1253 (2010).
32. Serra, R. *et al.* Hemorrhoids and matrix metalloproteinases: A multicenter study on the predictive role of biomarkers. *Surg. (United States)* **159**, 487–494 (2016).
33. Plackett, T. P., Kwon, E., Gagliano, R. A. & Oh, R. C. Case Report Ehlers-

Danlos Syndrome-Hypermobility Type and Hemorrhoids. (2014). doi:10.1155/2014/171803

34. Morgado, P. J., Suárez, J. A., Gómez, L. G. & Morgado, P. J. Histoclinical basis for a new classification of hemorrhoidal disease. *Dis. Colon Rectum* **31**, 474–480 (1988).

35. Johanson, J. F. & Sonnenberg, A. The prevalence of hemorrhoids and chronic constipation. An epidemiologic study. *Gastroenterology* **98**, 380–386 (1990).

36. Thomson, W. H. F. The nature of haemorrhoids. *Br. J. Surg.* **62**, 542–552 (1975).

37. Li, J., Lin, H. & Ren, D. Expression of collagen and elastin fibers in the rectum of patients with obstructed defecation syndrome and its significance. *Zhonghua Wei Chang Wai Ke Za Zhi* **18**, 1215–9 (2015).

38. Abramson, J. H., Gofin, J., Hopp, C., Makler, A. & Epstein, L. M. The epidemiology of inguinal hernia. A survey in western Jerusalem. *J. Epidemiol. Community Health* **32**, 59–67 (1978).

39. Ekici, U., Kartal, A. & Ferhatoglu, M. F. Association Between Hemorrhoids and Lower Extremity Chronic Venous Insufficiency. *Cureus* **11**, (2019).

40. Burkitt, D. P. Varicose Veins Deep Vein Thrombosis, and Haemorrhoids: Epidemiology and Suggested Aetiology. *Br. Med. J.* **2**, 556 (1972).

41. Heslop, J. PILES AND RECTOCELES. *ANZ J. Surg.* **57**, 935–938 (1987).

42. Miedel, A., Tegerstedt, G., Mæhle-Schmidt, M., Nyrén, O. & Hammarström, M. Nonobstetric Risk Factors for Symptomatic Pelvic Organ Prolapse. *Obstet. Gynecol.* **113**, 1089–1097 (2009).

43. Humphreys, D. M. Diverticular disease: Three studies: Part I—Relation to other disorders and fibre intake. *Br. Med. J.* **1**, 424–425 (1976).

44. S, R. J. vd L. G. D. Diverticular disease. Pathology and clinical aspects based on 368 autopsy cases. *Zentralbl Chir* **116**, 991–8 (1991).

45. Maguire, L. H. *et al.* Genome-wide association analyses identify 39 new susceptibility loci for diverticular disease. *Nat. Genet.* **50**, 1359–1365 (2018).

46. Massagué, J., Blain, S. W. & Lo, R. S. TGFβ signaling in growth control, cancer, and heritable disorders. *Cell* **103**, 295–309 (2000).

47. Derynck, R. & Akhurst, R. J. Differentiation plasticity regulated by TGF-β family proteins in development and disease. *Nat. Cell Biol.* **9**, 1000–1004 (2007).

48. Ono, M. Molecular links between tumor angiogenesis and inflammation: Inflammatory stimuli of macrophages and cancer cells as targets for therapeutic strategy. *Cancer Science* **99**, 1501–1506 (2008).

49. Derynck, R. & Zhang, Y. Intracellular signalling: The mad way to do it. *Curr. Biol.* **6**, 1226–1229 (1996).

50. Wells, R. G. Fibrogenesis. V. TGF-β signaling pathways. *American Journal of Physiology - Gastrointestinal and Liver Physiology* **279**, (2000).

51. Roberts, A. B., Russo, A., Felici, A. & Flanders, K. C. Smad3: A key player in pathogenetic mechanisms dependent on TGF-β. in *Annals of the New York Academy of Sciences* **995**, 1–10 (New York Academy of Sciences, 2003).

52. Flanders, K. C. Smad3 as a mediator of the fibrotic response. *International Journal of Experimental Pathology* **85**, 47–64 (2004).

53. Inagaki, Y. & Okazaki, I. Emerging insights into transforming growth factor β Smad signal in hepatic fibrogenesis. *Gut* **56**, 284–292 (2007).

54. Benke, K. *et al.* The role of transforming growth factor-beta in Marfan syndrome. *Cardiol. J.* **20**, 227–234 (2013).

55. Powell, D. W. *et al.* Myofibroblasts. II. Intestinal subepithelial myofibroblasts.

American Journal of Physiology - Cell Physiology **277**, 183–201 (1999).

56. Pucilowska, J. B., Williams, K. L. & Lund, P. K. Fibrogenesis IV. Fibrosis and inflammatory bowel disease: Cellular mediators and animal models. *Am. J. Physiol. - Gastrointest. Liver Physiol.* **279**, (2000).
57. Vetuschi, A. *et al.* Smad3-null mice lack interstitial cells of Cajal in the colonic wall. *Eur. J. Clin. Invest.* **36**, 41–48 (2006).
58. Mckaig, B. C., Hughes, K., Tighe, P. J. & Mahida, A. Y. R. Differential expression of TGF-β isoforms by normal and inflammatory bowel disease intestinal myofibroblasts. *Am. J. Physiol. - Cell Physiol.* **282**, (2002).
59. Latella, G. *et al.* Smad3 loss confers resistance to the development of trinitrobenzene sulfonic acid-induced colorectal fibrosis. *Eur. J. Clin. Invest.* **39**, 145–156 (2009).
60. Lakos, G. *et al.* Targeted disruption of TGF-β/Smad3 signaling modulates skin fibrosis in a mouse model of scleroderma. *Am. J. Pathol.* **165**, 203–217 (2004).
61. Inazaki, K. *et al.* Smad3 deficiency attenuates renal fibrosis, inflammation, and apoptosis after unilateral ureteral obstruction. *Kidney Int.* **66**, 597–604 (2004).
62. Zhao, J. *et al.* Smad3 deficiency attenuates bleomycin-induced pulmonary fibrosis in mice. *Am. J. Physiol. - Lung Cell. Mol. Physiol.* **282**, 585–593 (2002).
63. Lee, J. Il *et al.* Role of Smad3 in platelet-derived growth factor-C-induced liver fibrosis. *Am. J. Physiol. Physiol.* **310**, C436–C445 (2016).
64. Tsushima, H. *et al.* High levels of transforming growth factor in patients with colorectal cancer: Association with disease progression. *Gastroenterology* **110**, 375–382 (1996).
65. Slattery, M. L., Lundgreen, A., Herrick, J. S., Wolff, R. K. & Caan, B. J. Genetic variation in the transforming growth factor-β signaling pathway and survival after

diagnosis with colon and rectal cancer. *Cancer* **117**, 4175–4183 (2011).

66. Slattery, M. L. *et al. Genetic variants in the TGFβ-signaling pathway influence expression of miRNAs in colon and rectal normal mucosa and tumor tissue*.

67. Brewer, C. Endoglin expression as a measure of microvessel density in cervical cancer. *Obstet. Gynecol.* **96**, 224–228 (2000).

68. Akagi, K. *et al.* Estimation of angiogenesis with anti-CD 105 immunostaining in the process of colorectal cancer development. *Surgery* **131**, S109–S113 (2002).

69. Chung, Y. C., Hou, Y. C. & Pan, A. C. H. Endoglin (CD105) expression in the development of haemorrhoids. *Eur. J. Clin. Invest.* **34**, 107–112 (2004).

70. Frenckner, B. & Euler, C. V. Influence of pudendal block on the function of the anal sphincters. *Gut* **16**, 482–489 (1975).

71. Hancock, B. D. Internal sphincter and the nature of haemorrhoids. *Gut* **18**, 651–655 (1977).

72. Gibbons, C. P., Bannister, J. J. & Read, N. W. Role of constipation and anal hypertonia in the pathogenesis of haemorrhoids. *Br. J. Surg.* **75**, 656–660 (1988).

73. Lane, R. H. Measurement of anal pressure in patients with haemorrhoids. *Schweiz. Rundsch. Med. Prax.* **71**, 112–5 (1982).

74. Teramoto, T., Parks, A. G. & Swash, M. Hypertrophy of the external anal sphincter in haemorrhoids: a histometric study. *Gut* **22**, 45–48 (1981).

75. Hancock, B. D. & Smith, K. The internal sphincter and Lord's procedure for haemorrhoids. *Br. J. Surg.* **62**, 833–836 (1975).

76. Bhardwaj, R., Vaizey, C. J., Boulos, P. B. & Hoyle, C. H. V. Neuromyogenic properties of the internal anal sphincter: Therapeutic rationale for anal fissures. *Gut* **46**, 861–868 (2000).

77. Moszkowicz, David; Peschaud, Fredrique; Bessede, Thomas; Benoit, Gerard; Alsaid, B. Internal Anal Sphincter Parasympathetic-Nitrergic and Sympathetic-Adrenergic Innervation: A 3-Dimensional Morphological and Functional Analysis. *Dis Colon Rectum* **55**, 473–481 (2012).

78. O'Kelly, T., Brading, A. & Mortensen, N. Nerve mediated relaxation of the human internal anal sphincter: The role of nitric oxide. *Gut* **34**, 689–693 (1993).

79. Hallett, M. One Man's Poison — Clinical Applications of Botulinum Toxin. *N. Engl. J. Med.* **341**, 118–120 (1999).

80. Patti, R. *et al.* Randomized clinical trial of botulinum toxin injection for pain relief in patients with thrombosed external haemorrhoids. *Br. J. Surg.* **95**, 1339–1343 (2008).

81. Sun, W. M., Peck, R. J., Shorthouse, A. J. & Read, N. W. Haemorrhoids are associated not with hypertrophy of the internal anal sphincter, but with hypertension of the anal cushions. *Br. J. Surg.* **79**, 592–594 (1992).

82. Sun, WM; Read, NW; Shorthouse, A. Hypertensive anal cushions as a cause of the high anal canal pressures in patients with haemorrhoids. *Br. J. Surg.* **7**, 458–462 (1990).

83. Gretarsdottir, S. *et al.* Genome-wide association study identifies a sequence variant within the DAB2IP gene conferring susceptibility to abdominal aortic aneurysm. *Nat. Genet.* **42**, 692–697 (2010).

84. Jones, G. T. *et al.* Meta-Analysis of Genome-Wide Association Studies for Abdominal Aortic Aneurysm Identifies Four New Disease-Specific Risk Loci. *Circ. Res.* **120**, 341–353 (2017).

85. Foroud, T. *et al.* Genome-wide association study of intracranial aneurysm identifies a new association on chromosome 7. *Stroke* **45**, 3194–3199 (2014).

86. Low, SK; Takahashi, A; Cha, PC; Zembutsu, H; Kamatani, N; Kubo, M; Nakamura, Y. Genome-wide association study for intracranial aneurysm in the Japanese population identifies three candidate susceptible loci and a functional genetic variant at EDNRA. *Hum Mol Genet* **21**, 2102–2110 (2012).

87. van 't Hof, F. N. G. *et al.* Shared Genetic Risk Factors of Intracranial, Abdominal, and Thoracic Aneurysms. *J. Am. Heart Assoc.* **5**, (2016).

88. Yetkin, E. & Ileri, M. Dilating venous disease: Pathophysiology and a systematic aspect to different vascular territories. *Med. Hypotheses* **91**, 73–76 (2016).

89. Yetkin, E. & Waltenberger, J. Novel insights into an old controversy: Is coronary artery ectasia a variant of coronary atherosclerosis? *Clinical Research in Cardiology* **96**, 331–339 (2007).

90. Emeto, T. I., Moxon, J. V., Au, M. & Golledge, J. Oxidative stress and abdominal aortic aneurysm: Potential treatment targets. *Clin. Sci.* **130**, 301–315 (2016).

91. Cebral, J. *et al.* Flow conditions in the intracranial aneurysm lumen are associated with inflammation and degenerative changes of the aneurysm wall. *Am. J. Neuroradiol.* **38**, 119–126 (2017).

92. Lim, C. S. & Davies, A. H. Pathogenesis of primary varicose veins. *Br. J. Surg.* **96**, 1231–1242 (2009).

93. Kuhlencordt, P. J. *et al.* Accelerated Atherosclerosis, Aortic Aneurysm Formation, and Ischemic Heart Disease in Apolipoprotein E/Endothelial Nitric Oxide Synthase Double-Knockout Mice. *Circulation* **104**, 448–454 (2001).

94. Jacob, T., Hingorani, A. & Ascher, E. Overexpression of transforming growth factor-β1 correlates with increased synthesis of nitric oxide synthase in varicose veins. *J. Vasc. Surg.* **41**, 523–530 (2005).

95. Salnikova, L. E., Khadzhieva, M. B. & Kolobkov, D. S. Biological findings from

the PheWAS catalog: focus on connective tissue-related disorders (pelvic floor dysfunction, abdominal hernia, varicose veins and hemorrhoids). *Hum. Genet.* **135**, 779–795 (2016).

96. Gujral, D. M., Bhattacharyya, S., Hargreaves, P. & Middleton, G. W. Metastatic rectal adenocarcinoma within haemorrhoids: A case report. *J. Med. Case Rep.* **2**, 128 (2008).

97. Pfenninger, J. L. & Zainea, G. G. *Common Anorectal Conditions: Part I. Symptoms and Complaints*. *American Family Physician* **63**, (2001).

98. Koning, M. & Loffeld, R. Rectal bleeding in patients with haemorrhoids. Coincidental findings in colon and rectum. *Fam Pr.* **27**, 260–262 (2010).

99. Tol, R. R. *et al.* European Society of ColoProctology: guideline for haemorrhoidal disease. *Color. Dis.* **22**, 650–662 (2020).

100. Kune, G. A., Kune, S. & Watson, L. F. Colorectal Cancer Risk, Chronic Illnesses, Operations, and Medications: Case Control Results from the Melbourne Colorectal Cancer Study. *Cancer Res.* **48**, (1988).

101. Matsuyama, T. *et al.* MUC12 mRNA expression is an independent marker of prognosis in stage II and stage III colorectal cancer. *Int. J. Cancer* **127**, 2292–2299 (2010).

102. Byrd, J. C. & Bresalier, R. S. Mucins and mucin binding proteins in colorectal cancer. *Cancer and Metastasis Reviews* **23**, 77–99 (2004).

103. Li, J. *et al.* Elastin is a key factor of tumor development in colorectal cancer. doi:10.1186/s12885-020-6686-x

104. Slattery, M. L. & Lundgreen, A. The influence of the CHIEF pathway on colorectal cancer-specific mortality. *PLoS One* **9**, (2014).

105. Yu, J. *et al.* Disruption of NCOA2 by recurrent fusion with LACTB2 in colorectal

cancer. *Oncogene* **35**, 187–195 (2016).

106. Holzer, K. *et al.* Nucleoporin Nup155 is part of the p53 network in liver cancer. *Nat. Commun.* **10**, 1–13 (2019).

107. Kaidar-Person, O., Person, B. & Wexner, S. D. Hemorrhoidal Disease: A Comprehensive Review. *Journal of the American College of Surgeons* **204**, 102–117 (2007).

108. Johanson, J. F. & Sonnenberg, A. Constipation is not a risk factor for hemorrhoids: A case-control study of potential etiological agents. *Am. J. Gastroenterol.* **89**, 1981–1986 (1994).

109. Yang, J., Zeng, J., Goddard, M. E., Wray, N. R. & Visscher, P. M. Concepts, estimation and interpretation of SNP-based heritability. *Nature Genetics* **49**, 1304–1310 (2017).

110. Riss, S. *et al.* The prevalence of hemorrhoids in adults. doi:10.1007/s00384-011-1316-3

111. Lee, J.-H., Kim, H.-E., Kang, J.-H., Shin, J.-Y. & Song, Y.-M. Factors Associated with Hemorrhoids in Korean Adults: Korean National Health and Nutrition Examination Survey. *Korean J Fam Med* **35**, 227–236 (2014).

112. LeClere, F. B., Moss, A. J., Everhart, J. E. & Roth, H. P. Prevalence of major digestive disorders and bowel symptoms, 1989. *Adv. Data* 1–15 (1992).

113. Sandler, R. S. & Peery, A. F. Rethinking What We Know About Hemorrhoids. *Clinical Gastroenterology and Hepatology* **17**, 8–15 (2019).

.

3.7. Chapter Appendix

The appendix for this chapter is provided as an online supplement at the following URL: **bit.ly/WAhmed_C3Appendix**

Table of Contents

Chapter 4: The shared genetic architecture of hernia phenotypes

4.1. Introduction

4.1.1. Rationale and aims

In **Chapter 1** I provided evidence for hernia being a complex disease model, with known familial clustering. Patients with a positive family history are at an eight-fold increased risk of groin hernia[1,2], and have an increased susceptibility to both contralateral and recurrent inguinal hernia.[3–5] Moreover, both concordant and discordant standardised incidence ratios (SIR) for multiple abdominal wall hernia (AWH) subtypes have been found to be higher than 2 in a study by Zöller *et al*[6], suggesting multiple hernia susceptibility, which is supported by clinical observational data.[7,8]

The broad aim of this chapter is to study the shared genetic architecture between four hernia subtypes. My hypothesis is that there will be certain genetic regions that predispose to more than one hernia subtype.

I will investigate this by:

1) Performing individual GWAS of four hernia subtypes (inguinal, femoral, umbilical, and hiatus hernia) using the UK Biobank resource
2) Look for evidence of shared genetics between these hernia subtypes by performing:

   i) Combined GWAS analyses of all four individual hernia subtypes in UK biobank and participants with multiple overlapping hernia phenotypes, as well as a GWAS of multiple overlapping hernia phenotypes alone

ii) A multi-trait analysis of all four individual hernia phenotypes in UK Biobank to uncover genetic regions of shared susceptibility

iii) A multivariate meta-analysis of all four individual hernia phenotypes in UK Biobank to uncover genetic regions of shared susceptibility

4.2. Methods

4.2.1. Ethics and consent

The research ethics and consent procedures of the UK Biobank are provided in **Chapter 2 (Section 2.2.1.)**.[9]

4.2.2. Study participants

A complete description of the study participants of the UK Biobank cohort are provided in **Chapter 2 (Section 2.2.2.)**.[10]

The UK Biobank cohort was used to define three different sets of hernia case-control cohorts, as described below:

i) **Individual hernia** – these were four sets of hernia cases that had diagnostic and/or operative codes for only *one* of the four hernia types. i.e. ether inguinal, femoral, umbilical or hiatus hernia. In other words, for all four hernia cases, cases with phenotype coding for more than one hernia were removed from the cohort. All cases in this cohort were matched 1:5 to non-hernia controls.

ii) **Overlap hernia –** this cohort consisted of hernia cases with diagnostic and/or operative coding for *more than* one of the four hernia types. In other words, cases with phenotype coding for only one of the four hernia types were removed from the cohort. All cases in this cohort were matched 1:5 to non-hernia controls.

iii) **Umbrella hernia** – this cohort consisted of the full set of hernia cases in UK Biobank (i.e. any individual with at least one diagnostic code for any hernia subtype was included in this group). The umbrella cohort was therefore constructed by combining cohorts (i) and (ii). All cases in this cohort were matched 1:5 to non-hernia controls.

i) Individual hernia cohort

The four individual hernia cases were defined if they had at least one of the following diagnostic or operative codes consistent with either inguinal, femoral, umbilical or hiatus hernia (**Appendix Table 4.1)**:

1. Primary and/or secondary ICD-10 codes for either inguinal, femoral, umbilical or hiatus hernia.
2. Primary and/or secondary OPCS code for either inguinal, femoral, umbilical or hiatus hernia.
3. Self-reported operation code for either inguinal, femoral, umbilical or hiatus hernia surgery.
4. Self-reported non-cancer illness code for either inguinal, femoral, umbilical or hiatus hernia.

For the four hernia case cohorts, after quality control (described in **Section 4.2.4**), 23,007 participants had diagnostic or operative codes for inguinal hernia, 1,578 for femoral hernia, 7,432 for umbilical hernia, and 31,543 for hiatus hernia. The final individual hernia cohorts were then defined by removing all overlapping hernia cases (a total of 4,216 overlapping cases were removed from the inguinal hernia cohort, 605

from the femoral hernia cohort, 2,076 from the umbilical hernia cohort and 4,596 from the hiatus hernia cohort). The final four individual hernia cohorts consisted of 18,791 inguinal hernia, 973 femoral hernia, 5,356 umbilical hernia, and 31,543 hiatus hernia cases **(Figure 4.1)**.

All individual hernia cases were matched 1:5 to controls in the UK Biobank cohort based on i) age (+/- 5 years), ii) sex, iii) genotyping platform. All control cohorts contained completely distinct participants.

The final individual hernia cohorts therefore consisted of the following participants:

- **Inguinal hernia:** 112,746 participants (18,791 cases and 93,955 controls)
- **Femoral hernia:** 5,838 participants (973 cases and 4,865 controls)
- **Umbilical hernia:** 32,136 participants (5,356 cases and 26,780 controls)
- **Hiatus hernia:** 193,788 participants (32,298 cases and 161,490 controls)

ii) Overlap hernia cohort

The overlap hernia cases were those cases that had diagnostic or operative codes for two or more hernia types and were subsequently removed from the individual hernia cohort. The final overlap cohort consisted of 5,219 cases (**Figure 4.2**), which were matched 1:5 (using the above described approach) to 26,095 non-hernia controls (total cohort 31,314 participants).

iii) Umbrella hernia cohort

The umbrella hernia cases were defined if they had diagnostic or operative codes for any hernia types, including those with an individual or overlapping hernia. The final umbrella cohort consisted of 62,637 cases after quality control (described in **Section 4.2.4**) (**Figure 4.3**), which were subsequently matched 1:5 (using the approach described previously) to 313,185 non-hernia controls (total cohort 375,822 participants)

Figure 4.1: Venn diagram of the four individual hernia case cohorts in UK Biobank. Following quality control (described in **Section 4.2.4**), a total of 62,637 participants in UK Biobank possessed a diagnostic and/or operative code for at least one of the four hernia subtypes. 5,219 cases possessed coding for two or more hernia subtypes (i.e. overlapping hernia) and were therefore removed (*grey*) to define the four individual hernia case cohorts (total 57,418).

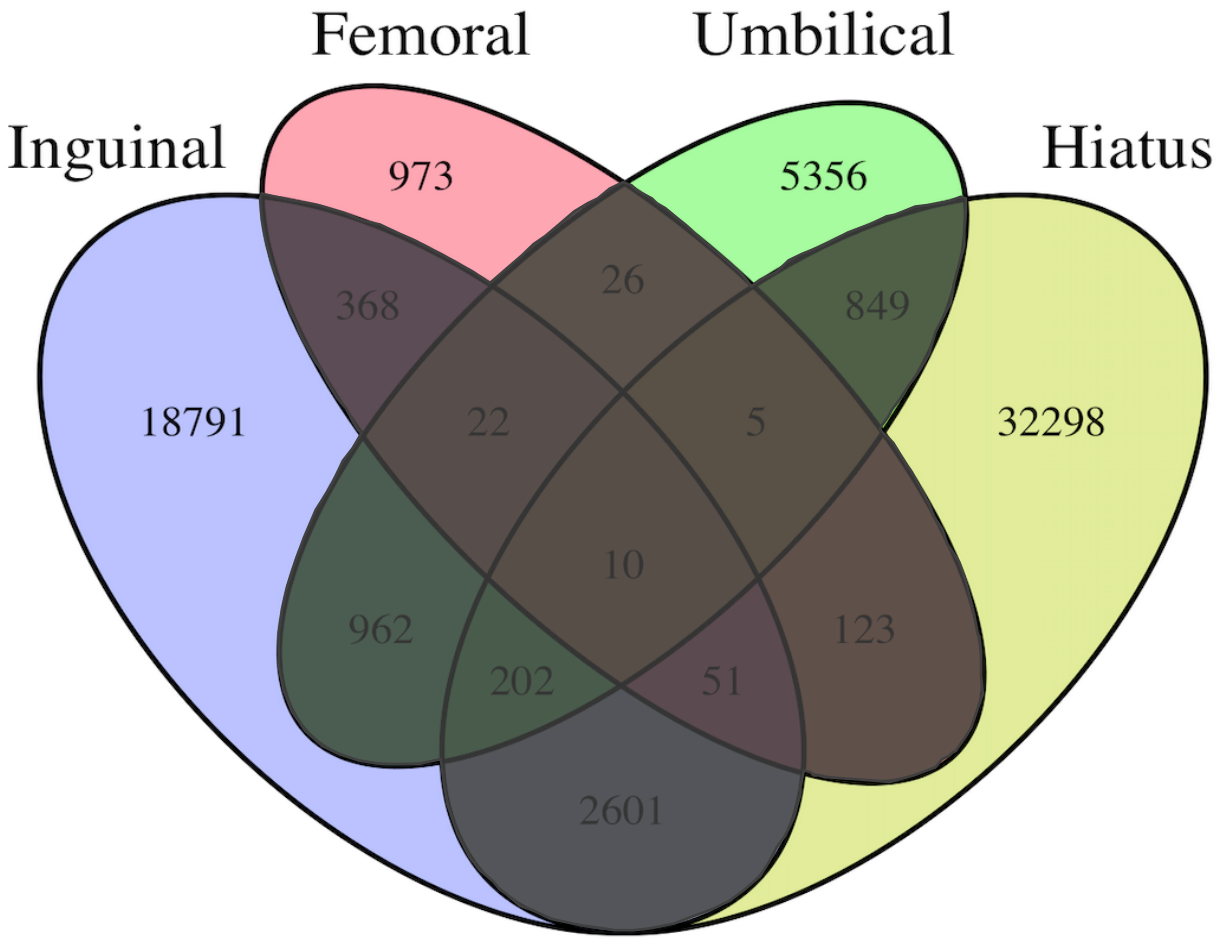

Figure 4.2: Venn diagram of the overlap hernia case cohort in UK Biobank. Following quality control (described in **Section 4.2.4**), a total of 5,219 cases possessed codes for two or more hernia subtypes (i.e. overlapping hernia) and were therefore included in the overlap hernia cohort. All cases with phenotype codes for only one hernia type were removed from this cohort (grey).

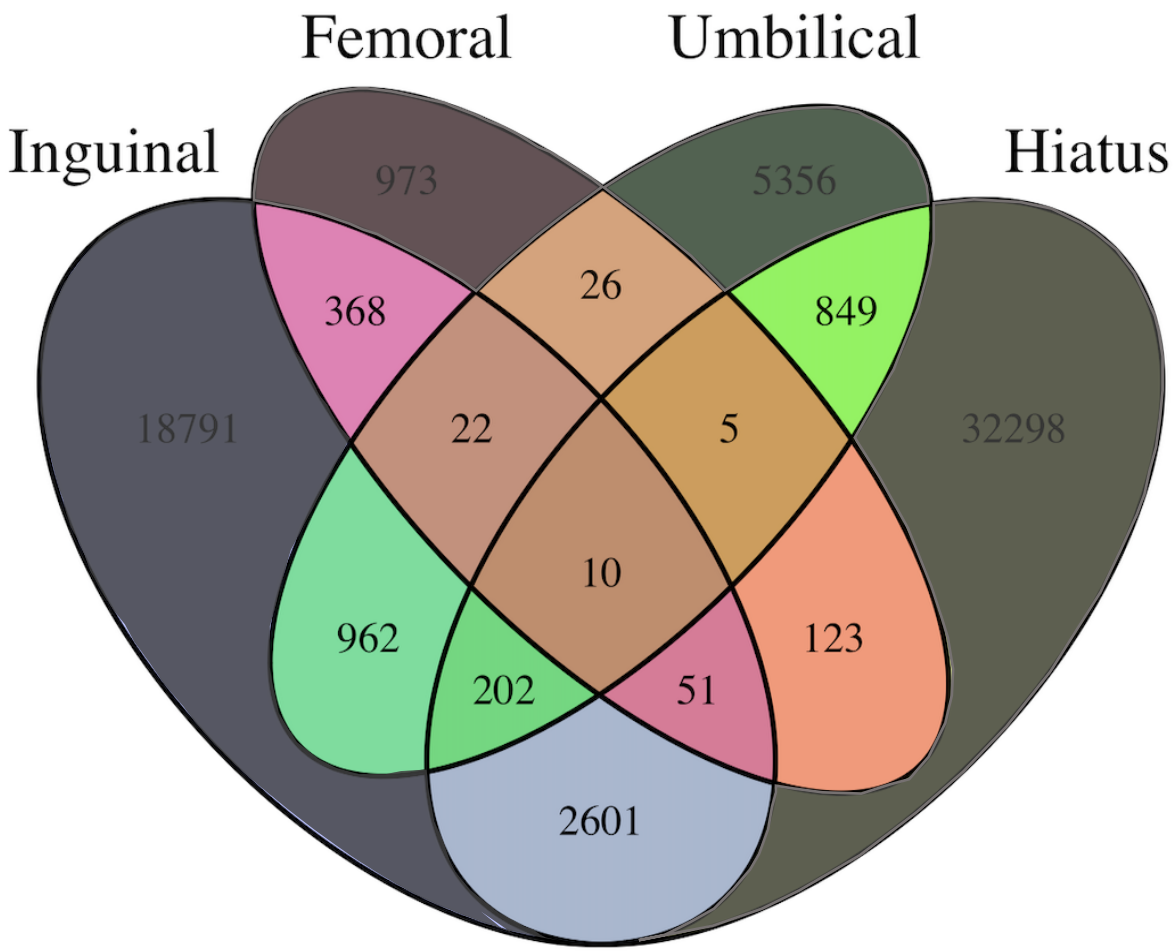

Figure 4.3: Venn diagram of the umbrella hernia case cohort in UK Biobank. Following quality control (described in **Section 4.2.4**), a total of 62,637 cases possessed codes for at least one hernia subtype and were therefore included in the umbrella hernia cohort.

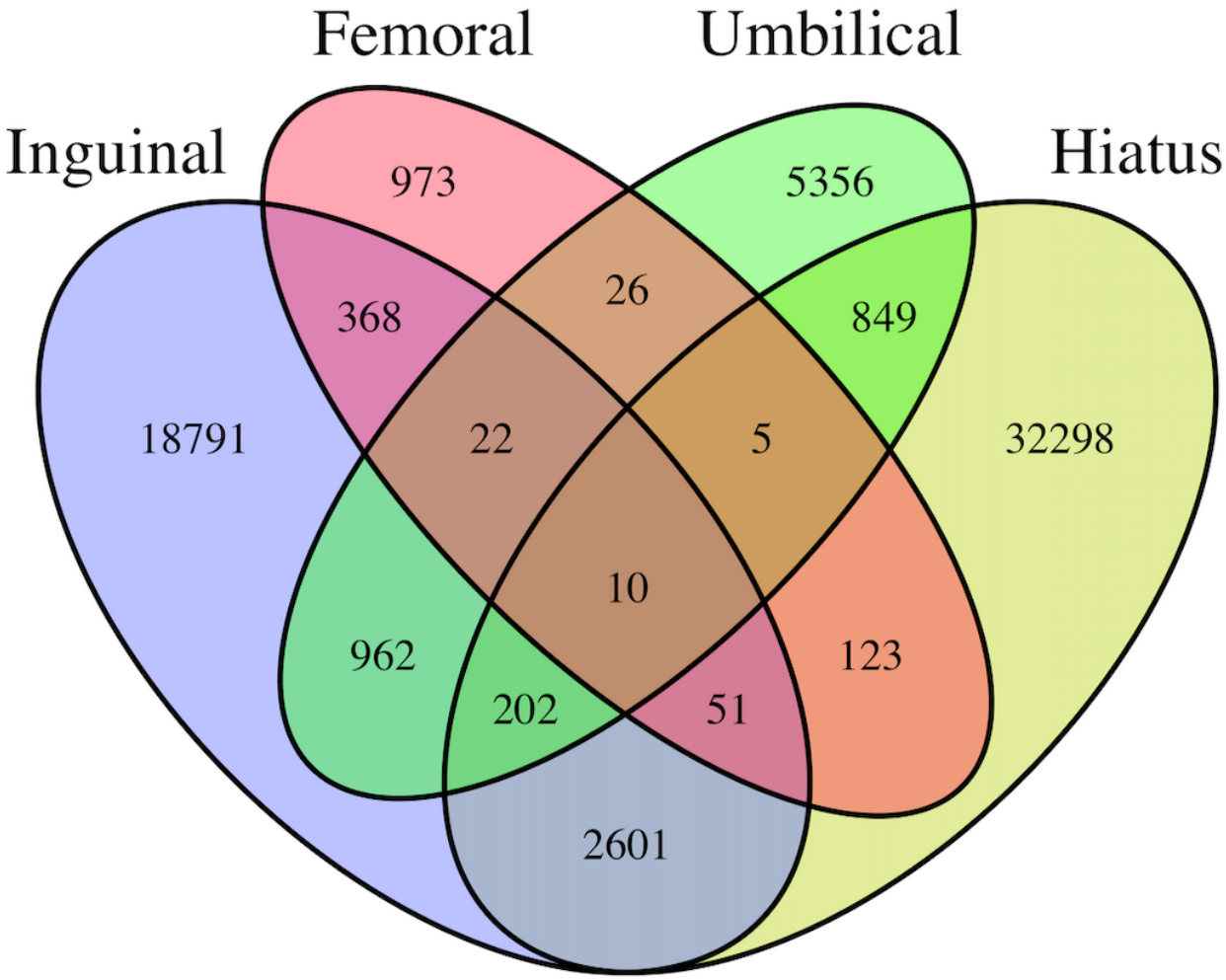

4.2.3. Genotyping

A complete description of the genotyping procedure for the UK Biobank cohort is provided in **Chapter 2 (Section 2.2.3.)**.[10]

4.2.4. Quality control

A complete description of the quality control (QC) procedure implemented centrally by UK Biobank and locally by our group is provided in **Chapter 2 (Section 2.2.4.).**[10]

After central (UK Biobank)[10], and local QC implementation, 86,794 participants and 230,562 genotyped SNPs were excluded from subsequent association analyses (See **Chapter 3**, **Figure 3.3**). In summary, a maximal set of 547,011 genotyped variants and 401,583 participants of white British ancestry passed the QC and were available for inclusion in the three hernia cohorts – matching was subsequently performed to define each cohort as described in **Section 4.2.2**.

4.2.5. Imputation

A complete description of the imputation methodology is provided in **Chapter 2 (Section 2.2.5)**.[10]

4.2.6. Association analyses in BOLT-LMM

Genome-wide association testing was performed across a total of ~9M SNPs (~500K genotyped (MAF ≥ 0 .01) and ~8.4M imputed SNPs (MAF ≥ 0.01, INFO Imputation score ≥ 0.90)) for each of the four individual, overlap and umbrella cohorts using a linear mixed non-infinitesimal model implemented in BOLT-LMM v2.323.[11,12]

Further methodological details pertaining to the association analysis performed using BOLT-LMM[11,12] in this chapter are provided in **Chapter 2 (Section 2.2.13)**.

4.2.7. Genomic risk loci definition for BOLT-LMM studies

A complete description of the methods used for genomic risk loci definition for the individual, overlap and umbrella BOLT-LMM[11,12] analysis results is provided in **Chapter 2 (Section 2.2.7)**.

4.2.8. Functional annotation of BOLT-LMM studies

A complete description of the methods used for the functional annotation of variants for the individual, overlap and umbrella BOLT-LMM[11,12] analysis results is provided in **Chapter 2 (Section 2.2.8)**.

4.2.9. Candidate gene mapping of BOLT-LMM studies

A complete description of the methods used for the candidate gene mapping approach for the individual, overlap and umbrella BOLT-LMM[11,12] analysis results is provided in **Chapter 2 (Section 2.2.9)**.

4.2.10. Gene set, tissue and pathway analyses of BOLT-LMM studies

These analyses were performed for the individual, overlap, and umbrella analyses. This section follows the methodology described in **Chapter 2 (Section 2.2.10)**.

4.2.11. SNP-based heritability of BOLT-LMM studies

Methodological details on the SNP heritability analysis for each of the individual, overlap and umbrella summary statistics is described in **Chapter 2 (Section 2.2.11.)**.

4.2.12. Genetic risk score for hernia

The weighted genetic risk score (wGRS) methodology implemented in this chapter mirrors those described in **Chapter 2** (**Section 2.2.14.)**.[13] For each of the individual, overlap and umbrella summary statistics, the wGRS was compared between six groups of participants from the GWAS: i) all cases vs all controls; ii) surgical cases vs non-surgical cases, ii) cases with a single hernia (i.e. individual hernia cases) vs cases with that particular hernia type plus at least one more hernia type (i.e. overlapping hernia cases).

4.2.13. Multi-trait analysis in MTAG

To unpick the shared genetics behind the hernia phenotypes, MTAG (multi-trait analysis of GWAS) was implemented across the four individual hernia cohorts (total

57,418 cases and 287,090 controls).[14] The MTAG method enables joint analysis of summary statistics by combining several genetically correlated traits to augment the power to discover new susceptibility loci. MTAG produces trait-specific effect estimates across each SNP and through inverse-variance-weighted meta-analysis for each single-trait GWAS, MTAG outputs trait-specific association statistics.[14] The MTAG analysis makes a homogeneity assumption across all SNPs, assuming an equal variance–covariance matrix of effect sizes across the traits. MTAG therefore works optimally when there is high genetic correlation between the input traits. The original authors have demonstrated analytically that even in scenarios where this assumption is not true, MTAG is a consistent and reliable estimator.[14] The final MTAG analysis was therefore performed across a shared 6,760,521 SNPs from each of the four individual hernia phenotypes. The genome-wide significant threshold for the MTAG association was set a $P < 5\times10^{-8}$. Pairwise testing was performed in GWAMA for all MTAG signals where the MTAG derived P-value was stronger than all four individual hernia trait P-values.[15]

4.2.14. Multivariate meta-analysis in metaUSAT

The metaUSAT multivariate method was used as an auxiliary meta-analysis method to further characterise potential regions of shared hernia susceptibility between the four individual hernia traits.[16] metaUSAT (meta-analysis unified score-based association test) performs a unified association test for each SNP (using the estimated correlation matrix to test association) across several trait summary statistics.[16] metaUSAT is data-adaptive, and was established to be robust to the association structure of correlated traits (less affected by the true (unknown) association structure)

and is not dependent on individual-level data.[16] Unlike MTAG[14], metaUSAT does not assume homogeneity of effects across traits. metaUSAT outputs an approximate asymptotic P-value for the meta-analysis association and has been shown to maintain a low type I error in simulation experiments.[16] The metaUSAT meta-analysis was performed across the four individual hernia cohorts (total 57,418 cases and 287,090 controls) and 8,896,286 SNPs. The genome-wide significant threshold for the metaUSAT association was set a $P < 5\times10^{-8}$.

4.2.15. URLs

metaUSAT, https://github.com/RayDebashree/metaUSAT; MTAG, https://github.com/JonJala/mtag

4.3. Results

The analytic workflow implemented to unpick shared genetic biology between hernia phenotypes is summarised in **Figure 4.4**.

4.3.1. Association analysis of individual hernia phenotypes in BOLT-LMM

Association analysis of inguinal hernia yielded 24 susceptibility loci (3076 variants), 20 of which were previously unreported (all four previously associated inguinal hernia loci replicated in UK Biobank[17]) (**Table 4.1**). Conditional regression analysis[11,12] provided evidence for a further four independent signals at three inguinal hernia susceptibility loci: **2p16.1** (*EFEMP1*), **8p21.2** (*EBF2*) and **11p13** (*WT1*). In the femoral hernia analysis, 43 genome-wide significant variants clustering in a single ~10kb region at one independent locus was identified, **1q41** (lead variant rs7538503; $P = 1.3\times10^{-10}$, OR = 1.42) (**Table 4.2**). Association analysis for umbilical hernia uncovered five novel independent susceptibility loci (277 variants) (**Table 4.3**). The statistically strongest signal was rs4846567, a predicted pathogenic, genotyped, regulatory region variant at **1q41** (*ZC3H11B*) ($P = 1.7\times10^{-18}$, OR = 1.22, CADD = 14.9). Lastly, for the hiatus hernia association analysis, eight independent signals were discovered at eight susceptibility loci (all novel) (**Table 4.4**). Locus Zoom plots for all associations can be found in **Appendix Figure 4.1**.

In summary, 52 independent signals across 38 loci (34 novel) were found to be associated with the four individual hernia phenotypes (**Figure 4.5**). The strongest associated signal across all hernia phenotypes was rs6983815, which associated with inguinal hernia ($P = 1.1\times10^{-54}$, OR = 1.19) at **8p21.2** (*EBF2*)— this region did not

associate with any of the other hernia phenotypes. The signal with the largest effect size was rs7538503 at **1q41** (*ZC3H11B*) ($P = 1.3\times10^{-10}$, OR = 1.42), which associated with femoral hernia. The λ_{GC} demonstrated nominal inflation levels across the four association analyses, ranging from 1.00-1.20 ($\lambda_{GC\text{-}femoral}$: 1.00; $\lambda_{GC\text{-}umbilical}$: 1.05; $\lambda_{GC\text{-}inguinal}$: 1.15; $\lambda_{GC\text{-}hiatus}$: 1.20), however the LDSC intercept range of 1.00-1.03 (Femoral: 1.00; Umbilical: 1.01; Inguinal: 1.02; Hiatus: 1.03) and an attenuation ratio of 0.08-0.19 (Umbilical: 0.08; Inguinal:0.11; Hiatus: 0.13; Femoral: 0.19) is fully in keeping with the effects of polygenicity and large sample size (**Appendix Figure 4.2**).[18]

Shared susceptibility between multiple hernia subtypes was seen at five loci (four loci demonstrating concordance in allelic effect directions). The most striking evidence of shared susceptibility was seen at **1q41** (near *ZC3H11B*), which associated with three of four hernia subtypes: inguinal hernia (lead variant rs2820441, $P = 6.6\times10^{-13}$, OR = 1.09, EAF = 0.32(G)), femoral hernia (rs7538503 ($P = 1.3\times10^{-10}$, OR = 1.42, EAF = 0.29(G)), and umbilical hernia (rs4846567, $P = 1.7\times10^{-18}$, OR = 1.22, EAF = 0.31(T)). A further four loci showed overlap between two hernia subtypes. Shared susceptibility was demonstrated between inguinal and hiatus hernia at three loci: **2p16.1** (*EFEMP1*) (rs11899888, $P_{Inguinal} = 2.2\times10^{-12}$, OR = 1.16, EAF = 0.16(G); rs10207635, $P_{Hiatus} = 1.3\times10^{-8}$, OR = 1.07, EAF =0.13)), **6p22.2** (*MHC region*) (rs13212652, $P_{Inguinal} = 3.1\times10^{-11}$, OR = 1.12, EAF=0.87(T); rs9393735, $P_{Hiatus} = 2.7\times10^{-8}$, OR = 1.07, EAF = 0.86(G)), and **11p13** (*WT1*) (rs4140413, $P_{Inguinal} = 2.4\times10^{-20}$, OR =1.11, EAF = 0.63(G); rs11031796, $P_{Hiatus} = 3.6\times10^{-16}$, OR = 1.07, EAF = 0.62(G)). A shared susceptibility locus was also demonstrated between umbilical and hiatus hernia at locus **7q33** (*CALD1*) (rs12707188, $P_{Umbilical} = 5.0\times10^{-15}$, OR = 1.19, EAF = 0.37(T); rs4728341,

P_{Hiatus} = 3.9×10^{-10}, OR = 1.06, EAF = 0.55(T)), although these associations were intriguingly in opposite effect directions.

Figure 4.4: Hernia GWA study design and shared genetics analysis workflow. The three analysis approaches to characterise the shared genetic biology of hernia in UK Biobank are depicted.

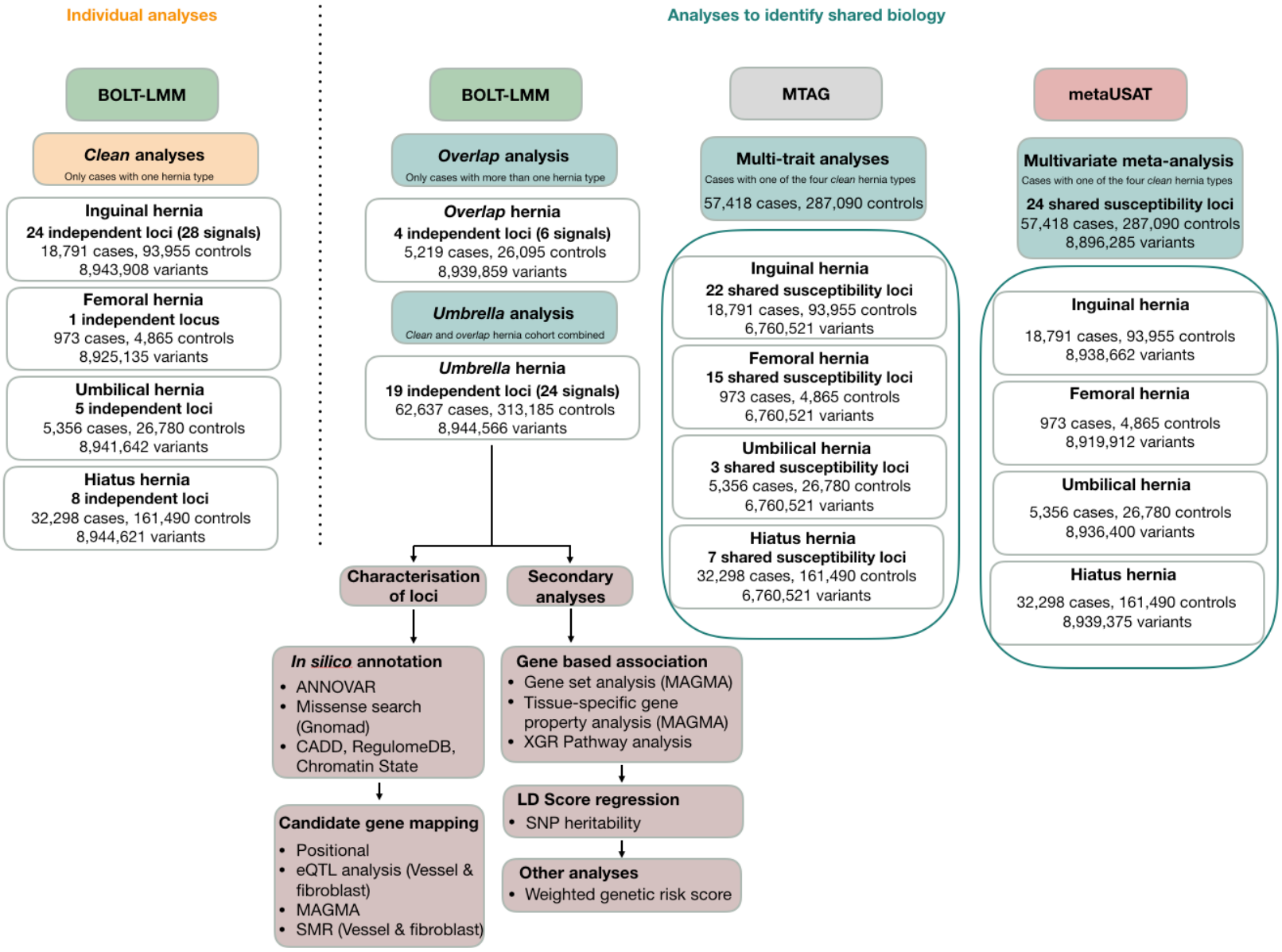

Table 4.1. Twenty-eight signals at 24 loci associated with inguinal hernia in 18791 cases and 93955 controls in UK Biobank

Chromosome	Position[a]	rsID	EA[b]	NEA[c]	EAF[d]	Info[e]	OR (95% CI)	P-value	Mapped genes[f]
1	**9443340**	**rs1106370**	**A**	**G**	**0.42**	**0.990**	**1.07 (1.04-1.09)**	**1.0×10^{-8}**	***SPSB1***
1	**219734960**	**rs2820441**	**C**	**A**	**0.32**	**G**	**1.09 (1.06-1.11)**	**6.6×10^{-13}**	**-**
2	**43665943**	**rs76684055**	**G**	**A**	**0.90**	**0.998**	**1.12 (1.08-1.16)**	**2.8×10^{-10}**	***THADA, ZFP36L2***
2[#]	56102744	rs11899888	G	A	0.16	0.987	1.16 (1.13-1.20)	2.2×10^{-12}	*EFEMP1, PNPT1*
2	56106928	rs59985551	C	T	0.78	0.998	1.19 (1.16-1.22)	4.7×10^{-40}	*EFEMP1, PNPT1*
2[#]	56197200	rs7564964	A	G	0.57	0.995	1.13 (1.10-1.15)	2.2×10^{-10}	-
3	**55602137**	**rs61613824**	**A**	**T**	**0.37**	**0.987**	**1.08 (1.05-1.10)**	**1.1×10^{-10}**	***ERC2***
3	**56141843**	**rs7647972**	**C**	**G**	**0.70**	**0.991**	**1.09 (1.06-1.11)**	**8.9×10^{-12}**	***CCDC66, ERC2***
3	**100297679**	**rs13083051**	**T**	**C**	**0.92**	**0.986**	**1.12 (1.08-1.17)**	**2.9×10^{-8}**	***TMEM45A***
4	**4949339**	**rs4330303**	**G**	**A**	**0.68**	**0.975**	**1.07 (1.04-1.09)**	**2.4×10^{-8}**	**-**
4	**174616174**	**rs56063997**	**C**	**T**	**0.36**	**0.988**	**1.07 (1.05-1.10)**	**3.6×10^{-10}**	**-**
5	64355060	rs370763	A	T	0.67	0.998	1.10 (1.08-1.13)	3.3×10^{-17}	*ADAMTS6, CWC27*
6	**6743149**	**rs1294421**	**T**	**G**	**0.40**	**G**	**1.07 (1.05-1.10)**	**5.6×10^{-10}**	**-**
6	**26099279**	**rs13212652**	**T**	**G**	**0.87**	**1.000**	**1.12 (1.08-1.15)**	**3.1×10^{-11}**	***BTN2A1, BTN3A2, C6orf15, HFE, HIST1H1A, HIST1H1B, HIST1H1C, HIST1H1T, HIST1H2AB, HIST1H2AC, HIST1H2AJ, HIST1H2AL, HIST1H2BB, HIST1H2BC, HIST1H2BL, HIST1H2BN, HIST1H3A, HIST1H3B, HIST1H3C, HIST1H3I, HIST1H3J, HIST1H4A, HIST1H4B, HIST1H4C, HIST1H4L, LRRC16A, OR2B2, PGBD1, SCGN, SLC17A1, SLC17A2, SLC17A3, SLC17A4, TRIM26, TRIM31, TRIM38, ZKSCAN3, ZKSCAN4, ZKSCAN8, ZNF165, ZNF322, ZSCAN12, ZSCAN16, ZSCAN31, ZSCAN9***

									APOM, BRD2, C4A, C4B, C6orf10, GPANK1, HLA-DMA, HLA-DMB, HLA-DOB, HLA-DQB1, HLA-DQB2, HLA-DRA, HLA-DRB5, LSM2, LY6G5B, MICB, MSH5, MSH5-SAPCD1, NOTCH4, PSMB8, PSMB9, RNF5, SKIV2L, TAP1, TAP2, VARS, VWA7, XXbac-BPG181M17.5
6	**32808299**	**rs45506201**	**G**	**A**	**0.90**	**0.996**	**1.11 (1.07-1.15)**	**5.6×10^{-9}**	
6	**45481873**	**rs62400367**	**A**	**G**	**0.85**	**0.983**	**1.09 (1.06-1.12)**	**2.9×10^{-8}**	***RUNX2***
6	**143676186**	**rs6570555**	**A**	**T**	**0.43**	**0.995**	**1.08 (1.06-1.11)**	**7.8×10^{-13}**	***AIG1***
7	**25681464**	**rs10951081**	**C**	**A**	**0.33**	**0.968**	**1.07 (1.05-1.10)**	**5.3×10^{-9}**	**-**
7	**73540726**	**rs3895707**	**C**	**T**	**0.91**	**0.987**	**1.11 (1.07-1.15)**	**2.3×10^{-8}**	***ELN, LIMK1***
8[#]	25435170	rs10481336	C	T	0.21	0.986	1.10 (1.08-1.13)	1.6×10^{-15}	*CDCA2, DOCK5, GNRH1, KCTD9*
8	25717620	rs6983815	A	T	0.41	0.996	1.19 (1.17-1.22)	1.1×10^{-54}	*EBF2*
9	**16766118**	**rs7850168**	**C**	**A**	**0.08**	**0.980**	**1.12 (1.08-1.17)**	**1.7×10^{-8}**	***BNC2***
11[#]	32350027	rs7924571	C	A	0.78	0.995	1.08 (1.06-1.11)	8.8×10^{-9}	*CCDC73, EIF3M*
11	32459228	rs4140413	G	T	0.63	0.988	1.11 (1.09-1.14)	2.4×10^{-20}	*CCDC73, EIF3M, WT1*
12	**66328027**	**rs12810758**	**T**	**C**	**0.23**	**0.991**	**1.08 (1.05-1.11)**	**3.2×10^{-9}**	***AC090673.2, HMGA2***
13	**32398964**	**rs796861335**	**C**	**CT**	**0.41**	**0.960**	**1.06 (1.04-1.09)**	**4.6×10^{-8}**	***FRY, RXFP2***
16	**84856552**	**rs4238714**	**C**	**T**	**0.42**	**0.992**	**1.09 (1.06-1.11)**	**2.8×10^{-13}**	***CRISPLD2***
17	**12191339**	**rs12453693**	**T**	**C**	**0.31**	**0.995**	**1.08 (1.06-1.11)**	**3.0×10^{-11}**	**-**

[a]Based on NCBI Genome Build 37 (hg19).
[b]The effect allele.
[c]The non-effect allele.
[d]The effect allele frequency.
[e]The SNP INFO score for imputed SNPs; G = genotyped SNP.
[f] The 101 genes prioritised at these loci based on positional mapping, eQTL mapping, MAGMA gene mapping and summary-based mendelian randomisation (see Methods).
[#]Denotes the four residual significant signals following conditional regression analysis at the lead SNP at the locus.
Bold loci are those that have not been previously reported.

Table 4.2. One previously unreported locus significantly associated with femoral hernia in 973 cases and 4865 controls in UK Biobank.

Chromosome	Position[a]	rsID	EA[b]	NEA[c]	EAF[d]	Info[e]	OR (95% CI)	P-value	Mapped genes[f]
1	219788530	rs7538503	G	A	0.29	0.995	1.42 (1.27-1.58)	1.3×10^{-10}	-

[a]Based on NCBI Genome Build 37 (hg19).
[b]The effect allele.
[c]The non-effect allele.
[d]The effect allele frequency.
[e]The SNP INFO score for imputed SNPs; G = genotyped SNP.
[f] No genes were prioritised at this loci based on positional mapping, eQTL mapping, MAGMA gene mapping and summary-based mendelian randomisation (see Methods).

Table 4.3. Five previously unreported loci significantly associated with umbilical hernia in 5,356 cases and 26,780 controls in UK Biobank.

Chromosome	Position[a]	rsID	EA[b]	NEA[c]	EAF[d]	Info[e]	OR (95% CI)	P-value	Mapped genes[f]
1	219750717	rs4846567	T	G	0.31	G	1.22 (1.17-1.28)	1.7×10^{-18}	-
2	146365492	Not available	C	CAA	0.56	0.990	1.13 (1.08-1.17)	2.5×10^{-8}	-
2	199676405	rs778276885	AT	A	0.51	0.996	1.12 (1.08-1.17)	3.9×10^{-8}	-
7	134591097	rs12707188	T	C	0.37	0.998	1.19 (1.14-1.24)	5.0×10^{-15}	*CALD1*
12	78154757	rs2887596	T	C	0.47	0.998	1.12 (1.08-1.17)	2.7×10^{-8}	-

[a]Based on NCBI Genome Build 37 (hg19).
[b]The effect allele.
[c]The non-effect allele.
[d]The effect allele frequency.
[e]The SNP INFO score for imputed SNPs; G = genotyped SNP.
[f] One gene was prioritised at these loci based on positional mapping and MAGMA gene mapping (see Methods).

Table 4.4. Eight previously unreported loci significantly associated with hiatus hernia in 32,298 cases and 161,490 controls in UK Biobank.

Chromosome	Position[a]	rsID	EA[b]	NEA[c]	EAF[d]	Info[e]	OR (95% CI)	P-value	Mapped genes[f]
2	56040035	rs10207635	T	A	0.13	1.000	1.07 (1.05-1.10)	1.3×10^{-8}	*EFEMP1*
3	70920485	rs4499560	A	T	0.31	0.984	1.07 (1.05-1.08)	8.9×10^{-12}	-
5	4977446	rs42202	A	G	0.08	0.986	1.14 (1.10-1.18)	8.0×10^{-16}	-
6	26582327	rs9393735	A	G	0.86	G	1.07 (1.05-1.10)	2.7×10^{-8}	*BTN2A1, BTN3A2, HIST1H2BN, HIST1H4L, HMGN4, OR2B2, ZNF311, ZNF391*
7	134605106	rs4728341	T	C	0.55	0.965	1.06 (1.04-1.07)	3.9×10^{-10}	*CALD1*
9	96624645	rs4075733	C	T	0.46	0.996	1.05 (1.04-1.07)	1.5×10^{-9}	-
11	32479807	rs11031796	G	A	0.62	0.998	1.07 (1.06-1.09)	3.6×10^{-16}	*WT1*
19	18787981	rs2891698	G	A	0.47	0.998	1.06 (1.04-1.07)	4.0×10^{-10}	*CRTC1, KLHL26, TMEM59L, UBA52*

[a]Based on NCBI Genome Build 37 (hg19).
[b]The effect allele.
[c]The non-effect allele.
[d]The effect allele frequency.
[e]The SNP INFO score for imputed SNPs; G = genotyped SNP.
[f]The 15 genes prioritised at these loci based on positional mapping, eQTL mapping and MAGMA gene mapping (see Methods).

Figure 4.5. Manhattan plots for the four individual hernia analyses in UK Biobank. Manhattan plots are annotated with the gene names of loci that demonstrate shared susceptibility across two or more individual analyses (*Bold*). The 6q24.2 (*AIG1)* locus is plotted for inguinal hernia because it shows shared susceptibility with the overlap hernia analysis (discussed later).

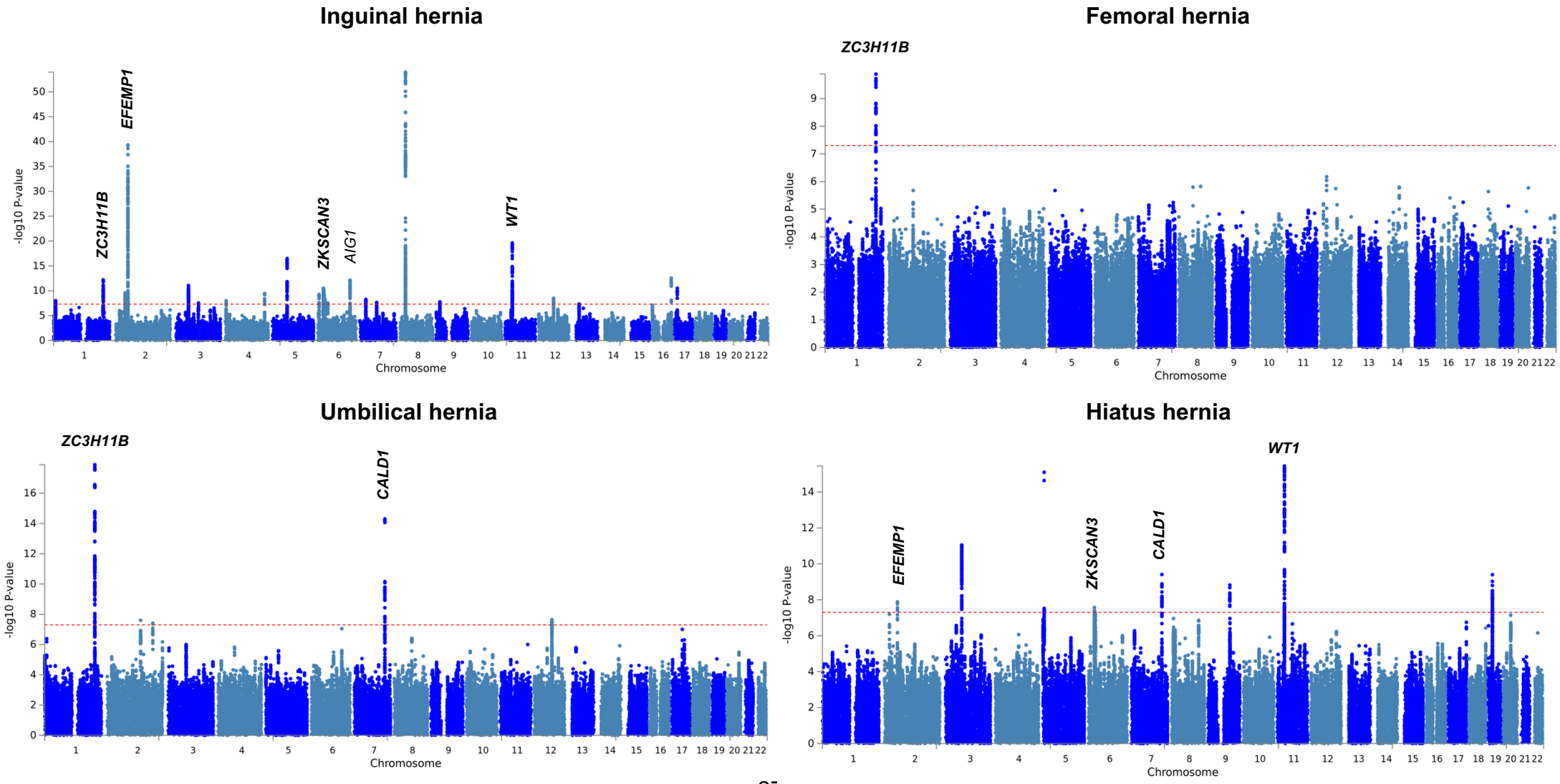

4.3.2. *In silico* annotation of individual hernia loci

Localisation of associated variants across the four individual hernia phenotypes was performed in FUMA *SNP2GENE* v1.3.6[19]. ANNOVAR[20] identified genome-wide significant exonic variants for three hernia subtypes: inguinal, umbilical and hiatus hernia. For inguinal hernia, 11 variants were exonic— five of which were non-synonymous variants (**Appendix Table 4.2**). Most notably, rs7578597 (P = 4.20×10-8, OR = 1.12), which is in high LD with the lead variant (rs76684055) at locus 2p21 (r^2 = 0.88), resides in an evolutionarily constrained region (Genomic Evolutionary Rate Profiling (GERP) Score = 4.0) within *THADA*. rs7578597 causes a p.Thr1187Ala substitution that is predicted to have a *'deleterious' (*SIFT[21]) and *'possibly damaging'* (PolyPhen[22]) consequence on THADA protein structure and function (**Appendix Table 4.3**). Moreover, three additional intronic/intergenic variants demonstrated strong pathogenic and regulatory potential (Combined Annotation Dependent Deletion (CADD) Score[23] > 12.37, RegulomeDB (RDB)[24] = 2B or less) near the *THADA* and *SPSB1* loci (all in high linkage with lead variant (r^2 > 0.89)). For both umbilical and hiatus hernia, one missense variant was identified which significantly associated with both hernia types: rs6973420 ($P_{Umbilical}$ = 2.70×10^{-10}, OR = 1.14 (G); P_{Hiatus}= 2.40×10^{-8}, OR = 1.05 (A)), which resides within exon 5 of *CALD1*, resulting in a p.His397Arg substitution that is predicted to have a '*tolerated (low confidence)'* effect on protein function (SIFT[21]) (**Appendix Table 4.2**). Aside from exonic variants, one intronic variant significantly associated with umbilical hernia was identified near *CALD1,* rs12532492 ($P_{Umbilical}$ = 1.4×10^{-8}, OR = 1.13, CADD = 16.02, RDB = 1F, r^2_{index} = 0.64) which suggests strong functionality (**Appendix Table 4.3**). Moreover, for hiatus hernia, one non-coding variant, rs1522552 (P = 3.40×10^{-11}, OR = 1.06, CADD = 19.71,

RDB = 2B) was suggested to have strong functionality at locus 3p13, and is in high LD with the lead variant at this locus (rs4499560, $r^2 = 0.96$) (**Appendix Table 4.3**). For femoral hernia, no exonic variants were identified; however, three potentially robust functional intergenic variants were recognised within a 47kb cluster (all in high LD with the index variant) at the 1q41 locus near *ZC3H11B*: rs2785986 ($P = 1.90\times10^{-8}$, OR= 1.34, $r^2_{index} = 0.66$, CADD = 14.7), rs4846567 ($P = 3.30\times10^{-9}$, OR = 1.38, $r^2_{index} = 0.83$, CADD = 14.9), and rs2820443 ($P = 2.20\times10^{-9}$, OR = 1.38, $r^2_{index} = 0.85$, CADD = 13.0) (**Appendix Table 4.3**).

4.3.3. Candidate gene mapping of individual hernia loci

Associated signals for the four hernia types were mapped to putative protein-coding genes using four mapping strategies (as previously described in **Section 4.2.9**). In total, 101 unique genes were mapped to 18 of the 24 inguinal hernia associated loci by positional mapping[19] (n = 53), eQTL mapping in GTEx[25] v8 Cells Transformed Fibroblast and Skeletal Muscle Tissue (n = 42), MAGMA[26] (n = 64), and Summary-based Mendelian Randomisation (SMR)[27] using GTEx v7 Cells Transformed Fibroblast and Skeletal Muscle Tissue (n = 3) (**Appendix Tables 4.4, 4.5 and 4.6**). Overlap was demonstrated across the mapping strategies with 29 genes mapped by two or more strategies, and four genes mapped by three mapping strategies (*THADA*, *EFEMP1*, *HLA-DMA*, *CRISPLD2*) (**Appendix Figure 4.3)**. For femoral hernia, no genes were prioritised at the **1q41** susceptibility locus, although the index signal rs7538503 ($P = 1.7\times10^{-18}$, OR = 1.22, CADD = 14.9) is a regulatory region variant narrowly residing outside the positional mapping window from *ZC3H11B (*~11.25kb downstream). For umbilical hernia, one gene (*CALD1*) was prioritised at the **7q33** locus by both positional and MAGMA mapping (**Appendix Table 4.7)**. For hiatus hernia, 15 unique genes were prioritised at five of eight genome-wide significant susceptibility loci by position (n = 5), eQTL (n = 4), and MAGMA mapping (n = 11) (**Appendix Tables 4.8 and 4.9**)., with five putative genes mapped by more than one approach (*BTN3A2*, *CALD1*, *WT1*, *KLHL26*, *CRTC1*) (**Appendix Figure 4.4)**. In summary, 117 unique genes were prioritised using the four mapping strategies at 12 of 38 susceptibility loci associated with the four individual hernia phenotypes.

4.3.4. SNP-based heritability of individual hernia phenotypes

The contribution of common variants to hernia risk for each of the individual GWAS were estimated using LD Score regression.[18] Using LD scores from ~1.2 million common low-LD variants from each of the studies, the SNP-based heritability (h^2g) for each individual hernia phenotype was calculated in UK Biobank for the first time. The largest h^2g was seen for femoral hernia at 12.79% (S.E. = 7.85%), followed by umbilical hernia which had a h^2g of 9.80% (1.67%). Interestingly, the association analyses which yielded the largest number of susceptibility signals— inguinal hernia and hiatus hernia, had the lowest SNP-heritability at 7.43% (0.83%) and 5.06% (0.34%).

4.3.5. Genetic risk score for the individual hernia phenotypes

The lead signals from all four individual hernia analyses in UK Biobank were used to calculate a weighted genetic risk score (wGRS) for each individual hernia phenotype (**Table 4.5**). As expected, the wGRS for all four hernia cases was higher than in controls (inguinal hernia: 3.070 vs 2.967 ($P = 5.53\times10^{-322}$); hiatus hernia: 0.455 vs 0.442 ($P = 9.54\times10^{-79}$); umbilical hernia: 0.650 vs 0.599 ($P = 2.02\times10^{-50}$); femoral hernia: 0.710 vs 0.565 (unweighted) ($P = 1.24\times10^{-9}$). Furthermore, it was also found that all hernia cases (across all four hernia phenotypes) that had undergone surgery had a higher wGRS compared to hernia cases that had not undergone surgery (inguinal hernia: 3.072 vs 3.013 ($P = 5.46\times10^{-6}$); femoral hernia: 0.739 vs 0.597 (*unweighted*) ($P = 6.69\times10^{-3}$); hiatus hernia: 0.464 vs 0.454 ($P = 4.77\times10^{-3}$); umbilical hernia: 0.653 vs 0.630 ($P = 2.13\times10^{-2}$).

Table 4.5. Genetic risk score for the four individual hernia phenotypes in the UK Biobank cohort.

Inguinal hernia

Group	Inguinal hernia cases	Controls	P-value†	Inguinal hernia cases with operation code	Inguinal hernia cases without operation code	P-value§
N	18,791	93,955		18,082	709	
Mean wGRS (standard deviation)	3.070 (0.332)	2.967 (0.334)	5.53×10^{-322}	3.072 (0.332)	3.013 (0.337)	5.46×10^{-6}

Femoral hernia

Group	Femoral hernia cases	Controls	P-value†	Femoral hernia cases with operation code	Femoral hernia cases without operation code	P-value§
N	973	4,865		774	199	
Mean GRS (standard deviation)	0.710 (0.681)	0.565 (0.636)	1.24×10^{-9}	0.739 (0.688)	0.597 (0.642)	6.69×10^{-3}

Umbilical hernia

Group	Umbilical hernia cases	Controls	P-value†	Umbilical hernia cases with operation code	Umbilical hernia cases without operation code	P-value§
N	5,356	26,780		4,749	607	
Mean wGRS (standard deviation)	0.650 (0.228)	0.599 (0.223)	2.03×10^{-50}	0.653 (0.228)	0.630 (0.229)	2.13×10^{-2}

Hiatus hernia

Group	Hiatus hernia cases	Controls	P-value†	Hiatus hernia cases with operation code	Hiatus hernia cases without operation code	P-value§
N	32,398	161,490		1,311	30,987	
Mean wGRS (standard deviation)	0.455 (0.115)	0.442 (0.114)	9.54×10^{-79}	0.464 (0.115)	0.454 (0.115)	4.77×10^{-3}

*wGRS: weighted genetic risk score. GRS: unweighted genetic risk score (for femoral hernia analysis only). †Unpaired two-tailed t-test between hernia cases and controls. §Unpaired two-tailed t-test between hernia cases with an operation code and hernia cases without an operation code.

4.3.6. Combined association analysis of hernia phenotypes in BOLT-LMM

To understand the shared genetic architecture of hernia risk, a second set of association analyses were performed in BOLT-LMM[11,12]: **i) Overlap hernia**: all participants in UK Biobank with diagnostic or operative codes for two or more hernia subtypes; **ii) Umbrella hernia**: a complete set (umbrella) of hernia cases from all four individual hernia cohorts (described in **Section 4.3.1**) and the overlapping hernia (overlap) cohort, i.e. all participants in UK Biobank with diagnostic or operative codes for at least one hernia subtype.

Overlap hernia analysis

5,219 cases with more than one hernia subtype and 26,095 matched controls in UK Biobank that were not included in the individual hernia analyses were tested for association. Association analysis across 8,939,859 imputed/genotyped common variants yielded four genome-wide significant loci (516 variants), with conditional regression analysis identifying a further two signals at locus **2p16.1** (*EFEMP1*) (**Table 4.6**). Regional Locus Zoom Plots for all six overlap hernia signals are provided in **Appendix Figure 4.5**. The three strongest association signals were seen at locus **2p16.1** (*EFEMP1*) (rs1346786 (P = 7.6×10^{-20}, OR = 1.24)), **1q41** (*ZC3H11B*) (rs1415287 (P = 1.2×10^{-16}, OR = 1.21)), and locus **11p13** (*WT1*) (rs3858458, P = 8.4×10^{-13}, OR = 1.17), all of which demonstrated shared susceptibility with individual hernia loci (**Figure 4.6**). The **1q41** (*ZC3H11B*) locus was associated with inguinal, femoral and umbilical hernia individually, with the **2p16.1** (*EFEMP1*) and **11p13** (*WT1*) loci being significantly associated in the individual analyses with inguinal and hiatus hernia. The final significant overlap hernia locus, **6q24.2** (*AIG1*) (rs4896643, P =

3.6×10^{-8}, OR = 1.12) only demonstrated a significant association with inguinal hernia in the individual association analysis (rs6570555, $P_{Inguinal} = 7.8\times10^{-13}$, OR = 1.08).

Umbrella hernia analysis

A combined cohort (umbrella) of 62,637 hernia cases with individual and overlap hernia phenotypes and 313,185 matched controls was tested for association in UK Biobank. The final umbrella analysis was performed across 375,822 participants and 8,420,566 imputed (MAF ≥ 0.01, INFO Imputation score ≥ 0.90) and 524,000 genotyped SNPs (MAF ≥ 0.01), and discovered 25 independent signals at 19 genome-wide significant loci (4785 variants) (**Table 4.7**) (Regional Locus Zoom Plots provided in **Appendix Figure 4.6**). Nine loci were not previously discovered in the individual or overlap hernia analyses (**Figure 4.6**), and the new top locus was **1q41** (*TGFB2*) (rs2799098, $P = 9.3\times10^{-15}$, OR = 1.06). Five of the 10 previously associated loci (in the individual and/or overlap cohort) demonstrated significant overlap in the umbrella analysis. The most striking overlap was seen at the **1q41** (*ZC3H11B*) locus (rs2820441, $P_{Umbrella} = 2.7\times10^{-23}$, OR = 1.07) which coincided with four previous hernia phenotypes (inguinal, femoral, umbilical, and overlap hernia). The **11p13** (*WT1*) locus was the strongest associated signal (rs66798575, $P = 1.6\times10^{-40}$, OR= 1.09) and showed overlap with three of the previous phenotypes (inguinal, hiatus and overlap hernia). This was followed by the **2p16.1** (*EFEMP1*) locus, which also showed commonality with three phenotypes (inguinal, hiatus and overlap hernia), and was the second most significant umbrella signal (rs75439645, $P = 2.4\times10^{-38}$, OR = 1.12). Two umbrella loci overlapped with two previous hernia phenotypes: the **6p22.2** (*MHC*) locus (rs28360634, $P_{Umbrella} = 1.7\times10^{-17}$, OR = 1.09) which overlapped with inguinal

and hiatus individual analyses and the **6q24.2** locus (*AIG1*) (rs6917403, $P_{Umbrella}$ = 2.9×10^{-12}, OR = 1.04) which overlapped with inguinal and overlap hernia analyses.

Across both overlap and umbrella hernia analyses, the λ_{GC} was 1.05 and 1.20, respectively, with an LDSC intercept of 1.01 and 1.03 and an attenuation ratio of 0.15 and 0.10 (**Appendix Figures 4.7 and 4.8)**.[18] These findings are consistent with the individual analyses performed in BOLT-LMM.

Table 4.6. Six signals (four loci) significantly associated with overlap hernia in 5,219 cases and 26,095 controls in UK Biobank

Chromosome	Position[a]	rsID	EA[b]	NEA[c]	EAF[d]	Info[e]	OR (95% CI)	P-value	Mapped genes[f]
1	219742537	rs1415287	T	C	0.31	0.998	1.21 (1.16-1.26)	1.2×10^{-16}	-
2[#]	56040099	rs10199082	C	T	0.14	G	1.29 (1.22-1.37)	1.9×10^{-10}	*EFEMP1*
2	56108333	rs1346786	C	T	0.71	0.994	1.24 (1.18-1.29)	7.6×10^{-20}	*EFEMP1*
2[#]	56194773	rs981037	T	C	0.58	0.993	1.21 (1.16-1.27)	1.0×10^{-9}	-
6	143670001	rs4896643	C	G	0.45	0.993	1.12 (1.08-1.17)	3.6×10^{-8}	*AIG1*
11	32484594	rs3858458	C	T	0.63	0.981	1.17 (1.12-1.22)	8.4×10^{-13}	*WT1*

[a]Based on NCBI Genome Build 37 (hg19).
[b]The effect allele.
[c]The non-effect allele.
[d]The effect allele frequency.
[e]The SNP INFO score for imputed SNPs; G = genotyped SNP.
[f]The four genes prioritised at these loci based on positional mapping, eQTL mapping and MAGMA gene mapping (see Methods). [#]Denotes the two residual significant signals following conditional regression analysis at the lead SNP at the locus.

Table 4.7. Twenty-five signals at 19 loci significantly associated in the umbrella hernia analysis

Chr	Position[a]	rsID	EA[b]	NEA[c]	EAF[d]	Info[e]	OR (95% CI)	P-value	Mapped genes[f]	Significant in individual or overlap GWAS[g]
1	51477643	rs13376700	A	T	0.43	0.992	1.04 (1.02-1.05)	1.3×10^{-8}	*CDKN2C, EPS15, FAF1, NRD1*	-
1	218521609	rs2799098	A	G	0.82	G	1.06 (1.05-1.08)	9.3×10^{-15}	*RRP15, TGFB2*	-
1	219734960	rs2820441	C	A	0.32	G	1.07 (1.05-1.08)	2.7×10^{-23}	-	*IH,FH,UH,OH*
2	20878406	rs3072	C	T	0.36	0.994	1.04 (1.02-1.05)	1.8×10^{-8}	*C2orf43, GDF7*	-
2	21239884	rs76622701	A	T	0.56	0.979	1.04 (1.02-1.05)	3.5×10^{-8}	*APOB*	-
2	56048944	rs75439645	A	G	0.13	0.999	1.12 (1.10-1.14)	2.4×10^{-38}	*CCDC104, EFEMP1, PNPT1, SMEK2*	*IH,HH,OH*
2#	56106928	rs59985551	C	T	0.78	0.998	1.09 (1.08-1.11)	5.1×10^{-9}	*CCDC104, CLHC1, EFEMP1, PNPT1, RTN4, SMEK2*	*IH,HH,OH*
2#	56193665	rs13431149	C	A	0.60	0.991	1.07 (1.05-1.08)	2.5×10^{-23}	*CCDC104, PNPT1, SMEK2*	*IH,HH,OH*
3	134372486	rs9883955	G	T	0.63	G	1.04 (1.02-1.05)	1.2×10^{-8}	*AMOTL2, ANAPC13, CEP63, EPHB1, KY*	-
5#	4881885	rs570260	G	A	0.34	G	1.03 (1.02-1.05)	6.2×10^{-10}	-	*HH*
5#	4977446	rs42202	A	G	0.08	0.986	1.08 (1.06-1.11)	1.7×10^{-11}	-	*HH*
5#	5145100	rs1834922	G	A	0.35	0.999	1.04 (1.02-1.05)	9.0×10^{-10}	*ADAMTS16*	
5	5350637	rs7715383	C	G	0.10	0.970	1.08 (1.06-1.10)	1.2×10^{-12}	-	
5	64355060	rs370763	A	T	0.67	0.998	1.05 (1.03-1.06)	8.3×10^{-12}	*ADAMTS6*	*IH*
6	27332891	rs28360634	T	C	0.89	1.000	1.09 (1.07-1.11)	1.7×10^{-17}	*ABT1, APOM, APOM, BTN1A1, BTN2A1, BTN2A2, BTN3A1, BTN3A2, BTN3A3, C4A, C4B, C6orf15, C6orf48, CCHCR1, CLIC1, DDR1, DPCR1, HCG27, HFE, HIST1H1A, HIST1H1B, HIST1H2AG, HIST1H2AI, HIST1H2AJ, HIST1H2AK, HIST1H2AL, HIST1H2AM, HIST1H2BC, HIST1H2BF,*	*IH,HH*

									HIST1H2BJ, HIST1H2BL, HIST1H2BM, HIST1H2BN, HIST1H2BO, HIST1H3C, HIST1H3H, HIST1H3I, HIST1H3J, HIST1H4A, HIST1H4J, HIST1H4K, HIST1H4L, HLA-A, HLA-B, HLA-C, HLA-DMA, HLA-DMB, HLA-DRA, HMGN4, LRRC16A, LSM2, MSH5, MSH5-SAPCD1, NKAPL, OR12D3, OR2B2, OR2B6, PBX2, PGBD1, POM121L2, POU5F1, PRRC2A, PRSS16, PSORS1C1, RNF5, SCAND3, SFTA2, SLC17A1, SLC17A2, SLC17A3, SLC17A4, TRIM26, TRIM27, TRIM31, TRIM38, TRIM39, TRIM39-RPP21, TUBB, VARS, VWA7, ZFP57, ZKSCAN3, ZKSCAN4, ZKSCAN8, ZNF165, ZNF184, ZNF192P1, ZNF322, ZNF391, ZSCAN12, ZSCAN16, ZSCAN23, ZSCAN31, ZSCAN9	
6	117507982	rs200889152	C	A	0.38	0.991	1.04 (1.03-1.05)	3.4×10^{-9}	-	-
6	143653287	rs6917403	A	G	0.42	0.987	1.04 (1.03-1.06)	2.9×10^{-12}	*AIG1*	*IH,OH*
7[#]	73445942	rs2356532	G	A	0.06	0.996	1.09 (1.06-1.11)	1.1×10^{-8}	*ELN*	*IH*
7	73474825	rs17855988	G	C	0.90	0.963	1.08 (1.05-1.10)	3.8×10^{-12}	*ELN, LIMK1*	*IH*
8	25693744	rs4368985	T	A	0.40	0.997	1.06 (1.05-1.07)	2.1×10^{-19}	*EBF2*	*IH*
9	133038387	rs9299329	G	A	0.50	0.979	1.04 (1.02-1.05)	1.7×10^{-8}	*HMCN2*	-
11	32451920	rs66798575	T	G	0.64	0.973	1.09 (1.08-1.10)	1.6×10^{-40}	*CCDC73, EIF3M, WT1*	*IH, HH,OH*
12	89767237	rs797267	G	A	0.19	0.996	1.05 (1.03-1.06)	2.6×10^{-9}	*DUSP6*	-
16	84855477	rs1874013	G	T	0.38	0.994	1.04 (1.03-1.05)	1.1×10^{-9}	*CRISPLD2*	*IH*
19	18824038	rs34482977	C	G	0.81	0.992	1.05 (1.03-1.06)	5.3×10^{-9}	*CRLF1, CRTC1, KLHL26, SSBP4*	*HH*

[a]Based on NCBI Genome Build 37 (hg19).
[b]The effect allele.
[c]The non-effect allele.
[d]The effect allele frequency.
[e]The SNP INFO score for imputed SNPs; G = genotyped SNP.
[f]The 138 genes prioritised at these loci based on positional mapping, eQTL mapping, MAGMA gene mapping and summary-based Mendelian randomisation (see Methods).
[g]where IH = Inguinal Hernia Individual, FH = Femoral Hernia Individual, UH = Umbilical Hernia Individual, HH = Hiatus Hernia Individual, OH = overlapping hernia analysis.
[#]Denotes the six residual significant signals following conditional regression analysis at the lead SNP at the locus

Figure 4.6. **Manhattan plots of the combined hernia analyses performed in BOLT-LMM.** Manhattan plots are annotated with the gene names of loci that demonstrate shared susceptibility across two or more individual analyses (*black*). For the umbrella plot, the nine loci that were not discovered in the individual or overlap analyses are highlighted with the gene name in green *(or ** where no gene was prioritised at this locus).*

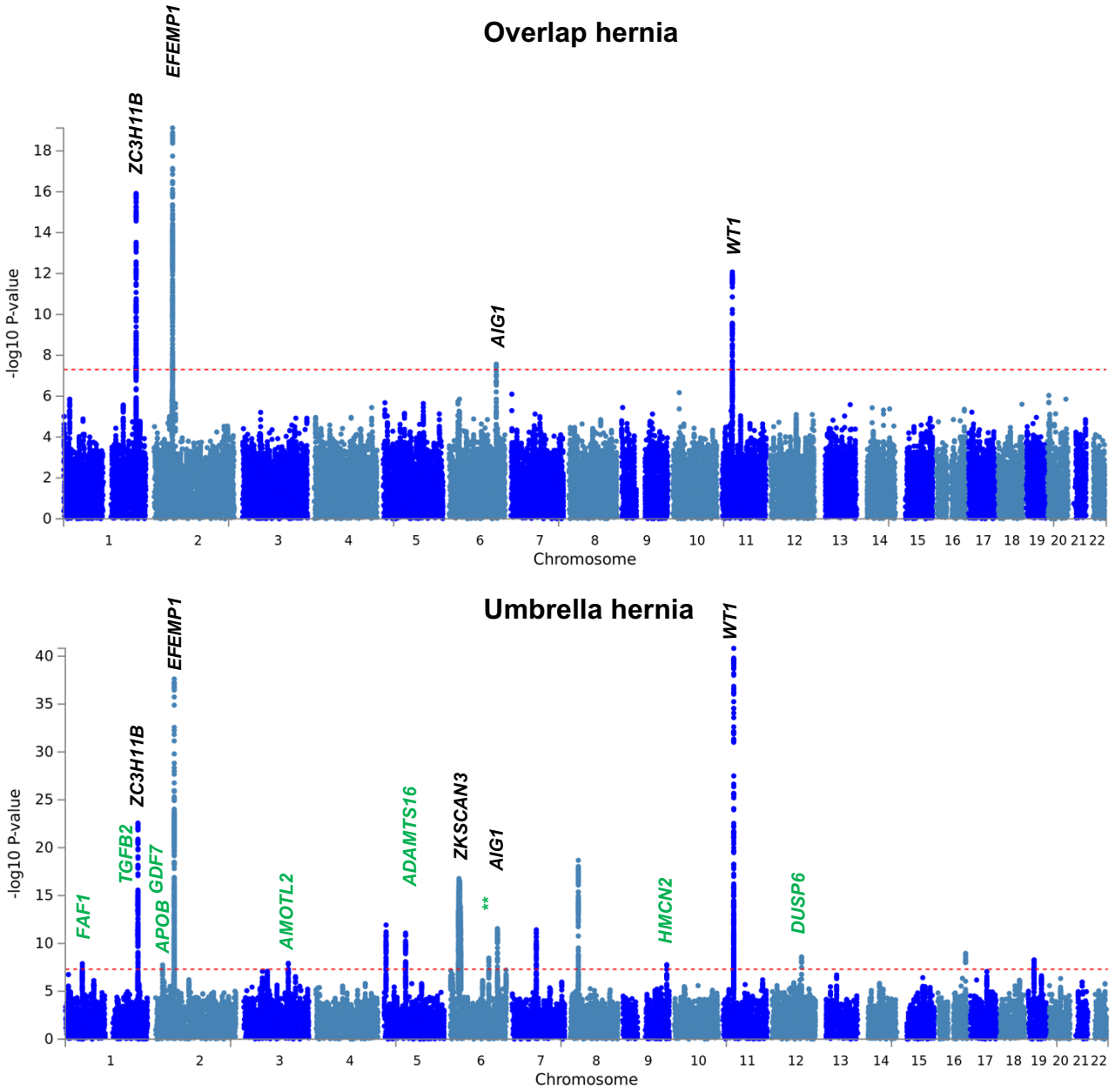

4.3.7. *In silico* annotation of combined hernia loci

Associated variants in the overlap and umbrella analyses were annotated within FUMA *SNP2GENE* v1.3.6.[19] 187 genome-wide significant ($P < 5\times10^{-8}$) candidate SNPs were identified by FUMA to be in LD ($r^2 > 0.6$) with the lead variant at each of the four overlap hernia loci. No exonic variants were localised, however, six intronic-intergenic variants had predicted deleterious effects and were in high LD with the index variant at each overlap hernia loci, including three at locus **1q41** (*ZC3H11B*) (rs4846567 ($P = 1.40\times10^{-16}$, $r^2_{index} = 0.99$, CADD[23] = 14.9); rs2820443 ($P = 3.40\times10^{-16}$, $r^2_{index} = 0.99$, CADD = 13.0); rs2785986 ($P = 1.60\times10^{-15}$, $r^2_{index} = 0.76$, CADD = 14.7), and two at locus **2p16.1** (*EFEMP1*) (rs3791679 ($P = 1.40\times10^{-17}$, $r^2_{index} = 0.66$, CADD =17.8) and rs7422809 ($P = 1.30\times10^{-14}$, $r^2_{index} = 0.68$, CADD=15.2) (**Appendix Table 4.10**).

For the umbrella association analysis, FUMA identified 877 genome-wide significant candidate SNPs in LD with the lead SNP at the 19 umbrella susceptibility loci. 18 high-LD exonic variants were discovered (**Appendix Table 4.11**), 15 of which resided at the MHC locus (**6p22.2**) — of these, four variants resulted in amino acid substitutions that were predicted to have damaging (PolyPhen[22]) and deleterious (SIFT[21]) consequences on *BTN2A1* (rs13195401, rs13195402) and *OR2B2* (rs34788973, rs61742093). Of the non-MHC exonic variants, rs17855988 (P=3.80E-12, OR=1.07, $r^2_{index} = 1.0$, CADD[23] = 25.9, RDB[24] = 2B), results in a p.Gly581Arg substitution in the 25th exon of *ELN* that is predicted by SIFT to have a deleterious (low confidence) consequence on elastin function. Predicted functional intronic and intergenic variants associated with umbrella hernia are provided in **Appendix Table 4.12**.

4.3.8. Candidate gene mapping of combined hernia loci

Genes were prioritised at the overlap and umbilical hernia associated loci using four mapping strategies (identical to individual hernia). In summary, three unique genes were mapped at the three of four of the overlap hernia associated loci, with two genes (*WT1* and *EFEMP1*) being prioritised by more than one mapping approach (**Appendix Tables 4.13 and 4.14; Appendix Figure 4.9**). A total of 129 unique genes were mapped to 20 of the 25 signals from the umbrella hernia analysis (**Appendix Tables 4.15 and 4.16**), with 38 genes being mapped by two strategies, and seven genes showing overlap across three mapping strategies (*EFEMP1*, *ADAMTS16*, *BTN2A1*, *HIST1H2BN*, *HMGN4*, *ZSCAN31*, *CRISPLD2*) (**Appendix Table 4.17; Appendix Figure 4.10)**.

4.3.9. Gene set, pathway and tissue enrichment analysis of combined hernia loci

Overlap hernia: Gene-set analysis performed in MAGMA v1.07[26] delineated the convergence of MAGMA mapped genes within 15,496 gene sets (5500 curated gene sets and 9995 GO terms) from MSigDB v8.0.[28] Two biological processes gene sets were significantly enriched: *'Negative regulation of cell proliferation in kidney development'* ($P = 5.76\times10^{-7}$, n = 5 genes) and *'Diaphragm development'* ($P = 3.00\times10^{-6}$, n = 9 genes) (**Appendix Table 4.18)**. Gene set enrichment analysis in FUMA *GENE2FUNC*, identified all three prioritised genes to cluster with GWAS Catalog reported genes related to pulse pressure. Moreover, XGR analysis enriched two canonical pathways[29]: *'Regulation of Telomerase'* ($P = 3.80\times10^{-4}$, Z = 4.88, FDR = 1.0×10^{-3}, *WT1*) and *'Genes encoding structural ECM glycoproteins'* ($P = 3.2\times10^{-3}$, Z = 2.7, FDR = 5.4×10^{-3}, *EFEMP1*) (**Appendix Table 4.19)**.

Umbrella hernia: MAGMA[26] gene-set analysis enriched 29 gene sets from MSigDB that met Bonferroni-correction (0.05/15496) (**Appendix Table 4.20**). The top biological processes gene ontology was *'Connective tissue development'* ($P = 8.05\times10^{-9}$, n = 262 genes); the top curated gene set was *'Elastic fibre formation'* ($P = 3.29\times10^{-8}$, n = 46 genes), and the top molecular functions gene ontology was *'BMP receptor binding'* (3.36×10^{-8}, n = 8 genes). Of note, enriched biological processes gene sets included *'Skeletal system development'* ($P = 3.28\times10^{-7}$, n = 498 genes) and *'Thorax and anterior abdomen determination'* ($P = 1.42\times10^{-6}$, n = 5 genes). Moreover, tissue expression analysis in MAGMA[26] using GTEx[25] v8.0 54 specific tissue types demonstrated adipose visceral omentum ($P = 6.77\times10^{-4}$, most enriched) and adipose subcutaneous tissues to be enriched ($P = 1.11\times10^{-3}$, 4th most enriched) (**Appendix**

Figure 4.11). GTEx v8.0 30 general tissue types analysis demonstrated Adipose tissue to be the most enriched tissue ($P = 6.31 \times 10^{-4}$) (**Appendix Figure 4.11**).

4.3.10. SNP-based heritability of combined hernia phenotypes

Using common, low-LD variants from the GWAS summary statistics, the narrow-sense SNP-based heritability (h^2g) for the overlap hernia phenotype in UK Biobank was 10.51% (1.85%), and for the umbrella hernia phenotype it was 3.35% (0.24%).

4.3.11. Genetic risk score to look for evidence of shared biology between hernia subtypes

As with the individual phenotypes, for both overlap and umbrella hernia analyses, a wGRS was constructed from the lead independent variants from the association analysis (**Table 4.8**). Again, as expected, both overlap (1.093 vs 1.005) and umbrella hernia cases (1.354 vs 1.325) had a higher wGRS than controls ($P = 1.17\times10^{-65}$ and $P = 4.20\times10^{-298}$, respectively). Moreover, as with the individual analyses, overlap cases that had undergone surgery (1.096 vs 1.036) and umbrella cases that had undergone surgery (1.366 vs 1.343) had a higher wGRS than cases that had not ($P = 3.98\times10^{-3}$ and $P = 4.87\times10^{-55}$, respectively).

For each of the four hernia types, the wGRS was compared between participants who only had that hernia type (individual) with those who had more than one hernia type (overlap) (**Table 4.9**). Across three of the four hernia phenotypes, the individual cases had a higher wGRS than for overlap cases: inguinal (3.070 vs 3.067, $P = 5.9\times10^{-1}$), femoral (0.710 vs 0.708, $P = 9.7\times10^{-1}$) and umbilical (0.650 vs 0.642, $P = 1.8\times10^{-11}$). However, for hiatus hernia (which was the best powered analysis), overlap cases had a higher wGRS than for individual cases (0.459 vs 0.455, $P = 1.70\times10^{-2}$).

Table 4.8. Weighted genetic risk score for combined hernia

Overlap hernia

Group	Overlap hernia cases	Controls	P-value†	Overlap hernia cases with operation code	Overlap hernia cases without operation code	P-value§
N	5,219	26,095		4,941	278	
Mean wGRS* (standard deviation)	1.093 (0.336)	1.005 (0.332)	1.17×10^{-65}	1.096 (0336)	1.036 (0.338)	3.98×10^{-3}

Umbrella hernia

Group	Umbrella hernia cases	Controls	P-value†	Umbrella hernia cases with operation code	Umbrella hernia cases without operation code	P-value§
N	62,637	313,185		29,857	32,780	
Mean wGRS* (standard deviation)	1.354 (0.180)	1.325 (0.179)	4.20×10^{-298}	1.366 (0.180)	1.343 (0.180)	4.87×10^{-55}

*wGRS: weighted genetic risk score. †Unpaired two-tailed t-test between hernia cases and controls. §Unpaired two-tailed t-test between hernia cases with an operation code and hernia cases without an operation code.

Table 4.9. Weighted genetic risk score comparing cases with a single hernia with those with multiple hernias

Inguinal hernia

Group	Inguinal hernia individual cases	Inguinal hernia overlap cases	P-value†
N	18,791	4,216	
Mean wGRS* (standard deviation)	3.070 (0.332)	3.067 (0.332)	5.85×10^{-1}

Femoral hernia

Group	Femoral hernia individual cases	Femoral hernia overlap cases	P-value†
N	973	605	
Mean wGRS* (standard deviation)	0.710 (0.681)	0.708 (0.705)	9.67×10^{-1}

Umbilical hernia

Group	Umbilical hernia individual cases	Umbilical hernia overlap cases	P-value†
N	5,356	2,076	
Mean wGRS* (standard deviation)	0.650 (0.228)	0.642 (0.227)	1.81×10^{-1}

Hiatus hernia

Group	Hiatus hernia individual cases	Hiatus hernia overlap cases	P-value†
N	32,398	3,841	
Mean wGRS* (standard deviation)	0.455 (0.115)	0.459 (0.115)	1.70×10^{-2}

*wGRS: weighted genetic risk score. †Unpaired two-tailed t-test between hernia cases with only one hernia type and hernia cases with a particular hernia type and at least one more.

4.3.12. Multi-trait analysis of the individual hernia phenotypes in MTAG to uncover shared genetic biology

To delineate the shared genetic biology between the four individual hernia phenotypes in greater detail, multi-trait analysis was performed in MTAG across 6,760,521 of the ~9M SNPs from each of the individual hernia phenotypes.[14] The final MTAG analysis consisted of 32,298 hiatus hernia cases, 18,791 inguinal hernia cases, 5,356 umbilical hernia cases, and 973 femoral hernia cases (total 57,418 individual hernia cases) and 287,090 matched controls from UK Biobank. Forty-seven loci were discovered across the four MTAG multi-trait analyses (22 inguinal (**Table 4.10**); 15 femoral (**Table 4.11**); 3 umbilical (**Table 4.12**); 7 hiatus (**Table 4.13**); Manhattan plots provided in **Figure 4.7**; Regional Locus Zooms Plots provided in **Appendix Figure 4.12**). Locus **2p16.1** (*EFEMP1*) and **11p13** (*WT1*) were significant across all four MTAG analyses (**Figure 4.8)**, and locus **1q41** (*ZC3H11B*) and **6p22.2** (*MHC*) were found to be significant in three of four analyses.

Of the twenty-two loci significantly associated with inguinal hernia in MTAG, 14 were more significant under multi-trait analysis (than any of the four individual phenotypes alone), providing evidence for shared genetics (**Table 4.10**). This includes locus **1q41** (*TGFB2*) which was sub-threshold across the four individual hernia phenotypes ($P_{Inguinal}$ = 3×10^{-7}, $P_{Femoral}$ = 8.8×10^{-1}, $P_{Umbilical}$ = 7.2×10^{-2}, P_{Hiatus} = 2.7×10^{-5}), but became significant under multi-trait analysis (rs3121580, P_{MTAG} = 3.41×10^{-8}), with pairwise testing confirming the signal at this locus to be contributed most significantly by inguinal and hiatus hernia (**Figure 4.9)**. Of note, **1q41** (*TGFB2*) was also discovered as a new locus in the femoral hernia MTAG analysis (rs2799098, P_{MTAG} =

4.66×10^{-8}; **Appendix Figure 4.13**) (with pairwise analysis demonstrating that both inguinal and femoral hernia contribute to the signal), as well as in the umbrella analysis, where it was the top associated signal (rs2799098, $P_{Umbrella} = 9.3\times10^{-15}$). Of the 15 loci discovered to associate with femoral hernia in MTAG (**Table 4.11**), 14 (bar **1q41** (*TGFB2*)) significantly associated with inguinal hernia in the individual analysis .

For the remaining two hernia phenotypes, no new loci became significant under multi-trait MTAG analysis that were not discovered in either of the four individual analyses.[14] For umbilical hernia, three loci were discovered under multi-trait analysis, with locus **1q41** (*ZC3H11B*) (rs4846567, $P_{MTAG} = 8.85\times10^{-24}$) becoming more significant under multi-trait analysis than for any individual traits (**Table 4.12**). Two loci were newly discovered to associate with umbilical hernia under multi-trait analysis (**2p16.1** (*EFEMP1*) and **11p13** (*WT1*)), both of which previously associated with inguinal and hiatus hernia in the individual analyses. Lastly, of the seven loci associated with hiatus hernia under multi-trait analysis (**Table 4.13**), three loci became more significant under MTAG than in the individual hiatus analysis alone (**2p16.1** (*EFEMP1*), **6p22.1** (MHC region), and **11p13** (*WT1*)) -- with **11p13** (*WT1*) becoming more significant under multi-trait analysis than across any of the individual individual analyses.

Table 4.10. Twenty-two loci significantly associated with inguinal hernia in the MTAG multi-trait analysis of 57,418 cases and 287,090 controls in UK Biobank. Statistically significant signals from the inguinal hernia MTAG analysis are shown in the left-hand column. The central column shows the association p-values for those SNPs in the individual hernia analyses, with the direction of effect indicated by a + or – sign. Pairwise testing was performed for MTAG signals that were more statistically significant than in any of the individual analyses (right-hand column). Colour code: Green = MTAG more significant than individual analysis, Red = MTAG less significant, Blue = new locus not previously associated with an individual trait.

Inguinal hernia MTAG								Four individual traits					Pairwise analysis between individual traits (P-value)		
Chr	Pos	rsID	EA	BETA	SE	P	Candidate genes	IH	FH	UH	HH	BETA Direction	FH and IH	UH and IH	HH and IH
1	94467 61	rs1213 4602	G	0.0086 5193	0.00 1539 76	1.92 E-08	*SPSB1*	1.2E-08	8.6E-01	2.7E-01	8.7E-01	+-++	-	-	-
1	21849 2121	rs3121 580	T	-0.0110 874	0.00 2008 88	3.41 E-08	*(TGFB2, RRP15)*	3.0E-07	8.8E-01	7.2E-02	2.7E-05	----	4.92E-07	8.08E-08	**1.12E-10**
1	21973 4960	rs2820 441	A	-0.0143 895	0.00 1609 64	3.91 E-19	*-(ZC3H11B)*	6.6E-13	2.7E-09	2.0E-15	4.5E-01	----	1.03E-16	**7.95E-24**	5.44E-07
2	43665 943	rs7668 4055	G	0.0151 3517	0.00 2488 42	1.19 E-09	*THADA, ZFP36L2*	2.8E-10	9.4E-01	2.3E-01	1.2E-01	+--+	-	-	-
2	56106 928	rs5998 5551	C	0.0246 1083	0.00 1801 93	1.81 E-42	*EFEMP1*	4.7E-40	1.0E-02	2.2E-02	7.2E-02	++++	**2.01E-41**	1.97E-37	1.53E-21
3	55585 396	rs4271 886	C	-0.0103 582	0.00 1578 03	5.24 E-11	*ERC2*	1.2E-10	1.6E-01	7.0E-01	5.4E-01	----	**4.55E-11**	4.26E-09	9.15E-06
3	56139 250	rs4974 167	A	0.0098 8327	0.00 1636 51	1.55 E-09	*ERC2*	1.3E-11	2.0E-01	3.6E-01	2.2E-02	+---	-	-	-
3	10029 7679	rs1308 3051	T	0.0157 0352	0.00 2810 45	2.30 E-08	*GPR128, NIT2, TMEM45A*	2.9E-08	3.7E-01	1.5E-02	1.8E-01	+-++	1.99E-07	**1.58E-09**	8.87E-06

4	49653 64	rs6446 301	C	- 0.0090 194	0.00 1634 58	3.43 E-08	-	2.6E-08	7.6E-01	8.4E-01	4.8E-01	----	-	-	-
4	17461 6174	rs5606 3997	T	- 0.0093 771	0.00 1568 48	2.25 E-09	-	3.6E-10	3.2E-01	1.4E-01	3.4E-01	-+-+	-	-	-
5	64351 146	rs4225 29	G	- 0.0133 784	0.00 1593 85	4.71 E-17	- *(ADAMTS6)*	5.7E-17	3.7E-01	5.6E-01	3.2E-01	----	**6.34E-17**	1.67E-14	3.28E-09
6	67431 49	rs1294 421	T	0.0093 173	0.00 1535 69	1.30 E-09	-	5.6E-10	8.0E-01	6.4E-01	4.4E-01	+-++	-	-	-
6	26099 279	rs1321 2652	T	0.0155 0491	0.00 2236 25	4.11 E-12	*HFE, HIST1H1A, HIST1H2AB, HIST1H3B, HIST1H4B, SCGN, SLC17A1, SLC17A2, SLC17A3, TRIM38*	3.1E-11	2.6E-01	9.7E-01	7.9E-05	++-+	1.79E-11	4.74E-09	**6.56E-13**
6	32343 236	rs2894 251	A	0.0130 9947	0.00 2156 32	1.24 E-09	*C2, BTNL2, C6orf10, HLA-DQA1, HLA-DQB1, HLA-DRA, NOTCH4, PSMB8, TAP2, TNXB*	1.3E-08	8.3E-02	9.4E-01	3.4E-04	++-+	3.25E-09	6.02E-07	**2.84E-10**
6	14365 3287	rs6917 403	A	0.0106 3646	0.00 1527 24	3.30 E-12	*AIG1*	9.9E-13	6.3E-02	1.5E-02	1.3E-01	+-++	-	-	-
7	25681 464	rs1095 1081	C	0.0090 193	0.00 1619 7	2.57 E-08	-	5.3E-09	9.7E-02	1.3E-03	9.5E-01	++--	-	-	-

7	73422593	rs76027228	C	0.0169	0.00	3.19 E-10	*ELN*	2.4E-08	5.5E-02	8.4E-04	2.0E-02	++++	4.75E-09	**8.81E-11**	1.46E-07
8	25707778	rs10746560	A	-0.0225	0.00	2.82 E-49	*EBF2*	1.5E-54	4.7E-01	3.8E-01	4.0E-01	-+++	-	-	-
11	32459228	rs4140413	G	0.0161	0.00	8.26 E-25	*WT1*	2.4E-20	2.1E-03	5.2E-02	1.7E-13	++++	3.46E-22	1.16E-19	**1.69E-30**
12	66328027	rs12810758	C	-0.0104	0.00	6.95 E-09	*AC090673.2, HMGA2*	3.2E-09	5.4E-01	5.2E-01	2.1E-01	-+--	-	-	-
16	84856552	rs4238714	T	-0.0113	0.00	1.20 E-13	*CRISPLD2*	2.8E-13	4.5E-01	1.0E-01	6.4E-01	----	**3.08E-13**	5.35E-13	1.31E-06
17	12191339	rs12453693	C	-0.0102	0.00	3.10 E-10	-	3.0E-11	6.0E-01	8.5E-01	8.1E-01	-+++	-	-	-

[a]Based on NCBI Genome Build 37 (hg19).
[b]The effect allele.
[c]The non-effect allele.
[d]The effect allele frequency.
[e]The SNP INFO score for imputed SNPs; G = genotyped SNP.
[f]Genes mapped to these loci based on positional mapping in FUMA (see Methods).

Table 4.11. Fifteen loci significantly associated with femoral hernia in the MTAG multi-trait analysis of 57,418 cases and 287,090 controls in UK Biobank. Statistically significant signals from the femoral hernia MTAG analysis are shown in the left-hand column. The central column shows the association p-values for those SNPs in the individual hernia analyses, with the direction of effect indicated by a + or – sign. Pairwise testing was performed for MTAG signals that were more statistically significant than in any of the individual analyses (right-hand column). Colour code: Green = MTAG more significant than individual analysis, Red = MTAG less significant, Blue = new locus not previously associated with an individual trait.

Femoral hernia MTAG								Four Individual Traits					Pairwise analysis between individual traits (P-value)		
Chr	Pos	rsID	EA	BETA	SE	P	Mapped genes	IH	FH	UH	HH	BETA Direction	IH and FH	UH and FH	HH and FH
1	218521609	rs2799098	G	-0.016653	0.0030478	4.66E-08	*TFGB2, RRP15*	1.1E-07	9.9E-01	9.6E-02	8.7E-06	-+--	**2.20E-07**	0.126445	1.21E-05
1	219734960	**rs282044 1**	A	-0.022452	0.0024803	1.40E-19	*- (ZC3H11B)*	6.6E-13	2.7E-09	2.0E-15	4.5E-01	----	1.03E-16	**6.79E-22**	0.078315
2	43451957	rs149290349	G	0.024353397	0.0042606 7	1.09E-08	*PLEKHH2, THADA, ZFP36L2*	3.5E-09	4.5E-01	3.2E-01	3.5E-02	++-+	-	-	-
2	56106928	rs59985551	C	0.036693374	0.0028200 8	1.05E-38	*EFEMP1*	4.7E-40	1.0E-02	2.2E-02	7.2E-02	++++	-	-	-
3	55585396	rs4271886	C	-0.015293 1	0.0024321 5	3.22E-10	*ERC2*	1.2E-10	1.6E-01	7.0E-01	5.4E-01	----	-	-	-
5	64351146	rs422529	G	-0.019360 3	0.0024517 3	2.87E-15	*- (ADAMTS6)*	5.7E-17	3.7E-01	5.6E-01	3.2E-01	----	-	-	-
6	67403 66	rs1294414	A	0.013317 08	0.0023843 7	2.33E-08	-	1.2E-09	9.0E-01	6.4E-01	3.7E-01	++++	-	-	-

6	26099472	rs3540 2046	G	0.0233 4313	0.003 4106 5	7.69E -12	*HFE, HIST1H1A, HIST1H2AB, HIST1H3B, HIST1H4B, SCGN, SLC17A1, SLC17A2, SLC17A3, TRIM38*	4.6E-11	2.3E-01	1.0E+00	2.4E-05	++++	**2.35E-11**	0.632349	1.29E-05
6	14362 5532	rs7383 094	G	0.0147 7797	0.002 3730 3	4.74E -10	*AIG1*	5.2E-12	3.3E-01	4.9E-02	4.1E-02	+-++	-	-	-
7	25681 464	rs1095 1081	C	0.0137 399	0.002 5077 1	4.28E -08	-	5.3E-09	9.7E-02	1.3E-03	9.5E-01	++--	-	-	-
7	73422 593	rs7602 7228	C	0.0258 8356	0.004 1995 5	7.12E -10	*ELN*	2.4E-08	5.5E-02	8.4E-04	2.0E-02	++++	**4.75E-09**	1.33E-04	0.008968
8	25706 115	rs1113 5895	A	-0.0315 961	0.002 3628 9	8.84E -41	*EBF2*	2.1E-54	5.1E-01	3.8E-01	4.4E-01	-+++	-	-	-
11	32459 228	rs4140 413	G	0.0249 1545	0.002 3898 9	1.90E -25	*WT1*	2.4E-20	2.1E-03	5.2E-02	1.7E-13	++++	**3.46E-22**	0.002738	7.03E-15
16	84856 552	rs4238 714	T	-0.0162 622	0.002 3533 5	4.84E -12	*CRISPLD2*	2.8E-13	4.5E-01	1.0E-01	6.4E-01	----	-	-	-
17	12191 339	rs1245 3693	C	-0.0142 353	0.002 5183 9	1.58E -08	-	3.0E-11	6.0E-01	8.5E-01	8.1E-01	-+++	-	-	-

[a]Based on NCBI Genome Build 37 (hg19).
[b]The effect allele.
[c]The non-effect allele.
[d]The effect allele frequency.
[e]The SNP INFO score for imputed SNPs; G = genotyped SNP.
[f]Genes mapped to these loci based on positional mapping in FUMA (see Methods).

Table 4.12. Three loci significantly associated with umbilical hernia in the MTAG multi-trait analysis of 57,418 cases and 287,090 controls in UK Biobank. Statistically significant signals from the umbilical hernia MTAG analysis are shown in the left-hand column. The central column shows the association p-values for those SNPs in the individual hernia analyses, with the direction of effect indicated by a + or – sign. Pairwise testing was performed for MTAG signals that were more statistically significant than in any of the individual analyses (right-hand column). Colour code: Green = MTAG more significant than individual analysis, Red = MTAG less significant, Blue = new locus not previously associated with an individual trait.

Umbilical hernia MTAG								Four Individual Traits					Pairwise analysis between individual traits (P-value)		
Chr	Pos	rsID	EA	BETA	SE	P	Mapped genes	IH	FH	UH	HH	BETA Direction	IH and UH	FH and UH	HH and UH
1	219750717	rs4846567	G	-0.0279967	0.0027847	8.85E-24	- *(ZC3H11B)*	9.3E-12	3.3E-09	1.7E-18	6.5E-01	----	3.99E-24	**3.22E-25**	1.65E-04
2	56048944	rs75439645	G	-0.028864	0.0038121	3.69E-14	*EFEMP1*	3.6E-21	2.3E-03	8.4E-04	1.7E-08	----	-	-	-
11	32459228	rs4140413	G	0.0183 0575	0.0026809 6	8.61E-12	*WT1*	2.4E-20	2.1E-03	5.2E-02	1.7E-13	++++	-	-	-

[a]Based on NCBI Genome Build 37 (hg19).
[b]The effect allele.
[c]The non-effect allele.
[d]The effect allele frequency.
[e]The SNP INFO score for imputed SNPs; G = genotyped SNP.
[f]Genes mapped to these loci based on positional mapping in FUMA (see Methods).

Table 4.13. Seven loci significantly associated with hiatus hernia in the MTAG multi-trait analysis of 57,418 cases and 287,090 controls in UK Biobank. Statistically significant signals from the hiatus hernia MTAG analysis are shown in the left-hand column. The central column shows the association p-values for those SNPs in the individual hernia analyses, with the direction of effect indicated by a + or – sign. Pairwise testing was performed for MTAG signals that were more statistically significant than in any of the individual analyses (right-hand column). Colour code: Green = MTAG more significant than individual analysis, Red = MTAG less significant, Blue = new locus not previously associated with an individual trait.

Hiatus hernia MTAG								Four individual traits					Pairwise analysis between individual traits (P-value)		
Chr	Pos	rsID	EA	BETA	SE	P	Candidate Genes	IH	FH	UH	HH	BETA Direction	IH and HH	FH and HH	UH and HH
2	56048944	rs7543645	G	0.0118023	0.0017 5903	1.95E-11	*EFEMP1*	3.6E-21	2.3E-03	8.4E-04	1.7E-08	----	-	-	-
3	70951405	rs6805430	C	0.0087604	0.0012 8815	1.04E-11	*FOXP1*	1.9E-01	1.2E-02	9.0E-02	1.0E-11	+---	-	-	-
5	49774466	rs42202	A	0.0175 8426	0.0022 514	5.70E-15	-	8.4E-01	9.4E-02	5.7E-01	8.0E-16	-+-+	-	-	-
6	28825573	rs3132387	G	0.0113 5776	0.0019 2355	3.54E-09	*HIST1H1B, HIST1H3I, OR12D2, OR12D3, OR2B2, OR2B6, PGBD1, ZKSCAN4, ZSCAN12, ZSCAN9*	6.8E-10	4.9E-01	3.4E-01	5.6E-08	++++	-	-	-
9	96624645	rs4075733	C	0.0070 6618	0.0011 9858	3.74E-09	-	5.9E-01	1.4E-01	4.6E-01	1.5E-09	--++	-	-	-
11	32479807	rs11031796	G	0.0107 3813	0.0012 2954	2.47E-18	*WT1*	2.1E-15	9.7E-04	4.6E-01	3.6E-16	++++	**1.36E-29**	8.75E-18	5.22E-15
19	18787981	rs2891698	G	0.0074 4858	0.0011 9487	4.55E-10	*CRLF1, CRTC1, KLHL26, TMEM59L*	6.2E-01	5.5E-01	4.8E-01	4.0E-10	++++	-	-	-

Figure 4.7. Manhattan plots for the inguinal, femoral, umbilical and hiatus hernia MTAG multi-trait analysis summary statistics. Manhattan plots are annotated with the gene names of loci that demonstrate shared susceptibility across two or more MTAG analyses (*black gene names* or ** where no genes are proximate to the lead signal). Blue gene names are those loci that were previously not discovered in any of the individual hernia analyses (i.e. new loci).

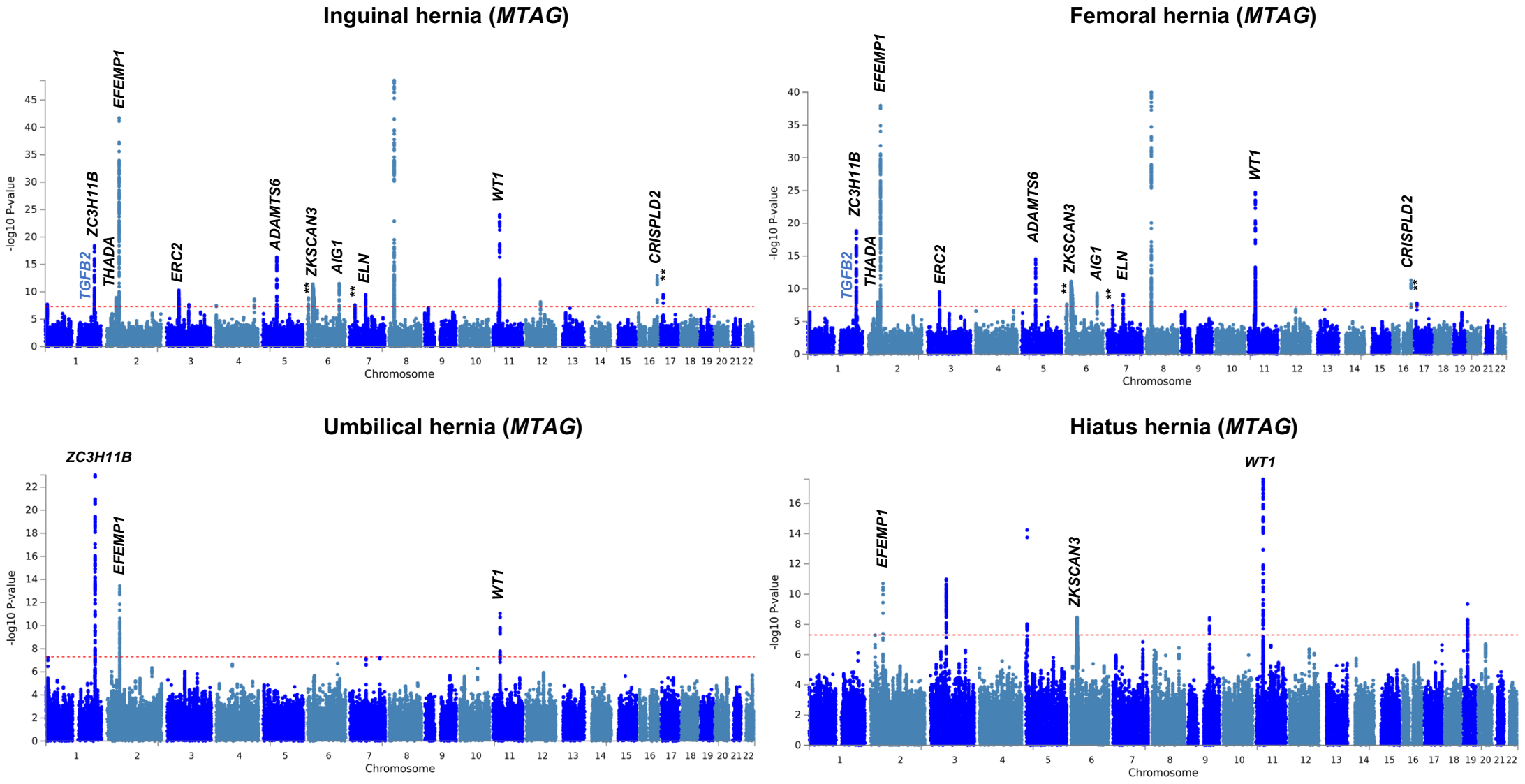

Figure 4.8. Two loci consistently significant across the four MTAG analyses.

2p16.1 *(EFEMP1)*

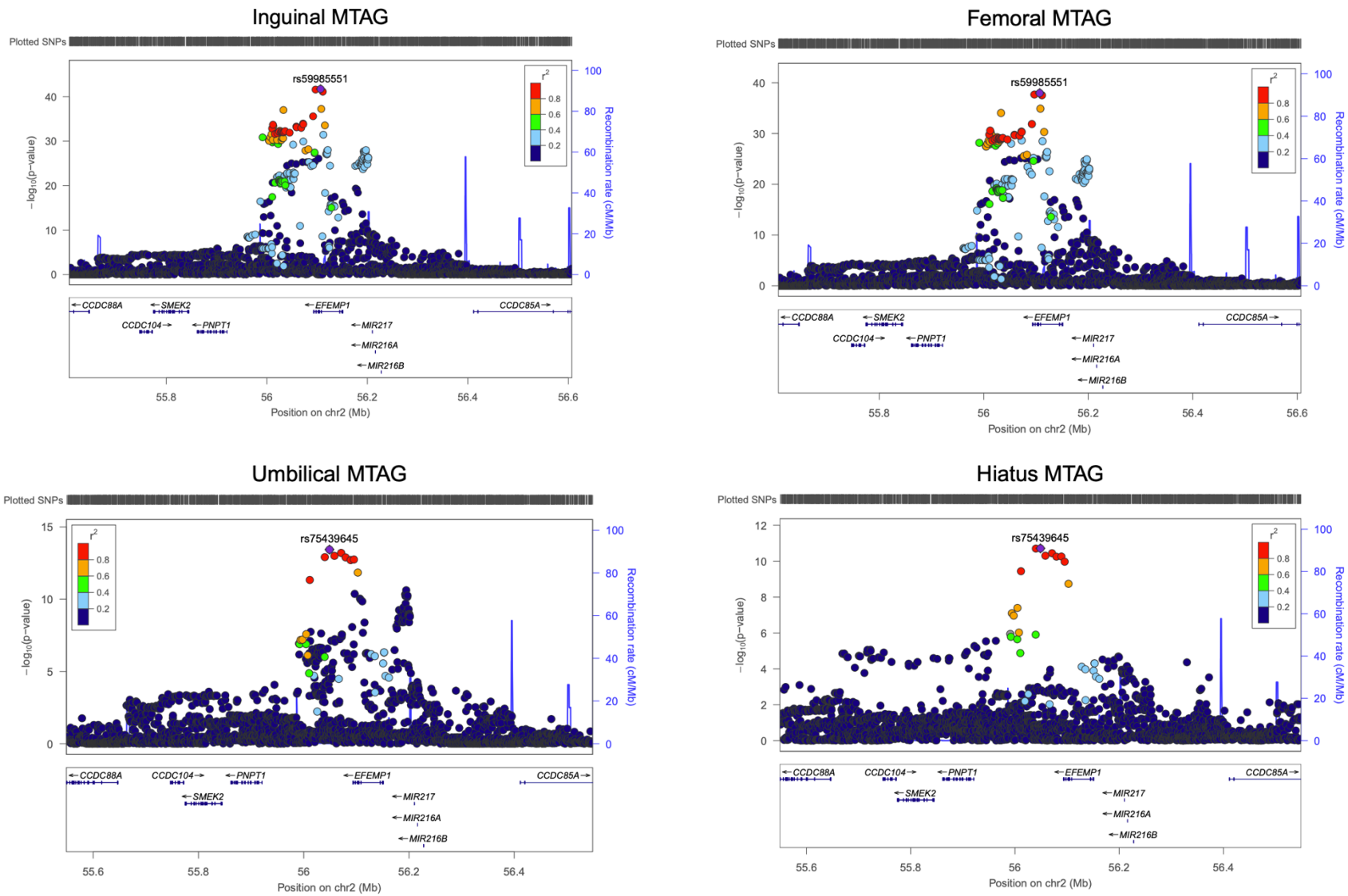

11p13 *(WT1))*

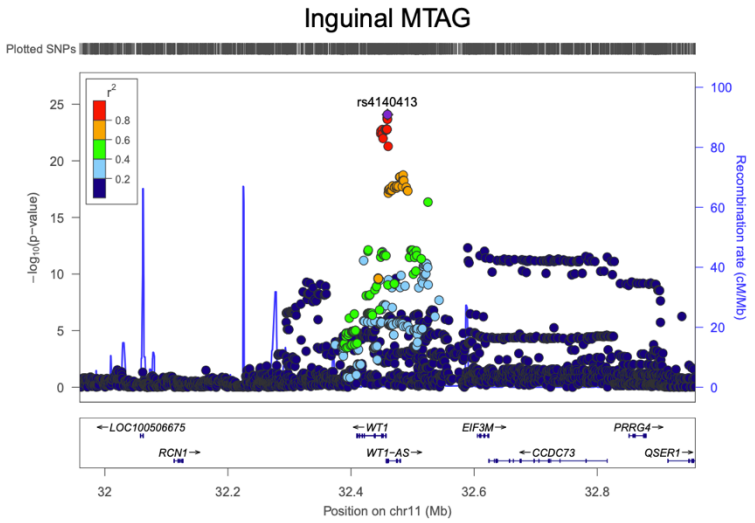
Inguinal MTAG
Plotted SNPs
rs4140413
r²
0.8
0.6
0.4
0.2
−log10(p−value)
Recombination rate (cM/Mb)
LOC100506675
WT1
EIF3M
PRRG4
RCN1
WT1−AS
CCDC73
QSER1
Position on chr11 (Mb)

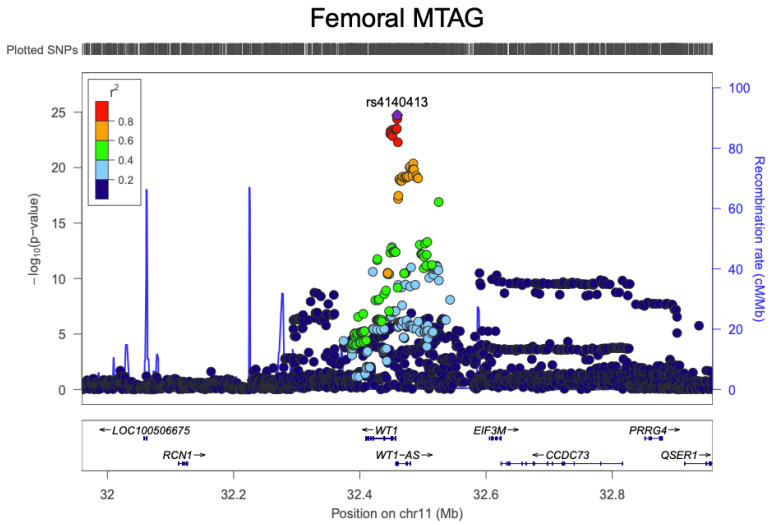
Femoral MTAG
Plotted SNPs
rs4140413
r²
0.8
0.6
0.4
0.2
−log10(p−value)
Recombination rate (cM/Mb)
LOC100506675
WT1
EIF3M
PRRG4
RCN1
WT1−AS
CCDC73
QSER1
Position on chr11 (Mb)

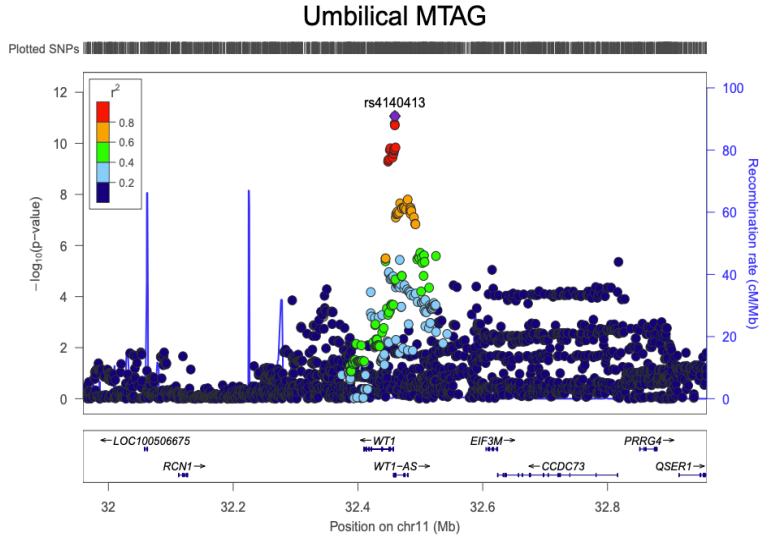
Umbilical MTAG
Plotted SNPs
rs4140413
r²
0.8
0.6
0.4
0.2
−log10(p−value)
Recombination rate (cM/Mb)
LOC100506675
WT1
EIF3M
PRRG4
RCN1
WT1−AS
CCDC73
QSER1
Position on chr11 (Mb)

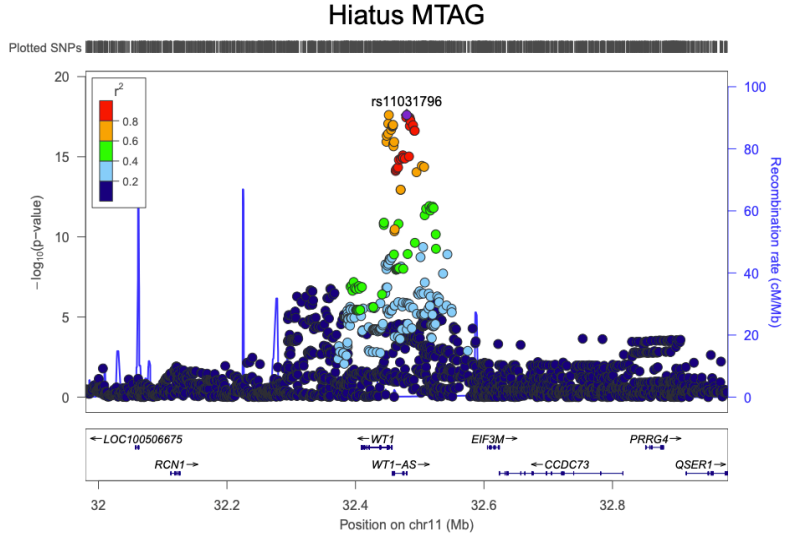
Hiatus MTAG
Plotted SNPs
rs11031796
r²
0.8
0.6
0.4
0.2
−log10(p−value)
Recombination rate (cM/Mb)
LOC100506675
WT1
EIF3M
PRRG4
RCN1
WT1−AS
CCDC73
QSER1
Position on chr11 (Mb)

Figure 4.9. New 1q41 (*TGFB2*) locus discovered to associate with inguinal hernia through MTAG multi-trait analysis.

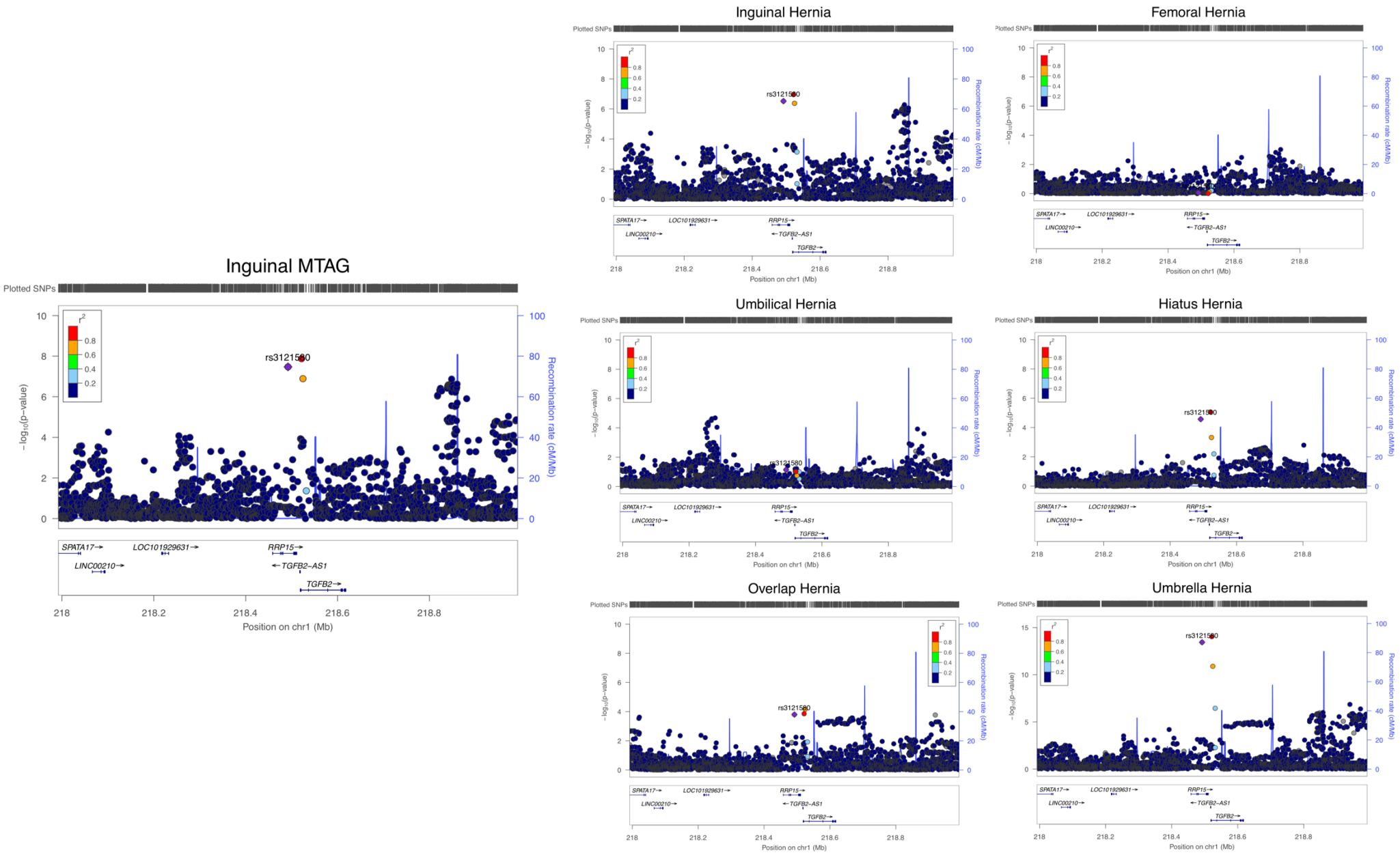

4.3.13. Multivariate meta-analysis of the individual hernia phenotypes in metaUSAT to uncover shared genetic biology

Multivariate meta-analysis of the four individual hernia traits was performed in metaUSAT[16], across a total of 57,418 individual hernia cases and 287,090 matched controls in UK Biobank. Twenty-four susceptibility loci (3645 variants) were discovered genome-wide significant ($P_{metaUSAT} < 5\times10^{-8}$), with one-third of metaUSAT loci (**1q41** (*ZC3H11B*); **2p16.1** (*EFEMP1*), **3p14.3** (*ERC2*); **3p13**; **5p15.33**; **6q24.2** (*AIG1*); **7p15.2** (*LOC646588*); **7q33** (*CALD1*)) becoming more significant than in any of the previous six BOLT-LMM analyses (4 x individual, overlap, and umbrella hernia), providing robust evidence of shared genetics (**Table 4.14; Figure 4.9**). Furthermore, six loci ((***1q41*** *(TGFB2),* **2p24.1** (*GDF7*), **5p15.33** (near *CEP72*), **5p15.32** (near *ADAMTS16*), **7q33** (*CALD1*), **12q21.33** (*DUSP6*)) were sub-threshold across the four individual analyses, and became significant under meta-analysis.

Intriguingly, the meta-analysis approach yielded an entirely new putative locus, **5p15.33** (rs72703080, $P_{metaUSAT} = 3.68\times10^{-8}$, ~20kb upstream from *CEP72*), which was sub-threshold across all six BOLT-LMM analyses and the four MTAG multi-trait analyses (**Figure 4.10**). Furthermore, for the majority of loci (n = 15), the metaUSAT association was more significant than all four MTAG analyses; importantly, metaUSAT discovered five loci that MTAG did not: **2p24.1** (*GDF7*), **5p15.33** (near *CEP72*), **5p15.32** (near *ADAMTS16*), **7q33** (*CALD1*), **12q21.33** (*DUSP6*) (the umbrella analysis was able to discover all loci except the new metaUSAT locus **5p15.33**) (**Table 4.14**).

As well as discovering new putative loci, metaUSAT demonstrated strong enrichment for loci that demonstrated significant overlap in the previous analyses.[16] This includes six loci that showed the greatest overlap with the individual and overlap susceptibility loci (**Figure 4.11**). This includes all five loci that imparted shared susceptibility to two or more hernia phenotypes in the individual analyses (discussed in **Section 4.3.1**): **1q41** (*ZC3H11B*); **2p16.1** (*EFEMP1*); **6p22.2** (*ZKSCAN3* (MHC region)); **11p13** (*WT1*); and **7q33** (*CALD1*) (note: three of these (**1q41** (*ZC3H11B*), **2p16.1** (*EFEMP1*), and **11p13** (*WT1*)) were also significant in the overlap analysis)**.** The sixth locus that metaUSAT enriched which showed the highest overlap in previous analyses was locus (**6q24.2** (*AIG1*) (**Table 4.14**), which happens to be the fourth and final overlap hernia locus and was also associated with inguinal hernia (discussed in **Section 4.3.6)** .

Table 4.14. 24 genome-wide significant loci discovered in the metaUSAT multi-trait meta-analysis of inguinal, femoral, umbilical, hiatus hernia in 57,418 cases and 287,090 controls in UK Biobank. Statistically significant signals from the metaUSAT analysis are shown in the left-hand column. The central column shows the association p-values for those SNPs in the BOLT-LMM analyses, with the direction of effect indicated by a + or – sign across the six BOLT analyses. The metaUSAT signals were compared against for their relevant association strength in the MTAG analysis. (right-hand column). Candidate genes are those selected from the prioritised genes (using the four mapping strategies described previously for all BOLT-discovered loci) or genes in proximity as identified within the UCSC genome browser.

metaUSAT analysis							BOLT-LMM analyses							MTAG analyses (P-value)				Candidate Gene
							Four individual hernias (P-value)				Combined Hernia (P-value)		BETA Direction[f]					
Chr[a]	BP[a]	SNP	A1[b]	A0[c]	T-statistic[d]	P-value[e]	IH	FH	UH	HH	OH	Umbrella		IH	FH	UH	HH	
1	218521609	rs2799098	G	A	3.53E-10	**5.18E-10**	1.10E-07	9.90E-01	9.60E-02	8.70E-06	1.40E-04	**9.30E-15**	-+----	**1.35E-08**	**4.66E-08**	1.14E-05	7.76E-07	*TGFB2*
1	219754012	rs559230165	C	CT	8.23E-33	**3.28E-34**	**1.50E-11**	**2.20E-09**	**1.30E-18**	7.90E-01	**1.70E-15**	**1.90E-21**	------	—[#]	—[#]	—[#]	—	*ZC3H11B*
2	20878406	rs3072	T	C	2.23E-08	**3.48E-08**	1.70E-02	9.40E-01	9.00E-01	6.30E-08	3.00E-02	**1.80E-08**	--+---	6.21E-03	3.61E-03	2.15E-02	5.24E-08	*GDF7*
2	43665943	rs76684055	G	A	6.96E-09	**1.07E-08**	**2.80E-10**	9.40E-01	2.30E-01	1.20E-01	8.30E-01	3.80E-05	+--+++	**1.19E-09**	**1.19E-08**	2.14E-01	6.36E-02	*THADA*
2	56106928	rs59985551	C	T	1.10E-39	**2.04E-41**	**4.70E-40**	1.00E-02	2.20E-02	**7.20E-02**[‡]	**8.30E-18**	**2.70E-33**	++++++	**1.81E-42**	**1.05E-38**	**9.23E-11**	1.80E-03	*EFEMP1*
3	56141843	rs7647972	C	G	1.71E-11	**6.97E-12**	**8.90E-12**	1.20E-01	4.90E-01	1.10E-02	2.70E-01	5.70E-02	+---++	—[#]	—[#]	—	—	*ERC2*
3	70951945	rs5007038	A	T	7.78E-12	**3.07E-12**	1.80E-01	9.90E-03	9.30E-02	**9.60E-12**	7.30E-01	1.80E-07	+-----	—	—	—	—[#]	- (~70kb from *FOXP1*)
4	174606591	rs12649191	T	C	1.17E-08	**1.81E-08**	**6.20E-10**	2.60E-01	1.60E-01	2.90E-01	2.00E-03	2.90E-04	-+-+--	**4.82E-09**	4.60E-07	8.48E-03	6.72E-01	- (~300kb *HAND-AS1*)
5	595238	rs72703080	A	G	2.35E-08	**3.68E-08**	4.40E-01	4.30E-01	5.00E-04	1.70E-07	7.40E-01	7.30E-03	+-+---	5.61E-01	9.41E-01	1.15E-01	3.55E-06	- (~20kb from *CEP72*)
5	4977446	rs42202	A	G	1.44E-15	**2.71E-14**	8.40E-01	9.40E-02	5.70E-01	**8.00E-16**	8.40E-04	**1.90E-11**	-+-+++	4.93E-01	1.31E-01	3.80E-02	**5.70E-15**	- (~100kb from *ADAMTS16*)
5	5350637	rs7715383	G	C	1.97E-09	**2.97E-09**	5.00E-05	7.00E-01	4.80E-02	2.30E-07	1.40E-01	**1.20E-12**	------	—	—	—	—	- (~25kb from *ADAMTS16*)
5	64355060	rs370763	T	A	5.98E-15	**2.84E-14**	**3.30E-17**	4.60E-01	6.00E-01	2.80E-01	7.70E-06	**8.30E-12**	------	—[#]	—[#]	—	—	*ADAMTS6*

6	27352750	rs71559024	G	A	3.17E-14	**3.64E-14**	**2.20E-10**	8.80E-01	3.30E-01	**8.10E-08**[±]	2.80E-03	**2.10E-17**	++++++	**2.04E-11**	**7.33E-11**	1.10E-05	**5.27E-09**	*ZKSCAN3*
6	143676186	rs6570555	A	T	8.89E-13	**3.42E-13**	**7.80E-13**	4.70E-02	1.80E-02	1.80E-01	**2.20E-07**[±]	**1.00E-11**	+-++++	__[#]	__[#]	__	__	*AIG1*
7	25681464	rs10951081	C	A	1.32E-09	**1.98E-09**	**5.30E-09**	9.70E-02	1.30E-03	9.50E-01	6.00E-01	1.40E-02	++--++	**2.57E-08**	**4.28E-08**	2.64E-01	9.60E-01	-(*LOC646588*)
7	73422593	rs76027228	C	T	3.32E-10	**4.83E-10**	**2.40E-08**	5.50E-02	8.40E-04	2.00E-02	7.20E-03	**8.60E-12**	++++++	**3.19E-10**	**7.12E-10**	8.74E-08	1.67E-03	*ELN*
7	134593511	rs4472440	C	G	9.20E-20	**1.54E-20**	3.10E-01	9.90E-01	**7.10E-15**	**1.30E-08**	1.10E-01	6.10E-02	---+++	__	__	__	__	*CALD1*
8	25717620	rs6983815	T	A	7.26E-52	**3.47E-54**	**1.10E-54**	4.10E-01	4.30E-01	4.40E-01	3.10E-04	**1.00E-18**	-+++--	__[#]	__[#]	__	__	*EBF2*
9	96624645	rs4075733	C	T	2.45E-09	**3.71E-09**	5.90E-01	1.40E-01	4.60E-01	**1.50E-09**	2.50E-01	3.20E-04	--++-+	8.31E-01	9.65E-01	1.81E-02	**3.74E-09**	- (~50kb from *BARX1*)
11	32458278	rs5030123	G	GT GT	3.73E-32	**1.60E-33**	**2.00E-19**	6.30E-03	1.40E-01	**7.70E-16**	**1.20E-12**	**1.50E-41**	++++++	__[#]	__[#]	__[#]	__[#]	*WT1*
12	89767237	rs797267	A	G	2.25E-08	**3.51E-08**	1.00E-02	5.60E-04	4.20E-01	1.70E-06	3.00E-01	**2.60E-09**	------	3.74E-04	2.89E-05	1.92E-03	4.31E-07	*DUSP6*
16	84856552	rs4238714	T	C	1.73E-11	**7.05E-12**	**2.80E-13**	4.50E-01	1.00E-01	6.40E-01	4.70E-04	**1.60E-09**	------	**1.20E-13**	**4.84E-12**	2.19E-04	2.19E-01	*CRISPLD2*
17	12191339	rs12453693	C	T	4.73E-09	**7.22E-09**	**3.00E-11**	6.00E-01	8.50E-01	8.10E-01	6.10E-02	1.20E-04	-+++--	**3.10E-10**	**1.58E-08**	1.00E-01	8.06E-01	-
19	18787981	rs2891698	G	A	6.85E-10	**1.02E-09**	6.20E-01	5.50E-01	4.80E-01	**4.00E-10**	1.00E-01	**1.60E-08**	++++++	2.44E-01	1.10E-01	5.31E-03	**4.55E-10**	*KLHL26*

[a]*Based on NCBI Genome Build 37 (hg19).*
[b]*The reference allele.*
[c]*The alternate allele.*
[d]*The metaUSAT test statistic (scalar)*
[e]*The p-value of association based on the metaUSAT statistic*
fThe effect size direction in the six BOLT-LMM association analyses (IH, UH, FH, HH, OH, Umbrella) with respect to the reference allele
[g]*Genes were selected based on those genes mapped in the six BOLT-LMM analyses, and subsequently prioritised based on the existing literature.*

Bold P-values are those variants identified by metaUSAT that are genome-wide significant ($P < 5\times10^{-8}$) in a particular analysis
[±]*Denotes three loci where the reference metaUSAT SNP is not significant in the* individual *BOLT-LMM hernia analysis, however the locus contains genome-wide significant SNP associations.*
__Denotes loci where the metaUSAT identified variant was not available in the MTAG Analysis
__[#] Denotes loci where the metaUSAT identified variant was not available in the MTAG Analysis, however the locus was significant in the analysis.

Green P-values depict those that are the most significant across the three analysis approaches (metaUSAT, BOLT-LMM. MTAG).
The following shorthand notations are used: Inguinal Hernia, IH; Femoral Hernia, FH; Umbilical Hernia, UH; Hiatus Hernia, HH; Overlap Hernia, OH; Umbrella Hernia, Umbrella.

Figure 4.9. 24 loci discovered to confer shared hernia susceptibility after multivariate meta-analysis in 57,418 cases and 287,090 controls in metaUSAT. Each metaUSAT locus is annotated according to whether it was genome-wide significant in the individual, overlap or umbrella analyses (legend).

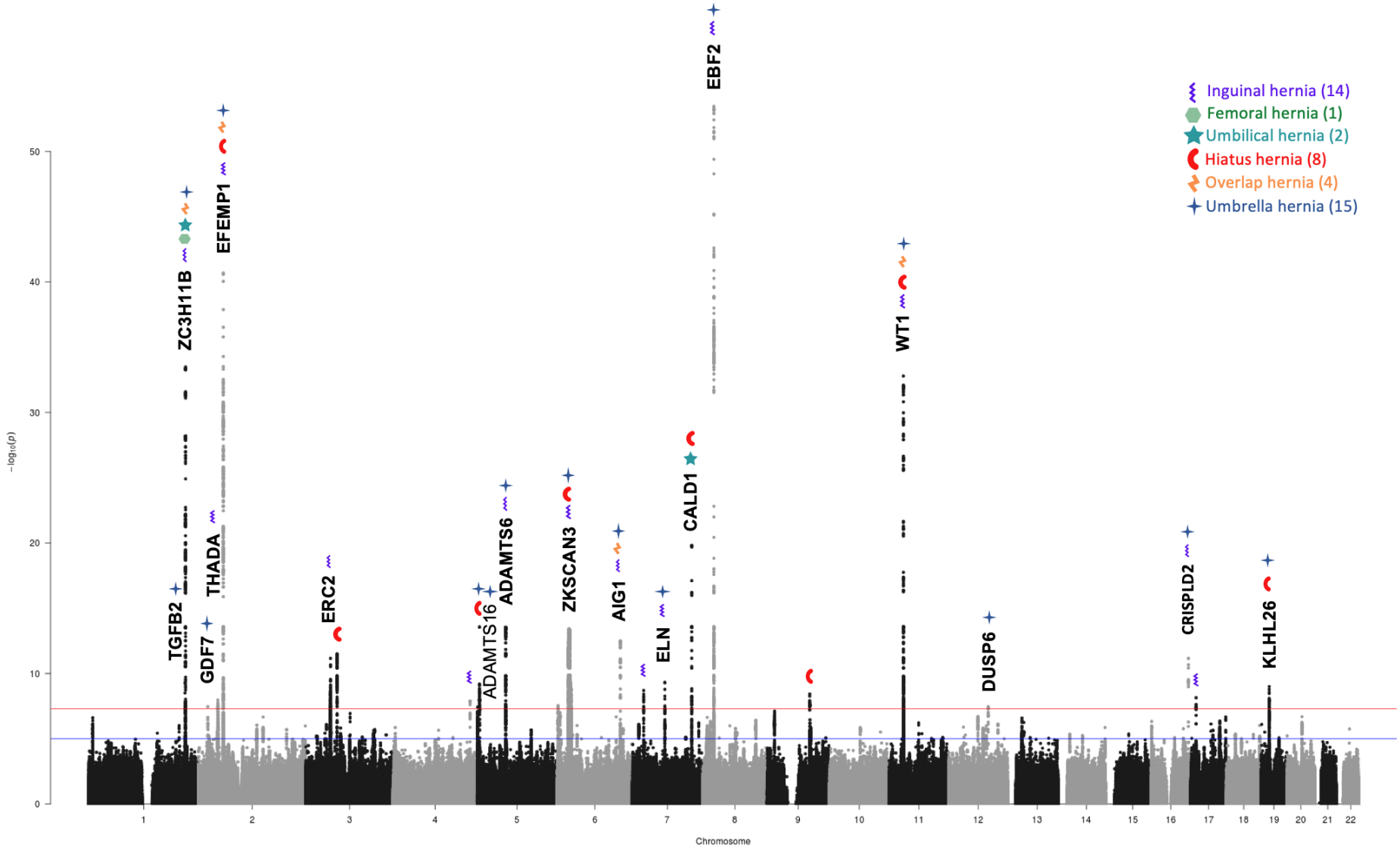

Figure 4.10. New putative shared hernia susceptibility locus 5p15.33 discovered through multivariate meta-analysis in metaUSAT

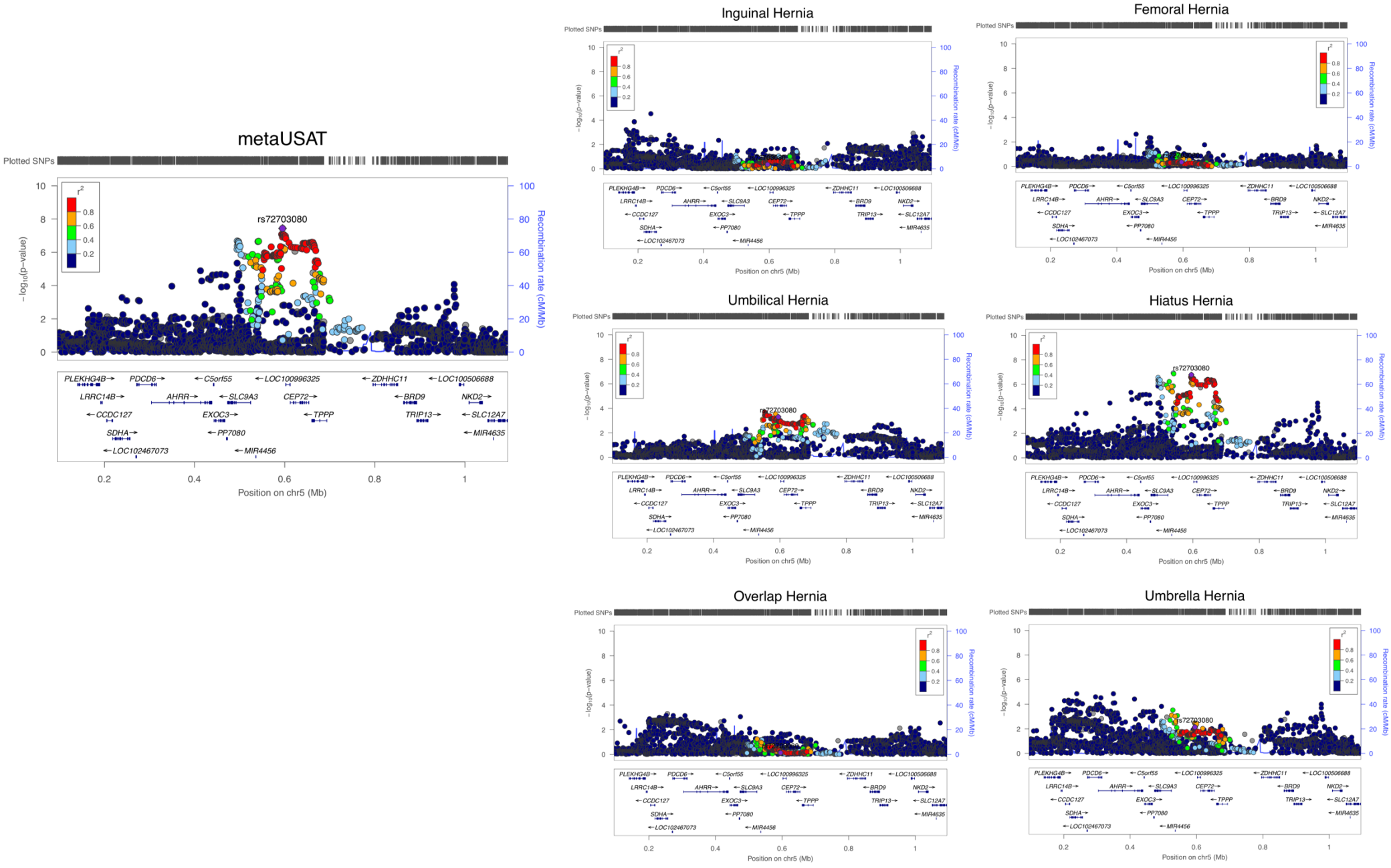

Figure 4.11. Six loci showing the greatest degree of overlap across all analyses.
1q41 (*ZC3H11B*) – metaUSAT SNP rs559230165 was not available in the reference panel hence the lowest P-value SNP was plotted for each Locus Zoom. *ZC3H11B* (the most proximal gene) was also not available in the gene panel.

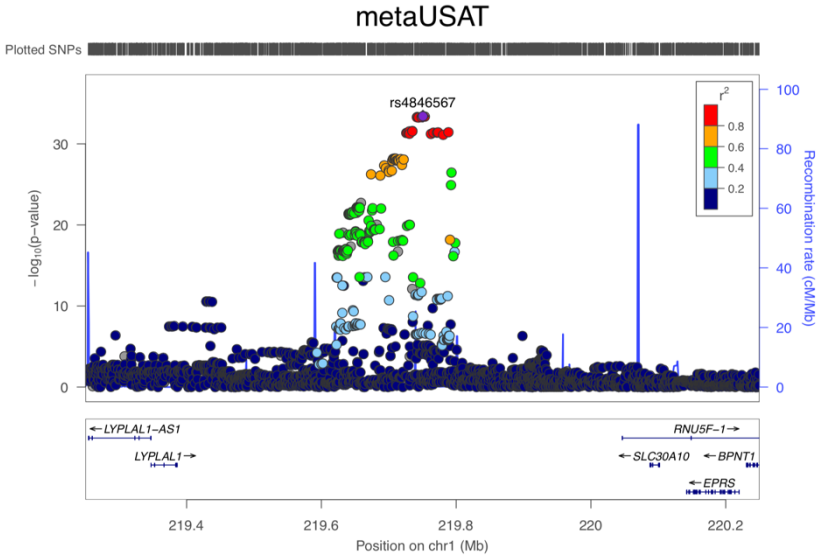

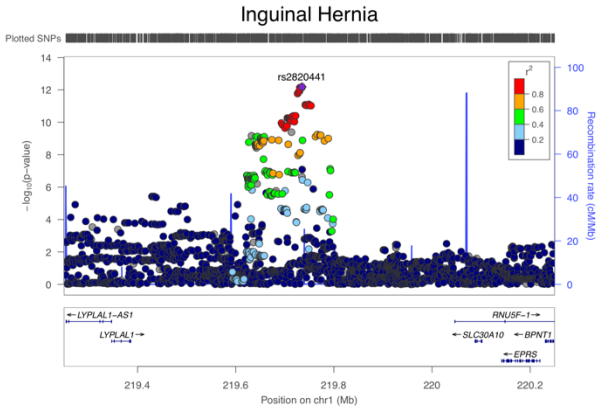

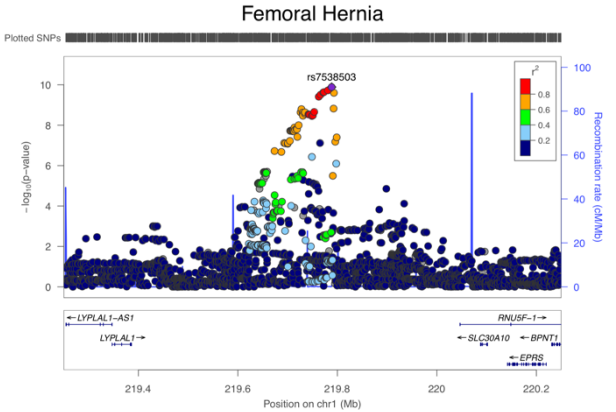

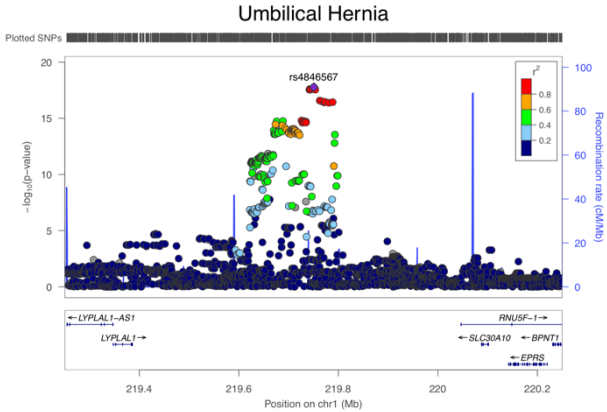

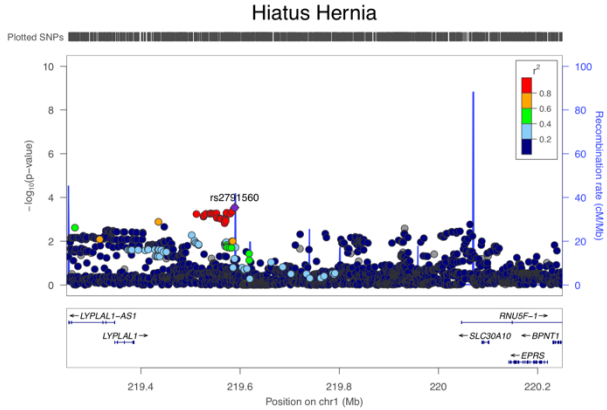

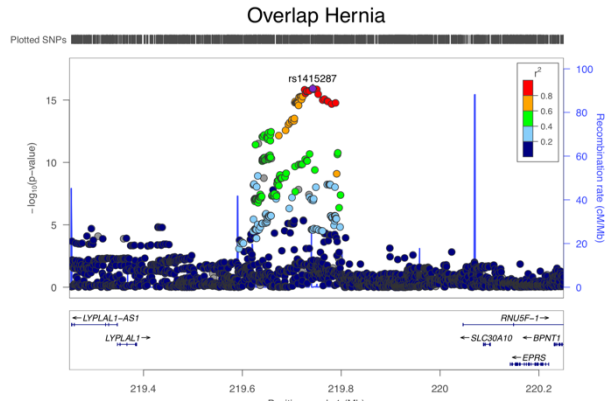

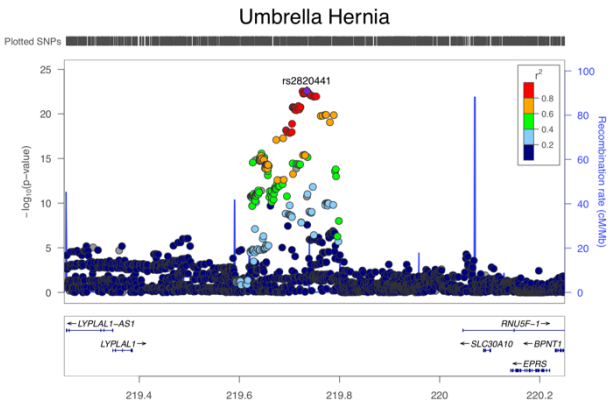

2p16.1 (*EFEMP1*)

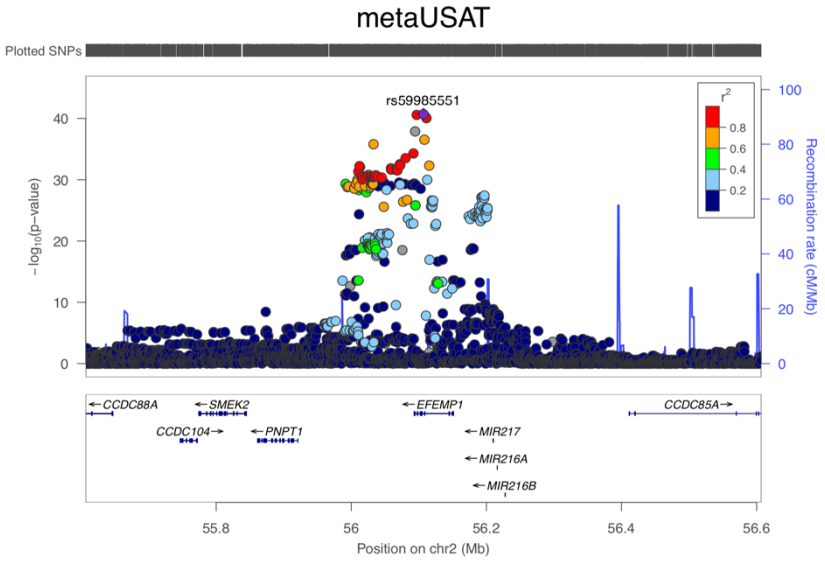

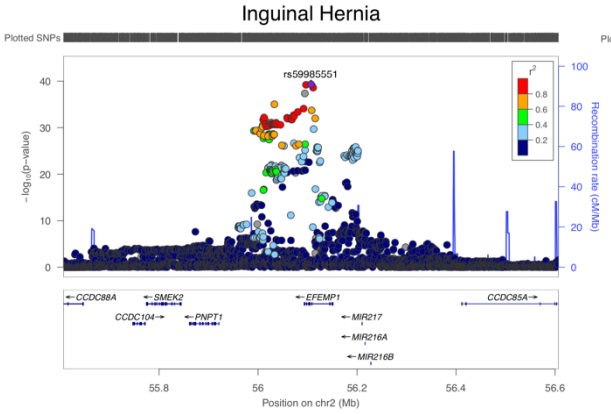

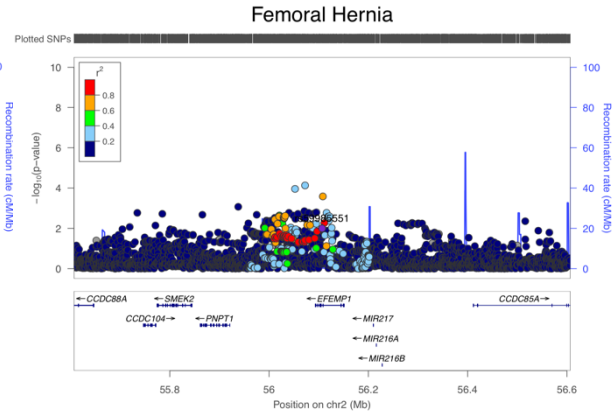

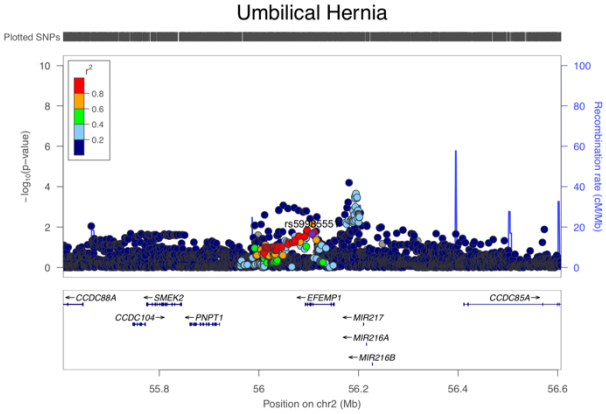

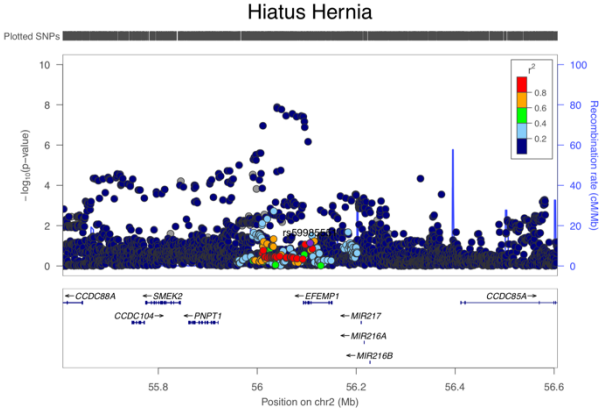

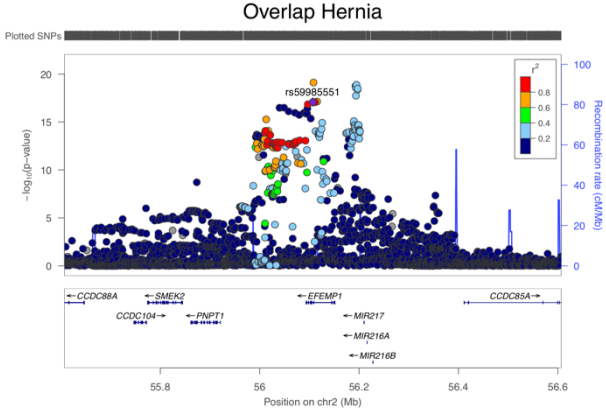

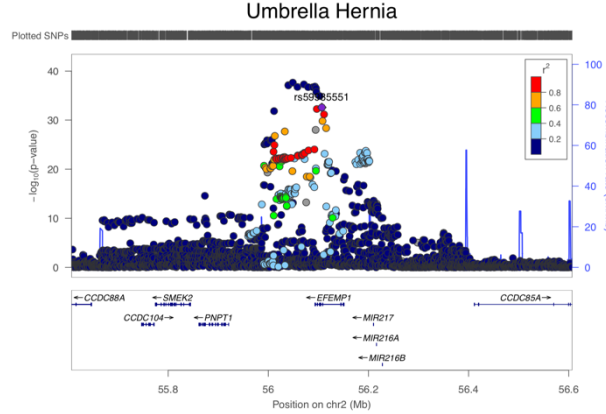

6p22.2 (*ZKSCAN3* (MHC region))

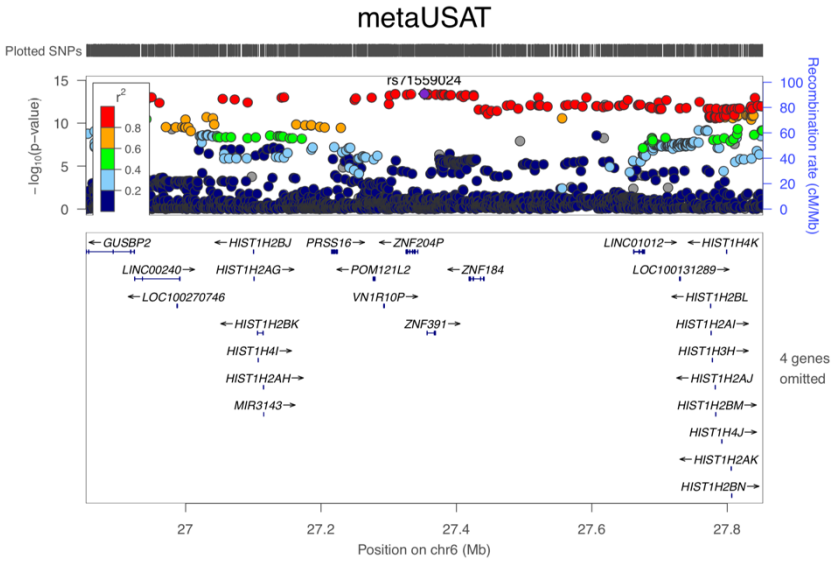

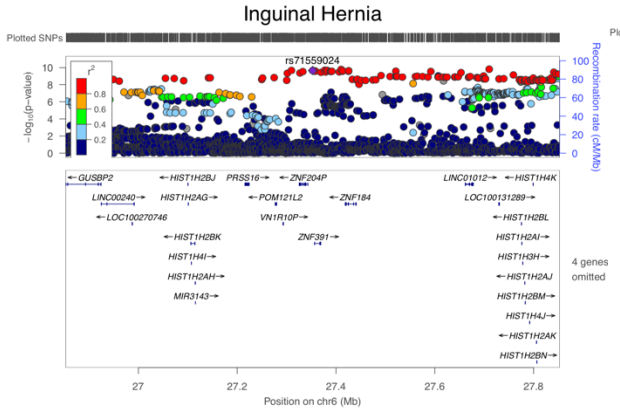

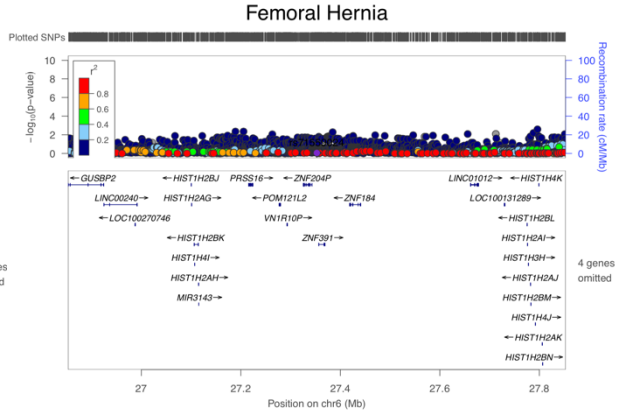

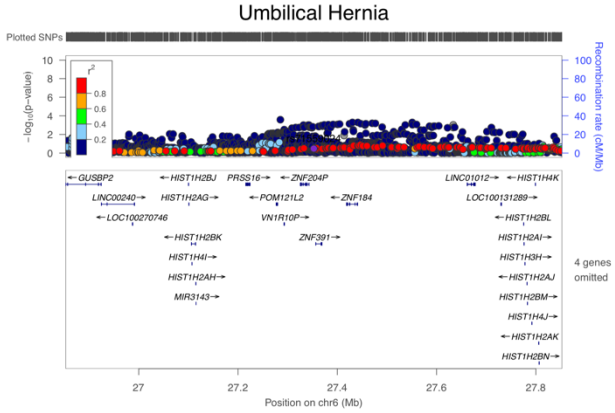

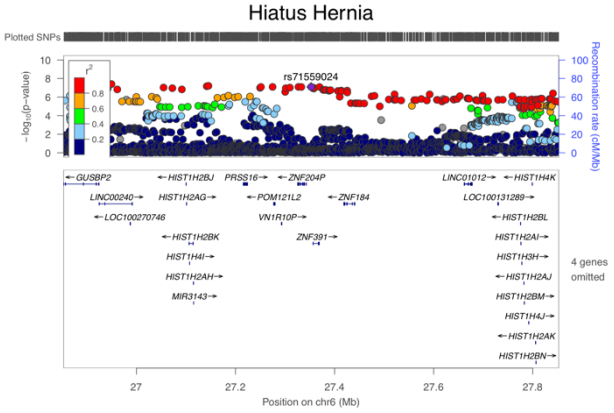

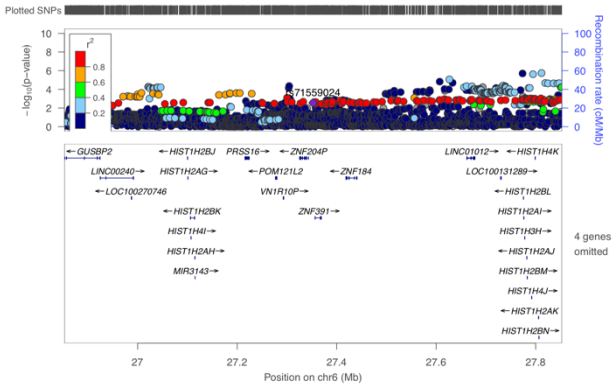

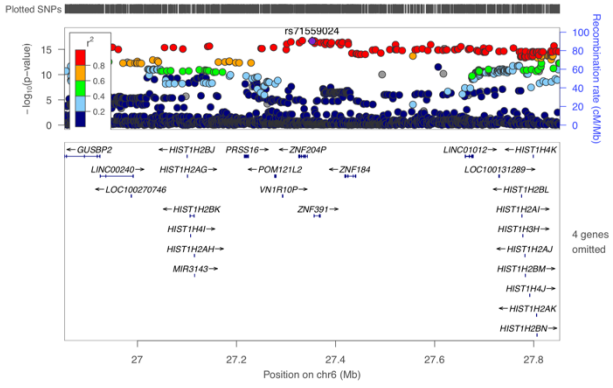

6q24.2 (*AIG1*)

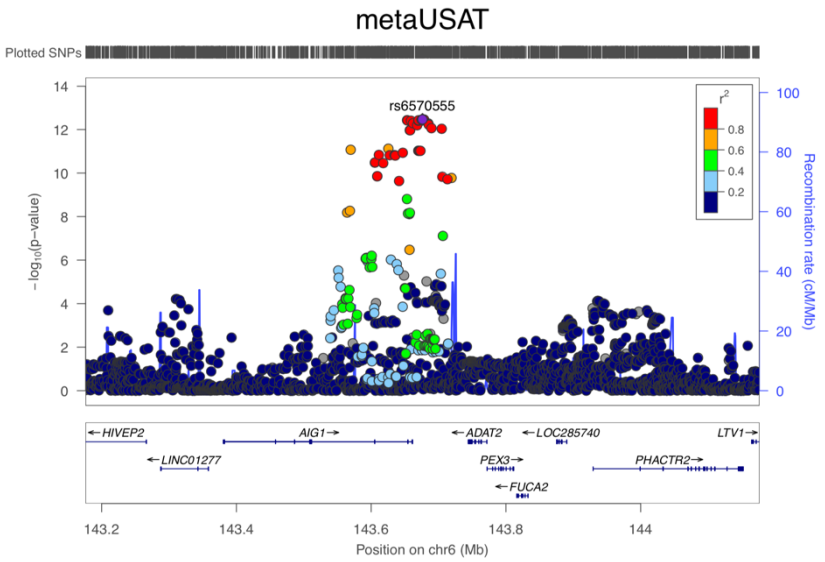
metaUSAT
Plotted SNPs
rs6570555
$-\log_{10}$(p-value)
Recombination rate (cM/Mb)
HIVEP2
AIG1
ADAT2
LOC285740
LTV1
LINC01277
PEX3
PHACTR2
FUCA2
143.2
143.4
143.6
143.8
144
Position on chr6 (Mb)

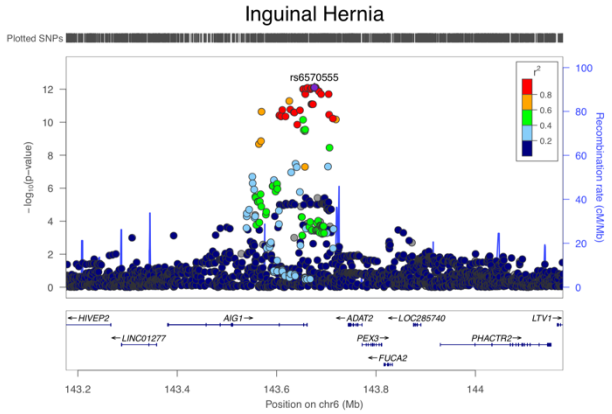
Inguinal Hernia
Plotted SNPs
rs6570555
$-\log_{10}$(p-value)
Recombination rate (cM/Mb)
HIVEP2
AIG1
ADAT2
LOC285740
LTV1
LINC01277
PEX3
PHACTR2
FUCA2
143.2
143.4
143.6
143.8
144
Position on chr6 (Mb)

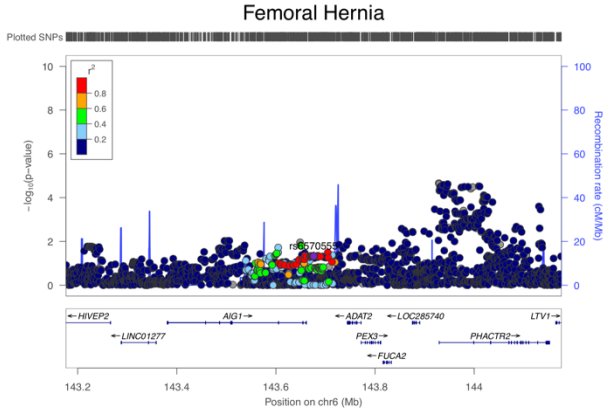
Femoral Hernia
Plotted SNPs
$-\log_{10}$(p-value)
Recombination rate (cM/Mb)
HIVEP2
AIG1
ADAT2
LOC285740
LTV1
LINC01277
PEX3
PHACTR2
FUCA2
143.2
143.4
143.6
143.8
144
Position on chr6 (Mb)

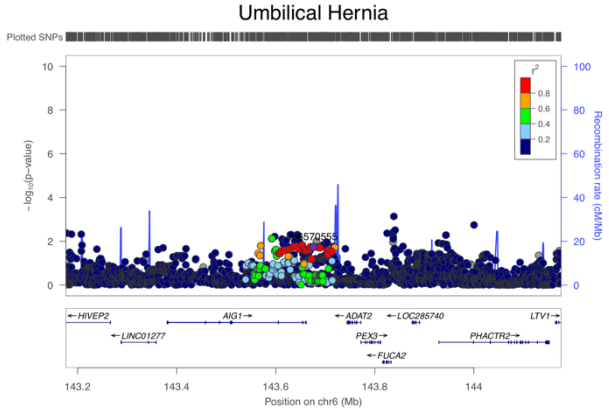
Umbilical Hernia
Plotted SNPs
$-\log_{10}$(p-value)
Recombination rate (cM/Mb)
HIVEP2
AIG1
ADAT2
LOC285740
LTV1
LINC01277
PEX3
PHACTR2
FUCA2
143.2
143.4
143.6
143.8
144
Position on chr6 (Mb)

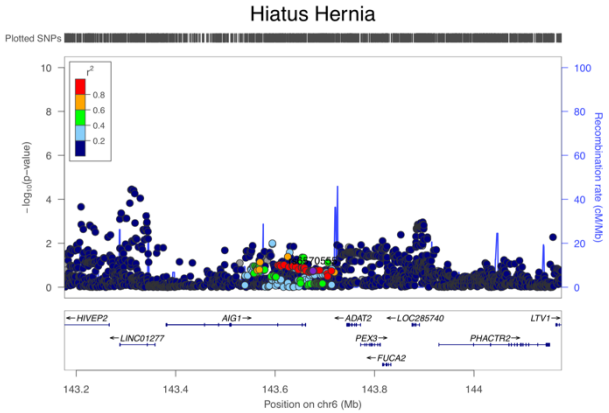
Hiatus Hernia
Plotted SNPs
$-\log_{10}$(p-value)
Recombination rate (cM/Mb)
HIVEP2
AIG1
ADAT2
LOC285740
LTV1
LINC01277
PEX3
PHACTR2
FUCA2
143.2
143.4
143.6
143.8
144
Position on chr6 (Mb)

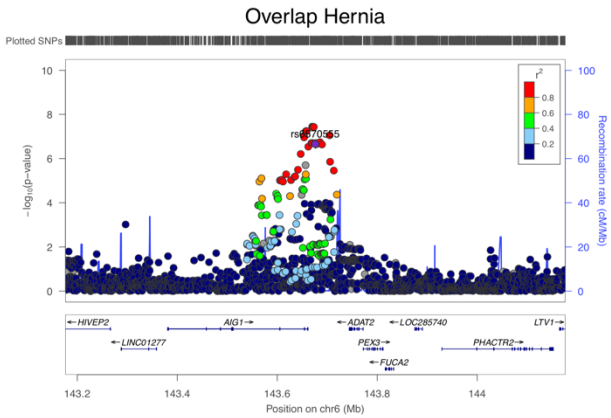
Overlap Hernia
Plotted SNPs
$-\log_{10}$(p-value)
Recombination rate (cM/Mb)
HIVEP2
AIG1
ADAT2
LOC285740
LTV1
LINC01277
PEX3
PHACTR2
FUCA2
143.2
143.4
143.6
143.8
144
Position on chr6 (Mb)

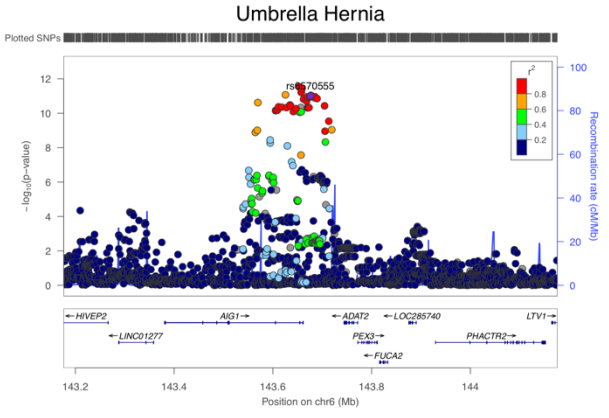
Umbrella Hernia
Plotted SNPs
rs6570555
$-\log_{10}$(p-value)
Recombination rate (cM/Mb)
HIVEP2
AIG1
ADAT2
LOC285740
LTV1
LINC01277
PEX3
PHACTR2
FUCA2
143.2
143.4
143.6
143.8
144
Position on chr6 (Mb)

7q33 (*CALD1*)

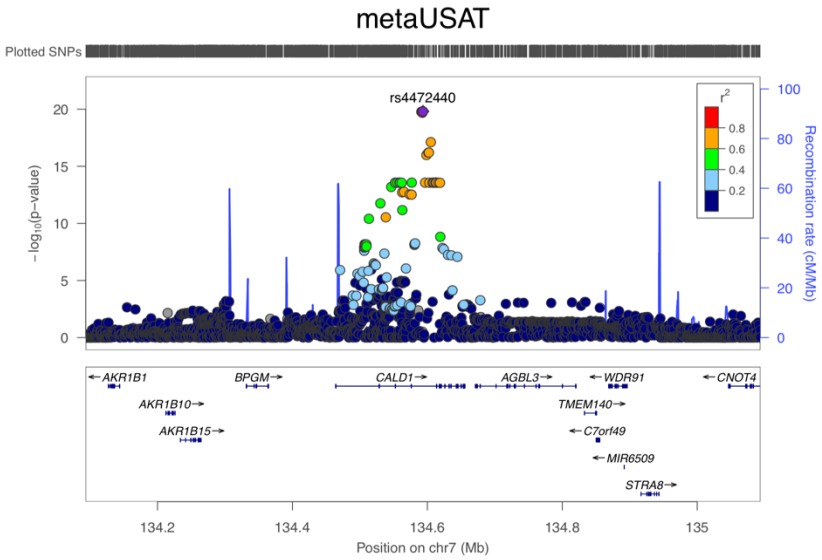
metaUSAT
Plotted SNPs
rs4472440
r^2
0.8
0.6
0.4
0.2
$-\log_{10}$(p-value)
Recombination rate (cM/Mb)
AKR1B1
BPGM
CALD1
AGBL3
WDR91
CNOT4
AKR1B10
TMEM140
AKR1B15
C7orf49
MIR6509
STRA8
134.2
134.4
134.6
134.8
135
Position on chr7 (Mb)

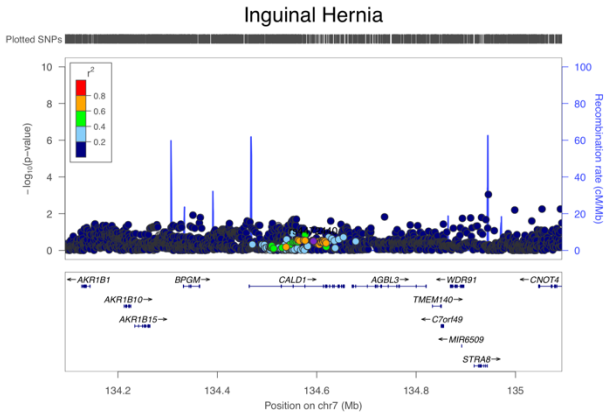
Inguinal Hernia
Plotted SNPs
r^2
0.8
0.6
0.4
0.2
$-\log_{10}$(p-value)
Recombination rate (cM/Mb)
AKR1B1
BPGM
CALD1
AGBL3
WDR91
CNOT4
AKR1B10
TMEM140
AKR1B15
C7orf49
MIR6509
STRA8
134.2
134.4
134.6
134.8
135
Position on chr7 (Mb)

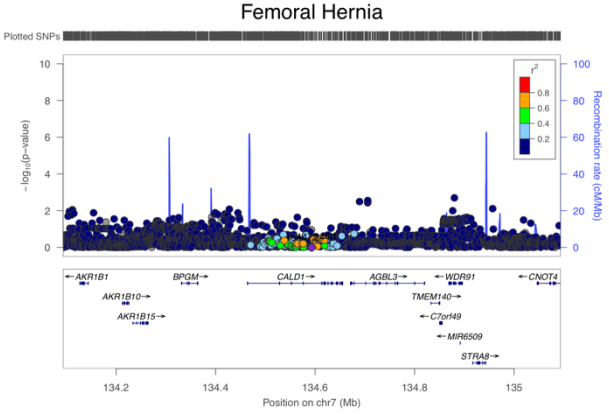
Femoral Hernia
Plotted SNPs
r^2
0.8
0.6
0.4
0.2
$-\log_{10}$(p-value)
Recombination rate (cM/Mb)
AKR1B1
BPGM
CALD1
AGBL3
WDR91
CNOT4
AKR1B10
TMEM140
AKR1B15
C7orf49
MIR6509
STRA8
134.2
134.4
134.6
134.8
135
Position on chr7 (Mb)

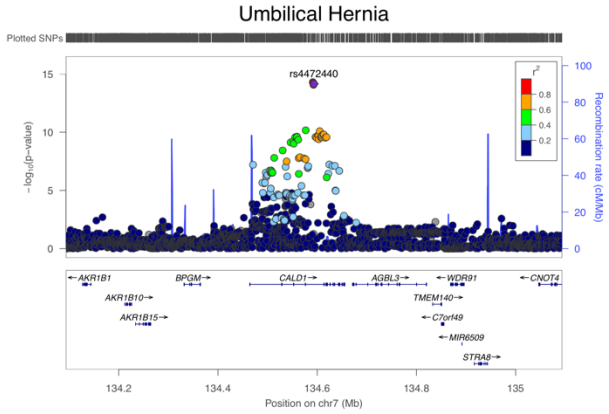
Umbilical Hernia
Plotted SNPs
rs4472440
r^2
0.8
0.6
0.4
0.2
$-\log_{10}$(p-value)
Recombination rate (cM/Mb)
AKR1B1
BPGM
CALD1
AGBL3
WDR91
CNOT4
AKR1B10
TMEM140
AKR1B15
C7orf49
MIR6509
STRA8
134.2
134.4
134.6
134.8
135
Position on chr7 (Mb)

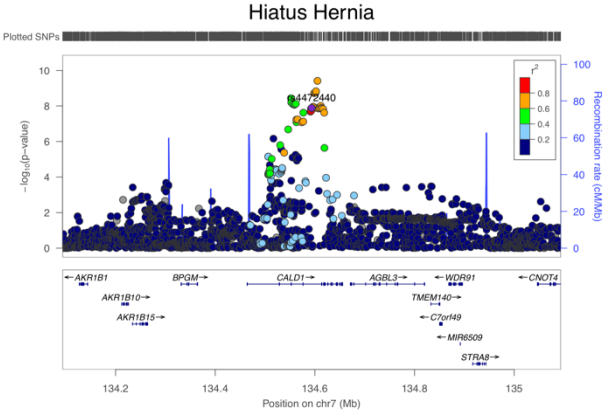
Hiatus Hernia
Plotted SNPs
r^2
0.8
0.6
0.4
0.2
$-\log_{10}$(p-value)
Recombination rate (cM/Mb)
AKR1B1
BPGM
CALD1
AGBL3
WDR91
CNOT4
AKR1B10
TMEM140
AKR1B15
C7orf49
MIR6509
STRA8
134.2
134.4
134.6
134.8
135
Position on chr7 (Mb)

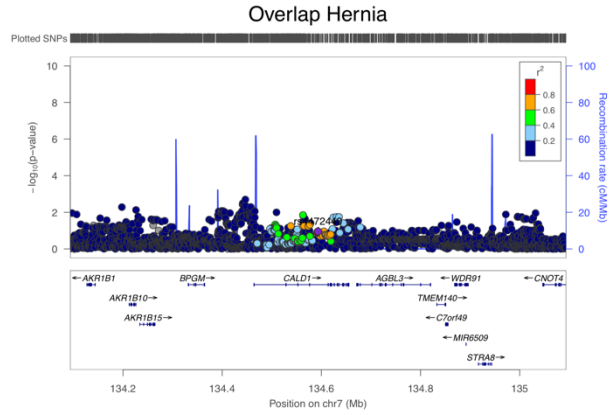
Overlap Hernia
Plotted SNPs
r^2
0.8
0.6
0.4
0.2
$-\log_{10}$(p-value)
Recombination rate (cM/Mb)
AKR1B1
BPGM
CALD1
AGBL3
WDR91
CNOT4
AKR1B10
TMEM140
AKR1B15
C7orf49
MIR6509
STRA8
134.2
134.4
134.6
134.8
135
Position on chr7 (Mb)

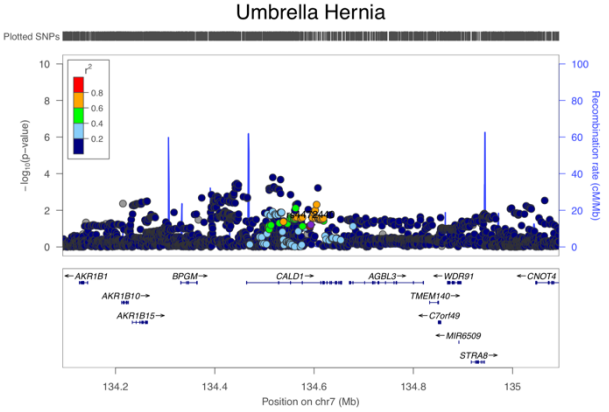
Umbrella Hernia
Plotted SNPs
r^2
0.8
0.6
0.4
0.2
$-\log_{10}$(p-value)
Recombination rate (cM/Mb)
AKR1B1
BPGM
CALD1
AGBL3
WDR91
CNOT4
AKR1B10
TMEM140
AKR1B15
C7orf49
MIR6509
STRA8
134.2
134.4
134.6
134.8
135
Position on chr7 (Mb)

11p13 (*WT1*). *LD information was not available for SNP rs5030123 in the reference panel.*

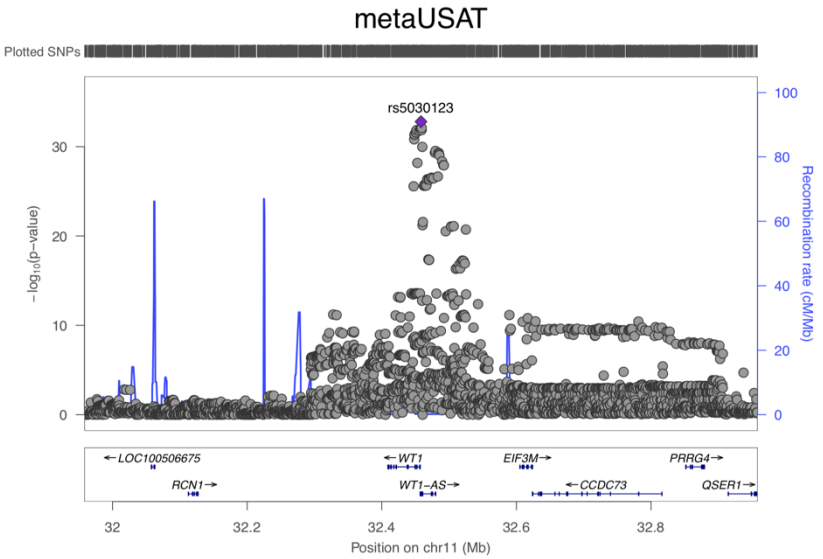

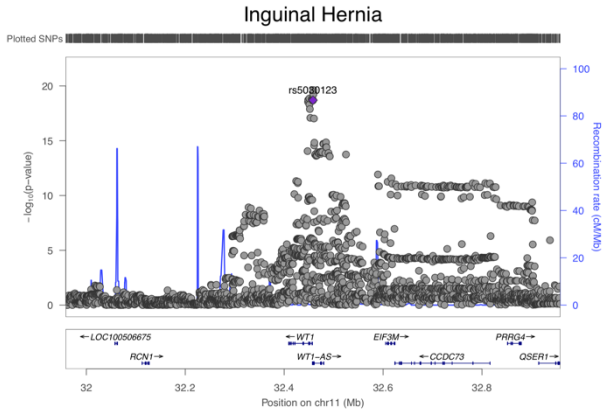

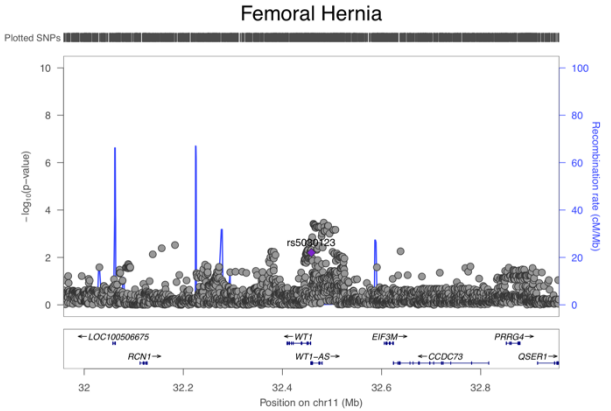

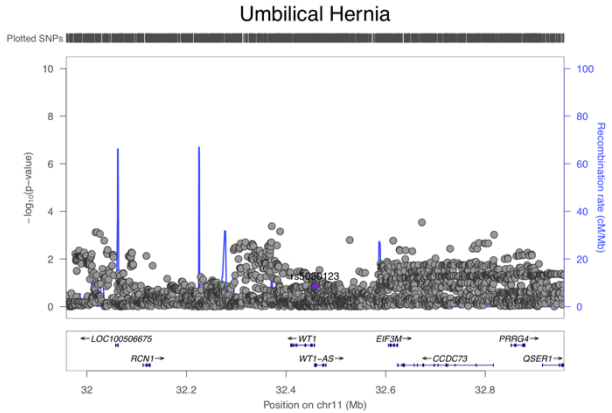

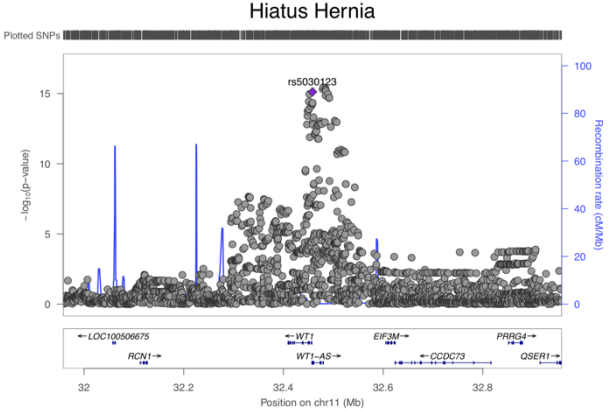

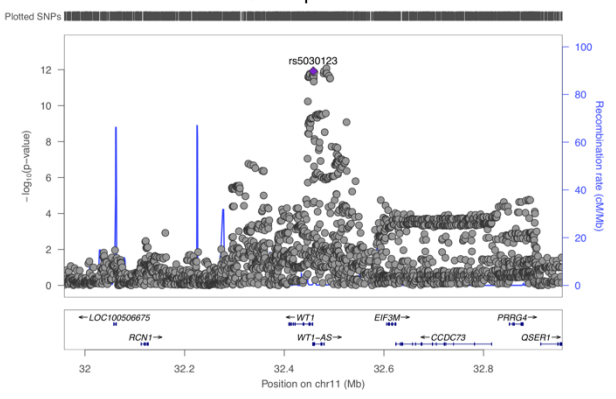

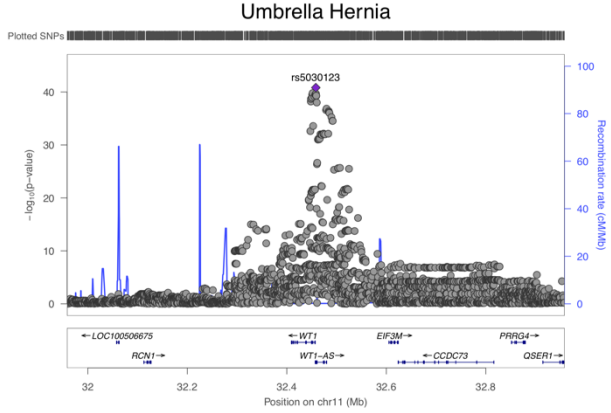

4.4. Discussion

4.4.1. Summary

Hernias are complex diseases with substantial genetic and non-genetic components. This chapter led to the discovery of fundamental molecular genetic candidates which collectively advance our existing understanding of the pathobiology of four common hernia subtypes, and more widely, hernia in general. In the first individual analyses, 38 susceptibility loci (34 of them novel) were found to associate individually with inguinal, femoral, umbilical, and hiatus hernia, representing substantial progress in characterising the genetic basis of these common diseases. Further, using both linear, multi-trait and multivariate analysis approaches to unravel the shared genetic biology of the four hernia phenotypes, six biologically-relevant loci (**1q41** (*ZC3H11B*); **2p16.1** (*EFEMP1*); **6p22.2** (*ZKSCAN3* (MHC region)); **11p13** (*WT1*); and **7q33** (*CALD1*), and **6q24.2** (*AIG1*)) were prioritised as putative loci demonstrating the highest evidence of shared susceptibility to multiple hernia phenotypes. Moreover, a further six loci (***5p15.33*** *(CEP72),* ***2p24.1*** *(GDF7),* ***1q41*** *(TGFB2),* ***3q22.2*** *(AMOTL2),* ***5p15.32*** *(ADAMTS16) and* ***12q21.33*** *(DUSP6))* were discovered under shared genetic analyses that were not discovered in the individual analyses and represent putative genetic elements in shared hernia biology. The *in silico* analyses provide data suggesting functional variants at the susceptibility loci. Pathway analyses enriched genes implicated in connective and elastic tissue biology, and thorax and anterior abdomen development, with tissue expression analyses markedly enriching adipose tissue. Finally, using genetic risk scoring, hernia severity (defined by surgical intervention) was discovered to correlate with genetic burden, highlighting the role of genetics in this unique complex disease model.

4.4.2. Six loci with evidence of shared susceptibility towards multiple hernia subtypes

1q41 (*ZC3H11B*). This locus imparted the highest susceptibility across three of four individual hernia phenotypes (umbilical, femoral and umbilical). Moreover, investigation for shared biology demonstrated this locus to be significant in the overlap and umbrella analyses, three of four MTAG analyses and the metaUSAT analysis. This locus also demonstrated strong evidence of functionality, with the highest effect size lead variant of all individual analyses, rs7538503 ($P_{Femoral} = 1.3\times10^{-10}$, OR = 1.42), associated with femoral hernia at this locus. Moreover, in the umbilical hernia individual analysis, the lead signal at this locus, rs4846567, is a predicted pathogenic regulatory region variant ($P = 1.7\times10^{-18}$, OR = 1.22, CADD = 14.9), and is also a genome-wide significant eQTL for *ZC3H11B* in GTEx v8 testis tissue ($P_{eQTL} = 1.5\times10^{-8}$). *ZC3H11B* demonstrates significant association with several myopia endophenotypes, including axial length, refractive error, corneal astigmatism, and spherical equivalent.[30] Accelerated connective tissue remodelling of the posterior sclera is thought to lead to axial elongation, which is a key feature of myopia. This pathological remodelling leads to stiffening of ocular connective tissue and is thought to be the underlying process behind myopia leading to glaucoma[31]. Intriguingly, at least two marfanoid-like syndromes, have been described with co-existing myopia and hernia.[32,33]

2p16.1 (*EFEMP1*). *EFEMP1* imparted susceptibility to inguinal and hiatus individual hernia phenotypes, as well as the overlap, umbrella, metaUSAT, and importantly, all four MTAG analyses. EFEMP1, which is discussed in detail in the previous two

chapters, encodes fibulin-3, a core extracellular matrix glycoprotein. Notably, an almost identical association profile is seen for *EFEMP1* as with *ZC3H11B*, with aberrant expression of *EFEMP1* associated with several ophthalmic phenotypes, including age-related macular degeneration, and several endophenotypes of myopia and glaucoma, as well as anthropometric measures of height and weight which are also associated with *ZC3H11B*. *EFEMP1* was discovered as a susceptibility locus by Jorgensen and colleagues in their GWA study of inguinal hernia (rs2009262, $P = 1.45\times10^{-17}$, OR = 1.15), and this signal was replicated in this larger study ($P = 6.1\times10^{-33}$, OR = 1.18).[34] Jorgensen demonstrated aberrant accumulation of EFEMP1 in mouse connective tissue[34], and suggested a role for EFEMP1 in hernia pathobiology through its role in collagen and elastin fibre homeostasis. Collagen is an important component of abdominal fascia[35], and indeed the transversalis fascia has been demonstrated to have a decreased type I:III collagen ratio in inguinal hernia[36], with heightened expression of type III collagen mRNA also described.[37] Disruption in the complex balance of collagen in fascia is therefore strongly implicated in inguinal hernia biology.[38] As well as collagen, fibulin-3 binds tropoelastin[39], the monomeric unit of elastin fibres. Diminished elastic fibre assembly in fascia of EFEMP1 knockout mice has been described, and these mice invariably develop inguinal hernia.[40] Therefore, the overexpression of collagen and decreased expression of elastin in fascial tissue may play a fundamental role in hernia biology.

11p13 (*WT1*). Alongside *EFEMP1*, locus 11p13 (*WT1*) was significantly associated in all four multi-trait MTAG analyses. WT1 was discovered by Jorgensen as one of four susceptibility loci associated with inguinal hernia in their GWA study ($P = 3.69\times10^{-14}$, OR = 1.11)[34], a signal which was replicated in the present study ($P = 4.0\times10^{-20}$, OR =

1.11). This locus was also associated with hiatus hernia ($P = 1.1\times10^{-13}$, OR = 1.07). Of note, several *WT1* deletion syndromes, including Denys-Drash[41], WAGR[42], and Meachem syndromes[43], are characterised by congenital hiatus hernia. Moreover, a variant near *WT1-AS* (~15kb from the lead variant at 11p13) has been discovered to significantly associate (rs3858461, $P = 1.0\times10^{-8}$) with medication use for peptic ulcer and gastro-oesophageal reflux disease (GORD)[44], which are the principal clinical sequelae of hiatus hernia. Of note, this variant was more significantly associated with hiatus and inguinal hernia in the individual analyses ($P_{Hiatus} = 2.4\times10^{-13}$, OR = 1.06; $P_{Inguinal} = 2.9\times10^{-9}$, OR = 1.07). WT1 is implicated in collagen homeostasis via its inhibition of MMP2 and activation of TIMP3, which lead to collagen accumulation. Deranged expression of MMPs which break down collagen, and their inhibitors, is noted in hernia fibroblasts.[37] EFEMP1 is thought to buttress the inhibitory effect of WT1 on MMPs through stimulating TIMP3 activity[45] - thus connecting these two shared loci. Taken together, these loci therefore impede MMPs and are suggested to disrupt the collagen make-up of fascia leading to hernia pathogenesis.

7q33 (*CALD1*). Susceptibility signals near *CALD1* were discovered to associate with umbilical and hiatus hernia (rs12707188, $P_{Umbilical} = 5.0\times10^{-15}$, OR = 1.19, EAF = 0.37(T); rs4728341, $P_{Hiatus} = 3.9\times10^{-10}$, OR = 1.06, EAF = 0.55 (T)), though intriguingly their effects are in opposite directions. The metaUSAT analysis further suggested shared genetic architecture for hernia at this locus. *CALD1* encodes caldesmon-1, which is a calmodulin- and actin-binding protein and is highly expressed in smooth muscle and non-muscle tissue[46], with important roles in cell motility, migration and reorganisation of actin cytoskeleton and smooth muscle contraction.[47] The patency of the processus vaginalis in inguinal hernia has been linked to smooth muscle cell

(SMC) persistence[48,49], and immunohistochemical studies have demonstrated smooth muscle phenotypic modulation to a synthetic phenotype in hernia; several markers for mature smooth muscle cells, including alpha-smooth muscle actin, desmin, and caldesmon, were found to be elevated in inguinal hernia sacs.[50,51] Moreover, new-born mice that are caldesmon-1 null have occasionally been demonstrated to be viable, however with fatalities occurring within the first 5-7 hours in the majority of homozygotes due to severe umbilical hernia.[52] *CALD1* has also been associated with diverticular disease, which is another elastic tissue disease characterised by SMC phenotypic switch to a secretory phenotype, specifically a reduction in smooth muscle myosin heavy chain (a marker of mature SMCs).[53,54] Therefore impaired contractility of smooth muscle and pathological SMC phenotypic transition may have an important role to play in hernia formation.

6q24.2 (*AIG1*). *AIG1* represents one of four overlap loci, demonstrating robust evidence of shared genetics via an association with inguinal and umbrella hernia and enrichment in the multivariate metaUSAT analysis. AIG1 (Androgen-inducible gene 1) has been cloned from human dermal papilla cells[55], where it has been shown to be inducible by dihydrotestosterone.[56] AIG1 mRNA shows high expression in testis, ovary, heart and colon.[55] Complete androgen insensitivity syndrome (CAIS) is characterised by masculinisation of the external genitalia caused by an inability to respond to androgens and a patent processus vaginalis.[57] Most characteristically, CAIS presents in young females with bilateral inguinal hernia; indeed, ~1-2% of all females with bilateral inguinal hernia are thought to have CAIS.[58] Disruption of AIG1 expression may therefore have some role to play in androgen sensitivity and therefore hernia pathobiology.

6p22.2 (*ZKSCAN3* (MHC region)). The MHC region imparted susceptibility to both inguinal and hiatus individual phenotypes (rs13212652, $P_{Inguinal} = 3.1\times10^{-11}$, OR = 1.12, EAF = 0.87(T); rs9393735, $P_{Hiatus} = 2.7\times10^{-8}$, OR = 1.07, EAF = 0.86(G)). The exact role of the MHC region in hernia is difficult to discern, however, common variants in the MHC locus have been found to heavily associate with Barrett's oesophagus[59], which is strongly linked with hiatus hernia.

4.4.3. Six loci discovered through multi-trait analysis that weren't discovered in the individual analyses

5p15.33 *(near CEP72).* A putative new locus **5p15.33** was discovered to associate with hernia in the multivariate analysis (rs72703080, $P_{metaUSAT}$ = 3.68×10^{-8}, ~20kb upstream from *CEP72*). *CEP72* encodes a centriolar satellite protein that is necessary for regulating microtubule-organising activity and centrosome integrity.[60] Using comparative genomic hybridisation, Choi *et al* discovered copy number aberrations (gains) at **5p15.33** in patients with ruptured intracranial aneurysms.[61] Moreover, the *CEP72* region was previously implicated in a GWA meta-analysis of Barrett's oesophagus and oesophageal adenocarcinoma.[62] Hiatus hernia plays a key role in oesophageal mucosal injury in GORD, which predisposes to Barrett's oesophagus.[63] Indeed, the size of hiatus hernia is significantly associated with progression of Barrett's oesophagus to high-grade dysplasia or malignancy.[64] To this end, a tangible contributor to shared hernia risk has been identified through multivariate meta-analysis.

2p24.1 *(GDF7).* Lead variant rs3072 resides in a 3'UTR of *GDF7* and was discovered to associate with hernia in the umbrella and metaUSAT analyses (P = 1.80×10^{-8}, P= 3.48×10^{-8}, respectively). Of note, this variant demonstrates strong functionality as a robust eQTL for *GDF7* in GTEx aorta tissue (P_{eQTL} =5.4×10^{-9}). GDF7 encodes BMP12, a ligand in the bone morphogenetic protein pathway, which is involved in neural system development[65] and in tendon and ligament development and repair.[66] BMP12 is tenogenic, and plays an important role in differentiating mesenchymal stem cells into tenocytes[67], and is therefore used in tissue engineering approaches to tendon

repair.[68] *GDF7* has been identified through GWAS to associate with eight traits, with three of these characterised by connective and elastic tissue dysfunction: pelvic organ prolapse (rs9306894-G, P = 3×10^{-17}, OR = 1.11)[69], abdominal aortic aneurysm (rs13382862-A, P = 1.0×10^{-6}, OR = 1.10)[70], and diverticular disease (rs7255-T, P = 4×10^{-6}, OR = 1.06).[71] The T allele of rs7255 was also found to confer risk of Barrett's Oesophagus in the GWAS by Gharahkhani *et al* (p=9.0e-11, OR=1.14).[62] The BMP pathway has been heavily implicated in Barrett's Oesophagus[72], and several studies have identified polymorphisms in the *TBX5-GDF7* genomic region demonstrating a considerable connection with Barrett's.[73–75] Further, the lead variant rs3072 at this locus was sub-threshold, but strongly suggestive of association in the individual hiatus hernia analysis (P = 6.30×10^{-8}), lending evidence for a potential role for this locus in hiatus hernia biology and a wider role in shared hernia susceptibility.

1q41 (*TGFB2*). Using the multi-trait MTAG analysis approach, this new locus was discovered to associate with inguinal ((rs3121580, $P_{MTAG} = 3.41\times10^{-8}$) and femoral hernia (rs2799098, P = 4.66×10^{-8}), and was identified in the metaUSAT and umbrella analyses, where it was the most significant locus (rs2799098, $P_{metaUSAT} = 5.8\times10^{-10}$, $P_{Umbrella} = 9.3\times10^{-15}$). *TGFB2* encodes the TGF-β2 ligand which is a core component of the TGF-β signalling pathway. A signature of increased TGF-β signalling is seen in Marfan syndrome, Loeys-Dietz, and cutis laxa which are associated with aneurysmal changes caused by mutations that hamper smooth muscle cell contractile proteins.[76] *TGFB2* haploinsufficiency pathologically activates the TGF-β signalling pathway[77] leading to Loeys-Dietz syndrome type 4 (LDS4)[78], which is characterised by arterial vasculopathy (arterial aneurysms, dissection and tortuosity), and other widespread connective tissue pathology including hernias.[79] Of note, several association studies

have found *TGFB2* to associate with glaucoma endophenotypes, including intraocular pressure[80], central corneal thickness[81]; as well as FEV1/FVC ratio[82] and severe COPD[83], which has also been suggested as an independent risk factor for hernia pathology and severity.[1,84]

3q22.2 *(AMOTL2).* The umbrella analysis revealed the **3q22.2** locus (rs9883955, P = 1.2×10^{-8}), which was not identified in any of the other analyses. The scaffold protein, AMOTL2, forms a complex with VE-cadherin which regulates endothelial cell shape through mechanical coupling of adherens junctions to contractile actin fibres, and has been shown to be required for aortic lumen expansion.[85] Additionally, AMOTL2 plays a fundamental role in endothelial cell polarity, migration and proliferation during angiogenesis.[86] Several associations of *AMOTL2* have also been described with myopia-related phenotypes, including refractive error, spherical equivalent, and vertical cup-disc ratio.[30] Moreover, proximal deletions in 3q have been described in the literature, which most commonly occur in 3q22-23. *De novo* mutations in 3q22.1 result in a syndromic presentation of bilateral inguinal hernia[87] and an interstitial deletion of 3q23 has been described to result in BPES syndrome, which is characterised by diaphragmatic hernia.[88] This region on the long arm of chromosome 3 may therefore be of considerable interest in multiple hernia pathobiology.

5p15.32 *(ADAMTS16).* Two signals were discovered in the metaUSAT analysis in proximity to the *ADAMTS16* gene at **5p15.32**: rs42202 ($P_{metaUSAT}$ =2.71×10^{-14}, ~100kb upstream from *ADAMTS16*) and rs7715383 ($P_{metaUSAT}$ = 2.97×10^{-9}, ~25kb downstream from *ADAMTS16*), both of which were discovered in the umbrella analysis (P = 1.7×10^{-11} and P = 1.2×10^{-12}, respectively). Intriguingly, only the upstream

signal (and not the downstream signal) was associated with hiatus hernia in the individual (rs42202, $P_{Hiatus} = 8.0\times10^{-16}$) and MTAG (rs42202, $P_{MTAG} = 5.70\times10^{-15}$) analyses. ADAMTS16 is a member of the ADAMTS family of multi-domain secreted metalloendopeptidases which are central remodelling enzymes of the extracellular matrix.[89] ADAMTS16 is co-expressed alongside WT1 in murine models and is thought to play an important role in murine genitourinary development.[90] Variants in *ADAMTS16* have been associated with urinary incontinence[91], a manifestation of pelvic floor dysfunction, which have been shown independently to lead to a higher prevalence of hiatus and inguinal hernia.[92] Several mutations have been described in the other 18 ADAMTS superfamily genes which result in distinct human genetic disorders.[89] Three additional ADAMTS proteins show striking implications for connective tissue biology. Mutations in *ADAMTS2* are responsible for dermatosparactic type Ehlers-Danlos Syndrome (type VIIC) by disrupting processing of procollagen molecules[93], and is typified by extreme skin fragility, joint laxity, and umbilical hernia. ADAMTS4 shows significant aggrecanase activity and is implicated in articular cartilage degradation and arthritis[94], and ADAMTS4 mRNA and protein have been found to be highly expressed in lumbar herniated intervertebral discs, suggesting their potential role in lumbar disc herniation.[95] ADAMTS6 protease converts procollagen to collagen[96]; using qRT-PCR and RNA-seq, Jorgensen and colleagues discovered ADAMTS6 to be a susceptibility locus for inguinal hernia and demonstrated reduced expression levels of *ADAMTS6 in* mouse connective tissue related to human transversalis fascia, suggesting a role for ADAMTS6 in collagen homeostasis and hernia biology.[34] These findings provide evidence for the role of ADAMTS proteins in susceptibility to hernia pathology and the potential role of *ADAMTS16* in shared hernia risk.

12q21.33 *(DUSP6).* rs797267 was discovered in the umbrella and metaUSAT analyses ($P = 2.6\times10^{-9}$ and $P = 3.51\times10^{-8}$, respectively), a variant which is a suggestive eQTL for *DUSP6* in tibial nerve tissue ($P_{eQTL}= 3.2\times10^{-5}$). *DUSP6* encodes MKP3, an extracellular signal regulated kinase (ERK)-specific MAPK phosphatase which is a key regulator of extracellular signals transduced to the nucleus. DUSP6 acts as a negative regulator of fibroblast growth factor receptor signalling and loss-of-function mutations in DUSP6 result in FGFR-like syndromes characterised by postnatal mortality, dwarfism, craniosynostosis and hearing loss.[97] Deletions of the 12q21 region have been attributed to cause cranio-facio-cutaneous syndrome[98], which, among other craniofacial manifestations, presents variably with umbilical hernia.[99]

4.4.4. Genetic risk scoring of hernia severity and multiple hernia risk

The lifetime risk of groin hernia is ~27% in males and 3% for females[100], and the incidence of surgical correction sits at 10 to 28 per 100,000 per year.[101] Due to the risk of complications such as postoperative pain, infection and recurrence, elective hernia repair is generally reserved for patients with more symptomatic disease. Moreover, emergency hernia surgery (associated with a substantial mortality rate[102]), is reserved for incarcerated and strangulated hernia, which are surgical emergencies. As expected, all individual, overlap and umbrella hernia cases had a higher genetic burden than matched controls. The genetic risk score analyses also correlated with disease severity, with surgical cases having a higher genetic burden than non-surgical cases in all analyses. These data provide insights into the role of genetic susceptibility in hernia development and severity, and provide an important proof-of-principle of genetic risk scoring in personalising therapeutic approaches to manage this highly prevalent disease. An important caveat is that the secondary genetic risk score analyses, by and large did not demonstrate a higher genetic burden among hernia patients with multiple hernia presentations compared to patients with only an individual hernia occurrence. The only case where multiple hernia was nominally associated with a higher genetic burden was for hiatus hernia, the best powered individual analysis. This may suggest that genetic risk scoring in a larger cohort and using the full extent of associated signals (i.e. a polygenic risk score) may enable more conclusive data. However, this remains to be determined, and in this study we were unable to determine genetic risk score correlation with multiple hernia.

4.4.5. Strengths and limitations

The approach described in this chapter has several limitations that must be addressed in future research. Firstly, despite multiple attempts, we were unable to source a replication cohort to test the many interesting associations discovered. In **Chapter 2**, ~1/3 of discovery loci replicated in an independent cohort, meaning some of the findings identified in this chapter may indeed be false positives. Secondly, the use of biobank-scale data for the study of shared genetic susceptibility to hernia means that invariably heterogeneity in cohort structure are apparent, meaning that hiatus and inguinal hernia (which are substantially more common in the UK population) were over-represented in our dataset and accounted for ~90% of the total cohort across the four hernia phenotypes. This means that in the several multi-trait approaches implemented to dissect shared genetics, many of the identified loci are only minimally associated with umbilical and femoral hernia, despite being highlighted as contributors of shared genetic susceptibility. A larger cohort size, with an equal balance across all four hernia subtypes, would prove useful in defining further the prioritised loci demonstrating high degrees of shared susceptibility as well as uncovering potentially new shared loci.

By using distinct analytic approaches to examine the genetic architecture of the four hernia subtypes, novel and informative insights were gained into the biology of hernia. This enabled sub-threshold (i.e. non-genome-wide significant) loci to be prioritised that would otherwise not have been discovered with traditional single-trait association analyses. Despite the evident lack of a replication cohort, by segregating the four hernia cohorts in UK Biobank to avoid overlap, one can have confidence in the validity

of several loci that were discovered across multiple hernia phenotypes. This is the case for the twelve loci that demonstrated the greatest degree of overlap across the different analyses, and the resulting clustering of many of these loci across functionally related ontologies. Furthermore, the enrichment of biological pathways previously implicated in hernia pathobiology provide further compelling evidence to support the veracity of these loci, and for a shared genetic susceptibility to hernia. Lastly, despite not correlating with shared hernia susceptibility, the genetic risk score correlated with disease severity, which provides important evidence for the role of genetics in hernia biology.

4.5. Conclusion

Herniae are a complex surgical disease with a substantial global health burden affecting patients across all age groups. This study represents an important advancement in the understanding of the genetic architecture of abdominal wall and hiatus hernia. Several loci were discovered as key genetic players in individual hernia susceptibility, and when analysed together, twelve loci demonstrated striking overlap across multiple hernia subtypes, representing fundamental candidates which confer a shared susceptibility to multiple hernia. These shared susceptibility loci cluster in functional categories, most prominently connective and elastic tissue homeostasis and dysfunction which were also enriched in the pathway analyses. Moreover, there is significant evidence of functionality in these shared regions, and the weighted genetic risk score constructed from the association signals also correlated with disease severity. This suggests that a *phenotypic* severity of hernia correlates with *genotypic* severity, which is an important finding to inform future personalised therapeutic approaches to hernia.

4.6. Chapter References

1. Lau, H., Fang, C., Yuen, W. K. & Patil, N. G. Risk factors for inguinal hernia in adult males: A case-control study. *Surgery* **141**, 262–266 (2007).
2. Burcharth, J., Pommergaard, H. C. & Rosenberg, J. The inheritance of groin hernia: A systematic review. *Hernia* **17**, 183–189 (2013).
3. Ikeda, H. *et al.* Risk of contralateral manifestation in children with unilateral inguinal hernia: Should hernia in children be treated contralaterally? *J. Pediatr. Surg.* **35**, 1746–1748 (2000).
4. Jansen, P. L., Klinge, U., Jansen, M. & Junge, K. Risk factors for early recurrence after inguinal hernia repair. *BMC Surg.* **9**, 18 (2009).
5. Maddox, M. M. & Smith, D. P. A long-term prospective analysis of pediatric unilateral inguinal hernias: Should laparoscopy or anything else influence the management of the contralateral side? *J. Pediatr. Urol.* **4**, 141–145 (2008).
6. Zöller, B., Ji, J., Sundquist, J. & Sundquist, K. Shared and nonshared familial susceptibility to surgically treated inguinal hernia, femoral hernia, incisional hernia, epigastric hernia, and umbilical hernia. *J. Am. Coll. Surg.* **217**, (2013).
7. Glassow, F. Femoral hernia. Review of 2,105 repairs in a 17 year period. *Am. J. Surg.* **150**, 353–356 (1985).
8. De Luca, L. *et al. Relationship Between Hiatal Hernia and Inguinal Hernia*. *Digestive Diseases and Sciences* **49**, (2004).
9. Sudlow, C. *et al.* UK Biobank: An Open Access Resource for Identifying the Causes of a Wide Range of Complex Diseases of Middle and Old Age. *PLoS Med.* **12**, (2015).
10. Bycroft, C. *et al.* The UK Biobank resource with deep phenotyping and genomic data. *Nature* **562**, 203–209 (2018).

11. Loh, P. Mixed-model association for biobank-scale datasets. **50**, 906–908 (2018).
12. Loh, P. R. *et al.* Efficient Bayesian mixed-model analysis increases association power in large cohorts. *Nat. Genet.* **47**, 284–290 (2015).
13. De Jager, P. L. *et al.* Integration of genetic risk factors into a clinical algorithm for multiple sclerosis susceptibility: a weighted genetic risk score. *Lancet Neurol.* **8**, 1111–1119 (2009).
14. Turley, P. *et al.* Multi-trait analysis of genome-wide association summary statistics using MTAG. *Nat. Genet.* **50**, 229–237 (2018).
15. Mägi, R. & Morris, A. P. GWAMA: Software for genome-wide association meta-analysis. *BMC Bioinformatics* **11**, (2010).
16. Ray, D. & Boehnke, M. Methods for meta-analysis of multiple traits using GWAS summary statistics. *Genet. Epidemiol.* **42**, 134–145 (2018).
17. Jorgenson, E. *et al.* A genome-wide association study identifies four novel susceptibility loci underlying inguinal hernia. *Nat. Commun.* **6**, 1–9 (2015).
18. Bulik-Sullivan, B. *et al.* LD score regression distinguishes confounding from polygenicity in genome-wide association studies. *Nat. Genet.* **47**, 291–295 (2015).
19. Watanabe, K., Taskesen, E., Van Bochoven, A. & Posthuma, D. Functional mapping and annotation of genetic associations with FUMA. *Nat. Commun.* **8**, 1–10 (2017).
20. Wang, K. L. M. H. H. ANNOVAR: functional annotation of genetic variants from high-throughput sequencing data. *Nucleic Acids Res.* **38**, e164 (2010).
21. Ng, P. C. & Henikoff, S. SIFT: predicting amino acid changes that affect protein function. *Nucleic Acids Res.* **31**, 3812–3814 (2003).

22. Adzhubei, I. A. *et al.* A method and server for predicting damaging missense mutations. *Nature Methods* **7**, 248–249 (2010).

23. Rentzsch, P., Witten, D., Cooper, G. M., Shendure, J. & Kircher, M. CADD: predicting the deleteriousness of variants throughout the human genome. *Nucleic Acids Res.* **47**, D886–D894 (2018).

24. Boyle, A. P. *et al.* Annotation of functional variation in personal genomes using RegulomeDB. *Genome Res.* **22**, 1790–1797 (2012).

25. Aguet, F. *et al.* Genetic effects on gene expression across human tissues. *Nature* **550**, 204–213 (2017).

26. de Leeuw, C. A., Mooij, J. M., Heskes, T. & Posthuma, D. MAGMA: Generalized Gene-Set Analysis of GWAS Data. *PLoS Comput. Biol.* **11**, 1–20 (2015).

27. Zhu, Z. *et al.* Integration of summary data from GWAS and eQTL studies predicts complex trait gene targets. *Nat. Genet.* **48**, 481–487 (2016).

28. Liberzon, A. *et al.* The Molecular Signatures Database Hallmark Gene Set Collection. *Cell Syst.* **1**, 417–425 (2015).

29. Fang, H., Knezevic, B., Burnham, K. L. & Knight, J. C. XGR software for enhanced interpretation of genomic summary data, illustrated by application to immunological traits. *Genome Med.* **8**, 1–20 (2016).

30. Welter, D. *et al.* The NHGRI GWAS Catalog, a curated resource of SNP-trait associations. *Nucleic Acids Res.* **42**, D1001–D1006

31. Grytz, R., Yang, H., Hua, Y., Samuels, B. C. & Sigal, I. A. Connective tissue remodeling in myopia and its potential role in increasing risk of glaucoma. *Current Opinion in Biomedical Engineering* **15**, 40–50 (2020).

32. Mégarbané, A. *et al.* Marfanoid habitus, inguinal hernia, advanced bone age, and distinctive facial features: A new collagenopathy? *Am. J. Med. Genet. Part*

A **158A**, 1185–1189 (2012).

33. Halal, F., Gervais, M.-H., Baillargeon, J., Lesage, R. & Opitz, J. M. Gastro-cutaneous syndrome: Peptic ulcer/hiatal hernia, multiple lentigines/café-aulait spots, hypertelorism, and myopia. *Am. J. Med. Genet.* **11**, 161–176 (1982).
34. Jorgenson, E. *et al.* A genome-wide association study identifies four novel susceptibility loci underlying inguinal hernia. *Nat. Commun.* **6**, (2015).
35. Antoniou, G. A. *et al.* Abdominal aortic aneurysm and abdominal wall hernia as manifestations of a connective tissue disorder. *J. Vasc. Surg.* **54**, 1175–1181 (2011).
36. Casanova, A. B., Trindade, E. N. & Trindade, M. R. M. Collagen in the transversalis fascia of patients with indirect inguinal hernia: a case-control study. *Am. J. Surg.* **198**, 1–5 (2009).
37. Rosch, R. *et al. A role for the collagen I/III and MMP-1/-13 genes in primary inguinal hernia? BMC Medical Genetics* (2002).
38. Bendavid, R. The Unified Theory of hernia formation. *Hernia.* **8**, 171–176 (2004).
39. Kobayashi, N. *et al.* A comparative analysis of the fibulin protein family: Biochemical characterization, binding interactions, and tissue localization. *J. Biol. Chem.* **282**, 11805–11816 (2007).
40. McLaughlin, P. J. *et al.* Lack of fibulin-3 causes early aging and herniation, but not macular degeneration in mice. *Hum. Mol. Genet.* **16**, 3059–3070 (2007).
41. Devriendt, K. *et al.* Diaphragmatic hernia in Denys-Drash syndrome. *Am. J. Med. Genet.* **57**, 97–101 (1995).
42. Scott, D. A. *et al.* Congenital diaphragmatic hernia in WAGR syndrome. *Am. J. Med. Genet. Part A* **134A**, 430–433 (2005).
43. Suri, M. *et al.* WT1 mutations in Meacham syndrome suggest a coelomic

mesothelial origin of the cardiac and diaphragmatic malformations. *Am. J. Med. Genet. Part A* **143A**, 2312–2320 (2007).

44. Wu, Y. *et al.* Genome-wide association study of medication-use and associated disease in the UK Biobank. *Nat. Commun.* **10**, (2019).

45. Klenotic, P. A., Munier, F. L., Marmorstein, L. Y. & Anand-Apte, B. Tissue inhibitor of metalloproteinases-3 (TIMP-3) is a binding partner of epithelial growth factor-containing fibulin-like extracellular matrix protein 1 (EFEMP1): Implications for macular degenerations. *J. Biol. Chem.* **279**, 30469–30473 (2004).

46. Hayashi, K. *et al.* Genomic structure of the human caldesmon gene. *Proc. Natl. Acad. Sci. U. S. A.* **89**, 12122–12126 (1992).

47. Mayanagi, T. & Sobue, K. Diversification of caldesmon-linked actin cytoskeleton in cell motility. *Cell Adh. Migr.* **5**, 150–159 (2011).

48. Tanyel, F. C., Talim, B., Kale, G. & Büyükpamukçu, N. A Reevaluation of the Structures Accepted to Represent the Postnatal Gubernaculum. *Urol. Int.* **69**, 116–119 (2002).

49. Tanyel, F. C. *et al.* Inguinal hernia revisited through comparative evaluation of peritoneum, processus vaginalis, and sacs obtained from children with hernia, hydrocele, and undescended testis. *J. Pediatr. Surg.* **34**, 552–555 (1999).

50. Sfoungaris, D. *et al.* Differences in the development of the processus vaginalis between children with undescended testis and inguinal hernia. *J. Clin. Neonatol.* **5**, 31 (2016).

51. Mouravas, V. K. *et al.* Smooth muscle cell differentiation in the processus vaginalis of children with hernia or hydrocele. *Hernia* **14**, 187–191 (2010).

52. Guo, H. & Wang, C. L. A. Specific disruption of smooth muscle caldesmon

expression in mice. *Biochem. Biophys. Res. Commun.* **330**, 1132–1137 (2005).

53. Mimura, T. *et al.* Up-Regulation of Collagen and Tissue Inhibitors of Matrix Metalloproteinase in Colonic Diverticular Disease. *Dis. Colon Rectum* **47**, 371–379 (2004).

54. Hellwig, I. *et al.* Alterations of the enteric smooth musculature in diverticular disease. doi:10.1007/s00535-013-0886-y

55. Seo, J., Kim, J. & Kim, M. Cloning of androgen-inducible gene 1 (AIG1) from human dermal papilla cells. *Mol Cells* 35–40 (2001). Available at: https://pubmed.ncbi.nlm.nih.gov/11266118/. (Accessed: 10th September 2020)

56. A Arai, von Hintzenstern, F Kiesewetter, H Schell & O P Hornstein. In vitro effects of testosterone, dihydrotestosterone and estradiol on cell growth of human hair bulb papilla cells and hair root sheath fibroblasts. *Acta Derm Venereol* 338–341 (1990).

57. Viner, R. M., Teoh, Y., Williams, D. M., Patterson, M. N. & Hughes, I. A. Androgen insensitivity syndrome: a survey of diagnostic procedures and management in the UK. *Arch Dis Child* **77**, 305–309 (1997).

58. Jagiello, G. & Atwell, J. D. PREVALENCE OF TESTICULAR FEMINISATION. *The Lancet* **279**, 329 (1962).

59. Su, Z. *et al.* Common variants at the MHC locus and at chromosome 16q24.1 predispose to Barrett's esophagus. *Nat. Genet.* **44**, 1131–1136 (2012).

60. Oshimori, N., Li, X., Ohsugi, M. & Yamamoto, T. Cep72 regulates the localization of key centrosomal proteins and proper bipolar spindle formation. *EMBO J.* **28**, 2066–2076 (2009).

61. Choi, J. S., Kim, S. R., Jeon, Y. W., Lee, K. H. & Rha, H. K. Identification of DNA copy number aberrations by array comparative genomic hybridization in patients

with ruptured intracranial aneurysms. *J. Clin. Neurosci.* **16**, 295–301 (2009).

62. Gharahkhani, P. *et al.* Genome-wide association studies in oesophageal adenocarcinoma and Barrett's oesophagus: a large-scale meta-analysis. *Lancet Oncol.* **17**, 1363–1373 (2016).

63. Gordon, C., Kang, J. Y., Neild, P. J. & Maxwell, J. D. Review article: The role of the hiatus hernia in gastro-oesophageal reflux disease. *Alimentary Pharmacology and Therapeutics* **20**, 719–732 (2004).

64. Weston, A. P., Badr, A. S. & Hassanein, R. S. Prospective Multivariate Analysis of Clinical, Endoscopic, and Histological Factors Predictive of The Development of Barrett's Multifocal High-Grade Dysplasia or Adenocarcinoma. *Am. J. Gastroenterol.* **94**, 3413–3419 (1999).

65. Lo, L., Dormand, E. L. & Anderson, D. J. Late-emigrating neural crest cells in the roof plate are restricted to a sensory fate by GDF7. *Proc. Natl. Acad. Sci. U. S. A.* **102**, 7192–7197 (2005).

66. Berasi, S. P. *et al.* Divergent activities of osteogenic BMP2, and tenogenic BMP12 and BMP13 independent of receptor binding affinities. *Growth Factors* **29**, 128–139 (2011).

67. Wang, Q. W., Chen, Z. L. & Piao, Y. J. Mesenchymal stem cells differentiate into tenocytes by bone morphogenetic protein (BMP) 12 gene transfer. *J. Biosci. Bioeng.* **100**, 418–422 (2005).

68. Hou, Y. *et al.* Tenomodulin highly expressing MSCs as a better cell source for tendon injury healing. *Oncotarget* **8**, 77424–77435 (2017).

69. Olafsdottir, T. *et al.* Genome-wide association identifies seven loci for pelvic organ prolapse in Iceland and the UK Biobank. *Commun. Biol.* **3**, (2020).

70. Jones, G. T. *et al.* Meta-Analysis of Genome-Wide Association Studies for

Abdominal Aortic Aneurysm Identifies Four New Disease-Specific Risk Loci. *Circ. Res.* **120**, 341–353 (2017).

71. Maguire, L. H. *et al.* Genome-wide association analyses identify 39 new susceptibility loci for diverticular disease. *Nat. Genet.* **50**, 1359–1365 (2018).
72. Castillo, D. *et al.* Activation of the BMP4 Pathway and Early Expression of CDX2 Characterize Non-specialized Columnar Metaplasia in a Human Model of Barrett's Esophagus. *J. Gastrointest. Surg.* **16**, 227–237 (2012).
73. Palles, C. *et al.* Polymorphisms near TBX5 and GDF7 are associated with increased risk for Barrett's esophagus. *Gastroenterology* **148**, 367–378 (2015).
74. Becker, J. *et al.* The Barrett-associated variants at GDF7< and TBX5 also increase esophageal adenocarcinoma risk. *Cancer Med.* **5**, 888–891 (2016).
75. Palles, C., Findlay, J. M. & Tomlinson, I. Common variants confer susceptibility to Barrett's esophagus: Insights from the first genome-wide association studies. *Adv. Exp. Med. Biol.* **908**, 265–290 (2016).
76. Loeys, B. L. *et al.* A syndrome of altered cardiovascular, craniofacial, neurocognitive and skeletal development caused by mutations in TGFBR1 or TGFBR2. *Nat. Genet.* **37**, 275–281 (2005).
77. Moustakas, A. & Heldin, C. H. The regulation of TGFβ signal transduction. *Development* **136**, 3699–3714 (2009).
78. Lindsay, M. E. *et al.* Loss-of-function mutations in TGFB2 cause a syndromic presentation of thoracic aortic aneurysm. *Nat. Genet.* **44**, 922–927 (2012).
79. Ritelli, M. *et al. Further delineation of Loeys-Dietz syndrome type 4 in a family with mild vascular involvement and a TGFB2 splicing mutation*. (2014). doi:10.1186/s12881-014-0091-8
80. Gao, X. R., Huang, H., Nannini, D. R., Fan, F. & Kim, H. Genome-wide

association analyses identify new loci influencing intraocular pressure. *Hum. Mol. Genet.* **27**, 2205–2213 (2018).

81. Gao, X. *et al.* Genome-wide association study identifies WNT7B as a novel locus for central corneal thickness in Latinos. *Hum. Mol. Genet.* **25**, 5035–5045 (2016).

82. Artigas, M. S. *et al.* Genome-wide association and large-scale follow up identifies 16 new loci influencing lung function. *Nat. Genet.* **43**, 1082–1090 (2011).

83. Cho, M. H. *et al.* Risk loci for chronic obstructive pulmonary disease: A genome-wide association study and meta-analysis. *Lancet Respir. Med.* **2**, 214–225 (2014).

84. Blatnik, J. A., Krpata, D. M., Novitsky, Y. W. & Rosen, M. J. Does a history of wound infection predict postoperative surgical site infection after ventral hernia repair? *Am. J. Surg.* **203**, 370–374 (2012).

85. Hultin, S. *et al.* AmotL2 links VE-cadherin to contractile actin fibres necessary for aortic lumen expansion. doi:10.1038/ncomms4743

86. Wang, Y. *et al.* Angiomotin-like2 gene (amotl2) is required for migration and proliferation of endothelial cells during angiogenesis. *J. Biol. Chem.* **286**, 41095–41104 (2011).

87. Brett, M. S. *et al.* De novo 3q22.1 q24 deletion associated with multiple congenital anomalies, growth retardation and intellectual disability. *Gene* **517**, 82–88 (2013).

88. Wolstenholme, J. *et al.* Blepharophimosis sequence and diaphragmatic hernia associated with interstitial deletion of chromosome 3 (46,XY,del(3)(q21q23)). *J Med Genet* **31**, 647–648 (1994).

89. Mead, T. J. & Apte, S. S. ADAMTS proteins in human disorders. *Matrix Biology* **71**–**72**, 225–239 (2018).

90. Jacobi, C. L. J., Rudigier, L. J., Scholz, H. & Kirschner, K. M. Transcriptional regulation by the wilms tumor protein, Wt1, suggests a role of the metalloproteinase Adamts16 in murine genitourinary development. *J. Biol. Chem.* **288**, 18811–18824 (2013).

91. Richter, H. E. *et al.* Genetic contributions to urgency urinary incontinence in women. *J. Urol.* **193**, 2020–2027 (2015).

92. Segev, Y. *et al.* Are women with pelvic organ prolapse at a higher risk of developing hernias? *Int. Urogynecol. J. Pelvic Floor Dysfunct.* **20**, 1451–1453 (2009).

93. Colige, A. *et al.* Novel types of mutation responsible for the dermatosparactic type of Ehlers-Danlos syndrome (type VIIC) and common polymorphisms in the ADAMTS2 gene. *J. Invest. Dermatol.* **123**, 656–663 (2004).

94. Tortorella, M. D. *et al.* Purification and cloning of aggrecanase-1: A member of the ADAMTS family of proteins. *Science (80-.).* **284**, 1664–1666 (1999).

95. Hatano, E. *et al.* Expression of ADAMTS-4 (aggrecanase-1) and possible involvement in regression of lumbar disc herniation. *Spine (Phila. Pa. 1976).* **31**, 1426–1432 (2006).

96. Brocker, C. N., Vasiliou, V. & Nebert, D. W. Evolutionary divergence and functions of the ADAM and ADAMTS gene families. *Hum. Genomics* **4**, 43–55 (2009).

97. Li, C., Scott, D. A., Hatch, E., Tian, X. & Mansour, S. L. Dusp6 (Mkp3) is a negative feedback regulator of FgF-stimulated ERK signaling during mouse development. *Development* **134**, 167–176 (2007).

98. Rauen, K. A., Cotter, P. D., Bitts, S. M., Cox, V. A. & Golabi, M. Cardio-facio-cutaneous syndrome phenotype in an individual with an interstitial deletion of 12q: Identification of a candidate region for CFC syndrome. *Am. J. Med. Genet.* **93**, 219–222 (2000).

99. Chrzanowska, K., Fryns, J.-P. & Van den Berghe, H. Cardio-facio-cutaneous (CFC) syndrome: Report of a new patient. *Am. J. Med. Genet.* **33**, 471–473 (1989).

100. Primatesta, P. & Goldacre, M. J. Inguinal hernia repair: Incidence of elective and emergency surgery, readmission and mortality. *Int. J. Epidemiol.* **25**, 835–839 (1996).

101. Kingsnorth, A. & LeBlanc, K. Hernias: Inguinal and incisional. in *Lancet* **362**, 1561–1571 (Elsevier Limited, 2003).

102. Dahlstrand, U., Wollert, S., Nordin, P., Sandblom, G. & Gunnarsson, U. Emergency femoral hernia repair: A study based on a national register. *Ann. Surg.* **249**, 672–676 (2009).

4.7. Chapter Appendix

*The appendix for this chapter is provided as an online supplement at the following URL: **bit.ly/WAhmed_C4Appendix***

Table of Contents

Appendix Table 4.14. Genes mapped to the overlap hernia-associated loci using the four mapping strategies

Appendix Table 4.15. Genome-wide gene-based association analysis for umbrella hernia in MAGMA

Appendix Table 4.16. Summary-based Mendelian Randomisation (SMR) for umbrella hernia using eQTL data from GTEx

Appendix Table 4.17. Genes mapped to the umbrella hernia-associated loci using the four mapping strategies

Appendix Table 4.18. Enriched gene sets from the genome-wide gene-based enrichment analysis of overlap hernia in MAGMA

Appendix Table 4.19. Gene-based enrichment analysis for overlap hernia associated genes in eXploring Genomic Relations.

Appendix Table 4.20. Enriched gene sets from the genome-wide gene-based enrichment analysis of umbrella hernia in MAGMA

2. Appendix Figures

Appendix Figure 4.1. Regional Locus Zoom plots for all four individual hernia associated signals

Appendix Figure 4.2. Quantile-quantile (Q-Q) plots for all four individual hernia analyses

Appendix Figure 4.3. Venn diagram for the 101 genes prioritised at the inguinal hernia associated loci

Appendix Figure 4.4. Venn diagram for the 15 genes prioritised at the hiatus hernia associated loci

Appendix Figure 4.5. Regional Locus Zoom plots of all overlap hernia associated signals

Appendix Figure 4.6. Regional Locus Zoom plots of all umbrella hernia associated signals

Appendix Figure 4.7. Quantile-quantile (Q-Q) plot of all overlap hernia associated signals

Appendix Figure 4.8. Quantile-quantile (Q-Q) plot of all overlap hernia associated signals

Appendix Figure 4.9. Venn diagram for the 3 genes prioritised at the overlap hernia associated loci

Appendix Figure 4.10. Venn diagram for the 129 genes prioritised at the umbrella hernia associated loci

Appendix Figure 4.11. MAGMA tissue expression analysis of umbrella hernia

Appendix Figure 4.12. Regional Locus Zoom plots for all four MTAG hernia associated signals

Appendix Figure 4.13. New 1q41(*TGFB2*) locus discovered to associate with femoral hernia through MTAG multi-trait analysis

Chapter 5: The shared genetic architecture of common elastopathies

5.1. Introduction

5.1.1. Rationale and aim

In **Chapter 1**, the disruption caused by perturbations in the tightly controlled intrinsic elastin: collagen composition of elastic tissues was explored, particularly within hollow viscera, which can disrupt their normal molecular and physiological properties.[1] This leads to disorders in which elastin dysfunction causes common macroscopic pathology[2]—principally characterised by a loss of resilience and elastic recoil—which I tentatively defined as 'elastopathies.'

In **Chapter 2** and **Chapter 3**, the complex disease nature of varicose veins and haemorrhoid disease was substantiated, unveiling novel genetic loci clustered near extracellular matrix (ECM)-regulating genes.[3] **Chapter 4** explored the genetic architecture of four common abdominal herniae, revealing not only genetic insights into each subtype, but also providing the first evidence for shared genetic architecture and common pathways.[4]

A natural progression of this research is to seek to delineate the common pathways linking all elastopathies. Despite an extensive array of single-trait genome-wide association studies (GWAS) for common elastopathies, no study has explored their shared genetic architecture. Uniting these disorders under the overarching grouping of 'elastopathies,' diseases that are macroscopically, pathologically, and conceptually related, may unveil critical shared variants, gene sets, and pathways.[5] This chapter's broad aim is to investigate the shared genetic architecture of the 12 common elastopathies identified in the UK Biobank (hiatus hernia, diverticular disease,

haemorrhoids, inguinal hernia, varicose veins, female genital prolapse, umbilical hernia, aneurysmal disease, emphysema, pneumothorax, anorectal prolapse, and femoral hernia), hypothesising that commonalities in genetic architecture will emerge linking several of these disorders.

This will be investigated by:

1. Performing individual GWAS of the 12 common elastopathies identified in the UK Biobank.

2. Looking for evidence of shared genetics between these elastopathies by performing:

i. A combined GWAS meta-analysis of the summary statistics from the 12 individual analyses.

ii. Structural equation modelling of the elastopathy phenotype based on summary data from the 12 analyses.

iii. Interrogating genes and biological pathways implicated in regions of shared genetic architecture.

5.1.2. Justification of trait selection

The 12 complex disorders selected from the UK Biobank and united under the grouping of ‘elastopathies’ are justified in that they result in either i. protrusion of abdominal viscera from the normal cavity in which they lay (hiatus hernia, inguinal hernia, umbilical hernia, femoral hernia)[6], ii. prolapsing of pelvic viscera from the pelvic cavity (female genital prolapse and anorectal prolapse)[3], iii. dilatations of hollow viscus (diverticular disease, varicose veins, aneurysmal disease)[7], iv. deterioration of elastic tissue preventing normal physiological functionality of bodily organs (haemorrhoids, emphysema, pneumothorax).[1] In all 12 traits, loss of elastic tissue integrity is known to contribute to disease pathobiology, meaning both macroscopically and conceptually these disorders are related, however, to date have not been classed as such.

5.2. Methods

5.2.1. Ethics and consent

The research ethics and consent procedures of the UK Biobank are available in **Section 2.2.1**.[8]

5.2.2. Study population and phenotype definition

A complete description of the study participants of the UK Biobank cohort are available in **Section 2.2.2**.[9]

The 12 individual elastopathy cohorts were defined from the UK Biobank data showcase (See **5.2.15. URLs**) using operative, diagnostic, and self-report codes in keeping with a diagnosis of hiatus hernia, diverticular disease, haemorrhoids, inguinal hernia, varicose veins, female genital prolapse, umbilical hernia, aneurysmal disease, emphysema, pneumothorax, anorectal prolapse, or femoral hernia (**Appendix Table 5.1**). Cases were defined if they had *at least one* of the following codes corresponding to each of the 12 disorders:

1. Primary and/or secondary ICD-10 codes
2. Primary and/or secondary OPCS codes
3. Self-reported operation codes
4. Self-reported non-cancer illness codes

5.2.3. Case-control matching

An overview of the full case-control matching methodology implemented in this chapter is presented in **Figure 5.1**. Firstly, the full post-QC UK Biobank participants were segmented into cases and controls according to the phenotype definitions provided in **Section 5.2.5**. A valid custom random-matching algorithm was implemented in R v.4.2.2 to randomise the entire group of cases and controls disparate from each other. Next, the controls were expanded to exactly twice as many unique cases available for matching by inserting missing data identifiers ("NA"). This expanded control group, and the unique cases were then randomised a second time, and a linking procedure was implemented. The sole purpose of the linking procedure was to ensure that for a particular case there is always the same set of controls that are attributed to this case, to ensure a uniform distribution of controls between the various analyses. The implementation for the linking procedure was such that all cases were linked to a maximum of two controls (either 2 controls or 1 control + 1 "NA"). It is important to note that, by virtue of the algorithm implemented, a case could not be matched to zero controls. The linking procedure concluded with the removal of the missing data identifiers from the matching link. Each case was matched to on average ~1:1.8 controls (137,549 cases: 264,034 controls). Using the phenotype codes provided in **Section 5.2.2**, the elastopathy cases were extracted with their respective matched controls – creating the matched cohorts for the subsequent analyses. The sole exception to this matching and linking algorithm was that 15,669 males were removed from the female genital prolapse controls post-hoc due to hyper-inflation of the Scalable and Accurate Implementation of Generalized mixed model (SAIGE)

genetic relationship matrix (GRM) (discussed further in **Section 5.2.6**). The final 12 elastopathy cohorts for analysis were established as below:

- **Hiatus hernia:** 105,493 participants (36,139 cases, 69,354 controls)
- **Diverticular disease:** 105,160 participants (36,020 cases, 69,140 controls)
- **Haemorrhoids:** 92,304 participants (31,652 cases, 60,652 controls)
- **Inguinal hernia:** 67,204 participants (23,007 cases, 44,197 controls)
- **Varicose veins:** 65,619 participants (22,467 cases, 43,152 controls)
- **Female genital prolapse:** 37,068 participants (18,049 cases, 19,019 controls)
- **Umbilical hernia:** 21,689 participants (7,432 cases, 14,257 controls)
- **Aneurysmal disease:** 14,654 participants (5,015 cases, 9,639 controls)
- **Emphysema:** 7,509 participants (2,580 cases, 4,929 controls)
- **Pneumothorax**: 7,122 participants (2,446 cases, 4,676 controls)
- **Anorectal prolapse:** 5,561 participants (1,902 cases, 3,659 controls)
- **Femoral hernia:** 4,586 participants (1,578 cases, 3,008 controls)

A separate matched cohort was created to account for all elastopathy cases and all the controls in the Post-QC data set, with the 15,669 male controls removed. This overarching cohort was used for the individual patient data (IPD) GWAS meta-analysis (**Section 5.2.6)** and the common-factor analysis (**Section 5.2.7)**:

- **IPD GWAS Meta-analysis:** 385,914 participants (137,549 cases, 248,365 controls)
- **Common factor analysis:** 385,914 participants (137,549 cases, 248,365 controls)

Figure 5.1. Case-control matching methodology. The post quality control (QC) UK Biobank cohort of (i) 401,583 participants was used to identify cases as per our phenotype definitions (see **Section 5.2.2**), the remaining participants were classified as controls (ii). Cases and controls were individually randomised using a random matching algorithm (iii). Cases and controls were then linked with each case matched to ~1.8 controls (matching each control uniformly across all the cases). Cases and controls were then randomised for a second time, with this link maintained. The final cohorts of individual cases, with codes for each of the 12 elastopathies, were then created with their respective linked controls. [+]For the female genital prolapse analysis, 15,669 male controls were removed post-matching, due to genomic inflation in the IPD GWAS analysis (see **Section 5.2.6**). The subsequent IPD GWAS meta-analysis and the common factor analysis were pruned of these controls to reflect this (137,549 cases, 248,365 controls (385,914 participants).

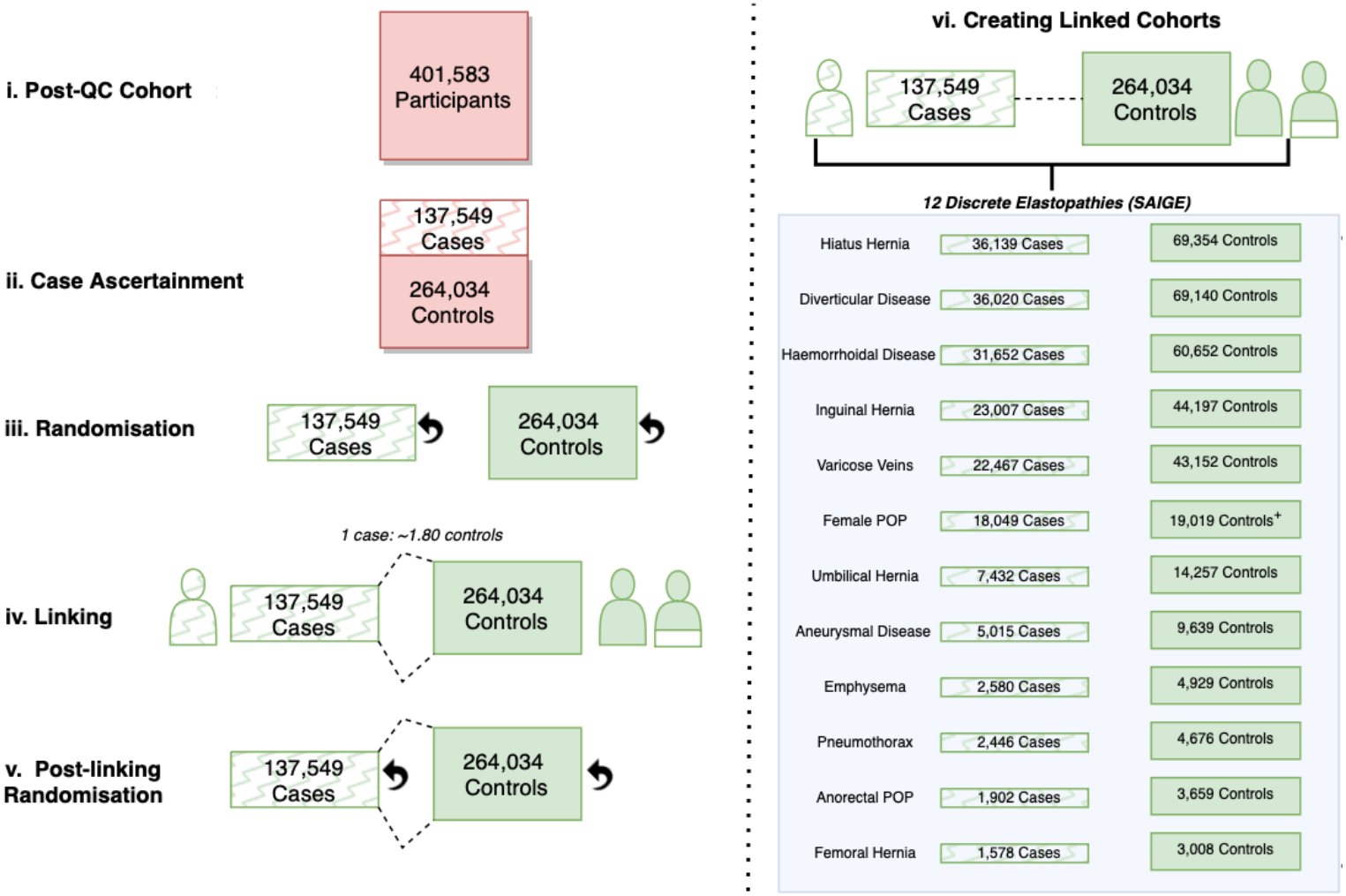

5.2.4. Genotyping

A complete description of the genotyping procedure for the UK Biobank cohort is available in **Section 2.2.3**.[10]

5.2.5. Quality control

A complete description of the UK Biobank quality control (QC) procedures, as well as additional QC parameters used on this dataset are available in **Section 2.2.4**.[10]

After QC, 86,794 participants and 230,562 genotyped variants were excluded from the subsequent association analyses (See **Chapter 3**, **Figure 3.3**). In summary, a maximal set of 547,011 genotyped variants and 401,583 participants of white British ancestry passed the QC and were available for inclusion in the 12 individual elastopathy cohorts, and the IPD GWAS meta-analysis–matching was subsequently performed to define each cohort as described in **Section 5.2.3**.

5.2.6. Imputation

A complete description of the imputation methodology performed is available in **Section 2.2.5.**[11]

5.2.7. Association analyses

Single-variant association analyses were performed using Scalable and Accurate Implementation of GEneralized mixed model (SAIGE) v1.1.6.3 (Nov 2022) (see **5.2.15. URLs**)[12], implemented in R v3.6.3 within an x86_64-conda-linux-gnu (64-bit) platform, running Ubuntu 22.04.1 LTS. SAIGE requires two steps to perform single-variant association tests. Firstly, owing to the fact that binary traits were analysed, and to account for sample relatedness, a null logistic mixed model was fitted using the step1_fitNULLGLMM.R script which can be located in the *extdata* directory within the SAIGE GitHub (see **5.2.15. URLs**). Genotype data for constructing the full genetic relationship matrix (GRM) and estimating the variance ratio was provided using PLINK binary files.[13] To adjust for inherent population structure biases, the null model was fitted using the full GRM, adjusting for the following covariates: Birth year (as a surrogate for age), genetic sex, genotyping platform, and the first ten genetic principal components provided by UK Biobank (Data Field 22009). For the female genital prolapse GWAS, parity status was included as an additional covariate (described in Data Field 2734 - Number of Live Births); for the emphysema GWAS, smoking was included as an additional covariate (as described in Data Field 20160 'Ever Smoked'). The minimal minor allele frequency (MAF) of variants to fit the GRM was defined as 0.01, with a maximum missingness rate defined as 0.15. Leave One Chromosome Out (LOCO) Analysis was performed in step 1. Standard settings were used to trace the coefficient of variation (CV) cut off (0.0025), the ratio for the CV cut off (0.001), the maxiter (20), the tol (0.02), and the saddle point approximation (SPA) cut off (2). The Generalized Linear Mixed Model Association Test (GMMAT) model file, and a variance ratio was outputted from step 1. For the female genital prolapse GWAS, the variance ratio was an inflationary outlier and therefore was corrected for (variance ratio for female genital prolapse (pre-correction): 0.76; median (range) variance ratio for

remaining 11 phenotypes: 0.96 (0.88 - 1.00)). Correction was made by removing all males (n = 15,669) from the controls for this analysis, which corrected the inflation (variance ratio for female genital prolapse (post-correction): 0.94).

In step 2, saddle point approximation (SPA) was used to account for case-control imbalance. Imputed and genotyped allelic dosages were provided in BGEN format.[14] The reference human genome assembly used was GRCh37 (hg19). The GMMAT model and variance ratio files from step 1 were integrated into the analysis. A minimum MAF of 0.01 was implemented, with the minimum minor allele count (MAC) set at 20, in keeping with recommendations from SAIGE implementation. Only good quality imputed/genotyped variants were maintained in the analysis (INFO > 0.90), with a maximum allowable missingness set at 0.15. Leave One Chromosome Out (LOCO) analysis was performed, with the association test executed chromosome-by-chromosome. Formal conditional analysis within SAIGE was not implemented (See **Section 5.2.10**). An effect size (BETA) and the standard error (SE) of the BETA for each variant was estimated using Firth's Bias-reduced logistic regression, with a maximum P-value cut-off for the effect-size calculation set at P = 0.05. A custom Perl script was used to compute an Odds Ratio (OR) and the confidence intervals for the ORs from these effect-sizes, where OR = exp(beta), OR_95L = exp(BETA - (1.96 * SE)), OR_95U = exp(BETA + (1.96 * SE)). In summary, genome-wide association testing was performed across a total ~9M variants (~500k of which were directly genotyped). The final summary statistics for each of the 12 elastopathies were pruned to remove around ~1M variants that were indels or multi-allelic variants from each summary statistic, leaving ~8M single nucleotide polymorphisms (SNPs) confirmed by the Pan-UKBB consortium [(range: 8,044,935 SNPs (femoral hernia) - 8,068,985

SNPs (varicose veins)] (See **5.2.15 URLs**). A final meta-analysis was performed in which all cases from all 12 elastopathies were combined, and their respective controls, meaning the final association test was performed in 385,914 participants (137,549 cases, 248,365 controls).

5.2.8. SNP-based heritability analysis

The SNP-based heritability analyses for all individual elastopathy and IPD GWAS meta-analysis summary statistics were calculated as previously described in **Section 2.2.11**.

5.2.9. Genetic correlation analysis

Pair-wise genetic correlations were computed between the 12 individual elastopathy summary statistics, using Linkage Disequilibrium SCore (LDSC) regression (see **5.2.15 URLs**).[15]

5.2.10. Common factor analysis

To project the 12 individual elastopathies onto a hypothetical 13th latent 'pan-elastopathy' trait, Genomic Structural Equation Modelling (Genomic SEM) was performed.[16] All 12 elastopathy summary statistics were implemented in the Genomic SEM package for R (see **5.2.15. URLs**). Input SNPs were filtered by MAF > 0.01 and INFO > 0.8. LD score regression was performed using European ancestry LD matrices from the Pan-UKBB consortium. The 'commonfactorGWAS' function was used to

model a hypothetical latent factor shared across all elastopathies examined with default parameters.

5.2.11. Multi-trait colocalisation

To determine multi-trait colocalisation across the 12 individual elastopathy phenotypes, an efficient deterministic Bayesian divisive clustering algorithm, Hypothesis Prioritisation in multi-trait Colocalisation (HyPrColoc) was implemented in R v4.2.2.[17] HyPrColoc enables the use of summary data to identify clusters of colocalised phenotypes. The key assumption of HyPrColoc is that, at most, there is one causal variant per trait in any analysis. HyPrColoc is also able to account for complete sample overlap in cases between the 12 traits.[17]

First, a matrix was created with common SNPs (n = 7,929,655) between all 12 traits. Regression coefficients and standard errors were extracted for each of the top signals from the IPD GWAS meta-analysis and the SEM analysis, across all 12 traits. 500kb blocks (1MB total) around each of the top independent signals from the IPD GWAS meta-analysis and the genomic SEM analysis were extracted. The co-localisation analysis was performed, taking into account the regression coefficients and the standard errors from each of the 1MB-block SNPs at each locus in both analyses. Signals were considered to colocalise if the posterior inclusion probability for co-localisation was 0.7 or higher, corresponding to a false discovery rate (FDR) ≤ 5%.[17]

5.2.12. Genomic risk loci borders

The full methodology for defining genomic risk loci borders in Functional Mapping and Annotation of Genome-Wide Association Studies (FUMA GWAS) v1.6.0 for all 12 individual elastopathy analyses, the IPD GWAS meta-analysis, and the common factor summary data are described in **Section 2.2.7**.[18]

5.2.13. Functional annotation of variants

All SNPs across the 12 individual elastopathy analyses, the IPD GWAS meta-analysis, and the common factor analysis were mapped and annotated in FUMA SNP2GENE v.1.6.0 (Sep 2023) as described in **Section 2.2.8**. [18]

5.2.14. Gene mapping

For the IPD GWAS meta-analysis, four mapping strategies were implemented to map candidate variants to putative genes: i. positional mapping implemented in FUMA[18], ii. expression quantitative trait loci (eQTL) mapping, iii. MAGMA gene-based, genome-wide association analysis (within 500kb from loci boundaries)[19], iv. summary-based Mendelian randomisation (SMR) (within 500kb from loci boundaries).[20] For the genomic SEM analysis, SMR was not performed due to SEM not outputting effect estimates.[16] The full candidate gene mapping approach is further described in **Section 2.2.9**.

5.2.15. URLs

ANNOVAR, www.annovar.openbioinformatics.org/en/latest/; CADD, www.add.gs.washington.edu/; CTG-VL, www.genoma.io ;Ensembl, www.ensembl.org/index.html; flashpca, www.github.com/gabraham/flashpca/; FUMA, www.fuma.ctglab.nl/; Genomic SEM, www.github.com/GenomicSEM/GenomicSEM, GERP, www.mendel.stanford.edu/SidowLab/downloads/gerp/; GnomAD, www.gnomad.broadinstitute.org/; GTEx Portal, www.gtexportal.org/home/; Human Genome Variation Society (HGVS), www.varnomen.hgvs.org/; HyPrColoc,, www.github.com/cnfoley/hyprcoloc; HRC, www.haplotype-reference-consortium.org/; LD Hub, www.ldsc.broadinstitute.org/ldhub/; LDStore2, www.christianbenner.com; MAGMA, www.ctg.cncr.nl/software/magma; PanUKBB, www.pan.ukbb.broadinstitute.org/; PLINK, www.pngu.mgh.harvard.edu/~purcell/plink/; Polyphen-2, www.genetics.bwh.harvard.edu/pph2; R, www.r-project.org; RegulomeDB, www.regulomedb.org/; rpy2, www.rpy2.github.io; SAIGE, www.saigegit.github.io/SAIGE-doc/; SHAPEIT3, www.jmarchini.org/shapeit3/; SIFT, www.sift.bii.a-star.edu.sg/; SusieR, www.github.com/stephenslab/susieR; UK Biobank, www.ukbiobank.ac.uk/; OPEN XGR, www.openxgr.com/; 1000 Genomes Project, www.1000genomes.org.

5.3. Results

The analytical approach implemented to establish the shared genetic basis of common elastopathies in this chapter is summarised in **Figure 5.2**.

Figure 5.2. Pan-elastopathy GWA study design and analytic workflow. In the first instance, genome-wide association analyses (GWAS) were performed in SAIGE across the 12 individual elastopathy cohorts **(1)**.[12] 85 distinct genome-wide significant loci ($P < 5\times10^{-8}$) across nine of the elastopathy phenotypes were discovered, eight of which have not before been reported. **(2)** Next, two subsequent GWA analyses were performed across the pan-elastopathy phenotype, by way of a IPD GWAS meta-analysis implemented in SAIGE[12], and a common factor analysis performed using Genomic SEM.[16] 37 independent loci (46 signals) were discovered in the IPD GWAS meta-analysis, and 31 susceptibility loci (40 signals) in the common factor analysis. These loci were subsequently characterised and analysed further.

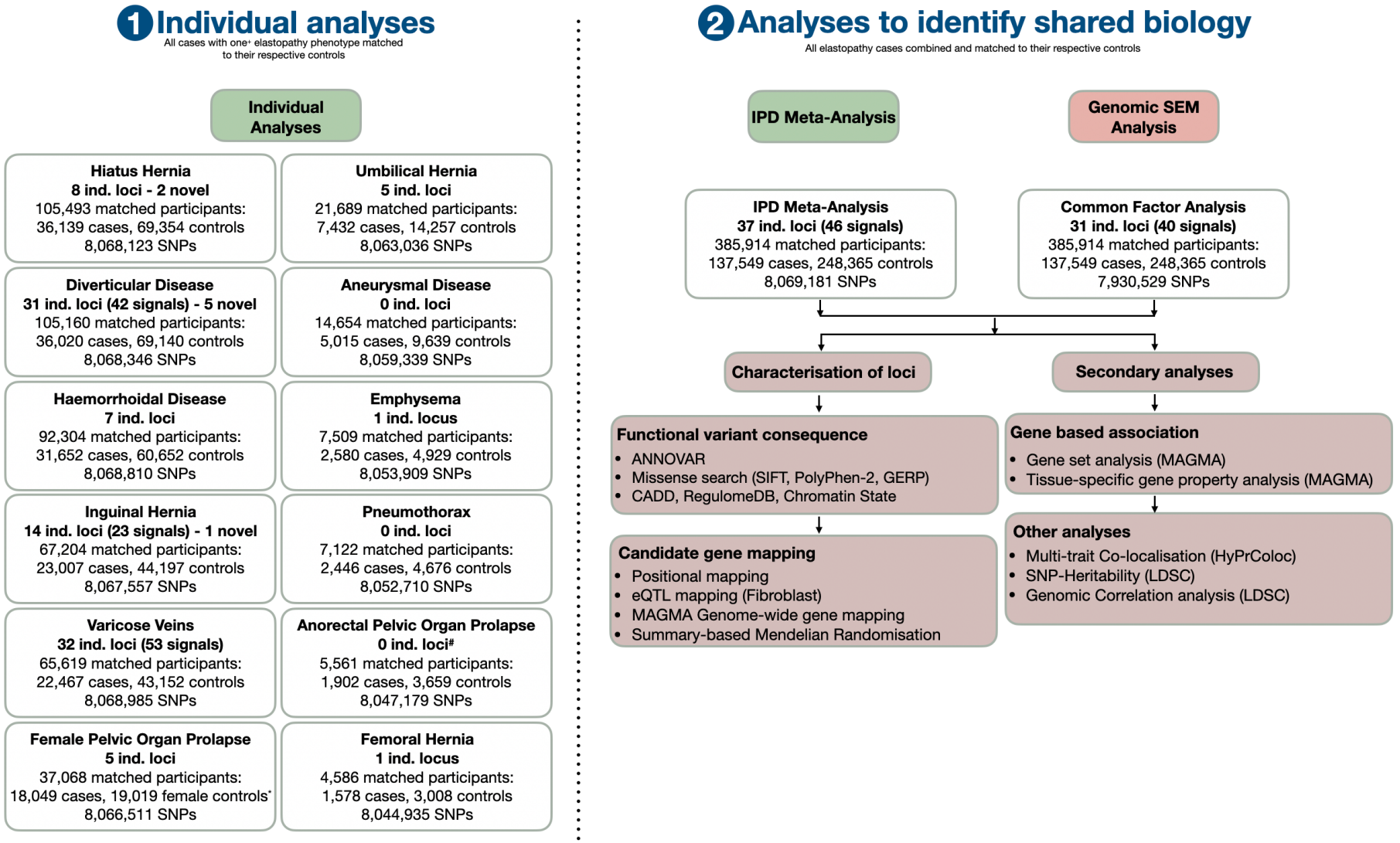

5.3.1. Case-control matching results

Following quality control (QC), 401,583 UK Biobank participants were included in the final analysis (**Section 5.2.5**). Across the 12 individual elastopathy cohorts, interrogating diagnostic or operative codes for the respective disorders following QC led to the identification of 36,139 hiatus hernia cases, 36,020 diverticular disease cases, 31,652 haemorrhoids cases, 23,007 inguinal hernia cases, 22,467 varicose veins cases, 18,049 female genital prolapse cases, 7,432 umbilical hernia cases, 5,015 aneurysmal disease cases, 2,580 emphysema cases, 2,446 pneumothorax cases, 1,902 anorectal prolapse cases, and 1,578 femoral hernia cases (**Figure 5.2**). Overlap between cases was allowed. In total, 137,549 unique cases were identified across the 12 cohorts, with significant overlap demonstrated between cases (**Figure 5.3**). The remaining 264,034 participants without diagnostic or operative codes for any of the 12 individual elastopathies were defined as controls from the 401,583 post-QC participants.

Figure 5.3: Case overlap across the 12 elastopathy case cohorts. This UpSet plot visually represents the intersection across the 12 sets of elastopathy cohorts. The horizontal bar plot shows the respective elastopathy case as a proportion of all unique cases from the 12 case groups, total, n (%). The number of cases in the intersection is shown in the vertical bar plot, with case overlaps greater than 50 depicted in this plot. Degrees of intersections between each case group are shown via two or more dots and a bridging line between the case groups. Where there are stand-alone dots, this indicates cases which do not intersect with any of the 11 other case groups.

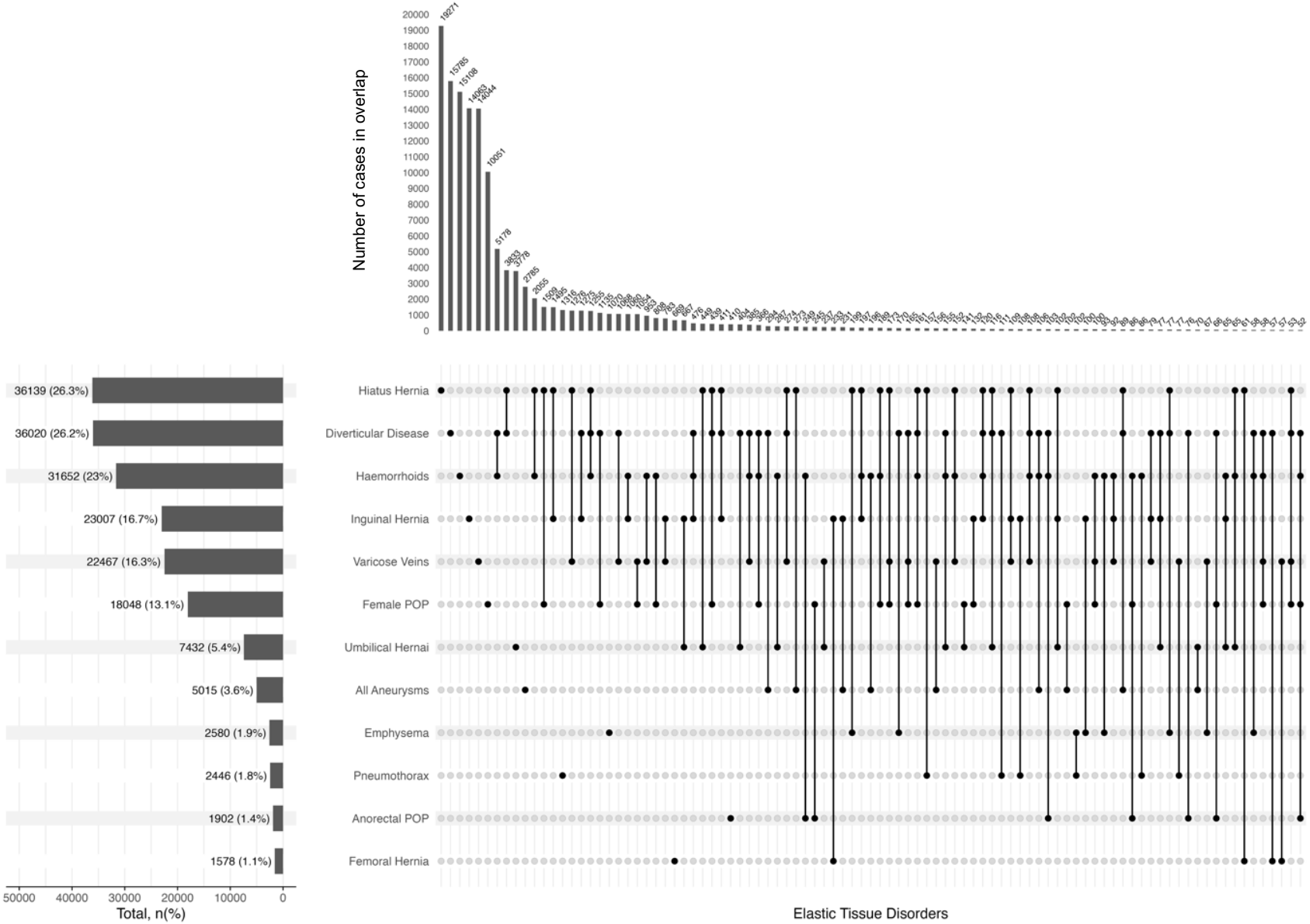

5.3.2. Individual association analysis of the 12 elastopathies

Genome-wide association analysis of the 12 individual elastopathies revealed 85 distinct genome-wide significant loci across nine individual phenotypes ($P < 5\times10^{-8}$), eight of which have not been previously described (**Table 5.1, Appendix Table 5.2, and Appendix Figure 5.1**). The GWA analysis results for all 12 individual elastopathy traits are presented in **Appendix Table 5.3, Appendix Figure 5.2** and **Appendix Figure 5.3**. Additionally, the QQ plots, λ_{GC} and intercepts for all individual association analyses are shown in **Appendix Table 5.4 and Appendix Figure 5.4**, with nominal evidence of inflation (λ_{GC} range: 1.01 - 1.18), suggesting consistency with the effects of polygenicity and a large sample size.[15]

Using LD Score regression[15], pair-wise genetic correlations were analysed between the elastopathy phenotypes, demonstrating significant positive genetic correlation between the 12 traits (**Table 5.2)**.

Table 5.1. **Summary of individual association analysis results**. Table depicting case-control distribution across the 12 individual elastopathy analyses across around ~8M SNPs (INFO ≥ 0.90, MAC ≥ 20, MAF ≥ 0.01), with the broad results summarised for each of the analyses. 85 distinct genome-wide significant loci (GWS, $P < 5\times10^{-8}$) were identified in nine of the analyses, with 8 loci not reported previously.

Elastopathy Phenotype	Total Participants	Cases	Controls	SNPs	GWS Loci (Ind. Signals)	Novel Loci	Notes
Hiatus Hernia	105,493	36,139	69,354	8,068,123	8	2	3p21.31 (*MYL3*) and 5q23.2 (*PRDM6*))
Diverticular disease	105,160	36,020	69,140	8,068,346	31 (42)	5	6p21.1 (*PTK7*), 7p15.3 (*NUPL2*), 11q24.3 (tolerated missense variant rs11222085 (p.Thr792Ala), exon 9 of *ADAMTS8*, CADD 20.9, GERP 1.01, SIFT: 0.45, PolyPhen: 0.01, also known eQTL in GTEx v6 testis for RP11-121M22.1 (7.0×10^{-13})), 13q12.2 (~50kb downstream of *POLR1D*), and 15q25.2 (~20kb away from *RP11-499F3.2*
Haemorrhoids	92,304	31,652	60,652	8,068,810	7	-	-
Inguinal hernia	67,204	23,007	44,197	8,067,557	14 (23)	1	15q26.2 (~250mb downstream of *MCTP2*)
Varicose veins	65,619	22,467	43,152	8,068,985	32 (53)	-	-
Female genital prolapse	37,068*	18,049	19,019*	8,066,511	5	-	-
Umbilical hernia	21,689	7,432	14,257	8,063,036	5	-	-
Aneurysmal disease	14,654	5,015	9,639	8,059,339	-		-
Emphysema	7,509	2,580	4,929	8,053,909	1	-	The top variant rs28929474-T/C (MAF 0.03, OR 1.94 (1.56-2.41)

							causes a predicted deleterious missense mutation at Exon 5 of *SERPINA1* (Glu342Lys, CADD: 20.2, SIFT: 0, PolyPhen: 1), with the homozygous genotype (TT) known to reduce pulmonary function and impart a greater likelihood of developing emphysema
Pneumothorax	7,122	2,446	4,676	8,052,710	-	-	First such GWAS in existing literature. The top SNP rs1022179 (C/A, MAF 0.18, INFO = 0.98, OR = 1.27 (1.15-1.39), P = 4.65×10^{-7}) is an intronic variant at intron 2 of *PDE10A*, which encodes phosphodiesterase 10A, a key mediator of lung inflammation
Anorectal prolapse	5,561	1,902	3,659	8,047,179	-	-	The top SNP rs2235707 (C/G, MAF = 0.08, OR = 1.50 (1.29 - 1.75)) did not meet the threshold of genome-wide significance (P = 7.87×10^{-8}), however, an intronic indel variant ~2kb further downstream at this 6p12.1 locus (*GCLC*) did meet genome-wide significance: rs750052398 (CAAA/C, MAF = 0.07, OR = 1.54 (1.32 - 1.80), P = 4.00×10^{-8})
Femoral hernia	4,586	1,578	3,008	8,044,935	1	-	-

Table 5.2. Genetic correlation estimates computed by LDSC regression for the 12 individual elastopathies. All correlation estimates were significant with a $P < 0.05$.

	Hiatus hernia	Diverticular disease	Haemorrhoidal disease	Inguinal hernia	Varicose veins	Female genital prolapse	Umbilical hernia	Aneurysmal disease	Emphysema	Pneumothorax	Anorectal prolapse	Femoral hernia
Hiatus hernia	**1.00**											
Diverticular disease	0.55	**1.00**										
Haemorrhoidal disease	0.48	0.49	**1.00**									
Inguinal hernia	0.37	0.32	0.32	**1.00**								
Varicose veins	0.30	0.25	0.30	0.20	**1.00**							
Female genital prolapse	0.56	0.55	0.48	0.33	0.33	**1.00**						
Umbilical hernia	0.36	0.45	0.30	0.30	0.18	0.43	**1.00**					
Aneurysmal disease	0.36	0.67	0.44	0.16	0.21	0.41	0.48	**1.00**				
Emphysema	0.39	0.40	0.33	-0.11	0.14	0.12	0.35	0.01	**1.00**			
Pneumothorax	0.37	0.08	0.09	0.05	0.15	0.29	0.39	0.48	0.54	**1.00**		
Anorectal prolapse	0.80	0.78	0.56	0.34	0.55	1.00	0.68	0.46	0.53	0.92	**1.00**	
Femoral hernia	0.31	0.36	0.23	0.44	0.07	-0.13	0.36	0.39	0.80	-0.29	0.45	**1.00**

5.3.2. GWAS meta-analysis of the 12 elastopathies

To scrutinise for possible evidence of shared genetic architecture across the 12 elastopathies, an individual patient data (IPD) GWAS meta-analysis was performed comprising 137,549 cases with a diagnosis of at least one of the 12 elastopathies matched with 248,365 controls without a diagnosis of an elastopathy. The final IPD GWAS meta-analysis was performed across a total of 385,914 participants and 8,069,181 SNPs (INFO ≥ 0.90, MAC ≥ 20, MAF ≥ 0.01). In total, 1,447 variants were found to be genome-wide significant ($P < 5\times10^{-8}$) and associated with the elastopathy phenotype at 37 loci (46 independent signals) (**Figure 5.4; Table 5.3, Appendix Figure 5.5**). Using LDSC regression[15], the total SNP heritability (h^2_g) was calculated for the elastopathy phenotype in UK Biobank to be 3.95% (S.E. = 0.25%) (**Appendix Table 5.5; Appendix Figure 5.6**).

Among the 46 independent signals discovered in the IPD GWAS meta-analysis, a non-synonymous missense variant was identified, rs17855988 (EAF (Effect Allele Frequency) = 0.90, OR = 1.06, $P = 1.16\times10^{-12}$), causing a glycine to arginine substitution within exon 25 of the elastin gene that is predicted to be deleterious (PolyPhen[21] = 1.00 (probably damaging), SIFT[22] = 0 (deleterious - low confidence), CADD[23] = 25).

To further delineate loci that confer a compelling *shared* risk for the elastopathy phenotype, comparison was made between the IPD GWAS meta-analysis-identified loci and the individual disease GWAS loci. Eighteen susceptibility loci (19 signals) were discovered to associate with the elastopathy phenotype on meta-analysis that

were not identified in any of the 12 individual analyses, 11 of which play a fundamental role in modelling and regulating the extracellular matrix (**Appendix Table 5.6; Appendix Figure 5.7**). Of note, four of these loci contain genes that are integral to the TGFβ and TGFβ-SMAD2/3 signalling pathway: *TGFB2* (1q41, rs2799097, EAF = 0.85, OR = 1.04, P = 3.78×10^{-8}*)*, *AFAP1* (4p16.1, rs11734860, EAF = 0.69, OR = 1.03, P = 1.63×10^{-8}), *NREP* (5q22.1, rs1379552, EAF = 0.77, OR =1.04, P = 1.85×10^{-10}), and *THBS2* (6q27, rs9505932, EAF = 0.32, OR = 1.03, P = 9.55×10^{-12}). A further two contain genes encoding core matricellular proteins: laminin B2 (encoded by *LAMB2 (3p21.31,* rs9586, EAF = 0.22, OR = 1.03, P = 3.17×10^{-9}) and CCN3 (encoded by *NOV, 8q24.12,* rs1599473, EAF = 0.76, OR = 1.03, P = 3.82×10^{-8}). Genes at four loci are involved in orchestrating chondrogenesis: *BMP6 (6p24.3,* rs12212270, EAF = 0.62, OR = 1.03, P = 3.72×10^{-10}), *DUSP6* (12q21.33, rs809973, EAF = 0.19, OR = 1.03, P = 3.77×10^{-8}), including the histone enzymes PHF2 (9q22.31, rs36174510, EAF = 0.37, OR = 1.03, P = 8.41×10^{-10}) and HDAC5 (17q21.31, rs4793079, EAF = 0.29, OR = 1.03, P = 6.56×10^{-10}) which are integral to chondrogenesis and osteoblast differentiation, and additionally FOXP2 (7q31.1, rs727644, EAF = 0.60, OR = 1.03, P = 3.18×10^{-9}), a transcription factor that exerts pleiotropic influences on skull shaping and bone remodelling in humans

Figure 5.4. Individual Patient Data Meta-Analysis Results. Manhattan plot demonstrating the 37 genome wide significant IPD meta-analysis loci (lead SNPs depicted by green circles). The corresponding 37 loci from the 12 elastopathy phenotypes are depicted in the plot by 12 colour coded shapes (see legend). The two dashed lines are the suggestive significance threshold ($P < 1\times10^{-5}$, blue) and the genome-wide significance threshold ($P < 5\times10^{-8}$, maroon). Annotated in black are the 18 loci which became significant under IPD meta-analysis and were *not* found to be significant in any of the 12 individual elastopathy GWA studies. Annotated in green are the seven loci which became more significant under IPD meta-analysis compared to any of the 12 individual elastopathy GWA studies, with at least one of the 12 individual elastopathy studies also finding this locus to be genome-wide significant. Annotations are based on the single best prioritised genes from the prioritisation methods used, or the top SNP from the IPD meta-analysis, where no gene was mapped at a particular locus.

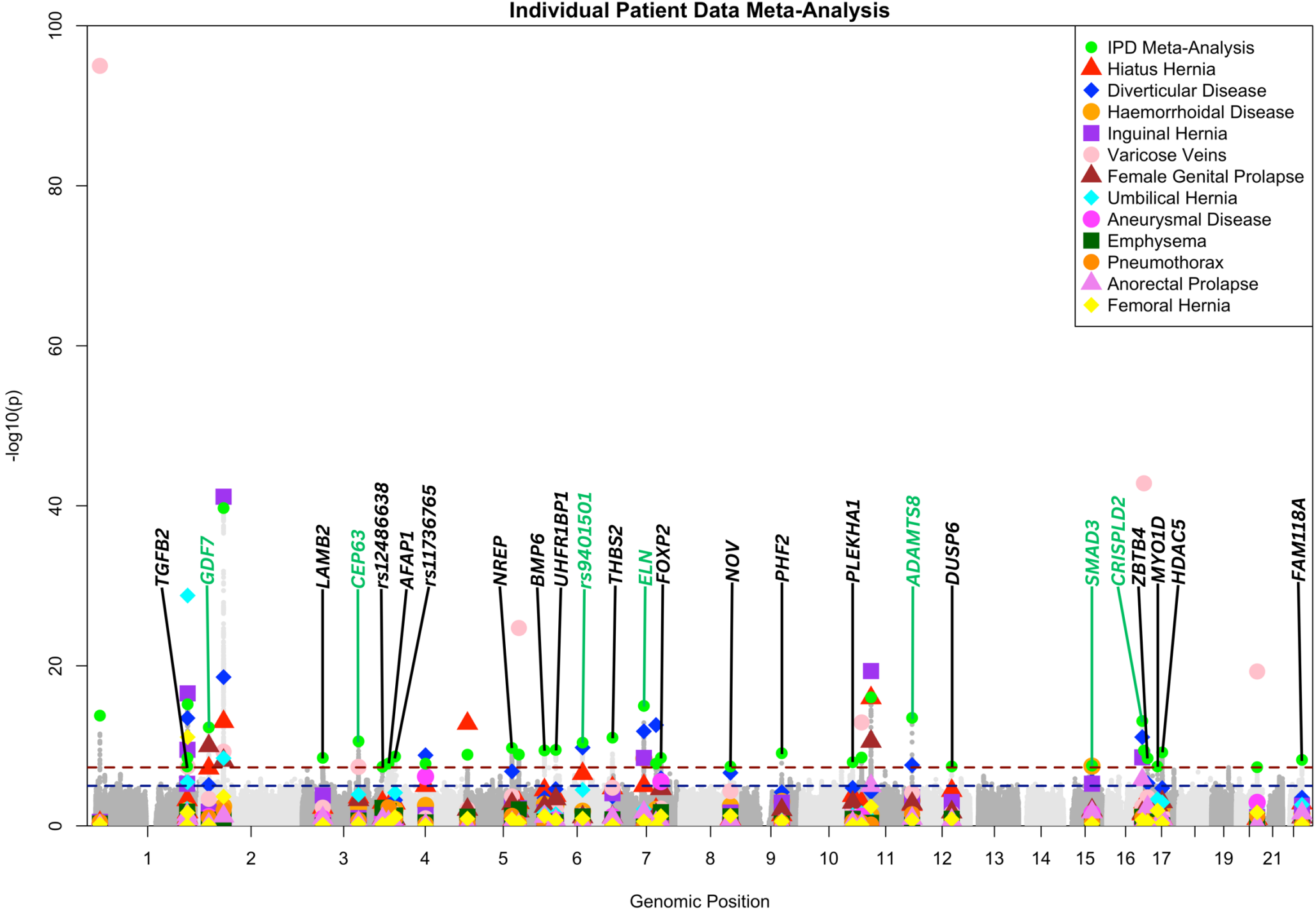
Individual Patient Data Meta-Analysis
IPD Meta-Analysis
Hiatus Hernia
Diverticular Disease
Haemorrhoidal Disease
Inguinal Hernia
Varicose Veins
Female Genital Prolapse
Umbilical Hernia
Aneurysmal Disease
Emphysema
Pneumothorax
Anorectal Prolapse
Femoral Hernia
-log10(p)
0
20
40
60
80
100
TGFB2
GDF7
LAMB2
CEP63
rs12486638
AFAP1
rs11736765
NREP
BMP6
UHFR1BP1
rs9401501
THBS2
ELN
FOXP2
NOV
PHF2
PLEKHA1
ADAMTS8
DUSP6
SMAD3
CRISPLD2
ZBTB4
MYO1D
HDAC5
FAM118A
1
2
3
4
5
6
7
8
9
10
11
12
13
14
15
16
17
19
21
Genomic Position

Table 5.3. Forty-six signals at 37 loci associated with the pan-elastopathy IPD GWAS meta-analysis of 137,549 cases and 248,365 controls in UK Biobank.

CHR[a]	POS [b]	MarkerID[c]	Allele2[d]	Allele1[e]	AF_Allele2[f]	Info[g]	OR[h]	OR_95L[i]	OR_95U[j]	P value[k]	Genes[l]
1	10825577	rs11121615	T	C	0.69	0.99	0.96	0.95	0.97	1.67×10^{-14}	*CASZ1*
1	218524632	rs2799097	G	A	0.85	0.99	1.04	1.02	1.05	3.78×10^{-8}	*TGFB2*
1	219294570	rs61823192	T	C	0.03	0.90	0.92	0.89	0.94	3.19×10^{-9}	
1	219734998	rs2785998	A	C	0.32	1.00	1.04	1.03	1.05	6.39×10^{-16}	
2	20878406	rs3072	C	T	0.36	0.99	1.04	1.03	1.05	4.97×10^{-13}	*GDF7*
2	55874811	rs12616982	T	C	0.05	1.00	1.07	1.04	1.09	2.80×10^{-10}	*EFEMP1*
2	55986569	rs1579494	G	A	0.16	0.96	0.96	0.95	0.97	9.39×10^{-10}	*EFEMP1*
2	56102744	rs11899888	G	A	0.16	0.99	1.09	1.08	1.10	1.92×10^{-40}	*EFEMP1*
2	56106928	rs59985551	T	C	0.22	1.00	0.93	0.92	0.94	3.19×10^{-38}	*EFEMP1*
2	56119510	rs727877	T	A	0.07	0.99	0.94	0.92	0.96	6.77×10^{-11}	*EFEMP1*
2	56190273	rs6735393	C	A	0.18	0.99	1.04	1.03	1.05	1.16×10^{-10}	*EFEMP1*
3	49213637	rs9586	T	C	0.78	G	0.97	0.96	0.98	3.17×10^{-9}	*LAMB2*
3	134379752	rs6762606	T	C	0.28	1.00	0.97	0.95	0.98	2.70×10^{-11}	*CEP63*
3	191337317	rs12486638	G	A	0.19	0.99	0.97	0.96	0.98	4.17×10^{-8}	
4	7828233	rs11734860	C	G	0.31	1.00	0.97	0.96	0.98	1.63×10^{-8}	*AFAP1*
4	23512757	rs11736765	T	A	0.33	0.97	0.97	0.96	0.98	2.17×10^{-9}	
4	96010061	rs1158368	A	G	0.71	1.00	0.97	0.96	0.98	1.71×10-8	*BMPR1B*
5	4977446	rs42202	G	A	0.92	0.99	0.95	0.93	0.97	1.28×10-9	
5	110979158	rs1379552	C	T	0.23	0.98	0.96	0.95	0.97	1.85×10^{-10}	*NREP*
5	127476971	rs1993878	A	C	0.75	1.00	0.97	0.96	0.98	1.23×10^{-9}	*SLC12A2*
6	7709341	rs12212270	A	C	0.38	0.99	0.97	0.96	0.98	3.72×10^{-10}	*BMP6*
6	34552797	rs2814944	A	G	0.15	G	1.04	1.03	1.06	3.23×10^{-10}	*UHRF1BP1*
6	98500712	rs9401501	C	T	0.39	1.00	0.97	0.96	0.98	4.00×10^{-11}	

6	169606389	rs9505932	A	C	0.32	1.00	1.03	1.02	1.04	9.55×10^{-12}	*THBS2*
6	169641383	rs73043897	T	C	0.14	0.99	0.96	0.95	0.97	4.35×10^{-9}	*THBS2*
7	73318286	rs13241670	C	T	0.25	0.98	0.97	0.96	0.98	4.20×10^{-9}	*ELN*
7	73431283	rs11762153	A	G	0.41	1.00	0.97	0.96	0.98	7.89×10^{-10}	*ELN*
7	73445942	rs2356532	G	A	0.06	1.00	1.08	1.06	1.10	1.02×10^{-15}	*ELN*
7	73474825	rs17855988	C	G	0.10	0.97	0.94	0.93	0.96	1.16×10^{-12}	*ELN*
7	102419805	rs2411048	G	A	0.34	0.97	1.03	1.02	1.04	1.68×10^{-8}	*FAM185A*
7	114109349	rs727644	G	A	0.60	1.00	1.03	1.02	1.04	3.18×10^{-9}	*FOXP2*
8	120475358	rs1599473	T	G	0.24	0.99	0.97	0.96	0.98	3.82×10^{-8}	*NOV*
9	96445224	rs36174510	G	A	0.37	0.99	1.03	1.02	1.04	8.41×10^{-10}	*PHF2*
10	124233181	rs79043147	T	C	0.07	0.99	0.95	0.93	0.97	1.12×10^{-8}	*PLEKHA1*
11	9947392	rs4910082	C	G	0.52	0.99	1.03	1.02	1.04	2.90×10^{-9}	*SBF2*
11	32459228	rs4140413	T	G	0.37	0.99	0.96	0.95	0.97	8.59×10^{-17}	*WT1*
11	130271209	rs1021205	C	T	0.19	0.99	0.96	0.95	0.97	3.19×10^{-14}	*ADAMTS8*
12	89767198	rs809973	C	T	0.19	1.00	1.03	1.02	1.05	3.77×10^{-8}	*DUSP6*
15	67561598	rs67872952	T	C	0.23	1.00	0.97	0.96	0.98	3.01×10^{-8}	*SMAD3*
16	84856552	rs4238714	C	T	0.42	0.99	1.04	1.03	1.05	7.94×10^{-14}	*CRISPLD2*
16	88835545	rs2911463	A	G	0.69	0.98	0.97	0.96	0.98	3.89×10^{-10}	*PIEZO1*
17	7366619	rs34914463	C	T	0.13	G	0.96	0.95	0.97	3.58×10^{-9}	*ZBTB4*
17	30987593	rs2640836	T	C	0.11	0.96	0.96	0.94	0.97	3.79×10^{-8}	*MYO1D*
17	42201956	rs4793079	A	C	0.71	1.00	0.97	0.96	0.98	6.56×10^{-10}	*HDAC5*
20	50065648	rs228836	A	G	0.59	0.99	1.03	1.02	1.04	4.66×10^{-8}	*NFATC2*
22	45723807	rs11556482	C	G	0.27	G	0.97	0.96	0.98	5.69×10^{-9}	*FAM118A*

[a]The chromosome number.
[b]Genomic position based on NCBI Genome Build 37 (hg19).
[c]The ID of the SNP.
[d]The effect allele.
[e]The non-effect allele.
[f]The effect allele frequency.
[g]The SNP INFO score for imputed SNPs. 'G' meaning genotyped SNP.
[h]The odds ratio.
[i]The 95% lower confidence bound of the odds ratio.
[j]The 95% upper confidence bound of the odds ratio.
[k]The SNP association P-value.
[l]From the genes identified from positional mapping, eQTL mapping, MAGMA gene mapping, summary-based Mendelian randomisation, a single best prioritised gene is presented here.
Red signals are a subset of the independent genome-wide significant SNPs (IndSigSNPs) that have an $r^2 < 0.1$ and are classified as independent lead SNPs (as discussed in **Section 5.2.10**, no formal Bayesian conditional analysis was performed).

5.3.3. Common factor analysis

Genomic structural equation modelling (SEM) was performed to identify the common factor genetic architecture of elastopathies.[16] The 12 elastopathy phenotypic subdomains were loaded onto a single latent common factor, revealing 40 shared susceptibility signals (31 loci) (**Figure 5.5; Table 5.4**). Sixteen loci (17 signals) were found to be *significant* or *more significant* under genomic SEM analysis than any of the individual elastopathy analyses (**Appendix Table 5.7, Appendix Figure 5.8**). Six loci were more significant under common factor analysis than any of the 12 individual elastopathies. A further ten loci (11 signals) were not significant in any of the individual analyses but reached genome-wide significance in the genomic SEM analysis. Among the ten newly identified common factor loci, six loci had also been discovered in the IPD GWAS meta-analysis (6p24.3 (*BMP6*), 6p21.31 (*UHRF1BP1*), 6q27 (*THBS2*), 7q31.1 (*FOXP2*), 10q26.13 (*PLEKHA1*), 17p13.1 (*ZBTB4*). Four loci were discovered which were not revealed in the IPD GWAS meta-analysis: 2p24.1 (*APOB*), 2q34 (*ERBB4*), 6p25.3 (*IRF4*), and 8q24.12 (~20kb upstream of *CCN3 (NOV)*).

Figure 5.5. Genomic Common Factor Results. Manhattan plot demonstrating the 31 genome-wide significant common factor loci (lead SNPs depicted by green circles). The corresponding 31 loci from the 12 elastopathy phenotypes are depicted in the plot by 12 colour coded shapes (see legend). The two dashed lines are the suggestive significance threshold ($P < 1\times10^{-5}$, blue) and the genome-wide significance threshold ($P < 5\times10^{-8}$, maroon). Annotated in black are the 10 loci which became significant under common factor analysis and were *not* found to be significant in any of the 12 individual elastopathy GWA studies. Annotated in green are the six loci which became more significant under common factor analysis compared to any of the 12 individual elastopathy GWA studies, with at least one of the 12 individual elastopathy studies also finding this locus to be genome-wide significant. Annotations are based on the single best prioritised genes from the prioritisation methods used, or the top SNP from the common factor analysis, where no gene was mapped at a particular locus.

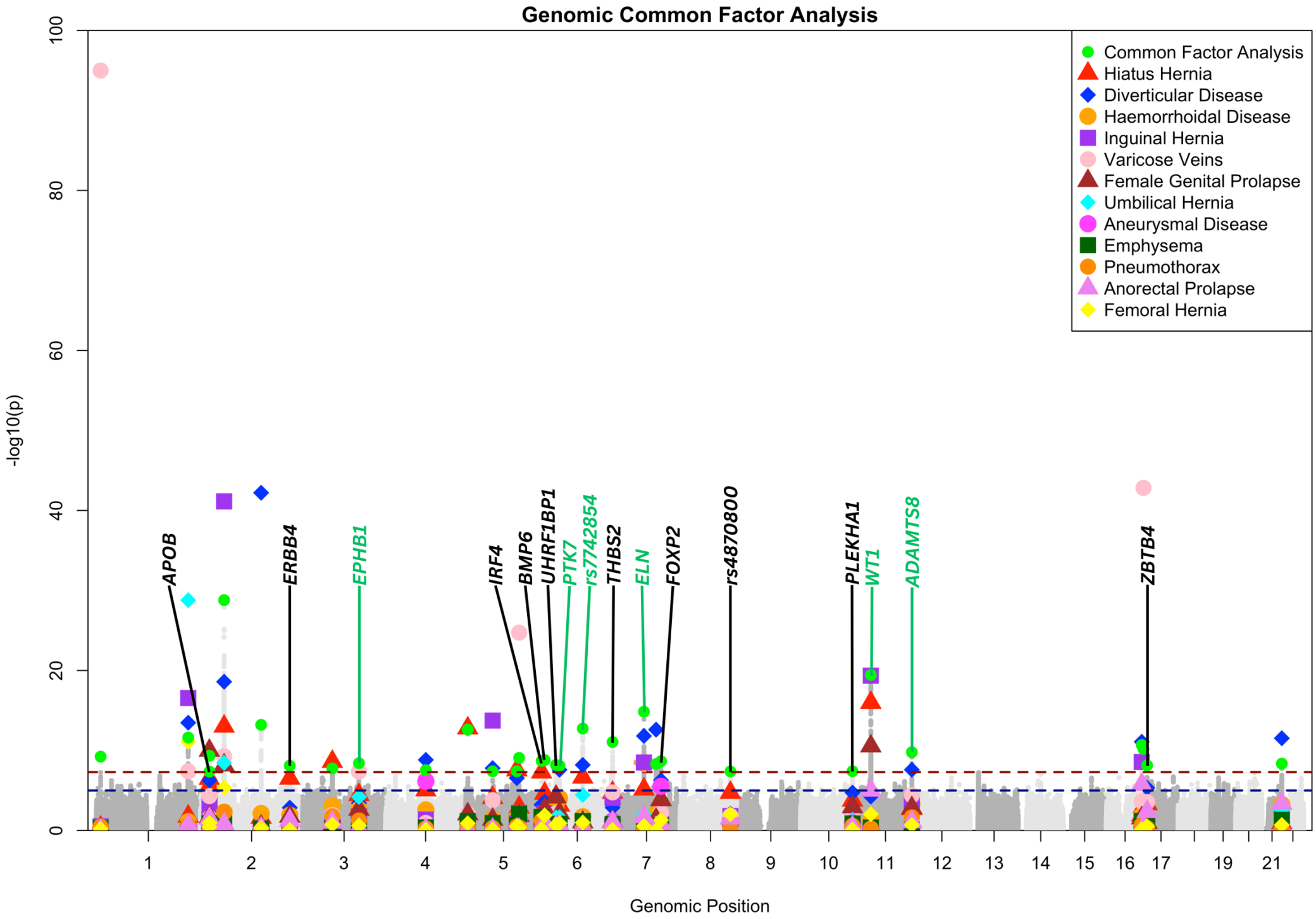
Genomic Common Factor Analysis
-log10(p)
Genomic Position
Common Factor Analysis
Hiatus Hernia
Diverticular Disease
Haemorrhoidal Disease
Inguinal Hernia
Varicose Veins
Female Genital Prolapse
Umbilical Hernia
Aneurysmal Disease
Emphysema
Pneumothorax
Anorectal Prolapse
Femoral Hernia
APOB
ERBB4
EPHB1
IRF4
BMP6
UHRF1BP1
PTK7
rs7742854
THBS2
ELN
FOXP2
rs4870800
PLEKHA1
WT1
ADAMTS8
ZBTB4

Table 5.4. Forty signals at 31 loci associated with the pan-elastopathy common factor analysis of 137,549 cases and 248,365 controls in UK Biobank.

CHR[a]	POS[b]	MarkerID[c]	Allele2[d]	Allele1[e]	SEM_Pval[f]	Genes[g]
1	10825577	rs11121615	T	C	5.85×10^{-10}	CASZ1
1	219704939	rs76926608	A	G	2.10×10^{-8}	
1	219707048	rs9431171	G	C	2.38×10^{-12}	
2	20881840	rs2289081	C	G	4.62×10^{-10}	GDF7
2	21239884	rs76622701	T	A	4.42×10^{-8}	APOB
2	56093204	rs1802575	C	G	1.61×10^{-29}	EFEMP1
2	56106928	rs59985551	T	C	7.30×10^{-26}	EFEMP1
2	56172646	rs12995908	T	C	1.07×10^{-10}	EFEMP1
2	56190273	rs6735393	C	A	1.27×10^{-12}	EFEMP1
2	144339654	rs10211096	G	A	6.21×10^{-14}	ARHGAP15
2	212590785	rs56405287	C	T	7.98×10^{-9}	ERBB4
3	70918127	rs1018340	A	G	1.76×10^{-8}	FOXP1
3	134369420	rs1868164	A	G	3.85×10^{-9}	EPHB1
4	96007656	rs17022989	G	A	2.82×10^{-8}	BMPR1B
5	4977446	rs42202	G	A	2.39×10^{-13}	
5	64390101	rs62369810	T	C	4.08×10^{-8}	(near ADAMTS6)
5	122104175	rs10041514	A	G	3.97×10^{-8}	SNX2
5	127476971	rs1993878	A	C	8.33×10^{-10}	SLC12A2
6	396321	rs12203592	T	C	2.04×10^{-9}	IRF4
6	7695418	rs12208776	T	G	1.55×10^{-9}	BMP6
6	34753748	rs112735232	T	C	6.53×10^{-9}	UHRF1BP1
6	43111445	rs3737185	C	T	8.01×10^{-9}	PTK7
6	98528143	rs7742854	T	C	1.81×10^{-13}	

6	169606389	rs9505932	A	C	8.80×10^{-12}	THBS2
6	169639426	rs55770539	T	C	5.98×10^{-10}	THBS2
7	73318286	rs13241670	C	T	3.26×10^{-9}	ELN
7	73431283	rs11762153	A	G	8.99×10^{-9}	ELN
7	73440985	rs55675441	C	T	1.42×10^{-15}	ELN
7	73504233	rs810536	A	G	3.27×10^{-11}	ELN
7	102412361	rs2261257	T	C	4.95×10^{-9}	FAM185A
7	114192545	rs7794413	C	T	2.14×10^{-9}	FOXP2
8	120508848	rs4870800	A	G	4.19×10^{-8}	
10	124233181	rs79043147	T	C	3.93×10^{-8}	PLEKHA1
11	32451003	rs3858447	G	A	3.63×10^{-20}	WT1
11	130262601	rs11606448	T	C	1.64×10^{-10}	ADAMTS8
16	84855477	rs1874013	G	T	2.11×10^{-11}	CRISPLD2
16	84884116	rs4783090	G	A	3.19×10^{-8}	CRISPLD2
16	88835545	rs2911463	A	G	6.41×10^{-11}	PIEZO1
17	7366619	rs34914463	C	T	7.28×10^{-9}	ZBTB4
21	47429769	rs2839078	G	C	4.36×10^{-9}	COL6A1

[a]The chromosome number.
[b]Genomic position based on NCBI Genome Build 37 (hg19).
[c]The ID of the SNP.
[d]The effect allele.
[e]The non-effect allele.
[f]The SNP association P-value.
[g]From the genes identified from positional mapping, eQTL mapping, MAGMA gene mapping, summary-based Mendelian randomisation, a single best prioritised gene is presented here.
Red signals are that subset of the independent genome-wide significant SNPs (IndSigSNPs) that have an $r^2 < 0.1$ and are classified as independent lead SNPs (as discussed in **Section 5.2.10**, no formal Bayesian conditional analysis was performed).

5.3.4. Multi-trait co-localisation

Across both the IPD GWAS meta-analysis and the genomic SEM analysis - one association signal, rs7255 at locus 2p41.1 (*GDF7)* co-localised across four individual elastopathy traits (hiatus hernia, diverticular disease, varicose veins, and female genital prolapse) with a posterior probability 0.79; this single SNP explained 93% of the posterior probability (**Appendix Table 5.8**). A second variant, rs59985551 at 2p16.1 (*EFEMP1*) co-localised across the IPD meta-analysis and genomic SEM in inguinal hernia, varicose veins, female genital prolapse, and umbilical hernia with a posterior probability of 0.91; 73% of the posterior probability was explained by this variant.

5.3.5. *In silico* annotation

In the IPD GWAS meta-analysis, FUMA identified 1,440 candidate SNPs ($P < 5\times10^{-8}$) at the 37 susceptibility loci (46 independent lead signals) (**Appendix Figure 5.9, Appendix Figure 5.10**).[18] Seventeen candidate SNPs were exonic, of which 12 were non-synonymous (**Appendix Table 5.9**). Among the non-synonymous missense variants, two were predicted to affect protein structure or function, and were in high linkage disequilibrium (LD) with the index lead signal:

i. rs1045920 (EAF = 0.05, INFO = 1, OR = 1.06 (1.04 - 1.08), r^2index = 0.94, P = 4.37×10^{-9}) causes a predicted deleterious p.Ile217Phe substitution within exon 8 of *CCDC104* (SIFT = 0.05 (deleterious), CADD = 22.6).

ii. rs17855988 (EAF = 0.90. INFO = 0.97, OR = 1.06 (1.04 - 1.08), P = 1.16×10^{-12}) is the index SNP at the 7q11.23 locus, causing a deleterious p.Gly581Arg mutation within exon 25 of *ELN* (SIFT = 0, PolyPhen = 0.999, CADD = 25.9, RDB = 2b).

In the genomic SEM analysis, FUMA identified 1,158 candidate SNPs ($P < 5\times10^{-8}$) at the 31 susceptibility loci (40 independent lead signals) (**Appendix Figure 5.11, Appendix Figure 5.12**). Ten SNPs were exonic, of which seven were non-synonymous (**Appendix Table 5.10**), with the same variant in *ELN* predicted to affect protein structure or function.

In the IPD GWAS meta-analysis, a total of 1,035 intronic and intergenic candidate variants were located at the susceptibility loci ($P < 5x10^{-8}$). 956 of these variants (92.4%) lay in open chromatin regions, and 56 variants possessed a Combined

Annotation-Dependent Depletion (CADD) score ≥ 12.37, suggesting putative evidence for deleterious effects. The regulatory activity of these variants was further examined with RegulomeDB (RDB)[24], with four of these predicted deleterious variants demonstrating regulatory activity with a RDB score of 2b or higher (likely to affect binding), and one variant having an RDB score of 1f or higher (likely to affect binding and linked to expression of a gene target) (**Appendix Table 5.11**).

In the common factor SEM analysis, 769 intronic and intergenic candidate variants were located at the discovered loci, and 696 variants (90.5%) resided in open chromatin regions. Thirty-seven intronic and intergenic variants (4.81%) demonstrated computational evidence of functionality with a CADD Score ≥ 12.37. Using RDB to delineate the regulatory effects of these prioritised variants, one SEM variant at 7q11.23, rs6964590 (28kb from *WBSCR28*; MAF = 0.24, $r^2 = 1$, $P = 2.21 \times 10^{-8}$, CADD = 12.75, RDB = 1f), was predicted likely to affect binding and linked to expression of a gene target (**Appendix Table 5.12**).

5.3.6. Gene Mapping

To map genes to the associated variants, several approaches were implemented. For the IPD GWAS meta-analysis, 55 genes were identified by FUMA SNP2GENE[18] to lie within a 10kb positional mapping window from at least one genome-wide significant candidate variant (**Appendix Table 5.13**). Twenty-six genes were mapped to one or more variants known to be a significant eQTL in cultured fibroblast cells in GTEx v8 ($P < 5\times10^{-8}$, $FDR < 5\times10^{-8}$) (**Appendix Table 5.14**).[25] A genome-wide, gene-set analysis implemented in MAGMA v1.08[19], discovered 64 protein-coding genes to be enriched in the IPD GWAS meta-analysis summary data (**Appendix Table 5.15**), forty-five of which lay within the boundaries of our risk loci**.**

Summary-based Mendelian randomisation (SMR) analyses were carried out for 6,679 probes with at least a single genome-wide significant cis-eQTL ($P < 5\times10^{-8}$).[20] The criteria for significance of each probe from the SMR test was defined as a $P_{SMR} < 7.49 \times10^{-6}$ (0.05/6679), with three genes passing this threshold. To exclude any significant associations from the SMR test due to linkage disequilibrium, HEterogeneity In Dependent Instrument (HEIDI) analysis was conducted across the three significant genes, one of which passed the HEIDI test ($P_{HEIDI} < 5\times10^{-2}$) and lay within the region of a known susceptibility locus 17q21.31 (*ASB16*), indicating an association with the elastopathy phenotype through pleiotropy rather than linkage and co-localisation (**Appendix Table 5.16**).

To *précis*, 80 unique genes were mapped to the IPD meta-analysis susceptibility loci by at least a single gene mapping strategy (**Table 5.5**). A pronounced convergence

was seen between mapping strategies, with most genes (n = 41) being mapped by two or more strategies. Four genes (*C6orf106*, *CRISPLD2*, *PIEZO1*, *FAM118A*) were mapped by three strategies, and a single gene was mapped by all four strategies (*ASB16*).

A total of 44 unique genes were mapped to the common factor susceptibility loci using positional mapping (**Appendix Table 5.17**)[18], eQTL mapping in cultured fibroblast cells from GTEx v8 (**Appendix Table 5.18**)[18], and a MAGMA v1.08 genome-wide gene association test (**Appendix Table 5.19**).[19] Again, there was a notable overlap between mapping strategies, with half of all genes (n = 22) mapped by two or more complimentary strategies, and three genes mapped by all three mapping strategies (*C6orf106*, *CRISPLD2*, *PIEZO1*) (**Table 5.6**).

Table 5.5. 80 unique genes mapped to 31 IPD meta-analysis loci using the four mapping strategies. Most loci are mapped to genes using multiple mapping strategies

Genomic Locus	CHR	POS	MarkerID	Allele2	Positionally Mapped Genes	eQTL-Mapped Genes	MAGMA Mapped Genes	SMR Mapped Genes	Number of Gene Mapping Approaches
1	1	10825577	rs11121615	T	*CASZ1*		*CASZ1*		**2**
2	1	218524632	rs2799097	G	*TGFB2*				**1**
2	1	218524632	rs2799097	G	*RRP15*				**1**
5	2	20878406	rs3072	C	*GDF7*				**1**
5	2	20878406	rs3072	C	*C2orf43*	*C2orf43*			**2**
6	2	56102744	rs11899888	G	*EFEMP1*		*EFEMP1*		**2**
6	2	56102744	rs11899888	G	*PNPT1*		*PNPT1*		**2**
6	2	56102744	rs11899888	G	*SMEK2*		*SMEK2*		**2**
6	2	56102744	rs11899888	G	*CCDC104*		*CCDC104*		**2**
7	3	49213637	rs9586	T	*CCDC71*				**1**
7	3	49213637	rs9586	T	*KLHDC8B*	*KLHDC8B*			**2**
7	3	49213637	rs9586	T	*C3orf84*		*C3orf84*		**2**
7	3	49213637	rs9586	T		*AMT*			**1**
7	3	49213637	rs9586	T		*DALRD3*			**1**
7	3	49213637	rs9586	T		*GMPPB*			**1**
7	3	49213637	rs9586	T		*GPX1*			**1**
7	3	49213637	rs9586	T		*NCKIPSD*			**1**
7	3	49213637	rs9586	T		*P4HTM*			**1**
7	3	49213637	rs9586	T		*WDR6*			**1**
7	3	49213637	rs9586	T		*TCTA*	*TCTA*		**2**

7	3	49213637	rs9586	T			*CCDC36*	**1**
7	3	49213637	rs9586	T			*RP11-3B7.1*	**1**
7	3	49213637	rs9586	T			*RHOA*	**1**
7	3	49213637	rs9586	T			*DAG1*	**1**
7	3	49213637	rs9586	T			*BSN*	**1**
8	3	134379752	rs6762606	T	*CEP63*	*CEP63*		**2**
8	3	134379752	rs6762606	T	*ANAPC13*	*ANAPC13*		**2**
8	3	134379752	rs6762606	T	*EPHB1*			**1**
8	3	134379752	rs6762606	T	*KY*			**1**
10	4	7828233	rs11734860	C	*AFAP1*		*AFAP1*	**2**
12	4	96010061	rs1158368	A	*BMPR1B*		*BMPR1B*	**2**
14	5	110979158	rs1379552	C	*NREP*			**1**
15	5	127476971	rs1993878	A	*SLC12A2*			**1**
16	6	7709341	rs12212270	A	*BMP6*			**1**
17	6	34552797	rs2814944	A	*UHRF1BP1*	*UHRF1BP1*		**2**
17	6	34552797	rs2814944	A	*SNRPC*			**1**
17	6	34552797	rs2814944	A	*C6orf106*	*C6orf106*	*C6orf106*	**3**
19	6	169606389	rs9505932	A	*THBS2*		*THBS2*	**2**
20	7	73445942	rs2356532	G	*ELN*		*ELN*	**2**
20	7	73445942	rs2356532	G	*LIMK1*			**1**
21	7	102419805	rs2411048	G	*FAM185A*		*FAM185A*	**2**
21	7	102419805	rs2411048	G	*FBXL13*		*FBXL13*	**2**
21	7	102419805	rs2411048	G		*LRRC17*		**1**
21	7	102419805	rs2411048	G		*POLR2J2*		**1**
21	7	102419805	rs2411048	G		*UPK3BL*		**1**
22	7	114109349	rs727644	G	*FOXP2*		*FOXP2*	**2**
23	8	120475358	rs1599473	T			*NOV*	**1**
24	9	96445224	rs36174510	G	*PHF2*			**1**

25	10	124233181	rs79043147	T	*PLEKHA1*				**1**
25	10	124233181	rs79043147	T	*HTRA1*				**1**
26	11	9947392	rs4910082	C	*SBF2*		*SBF2*		**2**
27	11	32459228	rs4140413	T	*WT1*		*WT1*		**2**
28	11	130271209	rs1021205	C	*ADAMTS8*		*ADAMTS8*		**2**
29	12	89767198	rs809973	C	*DUSP6*		*DUSP6*		**2**
30	15	67561598	rs67872952	T	*SMAD3*		*SMAD3*		**2**
30	15	67561598	rs67872952	T	*IQCH*	*IQCH*			**2**
30	15	67561598	rs67872952	T	*AAGAB*		*AAGAB*		**2**
31	16	84856552	rs4238714	C	*CRISPLD2*	*CRISPLD2*	*CRISPLD2*		**3**
32	16	88835545	rs2911463	A	*PIEZO1*	*PIEZO1*	*PIEZO1*		**3**
33	17	7366619	rs34914463	C	*ZBTB4*		*ZBTB4*		**2**
33	17	7366619	rs34914463	C	*CHRNB1*	*CHRNB1*			**2**
33	17	7366619	rs34914463	C		*TNFSF13*			**1**
33	17	7366619	rs34914463	C			*SLC35G6*		**1**
33	17	7366619	rs34914463	C			*POLR2A*		**1**
33	17	7366619	rs34914463	C			*MPDU1*		**1**
33	17	7366619	rs34914463	C			*FXR2*		**1**
33	17	7366619	rs34914463	C			*SHBG*		**1**
34	17	30987593	rs2640836	T	*MYO1D*				**1**
35	17	42201956	rs4793079	A	*HDAC5*		*HDAC5*		**2**
35	17	42201956	rs4793079	A	*ATXN7L3*		*ATXN7L3*		**2**
35	17	42201956	rs4793079	A	*TMUB2*		*TMUB2*		**2**
35	17	42201956	rs4793079	A	*ASB16*	*ASB16*	*ASB16*	*ASB16*	**4**
35	17	42201956	rs4793079	A	*LSM12*	*LSM12*			**2**
35	17	42201956	rs4793079	A	*C17orf53*		*C17orf53*		**2**
35	17	42201956	rs4793079	A	*G6PC3*		*G6PC3*		**2**
35	17	42201956	rs4793079	A	*UBTF*		*UBTF*		**2**

35	17	42201956	rs4793079	A			*TMEM101*	**1**
36	20	50065648	rs228836	A	*NFATC2*		*NFATC2*	**2**
37	22	45723807	rs11556482	C	*FAM118A*	*FAM118A*	*FAM118A*	**3**
37	22	45723807	rs11556482	C		*RIBC2*		**1**

Table 5.6. 44 unique genes mapped to 25 of the 31 common factor loci using the three mapping strategies. The majority of loci are mapped to genes using multiple mapping strategies

Genomic Locus	FUMA END	CHR	POS	MarkerID	Positionally Mapped Genes	eQTL Mapped Genes	MAGMA Mapped Genes	Number of Gene Mapping Approaches
1	10825577	1	10825577	rs11121615	*CASZ1*			**1**
2	219788530	1	219707048	rs9431171				**0**
3	20888265	2	20881840	rs2289081	*GDF7*			**1**
3	20888265	2	20881840	rs2289081	*C2orf43*	*C2orf43*		**2**
4	21239884	2	21239884	rs76622701	*APOB*		*APOB*	**2**
5	56218492	2	56093204	rs1802575	*EFEMP1*		*EFEMP1*	**2**
5	56218492	2	56093204	rs1802575	*PNPT1*		*PNPT1*	**2**
5	56218492	2	56093204	rs1802575	*SMEK2*		*SMEK2*	**2**
5	56218492	2	56093204	rs1802575	*CCDC104*		*CCDC104*	**2**
6	144403796	2	144339654	rs10211096	*ARHGAP15*		*ARHGAP15*	**2**
7	212591283	2	212590785	rs56405287	*ERBB4*		*ERBB4*	**2**
8	70955186	3	70918127	rs1018340				**0**
9	134385789	3	134369420	rs1868164	*EPHB1*			**1**
9	134385789	3	134369420	rs1868164	*KY*			**1**
9	134385789	3	134369420	rs1868164		*CEP63*		**1**
9	134385789	3	134369420	rs1868164		*ANAPC13*		**1**
10	96015307	4	96007656	rs17022989	*BMPR1B*		*BMPR1B*	**2**
11	4977446	5	4977446	rs42202				**0**
12	64390101	5	64390101	rs62369810				**0**
13	122104175	5	122104175	rs10041514	*SNX2*		*SNX2*	**2**

14	127544738	5	127476971	rs1993878	*SLC12A2*			**1**
15	396321	6	396321	rs12203592	*IRF4*			**1**
16	7727271	6	7695418	rs12208776	*BMP6*			**1**
17	34831761	6	34753748	rs112735232	*UHRF1BP1*	*UHRF1BP1*		**2**
17	34831761	6	34753748	rs112735232	*SNRPC*			**1**
17	34831761	6	34753748	rs112735232	*C6orf106*	*C6orf106*	*C6orf106*	**3**
18	43111445	6	43111445	rs3737185	*PTK7*			**1**
19	98546547	6	98528143	rs7742854				**0**
20	169652568	6	169606389	rs9505932	*THBS2*		*THBS2*	**2**
21	73566952	7	73440985	rs55675441	*ELN*		*ELN*	**2**
21	73566952	7	73440985	rs55675441	*LIMK1*			**1**
21	73566952	7	73440985	rs55675441			*WBSCR27*	**1**
21	73566952	7	73440985	rs55675441			*WBSCR28*	**1**
22	102481842	7	102412361	rs2261257	*FAM185A*		*FAM185A*	**2**
22	102481842	7	102412361	rs2261257	*FBXL13*		*FBXL13*	**2**
22	102481842	7	102412361	rs2261257		*UPK3BL*		**1**
22	102481842	7	102412361	rs2261257		*LRRC17*		**1**
22	102481842	7	102412361	rs2261257		*POLR2J2*		**1**
23	114194615	7	114192545	rs7794413	*FOXP2*		*FOXP2*	**2**
24	120508848	8	120508848	rs4870800				**0**
25	124233181	10	124233181	rs79043147	*HTRA1*			**1**
26	32543039	11	32451003	rs3858447	*WT1*		*WT1*	**2**
27	130281735	11	130262601	rs11606448	*ADAMTS8*			**1**
28	84884116	16	84855477	rs1874013	*CRISPLD2*	*CRISPLD2*	*CRISPLD2*	**3**
29	88846849	16	88835545	rs2911463	*PIEZO1*	*PIEZO1*	*PIEZO1*	**3**
30	7366619	17	7366619	rs34914463	*ZBTB4*		*ZBTB4*	**2**
30	7366619	17	7366619	rs34914463	*CHRNB1*	*CHRNB1*		**2**
30	7366619	17	7366619	rs34914463		*TNFSF13*		**1**

30	7366619	17	7366619	rs34914463			*POLR2A*	**1**
31	47453019	21	47429769	rs2839078	*COL6A1*			**1**

5.4. Discussion

5.4.1. Summary

This chapter investigated the shared genetic foundations of common elastopathies. Leveraging an individual patient data meta-analysis involving a prospective European cohort of ~400,000 participants[10], 18 susceptibility loci previously not associated with any of the individual elastopathies were discovered. Moreover, for a further seven susceptibility loci, the association strength became more significant under meta-analysis, implying their influence along shared pathways, contributing to an additive risk for elastic tissue disease. Employing genomic common factor analysis to unveil the latent elastopathy phenotype[16], ten susceptibility loci were identified, including four absent from the IPD GWAS meta-analysis, and a further six whose association signal became more significant under structural equation modelling.

This comprehensive approach, combining meta-analysis and common factor analysis, pinpointed core matrisomal genes associated with the elastopathy phenotype. Appreciably, the TGFβ signalling pathway and SMAD protein transduction is consistently implicated in the pathobiology of common elastopathies. Multi-trait co-localisation identified clusters of elastopathy traits co-localising at two distinct variants within 2p41.1 (*GDF7*) and 2p16.1 (*EFEMP1*), genes that are pivotal to the TGFβ signalling pathway and core matrisomal genes in elastic and connective tissue development.[26] Genomic correlation estimates provided evidence for a genetic overlap between the 12 individual elastopathies, pointing in the same causal direction. Lastly, employing *in silico* annotation, putative variants at the shared loci were prioritised.

5.4.2. Matrisome and matrisome-associated genes

The extracellular matrix (ECM) is a highly dynamic network of macromolecules and minerals that impart both biochemical and structural properties; it is necessary for the normal physiological function of bodily structures.[27] The matrisome constitutes the over 1000 genes which encode collagens, glycoproteins (including elastin), proteoglycans, regulators and affiliated proteins which make up the ECM in its entirety.[6,28] Of the 25 susceptibility loci that were newly discovered, or became more significantly associated, under meta-analysis, thirteen mapped to matrisome or matrisome associated genes; and of the 16 similar loci in the common factor analysis, seven mapped to matrisome or matrisome associated genes.

ELN

Elastin is a secreted matrisome glycoprotein which constitutes the principal protein in elastic fibres.[29] On account of its elastic properties, resilience and tensile strength afforded by extensive cross-linking, elastin is the *sole* protein in the human matrisome which imparts elastic recoil to tissues and organs. Elastin is highly robust: with a half-life of over seven decades, it is capable of persisting throughout the human lifespan under normal physiological conditions. Both transcriptional and post-transcriptional mechanisms are involved in the regulation of elastin, including promoter activation and inhibition, mRNA degradation, microRNA interaction, and alternative splicing.[30] Elastopathies can occur as a result of loss of quantity of elastic fibres (elastin haploinsufficiency and perturbed turnover) and quality of elastic fibres (abnormal elastin deposition and elastin dysfunction).[31] Elastin within elastic fibres accumulates irreversible damage from ageing, as well as chemical and enzymatic disintegration,

for example from aberrant expression of proteases/elastases, which may lead to pathological weakness within the elastin contractile unit, altering tissue properties and inevitably predisposing to elastopathies.

In both the IPD GWAS meta-analysis and the latent trait modelling of the elastopathy phenotype, the *ELN* locus at 7q11.23 which encodes tropoelastin, was found to be more significantly associated under combined analysis than any individual trait analysis suggesting a shared susceptibility to elastopathies at this locus. Of note, the index SNP at the 7q11.23 locus, rs17855988, causes a predicted deleterious p.Gly581Arg substitution within exon 25 of *ELN*. The glycine amino acid at this codon is known to be evolutionarily conserved among mammals.[32] Exon 25 of *ELN* encodes a KA cross-linking domain within the flexible bridge region of tropoelastin (linking the hinge and c-terminal domain), and is pivotal in interchain cross-linking in elastin fibres, with known variants within this exon understood to associate with supravalvular aortic stenosis and autosomal dominant cutis laxa.[33] It is intriguing that this particular variant has been identified in a patient with Williams–Beuren syndrome presenting with a bicuspid aortic valve, an elastic tissue disorder characterised by haploinsufficiency of the tropoelastin gene leading to short, fragmented and dysfunctional elastic fibres.[34]

ADAMTS8

As well as perturbing elastogenesis through haploinsufficiency of elastin and structural weaknesses in elastic fibres, variants within secreted elastases that cleave elastin can promote the solubilisation and deterioration of insoluble elastin fibres.[35] Aspartic, serine, and cysteine proteases, and metalloendopeptidases, such as matrix metalloproteinases (MMPs) and a disintegrin and metalloproteinases with

thrombospondin motifs (ADAMTS) proteases are all known to fragment elastin. ADAMTS proteins are zinc metalloendopeptidases that are central to the degradation and remodelling of the ECM, as well as cell-cell and cell-ECM signalling.[36]

There are 19 secreted ADAMTS proteins, with seven known to break down proteoglycans, three known to be pro-collagens, and several known to fragment elastin.[37] Maintaining the integrity of elastic tissues requires a balance of synthesis and degradation of matrix proteins, with tight regulation of elastin production, and more appreciably, its breakdown. Elevated ADAMTS1 expression causes thoracic aortic aneurysms and aortic dissection (TAAD) in mice due to disruption to the elastin contractile unit fragmenting elastin fibres, and perturbed collagen deposition and proteoglycan accumulation.[38] In a mouse model of Marfan's syndrome, targeting the the ADAMTS1-NOS2 axis has been shown to reduce TAAD formation.[39] Mutations in ADAMTS proteins have also been shown to lead to Weil-Merchesani Syndrome, dermatosparaxis Ehlers-Danlos Syndrome, and thrombotic thrombocytopenic purpura.

Among the matrisome-associated ADAMTS family, the protease sharing the greatest sequence homology and phylogenetic link with ADAMTS1 is ADAMTS8.[40] We identified the 11q24.3 (*ADAMTS8*) locus to associate more strongly with the elastopathy phenotype under IPD GWAS meta-analysis and common factor analysis than any of the individual trait analyses, suggesting shared risk at this locus. *ADAMTS8* demonstrates pronounced expression in heart and lung tissue Recombinant *ADAMTS8* has been shown to up-regulate MMP2, MMP9, MMP12 and MMP13 in pulmonary artery smooth muscle cells[41], with MMP2 and MMP9 known to

cleave elastin and collagen in aortic wall tissue. The substrate repertoire and post-translational regulation of ADAMTS8 has recently been described, with both TIMP2 and TIMP3 shown to inhibit its catalytic activity.[42] ADAMTS8 over-expression is pro-fibrotic in its effect, being shown to promote cardiac fibrosis following myocardial infarction.[43] Whilst no genome-wide significant loci were identified in the aneurysmal disease GWAS, and only diverticular disease associated with the 11q24.3 (*ADAMTS8*) locus (lead variant: rs11222085), it is possible that the pathological up-regulation of ADAMTS8 plays an important role in tissue remodelling towards an elastopathy state. The anthelmintic, mebendazole has been shown to suppress ADAMTS8 expression[41], and this may be worthy of further investigation in potential therapeutic applications in managing elastopathies.

CCN3 *(NOV)*

The cellular communication network (CCN) family of matrisome proteins comprise six members, most notably connective tissue growth factor (CTGF/ CCN2), and CCN3 (encoded by neuroblastoma over-expressed (*NOV*)).[44] This matricellular family play dynamic roles in fundamental cellular processes such as cell proliferation, migration, fibrosis, angiogenesis, and tumorigenesis.[45] The CCN glycoproteins attach to integrin receptors to coordinate cell-matrix communication in the ECM of several tissues. For instance, CCN3 attaches to integrins to induce migration in primary fibroblasts[46], as well as inducing angiogenesis in endothelial cells.[47] We identified the 8q24.12 (*NOV*) locus to associate with the pan-elastopathy phenotype under IPD GWAS meta-analysis, with this locus not being discovered in any individual analyses. Whilst CCN3 has been described as both promoting and inhibiting fibrosis in the literature, it is more extensively regarded as an inhibitor of fibrosis.[48] CTGF is a downstream mediator of

TGFβ signalling, modulating TGFβ, BMP and GDF signalling to promote ECM deposition, leading to fibrosis. CCN3 is known to inhibit CTGF[48], and perturb collagen deposition[48], moreover, in human mesangial cells, CCN3 promotes ECM breakdown by promoting the expression of MMPs and downregulating their natural inhibitors.[49] Therefore CCN3 plays an important role in countering matrix accumulation, but also hastening its breakdown. The protective role of CCN3 as an endogenous inhibitor of fibrosis has been demonstrated in glomerulosclerosis[50], where it has been found to downregulate TGFβ1-induced phosphorylation of SMADs 1, 5, and 8, therefore preventing downstream expression of pro-fibrotic genes.

5.4.3 TGFβ signalling pathway

The matrisome encodes not only a three-dimensional structure and elastic framework to support tissues and organs, but it furnishes a repository of growth factors and signalling peptides essential in cellular interaction and regulation.[51] The TGFβ superfamily of cytokines consists of two subgroups: i. the TGFβ subgroup (consisting of three TGFβ isoforms and several subunits of activin and inhibin) and ii. the bone morphogenetic protein (BMP) subgroup, consisting of over 20 growth differentiation factors (GDFs) and BMPs.[52] Within each group, ligands acting via their receptors impart secondary signalling cascades within target cells via intracellular SMAD transduction proteins (canonical) or SMAD-independent signalling (non-canonical) which alter transcription of effector genes that are implicated in the cell cycle, cell differentiation, migration and apoptosis, altering the extracellular matrix, fibrogenesis, neogenesis and angiogenesis.[53]

The extracellular matrix determines the availability of the Transforming Growth Factor β (TGFβ*)* superfamily of cytokines. TGFβ is among the most prolific regulators of both physiological and pathological elastin and collagen production.[54] In dermal and lung fibroblasts, TGFβ stabilises elastin mRNA levels.[55,56] TGFβ also plays a fundamental role in promoting elastin production through stabilising elastin mRNA and facilitating elastin synthesis in vascular tissues.[57] The main component of microfibrils is the ECM glycoprotein fibrillin-1, which is defective in Marfan's syndrome.[58] Fibrillin-1 attaches to the latent TGFβ complex to regulate TGFβ ligand availability[59], as well as sequestering BMPs in the matrix.[60] Fibronectin also has important roles in sequestering latent TGFβ as well as several other growth factors involved in tissue

regeneration and fibrosis.[61] With three known isoforms of the TGFβ ligand (TGFβ1, TGFβ2, and TGFβ3), the bioavailability of each ligand is intimately controlled in different tissues in normal physiology.[62] Mutations in genes encoding signalling peptides within the canonical TGFβ signalling pathway, such as SMAD3, TGFβ2, TGFβR1, TGFβR2, are known to lead to pathological remodelling and weaknesses in several elastic organs within the body, including the aorta.[63]

Of the 25 loci that became newly associated or more significantly associated in the IPD GWAS meta-analysis than the individual elastopathy analyses, six loci were involved in the TGFβ signalling pathway (1q41 (*TGFB2)*, 2p24.1 (*GDF7)*, 3p21.31 (*RHOA)*, 6p24.3 (*BMP6)*, 6q27 (*THBS2)*, 15q23 (*SMAD3)*). Two of these loci, 6p24.3 (*BMP6*) and 6q27 *(THBS2)* were also newly discovered in the genomic SEM analysis and had not been highlighted in any of the 12 individual elastopathy analyses.

TGFβ2

The TGFβ2 isoform is known to act as a pro-fibrotic cytokine, acting ubiquitously across the body. We identified the 1q41 locus (mapped to *TGFB2*) to significantly associate with the elastopathy phenotype under IPD GWAS meta-analysis. Intriguingly, this locus was not discovered in any of the individual elastopathy analyses and only became significant under meta-analysis, suggesting shared risk at this locus. Pathological variants in *TGFB2* are known to lead to Loeys-Dietz Syndrome (LDS) type IV[64], an inherited autosomal dominant disorder in close pathological relation to Marfan's and Ehlers-Danlos Syndrome.[65] LDS type IV is characterised by systemic features caused by disruption to the elastin contractile unit leading to craniofacial, musculoskeletal, cutaneous, ocular, and cardiovascular manifestations.[66] Elastin

fragmentation in LDS type IV leads to abdominal aortic aneurysms and dissection. Heterozygous knockout of a single *TGFB2* allele has been shown to be sufficient to cause aortic dissection in mice.[67] Paradoxically, *TGFB2* haploinsufficiency leads to activation of TGFβ expression and signalling, suggesting a complex pathobiology involved in TGFβ dysregulation.[67] Systemic sclerosis is a disorder characterised by refractory and progressive cutaneous and visceral fibrosis associated with a significant mortality-risk. Shin *et al.* discovered a novel enhancer at *TGFB2* which accelerates the fibrotic phenotype in *ex vivo* fibroblasts from systemic sclerosis patients, causing excess collagen deposition and down-regulation of MMP1.[68] This locus may therefore play an important role in ECM remodelling in elastic tissues, favouring fibrosis and elastin breakdown, and may be amenable to therapeutic targeting. Indeed, TGFβ2 targeting by antisense oligonucleotides has been found to reduce collagen deposition and αSMA expression, suggesting potential therapeutic rationale.[69] Treatment with the angiotensin II receptor blocker losartan has been shown to reduce TGFβ expression, and as a result reduce aortic root growth and prevent aortic aneurysms in mice.[70] TGFβ2 may be worth investigating further in the context of treating common elastopathies.

GDF7

GDF7 is a secreted autocrine and paracrine signalling glycoprotein that regulates the hedgehog and WNT signalling pathways.[71] GDF7 is involved in tissue maintenance and wound healing of ligaments and tendons.[72] Fragmentation of collagen fibrils has been found in the Achilles tendons of *GDF7* knockout mice.[73] We discovered the 2p24.1 locus (mapped to *GDF7)* to associate more strongly under IPD GWAS meta-analysis than any of the individual 12 elastopathies. Of note, the locus shows evidence

of co-localisation, with a cluster of four individual elastopathy traits (hiatus hernia, diverticular disease, varicose veins, and female genital prolapse) identified to colocalise at this 2p24.1 locus during HyPrColoc analysis in both IPD GWAS meta-analysis and the common factor analysis. GDF7 has been implicated to promote hepatic progenitor cell expansion in hepatic fibrosis to aid in regeneration.[74] Leucine-rich repeats and immunoglobulin-like domains (LRIG) proteins are known to regulate TGFβ signalling in humans—LRIG1 has been shown to suppress GDF7 expression and LRIG3 enhances GDF7 expression in a ligand-specific manner.[75] GDF7 is known to bind to BMPR1 to regulate gene transcription.[74] Intriguingly, the intronic variant rs1158368 within *BMPR1B* (encoding the 1B subunit of BMPR1) associated with the elastopathy phenotype in both the IPD meta-analysis and SEM analysis, however the association was stronger in the diverticular disease GWAS than the combined analyses. *GDF7* is a key elastopathy gene, being previously discovered to associate with several measures of aortic distension, abdominal aortic aneurysm, herniae, pelvic organ prolapse, diverticular disease, and Barrett's oesophagus.

BMP6

Aside from the aforementioned GDFs, the BMPs are the second largest constituent of the TGFβ superfamily, playing central roles in skeletal development and homeostasis.[76] BMP6 is among the primary BMPs expressed in hypertrophic chondrocytes, and is necessary to initiate normal endochondral bone development.[77] We discovered the 6p24.3 (*BMP6*) locus to associate significantly with the elastopathy phenotype in both the latent trait modelling and the IPD meta-analysis. This locus was sub-threshold in all 12 individual trait GWAS, suggesting that BMP6 contributes a latent propensity towards elastopathies. It is intriguing that rare disorders of elastic

tissue such as EDS and MFS present frequently with dysfunction in skeletal development typified by craniofacial abnormalities, suggesting the BMP-SMAD axis may also be an important player in the pathobiology of more common elastopathies.

RHOA

As well as being activated by canonical signalling pathways via SMAD transduction proteins, TGFβ receptors can be activated by non-canonical cascades via RhoA and the protein kinases ERK, p38, and JNK.[78] We discovered the 3p21.31 locus (mapped to *RHOA*) to associate with elastopathy under IPD meta-analysis, whereas it remained sub-threshold in all individual analyses. This shared risk locus encodes the RhoA GTPase, which is a matrisome-associated signalling G protein forming part of the Ras superfamily. In response to TGFβ signalling, RhoA acts as a molecular switch to regulate actin cytoskeletal assembly in fibroblasts and smooth muscle cells.[79] RhoA transduces signals intracellularly within these cells by alternating from the inactivated GDP form to the activated GTP-form to cascade downstream effects.[80] The RhoA/ROCK pathway is associated with several fibrotic phenotypes, including idiopathic pulmonary fibrosis.[81] RhoA expression is marked in vascular smooth muscle cells (VSMCs).[82] Moreover, its expression is reduced in the aortic wall in abdominal aortic aneurysms.[83] Conditional RhoA knock out leads to a greater burden of AAA, likely through impairing contractility of VSMCs, and causing elastin fragmentation.[83] Expression of RhoA is therefore likely to be decreased in elastopathies, and may be important in shared disease risk.

THBS2

Thrombospondins are a family of five secreted, calcium-binding, multi-domain, matrisome glycoproteins with considerable anti-angiogenic activity.[84] Thrombospondin-2 is a homotrimeric protein encoded by *THBS2*; it has defined roles in fibrogenesis, fibrin formation, blood clotting, tissue remodelling and wound repair.[85] The 6q27 locus (mapped to *THBS2*) shows shared genetic risk to elastopathies in both the IPD meta-analysis and the common factor analysis; again, this locus did not reach the significance threshold in any of the individual elastopathy GWAS analyses. THBS2 is known to associate with fibrosis in non-alcoholic fatty liver disease, altering expression of several collagen proteins.[86] Moreover, THBS2 deficiency in mice is associated with disruption in collagen fibre assembly.[87] Decreased function at this locus may therefore be of relevance to pathological extracellular matrix remodelling in elastopathies.

SMAD3

We identified the 15q23 locus (mapped to *SMAD3*) to associate more significantly with the pan-elastopathy phenotype under GWAS meta-analysis than any of the individual analyses—though this locus did not reach statistical significance under latent trait modelling. In the presence of SMAD7, an inhibitor of TGFβ signalling, SMAD3 activation has been shown to directly increase expression of several matricellular genes including *COL1A1*, *COL1A2*, *TIMP1*, *TIMP5*, and *TIMP6*.[88] Heterozygous mutations in six genes are currently known to lead to LDS[89], an elastic tissue disorder characterised by early aortic aneurysm and dissection[67], including two TGFβ ligands (TGFβ2 and TGFβ3), their receptors (TGFβR2 and TGFβR3), and their downstream SMAD transduction proteins (SMAD2 and SMAD3). ~5-10% of LDS patients have a milder form, LDS type-III (aneurysm-osteoarthritis syndrome) which is characterised

by heterozygous polymorphisms in *SMAD3*.[90] Recently, Baskin *et al*. identified for the first time LDS type-III caused by a novel inheritance pattern—biallelic variants in *SMAD3,* associated with more severe and earlier-onset symptoms.[91] There are three protein-coding domains within *SMAD3* (MH1, link-region, and, MH2). Whilst there is a lack of a mutational focal point within SMAD3, the majority of known pathological polymorphisms reside in the MH2 region, associated with an earlier onset of vascular complications.[66] SMAD3, and the SMAD axis more widely, may therefore represent an important pathway for susceptibility to elastopathy.

5.4.4. Strengths and limitations

While this study provides valuable insights into the shared genetic architecture of common elastopathies, it is important to acknowledge the inherent limitations associated with the chosen methodology. First, for the individual elastopathy analyses there was a substantial decrease in the power to detect susceptibility loci when case numbers fell below approximately 5,000 cases. Notably, genome-wide significant susceptibility loci were not identified for aneurysmal disease, pneumothorax, and anorectal prolapse. Second, the categorisation of these diseases as elastopathies is based on my hypothesis of their linkage, rooted in pathophysiological understanding and clinical perspectives. While I acknowledge the potential existence of other disorders with a common genetic architecture, my selection of the 12 elastopathies reflects a conceptual link defined by pathophysiology and clinical features. Third, limitations arise from the use of hospital self-report, medical, and surgical codes to define cases. GP codes, which were not accessible in the UK Biobank at the time of my analysis, have now become available. Though, inclusion of cases based on these codes would potentially serve to decrease the type II error rate and would not affect the validity of the loci we have discovered herein. Fourth, the modelling of the elastopathy phenotype stems from the hypothesis that these conditions are interconnected, despite the current absence of a diagnostic, surgical, or self-report code specifically assigned to this novel diagnosis. Consequently, I was unable to conduct an independent replication analysis of the identified loci.

However, I believe these limitations are off set by significant strengths pertaining to the study. First, the novelty in approach of jointly analysing these disorders has

enabled me to provide the first evidence that there are common pathways connecting nine of the 12 elastopathies that were previously classed under disparate disease categories. As we begin to imagine these disorders under a new grouping of elastopathies, it may be possible to develop common therapies. Second, the multitude of different techniques that I have used, all with differing assumptions, have highlighted similar key pathways and genes. Substantial clustering was observed across the discovered loci, notably along common pathways: the matrisome, TGFβ signalling, and SMAD protein transduction. I can therefore derive more confidence in concluding that these pathways are important in the genetic underpinnings of common elastopathies. Third, to my knowledge this is the first contribution to the literature of the use of genome-wide association testing to comprehensively study these disorders under the common grouping of elastopathies, and therefore prioritise novel genes that were not discovered when these disorders were studied independently, some of which may be amenable to therapeutic intervention.

5.5. Conclusion

5.5.1. Concluding remarks

In conclusion, my study, employing genome-wide association meta-analysis and structural equation modelling, delves into a novel category of pathologically linked disorders defined by elastic tissue dysfunction— the elastopathies. By uncovering shared susceptibility loci, key genes, and common pathways influencing elastic tissue homeostasis, I have significantly advanced our understanding of these interconnected conditions. Despite acknowledged limitations, the findings suggest a shared genetic architecture and a common pathophysiology, opening avenues for potential therapeutic interventions and contributing to a transformative shift in our comprehension of these disorders.

5.6. Chapter References

1. Hynes, R. O. & Naba, A. Overview of the matrisome-An inventory of extracellular matrix constituents and functions. *Cold Spring Harb. Perspect. Biol.* **4**, (2012).
2. Hynes, R. O. The extracellular matrix: Not just pretty fibrils. *Science* **326**, 1216–1219 (2009).
3. Frantz, C., Stewart, K. M. & Weaver, V. M. The extracellular matrix at a glance. *J. Cell Sci.* **123**, 4195–4200 (2010).
4. Ahmed, W. U. R. *et al.* Shared genetic architecture of hernias: A genome-wide association study with multivariable meta-analysis of multiple hernia phenotypes. *PLoS One* **17**, e0272261 (2022).
5. Miller, R. T. Mechanical properties of basement membrane in health and disease. *Matrix Biology* **57**–**58**, 366–373 (2017).
6. Naba, A. *et al.* The matrisome: In silico definition and in vivo characterization by proteomics of normal and tumor extracellular matrices. *Mol. Cell. Proteomics* **11**, (2012).
7. Yue, B. Biology of the extracellular matrix: An overview. *Journal of Glaucoma* **23**, S20–S23 (2014).
8. Lu, P., Takai, K., Weaver, V. M. & Werb, Z. Extracellular Matrix degradation and remodeling in development and disease. *Cold Spring Harb. Perspect. Biol.* **3**, (2011).
9. Sudlow, C. *et al.* UK Biobank: An Open Access Resource for Identifying the Causes of a Wide Range of Complex Diseases of Middle and Old Age. *PLoS Med.* **12**, (2015).
10. Bycroft, C. *et al.* The UK Biobank resource with deep phenotyping and

genomic data. *Nature* **562**, 203–209 (2018).

11. Auton, A. *et al.* A global reference for human genetic variation. *Nature* **526**, 68–74 (2015).
12. Zhou, W. *et al.* Efficiently controlling for case-control imbalance and sample relatedness in large-scale genetic association studies. *Nat. Genet. 2018 509* **50**, 1335–1341 (2018).
13. Purcell, S. *et al.* PLINK: A tool set for whole-genome association and population-based linkage analyses. *Am. J. Hum. Genet.* **81**, 559–575 (2007).
14. Band, G. & Marchini, J. BGEN: a binary file format for imputed genotype and haplotype data. *bioRxiv* 308296 (2018). doi:10.1101/308296
15. Bulik-Sullivan, B. *et al.* LD Score regression distinguishes confounding from polygenicity in genome-wide association studies. *Nat. Genet. 2015 473* **47**, 291–295 (2015).
16. Grotzinger, A. D. *et al.* Genomic structural equation modelling provides insights into the multivariate genetic architecture of complex traits. *Nat. Hum. Behav. 2019 35* **3**, 513–525 (2019).
17. Foley, C. N. *et al.* A fast and efficient colocalization algorithm for identifying shared genetic risk factors across multiple traits. *Nat. Commun. 2021 121* **12**, 1–18 (2021).
18. Watanabe, K., Taskesen, E., Van Bochoven, A. & Posthuma, D. Functional mapping and annotation of genetic associations with FUMA. *Nat. Commun.* **8**, 1–10 (2017).
19. de Leeuw, C. A., Mooij, J. M., Heskes, T. & Posthuma, D. MAGMA: Generalized Gene-Set Analysis of GWAS Data. *PLOS Comput. Biol.* **11**, e1004219 (2015).

20. Zhu, Z. *et al.* Integration of summary data from GWAS and eQTL studies predicts complex trait gene targets. *Nat. Genet.* **48**, 481–487 (2016).

21. Adzhubei, I., Jordan, D. M. & Sunyaev, S. R. Predicting Functional Effect of Human Missense Mutations Using PolyPhen-2. *Curr. Protoc. Hum. Genet.* **76**, 7.20.1-7.20.41 (2013).

22. Ng, P. C. & Henikoff, S. SIFT: predicting amino acid changes that affect protein function. *Nucleic Acids Res.* **31**, 3812–3814 (2003).

23. Rentzsch, P., Witten, D., Cooper, G. M., Shendure, J. & Kircher, M. CADD: predicting the deleteriousness of variants throughout the human genome. *Nucleic Acids Res.* **47**, D886–D894 (2018).

24. Boyle, A. P. *et al.* Annotation of functional variation in personal genomes using RegulomeDB. *Genome Res.* **22**, 1790–1797 (2012).

25. Aguet, F. *et al.* The GTEx Consortium atlas of genetic regulatory effects across human tissues. *Science (80-.).* **369**, 1318–1330 (2020).

26. Christiano, A. M. & Uitto, J. Molecular pathology of the elastic fibers. in *Journal of Investigative Dermatology* **103**, S53–S57 (1994).

27. Baldwin, A. K., Simpson, A., Steer, R., Cain, S. A. & Kielty, C. M. Elastic fibres in health and disease. *Expert Rev. Mol. Med.* **15**, (2013).

28. Harrison, P. & Wordsworth, P. Metabolic bone disease and inherited disorders of bone and connective tissue. in *The Rheumatology Handbook* 247–298 (Imperial College Press, 2011). doi:10.1142/9781848163218_0005

29. Milewicz, D. M., Urban, Z. & Boyd, C. *Genetic disorders of the elastic fiber system*. *Matrix Biology* **19**, (2000).

30. Wang, K., Meng, X. & Guo, Z. Elastin Structure, Synthesis, Regulatory Mechanism and Relationship With Cardiovascular Diseases. *Front. Cell Dev.*

Biol. **9**, (2021).

31. Parks, W. C. Posttranscriptional regulation of lung elastin production. *Am. J. Respir. Cell Mol. Biol.* **17**, 1–2 (1997).
32. Tassabehji, M. *et al.* Elastin: Genomic Structure and Point Mutations in Patients with Supravalvular Aortic Stenosis. *Hum. Mol. Genet.* **6**, 1029–1036 (1997).
33. Brown-Augsburger, P., Tisdale, C., Broekelmann, T., Sloan, C. & Mecham, R. P. Identification of an Elastin Cross-linking Domain That Joins Three Peptide Chains: POSSIBLE ROLE IN NUCLEATED ASSEMBLY. *J. Biol. Chem.* **270**, 17778–17783 (1995).
34. Delio, M. *et al.* Spectrum of elastin sequence variants and cardiovascular phenotypes in 49 patients with Williams–Beuren syndrome. *Am. J. Med. Genet. Part A* **161**, 527–533 (2013).
35. Mead, T. J. & Apte, S. S. ADAMTS proteins in human disorders. *Matrix Biology* **71**–**72**, 225–239 (2018).
36. Apte, S. S. ADAMTS Proteins: Concepts, Challenges, and Prospects. *Methods Mol. Biol.* **2043**, 1–12 (2020).
37. Kelwick, R., Desanlis, I., Wheeler, G. N. & Edwards, D. R. The ADAMTS (A Disintegrin and Metalloproteinase with Thrombospondin motifs) family. *Genome Biol.* **16**, 113 (2015).
38. Kemberi, M., Salmasi, Y. & Santamaria, S. The Role of ADAMTS Proteoglycanases in Thoracic Aortic Disease. *Int. J. Mol. Sci.* **24**, (2023).
39. Oller, J. *et al.* Nitric oxide mediates aortic disease in mice deficient in the metalloprotease Adamts1 and in a mouse model of Marfan syndrome. *Nat. Med.* **23**, 200–212 (2017).

40. Collins-Racie, L. A. *et al.* ADAMTS-8 exhibits aggrecanase activity and is expressed in human articular cartilage. *Matrix Biol.* **23**, 219–230 (2004).

41. Omura, J. *et al.* ADAMTS8 Promotes the Development of Pulmonary Arterial Hypertension and Right Ventricular Failure A Possible Novel Therapeutic Target. *Circ. Res.* **125**, 884–906

42. Santamaria, S. *et al.* Post-translational regulation and proteolytic activity of the metalloproteinase ADAMTS8. *J. Biol. Chem.* **297**, 101323 (2021).

43. Zha, Y. *et al.* ADAMTS8 Promotes Cardiac Fibrosis Partly Through Activating EGFR Dependent Pathway. *Front. Cardiovasc. Med.* **9**, 797137 (2022).

44. Holbourn, K. P., Acharya, K. R. & Perbal, B. The CCN family of proteins: structure–function relationships. *Trends Biochem. Sci.* **33**, 461–473 (2008).

45. Sun, C., Zhang, H. & Liu, X. Emerging role of CCN family proteins in fibrosis. *J. Cell. Physiol.* **236**, 4195–4206 (2021).

46. Ren, Z. *et al.* Effects of CCN3 on fibroblast proliferation, apoptosis and extracellular matrix production. *Int. J. Mol. Med.* **33**, 1607–1612 (2014).

47. Lin, C. G. *et al.* CCN3 (NOV) is a novel angiogenic regulator of the CCN protein family. *J. Biol. Chem.* **278**, 24200–24208 (2003).

48. Riser, B. L. *et al.* CCN3 (NOV) Is a Negative Regulator of CCN2 (CTGF) and a Novel Endogenous Inhibitor of the Fibrotic Pathway in an in Vitro Model of Renal Disease. *Am. J. Pathol.* **174**, 1725–1734 (2009).

49. Madne, T. H. & Dockrell, M. E. C. CCN3, a key matricellular protein, distinctly inhibits TGFβ1-mediated Smad1/5/8 signalling in human podocyte culture. *Cell. Mol. Biol. (Noisy-le-grand).* **64**, 5–10 (2018).

50. Liu, H. F. *et al.* CCN3 suppresses TGF-β1-induced extracellular matrix accumulation in human mesangial cells in vitro. *Acta Pharmacol. Sin. 2018*

392 **39**, 222–229 (2017).

51. Naba, A. *et al.* The extracellular matrix: Tools and insights for the ‘omics’ era. *Matrix Biol.* **49**, 10–24 (2016).
52. Moustakas, A. & Heldin, C. H. The regulation of TGFβ signal transduction. *Development* **136**, 3699–3714 (2009).
53. Massagué, J. TGFβ signalling in context. *Nat. Rev. Mol. Cell Biol.* **13**, 616–630 (2012).
54. Massagué, J., Blain, S. W. & Lo, R. S. TGFβ signaling in growth control, cancer, and heritable disorders. *Cell* **103**, 295–309 (2000).
55. Kucich, U., Rosenbloom, J. C., Abrams, W. R., Bashir, M. M. & Rosenbloom, J. Stabilization of elastin mRNA by TGF-beta: initial characterization of signaling pathway. *Am. J. Respir. Cell Mol. Biol.* **17**, 10–16 (1997).
56. Kuang, P. P. *et al.* Activation of elastin transcription by transforming growth factor-β in human lung fibroblasts. *Am. J. Physiol. - Lung Cell. Mol. Physiol.* **292**, 944–952 (2007).
57. Cocciolone, A. J. *et al.* Elastin, arterial mechanics, and cardiovascular disease. *Am. J. Physiol. - Hear. Circ. Physiol.* **315**, H189–H205 (2018).
58. Loeys, B. L. *et al.* The revised Ghent nosology for the Marfan syndrome. *J. Med. Genet.* **47**, 476–485 (2010).
59. Chaudhry, S. S. *et al.* Fibrillin-1 regulates the bioavailability of TGFbeta1. *J. Cell Biol.* **176**, 355–367 (2007).
60. Reinhardt, D. P. *et al.* Fibrillin-1: Organization in Microfibrils and Structural Properties. *J. Mol. Biol.* **258**, 104–116 (1996).
61. Zilberberg, L. *et al.* Specificity of latent TGF-β binding protein (LTBP) incorporation into matrix: Role of fibrillins and fibronectin. *J. Cell. Physiol.* **227**,

3828–3836 (2012).

62. Weiss, A. & Attisano, L. The TGFbeta Superfamily Signaling Pathway. *Wiley Interdiscip. Rev. Dev. Biol.* **2**, 47–63 (2013).

63. Bertoli-Avella, A. M. *et al.* Mutations in a TGF-β Ligand, TGFB3, Cause Syndromic Aortic Aneurysms and Dissections. *J. Am. Coll. Cardiol.* **65**, 1324–1336 (2015).

64. Loeys, B. L. *et al.* A syndrome of altered cardiovascular, craniofacial, neurocognitive and skeletal development caused by mutations in TGFBR1 or TGFBR2. *Nat. Genet.* **37**, 275–281 (2005).

65. Meester, J. A. N. *et al.* Differences in manifestations of Marfan syndrome, Ehlers-Danlos syndrome, and Loeys-Dietz syndrome. *Ann. Cardiothorac. Surg.* **6**, 582–594 (2017).

66. Schepers, D. *et al.* A mutation update on the LDS-associated genes TGFB2/3 and SMAD2/3. *Hum. Mutat.* **39**, 621–634 (2018).

67. Lindsay, M. E. *et al.* Loss-of-function mutations in TGFB2 cause a syndromic presentation of thoracic aortic aneurysm. *Nat. Genet.* **44**, 922–927 (2012).

68. Shin, J. Y. *et al.* Epigenetic activation and memory at a TGFB2 enhancer in systemic sclerosis. *Sci. Transl. Med.* **11**, (2019).

69. Dropmann, A. *et al.* TGF-β2 silencing to target biliary-derived liver diseases. *Gut* **69**, 1677–1690 (2020).

70. Habashi, J. P. *et al.* Losartan, an AT1 Antagonist, Prevents Aortic Aneurysm in a Mouse Model of Marfan Syndrome. *Science* **312**, 117 (2006).

71. Davidson, A. J. *et al.* Isolation of Zebrafish gdf7 and Comparative Genetic Mapping of Genes Belonging to the Growth/Differentiation Factor 5, 6, 7 Subgroup of the TGF-β Superfamily. *Genome Res.* **9**, 121–129 (1999).

72. Wolfman, N. M. *et al.* Ectopic induction of tendon and ligament in rats by growth and differentiation factors 5, 6, and 7, members of the TGF-beta gene family. *J. Clin. Invest.* **100**, 321–330 (1997).

73. Mikic, B., Bierwert, L. A. & Tsou, D. Achilles Tendon characterization in GDF-7 deficient mice. *J. Orthop. Res.* **24**, 831–841 (2006).

74. Kong, D. *et al.* Growth differentiation factor 7 autocrine signaling promotes hepatic progenitor cell expansion in liver fibrosis. *Stem Cell Res. Ther.* **14**, (2023).

75. Abdullah, A., Herdenberg, C. & Hedman, H. Ligand-specific regulation of transforming growth factor beta superfamily factors by leucine-rich repeats and immunoglobulin-like domains proteins. *PLoS One* **18**, (2023).

76. Wu, M., Chen, G. & Li, Y. P. TGF-β and BMP signaling in osteoblast, skeletal development, and bone formation, homeostasis and disease. *Bone Res. 2016 41* **4**, 1–21 (2016).

77. Kugimiya, F. *et al.* Involvement of Endogenous Bone Morphogenetic Protein (BMP) 2 and BMP6 in Bone Formation. *J. Biol. Chem.* **280**, 35704–35712 (2005).

78. Derynck, R. & Zhang, Y. E. Smad-dependent and Smad-independent pathways in TGF-β family signalling. *Nat. 2003 4256958* **425**, 577–584 (2003).

79. Huveneers, S. & Danen, E. H. J. Adhesion signaling – crosstalk between integrins, Src and Rho. *J. Cell Sci.* **122**, 1059–1069 (2009).

80. Haga, R. B. & Ridley, A. J. Rho GTPases: Regulation and roles in cancer cell biology. *Small GTPases* **7**, 207 (2016).

81. Knipe, R. S., Tager, A. M. & Liao, J. K. The Rho Kinases: Critical Mediators of Multiple Profibrotic Processes and Rational Targets for New Therapies for

Pulmonary Fibrosis. *Pharmacol. Rev.* **67**, 103–117 (2015).

82. Tang, L. *et al.* RhoA/ROCK signaling regulates smooth muscle phenotypic modulation and vascular remodeling via the JNK pathway and vimentin cytoskeleton. *Pharmacol. Res.* **133**, 201–212 (2018).

83. Molla, M. R. *et al.* Vascular smooth muscle RhoA counteracts abdominal aortic aneurysm formation by modulating MAP4K4 activity. *Commun. Biol.* **5**, (2022).

84. Adams, J. C. & Lawler, J. The thrombospondins. *Int. J. Biochem. Cell Biol.* **36**, 961 (2004).

85. Bornstein, P., Armstrong, L. C., Hankenson, K. D., Kyriakides, T. R. & Yang, Z. Thrombospondin 2, a matricellular protein with diverse functions. *Matrix Biol.* **19**, 557–568 (2000).

86. Kimura, T. *et al.* Thrombospondin 2 is a key determinant of fibrogenesis in non-alcoholic fatty liver disease. *Liver Int.* **44**, 483–496 (2024).

87. Kyriakides, T. R. *et al.* Mice That Lack Thrombospondin 2 Display Connective Tissue Abnormalities That Are Associated with Disordered Collagen Fibrillogenesis, an Increased Vascular Density, and a Bleeding Diathesis. *J. Cell Biol.* **140**, 419–430 (1998).

88. Verrecchia, F., Chu, M. L. & Mauviel, A. Identification of novel TGF-beta /Smad gene targets in dermal fibroblasts using a combined cDNA microarray/promoter transactivation approach. *J. Biol. Chem.* **276**, 17058–17062 (2001).

89. Velchev, J. D., Van Laer, L., Luyckx, I., Dietz, H. & Loeys, B. Loeys-Dietz Syndrome. In: Halper, J. (eds) Progress in Heritable Soft Connective Tissue Diseases. in *Advances in Experimental Medicine and Biology* **1348**, 251–264 (Springer, Cham, 2021).

90. Van Der Linde, D. *et al.* Aggressive Cardiovascular Phenotype of Aneurysms-Osteoarthritis Syndrome Caused by Pathogenic SMAD3 Variants. *J. Am. Coll. Cardiol.* **60**, 397–403 (2012).

91. Baskin, S. M., Morris, S. A., Vara, A., Hecht, J. T. & Farach, L. S. The first reported case of Loeys-Dietz syndrome in a patient with biallelic SMAD3 variants. *Am. J. Med. Genet. Part A* **182**, 2755–2760 (2020).

5.7. Chapter Appendix

*The appendix for this chapter is provided as an online supplement at the following URL: **bit.ly/WAhmed_C5Appendix***

Table of Contents

Appendix Table 5.15. Genome-wide gene-based association analysis for the IPD GWAS meta-analysis in MAGMA.

Appendix Table 5.16. Summary-based Mendelian Randomisation (SMR) for the IPD GWAS meta-analysis using eQTL data from GTEx.

Appendix Table 5.17. Positionally mapped genes for the common factor analysis.

Appendix Table 5.18. eQTL mapped genes for the common factor analysis.

Appendix Table 5.19. Genome-wide gene-based association analysis for the common factor analysis in MAGMA.

2. Appendix Figures

Appendix Figure 5.1. Regional locus zoom plots for the eight novel loci from the individual elastopathy analyses.

Appendix Figure 5.2. Manhattan plots for the 12 individual elastopathy analyses.

Appendix Figure 5.3. Regional locus zoom plots for all 12 individual elastopathy associated signals.

Appendix Figure 5.4. Quantile-quantile (Q-Q) plots for all 12 individual elastopathy analyses.

Appendix Figure 5.5. Regional locus zoom plots for the IPD GWAS meta-analysis.

Appendix Figure 5.6. Quantile-quantile (Q-Q) plots for the IPD GWAS meta-analysis.

Appendix Figure 5.7. Regional locus zoom plots for the IPD GWAS meta-analysis loci demonstrating compelling evidence of shared risk across the 12 elastopathy phenotypes.

Appendix Figure 5.8. Regional locus zoom plots for the common factor analysis loci demonstrating compelling evidence of shared risk across the 12 elastopathy phenotypes.

Appendix Figure 5.9. Summary of the FUMA SNP2GENE analysis of the IPD GWAS meta-analysis.

Appendix Figure 5.10. Functional annotation of the genome-wide significant variants at the 37 IPD GWAS meta-analysis loci.

Appendix Figure 5.11. Summary of the FUMA SNP2GENE analysis of the common factor analysis.

Appendix Figure 5.12. Functional annotation of the genome-wide significant variants at the 31 common factor loci.

Chapter 6: Conclusion

6.1. Conclusion

6.1.1. Summary

Chapter 1. I discussed the complexity of the extracellular matrix (ECM) and the mammalian matrisome, which has a fundamental role in structural integrity of tissues and roles exceeding far beyond this, including in important cellular processes. The ECM composition of tissues is delicately balanced by the complex interactions of proteases and their natural inhibitors. Dysfunction in the tightly controlled balance of elastic and collagen fibre components disrupts tissue homeostasis, which can alter the elastic properties of tissues and affect their ability to recover after deformation. This can prevent tissues from performing their normal physiological roles, which, in turn, can lead to a constellation of common diseases characterised by elastic tissue dysfunction which I coined as the "elastopathies". I then provided evidence for my twelve diseases of interest – hiatus hernia, diverticular disease, haemorrhoids, inguinal hernia, varicose veins, female genital prolapse, umbilical hernia, aneurysmal disease, emphysema, pneumothorax, rectal prolapse, and femoral hernia – being elastopathies with a complex aetiology and demonstrated a paucity in the understanding around their genetic susceptibility. Finally, I discussed the merits of GWAS as the current best way to study the genetic architecture of common disorders and introduced the UK Biobank as a truly ground-breaking resource that makes large-scale genetic association studies feasible.[1]

Chapter 2. To unravel the genetic architecture of varicose veins, I performed the largest two-stage GWAS of varicose veins in 135,514 cases and 675,111 controls

(810,625 participants) from the UK Biobank with independent replication in 23andMe.[2] I identified 49 signals at 46 risk loci (29 novel) associated with varicose veins, and using a plethora of bioinformatic tools, I prioritised functional variants and annotated these loci to over 200 genes, and demonstrated therapeutic tractability of several important genes including some pertaining to ECM regulation. Importantly, using the GWAS-derived variants as genetic predictors for varicose veins, I constructed a weighted genetic risk score (wGRS) that correlated with disease severity, which may foreseeably pave the way towards future personalised medicine approaches.

Chapter 3. I performed (at the time) the first ever GWAS of haemorrhoids disease in over 400,000 participants from the UK Biobank. I identified 12 novel loci associated with haemorrhoids, with prioritised genes showing remarkable clustering in pathways relating to ECM remodelling, TGF-β signalling, and smooth muscle biology. Moreover, almost one-fifth of prioritised genes had known pharmaceutical interactions and are currently being investigated in other disorders. Importantly, the wGRS again correlated with severity of haemorrhoids, and suggests that genetic susceptibility is an important contributor to haemorrhoids biology. The study findings reported in this chapter were subsequently confirmed by Zheng and colleagues though a large-scale GWAS in almost a million participants[3]

Chapter 4. I performed a novel GWAS to investigate the shared genetic susceptibility between multiple hernia phenotypes in UK Biobank (namely inguinal, femoral, umbilical, and hiatus hernia).[4] I performed this principally through two approaches: i) association studies of each hernia individually, ii) association analyses of the hernia phenotypes combined – using both linear mixed-model[5] approaches and multi-trait

meta-analyses approaches (MTAG and metaUSAT).[6,7] I uncovered 38 loci (52 signals) associated with the four hernia traits individually, and through multi-trait meta-analysis identified six biologically relevant putative loci that demonstrate the highest degree of shared susceptibility across the hernia phenotypes. The multi-trait meta-analysis approaches also uncovered six predisposing genetic variants that were not revealed by the individual analyses that demonstrate shared susceptibility. Through wGRS analysis, I demonstrate that genetic burden also correlates with disease severity across all examined hernia phenotypes. All in all, these results provide convincing new evidence of a shared genetic susceptibility to hernia risk.

Chapter 5. I extended my previous work by performing a comprehensive GWAS study of all 12 common elastopathies identified in UK Biobank (hiatus hernia, diverticular disease, haemorrhoids, inguinal hernia, varicose veins, female genital prolapse, umbilical hernia, aneurysms, emphysema, pneumothorax, rectal prolapse, and femoral hernia). This study leveraged an individual patient data (IPD) GWAS meta-analysis of ~400,000 participants to identify 18 susceptibility loci previously not associated with any of the individual elastopathies when studied alone. Employing genomic common factor analysis to unveil the latent elastopathy phenotype, an additional four susceptibility loci were identified. This comprehensive approach, combining both meta-analysis and common factor analysis, pinpointed core matrisomal genes associated with the elastopathy phenotype and highlights a shared genetic architecture and a common pathophysiology, opening avenues for potential therapeutic interventions and transforming out understanding of these disorders.

6.1.2. Implications

Despite the prominence of GWA studies over the past fifteen years, existing studies have largely overlooked the genetic susceptibility to common elastopathies.[8] In this DPhil thesis I presented data which advances the field of study around elastopathies and complex trait genetics. Collectively, I have identified a total of 85 distinct susceptibility loci (eight not before reported) associated with nine of the 12 elastopathy traits, and around a dozen loci which were not discovered in the individual analyses, to associate with the elastopathy phenotype. This plethora of rich associations would not have been possible without augmenting the case numbers through the use of operative codes to identify additional participants who had undergone surgery for the respective diseases. Indeed, the study of surgical disorders lends itself well to biobank-scale cohorts like the UK Biobank, due to the fact that participants undergoing surgery are more likely to be on the phenotypically severe end of the spectrum and are therefore more likely to be true cases. However, this is often neglected in existing GWA studies, resulting in misclassification bias and weak cohort definitions.[9]

For the pan-hernia and the pan-elastopathy analyses, several notable loci were identified only after multi-trait analysis, meta-analysis and common-factor analysis, and this finding is important in demonstrating the use of multi-trait approaches which are able to leverage larger sample sizes to delineate predisposing genetic variants that would not have been identified through single-trait approaches alone. In total, at the associated loci, I mapped over 500 putative genes, many of which demonstrated evidence of therapeutic tractability and warrant further investigation as potential drug targets. The most striking clustering of genes was seen for those pertaining to ECM components, meaning these complex disorders are ones in which elastic tissue dysfunction plays a central role in their pathobiology – this too is a novel and insightful

finding which helps to advance our understanding of their pathobiology. Among the putative genes identified in this thesis and subsequently shown to have good evidence of functionality and therapeutic potential is *PIEZO1*, which encodes a mechanosensitive cation channel involved in shear stress. Zhao *et al*.[10] leveraged this finding from GWAS (including my publication[2]) to demonstrate in a mouse model of varicose veins that a PIEZO1 agonist (Yoda1) exacerbates varicose veins with increased inflammatory cell infiltration, while endothelial Piezo1 deletion is protective. The authors conclude that PIEZO1 constitutes a potential therapeutic approach for the medical treatment of VVs. This study provides excellent proof-of-principle of the therapeutic potential of the disease-associated loci identified in this thesis, while also illustrating a fundamental raison d'être of GWAS.

6.2. Chapter references

1. Sudlow, C. *et al.* UK Biobank: An Open Access Resource for Identifying the Causes of a Wide Range of Complex Diseases of Middle and Old Age. *PLoS Med.* **12**, (2015).
2. Ahmed, W. U. R. *et al.* Genome-wide association analysis and replication in 810,625 individuals with varicose veins. *Nat. Commun. 2022 131* **13**, 1–11 (2022).
3. Zheng, T. *et al.* Genome-wide analysis of 944 133 individuals provides insights into the etiology of haemorrhoidal disease. *Gut* **70**, 1538–1549 (2021).
4. Ahmed, W. U. R. *et al.* Shared genetic architecture of hernias: A genome-wide association study with multivariable meta-analysis of multiple hernia phenotypes. *PLoS One* **17**, e0272261 (2022).
5. Loh, P. R. *et al.* Efficient Bayesian mixed-model analysis increases association power in large cohorts. *Nat. Genet.* **47**, 284–290 (2015).
6. Turley, P. *et al.* Multi-trait analysis of genome-wide association summary statistics using MTAG. *Nat. Genet.* **50**, 229–237 (2018).
7. Ray, D. & Boehnke, M. Methods for meta-analysis of multiple traits using GWAS summary statistics. *Genet. Epidemiol.* **42**, 134–145 (2018).
8. Grant, Y., Onida, S. & Davies, A. Genetics in chronic venous disease. *Phlebol. J. Venous Dis.* **32**, 3–5 (2017).
9. Fukaya, E. et al. Clinical and Genetic Determinants of Varicose Veins. *Circulation* 1–12 (2018). doi:10.1161/CIRCULATIONAHA.118.035584
10. Zhao, J. *et al.* Endothelium Piezo1 deletion alleviates experimental varicose veins by attenuating perivenous inflammation. *Mol. Cell. Biochem.* 1–13 (2024). doi:10.1007/S11010-024-05115-9/METRICS